JANUARY · 1953

Proceedings of the I·R·E

UHF ISSUE

UHF Commercial Television Pioneer

(RIGHT) Completed transmitter room of KPTV, the first commercial uhf TV station, now in operation at Portland, Ore.

(BELOW) KPTV's antenna about to be lifted to supporting tower as station neared completion last September.

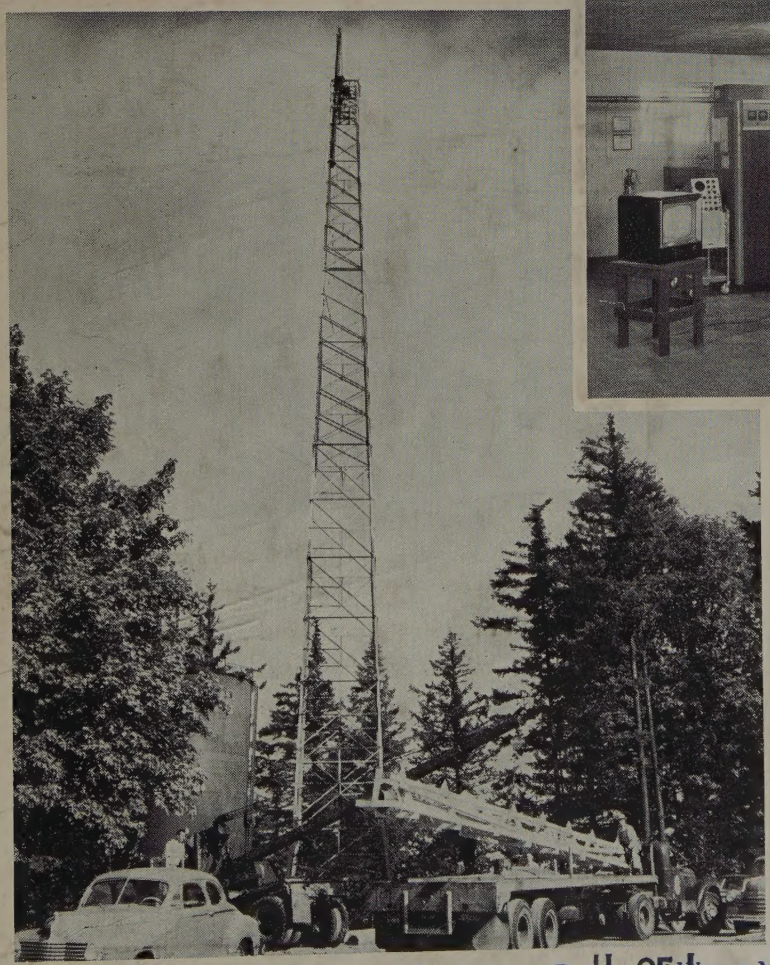

IN THIS ISSUE

Thirty UHF Papers on the Following Topics:

Transmitters	Antennas
Tubes	Relays
Receivers	Propagation
Transmission Lines	Instruments

The Institute of Radio Engineers

AMPEREX

AIR-COOLED TUBE AX9904-R/5924

"...Offers a maximum in kilowatts per dollar..." HARRY R. SMITH, Manager, Television Engineering, Standard Electronics Corporation

STANDARD ELECTRONICS CORPORATION uses this tube in Models TH653 High Band and TL653 Low Band Transmitters and also in their new 20 Kilowatt Transmitter, built on the exclusive S-E ADD-A-UNIT PRINCIPLE, and with special S-E features that insure dependable operation, maximum convenience, and minimum maintenance.

STANDARD ELECTRONICS CORPORATION
(A SUBSIDIARY OF CLAUDE NEON, INC.)

TELEVISION AND BROADCAST TRANSMITTERS AND AUXILIARY EQUIPMENT
AMERTRAN ELECTRONIC TRANSFORMERS AND TRANSTATS

TELEPHONE — BIGELOW 3-5540
BIGELOW 3-4444

285 EMMET STREET
NEWARK 5, N. J.

April 23, 1952

Mr. Sam Norris, Pres.
Amperex Electronics Corp.
25 Washington St.
Brooklyn 1, New York

Dear Mr. Norris:

As you know we have been working with the Amperex Type AX9904-R vacuum tube in the development of the various Standard Electronics television broadcast transmitters. The tube is being used in the currently manufactured Model TH653 and TL 653 Transmitters in both the aural and visual sections.

I believe you will be interested in knowing that we are very well satisfied with the performance of this tube as a broad band linear amplifier on all V.H.F. television channels. The low interelectrode capacitance and low internal impedance of the AX9904-R permit power output levels of 5KW and more, with band widths in excess of 5 megacycles. These conditions are readily obtainable from a single tube operating well within its published tube characteristics. The moderate cost of the tube leads us to believe that it offers a maximum in "kilowatts per dollar".

Yours very truly,
Harry R. Smith
Harry R. Smith
Mgr. Television Engineering

HRS:hg

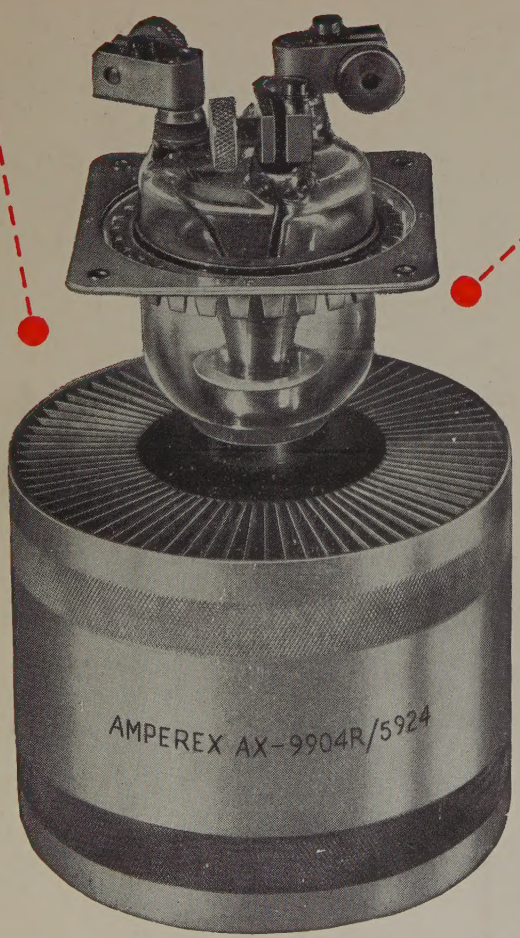

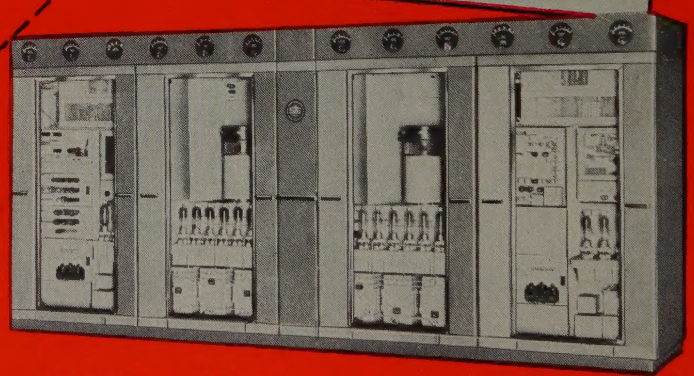

FEATURES INCLUDE . . . 14 MC band width at 220 MC . . . outputs of 5.7 KW . . . thoriated tungsten filament . . . non-emitting grid . . . disc type grid seal for mimimum inductance . . . minimum capacitance . . . and PROVEN *long life.*

Write for complete data sheets.

This tube is also available in a Water-Cooled Version, Type AX9904-5923.

***Re-tube with* AMPEREX**

AMPEREX ELECTRONIC CORP.
230 DUFFY AVENUE, HICKSVILLE, LONG ISLAND, N. Y.
In Canada and Newfoundland: Rogers Majestic Limited
11-19 Brentcliffe Road, Leaside, Toronto, Ontario, Canada
Cable: "AMPRONICS"

Changes of address (with advance notice of fifteen days) and communications regarding subscriptions and payments should be mailed to the Secretary of the Institute, at 450 Ahnaip St., Menasha, Wisconsin, or 1 East 79 Street, New York 21, N. Y.

* Numerals in parentheses following Directors' names designate Region numbers.

PROCEEDINGS OF THE I.R.E.

Published Monthly by

The Institute of Radio Engineers, Inc.

VOLUME 41 — *January, 1953* — NUMBER 1

PROCEEDINGS OF THE I.R.E.

INSTITUTE NEWS AND RADIO NOTES SECTION

James W. McRae

PRESIDENT, 1953

J. W. McRae was born on October 25, 1910, in Vancouver, British Columbia. He received the B.S. degree in electrical engineering from the University of British Columbia in 1933, and the M.S. and Ph.D. degrees from the California Institute of Technology in 1934 and 1937.

Dr. McRae joined the Bell Telephone Laboratories, Inc., in 1937, where he engaged in research on transoceanic radio transmitters and later worked on a microwave oscillator for National Defense Research Council.

During World War II, Dr. McRae was commissioned a major in the United States Signal Corps, assigned to the Office of the Chief Signal Officer in Washington, D. C. After working on development programs for airborne radar equipment and radar countermeasures devices, he transferred to the Signal Corps Engineering Laboratories at Bradley Beach, N. J., as chief of the engineering staff. There, he became deputy director of the division and attained the rank of colonel, before returning to civilian life and the Bell Telephone Laboratories in 1945.

In 1946, Dr. McRae was appointed director of radio projects and television research at Bell, with additional responsibility for electron dynamics research, and in 1947, he became director of electronics and television research. In 1949, he was appointed director of apparatus development I, and then director of transmission development. Dr. McRae became vice president in charge of systems development organization in 1951, the position he presently holds.

Dr. McRae joined the Institute in 1931, as an Associate and became an IRE Fellow in 1947. In addition to serving on various IRE Committees, he has been the Chairman of the New York IRE Section, has been a member of the IRE Board of Directors, and he has served on the IRE Board of Editors since 1946.

Dr. McRae holds membership in the American Institute of Electrical Engineers and Sigma Xi. He has received the United States Legion of Merit and the Eta Kappa Nu Honorary Mention for Outstanding Young Electrical Engineers.

The UHF Issue

In order that the membership may more readily keep abreast of the major developments in the radio engineering field, the Board of Directors of the Institute has authorized the publication, on a nonscheduled basis, of special issues of the PROCEEDINGS OF THE I.R.E., devoted to subjects of particular importance and timeliness. The present issue is the third such special issue to be published, and is devoted to a subject of far-reaching significance, namely, the ultra-high-frequency domain.

The recent action of the Federal Communications Commission in opening the uhf band for commercial television broadcasting in the United States is a matter of more than ordinary consequence. To the radio engineer, it is the signal for a marked acceleration in the development and use of apparatus for operation in this portion of the radio spectrum. And though attention will be focused primarily on television, the resulting new techniques will find important application in many other fields, leading to a general advancement of the radio-electronic art as a whole. To industry, the FCC's action obviously is of major commercial importance; it opens many new markets for products and services. To the man in the street, it signifies that truly "nationwide service" is an assured reality in the near future.

As noted above, the subject of ultra-high frequencies is considerably broader than that of uhf television. Hence, the scope of the papers presented herein is correspondingly broad, running the gamut of applications of the uhf and shf bands and encompassing the subjects of propagation, instrumentation, transmitting and receiving equipment, circuits, tubes, and components.

With this issue, the PROCEEDINGS OF THE I.R.E. marks the 40th anniversary of its first issue. It is particularly appropriate, therefore, that the present issue should be devoted to a subject which so well exemplifies the advances that have been made in radio since 1913, and the application of those advances to human needs. There is presented accordingly in the following pages a selection of papers which, it is felt, will substantially contribute to the further progress of the radio art and to the services rendered by it to society.

—The Technical Editor

Measurements of Some Operational Characteristics of an Amplitude-Modulated Injection-Locked UHF Magnetron Transmitter*

L. L. KOROS†, SENIOR MEMBER, IRE

Summary—**Measurements of the loop impedance of an amplitude-modulated injection-locked uhf magnetron looking from the transmission line toward the magnetron are presented. The loop impedance is computed from the voltage standing-wave ratio and the position of the minimum-voltage plane of the injection current reflected from the magnetron output loop. While the plate voltage is varied, the changes of the loop impedance are observed under specific conditions which are important for the proper performance of the resonant injection system.**

Analyses of the phenomena occurring in the output transmission line of the synchronized magnetron are described. Matched and decoupled resistive loads as well as a reactive load are presented to the magnetron at the high-power end of the modulation cycle. It is demonstrated that the load impedance seen by the magnetron steadily and substantially changes during an amplitude-modulation cycle. However, at the low-power end of a 100-per cent modulation cycle the load is constant, and the value of it for a given type of magnetron with a predetermined setting of the magnetron tuner depends only upon the carrier frequency. The changes of load during the modulation cycle are discussed. These are graphically represented by a special kind of circular diagram.

Introduction

THE PRODUCTION of amplitude-modulated ultra-high-frequency (uhf) carriers having stable frequency, low envelope distortion, and good efficiency is at present one of the interesting problems of the electronic industry. A similar but somewhat easier problem is the production of frequency- or phase-modulated (angular-modulated) carriers at the same high carrier-frequency regions. It is generally known that, if the carrier frequency is to be higher than about 500 mc conventional amplifier tubes are limited in use. One approach to the problem has been to apply frequency- and phase-controlled magnetron oscillators for amplitude modulated (AM) or angular-modulated transmitter services. Promising results have been previously reported.[1] Crystal control of the carrier frequency was achieved by means of a resonant injection system. The quality of the modulated output carrier met practical transmitter requirements and the measured plate-power efficiency was close to 60 per cent. As the emitted power level is varied, the dc plate-power input varies too, so the over-all efficiency during an AM cycle is substantially unchanged. Though the experiments were made at a 1-kw level, it is believed that the system has no inherent power limitations. A practical limit is set, however, by the power capacity of the RF injection source. Since the RF injection power must be about 5 to 10 per cent of the peak power of the magnetron, the magnetron peak power is, therefore, limited to about twenty to ten times the power output of the available injection-amplifier tube.

The basic properties of injection-locked modulated magnetrons have been previously reported. In some experiments the injection-source frequency was equal to one-half the carrier frequency, and in others it was equal to the carrier frequency itself.[1] An analytical study of the system by Donal and Chang[2] indicated a method by which some specific constants of the system might be predicted from the Rieke diagram of the magnetron, the system being operated with the injection frequency equal to the carrier frequency. Some earlier studies by others[3,4,5] in the injection-stabilizing field were discussed previously.[1]

In the present paper a method is described for obtaining some data on the amplitude-modulated magnetron while it is synchronized by an injection current at the frequency of the magnetron carrier. These data are considered to be necessary for a proper understanding of the operation of the resonant injection system.

The Measuring Setup

Fig. 1 is a block diagram of the experimental system, consisting basically of an injection-stabilized magnetron, and six tuners. The magnetron is amplitude modulated in the plate. All the tuners used in the experi-

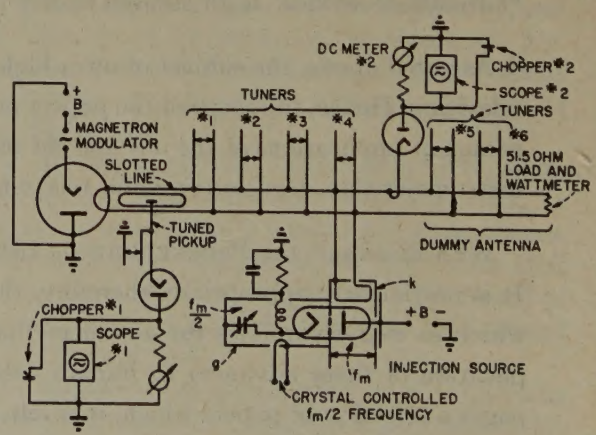

Fig. 1—The experimental setup to determine magnetron loop impedances and loading in a resonant injection system.

* Decimal classification: R355.912.1×R259. Original manuscript received by the Institute, September 26, 1952. Abstract presented at the National Electronics Conference, Chicago, Ill., Sept. 30, 1952.

† Radio Corporation of America, RCA Victor Div., Camden, N. J.

[1] L. L. Koros, "Frequency control of modulated magnetrons by resonant injection system," *RCA Rev.*, vol. XIII, pp. 47–57; 1952.

[2] J. S. Donal, Jr. and K. K. N. Chang, "An analysis of the injection locking of magnetrons used in amplitude-modulated transmitters," *RCA Rev.*, vol. XIII, pp. 239–257; June, 1952.

[3] I. Wolff, "Frequency-Controlled Electronic Oscillator," U. S. Patent 2,133,225; Application, July, 1936.

[4] J. C. Slater, M.I.T. Report No. 35, "The Phasing of Magnetrons," M.I.T., Cambridge, Mass.; April, 1947.

[5] E. E. David, Jr., M.I.T. Report No. 63, "Locking Phenomena in Microwave Oscillator," M.I.T., Cambridge, Mass.; April, 1948.

mental setup would not be necessary for operating a practical transmitter; they are, however, useful during measurements for changing the circuit constants without having to change the actual lengths of the transmission lines. A diode is coupled into the line at a point close to the dummy antenna, which is composed of a 51.5-ohm resistor and two tuners. The output of the detector is observed on an oscilloscope. A vibrating short circuit (chopper) is coupled to the load resistor of the detector to establish the zero-voltage line on the scope.[6] The amplitude-modulation factor can be measured from the scope picture in this way (Fig. 4). A similar detector system is coupled to the sliding pickup probe of the slotted line.

The injection power was produced by a Type-6161 grounded-grid frequency-doubler triode. The plate cavity "k" of the triode (Fig. 1) was tuned to the stabilized magnetron output frequency which was $f_m = 750$ or 825 mc, while the grid cavity "g" was excited with a crystal-controlled $f_m/2$ frequency.

The Measured Data

To keep the magnetron output frequency and phase under control, it is necessary to build up a high injection current in the output loop of the magnetron. To do this, it is necessary to know the loop impedance as seen from the injection source, in particular, at the low end of the AM cycle. The value of the loop impedance at the low end of an AM cycle is important design information since this impedance determines the distance of the injection junction from the magnetron loop, as will be discussed later. Methods used to measure the loop impedance of a magnetron in the nonoscillating condition with different plate voltages and at the low power end of an AM cycle will be described.

Another objective of this paper is to describe a method for determining the load seen by the synchronized magnetron. Whatever load is presented to the magnetron by the passive elements of the system shown in Fig. 1, this load is changed by the application of injection. This is in agreement with the analytical results of Donal and Chang.[2] It will be shown that the load seen by the magnetron also changes with the power level during the modulation cycle and, in general, at no power level must it be identical with the physical impedance of the dummy antenna itself.

A Method for Measuring the Loop Impedance of the Nonoscillating Magnetron

The loop impedance of the nonoscillating magnetron was computed from the voltage standing-wave ratio (vswr) and the position of the voltage minimum from the loop. The injection amplifier was used as the RF power source for the measurement. The reference plane of all the measurements is the plane L, as shown in Fig. 2, where the output loop of the magnetron is joined to the vacuum-sealed part of the transmission line in the multicavity magnetron. The developmental Type A-128 magnetron[7] was used during the experiments with a magnetic field of about 400 gausses. It is believed, however, that the qualitative results of the work are applicable also to different types of magnetrons. The loop impedance measured with operating magnetron-filament and magnetic field, but without

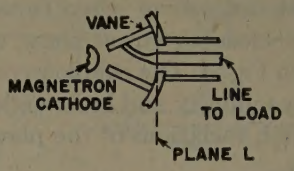

Fig. 2—Transmission-line coupling to the loop in plane L in the vacuum-sealed part of the magnetron.

plate voltage, is a typical high-Q impedance of high absolute value. As the plate voltage is applied and increased from zero towards the value where oscillation starts, the loop reactance continuously decreases. At the point where oscillation starts the reactance is typically low, but still of high Q. Fig. 3 shows the changes of the loop reactance with changes of plate

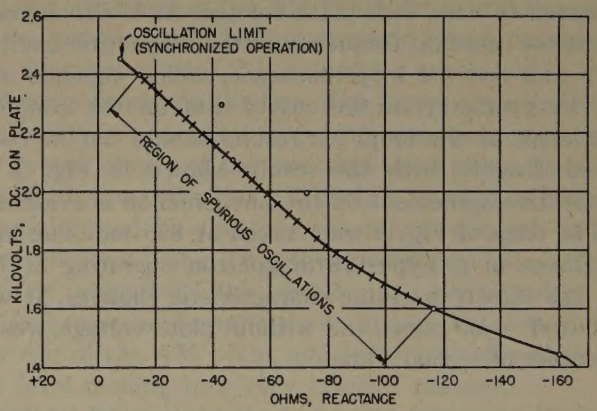

Fig. 3—Loop reactance at 825 mc at different plate voltages of a nonoscillating magnetron measured at plane L.

voltage. Oscillation starts when the plate voltage is between 2.4 and 2.5 kv. Between plate voltages of 1.6 and 2.4 kv, spurious oscillations at -50 to -60 db level below 1 kw at frequencies which were not the operational oscillation frequency of the magnetron were observed. When the plate voltage approaches the oscillation limit the spurious oscillations disappear and are no longer observed as the plate voltage in synchronized operation is further increased for higher power levels. Fig. 3 represents data measured on a cold magnetron. The magnetron tuner was adjusted during these measurements so that the loop reactance at the start of oscillation measured by the static method was close in value to the loop reactance measured by a dynamic method, to be discussed later. Close to cutoff, a condition approached at the low end of the AM cycle at 100-per cent modulation, the free-running magnetron fre-

[6] T. J. Buzalski, "Method of measuring the degree of modulation of a television signal," *RCA Rev.*, vol. VII, pp. 265–271; June, 1946.

[7] The Type A-128 magnetrons were built in the RCA Laboratories, Princeton, N. J. They include an electron beam for frequency modulation purposes, which, however, was not used during these experiments. See J. S. Donal, Jr., R. R. Bush, C. L. Cuccia, and H. R. Hegbar, "A 1-kilowatt frequency-modulated magnetron for 900 megacycles," Proc. I.R.E., vol. 35, pp. 664–669; July, 1947.

quency is several megacycles lower than the injection frequency. This results from "pushing," and the purpose of the injection system is to eliminate this frequency change. Now, since the loop impedance was measured at the injection frequency, the magnetron cavities at and below cutoff were inherently detuned from the measuring frequency. Impedance measurements on a cold magnetron when tuned to the measuring frequency close to cutoff show different results than indicated in Fig. 3. The cold loop reactance in such a case approaches infinity and is dependent only to a reduced degree upon variations of the plate voltage below the cut-off limit.

Welch[8] has shown on a different type of magnetron that the resonant frequency of the cavities below cutoff is a function of plate voltage. In the present work the frequency of the measuring signal, which was the same as the injection frequency, was constant, so that the magnetron loop-impedance was measured at a frequency which differed from the resonance frequency by varying amounts as the plate voltage was altered. Therefore, the measured reactance (Fig. 3) would be expected to vary with plate voltage. As Welch investigated the resonant frequency of the magnetron cavities only and not the loop reactance, which depends also on the geometry of the cavity and on the coupling coefficient of the loop, his results should not be compared directly with the results shown in Fig. 3. A qualitative agreement on the phenomenon is evident.

The data of Fig. 3 were taken at 825 mc. The loop reactance of a Type-128 magnetron operating at 750 mc has shown the same characteristic changes. It was at cutoff $-j33$ ohms, and without plate voltage, was of the order of $-j600$ ohms.

Loop Impedance Measurements at the Low End of an AM Cycle

The operation of the previously described measuring system becomes somewhat difficult at the oscillation limit. The measurement of the loop impedance close to cutoff, which resulted in a reactance of about $j10$ ohms, was repeated using a different technique. Somewhat more than 100 per cent AM was applied to the magnetron, with a frequency within the pass band of the

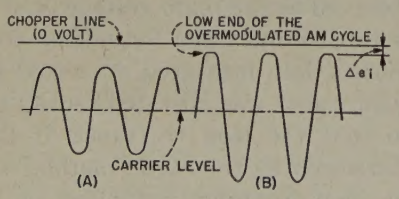

Fig. 4—Detected modulation envelopes at the load (A) at an intermediate level, (B) magnetron slightly overmodulated.

system. Scope No. 2, coupled to the load side, shows pictures as given in Fig. 4: (A) at an intermediate modulation level; (B) with the magnetron slightly overmodulated, where the sine-wave demodulated envelope becomes flat at the low modulation end. Between the distorted sine wave, which represents the overmodulated magnetron voltage (Fig. 4(B)), and the chopper line appears the remanent injection voltage at the low end of the AM cycle, Δe_i. In a properly adjusted system, Δe_i is very small compared with the peak amplitude; it is not more than a small percentage of it. The demodulated envelope is now observed along the slotted line on Scope No. 1 as shown in Fig. 5. As the pickup probe is moved in the slotted line, the d_1, d_2, d_3, $\cdots$ readings are made in time sequence during which the magnetron is cut off. Consequently, the d values correspond exactly to the injection voltage.

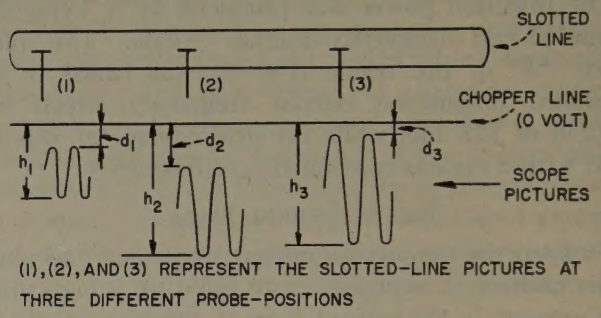

Fig. 5—Changes of detected modulation envelopes, as observed on the scope along the slotted line.

They are different at different pickup positions along the line. The d_1, d_2, d_3, $\cdots$ distances measured on the scope are plotted against the slotted-line probe positions, and the results give us the standing-wave pattern I in Fig. 6. The other patterns in Fig. 6 will be discussed later.

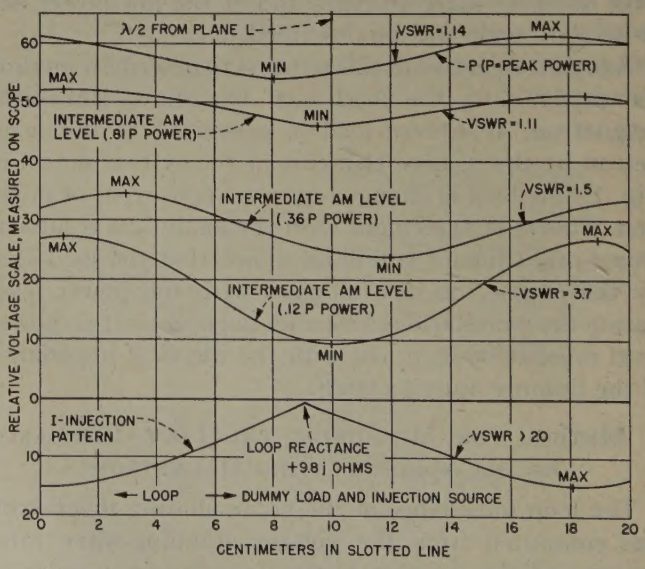

Fig. 6—Dynamic vswr patterns of an injection synchronized, amplitude-modulated Type A-128 magnetron at 825 mc (Case 1 in Table I and Fig. 8).

From the I curve may be computed the input impedance of the magnetron at the time instant when the oscillation stops, at the very low end of the modulation cycle. The vswr of the I pattern was considerably higher than 20. Consequently, the loop impedances at cutoff for

[8] H. W. Welch, Jr., "Effect of space-charge on frequency characteristic of magnetrons," Proc. I.R.E., vol. 38, pp. 1434–1449; 1950.

practical purposes are considered here as pure reactances. The absolute value of the loop reactance at the low end of the AM cycle is subject to changes with the setting of the internal magnetron tuner. The value of the inductive reactance, computed at $j9.8$ ohms, can be changed into a capacitive reactance of the same order of magnitude by changing the setting of this tuner. The setting of the tuner changes the capacitive loading of the cavities, and in this way influences the reactance of the loop which is inductively coupled to one cavity. The slightly inductive loop reactance at cutoff is typical for the investigated magnetron if the internal magnetron tuner is adjusted at the peak power level to produce a free-running magnetron frequency which is identical with the injection frequency. This kind of magnetron tuning, suggested by Wolff,[9] was used during experiments, with minor variations.

The loop reactance at cutoff depends also on the pushing of the free-running magnetron. When the magnetron is tuned for locked operation as described above, the loop reactance is measured more or less off resonance, depending on the amount of the free-running pushing—which is the difference between the frequency of the magnetron at the peak of the AM cycle (injection frequency) and at cutoff. As the pushing changes, the loop reactance seen from the line must also change.

Consequences of the Measurements

Important consequences arise from the fact that the magnetron loop is a high-Q circuit when measured at the injection source frequency and at the low end of an AM cycle. The absolute value and sign of the loop reactance are not important, and, as was shown, are different at different carrier frequencies. The importance of the low-loss character of the loop so far as the injection source is concerned can be understood from Fig. 7. The distance of the injection source joint from plane L must be selected in such a way that the vswr pattern of the injection voltage at the low end of a 100 per cent AM cycle must have a low point at the plane of the joint. The first possible injection-joint distance from plane L, a, is the distance of the first low-voltage point from plane L. Further half-wave lengths can be added to a, and in this way another mechanically proper injection-joint distance from the magnetron can be selected. If reactive elements (tuners) are coupled to the line, as is the case in Figs. 1 and 7, the physical length of the line added to a, to locate the proper injection joint, may be more or less than $\lambda/2$. By proper adjustment of the reactive elements, the low-voltage plane of the swr pattern may be moved to a previously established injection plane. In this way the carrier frequency can be changed within reasonable limits without changing the length of the connecting lines. If the low-voltage point of the vswr pattern is almost zero, the modulated RF output in the load at the low end of a 100-per cent magnetron AM cycle can be reduced almost to zero. An alternative experimental method is to use a line stretcher in the magnetron line to find the injection-joint plane with which the maximum AM can be obtained.

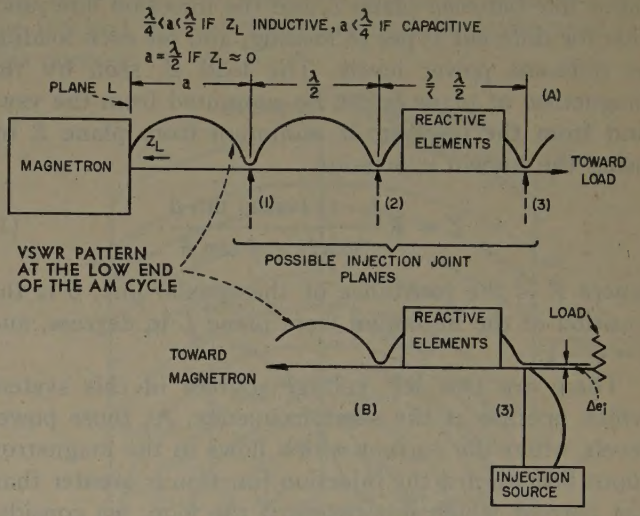

Fig. 7—Determining the proper plane of the joint of the main transmission line and injection line.

At the low end of the AM cycle the injection source works mainly into a high-Q network, which consists of the magnetron loop, the connecting transmission line, and some tuners on the line. The power absorbed from the injection source by these components is very low. By proper choice of the injection-joint plane, the load at the the low end of an AM cycle is as good as entirely short-circuited by the loop reactance reflected to the injection-joint plane. Thus the injection source is almost entirely unloaded. This results in a considerably increased injection-current circulation in the loop at the low end of the AM cycle, which helps to eliminate the low-level moding in a very efficient manner.

At higher power levels during the AM cycle, the loop impedance of the magnetron is changed, and consequently the low-voltage point of the injection pattern is not on the joint plane; thus the load at higher power levels absorbs not only magnetron power but also injection power. The loading of the injection source is consequently increased. The vswr patterns at the high-power end and for three intermediate power levels during the AM cycle in the line section a are represented in Fig. 6. In the line section, where reactive elements are located, the vswr patterns may have a high variety of forms, determined by the applied combination of the reactances. In the line section between the injection joint and the load, only the impedance of the load determines the swr pattern which remains unchanged at any power level. In the injection line a high standing wave is present at all power levels, but especially at the low end of the AM cycle. This condition is shown in Fig. 7(B). The length of the injection line must be selected to place the injection amplifier at a voltage plane which is within the safe operational value for the injection amplifier at the peak of a magnetron AM cycle. The optimum length can be experimentally determined with a line stretcher inserted in the injection line.

[9] Verbal communication to the author.

Measurements of the Loading of the Magnetron

To determine the load seen by the synchronized magnetron, the vswr was plotted in the magnetron input line between plane L and the injection line junction for different types of loading, and for each loading at different power levels. The load Z, seen by the magnetron at plane L, can be computed from the vswr and from the position of minimum from plane L by using the known expression

$$Z = R\frac{1 - j\,(\text{vswr})\tan\beta}{(\text{vswr}) - j\tan\beta}, \qquad (1)$$

where R is the resistance of the coaxial line, β is the position of the minimum from plane L in degrees, and $j=\sqrt{-1}$.

There are two RF voltage sources in this system which operate at the same frequency. At those power levels, where the current which flows in the magnetron input line toward the injection junction is greater than the current which flows toward the loop, we consider the system as a single RF generator—single-load network—and use (1) to compute Z. By this means, the effect of the injection source is expressed in values of Z. This Z is a dynamic loading which changes during an AM cycle, and, at any particular power level, is determined by the combined effects of (1) the dummy load, (2) the injection-source current which flows into the dummy load, (3) the injection current which flows into the magnetron loop, (4) the impedance of the injection line (looking toward the cavity k from the joint), and (5) by the tuners which may present different reactances. The combined effect of all the loading elements may present a large variety of loading which, at some power level, may match the transmission-line resistance, R.

The setup shown in Fig. 1 was also used for measuring the magnetron load, with a technique similar to that described previously in connection with the loop impedance measurement. The method consists in applying amplitude modulation to the magnetron carrier at different AM factors (not only at overmodulation, as before) and measuring on Scope No. 1 at different pickup positions in the slotted line the distances between the high end of the demodulated envelope and the chopper line and the low end of the demodulated envelope and the chopper line, which represent two different power levels. The distances to the chopper line at different pickup positions are compiled in vswr patterns. The thermal condition of the magnetron is substantially constant at different modulation factors, and therefore affects the measurements only at a low degree.

In Fig. 6 the vswr is plotted for three intermediate power levels which are expressed as parts of the peak power, P, delivered into the dummy load. The amplitudes of the vswr patterns do not serve to compare (or to measure if the scope is calibrated in volts) the power levels in the load during an AM cycle. This is the consequence of the factors that two RF sources are working into the same load and that the system contains nonlinear impedances—the magnetron loop and also, to a limited extent, the injection source.

As typical examples, in Table I are shown the values of the dynamic loads as seen by the magnetron, and as computed from Fig. 6 (Case 1), and also for two different types of loading (Case 2 and 3). In Case 1 the total load almost matches the magnetron line at the peak of the AM cycle. In Case 2 the load at the peak power output was selected higher than the line resistance (decoupled loading), but it is also in this case substantially resistive. In Case 3 a capacitive loading is used at the high-power end of the AM cycle. The three cases represent a few examples only from the practically infinite variety of possible loadings of the injection locked magnetron. Some of the loading combinations show lower incidental angular modulation during the AM cycle than others, and some combinations show better linearity in the AM envelope of the output-carrier versus input-voltage to the modulator in agreement with the analytical studies of Donal and Chang.[2] Nearly every passive load (antenna) can be transformed by reactive line elements at the peak of the AM cycle into a different impedance with which some additionally wanted advantage can be obtained during modulation, without imposing disturbing bandwidth limitations on the system. The magnetron does not require the transformation of the load into a pure resistance for efficient operation. This is a noteworthy difference between the synchronized magnetron oscillator and a tube amplifier, whereas, in other respects, both are similar in application.

TABLE I

Loading of a Type A-128 Magnetron at Different Power Levels During an AM Cycle. Carrier Frequency 825 mc.

Power relation to peak power (P) in dummy load	Load* seen by the magnetron at plane L, at 825 mc $Z=r\pm jx$ (ohms)	Load impedance $\sqrt{r^2+x^2}$ (ohms)
Case 1		
P	$46.4-j3.9$	46.56
$0.81P$	$46.5-j0.8$	46.51
$0.36P$	$37.0+j9.2$	38.13
$0.12P$	13.9	13.90
Cutoff	$-j9.8$	9.80
Case 2		
P	$62.3-j3.1$	62.38
$0.64P$	$62.6+j3.6$	62.70
$0.41P$	$47.9+j19.0$	51.53
$0.15P$	$21.9+j12.6$	25.26
Cutoff	$-j11.0$	11.00
Case 3		
P	$51.2-j57.5$	76.99
$0.83P$	$50.5-j53.5$	73.57
$0.53P$	$48.5-j42.8$	64.68
$0.11P$	$16.2-j26.6$	31.14
Cutoff	$-j13.3$	13.60

* Computed from (1).

In Table I the negative of the measured value of loop reactance is inserted as the load seen by the magnetron at cutoff. At cutoff, the magnetron loop was a passive load seen by the injection source and the magnetron was not a generator. This inverted repre-

sentation is, however, justified if we consider the meaning of the same, which is simply that the loop reactance of the magnetron must be inserted in an RF circuit which tunes it to the carrier frequency. The resonant RF circuit must be, of course, an active circuit which continues to sustain circulating injection currents in the loop when the magnetron stops oscillating. The low-level moding is suppressed in this way, a result which could not be achieved by a passive network.

The close agreement between the various reactance values at cutoff in all the cases in Table I indicates that the internal magnetron tuner was not changed considerably when operating with different loads. The adjustments were made almost exclusively by the tuners on the line; when the locked carrier frequency is changed, however, the magnetron tuner setting and also the loop reactance value at cutoff are changed. Thus, for a given magnetron and for a given peak-power output the load at the low end of an AM cycle, which is the negative value of the loop reactance, depends only on the carrier frequency.

The Loading Diagram

The important data given by the vswr patterns, as shown in Fig. 6, for different loading conditions of a magnetron can be represented in a common circular diagram. Fig. 8 shows a circular diagram wherein three loading conditions of Table I are drafted. The represented data are the vswr and the position of the minimum at the different power levels during an AM cycle. The circular diagram is made up of two parts to show the loading of two RF generators during the AM cycle, the magnetron and the injection source. The inner part of the diagram, which represents the vswr's from unity (as center point) to ∞, shows the changes of the vswr and position of the minimum for the major part of the AM cycle, where the current which flows towards the injection junction and dummy load is greater than the current flowing toward the magnetron loop. In the external part of the diagram the circle representing vswr $= \infty$ coincides with the circle for the internal part; the matched operation is, however, represented by any point of the circle of maximum diameter. In this external diagram are shown the vswr's and positions of minima for the condition where the higher currents flow toward the loop and the lower currents toward the injection junction thus the position of the generator is changed. A similar representation with a single circular diagram was previously used by the author.[1] In an analytical approach Donal and Chang[2] extended the load line beyond the ∞ vswr circle, making use, for the first time, of a double circular diagram. The difference between the representations is that in the external part of the diagram of Donal and Chang the matched condition of the injection source is at infinity and the vswr beyond the ∞ circle is considered as negative vswr produced by the magnetron. Both representations are equally applicable for the case where the generator, seen from the line, is a high-Q reactance. The diagram presented here, however, is also applicable for low-Q generators. The whole chart of Donal and Chang may be used for plotting resistance and reactance contours, whereas only the internal part of this chart may be easily used for this purpose.

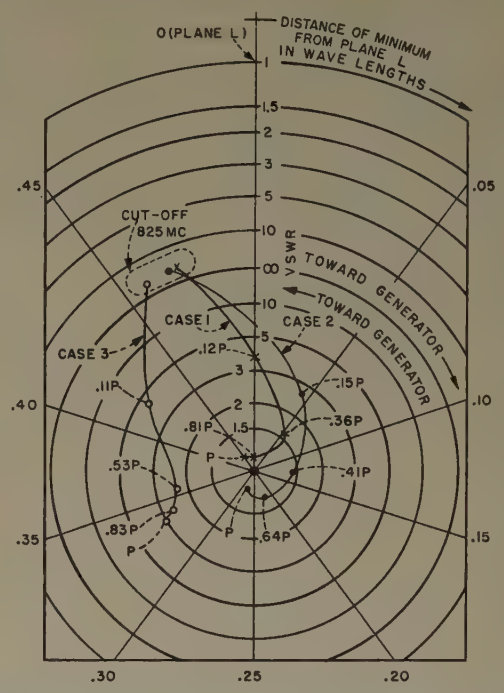

Fig. 8—VSWR and position of minimum during an amplitude-modulation cycle for three different loads of a type A-128 magnetron at 825 mc (Case 1, 2 and 3 in Table I), computed at plane L.

The values of the power delivered into the dummy antenna are shown along the load lines expressed as parts of the peak power P as parameters. At the end of the lines (cutoff) no magnetron power is transferred into the load, and the very low amount of power, if any, is furnished by the injection source only, as was discussed previously. All the load lines at a given carrier frequency must end close together. The angular position of this point is given by the reactance of the magnetron loop at cutoff, as explained above. As the carrier frequency is changed, the convergence point of all the load lines moves around the circle. For example, at 750 mc the convergence point, corresponding to a loop impedance of $-j33$ ohms, would appear for this type of magnetron near to 0.09λ instead of 0.47λ, which is the convergence point at 825 mc. For a given magnetron tuner position the high-end point is in any case determined by the choice of passive load. Consequently, the family of load lines for another carrier frequency may start in the same position, but must turn into a new position in Fig. 8. Note that the distance of the convergence point from plane L in Fig. 8 is identical with the distance a in Fig. 7.

The impedances represented by the points of Fig. 8 are calculated for the plane L of Fig. 2. There is reason to believe that the effective plane of the magnetron is as much as $\lambda/8$ to the left of plane L in Fig. 2. If, accordingly, the load lines of Fig. 8 are rotated 90 degrees clockwise, the resulting contours are generally similar

in position to those calculated by Donal and Chang[2] for the same Type A-128 magnetrons. The comparison cannot be exact since, in the present work, the load was not, in general, matched to the line as was assumed to be the case by the workers mentioned above.

Conclusions

The impedance of the magnetron loop was measured over a range of plate voltages below the point of oscillation. Whereas at low plate voltages the loop impedance was a high reactance with a low resistive component, at the oscillation limit it was found to be a typical low positive or negative reactance with a low resistive component.

The high-Q character of the magnetron loop reactance at cutoff results in a high vswr in the line at the bottom of an AM cycle. The coupling of the antenna in a low voltage plane of this vswr pattern prevents injection power flowing to the antenna at the low end of an AM cycle; thus an almost 100-per cent modulation of the carrier is feasible.

The loop reactance close to cutoff was also measured by use of a dynamic method to avoid errors arising from changes of magnetron temperatures. With the same dynamic method the swr and minimum positions were measured in the magnetron line at various power levels during an AM cycle and were plotted on a circular chart. All the points measured at the same carrier frequency lie on a continuous curve. In the internal part of the chart, conditions are represented where the net power flows towards the load; in the external part it flows towards the magnetron. The points of the load-line at cutoff lie close together, since, for a constant carrier frequency, these depend only on magnetron tuner position, which was constant. However, three different values of passive load were used, so that the high-power ends of the curves are at different positions on the chart.

This is the first time that experimental measurements have been made on the impedances presented to a phase-controlled magnetron, during variations in magnetron input, by the combination of the passive load and the locking source. If the impedances are calculated, it is seen that as the magnetron power level is reduced the successive loads presented are such as to progressively raise the frequency of an unlocked tube. This loading counteracts the pushing that would occur if the magnetron were unlocked. The incidental phase modulation and the linearity are functions of the passive load used. The total loading varies in both its resistive and reactive components. The changes in load are in general qualitative agreement with the analytical results of David and of Donal and Chang.[5,2]

Proper adjustments of the circuit and of the passive load yield a locking range sufficient to overcome the magnetron pushing. Good linearity and reasonable values of incidental phase modulation are obtained. Mode shifts at the low end of the modulation cycles are suppressed; thus the output carrier is similar to the carrier produced by a conventional amplifier tube.

Acknowledgments

The author is indebted to J. S. Donal, Jr. of the RCA Laboratories Division for special considerations on the content of this paper. Valuable discussions were held on several occasions with Irving Wolff, L. S. Neergard, and K. K. N. Chang of the RCA Laboratories Division. R. F. Schwartz, who designed several parts of the experimental setup, and D. E. Deuitch, both of the RCA Victor Division, co-operated with the author during the experimental work.

An X-Band Sweep Oscillator*

IRWIN D. OLIN†, ASSOCIATE, IRE

Summary—**A microwave sweep oscillator has been developed which sweeps the range of 8,500–9,500 mc. The RF amplitude over this band is maintained constant to within ±0.1 db by means of a ferrite modulator unit connected in an amplitude-stabilizing feedback circuit. In addition to providing amplitude control, the ferrite unit also provides amplitude modulation at 1,000 cps of the swept cw source. The generator sweeps the band in about 1.5 seconds, making practical the presentation of network transmission characteristics on an oscilloscope.**

I. Introduction

THE MEASUREMENT and adjustment of microwave networks may be greatly facilitated by employing a sweep generator which will display on a cathode-ray tube the pattern of RF amplitude versus frequency automatically. This device would permit rapid adjustment of a network for a prescribed transmission pattern or disclose the reflection characteristic at the input terminals. A generator for such service would be required, in addition to covering the proper frequency range, to maintain constant the energy incident upon the test network. There are, therefore, two principal phases involved in its design.

The available primary source of RF energy must be capable of being swept over the band in synchronism with the oscilloscope time base. Over most of the microwave range the klystron appears to be the most satisfactory signal source for low levels, its cavity dimensions being varied mechanically or electrically by means of thermal elements, to produce frequency sweep. However, even with accurate reflector tracking

* Decimal classification: R355.914.431. Original manuscript received by the Institute September 29, 1952.
† Naval Research Laboratory, Washington 25, D. C.

the output power is by no means constant and some form of amplitude control is required. The most common form of control would sample the primary source and use the variation in its level to control the amplitude of energy output by means of a variable attenuator placed in the transmission circuit. For visual display purposes the attenuator must be capable of fast response, so that mechanical arrangements are inadequate. Recent developments in the use of ferrites,[1] however, enable the construction of an attenuator in the microwave range which may be varied electrically. Moreover, this unit may be made to function as a modulator, producing 100 per cent modulation.

The device to be described operates at X-band, utilizing a mechanically swept klystron between the frequencies of 8,500–9,500 mc. The band is covered in about 1.5 seconds and the output power is maintained constant to within ± 0.1 db by employing a ferrite modulator. A modulation frequency of 1,000 cps is used, consistent with many of the tuned amplifiers available.

II. Component Performance

A block diagram of the essential components of the complete system is shown in Fig. 1. The primary RF source consists of a 2K48 reflex klystron mounted in an external coaxial cavity. Tuning is accomplished by moving a "noncontacting" short-circuit plunger within the cavity by an external cam and linkage assembly.

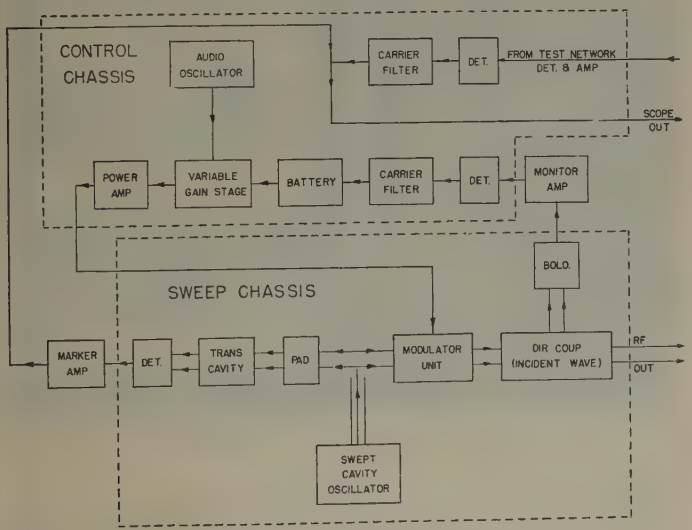

Fig. 1—Block diagram of the sweep generator.

A motor which is reversed at each end of the sweep band actuates the cam in addition to a reflector tracking potentiometer and a potentiometer supplying the time base for the oscilloscope. The cavity was produced for other equipments and is used here by replacing the cam with one providing the proper frequency coverage. Coupling of the cavity to the waveguide is provided by a magnetic probe in the cavity feeding an antenna in the waveguide. In order to provide a terminal for the marker cavity, the conventional short-circuit behind the antenna is replaced by a 15 db pad followed by the transmission-type marker cavity. It has been found that the RF signal output may be maintained constant, without control, to within 3 db over the sweep band by suitably adjusting the antenna length in the guide.

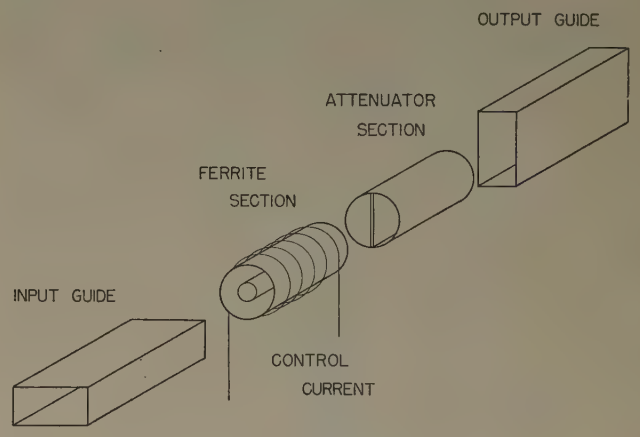

Fig. 2—Ferrite modulator unit.

A sketch of the modulator unit is shown in Fig. 2. The linearly polarized input wave, which may be considered as comprising left and right circular polarizations, enters the ferrite section. Depending upon the magnitude and direction of the controlling current, the velocity of one of the polarization components is reduced.[2] At the output of the ferrite section the equivalent plane wave has been rotated through an angle depending upon the amount of velocity reduction which has taken place.[3] The ferrite section is followed by an attenuator fin oriented in such a manner as to absorb all energy which would propagate in the plane of the input guide. The output guide, placed at right angles to the input guide, transmits the remaining component of the rotated plane wave. Thus, if there were no rotation in the ferrite all the energy in the input guide would be absorbed in the attenuator. With 90 degree rotation, all the input energy would be coupled to the output guide. With intermediate rotations, varying amounts of power are transmitted, the attenuator section always preventing reflection from the output guide from entering the ferrite section.

An idealized control characteristic of the modulator unit consisting of input and output guides, ferrite and attenuator sections, is shown in Fig. 3. With a sine wave current applied to the control coil, it is evident that the fundamental component of the modulated RF is twice the frequency of the excitation. In addition, whenever the coil current is zero no RF voltage is transmitted; with high currents, substantially all the RF is transmitted, so that the modulation at the output is 100 per cent. It should be pointed out, however, that the discussion

[1] C. L. Hogan, "The ferromagnetic Faraday effect at microwave frequencies and its applications," *Bell Sys. Tech. Jour.*, vol. 31, pp. 1–31; January, 1952.

[2] N. G. Sakiotis, A. J. Simmons, and H. N. Chait, "Microwave antenna ferrite applications," *Electronics*, vol. 25, p. 156; June, 1952.

[3] C. H. Luhrs, "Correlation of the Faraday and Kerr magneto-optical effects in transmission line terms," Proc. IRE, vol. 40, pp. 76–78; January, 1952.

has been confined to an idealized case. With the ferrites used there is always some unequal absorption of the circular components, hence ellipticity is observed at the output. This, combined with mechanical imperfections and residual fields, results in some energy, though small, being propagated in the absence of coil current. Similarly, the control characteristic may not be exactly linear or symmetrical for all currents. If the coil current is increased too much, the ferrite may tend to saturate or the rotation may exceed 90 degrees and thus alter the characteristic.

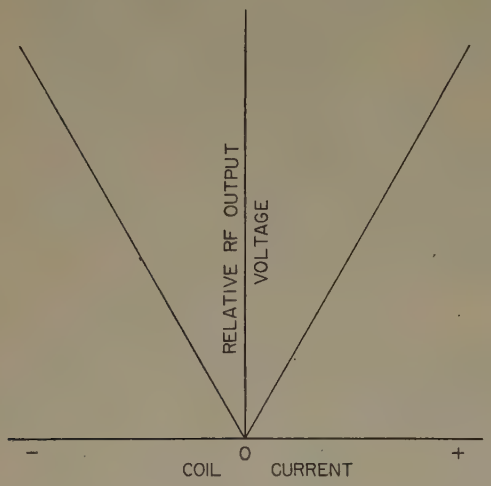

Fig. 3—Idealized modulator control characteristic.

A photograph of the sweep chassis which includes the modulator unit and oscillator is shown in Fig. 4. The metal shield covers the space occupied by the potentiometers.

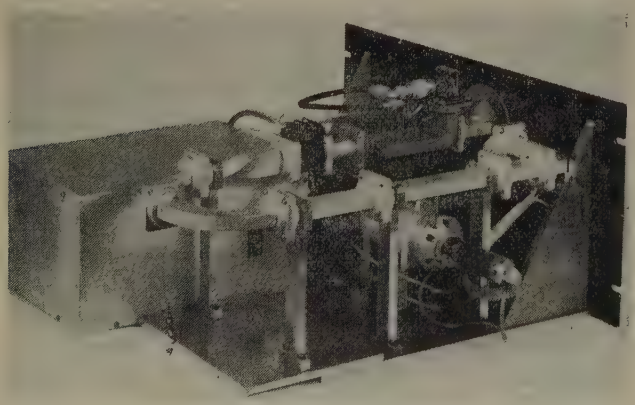

Fig. 4—Completed sweep chassis.

III. Control Chassis Operation

The control chassis receives a signal from the monitor amplifier (tuned to 1,000 cps) which varies in accordance with the power incident on the test network. The envelope is derived by means of the detector and filter, resulting in an increasingly negative voltage for an increase in RF power. A battery subtracts a fixed amount from the envelope to supply the variable gain stage with an error voltage from which to work. The variable gain stage, a single 6BA6, amplifies a 500 cps signal in accordance with the supplied bias, the error voltage. If the RF voltage tends to increase, the bias on the 6BA6 becomes more negative and decreases the magnitude of the 500 cps output signal. The 500 cps signal is supplied by a phase-shift type oscillator using a single 6SJ7. A power amplifier consisting of push-pull 6L6 tubes couples the signal to the control unit coil. With a coil impedance of about 10 ohms at 500 cps, the power amplifier supplies an average of 1 ampere when the entire unit is in operation.

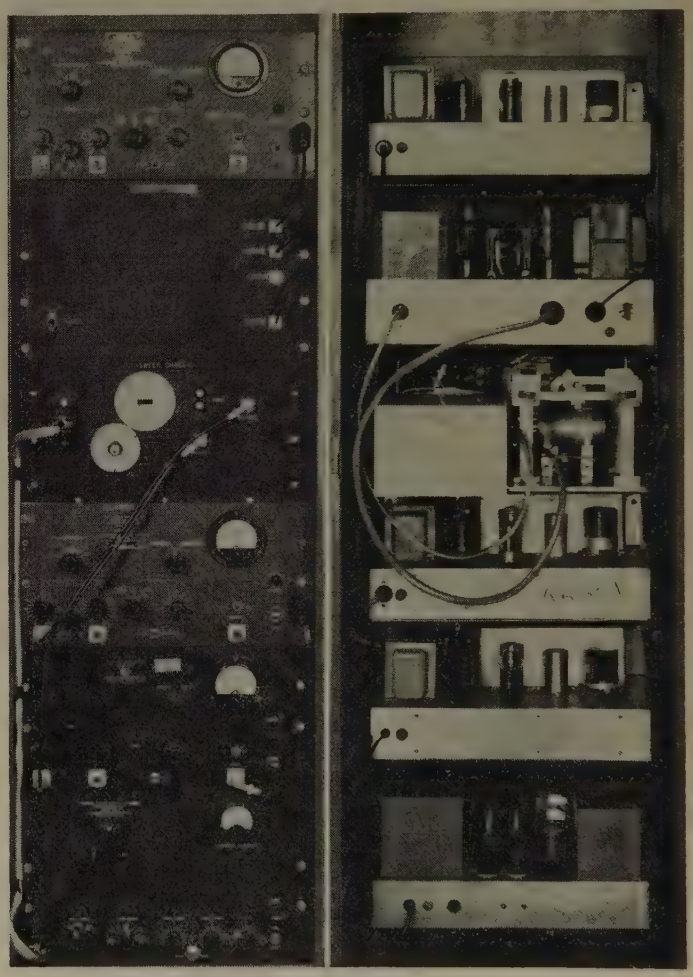

Fig. 5—Front and rear views of completed generator.

The actual power output uniformity, assuming the automatic control system is operating with small error, is dependent upon the characteristic of the directional coupler used in the monitor circuit. Most available types are not flat over this wide band, so that the detector used for measuring the transmitted power of the test network consists of another directional coupler, identical with the one in the monitor circuit.

IV. Marker Operation

The transmission cavity operates with a cw wave applied to the input. When the wavelength of the generated wave corresponds with the wavelength of the cavity, an RF pulse is applied to the detector. The width

of the pulse is a function of the sweep speed and the cavity Q. In the equipment constructed, it corresponds approximately to the period of a 200 cps sine wave. This pulse is amplified by a commercial variety amplifier which is arranged to overdrive, thus providing limiting and resulting in markers of equal height on the scope, regardless of RF frequency.

V. CRT Display

To provide a clearer indication of the test network transmission the associated amplifier output, also tuned to 1,000 cps, is connected to an envelope detector before display on the cathode-ray tube. The marker pulse is added to the presentation by capacitively coupling the marker amplifier to the scope terminals. The circuitry for the envelope detector and the marker coupling has been included on the control chassis. Photographs of the completed sweep generator are shown in Fig. 5 (see page 12). The only auxiliary equipment required is a scope with dc amplifiers and a long persistence screen. The directional coupler, detector and matched load which are attached to the test network are not shown in the photograph.

VI. Conclusion

The instrument is presently used for transmission adjustments on four terminal networks, for which the characteristics are suited. Transmission attenuations as great as 20 db may be clearly indicated. In other applications more rigid amplitude control may be desirable, or actual power uniformity required. Such requirements may be satisfied by increasing the loop gain and using a directional coupler in the monitor circuit which is flat over the band.

It should be pointed out that a phase change of 180 degrees occurs in the RF wave each time the control coil current reverses, since the rotations in the plane wave take place in opposite directions. For ordinary measurements this does not appear disadvantageous; however, another modulator scheme could be used if this is objectionable. The coil excitation current could be clamped in such a manner as to maintain the current unidirectional, zero current corresponding to no RF transmission and the maximum current of each modulating cycle adjusted to provide amplitude control. This scheme, of course, would produce 1,000 cps modulation with 1,000 cps excitation.

One-Kilowatt Tetrode for UHF Transmitters*

W. P. BENNETT†, member, ire, and H. F. KAZANOWSKI†, member, ire

***Summary*—A forced-air-cooled power tetrode capable of delivering 1,200 watts output in television service at frequencies up to 900 mc is described. Particular features of the design include a coaxial electrode structure, novel metal-to-ceramic seals, and a unipotential matrix-type cathode having a 120-volt heater.**

A discussion is included of the special parts-making techniques and precision assembly methods in which radio-frequency heating is used together with accurate jigging to maintain uniform electrode spacings.

A typical 900-mc circuit for use with the tube is described and tube performance data as a cathode-driven amplifier are given.

A NEW FORCED-AIR-COOLED transmitter tube' the 6181, has been developed to meet the needs of a rapidly expanding television industry for a power tetrode capable of delivering approximately one kilowatt at ultra-high frequencies. This tube combines the proven features of coaxial design with an improved tetrode structure having closely spaced, thermally efficient electrodes and an envelope structure utilizing low-loss ceramic-metal seals.

Although both the triode and tetrode types of negative-grid power tubes were originally considered, the tetrode construction was chosen for this uhf application because it appeared to offer the following advantages over the triode construction:

a. Reduced internal feedback effects.
b. Reduced driving power.
c. Reduced output capacitance because of increased screen-to-plate spacing.

Fig. 1—UHF power tetrode type 6181.

* Decimal classification: R331×R339.2. Original manuscript received by the Institute, November 11, 1952.

† Tube Dept., Radio Corporation of America, Lancaster, Pa.

In addition, the tetrode construction has been preferred by designers of television transmitting equipment.[1,2] Forced-air cooling, also a primary requirement for economical, trouble-free transmitter operation, was provided by the use of a conventional type of structure having an external plate and cooling fins. Radio-frequency losses and interelectrode coupling were minimized by the use of a coaxial arrangement of cylindrical electrodes, supports, and terminals. Use of ceramic insulators in place of glass was found desirable because it permitted higher processing and operating temperatures, provided lower dielectric losses, and simplified assembly methods.

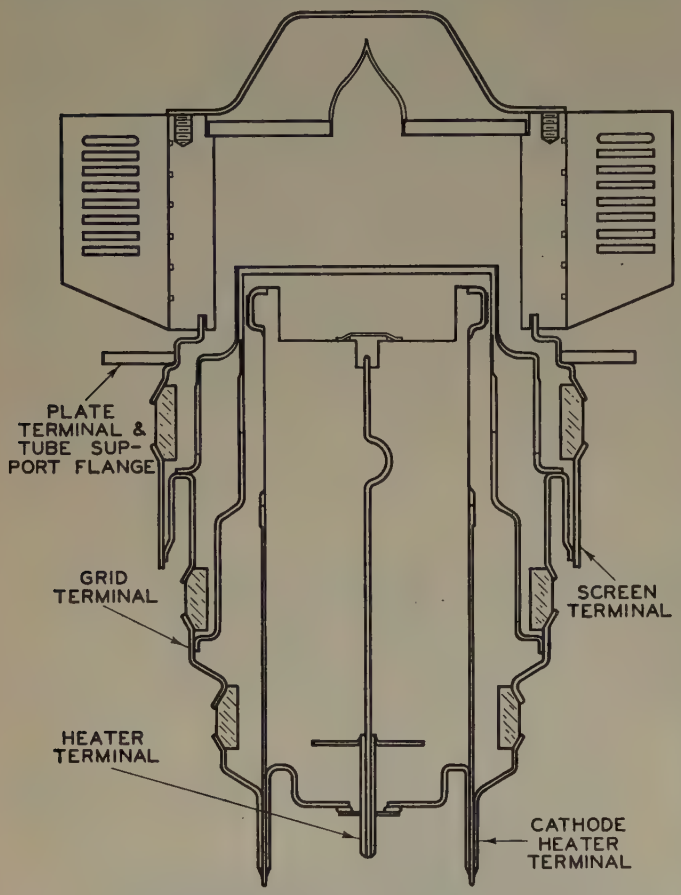

Fig. 2—Cross section of uhf power tetrode type 6181.

A photograph of the 6181 is shown in Fig. 1 (see page 13) and a cross-sectional view in Fig. 2. The cathode used for the 6181 is a low-temperature unipotential barium-oxide type having a high efficiency. Its physical structure is such that the alternating heater voltage is completely shielded from the tube input. The use of a cathode construction of the matrix[3] or sponge type permits the application of plate voltages in the order of 2 kv without sparking, provides good coating adherence, and yields long life under back-bombardment conditions.

[1] A. K. Wing and J. E. Young, "A new ultra-high-frequency tetrode and its use in a 1-kilowatt television sound transmitter," Proc. I.R.E., vol. 29, pp. 5–9; January, 1941.
[2] P. T. Smith and H. R. Hegbar, "Duplex tetrode uhf power tubes," Proc. I.R.E., vol. 36, pp. 1348–1353; November, 1948.
[3] C. E. Fay, D. A. S. Hale, and R. J. Kirchner, "A 1.5 kw. 500 mc. grounded grid triode," Proc. I.R.E., vol. 39, pp. 800–803; 1951.

The length of the cathode was limited for two reasons. First, the height of the active portion of the electrodes should be only a small percentage of a wavelength at the highest operating frequency in order to have uniform radio-frequency voltage along the active cathode. Second, short grid and screen structures are desirable because they provide good end or conduction cooling, thus allowing greater dissipation before instability occurs due to grid emission. The cathode diameter was selected to satisfy emission requirements for the specified power output at the specified cathode current density and cathode height.

General Features

The coaxial structure of the 6181 provides for easy insertion into a socket and eliminates the necessity for cumbersome circuit disassembly. Cylinders having progressively larger diameters provide the external contact surfaces for the cathode, the control grid, the screen grid, and the plate flange. Continuous contact can be made to the under surface of the plate flange by means of a lock-washer type spring or other suitable slightly flexible contact. During operation the tube is supported and held firmly by this plate flange. The plate contact surface is the reference for the axial locations of the various other contact surfaces. Perpendicularity of the plane of this surface with respect to the axis of the tube and the concentricity of the various terminals with respect to the axis of the tube are specified in terms of a standard cylindrical gauge, which all tubes must be capable of entering. The maximum movement required by the circuit contact fingers can be determined from a comparison of the minimum diameters of the various tube terminals and the corresponding diameters of the gauge. In circuits designed for use with this tube, lateral movement of the plate flange is not limited and the cylindrical terminals are allowed to seek their final positions freely.

Cathode and Heater

An adequate emitting surface area of approximately two-inch diameter and one-quarter-inch height is formed by the sintering of nickel powder matrix onto a drawn nickel cathode cup. This portion of the single-piece, re-entrant cathode (Fig. 3) is formed at high unit pressures in a precision die by an expanding punch. A

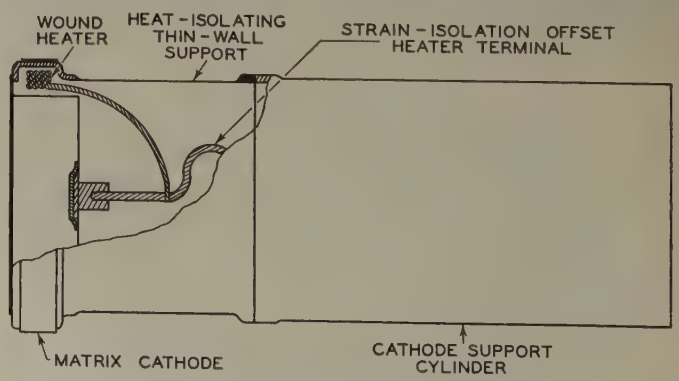

Fig. 3—Cutaway view of cathode assembly.

thin-wall heat-isolating section is rolled from the parent metal to provide a thermally and mechanically stable cylindrical support. After suitable washing processes, a pure nickel powder of fine particle size is bonded to the band-shaped cathode-surface area with the aid of differential expansion jigs and firing in a high-temperature hydrogen furnace. This sponge-like band, full of voids, will later form the "active" cathode after it is impregnated with emitting material and further processed. Prior to this impregnation, however, insulated receiving-tube type heater wire is wound inside the cathode offset section and the cathode is radio-frequency brazed to a cylindrical support member. An appropriate length of heater wire is used to provide the required cathode heating at approximately 120 volts and 1.5 amperes. This high-voltage, low-current heater-power requirement permitted the use of small-diameter wire for the heater winding. The use of an offset cathode, in which only the actual emitting area of the cathode is spaced close to the adjacent grid, greatly reduces the input capacitance of the structure and permits use of a less costly modulator.

Ceramic-Metal Seals

When high-power vacuum tubes are designed to be operated at ultra-high frequencies, high-conductivity metallic members and low-loss dielectric materials are used. The physical properties of the metals and ceramics used must be matched carefully to provide vacuum-tight envelope assemblies. A well-designed tube should

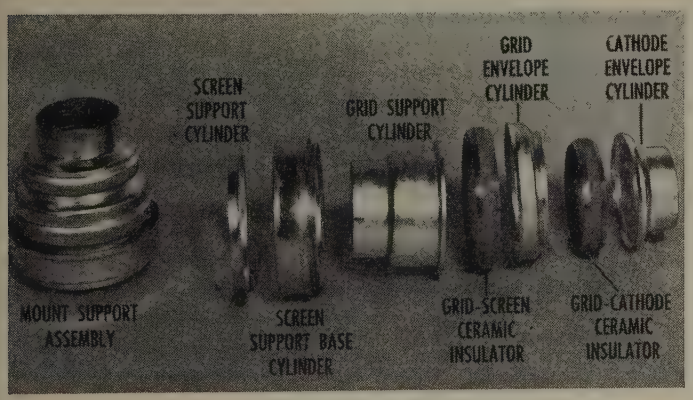

Fig. 4—Mount support; assembly and exploded view.

also be easy to assemble, should have internal cleanliness, and should be able to withstand repeated high thermal and electrical stresses without fractures or vacuum leaks.

The mount support assembly of the 6181, shown in Fig. 4, consists of tapered metal and metallized ceramic cylinders, seated together by the positioning of the adjacent tapers one upon another, and sealed as an assembly by conventional brazing of the component parts in a hydrogen atmosphere using a eutectic silver-copper brazing alloy. The ceramic material selected for the insulating cylinders is a high-alumina body. The metal parts may either be drawn from a high-conductivity low-expansion copper-clad alloy, or copper plated after fabrication. In preparation for envelope assembly, a 30-degree taper is ground on both ends of the ceramic cylinders which mate the 30-degree flared lips of the metal cylinders. The tapered ceramic is then metallized along the sealing edges to provide a suitable base for adherence of the brazing alloy. Very satisfactory metallizing is accomplished by painting a mixture of extremely fine tungsten and iron powders, with a binder, onto the tapered sections, and then hydrogen-firing the ceramics at 1,400°C. After this sintering process, the metallized area is wire-brushed to remove the nonadhering powders and the metallic surface is lightly plated with nickel or copper to promote solder flow on assembly.

Several theories may be advanced as to how a firmly adhering layer of metal is bonded to a ceramic surface. The reactions that occur, however, are complex, and none of the explanations appear complete enough to satisfy all conditions encountered. One hypothesis is that the action is a diffusion of metal into the ceramic and, possibly, the bond is created by a peculiar arrangement, or rearrangement, of the crystals at the interface. Another hypothesis is that solid reactions take place because of loosening of the atomic bonds by thermal agitation, permitting mutual diffusion of the different atoms into adjacent parts of the structure. In this case it is possible that large crystals grow from smaller ones, or a new type of crystal grows from two dissimilar ones. It is evident that a more extensive study of the interface, its composition and properties, is necessary before a complete explanation of the ceramic-metal bond can be made.

Grid and Screen

The close interelectrode spacings necessary for operation of electron tubes at ultra-high frequencies create problems of grid structure, grid-cathode spacing, and grid cooling. All of these factors must be considered in the tube design if thermionic emission from the grid wires during tube operation is to be minimized. Heating of the grid is caused primarily by heat radiated by the cathode, electron bombardment of the grid, and high radio-frequency currents charging the grid-cathode capacitance. The most desirable method of handling the grid-dissipation problem is to make the entire grid of one piece of material having high thermal conductivity and to provide for removal of the heat to the outside of the tube by thermal conduction. In addition, especially for large-diameter grids, considerable mechanical rigidity is desirable to prevent vibration or changes in interelectrode spacing. The 6181 uses grids of single-piece chrome-copper construction made by a special cold-forming process.[4]

In this process, a large number of grid strands, in this case 160 vertical wires, are rolled into a slotted mandrel. At the same time a reference surface is rolled along the base of the grid which will subsequently be used for jigging during induction brazing to the support surface.

[4] W. P. Bennett, E. A. Eschbach, C. E. Haller, and W. R. Keye, "A new 100 watt triode for 1000 megacycles," Proc. I.R.E., vol. 36, pp. 1296–1302; October, 1948.

After the grid is removed from the mandrel, it is acid-etched and is then ready for use. The same procedure is used for fabrication of the screen grid. This construction eliminates thermal barriers from welded joints or uneven thermal-mechanical strains, and provides for use of the outside cylinder of the grid or screen base as a reference surface concentric to close tolerances with the wire cylinders. The thermal "sink" necessary for grid and screen cooling is supplied by cooling air passing over envelope terminals and by the contacting circuit fingers.

General Assembly Methods

In the fabrication of parts and assembly of closely spaced uhf tubes, precision jigging and, often, novel tube-making techniques are required. The coaxial-type structure used in the 6181 uses the V-block-and-mandrel method of assembly,[4] together with accurate reference surfaces on the individual parts. During the assembly of the tube, as each element is induction-brazed to the main unit, its reference surface is aligned by the jigs with the primary reference surface, the inside cylindrical surface of the cathode support sleeve. This method provides for a reproducible construction and for accurate spacing of the four electrodes.

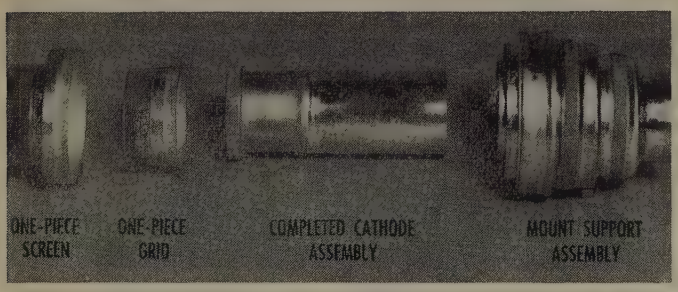

Fig. 5—Screen grid, control grid, cathode assembly, and mount support assembly.

A complete tube mount assembly is given in Fig. 5. Initially, the ceramic-metal mount is made into a support assembly and vacuum-tight envelope by the use of a precision firing jig and furnace brazing in hydrogen. A single-stepped fixture provides the necessary positioning for insertion of the cathode assembly into the mount to the proper depth and also provides a reference for the cathode surface with respect to the grid and screen supports. A radio-frequency braze, made while the assemblies are in the fixture, joins the cylindrical cathode support and the envelope cathode terminal. The brazing is done by a heavy surge of current through a single-turn induction coil which brings the metals up to temperature in a few seconds. Because the heating is concentrated and of short duration, the brazing is accomplished with a minimum of total heat, and the adjacent seal remains at low temperature, unharmed. After this brazing operation, the matrix cathode is impregnated with an appropriate carbonate coating. Next, the single-piece grid and screen are radio-frequency brazed to their support members; the ground V-blocks and mandrels are used for accurate alignment of parts. The brazes produced are symmetrical, continuous, and uniform, providing great mechanical strength and high thermal and

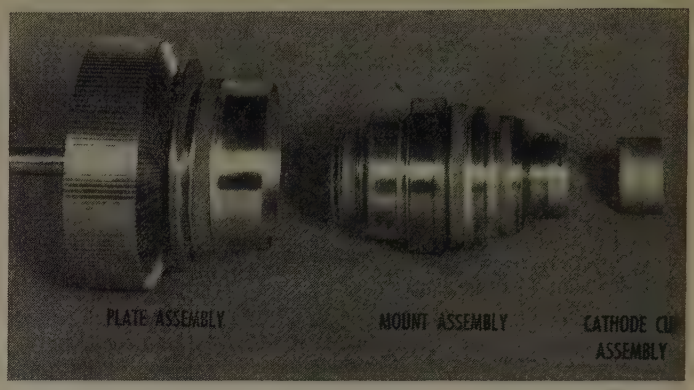

Fig. 6—Plate assembly, mount assembly, and cathode cup assembly.

electrical conductivity. All these joining operations are made in a reducing atmosphere to maintain tube cleanliness by preventing oxidation of the heated surfaces.

The plate assembly, shown in completed form in Fig. 6, is made by brazing all the parts together in one opera-

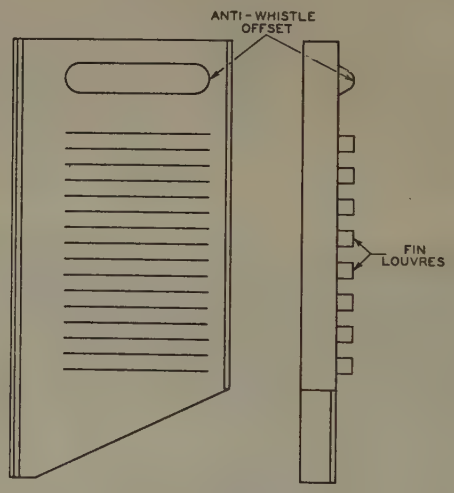

Fig. 7(a)—Radiator fin.

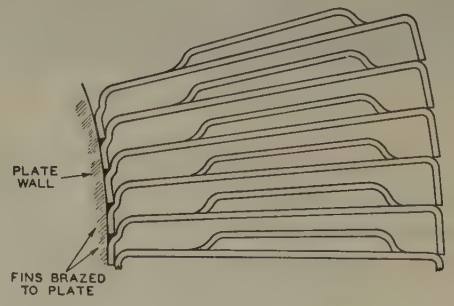

Fig. 7(b)—Radiator fin assembly.

tion in a hydrogen furnace. An unusual feature of this assembly is the high thermal efficiency of the radiator obtained by bonding the individual fins directly to the plate wall. (See fin and assembly, Fig. 7.) The rather high, heavy-wall, oxygen-free, high-conductivity copper plate further aids thermal conduction from the bom-

barded area and distributes heat efficiently over the entire length of fin. Louvres are stamped into each fin to aid the transfer of heat from the radiator to the plate air stream. All these factors combine to permit the use of smaller blowers and result in the relatively low cooling requirements of the 6181 as shown in Fig. 8.

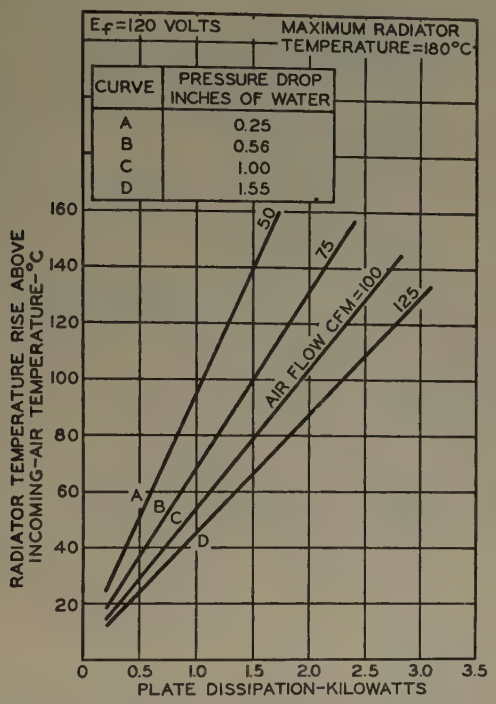

Fig. 8—Cooling requirements of Type 6181.

The main seal of the tube is made by inserting the mount assembly into the plate assembly to a fixed depth, and radio-frequency brazing the edge of the screen and screen-support cylinders. The final closure is made by placing the self-aligning cathode-cup assembly into the cathode support cylinder and radio-frequency brazing it in place. The heater rod is joined to the external terminal by means of a flame weld. The tube is then evacuated and a cold-metal pinch-off is made at the exhaust tubulation above the plate. After pinch-off, a protective cap is attached and the exterior of the entire tube is silver plated.

Circuit and Operation

In the original developmental design of this tube, an output space (screen-grid-to-plate spacing in the active area) of approximately 0.060 inch was provided. This relatively close spacing was considered necessary to minimize transit-time effects in the output region. However, developmental tubes having this spacing yielded a very low output. Measurements of circuit efficiency and bandwidth, made by the Lawson method involving a slotted line between the cavity and a matched load,[5] showed that this tube and cavity had extremely high radio-frequency losses. Even with the external load almost completely decoupled the load resistance presented to the electron beam was far too low for efficient operation. This poor circuit efficiency was believed to be due to the high circulating current required to charge the high plate-screen capacitance. This high capacitance was a result of the close output spacing of the tube. In later developmental tubes, the output space was increased and substantially higher outputs were obtained as a result of increased circuit efficiency. In subsequent tubes the output space was further increased to 0.200 inch and additional improvement in performance was obtained.

The total radio-frequency power generated by the tube is determined by adding the power lost in the circuit to that delivered to the load. When this total power was originally measured, it was found to agree substantially with the calculated low-frequency output. This agreement indicated that, in the output space, transit-time effects, even though present, did not cause serious reduction of efficiency.[6] However, there were evidences that transit-time effects were present, and were perhaps being compensated for automatically as circuit adjustments were made to obtain optimum power. As the output tank circuit was tuned, minimum plate current and optimum power output did not occur simultaneously. This phenomenon could be due to feedback effects, but this possibility seemed unlikely in view of the low internal feedback capacitance in a grounded-grid-grounded-screen type circuit. Furthermore, the measured bandwidth for a particular circuit and set of operating conditions was almost always lower in value than the corresponding calculated values. This reduction would be an indication that the electron beam was operating into a load resistance that was higher than expected and and that the plate-voltage swing had a value higher than expected. It is quite likely, as suggested by Dow,[7] that the reduction in fundamental component of the current pulse, which is brought about by transit-time effects, can be compensated by an over-voltage swing across the output space, and that suitable phase relationships prevent electron rejection by the plate.

Transit-time effects in the input or cathode-to-control-grid space are evidenced by back bombardment of the cathode. Although a matrix-type cathode is used to minimize the detrimental effect of cathode bombardment, the life of a tube can be further increased by proper control of heater power. During high-frequency operation the heater voltage should be maintained at as low a value as possible consistent with line-voltage fluctuations and power-output requirements.

[5] G. B. Collins, "Microwave Magnetrons," McGraw-Hill Book Co., Inc., New York, N. Y.; 1948.

[6] H. Rothe and E. Gundert, "The effect of electron transit time on the efficiency of tetrodes," *Telefunken-Zeit.*, vol. 25 pp. 75–87; June, 1952.

[7] W. G. Dow, "Transit time effects in ultra-high-frequency class-C operation," Proc. I.R.E., vol. 35, pp. 35–42; January, 1947.

TABLE I

GENERAL DATA

Heater, for unipotential cathode:		
voltage (ac or dc)	120 av	volts
	130 max	volts
Current at 120 volts	1.55	amperes
Mμ-factor, grid no. 2 to grid no. 1 for plate volts=1000, grid no. 2 volts=400, and plate amperes=1	8	
Direct interelectrode capacitances:		
Grid no. 1 to cathode	44	μμf
Plate to cathode	0.10 max	μμf
Grid no. 2 to plate	22	μμf
Maximum over-all length	7-7/16	inches

RATINGS AND TYPICAL OPERATION OF 6181 AS BIAS-MODULATED RF POWER AMPLIFIER

Synchronizing-level conditions per tube unless otherwise specified

Maximum CCS* ratings, absolute values:		
DC plate voltage	2000 max	volts
DC grid—no. 2 (screen) voltage	500 max	volts
DC grid—no. 1 (control-grid) voltage (white level)	−300 max	volts
DC plate current	1.75 max	amp
DC grid—no. 1 current	0.2 max	amp
Plate input	3500 max	watts
Grid—no. 2 input	40 max	watts
Plate dissipation	2000 max	watts

TYPICAL CATHODE-BIAS-MODULATED OPERATION IN CATHODE-DRIVE CIRCUIT AT 900 MC

Bandwidth† of 8 mc

Air flow through radiator:		
Minimum, with incoming air at 45°C	60	cfm
Static pressure	0.36	inch of water
DC plate-to-grid—no. 1 voltage	1875	volts
DC grid—no. 2-to-grid—no. 1 voltage	550	volts
DC cathode-to-grid—no. 1 voltage:		
Synchronizing level	75	volts
Pedestal level	105	volts
White level	210	volts
Peak RF cathode-to-grid—no. 1 voltage	120	volts
DC plate current:		
Synchronizing level	1.7	amp
Pedestal level	1.2	amp
DC grid—no. 2 current (pedestal level)	−0.025	amp
DC grid—no. 1 current (approx.):		
Synchronizing level	0.075	amp
Pedestal level	0.020	amp
Driver power output (approx.):		
Synchronizing level	200	watts
Output-circuit efficiency (approx.)	75	per cent
Useful power output (approx.):‡		
Synchronizing level	1200§	watts
Pedestal level	675§	watts

* Continuous commercial service.

† Measured between half-power points.

‡ The driver stage is required to supply tube losses, RF circuit losses, and RF power added to the plate input. The driver stage should be designed to provide an excess of power above the indicated value to take care of variations in line voltage, in components, in initial tube characteristics, and in tube characteristics during life.

§ This value of useful power is measured at load of output circuit having indicated efficiency.

The typical data as shown in Table I and Fig. 9 were obtained with the 6181 operating as an amplifier at a frequency of 900 mc in a cathode-driven circuit in which the control grid and screen grid are separated, similar to

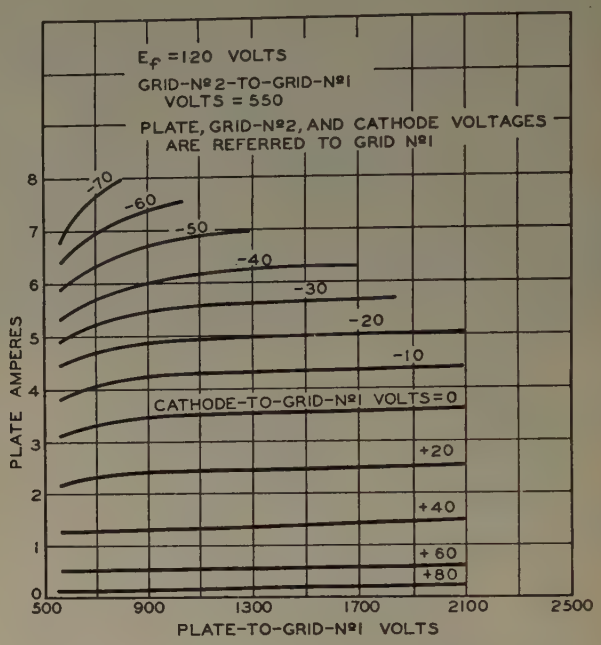

Fig. 9—Average plate characteristics of Type 6181

that shown in cross section in Fig. 10. The tube is driven by a 6161 amplifier stage which in turn is driven by a 6161 frequency doubler. The 6181 input circuit consists of a coaxial line having an effective electrical length of either three-quarter or five-quarter wavelength depending upon where the input coupling loop is located. The circuit is tuned by a contacting-type shorting bar at the end of the line. In the usual cathode-driven circuit it is desirable to maintain the control grid and screen grid at the same radio-frequency potential. Two different circuit variations were tried and found to be satisfactory so long as certain operating conditions were avoided. In one type of circuit a coaxial line having a movable shorting bar was placed between the grids. In this circuit, performance is not affected by the position of the shorting bar unless the length of the line is such as to cause it to be in parallel resonance. Another condition to be avoided is having the length of the line such as to allow a lower-frequency spurious mode of oscillation to build up whereby triode operation could exist with the screen acting as a plate. Such a spurious oscillation could be damped out without adversely affecting performance by loading the screen-grid and control-grid circuit with a high-loss material such as carbon. In other circuits, the region between the screen grid and control grid is simply left open. However, precautions must be taken to prevent the development of spurious resonances, as well as excessive radiation from this opening.

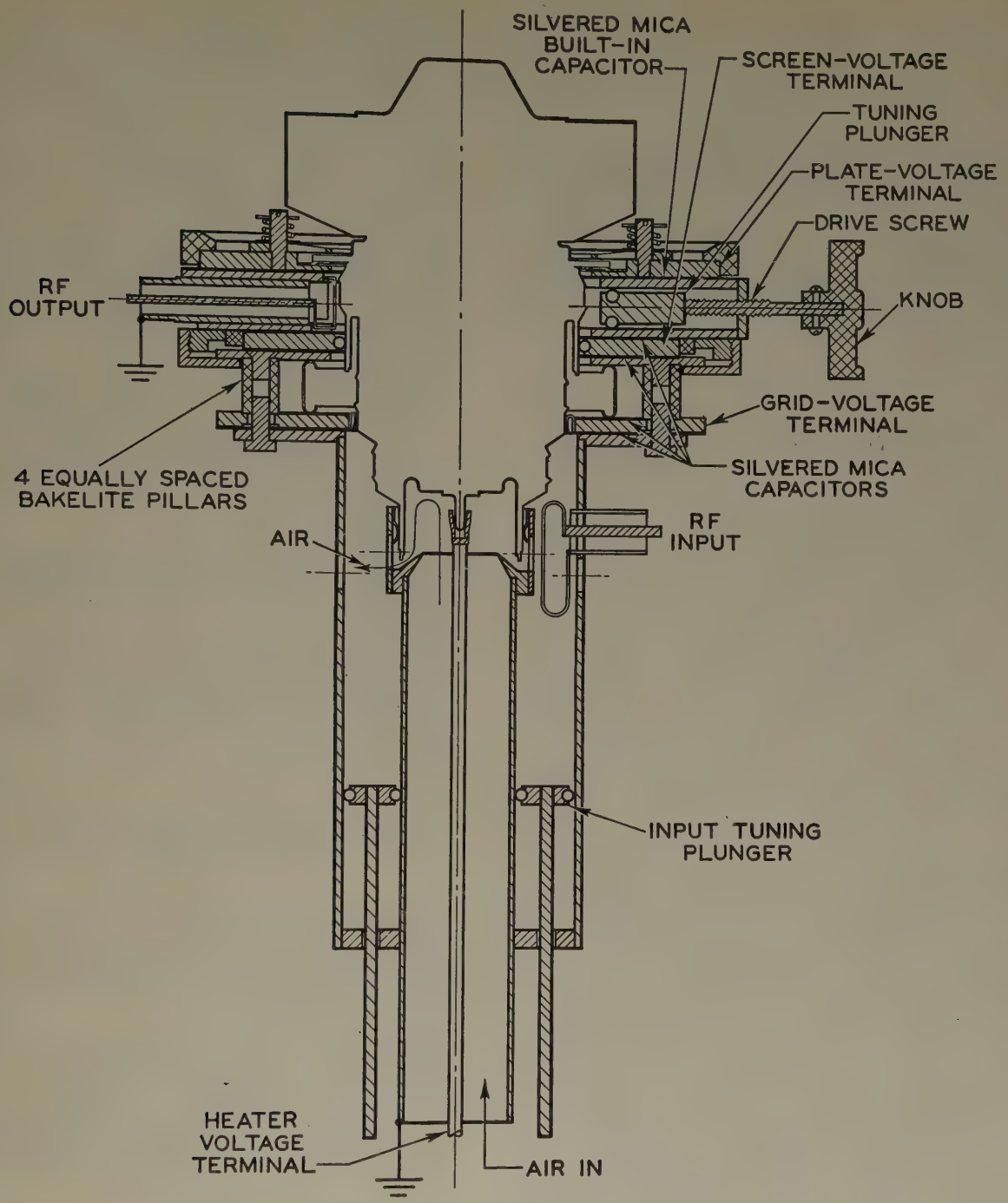

Fig. 10—Cross section of cathode-driven 900-mc circuit for Type 6181.

The output circuit connected between the plate flange and the screen-grid terminal is a simple quarter-wave type, fitting closely about the tube and providing uniform current distribution about the circumference of the tube and circuit. Output tuning is effected by moving a "slug" in a direction perpendicular to the tube axis. Power is fed out of the circuit by means of a coupling loop connected to an external adaptor, which is in turn terminated by a 50-ohm load. All power measurements were made calorimetrically by means of a calibrated water-cooled load.

Acknowledgment

The authors are indebted to Dr. D. G. Burnside for the development of a satisfactory ceramic-metal sealing technique, and to F. W. Peterson and G. S. Scholes for their aid in the design and construction of suitable uhf circuitry and for operational testing of the tubes.

High-Power Klystrons at UHF*

D. H. PREIST†, MEMBER, IRE, C. E. MURDOCK†, ASSOCIATE, IRE, AND J. J. WOERNER†

Summary—**A brief history of high-power cw klystron development and a classification of types of klystron are followed by a description of the three-cavity, gridless klystron amplifier with magnetic focusing, in general terms, and the Eimac 5-kw klystron for UHF-TV in more detail. This tube has cavities which are partly outside the vacuum system and contain ceramic "windows." The advantages of the klystron over the conventional negative-grid type of tube are reviewed from the standpoint of performance, and the main operational features are noted.**

Introduction

IN VIEW OF the increasing activity above 450 mc for such purposes as television, it may be of value to review the means of generating transmitter power presently available.

Of outstanding interest in this field is the post-World War II development of power amplifier klystrons. Although the klystron principle was discovered as far back as 1939,[1] its application to high-power generation was delayed, largely because of the 1939–1945 war and the need to concentrate on those lines of development which appeared the most promising for military purposes. The ultimate possibilities of the klystron were appreciated by few, and although a great deal of fundamental research on electron beams was carried on in various places, development in the field of high-power cw tubes was confined mainly to one group in California,[2,3] and one group in France.[4,5] As a result of this work the basic principles have been extended, and much progress has been made in techniques of construction, culminating in the recent appearance of high-power klystrons for commercial purposes in the United States,[2,6] and an increasing awareness of the great advantages of this type of tube for stable amplification at high-power levels.

The object of this paper is to review, briefly, from the point of view of the potential user, the performance of a modern high-power klystron, and to describe the special peculiarities and methods of operation of this type of tube. A brief survey will also be made of the factors limiting the performance of a klystron, compared with the factors limiting the performance of conventional negative-grid tubes.

* Decimal classification: R339.2×R583.6. Original manuscript received by the Institute, November 3, 1952.

† Eitel-McCullough, Inc., San Bruno, Calif.

[1] R. H. Varian and S. F. Varian, "A high frequency oscillator and amplifier," *Jour. Appl. Phys.*, vol. 10, p. 321; 1939.

[2] "High Power UHF Klystron," *Tele-Tech*, p. 60; October, 1952.

[3] W. C. Abraham, F. L. Salisbury, S. F. Varian, and M. Chodorow, "Transmitting Tube Suitable for UHF TV," paper presented at IRE National Convention; 1951.

[4] P. Guénard, B. Epsztein, and P. Cahour, "Klystron Amplificateur de 5 KW à large bande passante," *Ann. Radioelect.*, vol. VI, p. 24; 1951.

[5] R. Warnecke and P. Guénard, "Tubes à Modulation de Vitesse," Gauthier-Villards, Paris; 1951.

[6] J. J. Woerner, "A High Power UHF Klystron for TV Service," paper presented at IRE National Convention; 1952.

Klystron Types

Present-day klystrons fall into three categories:

1. *Reflex Klystron Oscillators*
   Most of these have low efficiency (of the order of 1 per cent) and generate relatively low power, and are suitable for receivers, local oscillators, test equipment, and the like.
2. *2-Cavity Klystrons*
   These may be used as amplifiers, oscillators, or frequency multipliers; as amplifiers they are capable of power gains of about 13 db and efficiencies of about 20 per cent, at frequencies of the order of 1,000 mc.
3. *3-Cavity Klystrons*
   These are useful, principally, as amplifiers, and are capable of power gains of about 20 to 30 db, and efficiencies of 30 to 40 per cent, together with bandwidths of several mc, at frequencies of the order of 1,000 mc. Because of the superior amplifier performance given by this type of klystron, the other two types will not be dealt with further in this paper.

3-Cavity Gridless Klystron Amplifier with Magnetic Focussing

A. Description

This type of tube, sometimes called a "cascade amplifier," is illustrated schematically in Fig. 1. It will be seen to consist of four essential parts:

1. *The Electron Gun*
   This has a source of electrons (the cathode), a means of accelerating the electrons to a high energy level (the anode), and a means of focussing the electrons into a parallel beam of high electron density emerging from the hole in the anode.

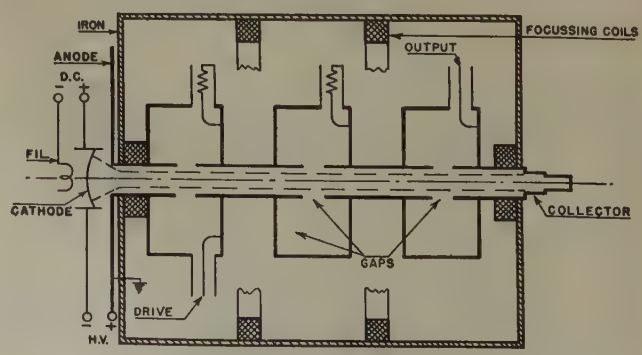

Fig. 1—Schematic diagram of 3-cavity klystron with magnetic focusing.

2. *The RF Resonant Cavities and Drift Tubes*
The first cavity is fed with RF energy from a driving source at low level. The second cavity is tuned to resonance, or near resonance, but is not fed with energy from outside. The function of these two cavities, in conjunction with the drift tubes, is to velocity-modulate the electron beam so as to produce "bunches" of electrons at the output cavity. The latter is tuned to resonance and coupled to the antenna, or other load, and serves to extract as much RF energy as possible from the "bunched" electron beam. Its function and operation are closely similar to those of the output circuit of a Class "C" amplifier using triodes or tetrodes.
3. *The "Collector" Electrode*
This collects the electrons after they have passed through the output cavity, and have given up part of their energy to the RF field, and thus to the load; because only about 30 per cent of the energy in the beam is converted to RF energy, this collector has to be capable of dissipating the remaining percentage, that is to say, 70 per cent of the product of the anode-cathode voltage and cathode current, when fully driven. (In practice the collector current is very slightly less than this because some electrons inevitably strike the anode and the drift-tube walls.) If the tube is used as a linear modulated amplifier, the collector will be required to dissipate 100 per cent of the input power under conditions of zero drive and zero output.
4. *External Magnetic Circuit*
This consists of suitably disposed electromagnets producing an axial magnetic field of controllable strength which tends to keep the beam parallel as it passes along the tube. Without this field the beam would expand because of the mutual repulsion of the electrons. The optimum field strength is fairly critical, and is not necessarily uniform along the length of the tube. It is usually prevented from penetrating the cathode, either by a metallic magnetic shield or by the use of a "bucking" coil, or by a combination of both.

B. Performance and Operational Features of This Type of Klystron

The 3-cavity klystron is a tube capable of generating a much larger power output at uhf than the conventional negative-grid tube. The deterioration of performance as the frequency is raised is slight. The power gain of the klystron is very much larger than that of a tetrode. It may be worthwhile to review briefly the reasons for this.

Considering the factors limiting the power output of a triode or tetrode, aside from external circuit losses, one finds that basically they are the total cathode emission, the anode voltage, the interelectrode spacing, and the RF loss in the materials used to make the electrodes and the envelope. Now the total cathode emission, assuming the best material is used and that a given life is required, depends on its area. This area is limited at uhf because the tube forms part of a resonant transmission line in which large changes of electric and magnetic field occur over distances which are small compared with the wavelength. Since nonuniform potentials between electrodes cause loss of efficiency, it is necessary to keep the electrode dimensions small compared with the wavelength; thus, the cathode area is limited, and has to be reduced as the wavelength is decreased. The anode voltage is limited by internal flash-arcs between electrodes. The electrode spacing must, however, be small enough to give small electron transit times, and must be decreased with the wavelength. The applied voltage must, therefore, be reduced also with the wavelength. Lastly, the RF losses in the tube materials increase as the wavelength decreases. All these factors added together give the well-known result that triodes and tetrodes get rapidly smaller as the wavelength decreases, and so does the power they will generate and the efficiency. In addition, the problem of manufacture becomes more and more serious, and ultimately becomes prohibitive. The two worst problems are caused by the small spacing between electrodes, of the order of 0.001 inch, and the mechanical weakness of the fine wire grids.

Considering now the power gain, this becomes less as the wavelength decreases because the tube requires more and more driving power to overcome the increasing electron transit-time effects, losses in materials, grid current, and (usually) inherent negative feedback.

In a klystron, on the other hand, some of these limitations do not occur at all, and others are less significant. The cathode area is not limited by the wavelength because it is outside the RF field. The anode-to-cathode spacing being of the order of 1 inch, extremely high anode voltages may be applied without internal flash-arcs; also, the cavity gap spacings may be about $\frac{1}{2}$ inch in a 5-kw tube at 1,000 mc. Again, because gridless gaps may be used without serious loss of coupling between the beam and the resonant cavities, there are no problems of fabrication or heating of grid wires. Furthermore, because the collector is outside the RF field, it may be designed solely for the purpose of dissipating heat, and this becomes a minor problem in practice. The losses in the conductive tube materials are small because all the metal parts carrying RF current may be made of high-conductivity metal. (There is no loss comparable to the RF losses in a triode due to RF current flowing through lossy cathode material or fine resistive grid wires.) Therefore, the only limiting factor approached in klystrons giving adequate power for present commercial applications is the loss in the dielectrics. Some dielectrics are inevitable either in the form of windows in the cavities, as in the Eimac tube, or in the other type of tube with integral cavities, the window between the

output cavity and the load. If the power level is raised high enough, these dielectrics will ultimately break down, either by cracking due to heat or by flashing over the outside surface which is at atmospheric pressure; however, this does not occur in a well-designed tube at power levels that are presently interesting.

Considering the power gain of a klystron, this is governed almost entirely by the geometry and is limited only by the small RF losses in the input cavity and the beam loading of the cavity, which is small. The transit-time loading experienced with a triode becomes a factor of minor importance, and the negative feedback disappears since there is no coupling between the input and output cavities.

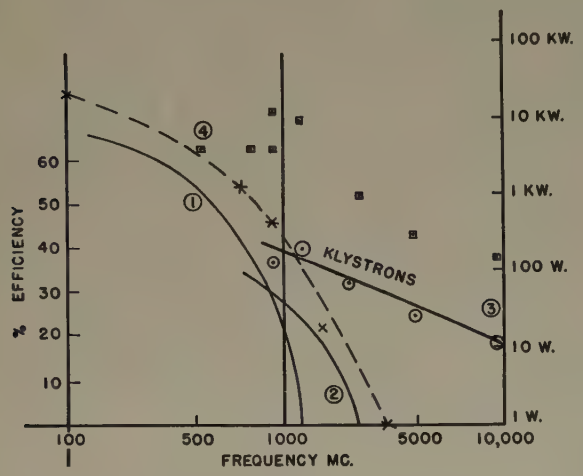

Fig. 2—Curve (1): Efficiency versus frequency for typical uhf tetrode —4X150G. (Plate dissipation 150 watts.)
Curve (2): Efficiency versus frequency for typical uhf triode —2C39. (Plate dissipation 100 watts.)
Curve (3): Typical efficiency of klystrons versus frequency (independent of output power). This is the efficiency at the optimum frequency for each tube.
Curve (4) (dotted): Maximum power output of the largest commercially available negative-grid tube at various frequencies.
Points ⊡ cw power output of various klystrons (not the largest possible).

It is, therefore, apparent that the efficiency and power gain of a klystron will fall off relatively slowly, compared with a triode or tetrode, as the wavelength is reduced. This is illustrated by the curves in Fig. 2. It is also clear that the maximum size and power output of a klystron are not determined by the wavelength. It follows that the klystron is ideally suited to high-power generation at uhf and microwave frequencies, and outclasses the conventional type of tube in every respect, including ease of manufacture.

Turning now to a typical performance obtainable from a 3-cavity klystron, the results given by the Eimac tube may be taken as representative of this type of tube. This tube will generate 5 kw of RF power in the uhf television band with an efficiency of more than 30 per cent when fully driven. The over-all bandwidth is about 5 mc and the power gain, under television conditions, is about 20 db. Salient features of operation are these:

The tuning of each of the 3 cavities is independent of the others since there is no feedback present. This makes for very simple lining-up procedure.

The output cavity is tuned to resonance at the midband frequency, and loaded for optimum performance by means of some variable coupling device external to the tube.

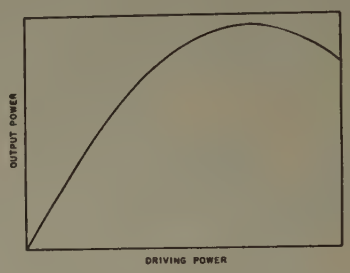

Fig. 3—Output power versus driving power for klystron.

A curve of power output against power input for this type of tube is a Bessel function of the first order and the first kind, and the first part of such a curve is very nearly linear. (See Fig. 3.) In television service, assuming that sync stretching is used in the driving stages, the klystron may be operated in such a way that the sync pulses drive the tube very nearly to the peak of the Bessel curve, so that the efficiency at sync pulse levels is nearly the fully driven efficiency.

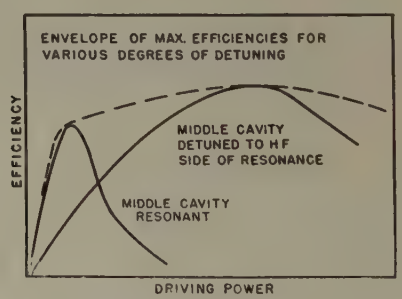

Fig. 4—Efficiency versus driving power, showing the effect of detuning the middle cavity.

The center cavity is detuned to a frequency slightly higher than the midband frequency, since this gives greater efficiency than resonant operation, and helps to broaden the pass band. This cavity may be loaded externally by resistance in some cases. This detuned operation requires greater driving power to the first cavity than resonant operation. (See Fig. 4.)

The input cavity may be either detuned on the low-frequency side of resonance or it may be tuned to resonance and loaded with external resistance in order to achieve the necessary bandwidth.

The relation between efficiency, power output, and anode voltage for a given tube is shown at Fig. 5. There is an optimum voltage for best efficiency because the voltage determines the speed of the electrons along the tube. Now a certain time is required for electron bunching to take place; this depends mainly on the frequency and determines the distance between the cavities. But this distance will be optimum for only one electron speed, and therefore only one voltage. Conversely, for a given voltage the relation between efficiency and frequency will also show a broad peak at a given frequency, and this fall-off at higher and lower frequencies will limit the useful frequency range of a given tube, even if the cavities are tunable over an indefinitely wide range.

The power input from the dc power supply feeding the anode of the tube is constant (about 1.5 amps at 13 kv), and independent of the drive voltage; therefore, the regulation of this power supply may be quite poor without adverse effects. Also, only simple circuits are necessary to reduce the hum to a low level. The filament may be heated by ac.

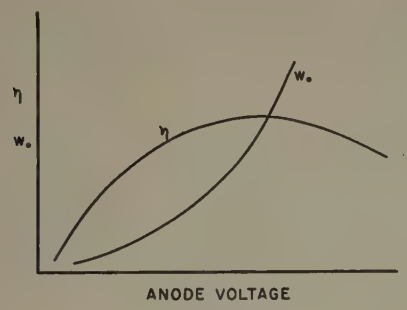

Fig. 5—Power output and efficiency versus anode voltage.

The magnetic field used for focussing the beam is simple to arrange, and relatively low in intensity, and consumes only a small amount of dc power in the coils. It must be made variable since the efficiency of the tube varies fairly rapidly with the field strength and reaches a maximum for an optimum setting of the magnetic field. The RF cavities, the drift tubes, and the anode are all in metallic contact and may be grounded. Thus, there is no problem of by-passing and dc isolation in the output circuit compared to the by-passing problem with a triode or tetrode amplifier. The collector is usually insulated from the main part of the tube in order to facilitate monitoring of the current division between the collector and the drift tubes. The anode voltage supply is grounded on the positive side, and the negative side is connected to the cathode of the tube.

Considering now the over-all problem of design, construction, installation, and operation of a high-power uhf amplifier, and the difference between the problem with a conventional type of tube and with a klystron, it is evident that the klystron scores heavily in all respects. The burden imposed on the transmitter designer is lessened because the klystron with its cavities forms a complete amplifier stage in itself. Because of the absence of feedback in the klystron, the circuit design is greatly simplified, compared with the conventional amplifier design. Also, when using a conventional tube at uhf, the designer is usually faced with the very difficult problem of obtaining the maximum efficiency from a stage in which the tube is run to its limit, and only by very careful design can the desired performance be obtained from it. With klystrons, on the other hand, the problem is easier because there is usually a greater margin of performance, both in respect to output and power gain. Also, the construction of a klystron stage is simpler than the conventional stage, and, as we have seen, the operation is also simpler.

Fig. 1 shows the more or less conventional type of klystron construction involving integral cavities, namely, cavities which are an integral part of the vacuum system. A unique feature of the Eimac tube, hereinafter described, is that part of the cavities are external to the tube envelope so that simple mechanical tuning of the cavities over a wider band of frequencies is possible. The tube itself is also simplified.

C. A Practical Example: Eimac UHF Klystron for TV

The photograph in Fig. 6 shows the Eimac uhf klystron, an example of a 3-cavity klystron in a form suitable for commercial manufacture, and now in produc-

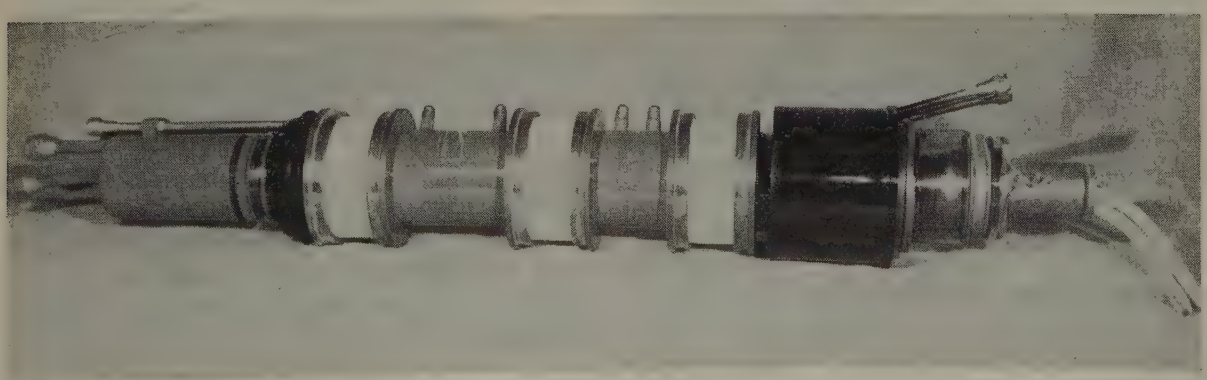

Fig. 6—The Eimac 5-kw uhf klystron for TV.

tion. Tube-cavity parts and drift-tube sections are shown in Fig. 7. Fig. 8 shows the tube and external cavities in a test setup.

Fig. 7—Tube cavity parts and drift tube sections.

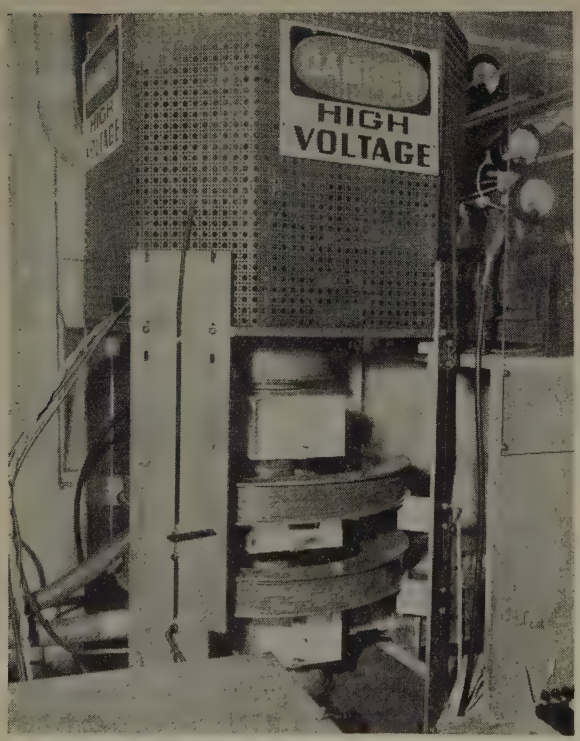

Fig. 8—The 5-kw klystron on test.

A feature of interest is the use of cavities which are tunable by means external to the vacuum system. This is made possible by use of ceramic "windows" which, if designed and fabricated correctly, will produce only a minor deterioration in the over-all performance of the tube because of their finite dielectric loss and high dielectric constant.

This means that part of each cavity is in vacuo and part is in air. The convenience of operating a tube of this type, compared with a tube in which the cavities are entirely in vacuo, is considerable. In the first place, the mechanism for varying the resonant frequency is simple and may involve straightforward shorting bars with sliding contacts with negligible losses. These slidable devices are outside the vacuum system, as shown in Fig. 8. The tuning range of such a cavity is large. With a totally evacuated cavity it has not yet been found possible to use such a means of tuning, because sliding contacts in vacuo are generally unsatisfactory. Therefore, tuning has to be done by distortion of some flexible metallic membrane. Such a membrane introduces mechanical weaknesses into the tube structure which then has to be stiffened by an external frame. Also, the range of tuning is relatively small, and usually the tuning is done by varying the gap spacing, and therefore, its capacitance. This can be done only to a limited extent. If the gap is made too wide, the electron transit time will become an appreciable fraction of 1 RF cycle, causing inefficiency; on the other hand, if the gap is too small, the bandwidth will suffer (bandwidth varies roughly as 1/c). With a ceramic window cavity the tuning is done by varying the inductance of the cavity, the capacitance across the gap is fixed, and the gap can be set for optimum performance over the frequency band.

Another point of difference is that the mechanical forces required to tune a cavity by means external to the vacuum system are small, being determined only by friction, whereas with the other type of cavity the tuning mechanism has to withstand the forces caused by the operation of atmospheric pressure against the flexible metallic membrane.

Fig. 9—Output cavity with one tuning plunger removed, showing ceramic and output coupling device.

Another desirable feature obtained with the ceramic windows is that the loading of the cavity may be accomplished outside the vacuum system, either by loops or a waveguide-to-cavity loading device, such as a quarter-wave transformer made from ridge waveguide. (See photograph of output cavity, Fig. 9.) The coupling may, therefore, be varied with ease. With a totally evacuated cavity it is very inconvenient to build in a variable load coupling, and it is common practice to use

a fixed loop; thus the benefit of variable coupling is lost.

Lastly, because of the relatively large frequency band that can be covered by a given klystron with ceramic windows, a smaller number of tube designs is required to cover a given frequency band, such as the uhf TV band. This simplifies the manufacturing problem and reduces the cost of the tube.

Another feature of interest is the use of a tantalum cathode heated by electron bombardment from a tungsten filament of relatively small size by means of a dc power supply (0.6 amps. at 2,000 volts) between the cathode and the filament. This constitutes a flexible system, and is much simpler to design and construct than a radiation-heated cathode.

Conclusions

The 3-cavity externally tunable klystron is excellently suited to high-power generation at uhf (and also at higher frequencies) because

1. it is relatively simple to manufacture,
2. it is easy to use and adjust,
3. the transmitter design and construction is simplified by its use,
4. its performance as an amplifier is greatly superior to other tube types.

It is likely that the future will see more and more such tubes in commercial service for an increasing variety of applications.

A Floating-Drift-Tube Klystron*

M. CHODOROW†, senior member, ire and S. P. FAN‡, associate, ire

Summary—**This paper describes a theoretical and experimental investigation of a special form of klystron which seems to have many important uses as a frequency-modulated oscillator. Basically, it is a single-cavity, two-gap klystron with a floating drift tube between the two gaps.**

By applying a separate voltage to the floating drift tube it is possible to produce frequency modulation by varying the transit angle between the gaps in a similar manner to the frequency modulation produced in a reflex klystron. An examination of the theory indeed indicates that the theory of the floating-drift-tube klystron (FDTK) and the reflex klystrons are essentially identical. One merely replaces the transit angle wherever it appears in reflex theory by the same number divided by a factor *H*, where *H* is the ratio of the effective voltages at the two gaps. However, in spite of this identity of theory, in practice the FDTK should have higher efficiency and power-handling capabilities merely because of its geometry. In addition, the absence of the reflection problem, i.e., of electrons transversing the same gap twice, eliminates all the difficulties connected with multiple transits which produce hysteresis, mode distortion, and the like, which are characteristic of many reflex klystrons. This prognosis fulfilled in the tube which was constructed.

When a detailed examination was made of the dependence of efficiency and electronic tuning bandwidth on the factor *H*, it was possible to vary the cavity shape so that one could get either high efficiency at relatively low bandwidth (22 per cent, 4 mc), or lower efficiency and greater bandwidth (6 per cent, 15 mc). In both cases the mode was very clean, showing no distortion or hysteresis, and the behavior of efficiency and bandwidth with change in parameters was in very close agreement with theory.

I. Introduction

THIS PAPER DESCRIBES a theoretical and experimental investigation of a special form of klystron which seems to have many important uses, particularly in communication, and specifically in microwave relay links. This type of tube has been previously described in the literature and has been worked on by a number of people.[1,2] Much of this work was done quite some time ago, however, when the interest was in exploring the simplest properties of this tube, and the emphasis was not on the particular properties which will be discussed in this paper.

This tube has been designated by various names, but it will be referred to here as the floating-drift-tube klystron, abbreviated as FDTK. A schematic diagram is shown in Fig. 1. From the configuration of the cavity it is obvious that the tube is generically related to a two-cavity klystron. Indeed, if one removes the common wall between the two adjacent resonators of such a

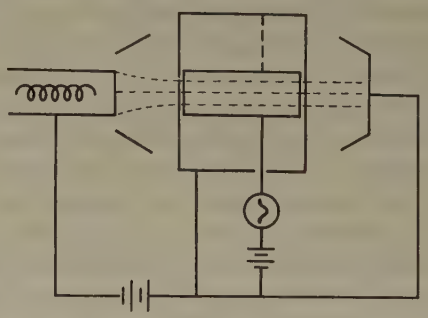

Fig. 1—Schematic diagram of floating-drift-tube klystron.

two-cavity klystron, one gets a single cavity which will resonate at the same frequency as the common frequency of its two constituents. The electronic behavior is also quite similar to that of a two-cavity oscillator; velocity modulation occurs at the first gap and for the right transit angle between the gaps, the voltage at the second gap will be of the right phase to extract energy

* Decimal classification: R355.912.3×R339.2. Original manuscript received by the Institute, December 10, 1951; revised manuscript received July 30, 1952. Presented, IRE National Convention, New York, N. Y., March 20, 1951.

† Stanford University, Stanford, Calif.
‡ Burroughs Adding Machine Co., Philadelphia, Pa.

[1] A. Arsenjewa-Heil and O. Heil, *Zeits. für Physik*, vol. 95, pp. 752–762; 1935.

[2] A. L. Samuel has done research on this tube at the Bell Telephone Laboratory. His work is described in G. C. Southworth's book, "Principles and Application of Waveguide Transmission," D. Van Nostrand Co., Inc., New York, N. Y.; 1950.

from the bunched beam. Thus, in many respects, particularly efficiency and power-handling capabilities, this type of tube will be very similar to a two-cavity oscillator. Of course, the drift tube must be supported in some manner, and, in particular, it may be insulated from the wall of the outside cavity, as shown in the figure, so that it is possible to apply a separate voltage to the drift tube. This changes the transit angle of the electrons between the two gaps without changing the input power, and in this type of operation one can get frequency modulation in a manner entirely analogous to that obtained in a reflex klystron when the reflector is modulated.

In this paper, a theoretical analysis of the operation of a FDTK is made, and the results obtained on an experimental tube are described. The results agreed very satisfactorily with the theory; in particular, the relation between the efficiency and electronic tuning bandwidth were verified. It was found possible to get a combination of the two, which is much better than has been heretofore obtained with a reflex tube in this frequency range.

II. Theory of Floating-Drift-Tube Klystron

A. Fundamental Equations

Since the FDTK has only one cavity, as in the reflex tube, the theory is, therefore, almost identical, with a few important differences. As in standard treatments of reflex tubes,[3,4] one defines an electronic admittance which is determined by the velocity modulation and bunching process and a circuit admittance which depends only on the cavity. The electronic admittance is a function of the voltage amplitude. In the steady state, this amplitude is such that the two admittances are equal. To get the electronic admittance, one can calculate the current at the output gap in terms of the voltage at the input gap in an obvious way from simple bunching theory. Since the circuit admittance of importance is the admittance across the output gap, one must write an electronic admittance using the *output* gap voltage. This can be easily written in terms of the input gap voltage since the ratio of the two gap voltages is a constant, depending only on cavity geometry. Using this ratio, one can equate the circuit admittance and electronic admittance for the output gap, and from the resultant complex equation one gets two real equations for the steady state,

$$y_e \frac{2J_1(x)}{x} \cos\phi = \omega C\left[\frac{1}{Q_0'} + \frac{G_L}{Q_{\text{ext}}}\right] \tag{1}$$

$$\left[\frac{1}{Q_0'} + \frac{G_L}{Q_{\text{ext}}}\right] \tan\phi = 2\delta + \frac{B_L}{Q_{\text{ext}}}, \text{ where} \tag{2}$$

x = bunching parameter $= \dfrac{M_1 V_1 \theta_0}{2V_0}$

V_1 = rf voltage gap 1

V_2 = rf voltage gap 2

M_1 = beam coupling coefficient for gap 1 $= \dfrac{\sin\theta_1/2}{\theta_1/2}$

M_2 = beam coupling coefficient for gap 2

$\theta_{1,2}$ = transit angle for input gaps 1, 2

θ_0 = drift-tube transit angle

$$\phi = \theta_0 - \frac{3\pi}{2}$$

$y_e = \dfrac{M_1 M_2 \theta_0 G_0}{2\beta} = \dfrac{M_2^2 \theta_0 G_0}{2H}$ = small-signal electronic conductance

$$G_0 = \frac{I_0}{V_0}, \quad \beta = \frac{V_2}{V_1}, \quad H = \frac{M_2}{M_1}\beta$$

I_0, V_0 = dc current and *drift-tube voltage*

$Y_C' = \omega C\left[\dfrac{1}{Q_0'} + j2\delta\right] \equiv G_C'[1 + j2Q_0'\delta]$ = equivalent circuit admittance at the second gap (including beam loading)

$Y_L' = \omega C\left[\dfrac{G_L}{Q_{\text{ext}}} + j\dfrac{B_L}{Q_{\text{ext}}}\right] = G_L' + jB_L'$ = equivalent load admittance at the second gap.

Equations (1) and (2) determine both the amplitude and frequency, and, consequently, also determine the modulation characteristics. Equations (1) and (2) are similar to those of the reflex tubes, except for the quantity H, which is the ratio of the effective gap voltages. It is obviously unity for the reflex tube. It is this quantity H which is the significant parameter in determining the behavior of the FDTK. It will be discussed in greater detail below.

B. Power and Efficiency

The RF power delivered to the second gap is

$$P_2 = \frac{M_2^2 I_0^2}{y_e} \times J_1(x) \cos\phi. \tag{3}$$

The power output to the load is

$$P_L = \frac{M_2^2 I_0^2}{y_e} \times \left[J_1(x)\cos\phi - \frac{1}{2} \times \frac{\omega C}{y_e Q_0'}\right]. \tag{4}$$

As in the reflex tube, the load for optimum power output can be found by differentiating (4) with respect to x. Then, x for optimum is given by $\omega C/y_e Q_0' = J_0(x_0)$ with $G_L' = J_2(x_0)$, the optimum power output is

$$P_{L\,\text{opt}} = V_0 I_0 \frac{M_2^2 G_0}{y_e} \frac{x_0^2}{2} J_2(x_0), \tag{5}$$

and the corresponding efficiency is

[3] J. C. Slater, "Microwave Electronics," chap. X, D. Van Nostrand Co., Inc., New York, N. Y.; 1950.

[4] J. Pierce and W. G. Shepherd, "Reflex oscillators," *Bell Sys. Tech. Jour.*, vol. 26, p. 460; July, 1947.

$$\eta_{L\,opt} = \frac{H}{\theta_0} x_0^2 J_2(x_0). \tag{6}$$

From the form of the equation it can be seen that H essentially determines the effective bunching angle, which can be defined as θ_0/H. The function $F_1(x_0) = x_0^2 J_2(x_0)$ is plotted against $J_0(x_0)$ in Fig. 2(a). The reason for choosing $J_0(x_0)$ instead of x_0 as abscissa is that $J_0(x_0) = \omega C/y_e Q_0'$ can be considered as a fundamental design parameter, whereas x_0 is only an operating parameter.

It should be pointed out that the efficiency in (6) uses drift-tube voltage as basis. Actually, the input power of the tube is determined by V_B, the anode voltage, so that the over-all efficiency should be multiplied by the factor V_0/V_B. The practical efficiency may be greater or less than the theoretical value.

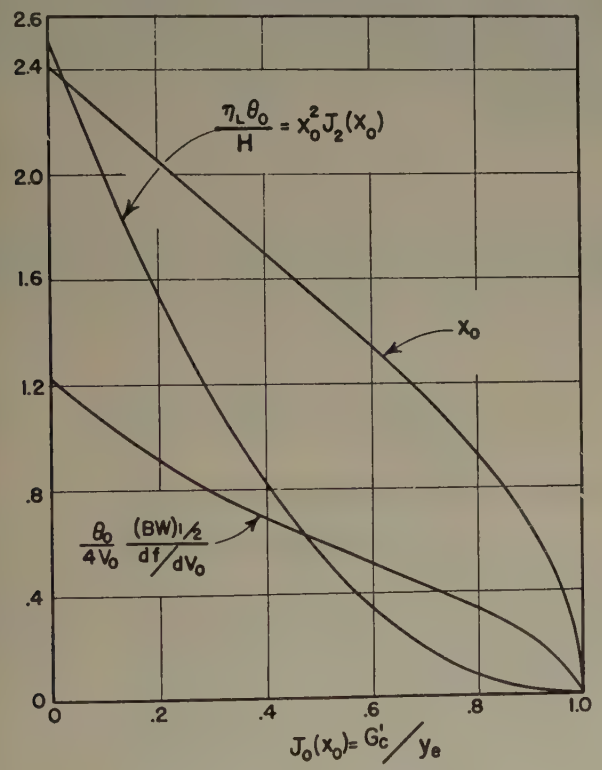

Fig. 2(a)—Performance curves I.

C. *Modulation Sensitivity and Electronic Tuning Bandwidth*

Since the drift tube is isolated from the outside cavity wall, it is possible to apply a voltage to it to change the electron transit time in the drift tube. This is similar to the effect of the repeller voltage of the reflex tube, and the analysis of the resulting frequency modulation can be carried out in an analogous way. In (2) ϕ is related to the operating drift-tube voltage, while $\delta = \Delta f/f_0$ is linearly proportional to the operating frequency. By simple differentiations and substitution, one gets for the modulation sensitivity

$$\frac{df}{dV_0} = \frac{f_0\theta_0}{4V_0} \frac{y_e}{\omega C} \frac{2J_1(x)}{x} \sec\phi, \tag{7}$$

and with optimum load,

$$\frac{df}{dV_0} = \frac{f_0\theta_0}{4V_0} \frac{G_L}{Q_{ext}} \frac{2J_1(x_0)}{x_0 J_2(x_0)}. \tag{8}$$

The half-power bandwidth (BW) can be found by the fact that the power output is always equal to $P_L = \frac{1}{2} V_2^2 G_L'$, and also $V_2 = \beta V_1$. Then at the center of the mode with $x = x_c$,

$$P_L = \frac{1}{2}\left[\frac{M_2 I_0}{y_e} x_c\right]^2 G_L'. \tag{9}$$

If the load does not change with frequency, x at the half-power point is $(1/\sqrt{2})x_c$. Substituting this value of x in (2) and solving for 2δ, the bandwidth is

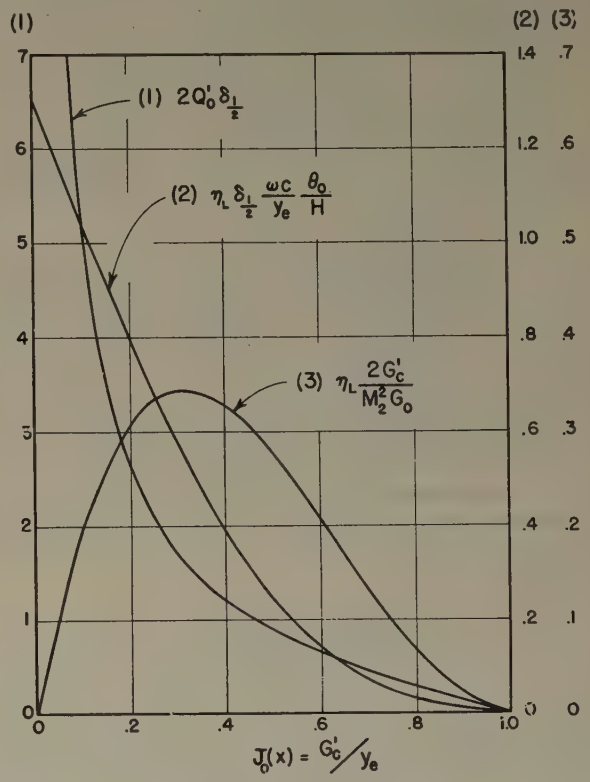

Fig. 2(b)—Performance curves II.

$$2\delta = \frac{G_0 f_0}{\omega C} \frac{M_2^2\theta_0}{H} \frac{1}{x_c}\left[2J_1^2\left(\frac{x_c}{2}\right) - J_1^2(x_c)\right]^{1/2}. \tag{10}$$

Equation (10) holds true with any load condition using the appropriate x. For the optimum loading condition, the product of efficiency and bandwidth is, with a slight rearrangement

$$\eta_{L\,opt}\,\delta \frac{\omega C}{y_e} \frac{\theta_0}{H} = x_0 J_2(x_0)\left[2J_1^2\left(\frac{x_0}{2}\right) - J_1^2(x_0)\right]^{1/2}. \tag{11}$$

Equation (11) is plotted in Fig. 2(b). The efficiency-bandwidth product $\eta_L\delta$ is similar to the gain-bandwidth product of the conventional video-amplifier circuit, $G(BW) = g_m/2\pi C$, in that they are both proportional to a similar factor $g/2\pi C$. From (11) it is apparent that to have high efficiency and wide bandwidth of electronic

tuning at the same time, the quantities G_0 and $1/\omega C$ should be as large as possible.

A rather useful equation which is particularly simple to verify experimentally, derived from (7) and (10), is

$$2\delta \Big/ \frac{df}{dV_0} = \frac{4V_0}{\theta_0} \frac{1}{J_1(x_c)} \left[2J_1^2\left(\frac{x_c}{2}\right) - J_1^2(x_c) \right]^{1/2}. \quad (12)$$

The operating parameter x can be calculated from the direct measurable quantities in the left-hand side of (12) and known quantities, V_0 and θ_0. Compared with other methods, this gives more accurate results because it involves only the measurements of the power, voltage, and frequency which can be rather accurately measured, while other methods involve the knowledge of the effective current which is difficult to measure accurately. The function of x in (12), i.e.,

$$\frac{\theta_0}{4V_0} \frac{2\delta}{df_0/dV_0},$$

is plotted in Fig. 2(a).

D. Gap Voltage Ratio

It was pointed out that the ratio of the effective RF gap voltages, $H=(M_2/M_1)\beta$, is important in the operation of the *FDTK*. The RF gap voltage ratio, β, is determined by the cavity configuration, and the beam-coupling coefficient depends on both electron velocity and the gap spacing. Therefore, the factor, H, will be a function of beam voltage and the cavity dimensions. Obviously, it is not necessarily unity, as in the reflex tube and, theoretically, it may have any value depending on adjustments.

The factor

$$\frac{M_2}{M_1} = \frac{\theta_1}{\theta_2} \frac{\sin \theta_2/2}{\sin \theta_1/2}$$

is greater than unity if $\theta_1 > \theta_2$, i.e., $S_1 > S_2$ with θ_1 (and θ_2) $< 2\pi$. Although the value of β decreases as d_1/d_2 increases, β depends on all dimensions of the cavity. With proper choice of the shape of the cavity, β can be made greater than unity over a considerable range of d_1/d_2. Thus, H can be adjusted over a rather wide range by changing both beam voltage and gap spacings. The calculation of β is given later.

As given by (6), the efficiency of the *FDTK* depends on the factor H, with x_0 for optimum loading, also related to H by the equation

$$J_0(x_0) = H \frac{2G_c'}{M_2^2 \theta_0 G_0}.$$

If all quantities on the right-hand side, except H, can be regarded as constant, then the expression for $\eta_{L\ opt}$ becomes

$$\eta_{L\ opt} = \frac{M_2^2 G_0}{2G_c'} x_0^2 J_0(x_0) J_2(x_0). \quad (13)$$

This can be optimized with respect to θ_0/H, using a the relation between this quantity and x_0. The corresponding efficiency is

$$\eta_{L\ opt\ max} = 0.169 \frac{M_2^2 G_0}{G_c'}, \quad (14)$$

when

$$H = 0.158 \frac{M_2^2 G_0}{G_c'} \theta_0. \quad (15)$$

Equation (14) gives the best efficiency which can be obtained. There is a similar expression for a reflex tube with $H=1$ and θ_0 as the only adjustable parameter.[5]

Equation (15) may lead one to a wrong conclusion that H can be made as large as possible to get high efficiency by increasing the value of G_0. There is actually a restriction on the magnitude of H because of the fact that the theory assumes no reflection of electrons. The restriction in that case is, $M_1 V_1(1+H) < V_B$. If $V_B = \alpha V_0$, it follows that

$$H < \frac{\theta_0 \alpha}{2x} - 1. \quad (16)$$

This equation gives an upper limit of H. In the practical design of the FDTK, (10), (11), (12), (14), (15), and (16) are the guiding equations. A universal efficiency curve, given by (13), together with the equation

$$2Q_0'\delta = \frac{2}{x_0 J_0(x_0)} \left[2J_1^2\left(\frac{x_0}{\sqrt{2}}\right) - J_1^2(x_0) \right]^{1/2}, \quad (17)$$

are plotted in Fig. 2(b) as functions of G_c'/y_e.

III. Design Considerations

Most of the design considerations for a FDTK are similar to those of the two-cavity klystron except for the problems involved in getting a suitable value of H. If efficiency and power output are important, the value of H must be greater than unity. If both efficiency and BW are desired, as in the case of frequency-modulated oscillators, the equivalent ωC should be as small as possible and the dc beam conductance G_0 should be large.

For a single cavity, as shown in Fig. 3, the equivalent RF gap voltage ratio β is constant if the cavity configuration is fixed. On the other hand, the beam-coupling coefficient depends on the beam voltage and the gap spacing. So, if both the cavity dimensions and the voltages are given, the value of H is definite. If large H is required, both β and M_2/M_1 must be large so that the product of them gives the required value.

For a capacity-loaded coaxial-line cavity, Fig. 3(a), a crude analysis shows that the condition $\beta > 1$ requires the capacity of gap 1 be greater than capacity of gap 2, i.e., $S_2 > S_1$. With transit angles $< 2\pi$, however, the value

[5] E. G. Linder and R. L. Sproull, "The maximum efficiency of reflex-klystron oscillators," Proc. I.R.E., vol. 35, pp. 241–248; March, 1947.

of $M_2/M_1<1$ for $S_2>S_1$, and therefore, the value of H for such a cavity would not be far from unity.

In order to have a large value of H one must get the required capacity ratio without adversely affecting the beam-coupling coefficients, and for this purpose the tapered-line cavity shown in Fig. 3(b) was used. An exact theoretical analysis of this cavity would have been difficult, and therefore two approximate methods were used. These consisted of using transmission-line theory for an exponentially tapered line, or replacing the tapered coaxial line by ordinary coaxial lines with abrupt change in the radii for the two halves of the cavity, the radii used being some suitable average over the taper. The accuracy of these approximations was checked by means of a sample cavity, and the measured frequencies agreed well with the calculated values.[6]

In addition to frequency, the RF gap voltage ratio, β, was also measured by a method similar to that proposed by Hansen and Post[7] for cavity-impedance measurement. This method measures, by perturbation of the cavity, the ratio of the gap field E to the energy stored, and can be extended in an obvious way to measure the ratio of the two gap fields.

The equivalent L/C ratio of the output gap can be easily derived by considering the resonator as being composed of two cavities separated by a nodal plane.

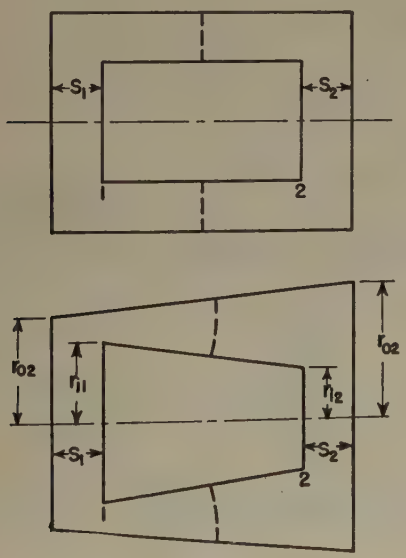

Fig. 3—Schematic cavities of FDTK. (a) Uniform coaxial cavity; (b) tapered cavity.

The resultant $\omega C=1/\sqrt{L/C}$ for the output gap can be represented by

$$\omega C = \frac{\omega C_1}{\beta^2} + \omega C_2,$$

where C_1 and C_2 are the capacities of the two gaps.

[6] S. P. Fan, "The Floating-Drift-Tube Klystron," Ph.D. Thesis, Department of Electrical Engineering, Stanford University, Stanford, Calif.; June, 1951.

[7] W. W. Hansen and R. F. Post, "On the measurement of cavity impedance," *Jour. Appl. Phys.*, vol. 19, pp. 1059–1061; 1948.

Based on the cavity measurements listed above, an experimental tube was built to operate at a wavelength of about 10 cm. It was designed to operate on a $3\frac{3}{4}$ mode with a drift-tube voltage of about 1,000 volts. A schematic diagram of the experimental assembly is shown in Fig. 4.

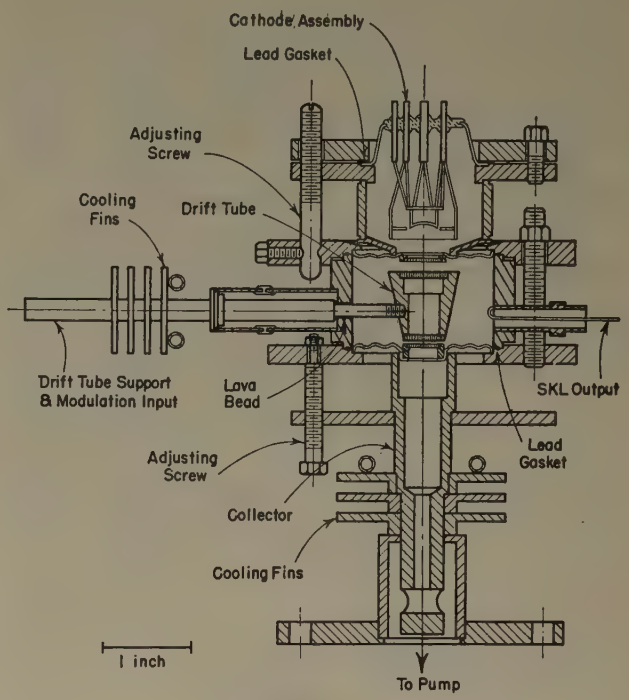

Fig. 4—Assembly of the experiment tube.

IV. Experimental Results

The experimental tube was not sealed off, but was continuously pumped. In the tests, it was possible to apply both ac and dc voltages to the drift tube. To check the theory of oscillation, cold-cavity measurements and power and frequency measurements with different external loads for different operating conditions of voltage and current were made for one mode with a fixed cavity configuration. The experimental results agree very well with the theoretical calculations. It is, therefore, possible to predict with good accuracy what the operating characteristics will be.

One of the most significant results of the theory is the dependence of the efficiency and the bandwidth on the gap ratio, H. This was studied by a set of experiments in which the value of H was varied by changing the gap spacings. The load was adjusted to optimum power output while all other quantities, such as voltage, current, and frequency remained unchanged. The results are shown in Fig. 5. The curve of bandwidth (BW) versus H shows that (BW) decreases with increasing H. The efficiency curve first increases and, after reaching a maximum, decreases. The decrease of experimental efficiency is caused by the decrease of x, as seen in Fig. 2(a). A

theoretical efficiency was calculated by using (6), and the values of x obtained from the BW and df/dV curves. The theoretical and experimental efficiency curves were plotted in Fig. 5 and showed close agreement.

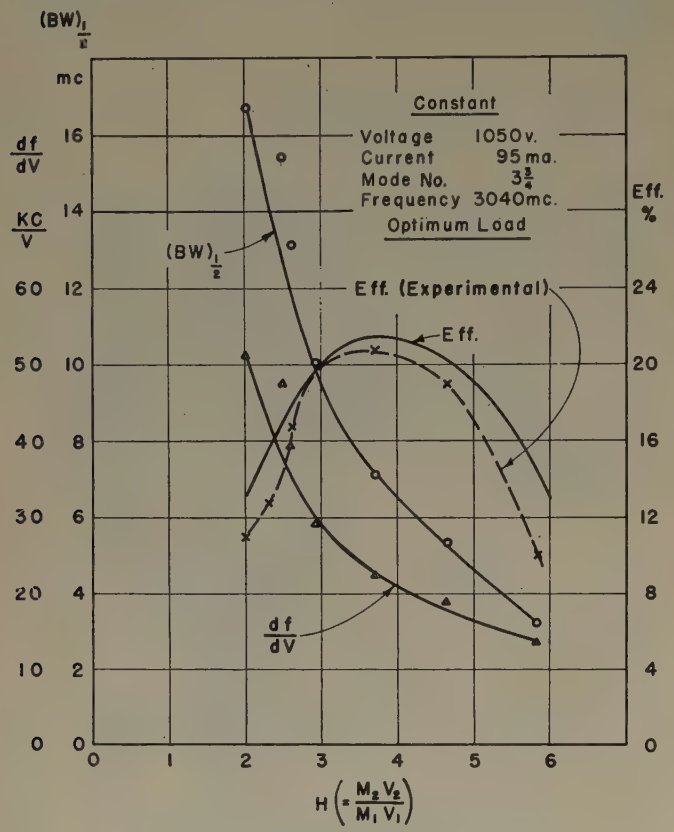

Fig. 5—Operating characteristics as function of gap voltage ratio H.

As an illustration that the FDTK can be adjusted to have either higher efficiency or large bandwidth, the data for two extreme adjustments of H are given here.

(A) High-Efficiency Operation

V_B=1,230 volts V_0=1,049 volts I_B=94 ma
S_1=0.366 cm S_2=0.208 cm H=4.98 f=3,012 mc
P_{out}=26.4 watts η_{theor}=26.8 per cent η_{total}=23 per cent
$G_{L(opt)}=0.49/Z_0$ (BW)=4 mc $\frac{df}{dV}$=0.0252 mc/v

(B) Wide BW Operation

V_B=1,560 volts V_0=1,040 volts I_B=145 ma
S_1=0.525 cm S_2=0.137 cm H=1.54 f=3,030 mc
P_{out}=14 watts η_{theor}=11.7 per cent η_{total}=6.2 per cent
$G_{L(opt)}=4.6/Z_0$ (BW)=14.8 mc $\frac{df}{dV}$=0.084 mc/v

The mode pattern for the wide BW operation is shown in Fig. 6.

It is apparent that there is no discontinuity or irregularity of the mode pattern. As said before, the FDTK may be used as a FM oscillator. To study its behavior in this respect, the linearity of frequency modulation was investigated. The frequency deviation from the center of the mode was measured and it is linear in the center portion of the mode, as shown in Fig. 7. To find the load presented to the modulator, the static capacitance and dynamic resistance of the drift tube were measured. The static capacitance depends mostly on the gap spacings, and its value ranged from 5 $\mu\mu$f to 10 $\mu\mu$f. The dynamic resistance was obtained from the curve of I_B versus V_{DDC} (Fig. 8). The S shape of the curve in the region of V_{DDC} <20 volts may be attributed mostly to the secondary electrons caused by the bombardment of the grids by the electron beam. The dynamic resistance for this tube was

$$R \doteq 7 \times 10^3 \text{ ohms with } |V_D| < 20 \text{ volts}$$
$$R \doteq 23 \times 10^3 \text{ ohms} \qquad |V_D| > 20 \text{ volts.}$$

Fig. 6—Mode pattern.

V_B = 1,560 v v_0 = 1,040 v I_B = 145 ma S_1 = 0.525 cm
$G_L = 4.7/Z_0$ = 3,030 mc H = 1.54 S_2 = 0.137 cm
P_{out} = 14 w $(BW)_{1/2}$ = 14.8 mc $\frac{df}{dV}$ = 84 kc/v
Eff $_{total}$ = 6.2 per cent Eff $_{(theor)}$ = 11.7 per cent

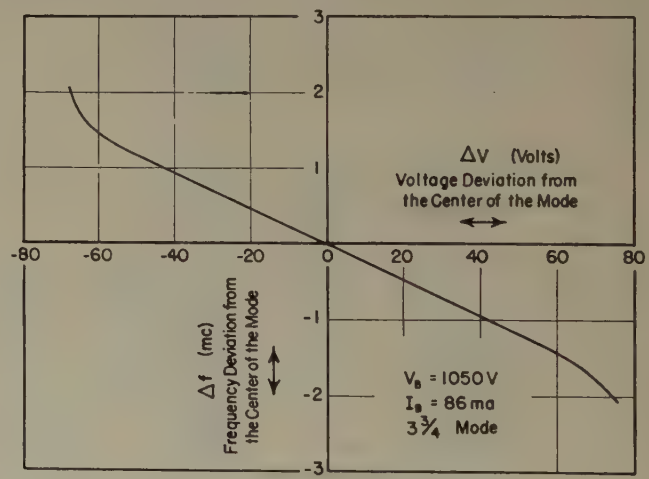

Fig. 7—Linearity of frequency modulation.

Hence, it is advisable to bias and to modulate this tube so that the drift-tube voltage is limited to $|V_D| > 20$ volts. The FDTK will then behave as a constant load, and the required driving power will be small.

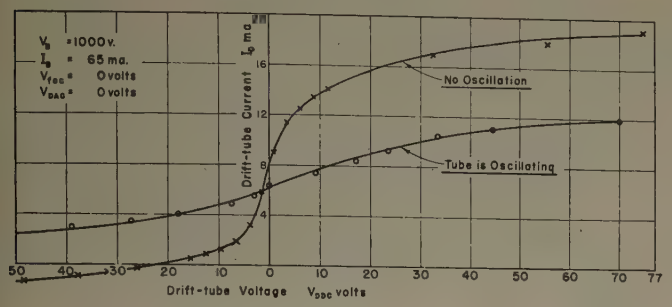

Fig. 8—Drift-tube voltage-current characteristics.

V. Conclusion

As stated in the introduction, the FDTK is similar to the two-cavity klystron in configuration and to the reflex tube in electronic behavior. Compared with the two-cavity klystron, the FDTK is easier to tune, both mechanically and electrically. The latter property renders the FDTK suitable for FM operation. As compared with the reflex tube, the FDTK has almost all the important properties of the reflex tube but not the disadvantages.

In the theory of the FDTK, H always occurs in combination with θ_0 as θ_0/H so that the effect of H is to modify the drift-tube transit angle. If one replaces the quantity θ_0 by θ_0/H in the equations of reflex-tube theory, except where θ_0 occurs in the phase angle ϕ, all these equations can be used for the FDTK, with the RF gap voltage V being the second gap voltage V_2. It is to be noted that the effective value of the bunching angle, θ_0, can be changed continuously in the FDTK by changing relative gap dimensions, while in the reflex tube one must go in discrete steps by changing modes. Thus, (16) can always be satisfied and the optimum efficiency can be obtained in the FDTK.

Although, theoretically, both types of tubes should have about the same optimum efficiency, and for circuit reasons (i.e., single-gap versus double-gap cavity), the reflex tube should have the greater BW, it turns out that there are a number of practical and almost insurmountable disadvantages in the reflex tube which do not occur in the FDTK which make the latter a very attractive alternative. Specifically, these disadvantages of the reflex tube all arise from the fact that one must return the beam to the same gap a second time by means of a reflector. The electron optics of such reflector regions are inherently difficult, and the requirements are such that the reflector must perform several almost incompatible functions. For example, it must focus the beam back through the gap without loss of current; the electrons must all be returned in the same phase in order to get optimum efficiency from the beam; and last and most difficult, the electrons must not go into the cathode region and return through the interaction region a second time,[8] since such multiple transits between the reflector and cathode will produce hysteresis, a property which is very undesirable for communication links. If one tries to put all of these factors into reflector design, it turns out that one usually has to compromise in such a way that there is either a loss of efficiency or a sacrifice of other desirable characteristics.

All the relatively insoluble problems connected with returning an electron beam are eliminated in the FDTK, and one can presumably get, as is borne out by the results of the paper, very close to the theoretically anticipated results, both for efficiency and for electronic tuning characteristics.

While no precise measurements of the linearity which is necessary for a relay system were made, the static measurements of modulation characteristic indicated that the FDTK has a good characteristic for FM operation. On the other hand, the power measurements showed that this tube could deliver a fairly high power output with reasonable operating efficiency. Such a combination of power and modulation characteristics should have interesting possibilities for microwave relay links.

Acknowledgment

We wish to thank the Sperry Gyroscope Company, which supported this research by a grant to Stanford University.

[8] D. R. Hamilton, J. K. Knipp and J. B. H. Kuper, "Klystrons and Microwave Triodes," M.I.T. Radiation Laboratory, Cambridge, Mass., vol. 7, chaps. 13 and 14; 1948.

FM Distortion in Reflex Klystrons*

ROBERT L. JEPSEN†, ASSOCIATE, IRE AND THEODORE MORENO†, ASSOCIATE, IRE

Summary—**The harmonic distortion introduced by a reflex klystron used as a frequency-modulated transmitter is computed. The method used is to make a power-series expansion of the theoretical expression of frequency as a function of reflector voltage, and then to relate the coefficients of the power series to the harmonic-distortion components. The design of a reflex klystron for low distortion is briefly discussed.**

A novel technique was used to measure the harmonic-distortion components experimentally. The experimental results were in good agreement with the theoretical predictions. The distortion is low enough for the reflex klystron to be useful for many transmitter and relay applications.

Introduction

REFLEX KLYSTRONS have been in use for a number of years as local oscillators in microwave receivers, and extensive work has been done on their theory.[1,2,3] More recently, they have been widely used as transmitting tubes in microwave-relay service.

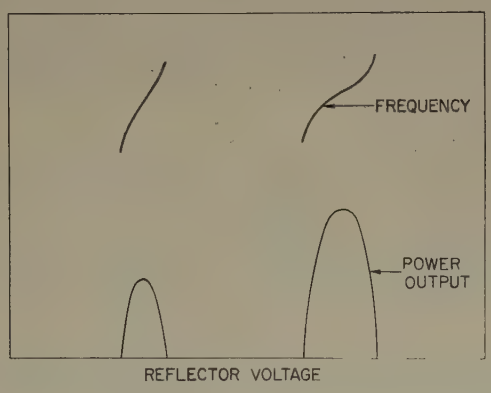

Fig. 1—Power and frequency versus reflector voltage.

In this application the frequency is controlled by the reflector voltage to produce frequency modulation; hence, the FM distortion properties of the tubes are of primary importance. To compute this distortion, it has been necessary to extend the existing theory. To measure the distortion a novel experimental method has been developed.

When the static reflector voltage of a reflex klystron is changed, the power output varies, as shown in Fig. 1. The frequency of oscillation is also controlled by the reflector voltage, typically over a range of many megacycles per second (again, see Fig. 1). In transmitter service, the quiescent operating voltages are usually set near the center of one of the modes of oscillation. The modulation voltage is then applied to the reflector electrode, which is a high-impedance electrode. Resulting frequency modulation is used to carry intelligence.

To minimize distortion, the tube should be operated at the most linear portion of the frequency versus reflector voltage characteristic. The points of minimum distortion and of maximum power do not necessarily coincide.

FM Distortion Theory

A schematic sketch of a reflex klystron is shown in Fig. 2. For this treatment the usual simple-theory approximations are made.[4]

1. The RF voltage across the gap is assumed small compared with the dc accelerating voltage.

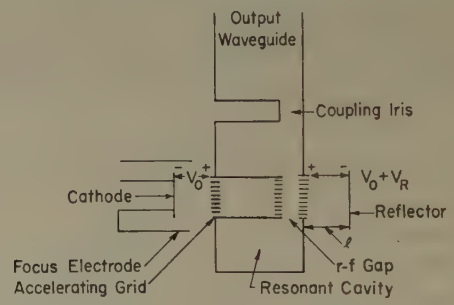

Fig. 2—Schematic sketch of reflex klystron.

2. Space-charge repulsion and interaction effects are neglected.
3. Variations in modulation coefficient and drift angle for various electron paths are neglected.
4. Sidewise deflections are neglected.
5. Thermal velocities are neglected.
6. The electron flow is considered to be a uniform distribution of charge.
7. Multiple transit electrons are ignored.
8. A linear reflecting voltage is assumed.

It is shown[5] that the fundamental frequency equation, with these approximations, may be written

$$f = f_0\left(1 + \frac{1}{2Q_L}\cot\theta\right) = f_0\left(1 - \frac{1}{2Q_L}\tan\phi\right), \quad (1)$$

where

$$\theta \cong \frac{4\pi f_0 l\sqrt{2\frac{m}{e}V_0}}{V_r + V_0} = \frac{a}{V_r + V_0}. \quad (2)$$

* Decimal classification: R355.912.3×R148.11. Original manuscript received by the Institute, October 8, 1952.

† Varian Associates, San Carlos, Calif.

[1] J. R. Pierce and W. G. Shepherd, "Reflex oscillators," *Bell. Sys. Tech. Jour.*, vol. 26, pp. 460–681; July, 1947.

[2] D. R. Hamilton, J. K. Knipp, and J. B. H. Kuper, "Klystrons and Microwave Triodes," M.I.T. Rad. Lab. Series, McGraw-Hill Book Co., Inc., New York, N. Y., no. 7, pp. 311–526; 1948.

[3] A. E. Harrison, "Klystron Tubes," McGraw-Hill Book Co., Inc., New York, N. Y., pp. 73–112; 1947.

[4] J. R. Pierce and W. G. Shepherd, *op. cit.*, p. 467.

[5] *Ibid.*, p. 487.

$$a \equiv 4\pi f_0 l \sqrt{2\frac{m}{e} V_0} \text{ (volts)}.$$

f = frequency of oscillation (cps).
f_0 = frequency of oscillation at the mode center (cps).
Q_L = loaded Q of the klystron cavity; this includes beam loading, both primary and secondary.
V_0 = dc beam voltage (volts).
V_r = reflector voltage. The reflector is at a potential $-V_r$ with respect to the cathode (volts).
m = electron mass (9.103×10^{-31} kg).
e = electronic charge (1.602×10^{-19} coulomb).
l = distance from reflector to RF gap (meters).
θ = drift angle in radians in the region between RF gap and reflector.
$\phi \equiv \theta - \theta_n$.
$\theta_n \equiv (n+3/4)2\pi$.
n = is the mode number.

Let us consider the case where the reflector voltage is the sum of a steady dc voltage V_r' and an alternating voltage $v = v_m \sin \omega_m t$, where $\omega_m = 2\pi f_m$, and f_m is the frequency of modulation. Thus

$$V_r = V_r' + v = V_r' + v_m \sin \omega_m t. \tag{3}$$

We can write f as a function of V_r using a Taylor series expansion around V_r'.

$$f(V_r) = f(V_r' + v) = f(V_r') + v \left.\frac{df}{dV_r}\right|_{V_r=V_r'} + \frac{v^2}{2} \left.\frac{d^2f}{dV_r^2}\right|_{V_r=V_r'} + \frac{v^3}{6} \left.\frac{d^3f}{dV_r^3}\right|_{V_r=V_r'} + \cdots. \tag{4}$$

Putting in $v = v_m \sin \omega_m t$, using appropriate trigonometric relationships, and restricting the analysis to small values of v_m, we obtain

$$f(V_r) \simeq f(V_r') + \left.\frac{df}{dV_r}\right|_{V_r=V_r'} v_m \sin \omega_m t - \frac{1}{4} \left.\frac{d^2f}{dV_r^2}\right|_{V_r=V_r'} v_m^2 \cos 2\omega_m t - \frac{1}{24} \left.\frac{d^3f}{dV_r^3}\right|_{V_r=V_r'} v_m^3 \sin 3\omega_m t + \cdots. \tag{5}$$

With an ideal FM detector, the output at a frequency nf_m will be proportional to the magnitude of the coefficient of $\sin n\omega_m t$ or $\cos n\omega_m t$. We define the nth harmonic distortion, D_n, as the magnitude of the ratio of detector output voltage at the nth harmonic frequency nf_m to that at the fundamental frequency f_m. Thus the second and third harmonic distortions are

$$D_2 = \frac{v_m}{4} \left| \frac{\dfrac{d^2f}{dV_r^2}}{\dfrac{df}{dV_r}} \right|_{V_r=V_r'} \tag{6}$$

and

$$D_3 = \frac{v_m^2}{24} \left| \frac{\dfrac{d^3f}{dV_r^3}}{\dfrac{df}{dV_r}} \right|_{V_r=V_r'}. \tag{7}$$

Using (1) and (2),

$$\frac{df}{dV_r} = \frac{f_0\theta^2}{2aQ_L \cos^2\phi} \tag{8}$$

$$\frac{d^2f}{dV_r^2} = -\frac{f_0\theta^3}{a^2Q_L \cos^2\phi}(1 + \theta \tan\phi) \tag{9}$$

$$\frac{d^3f}{dV_r^3} = \frac{3f_0\theta^4}{a^3Q_L \cos^2\phi}\left(1 + \frac{\theta^2}{3} + 2\theta \tan\phi + \theta^2 \tan^2\phi\right). \tag{10}$$

The peak modulating voltage v_m produces a peak frequency deviation Δf given by

$$\Delta f = \frac{v_m f_0 \theta^2}{2aQ_L \cos^2\phi}. \tag{11}$$

If, as V_r' is changed, v_m is adjusted to keep Δf constant, then

$$D_2 = \left(\frac{\Delta f Q_L}{f_0}\right) \left| \frac{\cos^2\phi}{\theta}(1 + \theta \tan\phi) \right|_{V_r=V_r'} \tag{12}$$

$$D_3 = \left(\frac{\Delta f Q_L}{f_0}\right)^2 \left| \frac{\cos^4\phi}{\theta^2}\left(1 + \frac{\theta^2}{3} + 2\theta \tan\phi + \theta^2 \tan^2\phi\right) \right|_{V_r=V_r'}. \tag{13}$$

If, however, v_m is set to produce a particular frequency deviation $\Delta f'$ at the mode center, and if v_m (rather than Δf) is thereafter held constant as V_r' is changed, then

$$\Delta f' = \frac{v_m f_0 \theta_n^2}{2aQ_L} \tag{14}$$

and

$$D_2' = \left(\frac{\Delta f' Q_L}{f_0}\right) \left| \frac{\theta}{\theta_n^2}(1 + \theta \tan\phi) \right|_{V_r=V_r'} \tag{15}$$

$$D_3' = \left(\frac{\Delta f' Q_L}{f_0}\right)^2 \left| \frac{\theta^2}{\theta_n^4}(1 + \frac{\theta^2}{3} + 2\theta \tan\phi + \theta^2 \tan^2\phi) \right|_{V_r=V_r'}. \tag{16}$$

A point of zero second harmonic distortion occurs near the mode center. The value of ϕ at which $D_2 = D_2' = 0$ is given approximately by

$$\left.\phi\right|_{D_2=0} \simeq -\frac{1}{\theta_n}. \tag{17}$$

At the mode center ($\phi = 0$),

$$D_2 = D_2' = \left(\frac{\Delta f Q_L}{f_0}\right)\frac{1}{\theta_n} \tag{18}$$

for ϕ large, i.e., for $\phi \gtrsim \pi/4$,

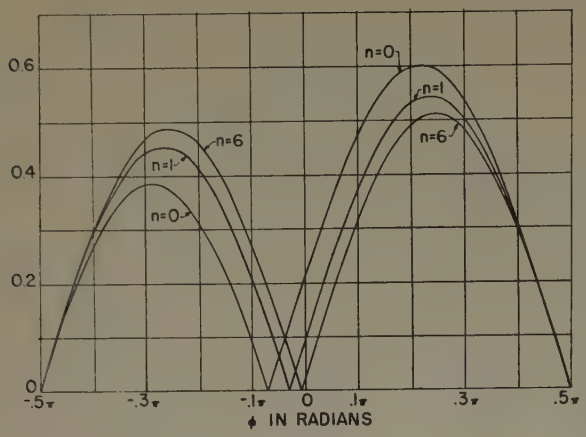

Fig. 3(a)—$|\cos^2\phi/\theta(1+\theta\tan\phi)|$ versus ϕ.

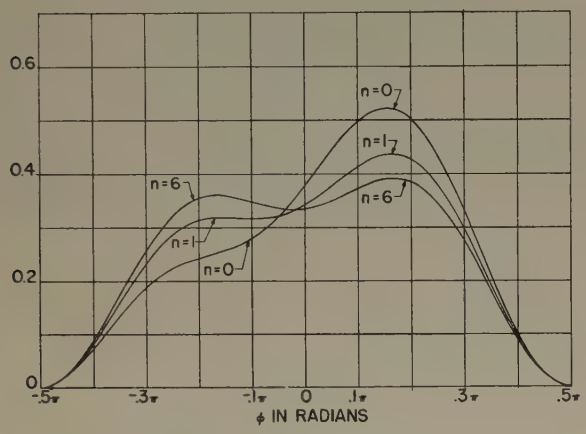

Fig. 3(c)—$|\cos^4\phi/\theta^2(1+\theta^2/3+2\theta\tan\phi+\theta^2\tan^2\phi)|$ versus ϕ.

$$D_2 \simeq \left(\frac{\Delta f Q_L}{f_0}\right)\left|\frac{\sin 2\phi}{2}\right|_{V_r=V_{r'}} \tag{19}$$

$$D_2' \simeq \left(\frac{\Delta f' Q_L}{f_0}\right)\left|\left(\frac{\theta}{\theta_n}\right)^2\tan\phi\right|_{V_r=V_{r'}}. \tag{20}$$

Third harmonic distortion is not zero near the mode center. For $\phi=0$,

$$D_3 = D_3' = \left(\frac{\Delta f Q_L}{f_0}\right)^2\frac{1}{\theta_n^2}\left(1+\frac{\theta_n^2}{3}\right) \simeq \frac{1}{3}\left(\frac{\Delta f Q_L}{f_0}\right)^2. \tag{21}$$

For ϕ large,

$$D_3 \simeq \left(\frac{\Delta f Q_L}{f_0}\right)^2\left|\cos^4\phi\left(\frac{1}{3}+\tan^2\phi\right)\right|_{V_r=V_{r'}} \tag{22}$$

$$D_3' \simeq \left(\frac{\Delta f' Q_L}{f_0}\right)^2\left|\left(\frac{\theta}{\theta_n}\right)^4\left(\frac{1}{3}+\tan^2\phi\right)\right|_{V_r=V_{r'}}. \tag{23}$$

If ϕ is large enough so that $\tan^2\phi \gg \frac{1}{3}$, then

$$D_3 \simeq \left(\frac{\Delta f Q_L}{f_0}\right)^2\left|\frac{\sin 2\phi}{2}\right|^2_{V_r=V_{r'}} \simeq D_2^2 \tag{24}$$

$$D_3' \simeq \left(\frac{\Delta f' Q_L}{f_0}\right)^2\left|\left(\frac{\theta}{\theta_n}\right)^2\tan\phi\right|^2_{V_r=V_{r'}} \simeq D_2'^2. \tag{25}$$

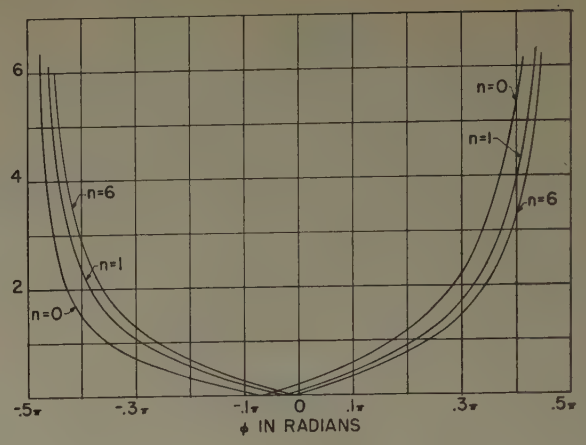

Fig. 3(b)—$(\theta/\theta_n^2)(1+\theta\tan\phi)|$ versus ϕ.

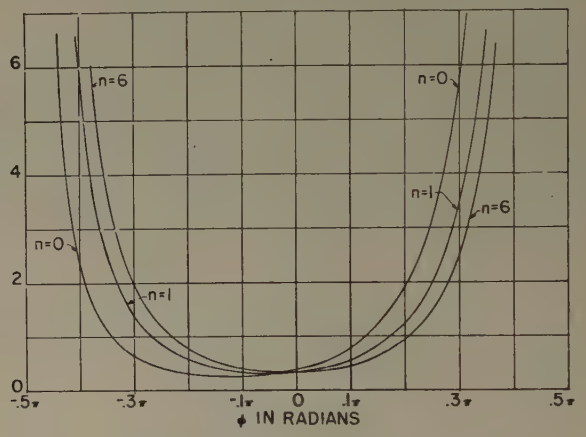

Fig. 3(d)—$|\theta^2/\theta_n^4(1+\theta^2/3+2\theta\tan\phi+\theta^2\tan^2\phi)|$ versus ϕ.

The portions of (12), (13), (15), and (16) that depend on θ (or ϕ and θ_n) are plotted as functions of ϕ for the $n=0$, 1, and 6 modes in Figs. 3(a), (b), (c), and (d). It is noted that the curves do not change greatly with mode number.

Klystron Design with Consideration of Distortion

In designing a reflex klystron for a specific application, there are many properties that need to be taken into account. These usually include frequency, power output and efficiency, and electronic tuning range, and may include modulation sensitivity (df/dV_r) and FM distortion, as well as a number of more subtle items. When a tube is designed for low distortion, a number of other characteristics must usually be compromised in the design.

From the expressions for D_2, and D_3 (see (19), (20), (24), and (25)), it is noted that, for a given Q_L, D_2 and D_3 are virtually independent of the mode number, n, especially for large n. D_2 and D_3 are made smaller chiefly by making Q_L smaller. For constant shunt impedance, Q_L can be reduced by increasing the L/C ratio of the cavity. This will also increase the electronic tuning range and modulation sensitivity. However, if the capacity is reduced (L/C ratio increased) by reducing the grid diameter, it becomes increasingly difficult to focus the beam current through the reduced aperture,

and debunching effects which can reduce power output are also more serious with a more concentrated electron beam.

For a fixed cavity and electron optics, Q_L can be reduced by loading the cavity more heavily. Electronic tuning range to half-power points has a maximum with respect to Q_L, and reducing Q_L below this optimum value results in reduced bandwidth. Power output also has a (different) maximum with respect to Q_L.

For a given Q_L, electronic tuning range can be increased at the expense of power by going to a larger value of n. Both output power and electronic tuning range will be increased by increasing beam current, or by increasing beam voltage at constant perveance.

A set of simple-theory parameters was assigned to a particular klystron operating in the $n=3$ mode.[6] The quantity l, and hence a, was chosen to give coincidence with the experimental points of minimum second harmonic distortion, and Q_L was selected to give agreement with the experimental modulation sensitivity, df/dV_r, at mode center. With $\Delta f=1$ mc (peak) (Δf held constant as V_r' was changed), D_2 and D_3 were calculated. D_3 nowhere exceeded -75 db. D_2 versus V_r is plotted along with the experimental curve in Fig. 4.

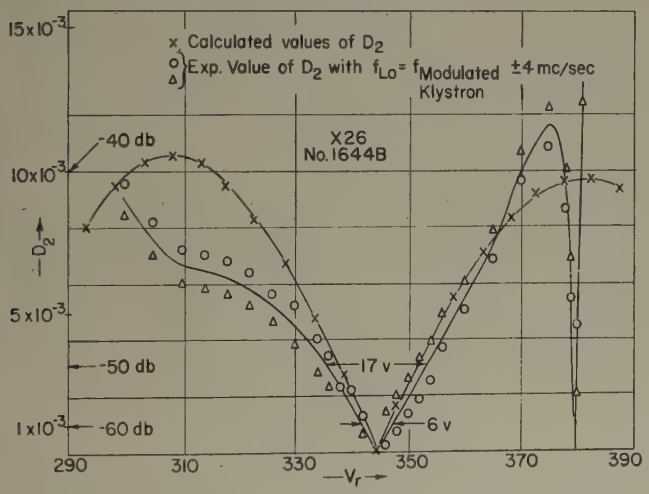

Fig. 4—Comparison between experiment and theory of second harmonic FM distortion.

Experimental Results

First-order theory of klystrons is usually no better than a rough approximation to their actual behavior. It was necessary to measure the distortion experimentally for comparison with the theoretical results.

In principle, it is a simple thing to measure distortion. The tube is modulated with a sine wave, which can be made arbitrarily pure with filters. The output of the klystron is then demodulated, and the distortion components of the demodulated output are measured with a wave analyzer. The chief experimental difficulty lies in finding a suitable limiter and demodulator. Wide-band microwave discriminators can be constructed, but good microwave limiters are not easily obtained. The microwave signal can be heterodyned to some intermediate frequency where conventional vacuum-tube limiters can be used, but the precision wide-band discriminator at intermediate frequencies offers a difficult problem.

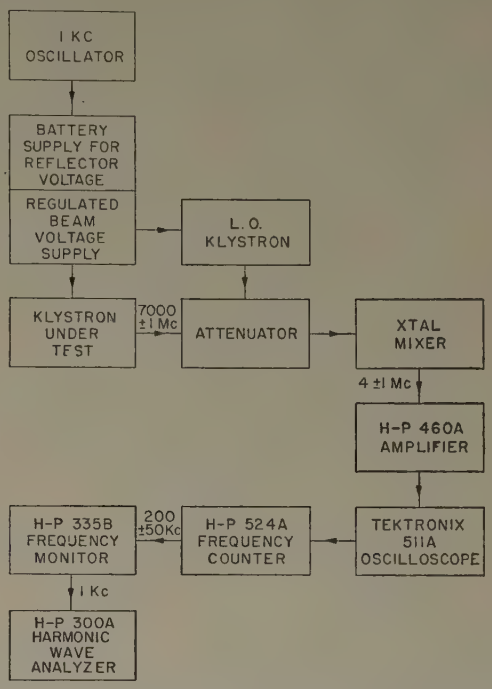

Fig. 5—Experimental setup used for measuring FM distortion.

The ideal type of linear discriminator is the counter type, used in some FM station monitors. These discriminators are usually designed for a center frequency of 200 kc/sec and a maximum frequency deviation of only ± 75 kc/sec, while the microwave frequency deviation of interest here was ± 1 mc/sec.

These problems were resolved with the experiment setup shown in Fig. 5. The tube under test, a Varian Associates X-26 Reflex Klystron, was modulated with a 1 kc/sec sine wave, with a frequency deviation of 1 mc/sec (peak). This signal was mixed with a local oscillator signal in a crystal, the two klystrons being isolated with a directional coupler and attenuators. The two klystrons were operated from a common, well-regulated beam voltage supply, and batteries were used to supply reflector voltage. The local oscillator frequency was adjusted until the output frequency from the crystal was 4 mc/sec, deviated ± 1 mc/sec. The signal was amplified by a Hewlett-Packard 460A Amplifier, and then amplified and displayed by a Tektronix 511A Oscilloscope. The amplified output from the oscilloscope was fed into a Hewlett-Packard 524A Frequency Counter.

This instrument is a high-speed counter, capable of counting at a maximum rate of 10 mc/sec. The gating circuits in the counter were disabled, and a special output connection was made after the first binary stage in the second decade counter. For every twenty cycles

[6] Simple-theory parameters used for Varian Associates Reflex Klystron X-26 #1644B; $f_0=7425$ mc, $Q_L=150$, $V_0=750$ volts, $a=25{,}738$ volts, $V_r=344.3$ volts at point of minimum distortion.

in, one cycle came out, so that the instrument served to divide the input frequency by a factor of twenty. The output frequency was therefore 200 kc/sec, deviated ±50 kc/sec. The modulating frequency was unchanged at 1 kc/sec. The 200 kc/sec signal was then demodulated by the discriminator of a Hewlett-Packard 335B FM Station Monitor, which was also used to set the 4 mc/sec intermediate frequency and the deviation level. The harmonic content of the demodulated output signal was measured with a harmonic wave analyzer.

With frequency deviation of ±1 mc/sec (peak), distortion components other than the second harmonic were −60 db or less, too small to be measured accurately. Second harmonic distortion was readily observable. Qualitatively, and even quantitatively, the results were in good agreement with the theoretical predictions.

Typical experimental results are shown in Fig. 4, along with the theoretical curve. It was observed that different values of distortion were measured when the local oscillator was tuned to the high and to the low side of the signal frequency. The source of this apparent error was traced to the small amount of distortion (estimated at −64 db) introduced by the amplifier which follows the discriminator in the FM monitor. This distortion can either add or subtract from the distortion introduced by the klystron. The relative phase of the two distortion components is changed by 180 degrees when the local oscillator is switched to one side or the other of the signal frequency. Similarly, the distortion introduced by the klystron is changed 180 degrees in phase when the static reflector voltage is tuned past the the point of minimum distortion. The true distortion of the klystron was judged to fall midway between the two experimental curves, as shown in Fig. 4.

Comparison of Experiment and Theory

One of the important considerations in the application of these klystrons is the range of reflector voltage or of operating frequency over which the distortion is less than some specified limit. Typical experimental results for ±1 mc/sec frequency deviation are tabulated below:

Second harmonic distortion (db)	Range of reflector voltage (volts)	Range of frequency (mc/sec)
−60	5	2
−50	15	6
−40	50	20

For different tubes, these ranges differed typically 10 to 20 per cent. The average ranges were in excess of the theoretical predictions by perhaps 20 per cent. Third harmonic distortion was an undetermined amount below −60 db. Theory predicted a value somewhat less than −75 db.

The reflector voltage of minimum distortion for this tube type was usually about 5 volts less than the voltage which gave maximum power. This was not in good agreement with the theory, which predicted that the minimum distortion point should fall about 3 volts above the maximum power point. Fortunately, it was found that the reflector voltage for minimum distortion was almost exactly halfway between the voltages corresponding to the half-power points. This simplified the tuning procedure for the tube, but there is no reason to expect this tuning procedure to apply equally well to other models of klystrons.

Relationship between Distortion, other Tube Characteristics, and System Design

It is advantageous for system design to specify distortion in terms of a permissible range of reflector voltage, or a permissible range of operating frequency. It is usually necessary to stabilize the operating frequency of the klystron by an afc circuit to compensate for changes in ambient temperature and of power-supply voltages. When the effects of changes in ambient temperature or of beam voltage upon the operating frequency of the klystron are also known, it is then possible to specify, for the system, temperature and voltage stability which will ensure adequately low distortion.

It has been found that when the distortion is too great, with reasonable stability of voltages and temperature, the distortion can be reduced by proper adjustment of the klystron load impedance. This adjustment has been incorporated into some relay systems.

Conclusions

With the growing use of reflex klystrons in relay systems, it has become important to know their distortion properties. Reflex klystron theory has therefore been extended so that, when other operating characteristics of the klystrons are known, the distortion can be computed with reasonable accuracy. A novel experimental technique was used to check the theoretical calculations, and theory and experiment were found to agree reasonably well. In general, the distortion of a reflex klystron used as a frequency-modulated transmitter is low enough for the tube to be satisfactory in many relay applications.

Theory of the Reflex Resnatron*

M. GARBUNY†

Summary—**A qualitative and quantitative description is given of the interaction phenomena between density-modulated groups of electrons and a field which permits them to cross the gap of a resonant cavity twice. Based on the method of Lagrangian parameters, resonance conditions of transit time and field parameters are derived for maximum energy transfer. The theory is extended to account for the specific behavior of the reflex resnatron in terms of efficiency, amplitude modulation, and bandwidth. The results are compared with experiment.**

I. Introduction

THE DEVICE that emerged during the past decade as the most powerful and efficient generator of continuous, uhf waves is the resnatron.[1] This potentiality of the resnatron is well understood[2] on the basis of its physical operation. This consists, in short, of the production of well-defined beams of density-modulated electron bunches in the gap of a tuned input cavity; the acceleration of these bunches by a high static potential toward a resonant output cavity; and the conversion of the resulting kinetic into field energy by the electrons while they are still sharply focused in phase and geometry in the output gap. These characteristics, which account for most of the notable efficiencies and power capabilities, are largely the result of the short transit times with which the electrons traverse the intervening fields between cathode and anode.[2] In view of this fact, it is interesting that a somewhat different operation, embodied in the reflex resnatron,[3] still produces substantially the high powers and efficiencies of the conventional device, although the transit times in the output cavity are much larger as a consequence of certain resonance conditions with respect to the field.

In the conventional resnatron the electrons surrender their energy to the high-frequency field in a single transit from the accelerating screen to the collecting anode; in the reflex resnatron (Fig. 1[4]) the anode is replaced by an electrode of sufficiently negative potential so that the electrons, after traversing most of the gap, are repelled to the screen where they are collected. It follows that transit times must stand in exact relationship with respect to field reversal and must, in fact, extend over most of the cycle, if maximum efficiency of energy conversion is to be achieved. A deviation from this condition will result in reduction of output energy, and therein lies the possibility of amplitude modulation by swinging the negative repeller with relatively little signal power. Moreover, as a consequence of the two-fold beam interaction with the field, this modulation can occur with relatively wide bandwidth, independent of the Q-value for the input cavity. The construction and performance of an experimental reflex resnatron, exhibiting these features, has been recently reported.[3] There remains, however, the need for a qualitative and quantitative description of the active transit-time phenomena to explain and derive the resonance conditions and performance characteristics for efficiency, modulation, and bandwidth.

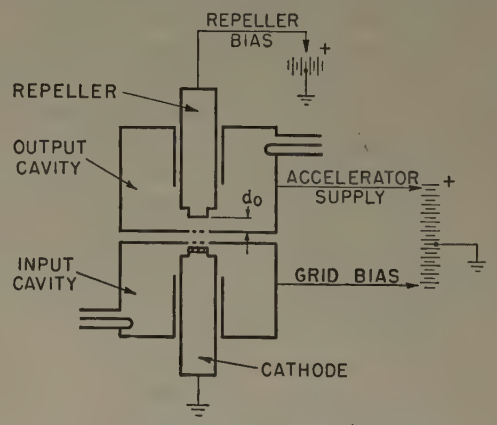

Fig. 1—Scheme of the reflex resnatron.

II. Outline of Procedure

The problem will be treated on the basis of the following assumptions, which are not only mathematically convenient but are in any case justified by the close correspondence to the actual experimental design.

First, the production of density-modulated bunches is effected in the same way as in the conventional resnatron. It will be sufficient to state here that during a periodically occurring time interval, called the "angle of flow," electrons of high, practically equal velocities enter the screen-repeller cavity which is tuned to the bunching frequency. Secondly, it is assumed that the field with which the electrons interact is homogeneous with only a negligible component normal to their velocity. The field is confined between two parallel plates, viz., the screen and the repeller. The effect of secondary electron emission from the screen is ignored as being,

* Decimal classification: R138×R339.2. Original manuscript received by the Institute, October 3, 1952. Based, in part, on a paper presented by M. Garbuny and G. E. Sheppard before the National IRE Convention, New York, N. Y., 1952.

† Westinghouse Research Laboratories, East Pittsburgh, Pa.

[1] D. H. Sloan and L. C. Marshall, "Ultra high frequency power," *Phys. Rev.*, vol. 58, p. 193; 1940. Also, D. H. Sloan, U. S. Patent 2,405,763.

[2] W. G. Dow and H. H. Welch, "The generation of ultra high frequency power at the fifty kilowatt level," *Proc. NEC* (Chicago), vol. 2, p. 603; October, 1946.

[3] G. E. Sheppard, M. Garbuny, and J. R. Hansen, "Reflex resnatron shows promise for UHF TV," *Electronics*, vol. 25, p. 116; September 1952.

[4] Reprinted with permission of the publisher from the *Electronics* article, *loc. cit.*

at any rate, unimportant in view of the retarding field conditions. Space charge will be a second-order effect. Finally, the electrons which pass through the screen again in the direction toward the cathode can be disregarded both with respect to their number and their individual effect. This treatment is, therefore, concerned only with the events in the interaction space between screen and repeller where the electrons describe one-dimensional paths $s(t)$.

It will be seen that the operation of the reflex resnatron is governed by density modulation, exhibiting therein the most contrasting feature with respect to the reflex klystron and the Barkhausen oscillator which produce velocity-grouped bunches and simultaneously extract energy from them. Unlike the theory of such effects, this treatment can afford to consider a single electron as representative of its group since the latter remains well focused in phase, with velocity modulation reduced to a secondary role. Thus a resonance condition for optimum operation will be derived on the basis of the transit-time phenomena of a single electron. The influence of all other electrons in the group will then be included by an approximation method to account for efficiencies, bandwidth, and the particular behavior of power modulation by variation of the static repeller potential.

III. Qualitative Description of the Operation

Qualitatively the production of radio-frequency power in the reflex resnatron can be understood by the following.

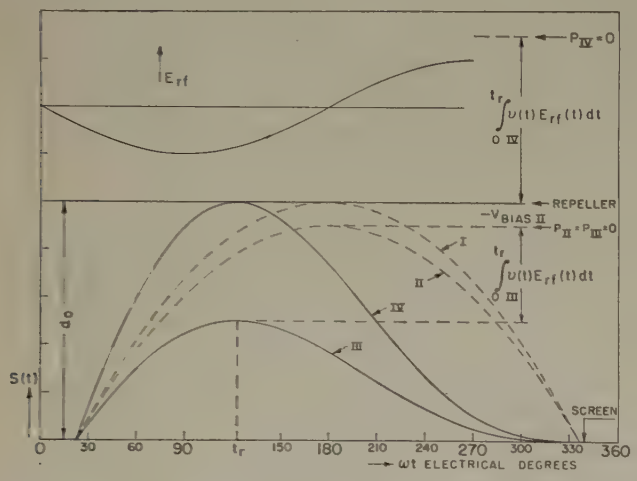

Fig. 2—Motion of single electron with time under the influence of a static retarding and oscillating field. I and II correspond to negligible radio-frequency field component, with two different values of repeller bias. III and IV represent, correspondingly, trajectories under the influence of optimal radio-frequency fields.

In Fig. 2 the position of the electron between screen and repeller is plotted against time, measured as the phase of the sinusoidally varying field to which work is rendered and which is indicated in the upper left corner. Curves I and II represent the limiting case of negligible radio-frequency power. The electron encounters then in the gap merely a retarding static potential, and its trajectory will be a parabola with the apex at that static potential line which corresponds to the cathode potential, except for the negligible net change in energy experienced in the previous interaction with time-variant fields. Curve I shows, for instance, that the electron nearly reaches the repeller, if the same is on cathode voltage. The time co-ordinate of the apex is given by the condition for maximum energy conversion which demands that the electron experience a retarding field over as much of its path as possible. The apex of the parabolas must therefore occur at field reversal, i.e., at 180 electrical degrees.

Another extreme case is represented by curves III and IV, for which the oscillating field is just large enough to extract the entire kinetic energy from the electron. It follows that the average velocities on the way to the apex are considerably larger than on the way from it because the descent begins, and asymptotically ends, with zero velocity. Hence there results the asymmetric shape of the trajectories with respect to time. The apex is traversed before field reversal and lies at a point positive with respect to the static cathode potential line by an amount equal to the net energy surrendered to the sinusoidal field, cf., curve III which corresponds to operation under the same repeller voltage as curve II. To utilize the cavity gap more fully, a suitable voltage between that of cathode and screen has to be applied to the repeller so that the electron penetrates most of the field space, yet yields all of its kinetic energy, cf., curve IV.

Between the two extreme cases of vanishingly small contribution and complete conversion of the kinetic energy, one finds, correspondingly, trajectories which vary gradually from the shape of parabolas to that of curves III and IV. It is obvious that the timing of beginning and end of the trajectories influences rather critically the ensuing interaction with the oscillating field. The transit time and field parameters will, in fact, have to fulfill a resonance condition between electron motion and field phase if the efficiency of energy conversion is to be a maximum.

IV. Quantitative Description of the Operation

A. The Conditions of Resonance

The following basic question has arisen from the merely qualitative arguments: What values have the field and time parameters to assume so that the energy given to the oscillating field by the electron is a maximum. Obviously this problem can be solved by finding a minimum for the kinetic energy or the square of the velocity with which the electron returns to the screen.

Writing the equations of motion for convenience in kinematic units, one obtains by successive integration

$$a = A \sin \omega t + B \tag{1}$$

$$v_2 = \frac{A}{\omega}(\cos \omega t_1 - \cos \omega t_2) + \frac{B}{\omega}(\omega t_2 - \omega t_1) + v_0 \tag{2}$$

$$s_2 = 0 = \frac{A}{\omega^2}\left[(\omega t_2 - \omega t_1)\left(\cos \omega t_1 + \frac{\omega v_0}{A}\right) + \sin \omega t_1 - \sin \omega t_2\right] + \frac{B}{2\omega^2}(\omega t_2 - \omega t_1)^2 \quad (3)$$

$0 \leqq t_1 < 2\pi, \quad t_1 < t_2, \quad s \geqq 0$, where

a = resultant electron acceleration
A = acceleration due to sinusoidal field with amplitude $(m/e)A$
B = acceleration due to static field $(m/e)B$
ω = circular frequency of sinusoidal field
t_1 = time of entering the field
t_2 = time of arrival at screen
v_0 = velocity at t_1
v_2 = arrival velocity at t_2
s_2 = position at t_2
e/m = specific charge of the electron.

It is seen that, v_0 being constant, the arrival velocity v_2 depends on the four variables t_1, t_2, A, and B, of which however only three are independent because of the condition of "restraint" (3). This corresponds exactly to this experimental situation: to achieve maximal power output with the reflex resnatron when input and driving conditions are fixed, three parameters are varied, viz., the two components of the complex impedance and the repeller bias. In computing the minimum of v^2, only those variables must be used for which there exists a true extreme value, i.e., at which the first derivative is still continuous. Thus the amplitude $(m/e)A$ of the sinusoidal field will be held constant at an arbitrary value. One obtains with the method of Lagrangian parameters

$$\frac{\partial(v_2^2)}{\partial t_1} + \Lambda \frac{\partial s_2}{\partial t_1} = 0 \quad (4)$$

$$\frac{\partial(v_2^2)}{\partial t_2} + \Lambda \frac{\partial s_2}{\partial t_2} = 0 \quad (5)$$

$$\frac{\partial(v_2^2)}{\partial B} + \Lambda \frac{\partial s_2}{\partial B} = 0 \quad (6)$$

$$s_2 = 0, \quad (7)$$

altogether four equations for the four unknowns t_1, t_2, B, and the Lagrangian parameter Λ. The solutions will contain values for maximum and minimum energy conversion and, in addition, such points of zero curvature for which variations vanish. Substituting v_2 and s_2 from (2) and (3) in (4) to (7), one easily finds by combination first two rather general relations between the time parameters which permit immediate evaluation of t_1 and t_2 for the various modes:

$$(\sin \omega t_2 + \sin \omega t_1)(\omega t_2 - \omega t_1) = 2(\cos \omega t_1 - \cos \omega t_2) \quad (8)$$

$$\sin \omega t_1[1 - \tfrac{1}{2}(\omega t_2 - \omega t_1)^2] + (\omega t_2 - \omega t_1) \cos \omega t_1 - \sin \omega t_2 = 0. \quad (9)$$

Equations (8) and (9) teach that the transit-time parameters t_1 and t_2 are independent of v_0 and A, a fact which is plausible since B has been allowed to assume the optimum value in terms of these constants. The solutions for (8) and (9) are expressed as sums and differences of t_1 and t_2:

$$\omega t_1 + \omega t_2 = n\pi \qquad n = 2, 3, 4, 5, \cdots, \quad (10)$$

n odd,

$$\frac{\omega t_2 - \omega t_1}{2} = \tan\left(\frac{\omega t_2 - \omega t_1}{2}\right), \quad \omega t_2 + \omega t_1 = 3\pi, 5\pi, \cdots; \quad (11)$$

n even,

$$\frac{2}{\omega t_2 - \omega t_1} - \frac{\omega t_2 - \omega t_1}{2} = ctn\left(\frac{\omega t_2 - \omega t_1}{2}\right), \quad \omega t_1 + \omega t_2 = 2\pi, 4\pi, 6\pi, \cdots. \quad (12)$$

Furthermore, one finds by expansion that approximately

$$\omega t_1 \cong \frac{2}{n\pi}, \quad \omega t_2 \cong n\pi - \frac{2}{n\pi}, \quad n = 2, 3, 4, 5, \cdots, \quad (13)$$

with improving accuracy as n increases. Finally, the optimal field parameter B also results from the combination of (4) to (7).

$$B = -\frac{2\omega v_0}{(\omega t_2 - \omega t_1)} - A \sin \omega t_1 \quad (14)$$

$$\cong -\frac{2}{n\pi}(\omega v_0 + A).$$

It is now possible to discuss the significance of the solutions for various values n. Here it is helpful to realize that parabolas, such as shown in Fig. 2 for $n=2$, form the limit curves of all optimal trajectories for various values A but of the same order number n. This follows from the invariance of (8) to (12) with respect to A. The electrons thus undulate under or above the limiting parabolas, depending on the negative or positive sign of the energy exchange.

The modes with n odd are symmetric to a field loop, the electrons spending equal times in retarding and accelerating phases of the oscillating field. Hence no net energy is transferred at all. This conclusion can be verified by inserting (10), (11), and (14) into (2), with the result that indeed $v_2 = -v_0$. The solutions represent therefore points of inflection rather than extreme values for the energy.

The modes with n even correspond to states in which t_1 and t_2 are symmetric with respect to a node of the field so that the electron spends equal times in phases of opposite polarity. The simplest example is that of the parabola for vanishing A and $n=2$ where the electron travels continuously with either a retarding or an accelerating phase of the oscillating field. These conditions

are characterized by maximum energy transfer to or from the electron. Again this result can be demonstrated by various tests.

It will be noted that the optimal times of entering and leaving the field converge towards 0 and $n\pi$ as the order increases. Thus, translating phases into electrical degrees, one obtains for $n=2$, $\omega t_1=22.8°$; $n=3$, $\omega t_1=12.5°$; $n=4$, $\omega t_1=9.5°$, and so on, with corresponding values for ωt_2. Similarly, the optimal static field parameter B is, at least approximately, inversely proportional to n. For positive A, i.e., for maximum electron acceleration, B assumes a more negative value than when maximum conversion into field energy is demanded. The choice of discrete values of B determines the mode and sign of the beam interaction. By the simple expedient of varying the repeller voltage in such manner that the order number changes by 1, the conversion efficiency fluctuates between a maximum value and zero, a fact pertinent to reflex resnatron modulation.

The computations have dealt with a fixed, although arbitrary, value for the oscillating field amplitude $(m/e)A$. The special case is of interest in which the electron surrenders all of its energy to the field, $v_2=0$. By inserting (14) and (12) or (13) into (2), one obtains

$$A = -\frac{\omega v_0}{(\omega t_2 - \omega t_1)\sin \omega t_1} \cong -\frac{\omega v_0}{2}. \qquad (15)$$

It should be mentioned here that it is of course possible to satisfy (2) and (3) for $v_2=0$ in case of a single electron, if other values for the variables are used. The point to be made, however, is that all other combinations of parameters lead to a greater value of A. Therefore, even if such modes of reflex operation were stable, they would lead to increased losses for the other electrons of the group. Hence the requirement of maximum conversion efficiency implies the choice of the optimal value (15) and the derivation given above. Similarly, if maximum power is to be transferred from the field to the electron, one will now apply as high an A as practically possible and then adjust for maximum electron acceleration at this fixed value.

Finally, the relation between field and time parameters (14) has to be expressed in terms of practical design. Replacing then in (14) accelerations by voltages, one obtains as condition of resonance

$$V_B = -4\pi \frac{d}{\lambda} \frac{\sqrt{2mc^2V_0/e}}{(\omega t_2 - \omega t_1)} + V_A \sin \omega t_1$$

$$\cong -\frac{4}{n}\frac{d}{\lambda}\sqrt{2V_0V_{Eq}} + \frac{2V_A}{n\pi},^{5} \qquad (16)$$

where

V_B = voltage difference between screen and repeller
V_0 = screen voltage
$-V_A$ = amplitude of sinusoidal voltage (retarding)
V_{Eq} = 511,000 volts, energy equivalent of electron mass $[eV_{Eq}=mc^2]$
d = cavity gap between screen and repeller
λ = wavelength of oscillating field.

Equation (16) is accessible to comparison with experiment, a subject taken up under Section V.

B. Extension to Multiple Electron Theory

The derivation of the resonance conditions was based on the transit-time phenomena of a single electron, physically embodied in a sufficiently small angle of flow. As long as no strong debunching occurs, the same relations will hold for a group of electrons with a spread in phase normally used in class C operation. As the order number of the mode increases and the electrons undergo several cycles of oscillations, defocusing effects mainly due to space charge will become more important and the treatment correspondingly complex. Hence the discussion of the transit-time phenomena for groups of electrons will be limited to the main mode, $n=2$. The salient features of efficiency, modulation, and bandwidth will already emerge from this practically most pertinent example.

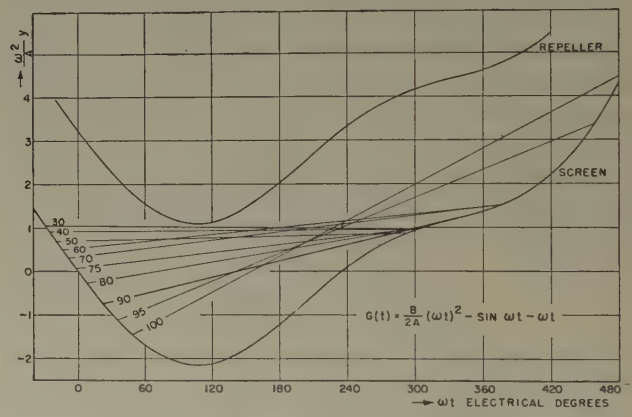

Fig. 3—Transformed electron trajectories in reflex space in fulfillment of the conditions of resonance.

A study of multiple trajectories is possible only with approximation methods. The graphical procedure used here (Fig. 3) has been described previously.[6] This method utilizes the fact that when particles move together through a homogeneous field of force which may be any function of time their trajectories describe straight lines when viewed from each other. Thus if a reference system, with respect to which positions and velocities are measured, is moving along with an electron such as represented by curve III or IV in Fig. 2, the trajectories of all electrons in its group, however complicated, are transformed into the straight lines shown in Fig. 3. The co-ordinates of screen and repeller, in turn, are now curves $G(t)$. Positions of the electrons at any time t during their motion are then measured as distances from

[5] It has been assumed in this derivation that d/λ is sufficiently large to accommodate the nth mode.

[6] M. Garbuny, *Jour. App. Phys.*, vol. 21, p. 1054; 1950.

$G(t)$ and velocities as differences between the slope of the straight line and that of $G(t)$.

The trajectories of electrons emitted from the cathode of a typical resnatron were followed through with this method, Fig. 3 showing only the phenomena occurring in the output gap. It is assumed that the control grid passes current between 30 and 100 electrical degrees. The diagram shows then that most electrons arrive at the screen with a spread over a relatively small time interval, showing only minor symptoms of velocity modulation and debunching. Furthermore, the curvature of $G(t)$ is positive during the arrival times, implying a field which is retarding to secondary electrons and which inhibits their effect.

The graphical evaluation of the arrival velocities permits determination of the individual conversion efficiencies $\eta = 1 - v^2(t_2)/v_0^2$ where $(v(t_2)/v_0)^2$ represents the fraction of the initial kinetic energy lost as heat to the screen. An evaluation of η for the different times of emergence from the cathode is shown in Fig. 4. The specific operating conditions chosen in this analysis were the optimum relations (15) and (16). Thus it is seen that the efficiency of most of the beam current can be very high, the average conversion efficiency amounting

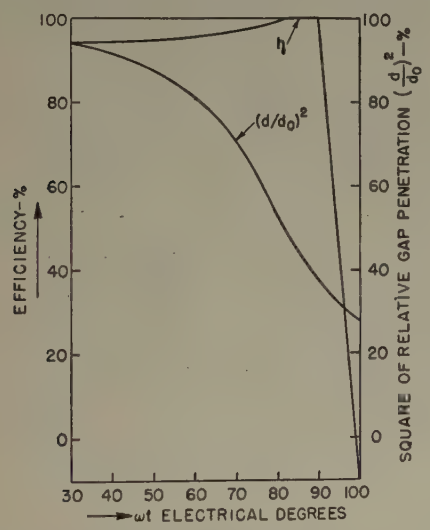

Fig. 4—Efficiencies η and the square of the maximum relative gap penetration plotted against phase of electron origin at the cathode. The curves, which have been graphically evaluated from Fig. 3, correspond to a choice of optimal conditions.

to 88.6 per cent. The sharp drop in the power contribution of the straggling electrons is of interest in view of the asymmetry with respect to the maximum. This has a direct bearing on the modulation characteristics of the reflex resnatron.

Power modulation in the output cavity can occur as the result of variations in the repeller voltage from the optimum value determined by (16). It would be possible to account for the resulting phenomena in Fig. 3 by altering the curvature of $G(t)$. Instead of this cumbersome process, it is easier to visualize the effect of the signal voltage as a small perturbation superimposed on the moving reference system. The straight lines become then parabolas of very small but varying curvature, and the following situation will result: As the repeller voltage is swung more positive, the trajectories curve upward so that the electrons are delayed in their arrival at the screen. They will therefore, in greater numbers, exhibit the behavior of the straggling electrons shown in Fig. 4. This implies that a variation in the repeller bias to more positive values results in a sharp reduction of power, and a sensitive control of the power level is possible in this region. For a single electron this merely corresponds to the transition from the second to the third mode, as outlined before. Fig. 4 also shows that a variation of the retarding potential to more negative values will lead only to a gradual reduction in the conversion efficiency. Thus the modulation characteristics of the reflex resnatron will show an asymmetric shape, and the positive branch will be the preferred region of operation.

The increased bandwidth of the reflex resnatron operation follows from the reduced oscillating voltage necessary to diminish the initial speed of the electrons. From an alternative point of view, the electrons traverse the gap twice, hence represent a twofold beam current. From this consideration results a gross approximation method to determine the bandwidth in the multiple trajectory picture. Fig. 4 shows a plot of the maximum penetration d of the gap d_0 for the trajectories of Fig. 3. Assuming that the resulting bandwidth is proportional to the mean square of the fractional penetration, one thus arrives at the theoretical estimate that an improvement by a factor of 2.7 is possible over the conventional operation.

V. Comparison with Experiment

The effect of space charge has been ignored in the treatment outlined in the preceding sections, and certainly only secondary corrections should be anticipated as necessary. A test of this conclusion is available by comparing (16) with the values measured for the maximum power points. Table I shows experimentally de-

TABLE I

d/λ	Output power (watts)	Oscillating voltage $-V_A$	Screen voltage V_s	Repeller voltage $-V_B$, meas	Theoretical repeller voltage $-V_B$, theor
0.0357	80	1030	3000	3700	4080
0.0357	120	1260	5000	5200	5310
0.0357	360	2180	3500	3850	4020
0.0357	900	3430	6000	5700	5030
0.0357	1100	3800	6000	5400	4900
0.0400	1800	4900	8000	6800	6400
0.0446	1800	4900	10,000	8700	9200

termined voltages for a great range of output powers corresponding to a number of beam current and voltage conditions. The frequency used was in the order of 600 mc. The ratio d/λ of gap to wavelength is, however, different for the two cases listed at the bottom of the

table because of constructional changes in the gap spacing. The oscillating voltage V_A was computed from the output power and the cavity characteristics, the screen voltage V_0 is measured directly, and V_B, the repeller potential with respect to the screen, represents the value adjusted for maximum output. The last column lists the theoretical values of V_B, computed from (16) with the use of the measured V_A, V_0, and d/λ, $n=2$.

It is seen that the discrepancy between the values of the last two columns is only in the order of 2–12 per cent. Experimental errors alone would account for these differences, and it is therefore correct to conclude that the available evidence does not warrant a correction of the derived expressions for space charge.

In comparing the results of the multitrajectory calculations with practice, one must be aware of the critical influence that the chosen driving conditions exert on the angle of flow and hence on the resulting efficiency. Moreover, it is difficult to establish the true conversion efficiency from measured values. The beam current to the screen, for instance, consists in the experimentally studied tube of two fractions with uncertain ratio, viz. the intercepted electron flow and the part succeeding to penetrate into the gap and interact with the field. It is however possible from an extrapolation of static screen current measurements with positive V_B to estimate this ratio. It was thus found that about 45 per cent of the current was prematurely intercepted by the screen under most reflex operating conditions. Even with this handicap, the total output efficiency was measured to be in the order of 40 per cent. Hence the conversion efficiency was about 73 per cent, which is quite close to the theoretical optimum of 89 per cent in view of the additional losses in the dielectrics.

The asymmetric behavior of the modulation curve predicted by the theory can be verified experimentally. Fig. 5 shows an example for low powers plotted against repeller voltage relative to ground. The sharp drop toward more positive values is indeed verified.

Finally, the bandwidth shows a consistent improvement by a factor of about 2.2 over that of the conventional resnatron. A bandwidth of about 8 mc at 2.5 kw was thus obtained with the experimental model.

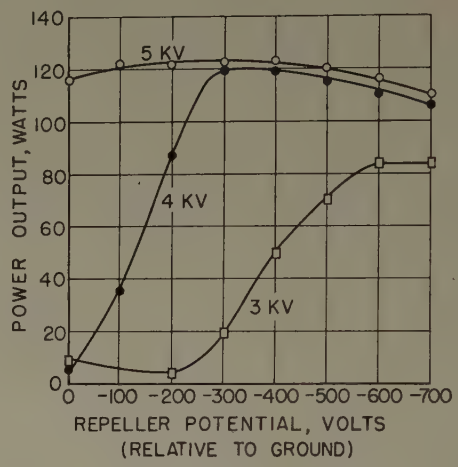

Fig. 5—Modulation curves at low currents. Repeller voltage is plotted relative to ground.

While these experimental results are quite encouraging, the theory points the way in which further advances can be made. Improved beam forming structures, specifically designed for reflex operation, should increase the over-all efficiency to about 75 per cent. Better input driving conditions, perhaps applied to higher modes of operation, should result in very steep modulation characteristics, permitting signal modulation at very small powers.

Acknowledgment

The author wishes to express his gratitude to G. E. Sheppard, who designed the first successful model of the reflex resnatron, to J. R. Hansen, who performed much of the experimental work, and to Dr. J. W. Coltman, who provided encouragement and many helpful suggestions.

An Axial-Flow Resnatron for UHF*

R. L. McCREARY†, SENIOR MEMBER, IRE, W. J. ARMSTRONG†, AND S. G. McNEES†, MEMBER, IRE

Summary—**A new design for a resnatron based on the axial flow of the electron stream has resulted in the development of a tube for uhf. The tube has been tested up to 29-kw cw power output at 420 mc with efficiencies from 45 to 75 per cent and power gains in excess of 10 db. The novel and general features of the mechanical design are described and the performance characteristics are given in curve and tabular form.**

* Decimal classification: R339.2. Original manuscript received by the Institute, November 12, 1952.
† Collins Radio Co., Cedar Rapids, Iowa.

Introduction

THE RESNATRON TUBE is uniquely applicable to the field of uhf in that it makes possible the use of high power for all types of applications in this frequency range. This tube can be used in service to provide power gains and efficiencies comparable to those obtainable at lower frequencies. For several years there has been in operation an extensive program of resnatron development to advance the design and per-

formance of this tube. As a part of this program, the design and performance features of various geometrical arrangements of the elements of the tube have been considered. A particular arrangement may be generally assigned to one of the two classifications consisting of (1) radial flow and (2) axial flow. In this sense a distinction is made according to whether the electron stream is directed perpendicular to or parallel to the axis of symmetry of the tube. This distinction is important when the requirements of constructional simplicity operational stability, and serviceability of the tube are considered.

The conventional resnatron design which has evolved from the original work of Sloan and Marshall[1] and which has been extended by other workers[2,3,4,5] is an example of the radial-flow resnatron. These tubes are high-power (50 kw), tetrode, cavity resonator types operating in the frequency range of 350 to 650 mc. Particular emphasis is placed upon the design of the electrodes in order to secure desirable beam-focusing characteristics. At uhf the electron transit-time effects require careful design consideration for the interelectrode spacings and for the electrode voltage if efficient operation is to be obtained.

A recent publication[6] describes a tube with an axial-flow arrangement of electrodes combined with a reflex principle of operation.

This paper presents a description of the design features and the performance of a resnatron amplifier utilizing the axial-flow arrangement. The design uses the basic information available from the previous works cited. However, because of the mechanical simplicity afforded by this arrangement, various critical parameters affecting the performance can be experimentally adjusted with a minimum of effort and time.

Design of the Axial-Flow Resnatron

A. General Design Objectives

The general objectives which were set up for this amplifier development are as follows:

1. A power output of 30 kw, cw.
2. A tuning range of 300 to 600 mc.
3. A power gain of at least 10 db with a 4-mc bandwidth and with a plate efficiency of at least 50 per cent.
4. A design which yields simplified construction, adaptable to variation of interelectrode spacing and accessible for rapid replacement of grids and cathode assemblies.

B. General Characteristics

As designed, this tube is continuously pumped during operation. Therefore, demountable vacuum gasket joints are employed at the flange connections. Tuning shafts are placed through vacuum seals to the outside of the tube. Fig. 1 is a photograph of the assembled tube. The flanged vacuum port is seen extending away from the main housing in the middle of this view. The anode and cathode cavity tuning shaft knobs are shown extending from the main housing. The lower section of the photograph of Fig. 1 includes the coaxial input line and the input stub tuner. The $3\frac{1}{8}$-inch flanged coaxial connector is shown on this section and the means for adjusting the stub tuner is seen at the bottom of the photograph. Fig. 2 is a schematic diagram showing the essential features of this design.

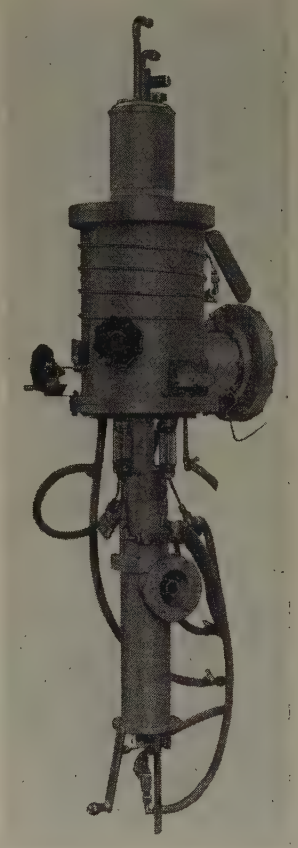

Fig. 1—Assembled axial-flow resnatron.

The tube is water cooled throughout. All water connections, with the exception of the anode, are made through the lower section of the tube. The anode water-cooling pipes are shown at the top of Fig. 1.

C. Cathode

The cathode of the axial-flow resnatron is comprised of twelve "U"-shaped, directly heated, thoriated tungsten filaments. The ends of the individual filaments

[1] D. H. Sloan and L. C. Marshall, "Ultra high frequency power," *Phys. Rev.* vol. 58, p. 193; 1940.
[2] W. W. Salisbury, "The resnatron," *Electronics*, vol. 19, pp. 92–97; February, 1946.
[3] W. G. Dow and H. W. Welch, "The generation of ultra high frequency power at the fifty kilowatt level," *Proc. NEC*, vol. II, pp. 603–614; October, 1946.
[4] W. G. Dow and H. W. Welch, "Very high frequency techniques," McGraw-Hill Book Co., Inc., New York, N. Y., chap. 19; 1947.
[5] D. B. Harris, "New UHF resnatron designs and applications," *Electronics*, vol. 24, pp. 86–89; October, 1951.
[6] G. W. Sheppard, M. Garbuny, and J. R. Hansen, "Reflex resnatron shows promise for UHF TV," *Electronics*, vol. 25, pp. 116–119; September, 1952.

are mounted to two concentric rings so that the angular spacing between the filaments is 30 degrees and the plane of the emitting surface is perpendicular to the

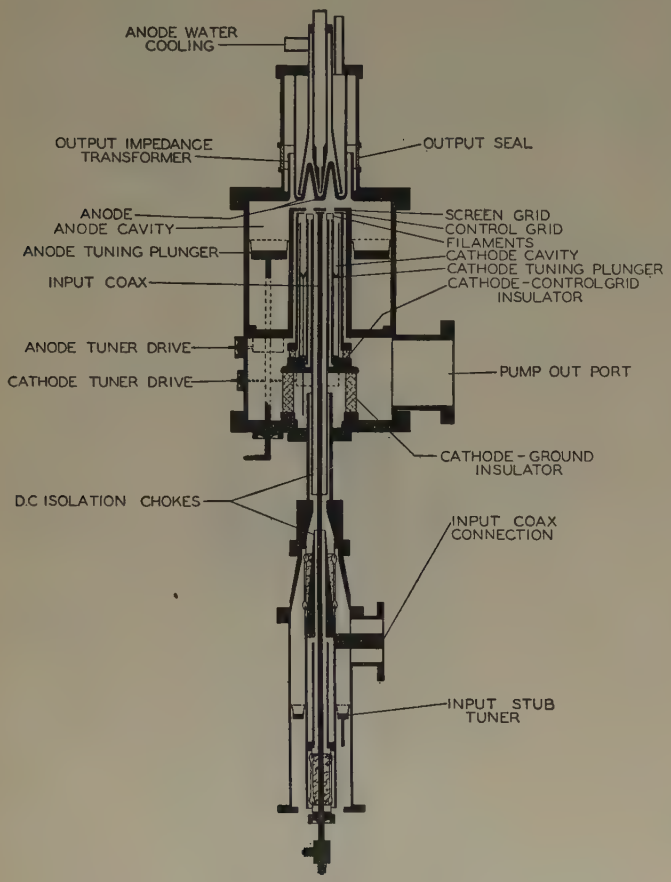

Fig. 2—Cross-section schematic of axial-flow resnatron.

axis of the rings. Fig. 3 is a photograph of the cathode, grid, screen grid- and anode elements removed from assembly and placed in their proper relative though expanded positions.

The individual filaments are made from thoriated tungsten ribbon 0.010 inch thick and 0.050 inch wide with an emitting length of 0.375 inch. The total emitting area of the cathode is 1.45 cm². The concentric copper rings on which the filaments are mounted are fastened to water-cooled surfaces by means of eight small screws.

The external filament connections are brought out of the tube through insulating glass seals shown in Fig. 1. Since the tube is operated with the cathode at a high negative potential relative to the grounded anode, these seals also furnish the insulation required by the plate voltage supply.

D. Control Grid and Screen Grid

The control and screen grids, as shown in Fig. 3, are flat copper plates with twelve radial slots milled through their surfaces. The control grid and screen grid are fastened to water-cooled tubes by means of screws and are oriented so that the slots of each are aligned and centered with the filaments of the cathode. By demounting the tube at the flanged joint which mounts the anode, (Fig. 1) the cathode, grid, and screen grid electrodes are readily accessible and may be accurately aligned and fixed in position before the final tube assembly is completed. This feature has proven valuable during the development period when effects of the variation of interelectrode spacings were studied.

Fig. 3—Axial-flow resnatron electrodes including anode, screen grid, grid, and cathode.

E. Anode

The anode of the axial-flow resnatron is unique in that it serves a two-fold purpose. It serves in its normal function as an anode as well as a power-output capacity probe.

The anode has 1.500 inches deep cylindrical "V" groove machined into its surface as shown in Fig. 2. The purpose of this "V" is to defocus and receive the electrons emitted and accelerated from the cathode. The anode is directly water cooled and has, under static tests, dissipated 60 kw of continuous power.

The anode is mounted to the tube through a glass or ceramic seal so that the "V" directly faces the grid slots. The anode, which is separated from the rest of the tube by an insulating seal, appears to have no return dc circuit (see Fig. 2). The circuit is actually completed by connecting the waveguide transmission line to the tube.

For the purpose of collecting data, the anode was isolated from the rest of the tube by means of a capacitor so that the screen and anode could be metered separately. This technique provides a means of determining the efficiency of the electron focusing. At high power, the screen current was found to be only 6 per cent of the total cathode current. This value remained constant under both dc and RF conditions.

F. Input Cavity and Coupling

The input cavity is a $\frac{1}{4}$-wavelength re-entrant coaxial cavity formed between the cathode and control grid. The actual electrode structures form part of the cavity and are located at the voltage maximum of the standing waves set up by cavity resonance. A choke, by-pass capacitor, and blocking arrangement is used to maintain RF continuity of the cathode cavity where it is broken to provide dc grid bias isolation from the cathode.

Tuning of the cathode cavity is accomplished by changing its length by means of a shorting plunger and tuner arrangement incorporated in the tube.

The inner conductor of the input coaxial line is connected directly to the center of the control-grid element and the outer conductor is connected directly to one side of the cathode wall. A choke, by-pass capacitor, and blocking system placed in the inner and outer conductors of the input coaxial line and within the vacuum envelope allow the input coaxial line to be at ground potential external to the tube. The external connection is designed to accommodate a standard $3\frac{1}{8}$-inch, 50-ohm coaxial transmission line.

The external grid bias connection is made to the grid water-cooling pipe. This water pipe is insulated by means of a glass seal from the tube housing which is operated at ground potential.

G. Output Cavity and Output Coupling

The output cavity is a $\frac{1}{4}$-wavelength re-entrant coaxial cavity concentric with and surrounding the cathode cavity. The screen and anode electrode structures form part of the cavity and are located at the RF voltage maximum point in the cavity.

The anode cavity extracts the power from the electrons that are accelerated into it from the cathode by the screen. Output power from the anode cavity is coupled into a waveguide or coaxial transmission system by means of a coaxial impedance transformer formed by the anode structure and a short length of tubing placed around it. The anode structure acts as a capacity probe for the output system.

As in the cathode cavity, the anode cavity is tuned by positioning a shorting plunger to alter the length. The position of the plunger is adjusted by means of a tuning arrangement incorporated in the tube.

Performance

Experimental curves of plate current as a function of plate voltage for a range of grid voltages are shown in Fig. 4. Constant plate current curves taken from these experimental data are shown in Fig. 5.

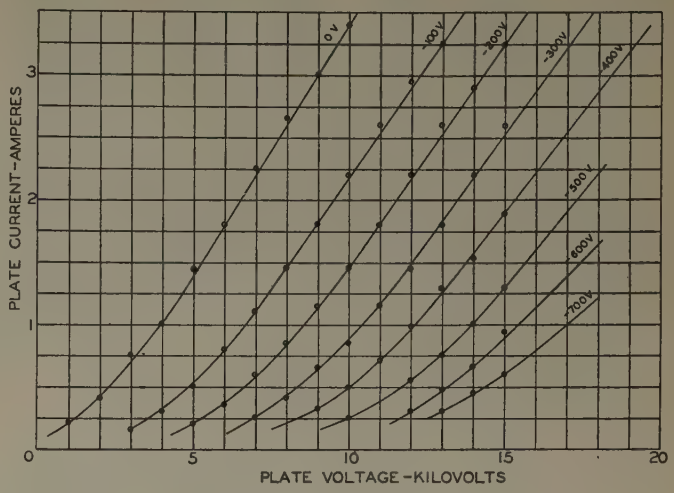

Fig. 4—Plate current versus plate voltage curves for constant-grid voltages as indicated.

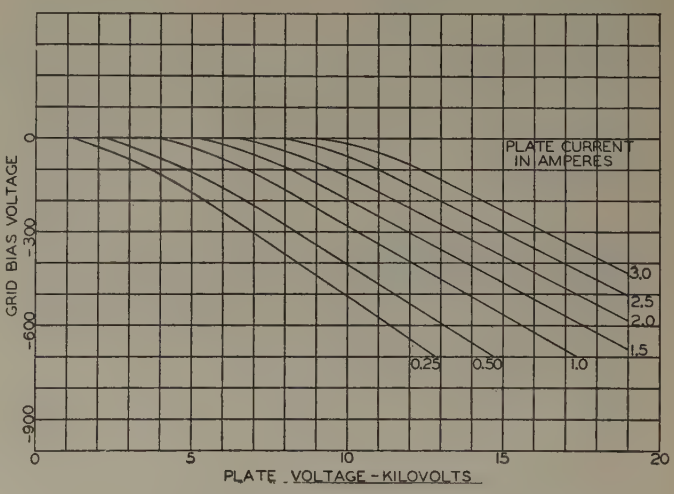

Fig. 5—Constant-plate current curves.

A compilation of typical RF operating conditions is given in Table I. For these data the grid-cathode spacing was fixed at a value which gave the most desirable over-all performance for power output, power gain, and efficiency. For these data a crystal-controlled amplifier was used to drive the axial-flow resnatron. The operating frequency was approximately 420 mc.

At this time, performance characteristics have not been acquired covering the frequency tuning range of the tube. However, the cathode and anode cavities have been tuned at signal generator level over the frequency range of 250 to 750 mc.

TABLE I

Power input watts	E_B kv	I_B amps	CW power output kw	Power gain	Plate efficiency
250	10.0	1.0	4.5	18.0	45 %
500	12.5	1.5	9.2	18.4	49 %
1000	15.0	2.7	18.5	18.5	45.6%
	15.0	2.0	16.0	16.0	53.3%
1500	15.0	2.8	22.0	14.7	52.3%
	17.0	3.05	25.5	17.0	49.2%
2000	15.0	2.8	23.5	11.75	56 %
2500	17.0	3.0	29.5	11.6	58 %
	15.0	2.15	24.0	9.6	74.7%

Conclusion

A resnatron amplifier has been developed which utilizes a geometrical arrangement of electrodes so that the electron stream is directed parallel to the axis of symmetry of the tube. When designed in this manner the construction of the tube is simplified. Novel means of coupling power into and out of the tube have been employed and have given satisfactory performance.

The performance characteristics of the tube have been measured, and these show that the tube will operate satisfactorily up to 29-kw cw output with a power gain in excess of 10 db at a bandwidth estimated to be approximately 4 mc. The measured plate efficiencies of the tube vary between 45 and 75 per cent depending upon the operating point of the tube.

The axial-flow resnatron design can be extended to tubes with considerably higher power output ratings than that covered in this paper. This will require new and improved cathode designs which are now under investigation. This design also holds promise for extending the resnatron principle to higher frequency operation as has been previously suggested.[5]

RF Performance of a UHF Triode*

H. W. A. CHALBERG†, SENIOR MEMBER, IRE

Summary—**The details of techniques of measurements and the dynamic results obtained with a uhf triode are discussed. Performance characteristics in the vhf and uhf television bands are covered, and a comparison of gain and noise figures made with tubes now available for vhf amplifier service.**

A DEVELOPMENTAL 9-pin miniature triode for grounded-grid RF amplifier applications in the vhf and uhf television bands has recently been announced by the General Electric Company. The developmental-type number of this tube is the Z-2103 (now Type 6AJ4). This paper will cover the measuring techniques used in evaluating the performance capabilities of the Z-2103. Results obtained on some of the early developmental samples will also be presented.

Early measurements were made with commercially available coaxial transmission-line equipment. This equipment permitted using simple tube chassis fitted with coaxial connectors. The coaxial system simplifies the measurement of standing-wave ratio, impedance, effect of feed-through coupling, and power gain.

It is common knowledge that power-gain measurements at frequencies from 400 to 1,000 mc are more reliable and reproducible than voltage-gain measurements where a mismatch exists between the components in the RF system, i.e., signal generator and tube or load. Therefore, power-gain measures have been used almost exclusively in order to eliminate the necessity for using matching transformers or circuits. However, since the television manufacturers are primarily interested in how many microvolts are required across the antenna to produce a given input to the grid of the RF system, additional experimental work has been done using lumped constant circuits in which the input and output were matched to the generator and load impedance.

The coaxial system is shown in block diagram form in Fig. 1. The output of the uhf signal generator, which is 30-per cent amplitude-modulated with a 1,000 cycle sine wave, is fed to a slotted line which in turn is connected to the input of the tube or to the output indicating system, as the case may be. The 1,000-cycle rectified output of the slotted-line probe is fed through a resistance attenuator calibrated in decibels, amplified, and observed on either a cathode-ray oscilloscope or meter.

The tube under test is mounted in a simple chassis fitted with RF input and output connectors and by-

* Decimal classification: R583.6×R333. Original manuscript received by the Institute March 18, 1952. Presented at the 1952 IRE National Convention in New York, N. Y.

† General Electric Co., Owensboro, Ky.

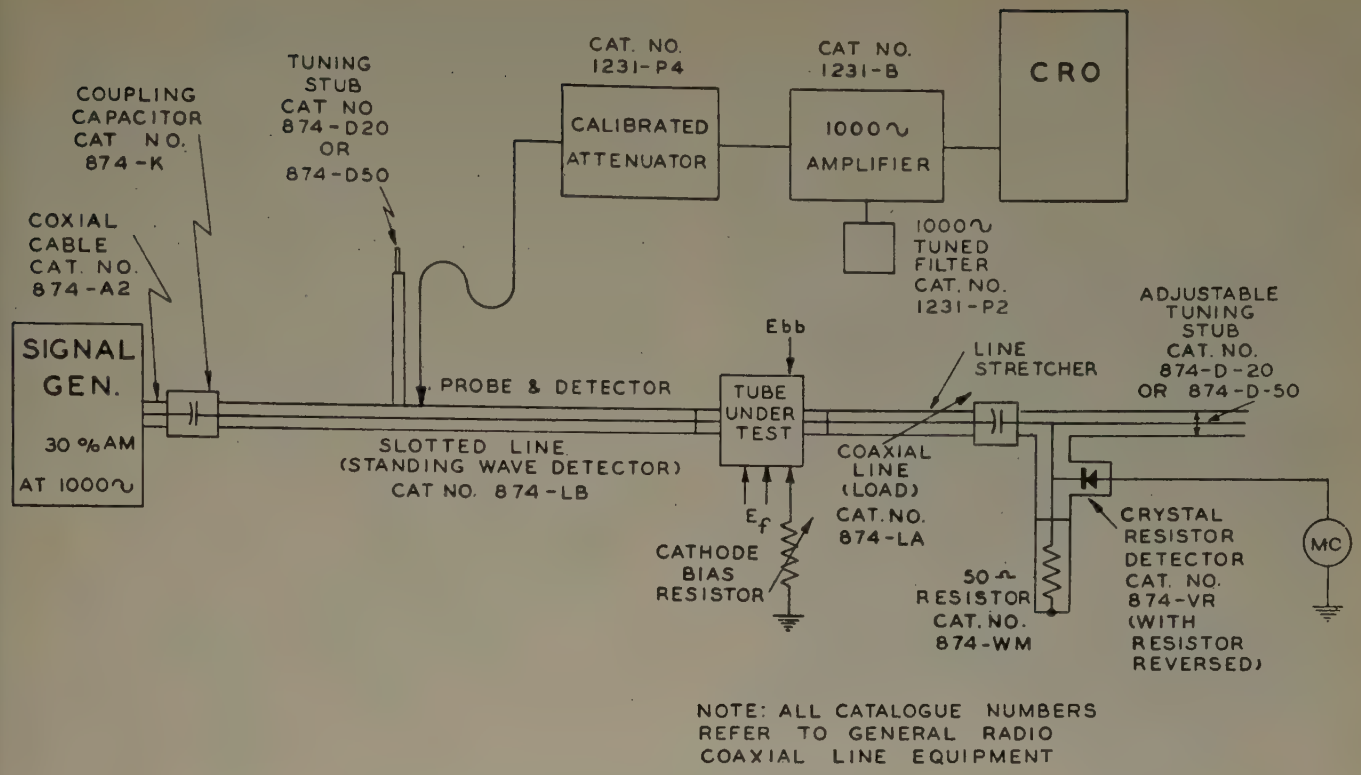

Fig. 1—UHF coaxial measuring system.

passed filament and plate leads which include RF chokes. The dc return for the cathode is also through a by-passed terminal with an RF series choke; this feature permits the use of different values of the self-bias resistor. The bottom view of this chassis is shown in Fig. 2. As can be seen in the figure, the RF cathode and plate leads have been made as short as possible; even with this precaution the electrical length from the connector to the cathode pin is approximately 0.4 of a wavelength at 900 mc.

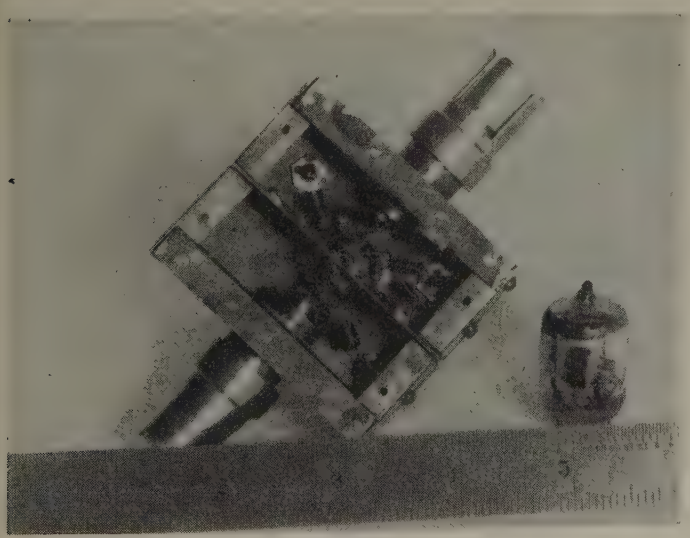

Fig. 2—Basic chassis for making Z-2103 RF measurements.

The output circuit consists of a line stretcher, coaxial "T," stubtuner, crystal rectifier, a 50-ohm coaxial-resistor, and dc microammeter. The RF tuned circuit connected to the plate consists of the line stretcher and shorting stub which are adjusted for the resonant frequency. Bandwidth of the system is adjusted by physically moving the position of the coaxial "T" crystal, and 50-ohm resistor along the coaxial line. This is similar to moving a pick-up loop in a cavity in varying the load presented to the plate.

The voltage-standing-wave ratio can be measured in decibels if the resistance attenuator in the slotted-line crystal circuit is calibrated in decibels. The dbswr is proportional to $A_{max}-A_{min}$, where A_{max} and A_{min} are the attenuator settings in decibels for constant indicator reading. In the case of the equipment being described here, the crystal probe is operated over its square-law region and a factor of $\frac{1}{2}$ must be used in measuring the dbswr. Thus, dbswr $=\frac{1}{2}(A_{max}-A_{min})$ db.

In measuring the impedance of a system, either short circuit or open circuit at the end of the slotted line can be used as the reference. When the tube and its tuned load are connected to the end of the slotted line, the position of voltage minimum will shift a distance of Δx from the reference point. This distance is plotted on a Smith chart as an angular shift equal to $(\Delta/\lambda)x$, using the zero impedance or infinite impedance reference on the Smith chart to correspond to the short-circuit or open-circuit slotted-line reference. If the position of the voltage minimum shifts toward the generator, the Δx vector is rotated in the clockwise direction from the reference position.

Of course, if the position of the voltage minimum moves away from the generator, the Δx is rotated in a counterclockwise direction. In either case the radial

length of the vector is proportional to the vswr of the system under investigation.

It is possible by this method to measure variation of input impedance for a system over a wide frequency range, and Fig. 3 is a plot of the input impedance of the Z-2103 from 400 to 900 mc. As stated before, these impedances are referred to the connector on the basic tube chassis and do not represent the impedance at the elements or even the tube's pins.

The effect of feed-through coupling on input impedance is also presented in Fig. 3. It is desirable to have as small a change of input impedance as possible when the signal generator is adjusted to the sidebands of plus and minus one-half the bandwidth. As can be seen in Fig. 3, the change in input impedance for this condition is virtually along the main impedance contour. If the impedance at the sidebands were to be greatly different than at the center frequency, the effect would result in narrowing the input bandwidth. This condition would also be indicative of greater regeneration or feed-through coupling, making the gain a function of the amplitude of the signal.

The Z-2103 does not appear to have any internal resonances, and the isolation between the output and input circuits appears to be very effective. With special socket arrangements, it is as high as −40 db.

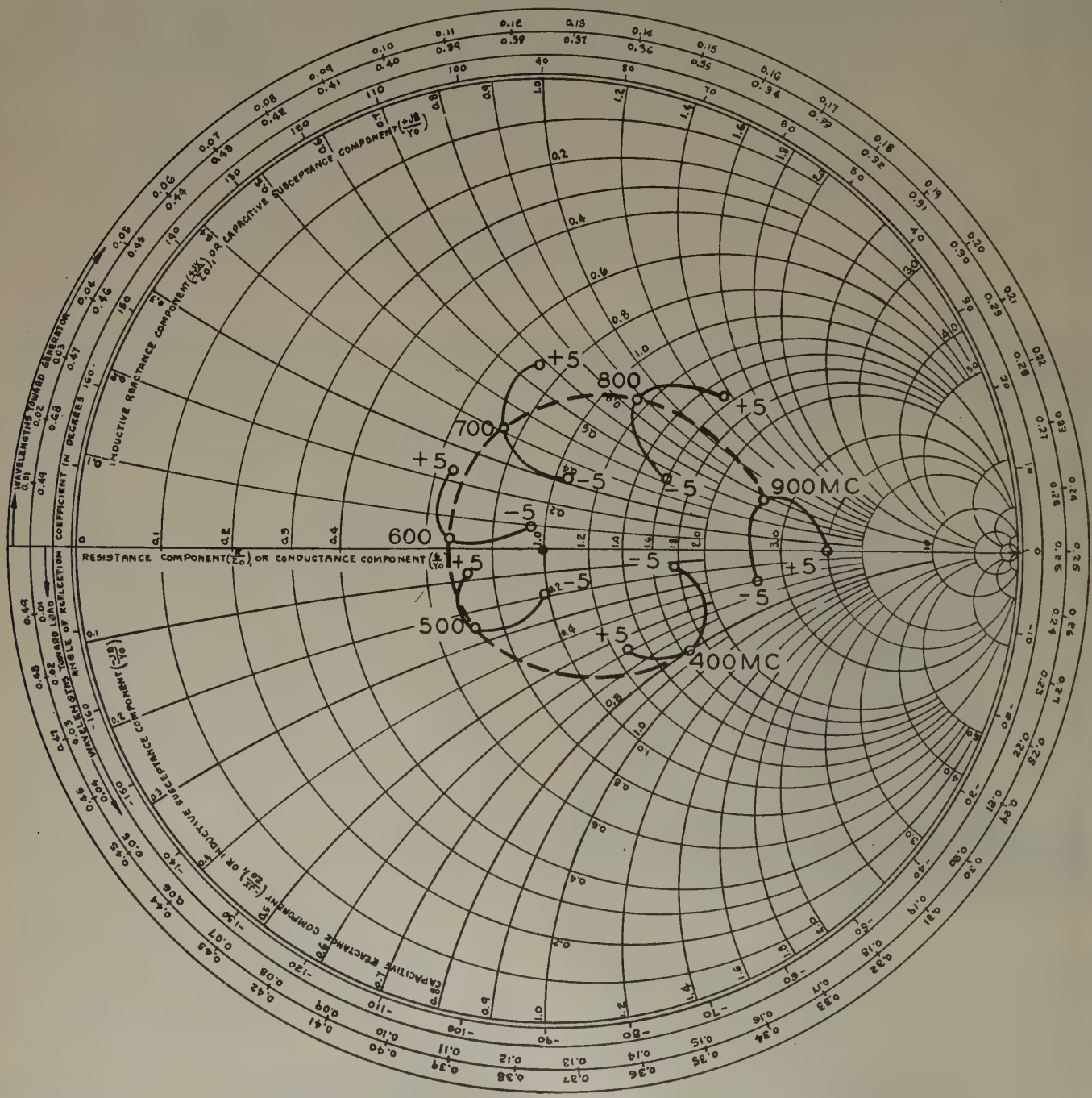

Fig. 3—Input impedance variations of the Z-2103 over the uhf range.

Power-gain measurements are made in the following manner: The maximum and minimum standing-wave voltages are measured for the combined tube and load and for the load alone. As in the case of measuring swr,

DERIVATION OF POWER GAIN EQUATION

$$P = \frac{V_{max} V_{min}}{2Z_0} \quad (1)$$

$$\text{P.G.} = \frac{P \text{ (load)}}{P \text{ (amplifier)}} \quad (2)$$

$$\text{P.G.} = \frac{V_{max} V_{min} \text{ (load)}}{V_{max} V_{min} \text{ (amplifier)}} \quad (3)$$

$$\text{P.G. (db)} = \frac{20}{2} [\log V_{max} + \log V_{min}] \text{ load} - \frac{20}{2} [\log V_{max} + \log V_{min}] \text{ amplifier} \quad (4)$$

$$V_{max}^2 = KR_{max}; \qquad V_{min}^2 = KR_{min} \quad (5)$$

$$\log R_{max} = \tfrac{1}{2} A_{max}; \qquad \log R_{min} = \tfrac{1}{2} A_{min} \quad (6)$$

$$\text{P.G. (db)} = \tfrac{1}{4}[A_{max} + A_{min}] \text{ load} - \tfrac{1}{4}[A_{max} + A_{min}] \text{ amplifier} \quad (7)$$

Fig. 4—Derivation of power gain equation.

the settings of the calibrated resistance attenuator are used. The power gain of the system is equal to PG(db) $= \frac{1}{4}(A_{max}+A_{min})$ load circuit $- \frac{1}{4}(A_{max}+A_{min})$ amplifier. The derivation of this equation is shown in Fig. 4. These same methods can be used in making similar measurements on other than coaxial systems.

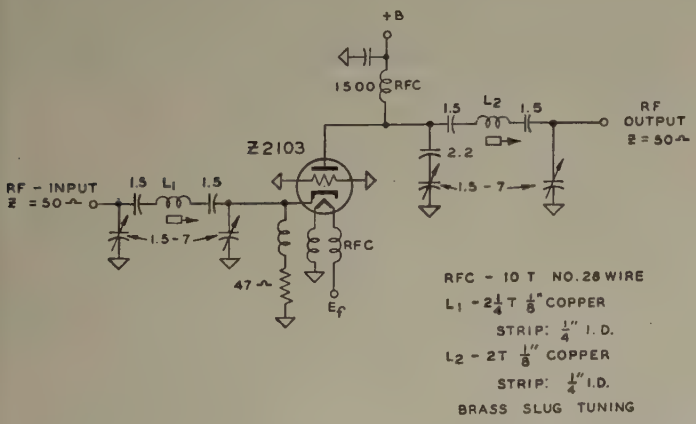

Fig. 5—Circuit diagram of a 900-mc amplifier using lumped constants.

One-tube RF amplifiers have been built for several frequencies in the uhf range using lumped constants for the input and output tuned circuits. The schematic diagram for a unit amplifier designed for operation at 900 mc is shown in Fig. 5. The input of this circuit has been adjusted to match the 50-ohm output impedance of the signal generator, and the output impedance has been matched to the load and detector circuit. Power-gain measurements are made in the same manner as previously described. Fig. 6 is a photograph of the 900-mc amplifier unit.

A third system for evaluating gain of the Z-2103 has been used. Two stages of RF amplification are connected in cascade and provision is made for connecting the RF signal to both tubes in series or to the input of

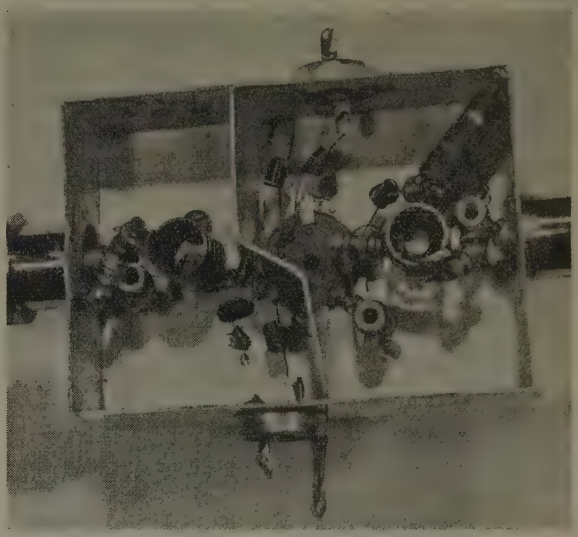

Fig. 6—900-mc chassis using lumped constants.

the second tube alone. Thus, the second tube is used as a calibrating or volt-meter tube. The circuit diagram of a complete 900-mc test unit is shown in Fig. 7.

The input impedance of both the test and calibrate positions are adjusted to match the 50-ohm signal generator impedance; and the gain, as a voltage ratio, is determined by the ratio of the settings of the signal generator attenuator at the calibrate position to that at

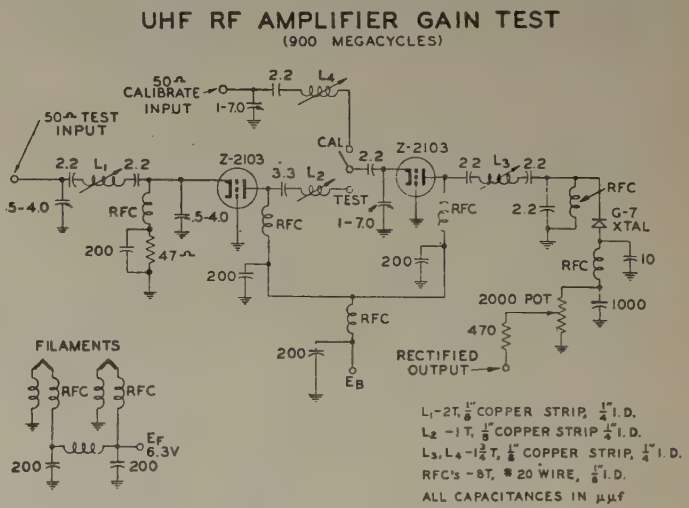

Fig. 7—Circuit diagram of a two 900-mc amplifier.

the test position for constant output indication. The calculated voltage db gain can be checked against the power gain (db) by measuring the maximum and minimum attenuator settings at the test and calibrate positions and substituting in the power-gain equation. A

bottom view of this two-stage amplifier is shown in Fig. 8.

Gain measurements using the three methods described above have been made on developmental samples of the Z-2103. The results obtained on the coaxial system and the single-stage lumped constant circuit are presented in tabulated form in Fig. 9.

The average voltage gain of several tubes as measured in the two-stage circuit of Fig. 7 gave gain of figures 3.5 times or calculated (db) gain of 11, at a frequency of 900 mc. This calculated value of gain in decibels checked within one-half of a decibel of the measured power gain in decibels.

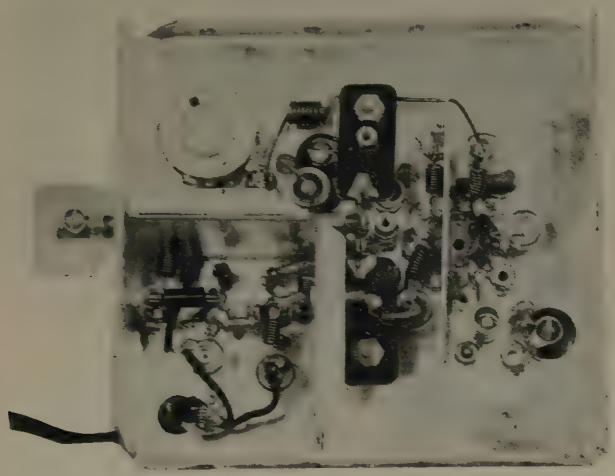

Fig. 8—900-mc two stage chassis.

In measuring the noise figure of the Z-2103 over the uhf range the single-stage lumped constant circuits were used ahead of a General Radio Crystal Mixer. A G-R Unit Oscillator served as the local oscillator source.

The measured noise figure of the Z-2103 amplifier stage plus crystal mixer varied from 12 db at 500 mc to 16.2 db at 900 mc. The noise figure of the tube alone was 10.7 db at 500 mc and 14.7 db at 900 calculated mc.

The vhf performance of the Z-2103 has been evaluated in a turret-type production tuner using a 6J6 mixer-oscillator and adapted for using a Z-2103 grounded-grid amplifier. The measured noise figures at channels 4 and 10 are 6.2 db and 8.2 db, respectively. The corresponding gains are 3.84 and 3.71 times in voltage. These figures compare favorably with other tubes now used in grounded-grid amplifiers in the vhf television bands.

FREQUENCY MC/S B.W.=6MC/S	COAXIAL LINE GAIN DECIBELS	LUMPED CONSTANT CIRCUITS GAIN DECIBELS	LUMPED CONSTANT CIRCUITS NOISE FIGURE DECIBELS
500	5.8	5.5	12.0
600	7.6	9.1	11.4
700	7.9	7.3	14.7
800	8.8	6.7	13.0
900	7.6	7.0	15.5
79	—	11.0	6.0
195	—	11.4	8.1

Fig. 9—RF performance of the Z-2103.

In conclusion, the preliminary data on measurements made over the uhf band of input and impedance, feed-through coupling, gain, and noise figure, together with performance figures over the vhf bands, indicate that the Z-2103 is a practical candidate for the RF amplifier position in combined vhf-uhf television tuners.

UHF Triode Design in Terms of Operating Parameters and Electrode Spacings*

L. J. GIACOLETTO†, SENIOR MEMBER, IRE AND H. JOHNSON†, SENIOR MEMBER, IRE

Summary—**An approximate triode theory has been organized in terms of the operating parameters and electrode spacings so that, with the aid of graphical representations, the tube designer can readily and very quickly predict the RF performance of a grounded-grid amplifier or the effect thereon of changes in design parameters. It is thus possible to minimize the experimental work required to achieve a desired performance. The effects of changes in design parameters are shown by illustrative examples, and a study of these examples confirms that substantial improvements in the performance of present-day tubes cannot be obtained by minor changes in one or two parameters. Significant improvements may only be obtained by pushing all design parameters to the limit of practicability. The performance predicted by this theory is compared with experimental measurements of other workers with satisfactory agreement. It is concluded that the theory is quite adequate for design work.**

Introduction

THIS STUDY of triode design emphasizes applications to the RF input stages of uhf television receivers. It is well known that extremely close-spaced triodes can be constructed to give excellent performance at ultra-high-frequencies (uhf). It is equally well recognized that the difficulties of constructing such triodes cannot be dismissed lightly. Thus, in order to evaluate the triode for uhf television applications, it is necessary to have some idea of the design and constructional difficulties imposed by the performance requirements for this application.

The various aspects of triode performance at ultra-high-frequencies have been discussed by many workers. These analyses have generally related the rf performance to the electrical parameters of the triode. The present study is an attempt to relate the RF performance more directly to the fundamental design parameters, such as electrode spacing, current density, and operating voltages. Somewhat similar design considerations have been published for tube designs in which the gain-bandwidth product is of paramount interest. However, in the present case, the noise performance and gain are of paramount interest and the present study is organized with this in mind.

While it is possible to set up explicit expressions for the RF performance as functions of the basic design parameters, these expressions are so involved that they contribute little to the understanding of the design problem. The present solution has set up graphical representations from which the ratio of the electrical parameters, transconductance and electronic grid input conductance, can be determined from the fundamental design parameters. Another set of graphs then gives the RF performance (gain and noise factor) from this ratio. To illustrate the trend in RF performance directly as a function of the fundamental design parameters, typical curves are given for the variation of gain and noise factor with changes in selected design parameters.

* Decimal classification: R333×R583.6. Original manuscript received by the Institute, October 1, 1952.

† Radio Corp. of America, RCA Laboratories Division, Princeton, New Jersey.

Circuit Considerations

Vacuum tubes are inevitably a part of a circuit; therefore, a tube designer has to consider the design of a tube in association with the circuit. Insofar as possible, circuit considerations will not be treated in this paper unless they relate directly to the tube-design problem. The circuit application for which a tube is to be designed is a Class A uhf grounded-grid amplifier, shown in Fig. 1.[1] The choice of a grounded-grid amplifier at uhf can generally be justified on the basis of the input-output shielding provided.

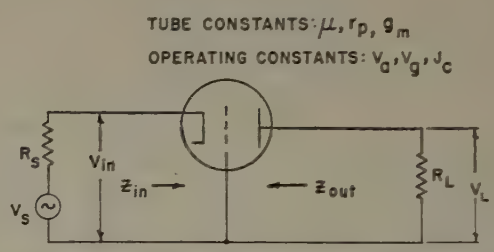

Fig. 1—Grounded-grid amplifier circuit. Tube constants: A = cathode area, μ = amplification factor, r_p = anode resistance, g_m = transconductance. Operating constants: V_a = anode voltage, V_g = grid voltage, J_c = cathode current density.

An accurate treatment of the circuit of Fig. 1 results in equations that are so complex as to be of little value as an aid in tube design. Therefore, various assumptions have been made to reduce these circuit equation complexities to a minimum while still retaining those factors that are of importance in a television uhf Class A amplifier. It is important that these assumptions be clearly defined and well understood in order that the final results may be properly interpreted. These assumptions are:

1. Tube lead and circuit losses are neglected.
2. Cathode-anode capacitance is negligible. This assumption is justified primarily on the basis of the resulting simplification of circuit equations. In addition, it is generally believed that C_{k-a} does not alter the noise factor of the amplifier since its most important role is to introduce feedback. Finally,

[1] The circuit shown indicates a source of internal resistance, R_s, delivering power to a load resistance, R_L, through a vacuum tube. In practice it will usually be necessary to employ an inout transformer of turns ratio $N_1 = R_s/R_1$ to match a generator resistance, R_1, and an output transformer of turns ratio $N_2 = R_2/R_L$ to match a terminating resistance, R_2.

this assumption must be again examined upon the completion of the tube design to ascertain its validity. The input and output tube capacitances can generally be accommodated as part of the input and output circuits.

Several other assumptions will be employed, but these will be recited during the course of the development.

The following equations concerning the circuit of Fig. 1 are either taken from or can easily be derived from published results,[2] and are therefore given here without proof. The input resistance in terms of anode resistance, r_p, load resistance, R_L, amplification factor, μ, and electronic grid input conductance, g_e, is

$$R_{\text{in}} = \frac{(r_p + R_L)}{1 + \mu + (r_p + R_L)g_e}, \tag{1}$$

and the output resistance is

$$R_{\text{out}} = r_p + \frac{\mu + 1}{\dfrac{1}{R_s} + g_e}. \tag{2}$$

From these, and the voltage ratio, V_L/V_S, the power gain is

$$\text{power gain} = G_p = \left(\frac{V_L}{V_S}\right)^2 \frac{(R_S + Z_{\text{in}})^2}{Z_{\text{in}} R_L} = \frac{R_L(1+\mu)^2}{r_p + R_L[1 + \mu + (r_p + R_L)g_e]}. \tag{3}$$

In order to get maximum power gain,[3] it is necessary to conjugately match the input and output circuits. The output resistance for maximum power gain can be obtained by differentiating G_p with respect to R_L and setting this equation equal to zero. The result is

$$R_L = r_p\left(1 + \frac{1+\mu}{r_p g_e}\right)^{1/2} \approx r_p\left(1 + \frac{g_m}{g_e}\right)^{1/2}. \tag{4}$$

In this equation as well as in several following equations μ is assumed to be much larger than unity, and the appropriate approximation is used. The maximum power gain is

$$G_{mp} = \frac{1}{r_p g_e}\left\{\frac{1+\mu}{1 + \left(1 + \dfrac{1+\mu}{r_p g_e}\right)^{1/2}}\right\}^2 \approx \mu \frac{g_m/g_e}{\left\{1 + \left(1 + \dfrac{g_m}{g_e}\right)^{1/2}\right\}^2}. \tag{5}$$

The power delivered to R_L will depend upon R_S and will be maximum when the source generator is conjugately matched. The source resistance for an input match can be obtained either by substituting (4) into (1), or by setting $R_{\text{out}} = R_L$ in (2) and solving for R_S. In either event,

$$R_S = \frac{1}{g_e\left(1 + \dfrac{1+\mu}{r_p g_e}\right)^{1/2}} \approx \frac{1}{g_e\left(1 + \dfrac{g_m}{g_e}\right)^{1/2}}. \tag{6}$$

When the product of the electronic grid input conductance and the equivalent noise resistance (R_{eg}) is greater than unity, it is well known that the improvement in the noise factor that can be obtained by mismatching the input is insignificant. Therefore, throughout the remainder of this article it will be assumed that the circuit of Fig. 1 is operated with a conjugate impedance match at both the input and the output.

To the above collection of formulas there should be added the approximate noise factor,[4] F, of a grounded-grid triode amplifier,

$$F - 1 = \frac{5 + 2.5\dfrac{g_e}{g_m}\left\{1 + \left[1 + \dfrac{g_m}{g_e}\right]^{1/2}\right\}^2}{\left[1 + \dfrac{g_m}{g_e}\right]^{1/2}}. \tag{7}$$

The preceding four equations relate the important circuit relations in terms of a dimensionless ratio of transconductance to electronic grid input conductance.[5] This ratio is determined by the grid-cathode and grid-anode transit angles so that the RF performance is solely a function of these angles and is independent of cathode area. Although g_m and g_e are proportional to the cathode area, since only their ratio is used here, they can be considered per unit area quantities.

[2] M. Dishal, "Theoretical gain and signal-to-noise ratio of the grounded-grid amplifier at ultra-high frequencies," PROC. I.R.E., vol. 32, pp. 276–284; May, 1944.

[3] At low frequencies it is customary to consider the voltage gain of an amplifier. When the electronic grid input conductance becomes appreciable, voltage gain loses significance, and it is preferable to consider the power gain. For reference, the voltage gain and the maximum voltage gain are

$$G_v = \frac{V_L}{V_S} = \frac{(1+\mu)R_L}{r_p + R_L + R_S[1 + \mu + (r_p + R_L)g_e]}$$

$$G_{mv} = \frac{1+\mu}{2\left[1 + \left(1 + \dfrac{1+\mu}{r_p g_e}\right)^{-1/2}\right]},$$

respectively.

The maximum power gain and maximum voltage gain are related as follows:

$$G_{mp} = \left(\frac{2r_p G_{mv}}{R_L}\right)^2 = \frac{4}{1 + \dfrac{1+\mu}{r_p g_e}} G_{mv}^2 \approx \frac{4}{1 + \dfrac{g_m}{g_e}} G_{mv}^2.$$

[4] The noise factor of a grounded-grid triode amplifier is usually given as

$$F = 1 + g_\Omega R_s + 5 g_e R_s + \left(\frac{\mu}{1+\mu}\right)^2 (1 + g_\Omega R_s + g_e R_s)^2 \frac{R_{eg}}{R_s}.$$

(See G. E. Valley and H. Wallman, "Vacuum Tube Amplifiers," McGraw-Hill Book Co., Inc., New York, N. Y., p. 634; 1948.) Since circuit losses are neglected, $g_\Omega = 0$. Since μ is much greater than unity, $\mu/1+\mu$ is approximately equal to unity. For an impedance match at the input, R_s is given by (6). Finally, R_{eg} for an oxide cathode operating at approximately 1000°K is usually taken as $2.5/g_m$. (See B. J. Thompson, D. O. North, and W. A. Harris, "Fluctuations in space-charge-limited currents at moderately high frequencies," *RCA Rev.*, vol. 4, p. 471; April, 1940; and vol. 5, p. 516; April, 1941.)

[5] This dimensionless ratio can be looked upon as an anode-to-grid current amplification factor, α_{ag}, similar to a collector-to-base current amplification factor, α_{cb}, often employed in transistors.

Introduction of Fundamental Design Parameters

Having expressed the RF performance in terms of the ratio, g_e/g_m, the next step is to express g_e/g_m in terms of the fundamental design parameters. This can readily be done with the aid of North's expression[6] for g_e/g_m in terms of the transit times, τ_1 and τ_2, in the cathode-grid and grid-anode regions, respectively, and is

$$g_e/g_m = \frac{\omega^2\tau_1^2}{180}\left(9 + 44\frac{\tau_2}{\tau_1}\right)$$

where ω is the angular frequency and second-order terms have been neglected. Using Ferris' expressions[7] for transit times in terms of the electrode spacing and effective electrode voltages, this becomes

$$\frac{g_e}{g_m} = \frac{45 \times 10^5\,(a/\lambda)^2}{V_1}\left\{1 + \frac{3.3b/a}{1 + \sqrt{V_a/V_1}}\right\}, \qquad (8)$$

where a is the cathode-grid spacing (cm), b is the grid-anode spacing (cm), V_1 is the effective grid-plane voltage (volts), V_a is the anode voltage (volts), and λ is the wavelength (cm). The following assumptions apply to this relation

"1. The electrodes are parallel planes.
2. The initial velocity of the emitted electrons is zero and the emission is ample, so the three-halves-power equation holds in the cathode-grid region.
3. The grid is an equipotential plane surface.
4. The amplification factor of the grid is high, ...
5. The alternating voltage at the plate is zero.
6. The alternating voltage at the grid is very small with respect to the effective static potential there.
7. The space-charge density in the grid-anode space is so slight that the potential distribution between grid and plate is substantially linear."[7]
8. The transit angles in both the cathode-grid and grid-anode regions are small, and second-order terms involving these transit angles may be neglected.

Under assumption (2) above the effective grid-plane voltage is given by the usual Child-Langmuir 3/2 power law,

$$V_1 = 5.69 \times 10^3\, a^{4/3} J_c^{2/3}, \qquad (9)$$

where J_c is the cathode current density (amp/cm²).

Thus, when the parameters J_c, a, b, V_a, and the wavelength are specified, g_e/g_m can be determined using (8) and (9). The noise factor, F, and the normalized maximum power gain, G_{mp}/μ, can in turn be determined from (7) and (5). To aid in the calculation of the desired quantities, the graphs of Figs. 2, 3, and 4 have been prepared. Normally, the design of a tube would begin with a choice of a, and J_c V_1 is then determined using (9) or the graph, Fig. 2. Next, b, V_a, and λ are chosen and g_e/g_m determined by means of (8) or with the aid of the graph, Fig. 3. Finally, F and G_{mp}/μ can be determined using (7) and (5) or the graph, Fig. 4.

This design procedure has thus far been carried out without detailed knowledge of the grid structure and of the tube amplification factor, μ. It is convenient to proceed with the tube design in this manner in order to

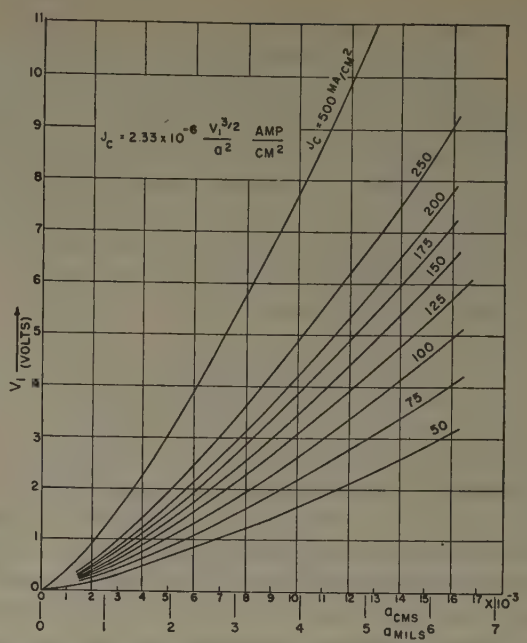

Fig. 2—Equivalent diode characteristics. J_c=cathode current density, amperes/cm², V_1=grid plane equivalent voltage, volts, and a=grid-cathode spacing, cm.

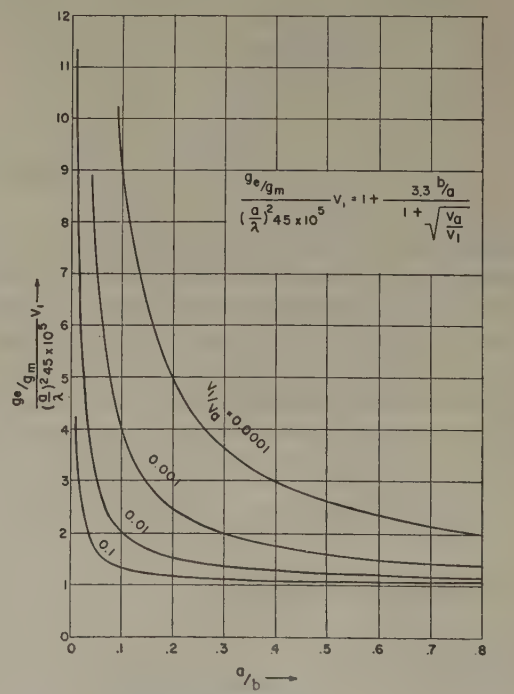

Fig. 3—Electronic grid conductance to transconductance ratio. g_e=electronic grid conductance, g_m=transconductance, V_1=grid plane equivalent voltage, volts, V_a=anode voltage, a=grid-cathode spacing, b=grid-anode spacing, and λ=operating wavelength.

[6] D. O. North, "Analysis of the effects of space charge on grid impedance," Proc. I.R.E., vol. 24, pp. 108–136; January, 1936. See North's equation (23), where it is assumed that both transit angles are small.

[7] W. R. Ferris, "Input resistance of vacuum tubes as ultra-high-frequency amplifiers," Proc. I.R.E., vol. 24, pp. 82–105; January, 1936.

simplify the development. However, if one wishes to determine the actual maximum power gain and to complete the design of the tube, detailed consideration must be given to the grid structure. There are several ways to do this. The most logical is for the tube designer to choose a power gain consistent with the application requirements. The power gain should be chosen so that the noise contribution of the succeeding stage, $(F_2-1)/G_{mp}$, is negligible compared with the over-all noise factor, F_{12}, given below:

$$F_{12} = F_1 + \frac{F_2 - 1}{G_{mp}}. \tag{10}$$

Care must be exercised in applying this relation when a wide-band RF amplifier is placed ahead of a receiver having appreciable image or other spurious responses. Even though the power gain is sufficient to make the second term of (10), negligible, the over-all receiver noise factor will not reduce to F_1 if the RF amplifier possesses gain at these undesired responses, but will be greater than F_1 due to the noise contribution of the undesired responses.

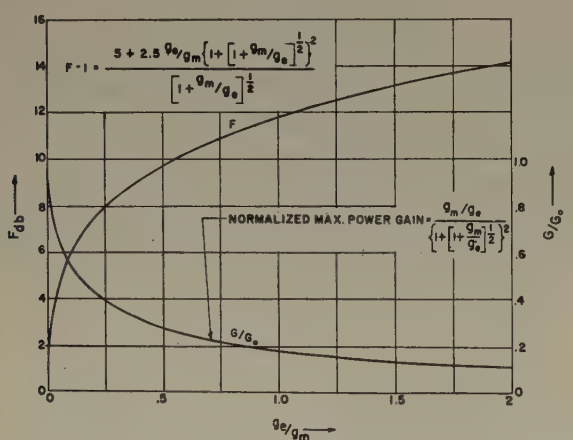

Fig. 4—Noise factor and normalized power gain.

Having selected G_{mp}, the normalized maximum power gain determines the amplification factor required. However, the resulting amplification factor may be so large that the grid draws current for the specified operating conditions. The limiting value of μ is determined by setting the control grid voltage, V_g, equal to zero in the expression[9] for the cathode current density of a triode, and is

$$\mu_{\max} = 1.76 \times 10^{-4} \frac{V_a}{J_c^{2/3} a^{4/3}} - \left(\frac{a+b}{a}\right)^{4/3} = \frac{V_a}{V_1} - \left(\frac{a+b}{a}\right)^{4/3}. \tag{11}$$

[9] The expression given by J. H. Fremlin, footnote reference 12, is

$$J_c = \frac{2.34 \times 10^{-6}\left(V_g + \frac{V_a}{\mu}\right)^{3/2}}{a^2\left[1 + \frac{1}{\mu}\left(\frac{a+b}{a}\right)^{4/3}\right]^{3/2}}.$$

The value of μ obtained from (11) should be larger than the value of μ required to give the desired power gain. If this condition is not satisfied, the design of the tube must be revised.

Next, the grid structure must be designed to give the desired μ. There are numerous formulas[10] that can be used for this purpose. A convenient empirical formula that yields reasonably good results has been given, by Herold,[11] and is

$$\mu = 2\pi N b[0.2 + 6.8Nd + 680(Nd)^5], \tag{12}$$

where N is the turns per unit length of the grid, d is the grid-wire diameter in the same units as N, and b is the grid-anode spacing also in the same units as N. For use with a mesh grid, Nd is interpreted as the fraction of the total area covered by the grid, and N is the total lineal length of exposed grid conductor per unit area of the grid. Since b has already been chosen, either N can be chosen and d determined, or vice versa, to yield the desired μ. According to Fremlin,[12] experiments indicate that if the cathode current density is held constant, the g_m of a triode is maximum when the grid-cathode spacing is approximately 3/4 of the grid pitch. Accordingly, N can be chosen as 3/4 a and d determined using (12).

The preceding development completes the basic tube design except for the cathode area. As noted above, the noise factor and power gain are independent of cathode area. The cathode area and therefore the cathode current and interelectrode capacitances are determined by bandwidth considerations provided the bandwidth required is not too large.

It is not possible to derive a simple solution for the cathode area in terms of known quantities. A suitable method of procedure is to assume a cathode area, A. The tube output capacitance, C_T, is given approximately by

$$C_T = \frac{0.0885A}{b}, \tag{13}$$

where A is in cm², b is in cm, and C_T is in micromicrofarads. For a more realistic calculation, it is well to add to C_T a fixed capacitance representing tube lead capacitance.

It is next necessary to obtain an expression for the anode resistance of a triode. The anode resistance can be determined from the transconductance since μ for the tube has already been specified. The usual expression for the transconductance of a triode obtained by differentiating the theoretical expression for anode current gives results that are considerably larger than measured values. A more exact method of evaluating the transconductance of a triode has been given by

[10] A good summary of μ equations can be found in K. R. Spangenberg, "Vacuum Tubes," McGraw-Hill Book Co., Inc., New York, N. Y., chap. 7; 1948.

[11] E. W. Herold, "Empirical formula for amplification factor," Proc. I.R.E., vol. 35, p. 493; May, 1947.

[12] J. H. Fremlin, "Calculation of triode constants," *Phil. Mag.* vol. 27, pp. 709–741; June, 1939.

Liebmann.[13] This method consists of determining the unit-area conductance to current density ratio, g_c/J_c,

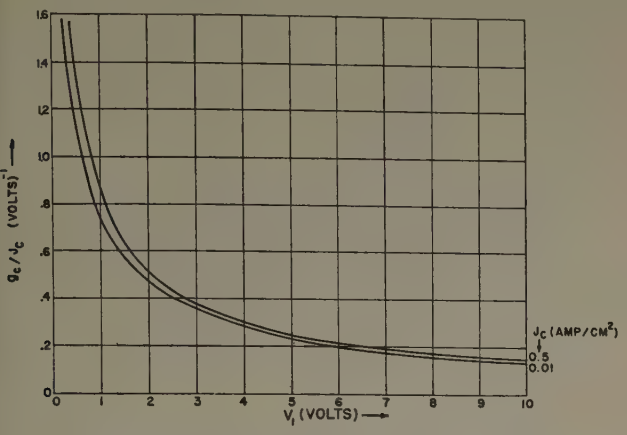

Fig. 5—Equivalent diode conductance per unit area to current density ratio.

of the equivalent diode and of correcting this ratio to give the transconductance-to-current ratio of the triode. For convenience, the data given by Liebmann is replotted in Fig. 5. In this figure, the ratio g_c/J_c of an oxide-cathode diode is given as a function of the effective grid-plane voltage (equivalent diode anode potential, V_1). It is noted that the value of g_c/J_c does not change rapidly as a function of the cathode current density. Using the appropriate value of g_c/J_c, the transconductance of the triode is[14]

$$g_m = \left.\frac{g_c}{J_c}\right|_{V_1} \frac{1}{\left[1+\frac{1}{\mu}\left(\frac{a+b}{a}\right)^{4/3}\right]} J_c A. \qquad (14)$$

Using (14), the anode resistance, r_p, of the triode can be obtained from $g_m r_p = \mu$. The output resistance, R_L, is then determined using (4). This output resistance is to be matched to another vacuum tube or similar device having an input resistance, R_T', and an input capacitance, C_T'. If a transmission line is used to effect the impedance match, the circuit configuration will be as shown in Fig. 6. For a given characteristic impedance, Z_0, the lengths of the transmission lines, l_1 and l_2, can be determined (for a given center frequency); the bandwidth at the tube terminals can then be computed, and the over-all bandwidth obtained. If the bandwidth is too small, a larger cathode area can be chosen, and the calculations repeated. These calculations should be carried out for the lowest frequency to be employed as the bandwidth increases for larger frequencies.

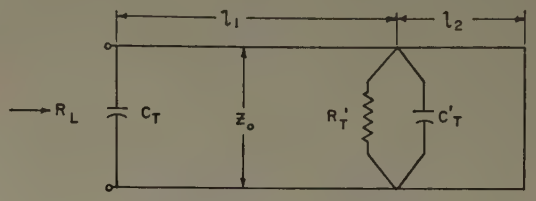

Fig. 6—Output matching circuit.

The procedure indicated above is tedious and time consuming. It is possible to shorten the calculations by making some simplifying assumptions concern-the transmission line. Usually, R_L will be much larger than R_T'. In this event, l_2 will be small and the transmission line will not differ appreciably from a short-circuited resonant line. A short-circuited resonant line can be approximated over a narrow frequency range by a parallel L_p, C_p lumped circuit where the total lumped capacitance[15] is

$$C = C_T + C_p = 1/2\left[C_T + \frac{1+(\omega Z_0 C_T)^2}{\omega Z_0}\sin^{-1}\left(\frac{1}{1+(\omega Z_0 C_T)^2}\right)^{1/2}\right]. \qquad (15)$$

The input circuit of the amplifier will normally have a large bandwidth because of the loading effect of the matched source resistance. It is assumed therefore that the amplifier bandwidth is determined solely by the output circuit. Since the output circuit is matched, the loading resistance is $R_L/2$ and the bandwidth for a single-tuned output circuit will be

$$\Delta f = \frac{1}{\pi C R_L}, \qquad (16)$$

where C is given by (15) and R_L is determined as indicated above. The bandwidth can now be computed as a function of the cathode area. When this is done, it is found that the bandwidth approaches a limiting value, Δf_{max}, as the cathode area is made larger and larger. The limiting bandwidth is obtained when the tube capacitance is the entire output capacitance. Therefore,

$$\Delta f_{max} = \frac{\left.\frac{g_c}{J_c}\right|_{V_1} J_c}{\frac{0.0885\times 10^{-12}}{b}\left[\mu+\left(\frac{a+b}{a}\right)^{4/3}\right]\left[1+\frac{g_m}{g_c}\right]}. \qquad (17)$$

This equation indicates that Δf_{max} is independent of cathode area. If the bandwidth desired exceeds Δf_{max}, a redesign of the tube is required, or alternatively, power gain can be traded for bandwidth by operating the tube with a mismatched output. Likewise, if the cathode

[13] G. Liebmann, "The Calculation of Amplifier Valve Characteristics," *Jour. IEE* (London), vol. 93, pt. III, pp. 138–152; May, 1946.

[14] The diode to triode correction factor employed here is obtained from J. H. Fremlin's formulation of an equivalent diode and differs slightly from that used by G. Liebmann.

[15] E. W. Herold and L. Malter, "Some aspects of radio reception at ultra-high frequency," PROC. I.R.E., vol. 31, p. 437; August, 1943.

area required to give the desired bandwidth is larger than can be tolerated because of cathode power requirement or anode power dissipation, a redesign of the tube is required. Unfortunately, tubes designed for larger Δf_{max} will usually have smaller power gains, greater noise factors, or both.

Computations to Illustrate the Effect of Changes in Design Parameters

It is apparent from the preceding development that there is no optimum set of parameters upon which the design of a tube can be based. The final design will depend upon a judicious compromise between desired RF performance, mechanical limitations, and practical operating conditions. In order to effect a compromise design, it is expected that several tubes will be designed and their expected characteristics compared.

The manner in which the design parameters affect the power gain and noise factor is sufficiently involved so that it is difficult to see from the expressions just how fast the RF performance varies as one of the design parameters is changed. A better understanding of this can be obtained by studying the following numerical illustrations.

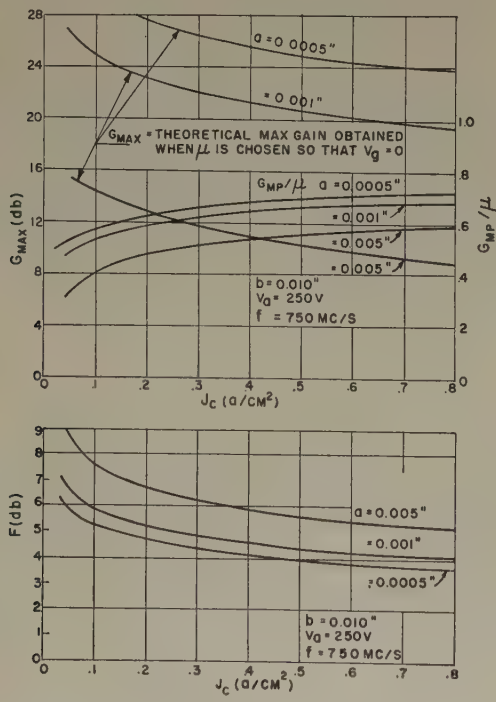

Fig. 7—Triode operating characteristics as a function of cathode current density and grid-cathode spacing.

The calculated data of Fig. 7 illustrate the effect of changing the cathode current density on the noise factor for tubes with several grid-cathode spacings. These calculated data are for a particular frequency (750 mc/s), a grid-anode spacing of 0.010 inches, and an anode voltage of 250 volts. For these chosen parameters, it is seen that for current densities above about 0.2 a/cm² the noise factor varies but slowly with increasing current density. However, at current densities below 0.2 a/cm² and particularly below 0.1 a/cm², the noise factor degrades rapidly with decreasing current density.

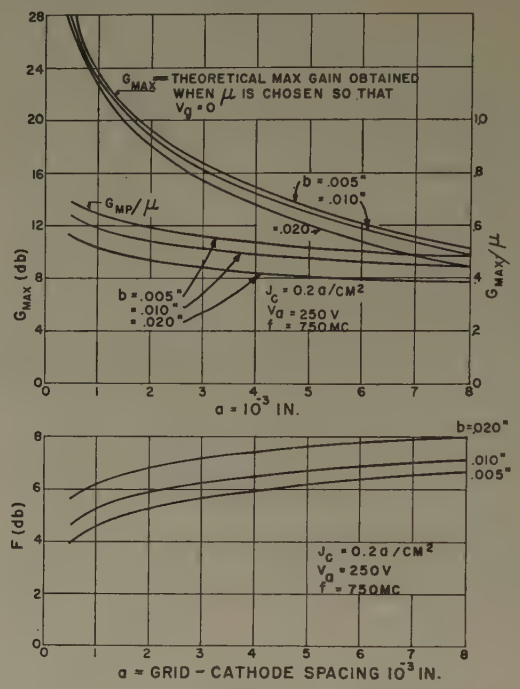

Fig. 8—Triode operating characteristics as a function of grid-cathode and grid-anode spacing.

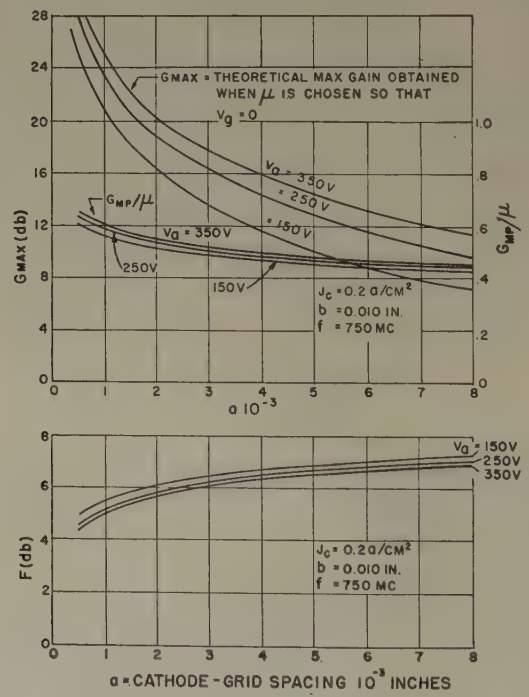

Fig. 9—Triode operating characteristics as a function of grid-cathode spacing and anode voltage.

The RF performance as a function of grid-cathode spacing for several grid-anode spacings is illustrated in Fig. 8 and for several anode voltages in Fig. 9. In both of these figures, the current density is fixed at 0.2 a/cm², and the frequency is 750 mc/s. In addition, the anode voltage is chosen as 250 volts in Fig. 8 and the grid-anode spacing is chosen as 0.010 inch in Fig. 9. Again, the noise factor does not vary particularly rapidly with a change in grid-cathode spacing, nor does a change in

grid-anode spacing or anode voltage change the noise factor rapidly. Similar statements apply to the normalized power gain G_{mp}/μ. However, the theoretical maximum power gain (μ being adjusted so that $V_g=0$) increases fairly rapidly as the grid-cathode spacing is reduced. This is because the maximum μ is correspondingly larger and indeed may be so large as to be impractical. A variation in grid-anode spacing does not radically affect the theoretical maximum power gain. A greater effect is shown by a variation in voltage.

It thus appears that, in so far as the noise performance is concerned, there is no one design parameter that produces a rapid change in the noise factor. To achieve a good noise performance, one can only adjust each of the design parameters to a limit indicated by practical constructional difficulties and economic considerations. The point to be emphasized, however, is that noise performance will not be greatly altered by a small change in only one of the design parameters, and that for the improvement to be worthwhile, one must add together the results of changes in several design parameters. Again these statements can be applied to the normalized power gain, G_{mp}/μ. However, in order to secure large absolute power gains, Figs. 8 and 9 show that a small grid-cathode spacing is required together with a suitable grid structure and grid-anode spacing to provide a large μ.

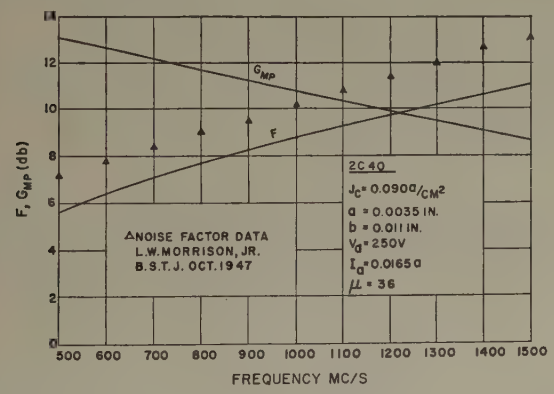

Fig. 10—Computed and measured performance of 2C40 triode.

Comparison of Calculated and Measured Results

In order to show the correlation between the above theoretical design calculations and experimental results, calculations will be made on some typical tubes and the results compared with measurements on the same tubes. The measured data available are very meager so that the only conclusion that can be reached at the moment is that the theory gives reasonably good checks with the measured data available.

A tube that has been used extensively as a grounded-grid amplifier is the 2C40. Calculations of power gain and noise factor of this tube are shown in Fig. 10. The electrode spacings and operating parameters used for these calculations are also shown on the figure. Similar calculations for the WE 416A and the RCA 5876 tubes are shown in Figs. 11 and 12, respectively. Although the RCA 5876 tube is a cylindrical tube, the theory developed herein for a planar tube has been used without correction. Such measured data as were available are shown on the figures. It is not known under what operating conditions the data on the 2C40 were taken, and in fact it is not clear whether these represent actual measured data. The data for the WE 416A and RCA 5876 were taken with the output mismatched, and this doubtlessly accounts for part of the discrepancy between computed and measured power gain.

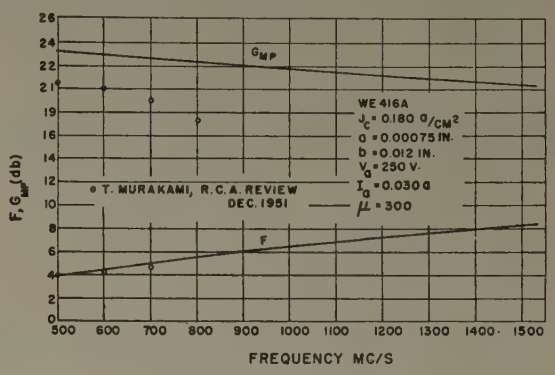

Fig. 11—Computed and measured performance of WE 416A triode.

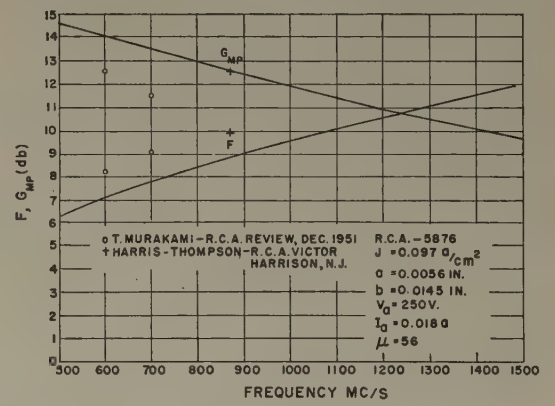

Fig. 12—Computed and measured performance of RCA 5876 triode.

Approximate bandwidth calculations were also made on these tubes, assuming a 100-ohm short-circuited resonant line. The calculations were made using measured values of tube capacitance and anode resistance. The results are shown in Fig. 13. It is seen that the present tubes (area ratio = 1) will not give a large enough bandwidth for a television signal when the output is matched. Tubes with something like twice the present cathode area are required for a television signal when operated under this condition.

Design of a Television RF Amplifier Tube

In this section, the design principles that have been outlined will be used to design a television RF amplifier tube that represents a compromise between optimum RF performance and practical manufacturing limits.

1. Choose $a=0.002$ inch $=0.00508$ cm. This represents about the minimum practical grid-cathode spacing for commercial receiver tube design.
2. Choose $J_c=0.2a/\text{cm}^2$. A larger cathode current density might be desirable, but this is about the

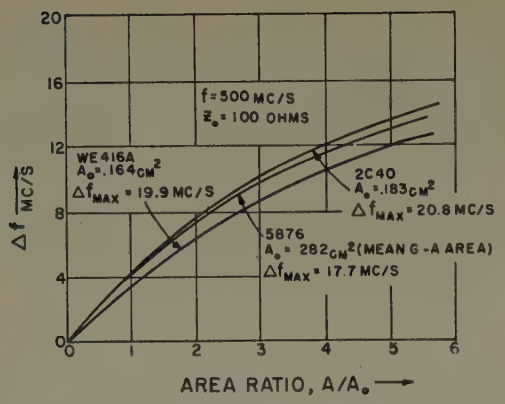

Fig. 13—Operating bandwidths as a function of area ratios. A_0=cathode area of individual commercial tube. A=cathode area of hypothetical tube.

maximum that can be used with an oxide cathode and still have a reasonable life.

3. Then, $V_1=1.67$ volts.
4. Choose $V_a=250$ volts. From past usage, this is about the maximum voltage that is employed in receivers.
5. For maximum g_m, $N=\frac{3}{4}\times 1/a=375$ turns/inch. This grid pitch is somewhat larger than what might be considered practical for commercial receiver tube usage, particularly because the grid wire diameter would then be prohibitively small. Therefore, pic, $N=250$ turns/inch rather arbitrarily and accept a small loss in g_m.
6. A grid-wire diameter should be chosen to give from 10- to 20-per cent coverage. For 10-per cent coverage the grid-wire diameter would be 0.0004 inch. This small size is beyond commercial practicability. A grid-wire diameter of 0.0008 inch representing 20-per cent coverage is near the commercially practical limit. For this grid-wire diameter, $\mu=2795b$. This can be equated to the maximum permissible μ to give $b_{max}=0.036$ inch. In order to provide for a small grid bias, choose $b=0.025$ inch. Then $\mu=70$ and $V_g=-1.1$ volt.
7. $g_c/g_m=0.318\times 10^{-6}\times f_{mc}^2$.
8. Noise factor and power gain as a function of frequency are shown in Fig. 14.
9. Using Fig. 5, $g_c/J_c=0.57$. Therefore, $g_m=0.0781A$, $r_p=897/A$. At 500 mc/s, $R_L=3310\ (1/A)$. Allowing 0.75 $\mu\mu$fd for lead capacitance, the anode-grid capacitance is $C_{a-g}=0.75+1.392A$ $\mu\mu$fd. Using the approximations indicated above and assuming an output line impedance, $Z_0=100$ ohms, then a few trials indicate that a cathode area, $A=0.17$ cm², will give approximately 6 mc/s bandwidth at 500 mc/s. This cathode area will be used for all calculations indicated below.
10. $C_{c-g}=2.96$ $\mu\mu$fd.
11. $C_{a-g}=0.75+0.25=1.00$ $\mu\mu$fd.
12. $I_a=34$ ma. $P_a=8.5$ watts.
13. $g_m=13.28$ ma/v.

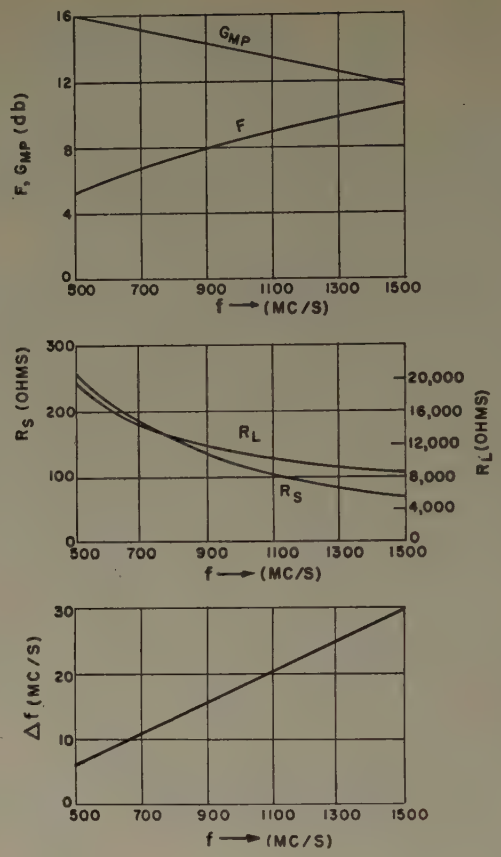

Fig. 14—Computed performance of hypothetical uhf television triode.

14. $r_p=5{,}280$ ohms.
15. R_s, R_L, and Δf as a function of frequency are shown in Fig. 14.

Conclusions

The RF performance of a grounded-grid uhf amplifier has been related to the tube-operating parameters and electrode spacings. Using the design information provided, the design of a tube can be carried out step-by-step, and its RF performance predicted. The noise factor and "normalized" power gain (G/μ) depend only on the ratio (g_e/g_m) of the electronic input conductance to the transconductance, i.e., on the electron transit angles, and are independent of cathode area. For this reason, the noise factor may be improved only by a decrease in transit angles; this is possible either by decreased spacings for the same effective electrode potentials or by increased electrode potentials for the same spacings. Either change requires an increase in cathode current density, but the same reduction in g_e/g_m can be effected by a smaller increase in current density if the grid-cathode spacing is decreased than if the voltage is increased.

Although sufficient experimental data available to evaluate the reliability of the theoretical results, there is every reason to believe that the theoretical performance can serve as a good guide for the design work. This should make it possible to reduce the amount of experimental work required to achieve a desired performance.

On Transformations of Linear Active Networks with Applications at Ultra-High Frequencies*

H. HSU†, ASSOCIATE, IRE

Summary—**A relation similar to the familiar Star-Delta transformation is developed for linear active networks. Transformation formulas are derived for triode circuits under both negative-grid and positive-grid conditions. The result can be extended to tetrodes and pentodes. Applications of the analysis to vacuum tubes and circuits are given for illustration, with special considerations to uhf problems.**

Part I. Theory

I. Introduction

A RELATION similar in nature to the familiar Star-Delta or Wye-Delta transformation is pointed out. This relation is believed to be helpful for the analysis of vacuum tubes and circuits.

Three types of the triode Star-Delta transformations are treated in detail in this paper. As shown in Figs. 1 to 3, a triode appears in all the Star-Delta circuits. In the Star-circuits, the triode electrode common to the input and output circuits is seen to be not grounded. This common electrode becomes grounded in their equivalent Delta networks which are the conventional grounded-grid, grounded-cathode, or grounded-plate (or cathode-follower) circuits. The Star-Delta circuits are, however, identical irrespective of the ground connections. Furthermore, the triode is taken here only as a typical linear active element which may be actually, for example, a transistor or a magnetic amplifier. The transformations are not limited to triode networks. The method can be generalized to Star and Delta circuits with a tetrode or pentode in the circuit. The triode case is however more fundamental for practical use, and therefore deserves special attention.

II. Transformations for Negative-Grid Triodes

There are three kinds of star networks depending upon whether the grid, cathode, or plate is connected to the common junction. Accordingly, there can be three types of transformations which, in this paper, are called "common-grid," "common-cathode," and "common-plate" transformations as in Figs. 1 to 3.

In the following sections the three types of transformations are analyzed separately. The constant current generator representation[1] of the vacuum tube is used for the convenience of the analysis. The plate resistance which should be connected in parallel with the constant-current generator is not shown in any of Figs. 1 to 3. The effect of the plate resistance can always be included in Y_{pk} and added to Y_{pk}' directly. Therefore, there is no loss of generality regarding the omission of the plate resistance, e.g., in Fig. 1.

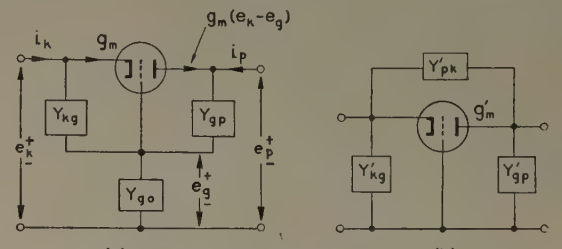

Fig. 1—Common grid transformation. (a) Star connection. (b) Delta connection.

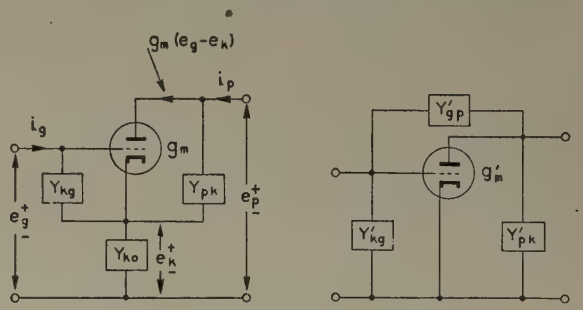

Fig. 2—Common cathode transformation. (a) Star connection. (b) Delta connection.

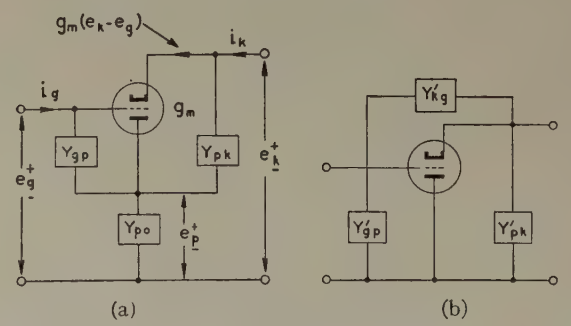

Fig. 3—Common plate transformation. (a) Star connection. (b) Delta connection.

A. Common-Grid Transformation. Referring to Fig. 1(a), we get

$$i_k = e_k(g_m + Y_{kg}) - e_g(g_m + Y_{kg}) \tag{1}$$

$$i_p = e_k(-g_m) + e_g(g_m - Y_{gp}) + e_p(Y_{gp}), \tag{2}$$

and, at the junction,

$$0 = -Y_{kg}e_k + (Y_{g0} + Y_{kg} + Y_{gp})e_g - Y_{gp}e_p \tag{3}$$

* Decimal classification: R139.1×R143. Original manuscript received by the Institute, November 3, 1952.

† General Electric Co., Owensboro, Ky.

[1] F. E. Terman, "Radio Engineer's Handbook," McGraw-Hill Book Co., Inc., New York, N. Y., p. 354; 1943.

or

$$e_g = (Y_{kg}e_k + Y_{gp}e_p)/\sum Y_g, \tag{3a}$$

where

$$\sum Y_g = Y_{g0} + Y_{kg} + Y_{gp}. \tag{4}$$

Eliminating e_g by substituting (3a) into (1) and (2), we have

$$i_k = Y_k{}^k e_k + Y_p{}^k e_p \tag{5}$$

$$i_p = Y_k{}^p e_k + Y_p{}^p e_p, \tag{6}$$

or, by means of the matrix algebra,

$$\begin{Bmatrix} i_k \\ i_p \end{Bmatrix} = \begin{Vmatrix} Y_k{}^k & Y_p{}^k \\ Y_k{}^p & Y_p{}^p \end{Vmatrix} \cdot \begin{Bmatrix} e_k \\ e_p \end{Bmatrix} \equiv \|Y_g\| \cdot \begin{Bmatrix} e_k \\ e_p \end{Bmatrix}. \tag{7}$$

$\|Y_g\|$ is used as an abbreviation of the admittance matrix, and

$$Y_k{}^k = g_m + Y_{kg} - (g_m + Y_{kg}) \cdot Y_{kg}/\sum Y_g \tag{7a}$$

$$Y_p{}^k = -(g_m + Y_{kg}) \cdot Y_{gp}/\sum Y_g \tag{7b}$$

$$Y_k{}^p = -g_m + (g_m - Y_{gp}) \cdot Y_{kg}/\sum Y_g \tag{7c}$$

$$Y_p{}^p = Y_{gp} + (g_m - Y_{gp}) \cdot Y_{gp}/\sum Y_g. \tag{7d}$$

The admittance matrix in (7) can be expanded as follows:

$$\|Y_g\| = \begin{Vmatrix} g_m & 0 \\ -g_m & 0 \end{Vmatrix} + \begin{Vmatrix} Y_{kg} & 0 \\ 0 & 0 \end{Vmatrix} + \begin{Vmatrix} 0 & 0 \\ 0 & Y_{gp} \end{Vmatrix}$$

(1st) (2nd) (3rd)

$$- (Y_{kg} + Y_{gp})/\sum Y_g \cdot \begin{Vmatrix} g_m & 0 \\ -g_m & 0 \end{Vmatrix}$$

(4th)

$$- (Y_{kg} + Y_{gp})/\sum Y_g \cdot \begin{Vmatrix} Y_{kg} & 0 \\ 0 & 0 \end{Vmatrix}$$

(5th)

$$- (Y_{kg} + Y_{gp})/\sum Y_g \cdot \begin{Vmatrix} 0 & 0 \\ 0 & Y_{gp} \end{Vmatrix}$$

(6th)

$$+ (g_m + Y_{kg}) \cdot Y_{gp}/\sum Y_g \cdot \begin{Vmatrix} 1 & -1 \\ -1 & 1 \end{Vmatrix}, \tag{8}$$

(7th)

and, by combining the matrices of similar nature,

$$\|Y_g\| = \begin{Vmatrix} g_m' & 0 \\ -g_m' & 0 \end{Vmatrix} + \begin{Vmatrix} Y_{kg}' & 0 \\ 0 & 0 \end{Vmatrix} + \begin{Vmatrix} 0 & 0 \\ 0 & Y_{gp}' \end{Vmatrix} + \begin{Vmatrix} Y_{pk}' & -Y_{pk}' \\ -Y_{pk}' & Y_{pk}' \end{Vmatrix}, \tag{9}$$

where

$$g_m'/g_m = Y_{kg}'/Y_{kg} = Y_{gp}'/Y_{gp} = Y_{g0}/\sum Y_g \tag{10}$$

and

$$Y_{pk}' = (g_m + Y_{kg}) \cdot Y_{gp}/\sum Y_g. \tag{11}$$

From (8) and (9), the equivalent circuit of the Delta type can be identified and constructed because each matrix corresponds to one branch of the Delta circuit (Fig. 1(b)).

Thus the first three terms in (8) represent an ideal grounded-grid amplifier with no feedback coupling. This is also the case for the first three terms in (9). When Y_{g0} is infinite, i.e., short-circuited, they are identical with each other. The effect of a finite Y_{g0} on g_m is indicated by the fourth term of (8), similarly for Y_{kg} in the fifth term and likewise Y_{gp} in the sixth term and finally for Y_{pk} in the seventh term. The presence of Y_{g0} thus effectively changes the transconductance of the tube, the input and output loadings, and the feedback coupling.

Since (9) indicates an equivalent Delta circuit as Fig. 1(b), (10) and (11) are the conditions of the Star-Delta transformation for the common-grid networks. The transformation formulas derived from (10) and (11) are

Common-Grid Star-Delta Transformation

$$g_m' = g_m Y_{g0}/\sum Y_g \tag{12}$$

$$Y_{kg}' = Y_{kg} Y_{g0}/\sum Y_g \tag{13}$$

$$Y_{gp}' = Y_{gp} Y_{g0}/\sum Y_g \tag{14}$$

$$Y_{pk}' = Y_{gp}(g_m + Y_{kg})/\sum Y_g, \tag{15}$$

where

$$\sum Y_g = Y_{g0} + Y_{kg} + Y_{gp}. \tag{4}$$

Common-Grid Delta-Star Transformation

$$g_m = g_m'(\sum Y'Y')_g/[Y_{gp}'(g_m' + Y_{kg}')] \tag{16}$$

$$Y_{kg} = Y_{kg}'(\sum Y'Y')_g/[Y_{gp}'(g_m' + Y_{kg}')] \tag{17}$$

$$Y_{gp} = (\sum Y'Y')_g/(g_m' + Y_{kg}') \tag{18}$$

$$Y_{g0} = (\sum Y'Y')_g/Y_{pk}', \tag{19}$$

where

$$(\sum Y'Y')g = Y_{kg}'Y_{gp}' + Y_{gp}'Y_{pk}' + Y_{pk}'Y_{kg}' + g_m'Y_{gp}'. \tag{20}$$

It is interesting to see that g_m appears in the fourth and seventh terms of (8) and also in the above transformation formulas. Being a direct consequence of the presence of the vacuum tube, this indicates the marked difference from the Star-Delta transformation of the passive circuits.

B. Common-Cathode Transformation. Referring to Fig. 2(a), we get

$$i_g = Y_{kg}e_g - Y_{kg}e_k \tag{21}$$

$$i_p = g_m e_g - (g_m + Y_{pk})e_k + Y_{pk}e_p \tag{22}$$

and

$$e_k = [(Y_{kg} + g_m)e_g + Y_{pk}e_p]/\sum Y_k, \quad (23)$$

where

$$\sum Y_k = g_m + Y_{k0} + Y_{kg} + Y_{pk}. \quad (24)$$

By eliminating e_k in (21) to (23), the admittance matrix $\|Y_k\|$ can be obtained and expanded as follows:

$$\begin{aligned}\|Y_k\| = &\begin{Vmatrix} Y_{kg} & 0 \\ 0 & 0 \end{Vmatrix} + \begin{Vmatrix} 0 & 0 \\ 0 & Y_{pk} \end{Vmatrix} + \begin{Vmatrix} 0 & 0 \\ g_m & 0 \end{Vmatrix} \\ &+ Y_{kg}Y_{pk}/\sum Y_k \cdot \begin{Vmatrix} 1 & -1 \\ -1 & 1 \end{Vmatrix} \\ &- (Y_{kg} + g_m + Y_{pk})/\sum Y_k \cdot \begin{Vmatrix} Y_{kg} & 0 \\ 0 & 0 \end{Vmatrix} \\ &- (Y_{kg} + g_m + Y_{pk})/\sum Y_k \cdot \begin{Vmatrix} 0 & 0 \\ 0 & Y_{pk} \end{Vmatrix} \\ &- (Y_{kg} + g_m + Y_{pk})/\sum Y_k \cdot \begin{Vmatrix} 0 & 0 \\ g_m & 0 \end{Vmatrix}. \end{aligned} \quad (25)$$

On the other hand, from Fig. 2(b), we have

$$\begin{aligned}\|Y_k\| = &\begin{Vmatrix} Y_{kg}' & 0 \\ 0 & 0 \end{Vmatrix} + \begin{Vmatrix} 0 & 0 \\ 0 & Y_{pk}' \end{Vmatrix} + \begin{Vmatrix} 0 & 0 \\ g_m' & 0 \end{Vmatrix} \\ &+ \begin{Vmatrix} Y_{gp}' & -Y_{gp}' \\ -Y_{gp}' & Y_{gp}' \end{Vmatrix}. \end{aligned} \quad (26)$$

By equating the corresponding matrices in (25) and (26), the following transformation formulas are obtained:

Common-Cathode Star-Delta Transformation

$$g_m' = g_m Y_{k0}/\sum Y_k \quad (27)$$
$$Y_{kg}' = Y_{kg}Y_{k0}/\sum Y_k \quad (28)$$
$$Y_{gp}' = Y_{pk}Y_{kg}/\sum Y_k \quad (29)$$
$$Y_{pk}' = Y_{pk}Y_{k0}/\sum Y_k, \quad (30)$$

where

$$\sum Y_k = g_m + Y_{k0} + Y_{kg} + Y_{pk}. \quad (24)$$

Common-Cathode Delta-Star Transformation

$$g_m = g_m'(\sum Y'Y')_k/Y_{kg}'Y_{pk}' \quad (31)$$
$$Y_{kg} = (\sum Y'Y')_k/Y_{pk}' \quad (32)$$
$$Y_{pk} = (\sum Y'Y')_k/Y_{kg}' \quad (33)$$
$$Y_{k0} = (\sum Y'Y')_k/Y_{gp}', \quad (34)$$

where

$$\begin{aligned}(\sum Y'Y')_k = &\ Y_{kg}'Y_{gp}' + Y_{gp}'Y_{pk}' \\ &+ Y_{pk}'Y_{kg}' + g_m'Y_{gp}'. \end{aligned} \quad (35)$$

C. Common-Plate Transformation. From the common-plate star circuit in Fig. 3(a), we get

$$i_g = Y_{gp}e_g - Y_{gp}e_p \quad (36)$$
$$i_k = -g_m e_g + (g_m + Y_{pk})e_k - Y_{pk}e_p \quad (37)$$

and

$$e_p = [(Y_{gp} - g_m)e_g + (g_m + Y_{pk})e_k]/\sum Y_p, \quad (38)$$

where

$$\sum Y_p = Y_{gp} + Y_{pk} + Y_{p0}. \quad (39)$$

By eliminating e_p, the admittance matrix $\|Y_p\|$ can be obtained and expanded as

$$\begin{aligned}\|Y_p\| = &\begin{Vmatrix} Y_{gp} & 0 \\ 0 & 0 \end{Vmatrix} + \begin{Vmatrix} 0 & 0 \\ 0 & Y_{pk} \end{Vmatrix} + \begin{Vmatrix} 0 & 0 \\ -g_m & g_m \end{Vmatrix} \\ &+ Y_{gp}(Y_{pk} + g_m)/\sum Y_p \cdot \begin{Vmatrix} 1 & -1 \\ -1 & 1 \end{Vmatrix} \\ &- (Y_{pk} + Y_{gp})/\sum Y_p \cdot \begin{Vmatrix} Y_{gp} & 0 \\ 0 & 0 \end{Vmatrix} \\ &- (Y_{pk} + Y_{gp})/\sum Y_p \cdot \begin{Vmatrix} 0 & 0 \\ 0 & Y_{pk} \end{Vmatrix} \\ &- (Y_{pk} + Y_{gp})/\sum Y_p \cdot \begin{Vmatrix} 0 & 0 \\ -g_m & g_m \end{Vmatrix}. \end{aligned} \quad (40)$$

The admittance matrix obtained from Fig. 3(b) is

$$\begin{aligned}\|Y_p\| = &\begin{Vmatrix} Y_{gp}' & 0 \\ 0 & 0 \end{Vmatrix} + \begin{Vmatrix} 0 & 0 \\ 0 & Y_{pk}' \end{Vmatrix} + \begin{Vmatrix} 0 & 0 \\ -g_m' & g_m' \end{Vmatrix} \\ &+ \begin{Vmatrix} Y_{kg}' & -Y_{kg}' \\ -Y_{kg}' & Y_{kg}' \end{Vmatrix}. \end{aligned} \quad (41)$$

By equating the corresponding matrices in (40) and (41), the following transformation formulas are obtained:

Common-Plate Star-Delta Transformation

$$g_m' = g_m Y_{p0}/\sum Y_p \quad (42)$$
$$Y_{kg}' = Y_{gp}(g_m + Y_{pk})/\sum Y_p \quad (43)$$
$$Y_{gp}' = Y_{gp}Y_{p0}/\sum Y_p \quad (44)$$
$$Y_{pk}' = Y_{pk}Y_{p0}/\sum Y_p, \quad (45)$$

where

$$\sum Y_p = Y_{p0} + Y_{gp} + Y_{pk}. \quad (39)$$

Common-Plate Delta-Star Transformation

$$g_m = g_m'(\sum Y'Y')_p/[Y_{gp}'(g_m' + Y_{pk}')] \quad (46)$$
$$Y_{gp} = (\sum Y'Y')_p/(g_m' + Y_{pk}') \quad (47)$$
$$Y_{pk} = Y_{pk}'(\sum Y'Y')_p/[Y_{gp}'(g_m' + Y_{pk}')] \quad (48)$$
$$Y_{p0} = (\sum Y'Y')_p/Y_{kg}', \quad (49)$$

where

$$\begin{aligned}(\sum Y'Y')_p = &\ Y_{kg}'Y_{gp}' + Y_{gp}'Y_{pk}' \\ &+ Y_{pk}'Y_{kg}' + g_m'Y_{gp}'. \end{aligned} \quad (50)$$

D. Analogue Between Transformations of Active and Passive Networks. For the convenience of comparison, a generalized form of the Star-Delta circuits is shown in Fig. 4. The connection of the triode is not specified.

Thus, Fig. 4 may represent Fig. 1, 2, or 3, depending upon the actual connections of the triode electrodes. The three types of triode connections are distinguished by defining the following symbols for g_m and g_m' of the respective types. Thus

$g_g, g_k, g_p = g_m$ of the common-grid, common-cathode, and common-plate star networks, respectively

$g_g', g_k', g_p' = g_m'$ of the common-grid, common-cathode, and common-plate delta networks, respectively.

The above notation implies the following conditions: For common-grid connection,

$$g_m = g_g, \quad g_m' = g_g' \tag{51}$$

$$y_k = g_p = g_k' = g_p' = 0. \tag{51a}$$

For common-cathode connection,

$$g_m = g_k, \quad g_m' = g_k' \tag{52}$$

$$g_g = g_p = g_g' = g_p' = 0. \tag{52a}$$

For common-plate connection,

$$g_m = g_p, \quad g_m' = g_p' \tag{53}$$

$$g_g = g_k = g_g' = g_k' = 0. \tag{53a}$$

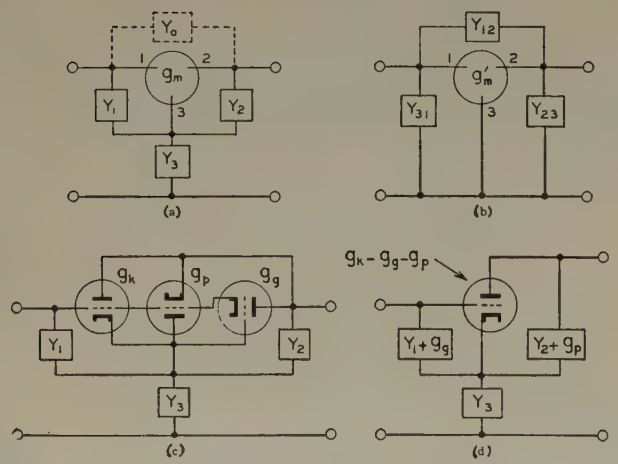

Fig. 4—General triode transformation. (a) Star connection. (b) Delta connection. (c) Equivalent star. (d) Transformed star.

By using the above notation and the symbols in Fig. 4, the three types of transformations can be combined into one set of formulas which become identical with the previous forms under the respective conditions of (51) to (53). Thus,

General Star-Delta Transformation

$$g_m' = g_m Y_3 / \sum Y \tag{54}$$

$$Y_{12} = (Y_1 + g_g)(Y_2 + g_p)/\sum Y \tag{55}$$

$$Y_{23} = Y_2 Y_3 / \sum Y \tag{56}$$

$$Y_{31} = Y_3 Y_1 / \sum Y, \tag{57}$$

where

$$\sum Y = (g_k + Y_1) + Y_2 + Y_3. \tag{58}$$

General Delta-Star Transformation

$$g_m = g_m' \sum YY / [(Y_{23} + g_p')(Y_{31} + g_g')] \tag{59}$$

$$Y_1 = Y_{31} \sum YY / [(Y_{23} + g_p')(Y_{31} + g_g')] \tag{60}$$

$$Y_2 = Y_{23} \sum YY / [(Y_{23} + g_p')(Y_{31} + g_g')] \tag{61}$$

$$Y_3 = \sum YY / Y_{12}, \tag{62}$$

where

$$\sum YY = Y_{12}(g_k' + Y_{31}) + (Y_{31} + g_g')(Y_{23} + g_p') + Y_{23}Y_{12}. \tag{63}$$

In the special case when the triode is absent or nonconducting, i.e.,

$$g_m = g_g = g_k = g_p = 0 \tag{64}$$

$$g_m' = g_g' = g_k' = g_p' = 0, \tag{64a}$$

(54) to (63) reduce to the familiar Star-Delta formulas for passive circuits as expected. A marked analogue between the passive case and the active case can be observed for the common-cathode transformations by substituting (52) and (52a) into (54) to (62).

As far as the analogue relations are concerned, it is interesting to consider the common-cathode transformation as a basic representation. The other two cases can be derived by effectively transforming the tube itself to the equivalent common-cathode connection, or vice versa. To indicate the process, only the transconductance matrices of the three types need to be considered. They are

$$\begin{Vmatrix} 0 & 0 \\ g_m & 0 \end{Vmatrix} \quad \text{for common-cathode}$$

$$\begin{Vmatrix} g_m & 0 \\ -g_m & 0 \end{Vmatrix} \quad \text{for common-grid}$$

$$\begin{Vmatrix} 0 & 0 \\ -g_m & g_m \end{Vmatrix} \quad \text{for common-plate}$$

since

$$\begin{Vmatrix} g_m & 0 \\ -g_m & 0 \end{Vmatrix} = \begin{Vmatrix} g_m & 0 \\ 0 & 0 \end{Vmatrix} + \begin{Vmatrix} 0 & 0 \\ -g_m & 0 \end{Vmatrix}, \tag{65}$$

and

$$\begin{Vmatrix} 0 & 0 \\ -g_m & g_m \end{Vmatrix} = \begin{Vmatrix} 0 & 0 \\ 0 & g_m \end{Vmatrix} + \begin{Vmatrix} 0 & 0 \\ -g_m & 0 \end{Vmatrix}. \tag{66}$$

The common-grid tube of transconductance g_m is thus equivalent to a common-cathode tube of transconductance $-g_m$ and an extra input admittance of the amount g_m between the grid and cathode. Similarly, for the common-plate tube its equivalent common-cathode transconductance is also $-g_m$, but the extra admittance of g_m is at the output side between the plate and cathode. These extra admittances give a clear indication of the impedance transformation characteristics for the grounded-grid and grounded-plate amplifiers. They also help to explain the appearance of g_g, g_g', and g_p, g_p' in (55) and (59) to (63). In fact, Fig. 4(a) can be redrawn

as Figs. 4(c) and (d). Then by applying (27) to (35), (54) to (63) can be verified.

The presence of g_k and g_k' in (58) and (63) can also be explained by the following identity:

$$\begin{Vmatrix} 0 & 0 \\ g_k & 0 \end{Vmatrix} \cdot \begin{Bmatrix} e_1 \\ e_2 \end{Bmatrix} = \begin{Vmatrix} g_k & 0 \\ 0 & 0 \end{Vmatrix} \cdot \begin{Bmatrix} e_1 \\ e_2 \end{Bmatrix} + \frac{g_k e_1}{e_2 - e_1} \cdot \begin{Vmatrix} 1 & -1 \\ -1 & 1 \end{Vmatrix} \cdot \begin{Bmatrix} e_1 \\ e_2 \end{Bmatrix}. \quad (67)$$

Equation (67) indicates a remarkable characteristic in that an active element of g_k can be represented by an extra admittance g_k across the input and a "pseudo" passive coupling admittance which can be handled as if it were passive. This interesting relation was observed and reported in a similar form by Keen.[2] Now, the extra admittances g_k and g_k' are added to the admittances Y_1 and Y_{31}, respectively, because they are in parallel connection.

In (54) to (63), the idea of considering g_m and g_m' as extra admittances is indicated by the parentheses which factor out g_m and g_m' with their respective correlated admittances.

By applying (67), the active Star-Delta circuits can both be expressed by pseudo-passive circuits. In this way, the transformation formulas for the common cathode circuit can actually be verified by applying the familiar Star-Delta formulas for passive networks. It is, however, difficult to detect the transformation relations. The matrix method is still far more clear and straightforward.

In Fig. 4(a), a coupling admittance Y_0 is shown by dotted lines. If Y_0 is present, (55) becomes

$$Y_{12} = Y_0 + (Y_1 + g_g)(Y_2 + g_p)/\sum Y. \quad (68)$$

Equation (68) is sometimes useful because it gives the total feedback coupling of the complete circuit.

III. Transformations for Positive-Grid Triodes

The previous analysis for negative-grid triodes can be generalized to positive-grid triodes provided the operation is linear.

Let g_n be the inverse (or reflex) transconductance. Then, using the symbols in Fig. 4 and the constant-current generator representation for a positive-grid triode,[3] (21) to (24) for the common-cathode case become

$$i_g = Y_1 e_g - (g_n + Y_1)e_k + g_n e_p \quad (69)$$

$$i_p = g_m e_g - (g_m + Y_2)e_k + Y_2 e_p \quad (70)$$

and

$$e_k = [(g_m + Y_1)e_g + (g_n + Y_2)e_p]/\sum Y, \quad (71)$$

where

$$\sum Y = g_m + g_n + Y_1 + Y_2 + Y_3. \quad (72)$$

In the above equations, the effects of the grid and plate resistances are supposed to be included in Y_1 and Y_2, respectively. By eliminating e_k in (69) to (71), the admittance matrix becomes

$$\|Y_k\| = \begin{Vmatrix} [Y_1(Y_2 + Y_3) - g_m g_n]/\sum Y, & [g_n(g_m + Y_3) - Y_1 Y_2]/\sum Y \\ [g_m(g_n + Y_3) - Y_1 Y_2]/\sum Y, & [Y_2(Y_1 + Y_3) - g_m g_n]/\sum Y \end{Vmatrix}. \quad (73)$$

Equation (73) can be expanded as

$$\|Y_k\| = Y_1 Y_3/\sum Y \cdot \begin{Vmatrix} 1 & 0 \\ 0 & 0 \end{Vmatrix} + Y_2 Y_3/\sum Y \cdot \begin{Vmatrix} 0 & 0 \\ 0 & 1 \end{Vmatrix} + g_m Y_3/\sum Y \cdot \begin{Vmatrix} 0 & 0 \\ 1 & 0 \end{Vmatrix} + g_n Y_3/\sum Y \cdot \begin{Vmatrix} 0 & 1 \\ 0 & 0 \end{Vmatrix} + (Y_1 Y_2 - g_m g_n)/\sum Y \cdot \begin{Vmatrix} 1 & -1 \\ -1 & 1 \end{Vmatrix}. \quad (74)$$

The Delta circuit can then be identified from (74). Thus, we get

Common-Cathode Star-Delta Transformation

$$g_m' = g_m Y_3/\sum Y \quad (75)$$

$$g_n' = g_n Y_3/\sum Y \quad (76)$$

$$Y_{12} = (Y_1 Y_2 - g_m g_n)/\sum Y \quad (77)$$

$$Y_{23} = Y_2 Y_3/\sum Y \quad (78)$$

$$Y_{31} = Y_3 Y_1/\sum Y. \quad (79)$$

Now, by applying the circuit transformations obtnedai from (65) and (66) for g_m and the similar relations for g_n, i.e., for common-grid circuit

$$\begin{Vmatrix} g_n & -g_n \\ 0 & 0 \end{Vmatrix} = \begin{Vmatrix} g_n & 0 \\ 0 & 0 \end{Vmatrix} + \begin{Vmatrix} 0 & -g_n \\ 0 & 0 \end{Vmatrix} \quad (65a)$$

and for common-plate circuit

$$\begin{Vmatrix} 0 & -g_n \\ 0 & g_n \end{Vmatrix} = \begin{Vmatrix} 0 & 0 \\ 0 & g_n \end{Vmatrix} + \begin{Vmatrix} 0 & -g_n \\ 0 & 0 \end{Vmatrix}, \quad (66a)$$

the common-grid and common-plate transformations can also be obtained. They can be combined into a generalized form,

General Star-Delta Transformation

$$g_m' = g_m Y_3/\sum Y \quad (80)$$

$$g_n' = g_n Y_3/\sum Y \quad (81)$$

$$Y_{12} = [(Y_1 + g_g + g_h)(Y_2 + g_p + g_q) - g_m g_n]/\sum Y \quad (82)$$

$$Y_{23} = Y_2 Y_3/\sum Y \quad (83)$$

$$Y_{31} = Y_3 Y_1/\sum Y, \quad (84)$$

[2] A. W. Keen, "Triode transmission networks," *Wireless Eng.*, pp. 56–66; February, 1951.

[3] E. L. Chaffee, "Theory of Thermionic Vacuum Tubes," McGraw-Hill Co., Inc., New York, N. Y., p. 200; 1933.

where

$$\sum Y = g_k + g_l + Y_1 + Y_2 + Y_3. \tag{85}$$

In the above equations, the notations in (51) to (53) are again used, but extended to include g_n so that

For Common-Cathode Connection

$$g_m = g_k, \qquad g_n = g_l \tag{86}$$

$$g_g = g_h = g_p = g_q = 0. \tag{86a}$$

For Common-Grid Connection

$$g_m = g_g, \qquad g_n = g_h \tag{87}$$

$$g_k = g_l = g_p = g_q = 0. \tag{87a}$$

For Common-Plate Connection

$$g_m = g_p, \qquad g_n = g_q. \tag{88}$$

$$g_k = g_l = g_g = g_h = 0. \tag{88a}$$

Naturally (80) to (85) become identical to (54) to (58) when g_n vanishes.

The common-cathode transformation of (75) to (79) can again be verified from the familiar Star-Delta formulas for passive circuits by the idea expressed in (67). Nevertheless, as can be observed from (73) and (74), the above transformation is not the only solution. Various other Delta circuits can be obtained by expanding (73) into different forms. From (73) itself, for example, a Delta circuit can be obtained as

$$g_m' = [g_m(g_n + Y_3) - Y_1Y_2]/\sum Y \tag{89}$$

$$g_n' = [g_n(g_m + Y_3) - Y_1Y_2]/\sum Y \tag{90}$$

$$Y_{12} = 0 \tag{91}$$

$$Y_{23} = [Y_2(Y_1 + Y_3) - g_mg_n]/\sum Y \tag{92}$$

$$Y_{31} = [Y_1(Y_2 + Y_3) - g_mg_n]/\sum Y. \tag{93}$$

Equations (89) to (93) can be considered as representing particular type of Delta circuit having no Y_{12}. Similarly, other forms of equivalent Delta circuits can be obtained by arbitrarily setting a value for one of the five admittances, i.e., g_m, g_n, Y_{12}, Y_{23}, or Y_{31}. This value may be zero, but may also be any other values, positive or negative. The reason for this uncertainty is that the five admittances are actually determined by only four equations corresponding to the conditions given by the four elements of the matrix of (73). As an example, a Delta circuit can be formed from (73) so that Y_{31} is zero, i.e.,

$$g_m' = Y_3(g_m + Y_1)/\sum Y \tag{94}$$

$$g_n' = Y_3(g_n + Y_1)/\sum Y \tag{95}$$

$$Y_{12} = [Y_1(Y_2 + Y_3) - g_mg_n]/\sum Y \tag{96}$$

$$Y_{23} = Y_3(Y_2 - Y_1)/\sum Y \tag{97}$$

$$Y_{31} = 0. \tag{98}$$

Similarly, by setting Y_{23} to zero, the equivalent Delta circuit becomes

$$g_m' = Y_3(g_m + Y_2)/\sum Y \tag{99}$$

$$g_n' = Y_3(g_n + Y_2)/\sum Y \tag{100}$$

$$Y_{12} = [Y_2(Y_1 + Y_3) - g_mg_n]/\sum Y \tag{101}$$

$$Y_{23} = 0 \tag{102}$$

$$Y_{31} = Y_3(Y_1 - Y_2)/\sum Y. \tag{103}$$

Also, by setting Y_n' to zero, the following Delta circuit is obtained:

$$g_m' = Y_3(g_m - g_n)/\sum Y \tag{104}$$

$$g_n' = 0 \tag{105}$$

$$Y_{12} = [Y_1Y_2 - g_n(g_m + Y_3)]/\sum Y \tag{106}$$

$$Y_{23} = Y_3(g_n + Y_2)/\sum Y \tag{107}$$

$$Y_{31} = Y_3(g_n + Y_1)/\sum Y. \tag{108}$$

The condition that g_n' be zero corresponds to an ideal negative-grid triode. Therefore, (104) to (108) indicate that it is possible to represent a positive-grid triode by an ideal negative-grid triode, and vice versa.

Several forms of the Delta circuit described here have also been suggested by Peterson.[4] Nevertheless, as regards the analogue to the transformation of passive circuits, (75) to (79) or (80) to (84) is probably the best choice. In the practical applications, however, it may be advantageous to make other choices.

IV. Transformations for Tetrodes and Pentodes

The analysis for triodes can be extended to tetrodes and pentodes and other multi-electrode tubes. For tetrodes, the admittance matrix has the rank of three. For pentodes, the rank is four. By means of the matrix expansion, equivalent circuits can be constructed in the same way as for triodes.

In practice, the screen and suppressor grids are usually grounded. The problem is then actually reduced to the triode case. The triode transformation formulas can be applied.

In this paper, no attempt will be made to generalize the transformations to tubes of any number of electrodes. In fact, even for the passive circuits, it is not always possible to transform the Delta of more than three terminals to an equivalent Star circuit. The reason is that there are more branches in a Delta circuit than in its equivalent Star circuit when the number of terminals is more than three. As far as any particular solution of a general network is concerned, there are other articles in the literature[5,6,7,8] which may be of interest to the reader.

[4] L. C. Peterson, "Equivalent circuits of linear active four-terminal networks," *Bell Sys. Tech. Jour.*, vol. 27, pp. 593–622; October, 1948.

[5] N. R. Campbell, V. R. Francis, and E. G. James, "Linear single-stage valve circuits," *Wireless Eng.*, pp. 333–338; July, 1945.

[6] U. Kirschner, "Allegemeine Netzwerktheorie," *Arch. Elekt. Uebertragung*, vol. 4, pp. 367–373; 1950.

[7] U. Kirschner; "Darstellung einer allgemeinen Roehrenschaltung durch eine Kettenmatrix," *Arch. Elekt. Uebertragung*, vol. 5, pp. 190–196; 1951.

[8] U. Kirschner: "Einiges über Gegengekoppelte Verstaerker," *Frequenz*, vol. 5, no. 8, pp. 223–230; 1951.

Part II—Applications

I. Introduction

The previous analysis indicates that a Star circuit (Fig. 4(a)) can always be transformed into a Delta circuit (Fig. 4(b)), and vice versa. Fig. 4(a) (including Y_0) is actually a single-stage feedback amplifier having both current and voltage regenerations. By means of the transformations it is possible to obtain an equivalent circuit with either a current or a voltage regeneration only. The transformation usually simplifies the analysis.

There are other views regarding the transformations. Since (a) and (b) of Fig. 4 are electrically identical, there is no limitation in the transformations as to which of the terminals of the circuits are for the input or output. In particular, the transformations can be applied even though Y_3 is actually in series with the input or the output electrode, as is shown in Fig. 5. In order to transform these circuits to their equivalent Delta circuits, for example, the common-grid formulas can be applied to Fig. 5(a) and the common-plate formulas to Fig. 5(b). Consequently, even if there are series admittances at each of the three electrodes, an equivalent Delta circuit can still be obtained by three successive transformations. Similarly, by means of the Delta-to-Star transformations, it is possible to get an equivalent circuit having only three series admittances with one at each electrode.

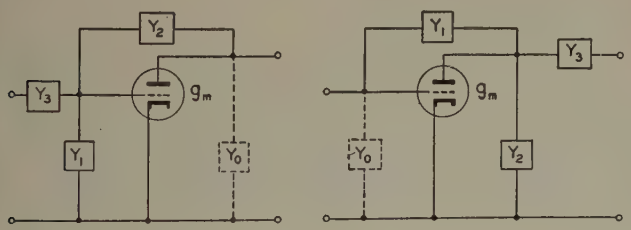

Fig. 5—Alternate star connections. (a) Common grid star. (b) Common plate star.

In general, the Star-to-Delta transformations are useful for effectively eliminating the series admittance Y_3, while the Delta-to-Star transformations provide the way for eliminating the shunt admittance Y_0.

There is no restriction regarding the circuit elements. The admittances Y_0, Y_1, Y_2, and Y_3 are not necessarily outside of the tube. For instance, Y_3 may be the admittance due to the oxide cathode interface or the electrode lead inductance. The admittances in Fig. 4(a), including the transconductance, may also have complex values.

At low frequencies, the triode can be represented as follows:

$$g_m = g_{m0} \tag{109a}$$

$$Y_{kg} = j\omega c_{kg} \tag{109b}$$

$$Y_{gp} = j\omega c_{gp} \tag{109c}$$

$$Y_{pk} = j\omega c_{pk} + 1/r_p = j\omega c_{pk} + g_{m0}D_p, \tag{109d}$$

where

C_{kg}, C_{gp}, C_{pk} = capacitances between the respective electrodes k, g, and p

ω = the angular frequency

r_p = the plate resistance

g_{m0} = the static transconductance

D_p = the inverse amplification factor $= 1/\mu$.

In (109d), D_p is used instead of the amplification factor μ simply for the convenience of comparison with the subsequent equations.

At high frequencies when the transit time becomes appreciable, (109a) to (109d) should be modified. The more general equations for a triode electrode, not taking into account the effect of the leads, are

$$g_m = g_{m0}\{Q - D_p(P - Q) + D_kR\} \tag{110a}$$

$$Y_{kg} = g_{m0}\{(1 + D_p)(P - Q) - D_kR\} + j\omega c_{kg} \tag{110b}$$

$$Y_{gp} = g_{m0}\{-D_p(P - Q) + (1 + D_k)R\} + j\omega c_{gp} \tag{110c}$$

$$Y_{pk} = g_{m0}D_pP + j\omega c_{pk}. \tag{110d}$$

These equations are stated as (53) to (56) in a recent paper by Rodenhuis,[9] except the introduction of the capacitances. The definitions of D_k, P, Q, and R can be found in Rodenhuis' paper.[10]

When the transit time approaches zero, we get

$$P = Q = 1$$

$$R = 0.$$

Then (110a) to (110d) reduce to (109a) to (109d), as expected.

In the following, a few examples are given to illustrate the application of the transformations to vacuum tubes and circuits.

II. Application to UHF Triodes

At ultra-high frequencies, the transit-time loading and the lead inductance become the factors of primary importance. Due to the lead inductances, none of the electrodes is perfectly grounded. Accordingly, it becomes necessary to treat separately the admittances between the electrodes, the admittances of the individual leads, and also the admittances between the individual electrodes and the common ground. The equivalent circuit is very complicated, but it is of the typical forms of Figs. 4(a) and 5(a) and (b). The circuit can be considerably simplified by the transformations, for example, by considering Y_3 in Fig. 4(a) as the admittance of the common electrode lead. Furthermore, the effect of Y_3 on g_m', Y_{12}, Y_{23}, and Y_{31} in the transformed circuit

[9] K. Rodenhuis, "The limiting frequency of an oscillator triode," *Philips Res. Rep.*, vol. 5, no. 1, pp. 46–77; February, 1950.

[10] In his paper, Rodenhuis did not consider C_{kg}. There is also a slight error in his treatment of the capacitance effect. To detect the error one needs only to check his results for the special case at low frequencies where the transit-time effect is negligible. With his equations expressed as (110a) to (110d), the only difference in P, Q, and R is to drop the second term of his (59) for R. The reader should also be cautious of the misprints in his equations.

(Fig. 4(b)) can be observed separately from (54) to (58) and (68). In this way, the analysis is usually less complicated but more instructional. When the total feedback coupling is being investigated, for instance, one needs only to evaluate Y_{12} alone. A solution can be obtained directly from (68) with the appropriate substitution of (109a) to (109d) or (110a) to (110d). Thus, the tube is considered as hot or conducting, and the transit-time effect can be included. It can be shown that, for example, the total feedback coupling of a grounded-grid triode may be dominantly determined by the grid-lead inductance instead of the plate-to-cathode capacitance. A condition of minimum regeneration can also be derived. This relation has been observed and analyzed by Diemer,[11] but his analysis was confined to cold tubes only because the action of the tube was neglected.

There is no restriction in the application of the transformations regarding the interpretation of the lead inductances.[12] In fact, the conception of the lead inductance can be generalized to tubes having multiple grid leads, even though there are mutual couplings among the leads of all the three electrodes.[13] The result provided a basis for the analysis of the type of uhf tubes similar to the 6AJ4, a miniature tube having five grid leads.

III. On Input and Output Admittances of Amplifiers

One rather interesting application of the transformations pertains to the input and output admittances of amplifiers.

In (54) to (58), let Y_3 be zero, that is, open circuit. Then g_m', Y_{23}, and Y_{31} vanish altogether; only Y_{12} is left. Accordingly, the equivalent Delta circuit in Fig. 4(b) reduces to a single admittance Y_{12}, which is, by putting Y_3 equal to zero in (68),

$$Y_{12}' = Y_0 + (Y_1 + g_g)(Y_2 + g_p)/(g_k + Y_1 + Y_2). \quad (111)$$

In this equation Y_{12}' is used to distinguish it from Y_{12} in (68). With Y_3 reduced to zero, the circuit in Fig. 4(a) becomes effectively a Delta circuit formed by Y_0, Y_1, and Y_2. Therefore, Y_{12}' is equal to the admittance of that Delta circuit looking at the terminals 1 and 2. As an example, the equivalent admittance of a triode between the grid and plate can be obtained from the common-cathode formula given by (111). The result has been applied to analyze uhf oscillators by Bell, Gavin, James, and Warren,[14] and by Kamphoefner.[15] By means of the transformations, the analysis can be extended to explain the effect of the lead inductances also.

[11] G. Diemer, "Passive feedback admittance of disc-seal triodes," *Philips Res. Rep.*, vol. 5, no. 6, pp. 423–434; December, 1950.
[12] E. E. Zepler, "Valve input conductance at VHF," *Wireless Eng.*, vol. 28, pp. 51–53; Feb. 1951.
[13] Unpublished notes.
[14] J. Bell, M. R. Gavin, E. G. James, and G. W. Warren, "Triodes for Very Short Waves—Oscillators," *Jour. IEE* (London), vol. 93, pp. 833–846; pt. IIIA; 1946.
[15] F. J. Kamphoefner, "Feedback in very-high frequency and ultra-high frequency oscillators," PROC. I.R.E., vol. 38, pp. 630–632; June, 1950.

The previous reasoning can further be applied to the circuits shown in Fig. 5. When Y_3 is zero, (111) gives the equivalent admittance at the output terminals of Fig. 5(a) and also the equivalent admittance at the input terminals of Fig. 5(b). In the special case of a grounded-cathode circuit, the common-grid formula of (111) is used for Fig. 5(a) and the common-plate formula for Fig. 5(b). Now, let Y_s = the source admittance and Y_L = the load admittance. Then, by considering Y_s as a part of Y_1 in Fig. 5(a), the equivalent admittance becomes actually the output admittance of a grounded-cathode amplifier. Similarly, Y_L can be included in Y_2 of Fig. 5(b) and get the actual input admittance of the amplifier.

The triode amplifier in Fig. 5 can also be considered as a general circuit representing grounded-grid and grounded-plate amplifiers as well. With reference to (65) and (66) and also to Figs. 4(c) and 4(d), the following relations can be observed.

For Fig. 5(a),

$$g_m = g_k' - g_g' - g_p' \quad (112a)$$
$$Y_0 = Y_{23} + g_p' \quad (112b)$$
$$Y_1 = Y_{31} + Y_s + g_g' \quad (112c)$$
$$Y_2 = Y_{12}. \quad (112d)$$

For Fig. 5(b)

$$g_m = g_k' - g_g' - g_p' \quad (113a)$$
$$Y_0 = Y_{31} + g_g' \quad (113b)$$
$$Y_1 = Y_{12} \quad (113c)$$
$$Y_2 = Y_{23} + Y_L + g_p', \quad (113d)$$

where the notations follow Fig. 4(b), with the electrode 1 as the input terminal and the electrode 2 as the output terminal. Now by substituting (113a) to (113d) into the common-plate formula of (111), a general expression of the input admittance can be obtained as

$$Y_{in} = Y_{31} + g_g' + \frac{Y_{12}(Y_{23} + Y_L + g_k' - g_g')}{g_p' + Y_{12} + Y_{23} + Y_L}. \quad (114)$$

Similarly, by substituting (112a) to (112d) into the common-grid formula of (111), we get the output admittance as

$$Y_{out} = Y_{23} + g_p' + \frac{Y_{12}(Y_{31} + Y_s + g_k' - g_p')}{g_g' + Y_{12} + Y_{31} + Y_s}. \quad (115)$$

Equations (114) and (115) are valid for the three types of grounded amplifiers. Furthermore, by substituting (54) to (58) into (114) and (115), the input and output admittances of ungrounded amplifiers shown in Fig. 4(a) can also be obtained.

In (114) and (115), Y_s and Y_L may also be the admittances of the preceding and following amplifier stages, respectively. By successive application of (114) and (115) for each stage, the input and output admittances of cascade amplifiers can be obtained. For example, the equations can be applied to a two-stage

grounded-plate to grounded-grid amplifier (i.e., a cathode coupled amplifier).

In deriving (114), Y_3 in Fig. 5(b) may also be considered as being equal to Y_L, but the output terminals are shorted. Similarly, (115) can be derived by putting Y_3 in Fig. 5(a) as Y_s. The results are of course the same as before.

IV. On the Gain of Amplifiers

As a further illustration of the transformations, a general expression is derived for the voltage gain of amplifiers.

The voltage gain of a grounded-cathode amplifier of Fig. 5(b) (Y_3 being zero) can be shown as

$$\text{voltage gain} = (-g_m + Y_1)/(Y_1 + Y_2). \quad (116)$$

Now by substitution of (113a) to (113d) into (116), a general expression can be obtained as

$$\text{voltage gain} = \frac{g_g' + g_p' - g_k' + Y_{12}}{g_p' + Y_{12} + Y_{23} + Y_L}. \quad (117)$$

Equation (117) is valid for all three types of grounded amplifiers. By substituting (54) to (58) into (117) the equation can be generalized for ungrounded amplifiers. Furthermore, Y_L in (117) may be actually Y_{in} in (114). Thus, (117) can be applied to cascade amplifiers as well.

Equation (117) gives not only the absolute value of the voltage gain but also the phase between the input and output voltages. With reference to (114) and (117), the relation of the absolute value of the voltage gain and the power gain can also be obtained as

$$\text{power gain} = |\text{voltage gain}|^2 \cdot \frac{\text{Re}\,(Y_L)}{\text{Re}\,(Y_{in})}. \quad (118)$$

Equation (118) can be applied to evaluate the power gain of grounded and ungrounded amplifiers.

Acknowledgment

The author takes this opportunity to express gratitude to his many associates at the General Electric Company, especially the members of the development and design engineering sections who were directly connected with the development work of the 6AJ4 uhf amplifier tube. Special thanks are extended to A. P. Haase and C. E. Horton for their co-operation, and also to Dr. K. Fong for his beneficial discussions.

Tuner for Complete UHF-TV Coverage Without Moving Contacts*

RICHARD J. LINDEMAN†, ASSOCIATE, IRE AND CHARLES E. DEAN†, SENIOR MEMBER, IRE

Summary—**A tuner covering the uhf television band continuously and having essentially constant selectivity over all of this band is described. A unique feature is that the tuner employs no moving contacts in the tuned circuits, and so avoids the well-known contact troubles.**

The circuit consists of a double-tuned preselector, a crystal mixer, a triode oscillator, and a cascode-type first intermediate stage. The two preselector circuits and the oscillator employ balanced parallel-rod constructions, each tuned with a movable capacitor element having surfaces shaped to give a linear displacement-frequency characteristic. Shielded compartments are provided for the three tuned circuits. The tuner input matches a 300-ohm antenna, and the output is suitable for feeding the conventional "40-mc" intermediate-frequency amplifier of a television receiver.

Measurements of the performance show the noise figure to be 15 db or better over the band, the image rejection at least 43 db, and the transadmittance (which is a measure of sensitivity) 11 db, or better, above 1 millimho. Oscillator signal at the antenna terminals averages approximately 43 db below 1 volt.

Introduction

IN A PROGRAM of development work in a field which is new to commercial exploitation, the form which apparatus should take to be best suited to the needs of the customer is usually not clear. The work on this tuner, therefore, was preceded by some consideration of the general aspects of the tuner problem. This led to certain rules, which may or may not be considered to hold in other commercial situations. However, they were controlling in this development and are stated, therefore, as follows:

1. The tuning system shall be continuous rather than switched. If preset tuning is wanted, it can be added as a mechanical auxiliary feature.
2. Sliding or switched contacts in the tuned circuits shall not be used.
3. The tuning motion shall be suitable for operation ganged with a continuously tuned vhf system, thus permitting a single drive mechanism for both frequency ranges.

It was found possible to comply with these rules and, at the same time, obtain a tuner with good electrical performance.

The chief electrical characteristics desired are low noise figure, adequate rejection of unwanted signals, and low oscillator radiation. To achieve these, certain principles should be observed, as follows:

For low noise figure. (1) Losses in the signal-frequency circuits are detrimental to noise figure, and therefore should be kept as low as possible (this applies to both mismatch losses and losses resulting from the use of

* Decimal classification: R583.5. Original manuscript received by the Institute, October 6, 1952.

† Hazeltine Corporation, Little Neck, L. I., N. Y.

low-Q circuits). (2) Crystal conversion loss should be kept as low as possible. (3) A low-noise intermediate-frequency amplifier of adequate gain following the crystal mixer is necessary.

For adequate rejection of unwanted signals. (1) The bandwidth of the signal-frequency circuits should be as narrow as is consistent with good signal reception. (2) All spurious resonances, located in or near the band, should be eliminated.

For low oscillator radiation. (1) The oscillator injection level should be as low as good conversion efficiency allows. (2) The path between the oscillator injection circuit and the antenna terminals should present a high impedance to oscillator signals. (3) The oscillator should be well shielded.

A general view of the tuner, resulting from this approach, is given in Fig. 1, and the chief mechanical and electrical features are shown in Figs. 2 and 3.

Signal-Frequency Circuits

Each of the two tuned circuits, which select the desired signal frequency, is made up of two silver-plated copper rods which are placed next to each other and tuned by a movable capacitor member, as shown in Figs. 2 and 4. It should be noted that the lowest frequency is reached when the maximum amount of capacitance is in the circuit, which is with the capacitor block furthest to the right on the rods. This is where the shortest portions of the rods are exposed. Therefore, in relation to short-circuited transmission lines, which give the lowest frequency with the greatest length, the tuning is in the opposite direction. Of course, there is some tuning similar to that on transmission lines due to the decrease in distributed inductance and capacitance as the sliding capacitor is moved further to the right over the rods, but this effect is small and does not materially affect the main tuning characteristic. The inductive path of each tuned circuit is completed by grounding its two rods to the chassis at their extreme right-hand ends.

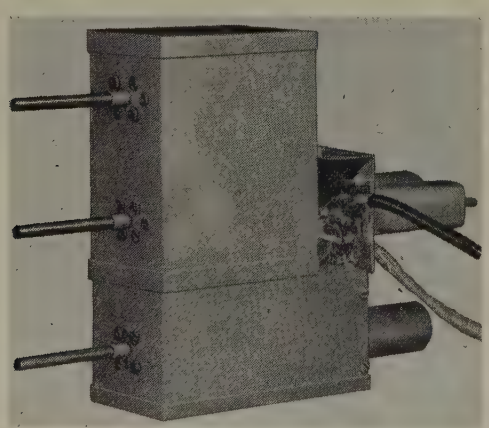

Fig. 1—General view of tuner.

Capacitive tuning of the signal-frequency circuits allow full coverage of the band (470–890 mc) in approximately three-quarters inch of travel. This reduces the physical size of the tuned circuits to about one quarter of what they would be if short-circuited transmission lines were used, but also increases tracking problems. To facilitate tracking of the two preselector circuits and the oscillator circuit, all three are made with capacitor elements having inner-curved surfaces shaped to provide linear frequency-displacement curves. Capacitors C_1 and C_4 (shown in Figs. 2 and 3) afford adjustment of the preselector circuits at the high-frequency end of the band. A two-point alignment can be obtained by providing also a mechanical adjustment in the attachment of tuning push rod to gang-tuning control.

The preselector lines are high-Q circuits, varying from an unloaded Q of 1,500 to 470 mc to 900 at 890 mc. This characteristic is obtained by using large surface areas in the lines, by shielding properly, and by silver plating the metal used for the lines and shielding.

The use of a balanced system in the signal-frequency circuits has two advantages: First, for those viewers in strong signal areas who wish to use their present vhf antenna for uhf pickup it may be possible to put both vhf and uhf tuners on the same lead in, which in most cases is balanced 300-ohm twin lead. Second, balanced twin lead has less loss than the coaxial type.

The stainless-steel push rod which drives each capacitor element is grounded by contact fingers at the point where it protrudes from the left end of the box. This point is, of course, not in the tuned circuit. The introduction of grounded metal push rods was found necessary to eliminate an unbalanced resonance between the lines and the box.

The positioning of loop L_3, which couples the antenna to the input section of the preselector, varies the amount of loading introduced into this tuned circuit by the antenna circuit. The two small series inductors, L_1 and L_2, wound of the same piece of wire as L_3, are provided to compensate for the increase in coupling which would otherwise occur at the higher frequencies. By adjustment of these inductances and the position of loop L_3, the 3-db bandwidth of the input section of the preselector can be held between 9 and 11 mc across the entire band.

Polytetrafluoroethylene feed-through insulators of low capacitance to ground (made of Teflon Poly F#1114 of DuPont, or Fuoroflex T of Resistoflex Corporation, Belleville, N. J.) are used to bring the antenna lead-in wires through the compartment wall, and are so arranged that the coupling loop in parallel with the feed-through capacitance does not become resonant within the band. (Similar feed-through insulators at other points are shown in the schematic; these are distinct from feed-through capacitors, C_5, C_9, and C_{10}, whose capacitance values are shown.)

In the adjustment of the coupling between the output section of the preselector and the crystal mixer, the crystal itself can be used as a signal detector. The short at F in Fig. 3 is replaced by a potential of about 150 volts applied through a 150-kilohm resistor so as to produce a current of about 1 ma through the crystal. The normal intermediate-frequency load on the crystal is replaced by a resistive load of approximately 200 ohms,

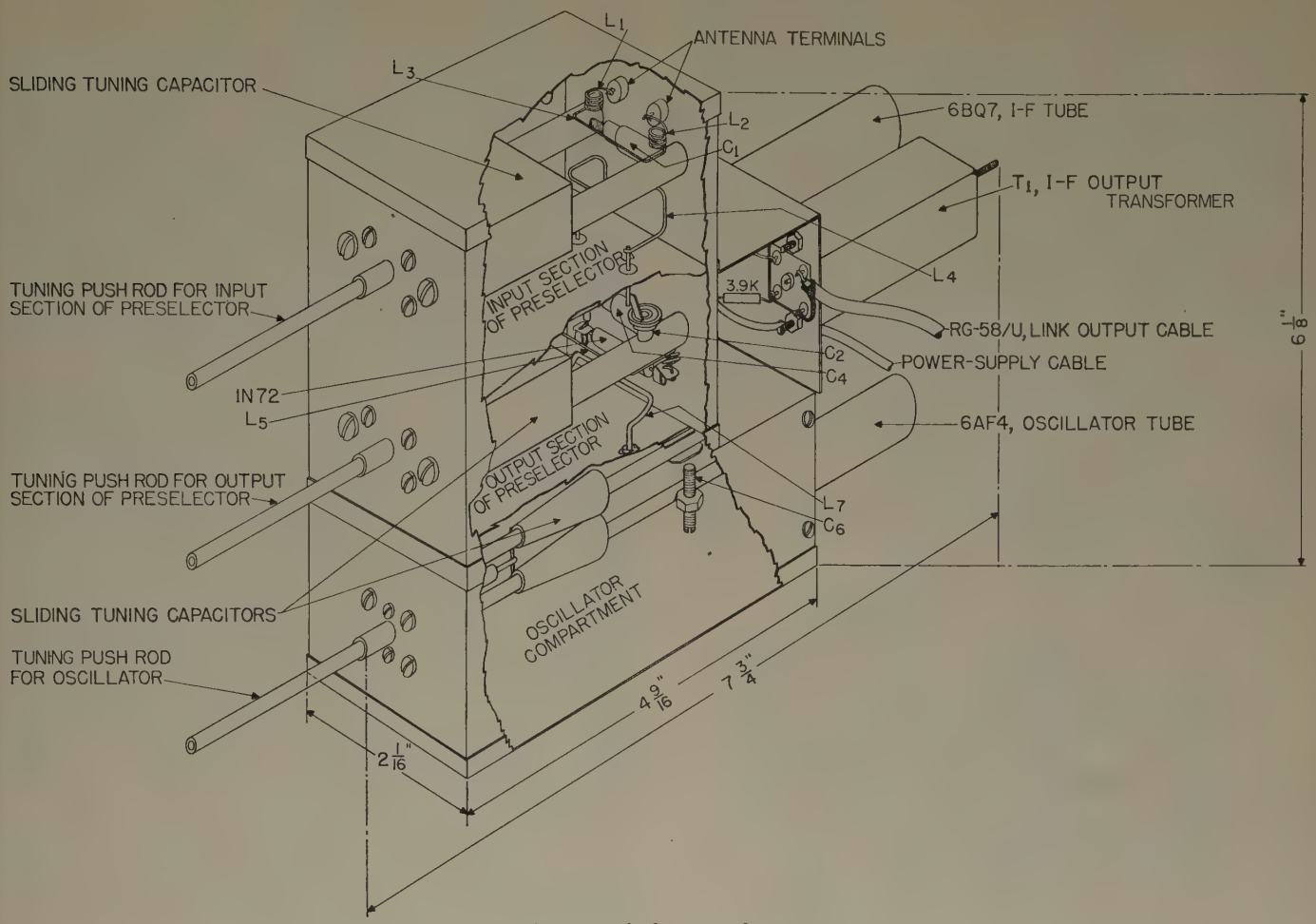

Fig. 2—Main features of tuner.

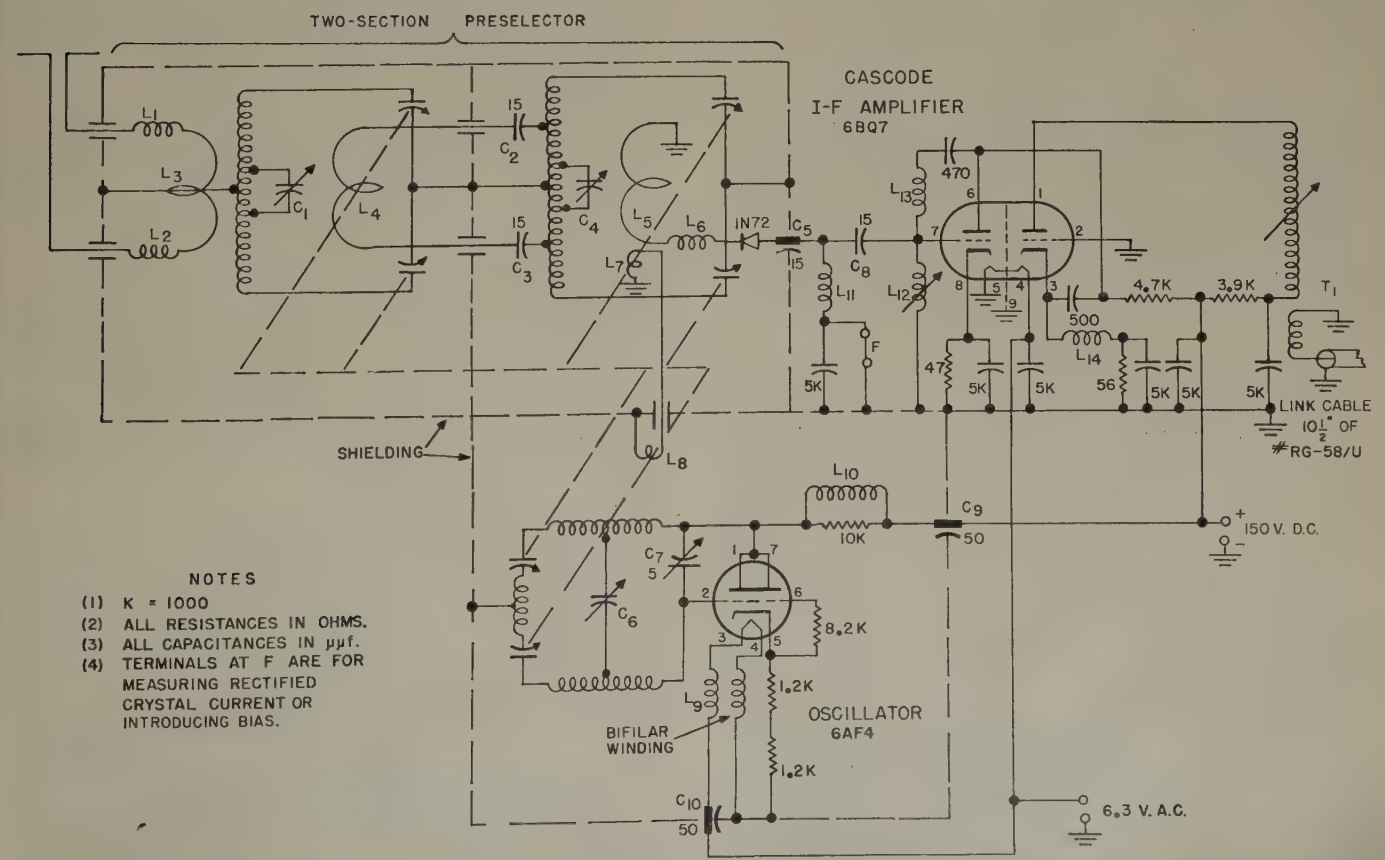

Fig. 3—Schematic circuit.

across part of which a tuned audio amplifier and output meter are connected to serve as indicator. The position of loop L_5 (shown in Figs. 2 and 3) is then varied, while the uhf signal is loosely coupled to the preselector line and the position located, giving a 3-db bandwidth of about 10 mc across the band. Inductance L_6, which is in series with L_5, gives a resonance outside the band in such a way as to prevent an increase of coupling which otherwise occurs at the low-frequency end of the range.

The coupling between the input and output sections of the preselector is obtained by inductively coupling from the input section with loop L_4, and feeding the signal to the output section through capacitors C_2 and C_3, as shown in Figs. 2, 3, and 4. Loop L_4 is adjusted to give approximately critical coupling between the two preselector sections at the low-frequency end of the band, with the result that they are slightly overcoupled at the high-frequency end.

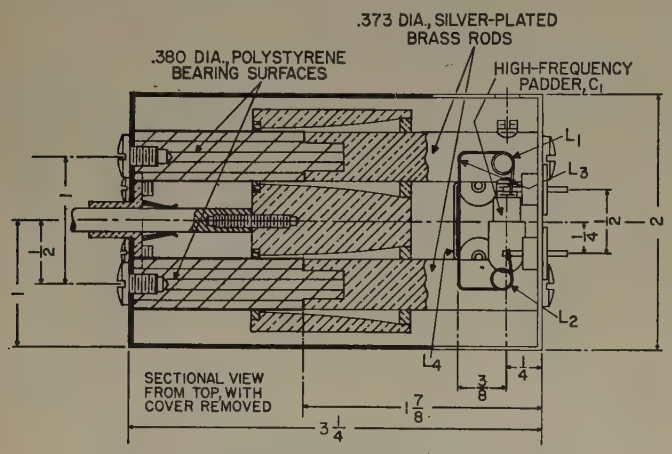

Fig. 4—Details of input section of preselector.

With the various couplings in proper adjustment, a good match is obtained between the antenna and the crystal mixer. The over-all bandwidth of the signal-frequency circuits is 14 to 16 mc, which is adequate for good signal reception, allows some tracking error without undue harm, and still provides the necessary rejection of unwanted signals.

Oscillator Circuit

A 6AF4 tube is used as oscillator with a grid-plate tuned circuit, which is much like the preselector lines, but is essentially half wave rather than quarter wave in characteristics. In order to obtain frequency stability through the use of high Q, silver plating is provided on the line, the movable tuning element, and the shield box.

The two socket connections to the grid of the 6AF4 are joined together by a silver-plated copper band. The plate pins are similarly joined, and the line is then soldered to these bands.

The inner curved surface of the movable tuning member is designed to give a linear frequency-displacement characteristic corresponding to that of the preselector tuned circuits. Full coverage of the 470–890 uhf band (oscillator 514–934) cannot be obtained by capacitive variation alone because of the effect produced by that part of the line which lies within the tube. Therefore, it is necessary to add inductance in series with the variable capacitor. This is provided by dividing the capacitor element into two parts and connecting them with a rod of one-sixteenth-inch diameter, which furnishes the desired inductance. As a result of the capacitance variation during tuning, the impedance added at the end of the line by the tuning member is capacitive at the higher frequencies, becomes resistive, and is then inductive for the lower part of the band.

To drive the tuning element, a metal rod is fastened to the center of the added inductance element.

It may be noted from the circuit diagram (Fig. 3) that the cathode of the oscillator tube is returned to ground through two 1.2-kilohm resistors connected in series. The use of resistance in place of the usual cathode inductance gives more uniform oscillator operation because the resonances of a coil are not present. Two resistors in series are desirable to keep the capacitance to ground small, for the inherent capacitances of the resistors are also in series. The heater is kept above ground by a bifilar choke L_9 which also aids in reducing the capacitance between the cathode and ground. The plate potential (150 volts) is fed through a choke L_{10}, which is damped by a 10-kilohm resistor. The 50-$\mu\mu$f bypass capacitors used on the plate and heater leads are a low-inductance feed-through type.

The oscillator output is delivered inductively and conductively by L_8 and L_7 to the 1N72 crystal modulator.[1] Loop L_7 is so positioned that the capacitive coupling, which is present, aids the inductive coupling to L_5, the desired path, but opposes any inductive coupling to the preselector line, thus providing additional attenuation of oscillator signal going toward the antenna terminals.

The amount of oscillator injection to the crystal is important. The optimum produces approximately 1 ma of rectified crystal current, as measured by inserting a meter in place of the short at terminals F in the schematic. Slightly less injection can be used satisfactorily if some dc bias[2] is applied to the crystal. These conclusions were arrived at by noting that noise originating in the crystal increases considerably at high-injection levels[3] (such as producing 2 ma of rectified crystal current); on the other hand, the conversion efficiency goes down rapidly if the rectified crystal current is allowed to fall below 0.5 ma.

The oscillator is provided with two alignment padders, one of which (C_6 in Figs. 2 and 3) is effective at the high-frequency end of the range. The other (C_7 in Fig. 3) is located near the vacuum-tube end of the line, and is effective at the low-frequency end. About 25 mc, at the extreme ends of the band, is the maximum obtainable variation if the general oscillator operation is to be unaffected. With the proper curves on the inner surfaces of the three tuning elements, this is sufficient to

[1] R. V. Pound, "Microwave Mixers," Radiation Laboratory Series McGraw-Hill Book Co., Inc., New York, N. Y., vol. 16, pp., 119–122; 1948.
[2] *Op. cit.*, pp. 249–256.
[3] *Op. cit.*, pp. 235–241.

obtain linear frequency displacement curves for the three circuits, and thus facilitate unicontrol.

Cascode First Intermediate Stage

The "cascode" circuit[4,5] (having two cascade triodes with the first operating grounded cathode and the second grounded grid) has been utilized to provide a low-noise intermediate-frequency amplifier. The circuit is arranged with ac coupling so that the same plate voltage may be used for both the oscillator and amplifier tubes. The common 150-volt supply is reduced by resistors to approximately 110 volts at the plate of each triode section of the cascode amplifier. The plate current of each section is about 10 ma.

The coupling into the cascode amplifier from the mixer consists of an LC network, L_{12} and C_8 (Fig. 3). The proportioning of this coupling is an important part of the design. It is a well-known fact that overcoupling at the grid of the input section of the cascode stage improves (that is, reduces) the noise figure of the amplifier. However, the impedance presented to the crystal mixer by the cascode input circuit affects the crystal conversion efficiency, so that a compromise is necessary to produce the best over-all noise figure.[6,7] A mathematical analysis to locate the optimum-compromise point was made and gave the result that the best noise performance is obtained when there is sufficient overcoupling to produce approximately a 3-to-1 impedance mismatch. Then, however, a new difficulty was encountered, namely, that the bandwidth was inadequate. To correct this, a further increase of coupling was necessary, and it was found that a deterioration of less than 1 db in the noise figure occurred when the coupling was increased enough to give the required bandwidth.

If this adjustment is made for crystals with high impedance, the bandwidth will remain adequate for all crystals. Care regarding this appears to be necessary due to the tolerance range of impedance in germanium diodes.

The grid-to-plate capacitance of the input section of the 6BQ7 is neutralized by an inductance L_{13}, which gives parallel resonance with the neutralized capacitance. This changes the interelectrode capacitance to a high impedance, and so reduces amount of feedback.

The output transformer T_1 is part of a link system which couples the output of the cascode amplifier to a conventional "40-mc strip," which is the intermediate-frequency amplifier such as found in the usual present-day television receiver. A similar transformer is used at the other end of the link to match the first grid of this amplifier. The couplings between the windings of these transformers were adjusted to obtain a 3-db bandwidth of about 4.75 mc. This provided, in conjunction with the succeeding stages, a typical television-receiver response characteristic.

The gain of the cascode amplifier is about 26.5 db at midband (44 mc). The noise figure, when the cascode input is matched to a 50-ohm noise diode, is between 2.5 and 3 db. Over-all noise figures indicate that the noise performance remains substantially the same when the input is obtained from the crystal mixer.

Figs. 1 and 2 show how the cascode stage and its components are mounted as a subchassis. The chosen location of the subchassis reduces the length of the lead from the crystal mixer to the cascode input grid, and appears desirable from the standpoint of reducing oscillator radiation.

TABLE I

Noise Figure Image Rejection, and Tuner Transadmittance

Frequency mc	Noise figure db	Balanced image rejection db	Trans-admittance db above 1 millimho
470	14	44	12
500	14.5	44	11
550	14.5	43.5	12
600	14	45	14
650	13.5	48	14
700	13.5	51	13.5
750	13.5	47	14.5
800	13	51	14
850	13	51.5	14
900	14.5	56	11

Performance

Noise figure, image rejection, and tuner transadmittance data are given in Table I. These measurements were made with perfect tracking.

Tuner transadmittance, as for vhf tuners, is defined as the ratio of short-circuit tuner-output intermediate-frequency plate current to the open-circuit antenna voltage required to produce it. It has, therefore, the dimensions of admittance and is usually expressed in millimhos; the values are then numerically equal to the voltage gain per kilohm of intermediate-frequency output load impedance. Transadmittance is most readily measured by first observing the intermediate-frequency plate current (ac only) in the tuner output which produces a chosen standard test output from a following amplifier. When this standard output is duplicated with a uhf signal fed from a signal generator through a dummy antenna to the tuner input, the transadmittance can be directly obtained as the ratio of the observed plate current divided by the observed uhf-signal voltage.

In the present case the output intermediate-frequency plate current was determined by applying an intermediate-frequency signal to the cascode input with its output link coupled in normal fashion to a following amplifier. The required input (e) to the cascode to obtain the standard test output was measured, as was the transconductance (g_m) of the input section of the cascode. The product ($g_m e$) of these two is the intermediate-frequency plate current of the first cascode section, which closely approximates that of the second.

[4] G. E. Valley, Jr., and H. Wallman, "Vacuum Tube Amplifiers," Radiation Laboratory Series, McGraw-Hill Book Co., Inc., New York, N. Y., vol. 18, pp. 615–694; 1948.
[5] H. Wallman, A. B. MacNee, and C. P. Gadsden, "A low-noise amplifier," Proc. I.R.E., vol. 36, pp. 700–708; June, 1948.
[6] L. A. Moxon, "Recent Advances in Radio Receivers," University Press, Cambridge, England, pp. 54–56; 1949.
[7] F. E. Terman, "Radio Engineers' Handbook," McGraw-Hill Book Co., Inc., New York, N. Y., pp. 204–208; 1943.

Care is necessary in making transadmittance measurements on uhf tuners to avoid over-all regeneration in the cascode stage, which may raise the observed values above the computed ones and may also cause de-

TABLE II

BALANCED-SIGNAL SPURIOUS RESPONSES

Frequency of tuner	Local-oscillator frequency, f_0	Input frequency, f_x	Rejection ratio, db	How formed
550 mc	594 mc	44 mc	60	$f_x=f_{IF}$
		183	60	$f_0-3f_x=f_{IF}$
		275	53	$f_0-2f_x=f_{IF}$
		572	66	$2f_0-2f_x=f_{IF}$
650	694	44	62	$f_x=f_{IF}$
		130	76	$f_0-5f_x=f_{IF}$
		163	70	$f_0-4f_x=f_{IF}$
		217	57	$f_0-3f_x=f_{IF}$
		325	53	$f_0-2f_x=f_{IF}$
750	794	44	65	$f_x=f_{IF}$
		107	75.5	$f_0-7f_x=f_{IF}$
		125	80	$f_0-6f_x=f_{IF}$
		150	70	$f_0-5f_x=f_{IF}$
		188	66	$f_0-4f_x=f_{IF}$
		250	65.5	$f_0-3f_x=f_{IF}$
		375	53.5	$f_0-2f_x=f_{IF}$
		816	50.5	$2f_x-2f_0=f_{IF}$
850	894	44	68	$f_x=f_{IF}$
		213	66.5	$f_0-4f_x=f_{IF}$
		283	61	$f_0-3f_x=f_{IF}$
		425	51	$f_0-2f_x=f_{IF}$

f_{IF} = intermediate frequency = 44 mc.

TABLE III

UNBALANCED-SIGNAL SPURIOUS RESPONSES

Frequency of tuner, f_s	Local-oscillator frequency f_0	Input frequency, f_x	Unbalanced-rejection ratio, db*	How formed
550 mc	594 mc	44 mc	77	$f_x=f_{IF}$
		550	47.5	$f_x=f_s$
		638	63	$f_x-f_0=f_{IF}$
650	694	44	75	$f_x=f_{IF}$
		650	43	$f_x=f_s$
		738	73	$f_x-f_0=f_{IF}$
750	794	44	79.5	$f_x=f_{IF}$
		750	42.5	$f_x=f_s$
		838	60	$f_x-f_0=f_{IF}$
850	894	44	79	$f_x=f_{IF}$
		850	38	$f_x=f_s$
		938	58	$f_x-f_0=f_{IF}$

f_{IF} = intermediate frequency = 44 mc.
* Values are for unbalanced interfering signal to produce same output as balanced desired signal.

tuning of the cascode-input circuit.[8] Such regeneration was substantially eliminated in the present design by placing a shield across the cascode socket to isolate the output circuit.

Tables II and III present the rejection ratio to spurious responses for balanced and unbalanced signals, respectively. The distinction between these lies in whether the interfering signal is present between the two balanced input terminals, or between both terminals and ground. The recorded value is the number of decibels corresponding to the ratio of open-circuit signal-generator voltage at the undesired frequency to the corresponding voltage at the desired frequency required to produce equal output. These tables include all responses with smaller rejection ratios than 80 db, except the balanced-image rejection which is shown in Table I. It should be realized that all rejection ratios, except for $f_x=f_s$ in Table III, are 6 db better than when measured in a television receiver due to the 6-db carrier attenuation normally provided in the receiver for vestigial-sideband reception.

Table IV gives the amplitude of balanced and unbalanced oscillator voltage at the antenna terminals of the tuner when they are terminated in a 300-ohm dummy-antenna impedance. A uhf converter feeding a low-frequency receiver was used to pick up and measure this voltage. Oscillator-injection level determines, to a great extent, how much voltage will appear at the antenna terminals. (When the injection was raised to give 2 ma of crystal-rectified direct current at 800 mc, the balanced-oscillator voltage at the antenna terminals increased 17 db.) The increase in voltage at the high-frequency end shown in Table IV is believed to be due, in part, to some increase in oscillator injection. The increase at the low-frequency end is believed to be due to an increase in preselector bandwidth.

TABLE IV

OSCILLATOR VOLTAGE AT THE ANTENNA TERMINALS

Signal frequency, mc	Oscillator frequency, mc	Oscillator signal at antenna db below 1 volt	
		Balanced	Unbalanced
500	544	38.5	32.5
550	594	54.5	48
600	644	48.5	62
650	694	44	45
700	744	48	52
750	794	44.5	36
800	844	33	38
850	894	28	34.5

While no definite limits for oscillator radiation have yet been established for the uhf band, a figure of 500 μv/m seems reasonable, based on the RTMA-suggested vhf limits of 50 μv/m for the range of 54–88 mc, and 150 μv/m for 174–216 mc. The value of 500 μv/m corresponds to an antenna-terminal voltage of about 36 db below 1 volt. Therefore, it appears that the voltage as measured at the antenna terminals is not excessive over most of the uhf-television band.

ACKNOWLEDGMENT

The contributions of I. B. Tiedeman, Jr., particularly to the oscillator design, are gratefully acknowledged.

[8] M. J. O. Strutt and A. van der Ziel, "The causes for the increase of the admittances of modern high-frequency amplifier tubes on short waves," PROC. I.R.E., vol. 26, pp. 1020–1025; August, 1938.

Development of A UHF Grounded-Grid Amplifier*

C. E. HORTON†, MEMBER, IRE

Summary—**The 6AJ4 is a nine-pin miniature, grounded-grid triode designed to operate as the radio-frequency amplifier in uhf television receivers. This paper reviews the development of this tube, treats the special problems encountered in extending the useful frequency range of a miniature tube to beyond 890 mc, and discusses the methods employed in arriving at a useful solution. Special attention is given the problem of isolation between input and output circuits. The techniques of the measurements involved in the development of this tube are also discussed.**

Introduction

THE ANNOUNCEMENT of commercial television channels in the uhf region created a new demand for a radio-frequency amplifier tube usable in television tuners at frequencies up to 900 mc. The desirability of using such a tube arises from the advantages of improved selectivity, reduced local oscillator radiation, additional gain, and improved noise figure. From the standpoint of electrical requirements, tubes which are more than suitable for this application have been available for some time in the form of lighthouse types and the like. However, the cost of these tubes is such as to outweigh the advantages in all but the most expensive sets. For this reason it has been found desirable to extend the frequency limitations of the less expensive miniature-type tubes to beyond 900 mc. This paper will describe the problems encountered in the development of the 6AJ4, one of the new miniature types designed for use as a grounded-grid, radio-frequency amplifier at frequencies up to 900 mc.

Investigation of Miniature-Tube Capabilities

Early models of this type were rather crudely made, designed only to indicate how far the upper frequency limit of 9-pin miniature tubes could be extended by the use of new mounting techniques. These tubes used the basic electrode structure—grid, plate, and cathode—of the 6AF4, because this was a relatively good high-frequency tube and the parts were readily available. The electrodes were mounted horizontally and in such a way as to reduce lead inductances and the plate-cathode capacitance as completely as seemed feasible. The tube was placed so close to the button stem that the plate radiating fins actually extended below the tops of the glass fillets which surround the tube pins.

Measurements made on these tubes indicated that at 1,000 mc (equipment limitations prevented measuring at higher frequencies) the tubes still had a gain greater than unity. Effort was then directed toward obtaining similar results with a structure better adapted to the established manufacturing techniques for miniature tubes.

* Decimal classification: R333×R583.6×R262. Original manuscript received by the Institute, November 3, 1952.

† Tube Dept., General Electric Co., Owensboro, Ky.

Problem of Internal Coupling

Although these first tubes indicated the possibility of success, at the same time they revealed a serious problem to be overcome before the design could be considered satisfactory. It was found that excessive coupling existed between input and output circuits when this tube was used as a grounded-grid amplifier. One effect of this coupling was to give a certain amount of regeneration. This was sufficient to give the tubes a gain of 1 or 2 db higher than they would otherwise have had, indicating a tendency towards instability. Another effect of this coupling is to give an excessive variation of input impedance over the pass band of the amplifier, due to coupling of the change in impedance of the plate load.

The plate-to-cathode capacitance was suspected to be the cause of this trouble, but improving the shielding so as to reduce this capacitance from its original value of 0.25 $\mu\mu$f to less than 0.07 $\mu\mu$f actually caused greater coupling between input and output circuits than before. The greatest source of coupling was found to be the grid lead inductance, which is an impedance common to both input and output circuits. This was in spite of the fact that the grid was grounded by means of parallel connections to four of the tube pins.

Although the effect of grid-lead inductance in grounded-grid amplifiers has been recognized for years, it has been found that engineers are often inclined to attach much more importance to plate-to-cathode capacitance than to grid-lead inductance. This is quite possibly because the latter difficulty has been virtually eliminated in lighthouse tubes, and therefore has never before been a common problem for grounded-grid amplifiers operating at 900 mc. Because of the importance of this effect in the development of a 9-pin miniature uhf amplifier, the basic theory will be reviewed.

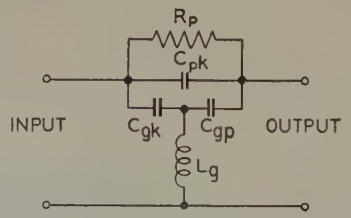

Fig. 1—The approximate equivalent circuit responsible for coupling in a conventional triode used as a grounded-grid amplifier.

Fig. 1 shows an approximate circuit to illustrate the factors which cause coupling between the input and output circuits of a grounded-grid amplifier. Coupling can occur through the plate resistance of the tube, the plate-to-cathode capacitance, and a third path consisting of the grid-plate and grid-cathode capacitances and the grid-lead inductance. By improving the electrostatic shielding of the tube, the plate-cathode ca-

pacitance can be cut drastically, but the additional shielding will increase the grid-cathode and grid-plate capacitances and thereby lower the impedance of the feed-through path they provide. This accounts for the experimental results obtained when an improvement of the electrostatic shielding gave poorer rather than better isolation.

As already mentioned, one of the effects of coupling between the input and output circuits is that with the plate-load impedance tuned to a fixed frequency, the input impedance varies widely over the amplifier pass band. This is much like the Miller effect in a grounded-cathode amplifier. Because of the gain of the tube, the voltage applied to the cathode causes a larger voltage to appear at the plate. As the plate-load impedance changes over the pass band, there is a change in the amplitude and phase of the plate voltage with respect to the input voltage. The difference between the input voltage and the output voltage is impressed across the feed-through circuits indicated in Fig. 1, and current will flow through these various paths as a result. As this current flows in the input circuit, it modifies the apparent input impedance of the amplifier. Changes in phase and amplitude of this current as the plate-load impedance varies over the frequency pass band can, under certain conditions, cause excessive variations of the input impedance. As a result, with the impedance of the input circuit matched at the center frequency, the mismatch at frequencies away from the center frequency may be so great that the bandwidth of the sys-

Fig. 2—Smith chart plot showing the excessive input impedance variations of an early developmental tube.

tem is limited by the input circuit impedance change rather than by the bandwidth of the plate circuit.[1]

Several observations which should help to avoid misinterpretations may be made regarding this effect.

1. The magnitude of the effect on the input impedance is a function of the voltage gain as well as the equivalent admittance of the feed-through path. A tube which is relatively poor from the standpoint of isolation between input and output circuits will show a satisfactory input impedance characteristic if it is put in a circuit which causes it to have a low gain. A tube operating at a high gain will amost always show considerable input admittance variation over the pass band, because the high radio-frequency plate voltage developed is sufficient to produce appreciable current in the feed-through paths even if these paths have a relatively high impedance.

2. In even the best tubes coupling through the plate resistance of the tube is noticeable at high gain levels.

3. Bandwidth is a much less important factor than gain in determining the amount that the input admittance changes over the band. The plate-load impedance will change the same amount between the half-power points, regardless of the actual bandwidth. Of course, the variation of the static or "cold" component of the input impedance will have a greater effect over the wider bandwidth. This change is usually small compared to other impedance changes involved.

Fig. 2 indicates approximately the input impedance characteristic obtained with the early models of this tube. This is a Smith chart showing the input impedance of the amplifier circuit as seen looking into the circuit through a 50-ohm transmission line. The large arc drawn with a solid line shows the operation of the tube at a center frequency of 900 mc and a bandwidth of 20 mc. As the frequency is varied over the pass band of the amplifier, the input impedance changes as shown over the frequency range from 890 to 910 mc. Other arcs show the operation of the tube with the plate circuit tuned to center frequencies of 700, 500, and 400 mc. The dashed line shows the locus of the input impedance over the uhf band for the condition that the plate load impedance is tuned to resonance at the input frequency.

It should be mentioned that Fig. 2 does not represent actual data on a specific tube. Due to measurement difficulties encountered with the earliest tubes, exact data on input impedance are not available; and the curves shown are meant only to be representative of characteristics of the first design. It should also be emphasized that the input impedance of the amplifier circuit, not of the tube itself, is shown. The connections between the tube and the 50-ohm transmission line represent discontinuities which introduce impedance transformations in the measured input impedances. However, it is evident that excessive impedance variations are encountered in these tubes at the high end of the uhf band. Another difficulty, also due to poor isolation between input an output circuits, will be encountered with large variations of input impedance. Tube will be found inferior with regard to attenuation of local oscillator signal.

Redesign to Reduce Internal Coupling

Fig. 1 represents approximately the circuits which produce unwanted coupling between the input and output circuits. The circuit shown in Fig. 3 represents an idealized solution to the problem of coupling. The unavoidable plate-to-cathode capacitance and plate resistance are of course still present. Neither has the grid-lead inductance been eliminated; if the tube is to remain a 9-pin miniature, it is unlikely that the grid-lead inductance can be made negligible. However, without eliminating this inductance, this circuit does eliminate any transmission of energy through the path associated with the grid-lead inductance.

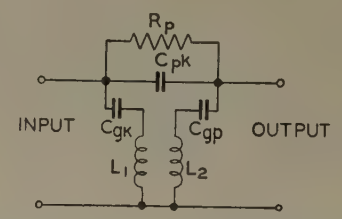

Fig. 3—Idealized equivalent circuit showing a method of eliminating the coupling caused by grid-lead inductance.

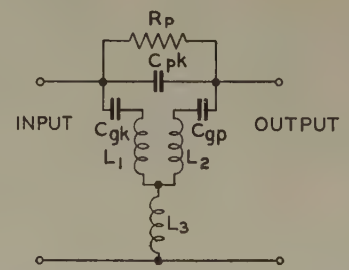

Fig. 4—The approximate equivalent circuit responsible for coupling between input and output circuits of the 6AJ4.

Fig. 5—Tube and mounts showing the construction of the 6AJ4.

[1] An analytical expression for input impedance is easily derived from equations developed in a companion paper by H. Hsu, "On transformations of linear active networks with applications at ultra-high frequencies," Proc. I.R.E., vol. 41, pp. 59–66, this issue. His equations 114 and 117, for the grounded-grid case ($g_p' = g_k' = 0$), may be combined to give

$$Y_{in} = Y_{31} + A(Y_{23} + Y_2),$$

where A is the voltage gain and Y_2 is the load admittance. Y_{31} and Y_{23} refer to constants of the circuit shown in his figure 4(b), which is a transformed equivalent circuit including the effect of grid-lead inductance.

This circuit is not actually obtainable because there will always be a small amount of mutual inductance or inductance common to both paths. However, by a careful redesign of the tube it has been possible to obtain the circuit of Fig. 4, where the inductance I_3 is relatively small. The isolation between input and output circuits is very much improved as a result.

A number of different tube designs were tried to determine which would give the isolation between input and output circuits. The most effective design was also, with a few modifications, the easiest design to manufacture. See present tube design (Fig. 5). Two large metal sheets provide a low inductance path between grid and ground, and give electrostatic shielding between cathode and heater connectors and plate.

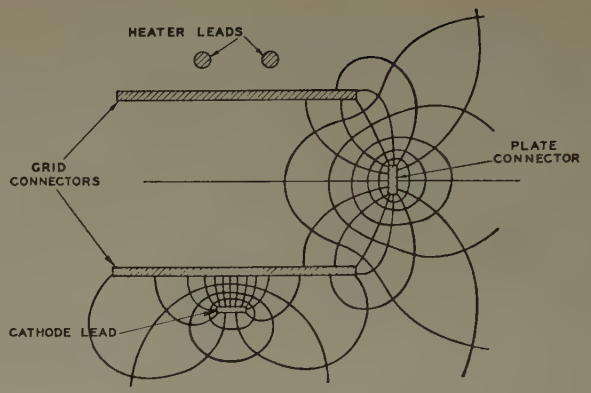

Fig. 6—Approximate cross section of the 6AJ4 lead configuration with a flux plot to indicate the degree of inductive isolation between input and output current paths.

Fig. 7—Smith chart representation of the input impedance of a 6AJ4 grounded-grid amplifier circuit over the frequency range of 400–900 mc.

It was mentioned that the improved performance of this tube is not primarily due to decreasing the grid-lead inductance, but rather is due to separation of the inductance through which the currents in the input and output circuits flow. To illustrate why this is so, a flux plot has been sketched in Fig. 6, which shows an approximate cross-sectional view of the tube. At high frequencies the currents flowing in the grid-cathode circuit are largely confined to the area in the grid lead just opposite the cathode connector. The currents flowing in the grid-plate circuit tend to travel along the right-hand edges of the grid connectors as shown in the sketch. The flux plot gives some indication of the area of influence of the two current paths. There is some overlap, but this construction gives the practical equivalent of separate transmission-line connections to the input and output circuits, with only a small degree of coupling between the two lines.

Fig. 7 illustrates the effectiveness of this arrangement. It shows the input impedance of a 6AJ4 tube over the uhf spectrum. Although the arcs over the amplifier bandwidth are moderately large in size, this tube is operating at a considerably higher gain. Considering this fact, the Smith chart plot in Fig. 7 indicates much better performance than the Smith chart plot in Fig. 2. A large part of the change in input impedance is due to energy fed through the plate resistance of the tube. This is indicated by the fact that the effect is about the same at all frequencies. The reactive coupling circuit that gave such a large impedance variation at 900 mc in the earlier tubes now has very little effect. The only reason that tubes of earlier design showed very little effect from coupling through the plate resistance was that the gain was not high enough for this effect to be noticeable. Tubes of the present design are also better from the standpoint of attenuation of local oscillator radiation.

Test Equipment

At ultra-high frequency it is impossible to separate tube design and circuit work; hence it was necessary to develop testing equipment as a part of the tube development program. This paper will describe the type of circuit which was first constructed and which is still found most convenient for routine testing. The work done on practical circuits, such as might be found in uhf television tuners, will not be discussed in this paper.

Essentially, all that was done to set up the amplifier circuit was to make the simplest possible connections from the tube elements to 50-ohm transmission lines. Aside from the chassis, which holds the tube under test, almost all parts of the test setup are standard components coupled together with General Radio Type 874 Universal Coaxial Connectors. No attempt is made to match the input impedance of the tube to the 50-ohm line, because, with a standing-wave detector, the power being fed into the tube can be measured whether the impedances are matched or not—the power is proportional to the product of the maximum and the minimum voltages of the standing-wave pattern.

Fig. 8 shows the essential features of the circuit. DC potentials are applied to the tube through radio-frequency chokes, and blocking capacitors are placed in the transmission-line system. The signal generator feeds

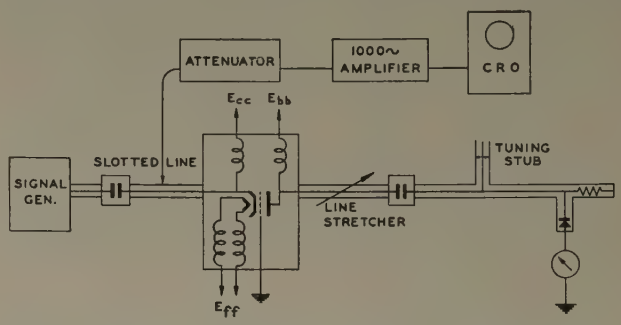

Fig. 8—Schematic diagram of the 6AJ4 coaxial-line test circuit.

a modulated signal to the tube through the standing-wave detector (or slotted line). The slotted-line crystal responds to the envelope of the modulated signal. The amplitude of the signal at any point is indicated by setting the calibrated attenuator so that a certain deflection is obtained on the oscilloscope.

The output load is a 50-ohm resistor. A crystal detector and a microammeter give an indication of the radio-frequency voltage across this resistor. A tuning stub and a line stretcher make it theoretically possible to transform the 50-ohms to any desired impedance, so there is no difficulty in adjusting it to the impedance necessary for proper performance. Although there is some interaction between the two variable elements used to control the load impedance, it is convenient to think of the tuning stub as the bandwidth control and the line stretcher as the adjustment for the resonant frequency of the load.

The method of measuring gain is very straightforward. The input power level is adjusted until the desired output indication is obtained on the microammeter. The input power is measured by means of the slotted line. The chassis holding the tube under test is then unplugged from the system, and the load is connected directly to the slotted line. The signal generator is adjusted to give the same deflection as before on the microammeter. It is then supplying the same power to the load that the amplifier tube was previously delivering. This power is measured with the slotted line. The power gain may then be found as the ratio of the power delivered to the load to the power input to the tube.

Fig. 9 shows the chassis which holds the tube under test. The input and output transmission lines are connected directly to the tube socket. DC power is fed in through radio-frequency chokes. The input and output circuits are separated by the shield which is placed horizontally to divide the chassis into two separate compartments, plus the smaller shield which extends downward and to the left from the center of the horizontal shield. A cover goes over the assembly to make the shielding complete. The cathode connection is at the

top. At the lower left are the heater leads, and the plate lead is at the lower right.

The main advantage of this type of circuit lies in its adaptability. It is not necessary to match the input, and the circuit can be adjusted for use with any output impedance. Therefore, neither the input nor the output impedances of the tube need to be considered. However, this can be a disadvantage as well as an advantage. For instance, the circuit may appear to give perfect performance with a tube having some serious defect, such as an input impedance which varies excessively with small changes in frequency.

Probably the biggest disadvantage of this type of circuit is that all of the transmission-line components which make up the load impedance—the line stretcher, the tuning stub, and so forth—can easily add up to one and a half wavelengths of transmission line unless very careful steps are taken to hold these lengths to a minimum. The bandwidth of such a system is much narrower than could be obtained with a more compact arrangement, and the circuit does not give an accurate picture of the full capabilities of the tube. With the particular arrangement which was chosen this is apparently more troublesome at the lower frequencies, and the test results actually show a slight dropping off in performance at the low end of the UHF television band.

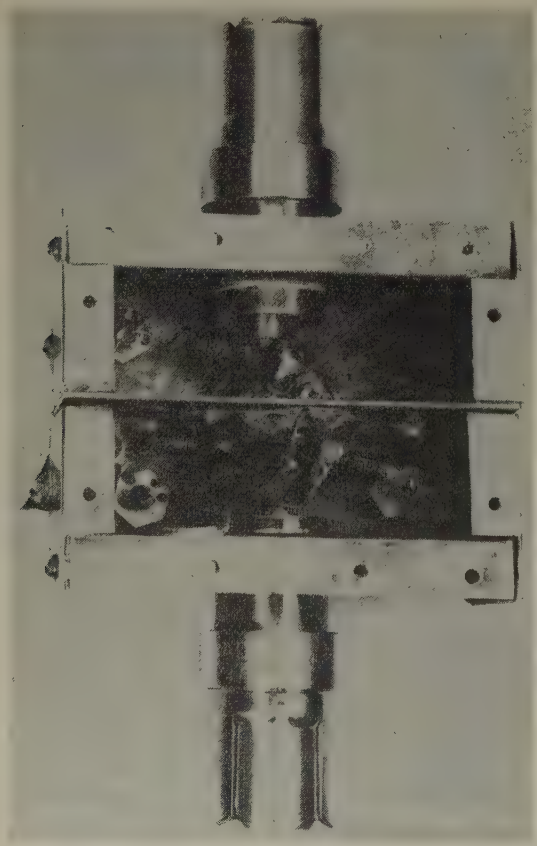

Fig. 9—Amplifier test chassis.

As an example of the improvement possible by a redesign of the plate-load impedance, the load shown in Fig. 10 was made which used for the bandwidth control a specially designed tuning stub which was a very small fraction of a wavelength long (rather than approximately a half wavelength long as dictated by convenience in the present arrangement). Control of the resonant frequency over a limited range was obtained by replacing the line stretcher (about a wavelength long) with an adjustable short-circuited stub about a quarter-wavelength long. This second stub was located about a

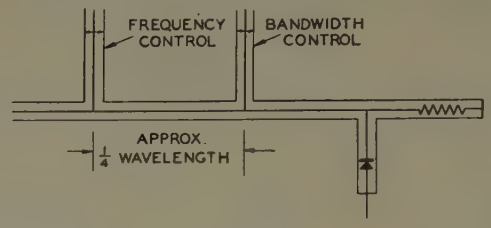

Fig. 10—Modified load circuit designed for improved bandwidth.

quarter wavelength from the stub controlling bandwidth, i.e., near a voltage maximum. In this position it is almost exactly equivalent to a line stretcher over a limited range. When compared to the system shown in Fig. 8, this load gave a 70-per cent increase in bandwidth with no loss in gain. Other improvements are of course possible. For instance, the quarter-wavelength adjustable short-circuited stub used for control of the resonant frequency could be replaced by an open-circuit adjustable stub a small fraction of a wavelength long. The short open-circuited stub would be less frequency sensitive than the longer short-circuited stub.

The convenience of the somewhat less efficient system outweighs many of its disadvantages. One load circuit can be used to cover the entire uhf band. Its components are all standard parts, and its construction is simple and easily duplicated. Although this arrangement does not reveal the maximum capabilities of the tubes tested, relative indications showing the difference between tubes are accurately obtained. The disadvantages of the system are serious only so long as these disadvantages are not recognized in interpreting the test results.

The gain measured with a 10-mc bandwidth is given in the coaxial-line test setup described, and also in what might be termed a "practical" circuit, using lumped-constant circuit elements.

TABLE I

Radio-Frequency Performance of the 6AJ4

Frequency in megacycles	Gain in coaxial-line circuit in decibels (bandwidth = 10 mc)	Performance in lumped-constant circuits	
		Gain in decibels (bandwidth = 10 mc)	Noise figure in decibels (stage bandwidth = 10 mc. Over-all noise bandwidth = 4 mc)
500	6.2	6.9	12.2
600	6.8	7.6	13.4
700	7.6	7.4	15.2
800	7.8	6.9	15.3
900	7.0	6.0	15.2

Acknowledgment

I would like to express my appreciation to the many people who have co-operated during the development

of this tube. Dr. Hsiung Hsu did much of the work in setting up the original test equipment, and made important fundamental contributions in the design of the tube itself. A. P. Haase, under whose direction this work was carried on, made many helpful suggestions. H. W. A. Chalberg has worked on the circuit developments and supervised the testing associated with this project. An investigation of the noise characteristics was carried out by J. W. Rush, and most of the other measurements made on the tube have been made by R. L. Bailey. Additional development work leading to the commercial version of this tube was carried out at Owensboro by J. G. Tucker, under the supervision of W. T. Millis.

Multichannel Crystal Control of VHF and UHF Oscillators*

ALWIN HAHNEL†

Summary—**Single-crystal control of a multiplicity of uhf channel frequencies is obtained by periodic phase control of a variable oscillator. Its output consists of a spectrum of harmonically related frequencies. The bandwidth of the spectrum envelope can be kept so narrow that the amplitude of any single desired frequency of the very large number of available ones is emphasized up to 40 db over the amplitudes of the adjacent harmonics. Suppressions of the undesired frequencies in this order of magnitude are obtained in oscillators which cover a frequency range of from 250 to 900 mc and are simultaneously excited at a crystal-controlled fundamental frequency in the range of from 1 to 10 mc. Thus, utilizing one single triode this uhf oscillator may put out any desired one of a very large number of crystal-controlled frequencies. It is continuously tunable over a wide frequency range, acting as though it were electronically detented.**

Introduction

A HIGH DEGREE of frequency accuracy is difficult to obtain if a multiplicity of frequency channels is required under conditions which do not allow the use of a separate crystal for each one. A relatively little known method of solving these problems at uhf or lower frequencies exists by the periodic phase control of a variable frequency oscillator at a frequency which is the fundamental of the desired harmonic frequencies. The output of this oscillator constitutes a spectrum of harmonically related frequencies whose envelope is peaked at the frequency to which the tank circuit of the variable frequency oscillator is tuned. In this phase-controlled mode of operation, the oscillator is termed a "spectrum generator." It may consist of a uhf oscillator tuned to the center of the desired spectrum, which is keyed by pulses at the crystal-controlled fundamental frequency.

Principle of Operation

The pulse repetition interval (T) is divided into a regenerative and a degenerative period. If a sufficiently high ratio of the time of pulse duration (T_p) to the time of one uhf period (T_0) can be realized, the oscillations increase during the regenerative period until a non-linear range of the tube characteristic becomes involved and a constant amplitude condition is reached. The oscillations of the free-running oscillator are quenched in the degenerative interval because of the pulse-controlled decrease of the transconductance of the oscillator tube, resulting in a positive damping of the tuned circuit.

To obtain a harmonic frequency spectrum it is essential that the uhf oscillator is pulsed so that its output waveform is periodic at the repetition frequency of the pulses. The oscillations must start with the same phase at the edge of each pulse, requiring that at the end of the degenerative period the oscillations have decayed to noise level and that the pulse harmonics have in the vicinity of the frequency to which the tank circuit is tuned an amplitude sufficiently large compared to the noise level. The resulting uhf wave shape is shown in Fig. 1.

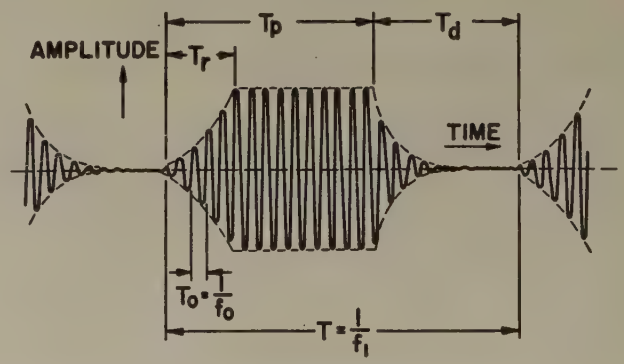

Fig. 1—Periodic time function as derived from the pulsed oscillator.

A Fourier analysis of the output waveform was made. An approximate solution was obtained by breaking up the RF waveform into periods of exponential build-up, constant-amplitude, and exponential decay. However, even with simplifying assumptions, the formula describing the spectrum envelope as a function of the oscillator waveform becomes an expression too cumbersome to be of much value at frequencies which are too high for direct observation of the periodic time function on an oscilloscope.

* Decimal classification: R355.6×R355.912. Original manuscript received by the Institute, October 9, 1952.
† Signal Corps Engineering Laboratories, Fort Monmouth, N. J.

The Fourier analysis of the periodic time function shows that, in order to obtain a spectrum of minimum envelope bandwidth, it is necessary to extend the constant amplitude period to a practical limit. This requires build-up and decay periods which are short compared to the intervals between two successive pulses. The build-up time can be shortened by increasing the regenerative coupling, but it depends upon the amplitude of the pulse harmonics in the vicinity of the oscillator frequency. To shorten the decay time a low circuit Q is required.

Circuit Details

The RF oscillator may be of any type which permits periodic phase control. The cathode-coupled oscillator shown in Fig. 2 was chosen in order to get high power output at very high frequencies. The grounded-grid amplifier is keyed at a crystal-controlled repetition frequency. The magnitude of feedback and, with this, the rise time of the oscillations is controlled by the cathode follower section. The conventional method of reducing

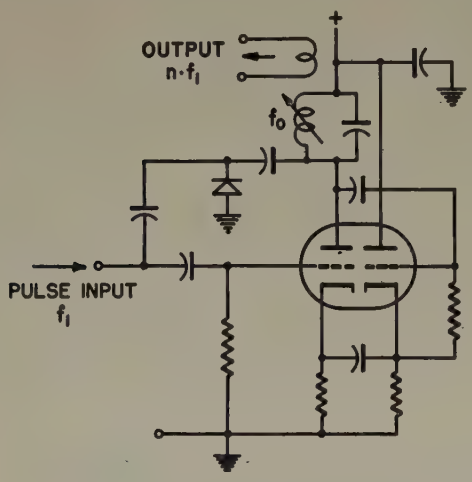

Fig. 2—Schematic diagram of a vhf spectrum generator.

decay time by low resistance shunting of the tuned circuit is not applicable in the case where maximum suppression of unwanted frequencies and large amplitude of the desired harmonic frequencies are important; a synchronously controlled diode paralleling the oscillator tank circuit was therefore provided. This diode is keyed so that it is in cutoff condition during the regenerative periods and is heavily conducting in between. This type of circuit was used in experimental vhf spectrum generators up to a frequency of 300 mc. It allowed an extension of the regenerative phase of operation to more than 90 per cent of the pulse repetition period.

The attempt to simplify the spectrum generator to a practical limit led to the development of a feedback oscillator consisting of two resonant circuits and two feedback paths so as to permit simultaneous excitation of two frequencies. A schematic diagram of an experimental spectrum generator of this type is shown in Fig. 3. The butterfly circuit is tunable over the frequency range from 250 to 900 mc. The other tuned circuit and the crystal are resonant at the desired fundamental frequency (f_1). The oscillation characteristic for f_1 represents the relation between the average plate current and the average grid voltage during the oscillation at the

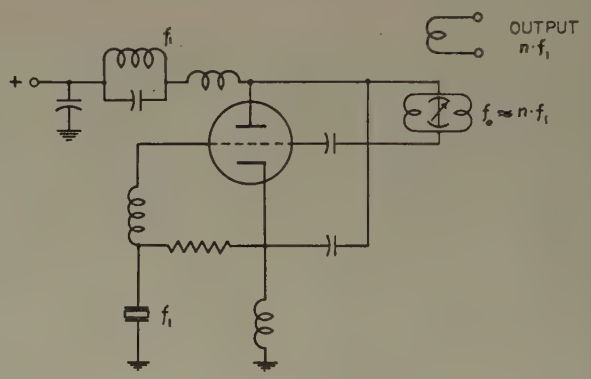

Fig. 3—Schematic diagram of a complete uhf spectrum generator.

higher of the two frequencies. For the higher frequency f_0, the point of operation shifts along the oscillation characteristic synchronously with the lower frequency. The frequency f_0 is thereby modulated with the lower one. By proper choice of circuit parameters it is possible to establish quenching at the lower frequency so that, during the degenerative period, the f_0 oscillation decays to noise level and the output waveform is phase-controlled at f_1. In this case, the output frequencies are exact harmonics of the crystal-controlled lower frequency.

Results

The various operation conditions are shown in the following oscillograms made at $f_0=10$ mc, particularly choosing that frequency for easier observation of the periodic time function. Fig. 4(a) shows a wave shape

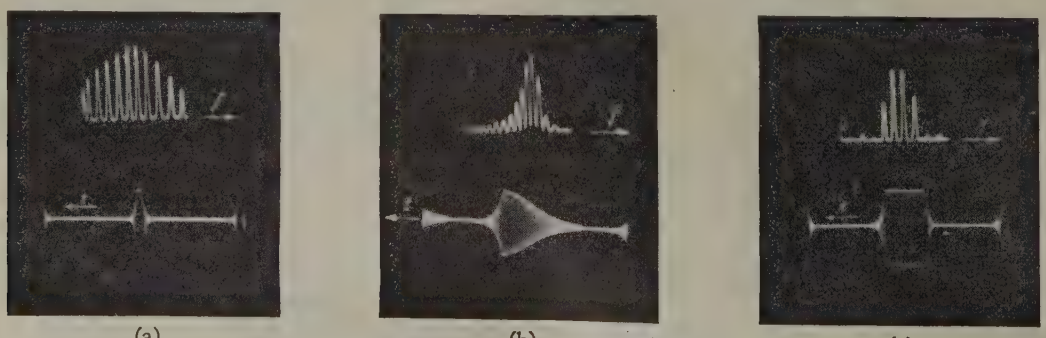

(a) (b) (c)

Fig. 4—Wave shape and frequency spectrum for relatively short pulses; $f_0=10$ mc.

with short rise and decay times, obtained with a pulse duration (T_p) of 2 μsec, at a pulse repetition rate (f_1) of 40 kc, which results in a broad spectrum envelope. The middle picture shows long rise and decay times of the wave shape which was obtained at $f_1 = 20$ kc, with pulses of 30-μsec duration. The spectrum envelope is unsymmetrical with respect to the frequency f_0 to which the oscillator is tuned. A pulse duration equal to half the pulse repetition interval, at $T = 25$ μsec, gives, under conditions resulting in the sharp rise and decay slopes of the periodic function pictured in Fig. 4(c), a spectrum envelope of narrow bandwidth. The oscillograms "a" and "c" were taken with the oscillator tuned to a frequency between two adjacent harmonics of f_1.

Single frequency output is attained by the generation of a wave shape with rapid increase and decrease of the oscillations, having a relatively long period of constant amplitude, as can be seen from Fig. 5(a). Tuning the oscillator from a frequency which is an integral multiple of the keying frequency to a point between two adjacent harmonics modifies the output spectrum to the one shown in Fig. 5(b).

Spectrum generators of the type which is phase-controlled by an external pulse source were tested over the frequency range from 1 to 900 mc. When designed for operation as frequency multipliers, with widely variable multiplication factors, differences of up to 40 db between the amplitude level of the desired harmonic frequency and those of unwanted harmonics of a similar order are obtained.

Triode oscillator circuits which were designed for simultaneous excitation of the uhf (250 to 850 mc) and the crystal-controlled fundamental frequency (1 to 10 mc) gave up to 40-db emphasis of the harmonic frequency to which they were tuned.

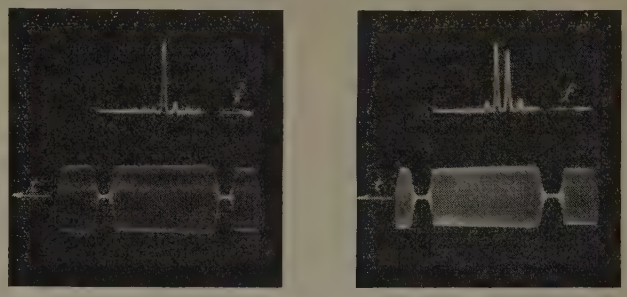

(a) (b)

Fig. 5—Effect of oscillator tuning on the frequency spectrum obtained with relatively long pulses; $f_0 = 10$ mc and $f_1 = 40$ kc.

Conclusions

The described spectrum generator has a wide range of applications. It was successfully applied in models of multichannel equipment in which it allowed considerable simplification of the frequency-control circuits. Operating the spectrum generator as a frequency multiplier, it may be used directly as a crystal-controlled master-oscillator. In such a system, frequency modulation may be introduced in the pulse circuit. Another application is in intermediate frequency receivers where it may replace the local oscillator; thus the receiver becomes tunable in discrete steps.

A Wide-Band Hybrid Ring for UHF*

WALTER V. TYMINSKI†, ASSOCIATE, IRE AND ALBERT E. HYLAS†, ASSOCIATE, IRE

Summary—**A $6\lambda/4$ hybrid ring was modified by replacing the $3\lambda/4$ long arm, with a $\lambda/4$ line and a frequency insensitive π phase shift. Calculations are shown for input and transfer admittances, insertion loss, and the effect of capacitance across the loads. Some experimental results are given and applications for the wide-band hybrid ring are suggested.**

Introduction

THE HYBRID RING[1–4] has been employed at microwave frequencies primarily as a mixer, and also has been utilized at ultra-high television frequencies to combine power in experimental transmitters.[5] However, its application to small signals at uhf has received relatively little attention and its inherent properties which include isolation of sources, sensitivity to unbalance, and practical physical size make it a useful and convenient tool for designers and experimenters at uhf.

The balance of the conventional $6\lambda/4$ hybrid ring shown in Fig. 1(a) is sensitive to frequency deviations, and thus it is essentially a narrow-band device. Another version of the hybrid ring, where the $3\lambda/4$ arm of the $6\lambda/4$ hybrid ring is replaced by a $\lambda/4$ arm and a frequency insensitive reversal of phase, is shown in Fig. 1(b). Since the balance of this ring is not a function of frequency, its bandwidth can be expected to be very wide, thus the term *wide-band hybrid ring*.

* Decimal classification: R310. Original manuscript received by the Institute, October 16, 1952.

† Allen B. Du Mont Laboratories, Inc., Research Division, Passaic, N. J.

[1] W. A. Tyrrell, "Coupling Arrangement for Use in Wave Transmission Systems," U. S. Patent 2,445,895.

[2] W. A. Tyrrell, "Hybrid circuits for microwaves," PROC. I.R.E., vol. 35, pp. 1294–1306; November, 1947.

[3] H. T. Budenbon, "Analysis and performance of waveguide hybrid rings for microwaves," *Bell Sys. Tech. Jour.*, vol. 27, pp. 473–486; July, 1948.

[4] R. V. Pound, "Microwave Mixers," Radiation Laboratory Series, McGraw-Hill Book Co., Inc., New York, N. Y., vol. 16, pp. 257–289; 1948.

[5] G. H. Brown, W. C. Morrison, W. L. Behrend, and J. G. Reddeck, "Method of multiple operation of transmitter tubes particularly adapted for television transmission in the ultra-high-frequency band," *RCA Rev.*, vol. 10, pp. 161–172; June, 1949.

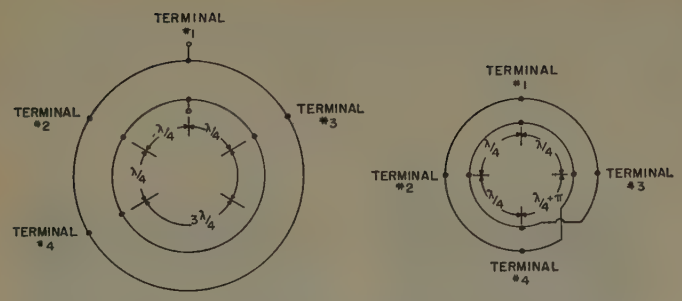

Fig. 1—(a) 6λ/4 hybrid ring. (b) Wide-band hybrid ring.

Analysis

By replacing each arm of the hybrid ring shown in Fig. 1(b) with its π equivalent circuit, the pertinent equations may be obtained by employing Kirchoff's laws. However, before setting down the equations to be derived from the equivalent circuit shown in Fig. 2, there are several items that should be mentioned. First, for generality, the load conductances at terminals two and three are related to the source conductance at terminal one by a factor of k. Furthermore, the line conductance is a function of k so that the input conductance of the ring will match the source conductance at the design center frequency of the ring. Because the equivalent circuit is balanced with respect to ground, only four of the possible eight nodal equations are necessary to describe operation of the ring. The simultaneous equations are

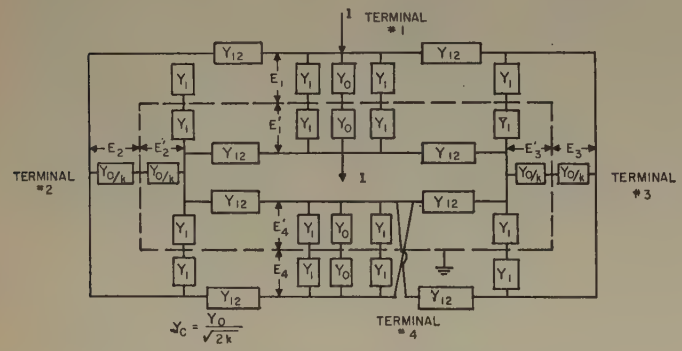

Fig. 2—Equivalent circuit of wide-band hybrid ring.

$$I = E_1Y_{11} - E_2Y_{12} - E_3Y_{12}, \tag{1}$$

$$O = -E_1Y_{12} \quad E_2Y_{22} \quad -E_4Y_{12}, \tag{2}$$

$$O = -E_1Y_{12} \quad E_3Y_{33} \quad E_4Y_{12}, \tag{3}$$

$$O = -E_2Y_{12} \quad E_3Y_{12} \quad E_4Y_{44}, \tag{4}$$

where

$$Y_{11} = Y_{44} = Y_0 + 2Y_1 + 2Y_{12},$$

$$Y_{22} = Y_{33} = Y_0/k + 2Y_1 + 2Y_{12},$$

and

$$Y_1 = JY_c \tan\frac{\theta}{2} = J\frac{Y_0}{\sqrt{2k}}\tan\frac{\theta}{2},$$

$$Y_{12} = -J\frac{Y_c}{\sin\theta} = -J\frac{Y_0}{\sqrt{2k}\sin\theta}.$$

By solving (1), (2), (3), and (4) for E_4 there is obtained the result that is intuitively obvious, namely,

$$E_4 = 0. \tag{5}$$

This result is independent of frequency and load conditions at terminal 4. By substituting (5) in (4), it is also apparent that for all frequencies

$$E_2 = E_3. \tag{6}$$

The condition of (5) also simplifies (1), (2), (3), and (4) so that the operation of the circuit may be described by two equations.

$$I = E_1Y_{11} - 2E_2Y_{12}, \tag{1a}$$

$$O = -E_1Y_{12} + E_2Y_{22}. \tag{2a}$$

From (1(a)) and (2(a)), the input and transfer admittance may be derived and power relationships obtained. Deriving first the normalized input admittance,

$$y_{in}' = \frac{Y_{in}}{Y_0} = \frac{I}{E_1Y_0} = \frac{Y_{11}}{Y_0} - 2\frac{\dfrac{Y_{12}^2}{Y_0^2}}{\dfrac{Y_{22}}{Y_0}}. \tag{7}$$

After substituting the equivalent for Y_{11}, Y_{22}, and Y_{12}, (7) becomes

$$y_{in}' = 1 + \frac{1}{1 + (2k-1)\cos^2\theta} + J\frac{\sqrt{2}}{\tan\theta}\left[\frac{\sqrt{k}}{1 + (2k-1)\cos^2\theta} - \frac{1}{\sqrt{k}}\right]. \tag{8}$$

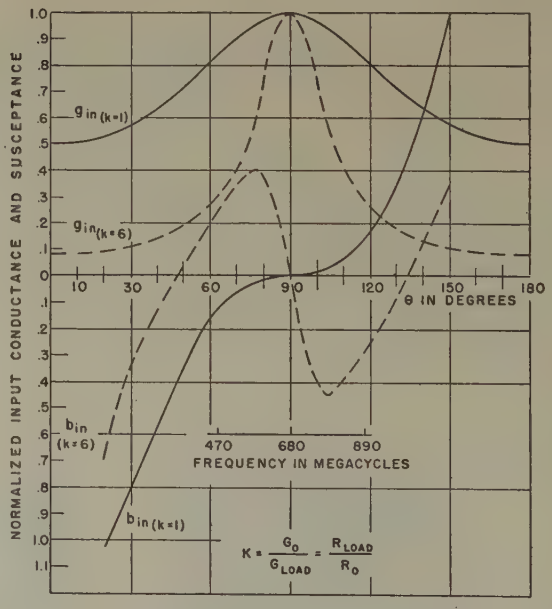

Fig. 3—Input admittance vs. frequency for wide-band hybrid ring.

It should be noted here that the source conductance is included in the input admittance equation. If the input admittance of the ring is desired, then it may be obtained by subtracting 1 from (8) so that (see Fig. 3)

$$y_{in} = y_{in}' - 1. \tag{9}$$

The transfer admittance may be expressed by

$$y_T = \frac{Y_T}{Y_0} = \frac{I}{E_2 Y_0} = \frac{\frac{Y_{11}}{Y_0}\frac{Y_{22}}{Y_0}}{\frac{Y_{12}}{Y_0}} - 2\frac{Y_{12}}{Y_0}, \qquad (10)$$

and once again substituting the equivalent for Y_{11}, Y_{22}, and Y_{12}, (10) becomes

$$y_T = \left(2 + \frac{2}{k}\right)\cos\theta + J\sqrt{\frac{2}{k}}\sin\theta\left(2 - \frac{1}{\tan^2\theta}\right). \qquad (11)$$

The power absorbed by the ring exclusive of that absorbed by the source impedance may be expressed as

$$P_{in} = |E_1|^2 \,\mathrm{Re}\,(Y_{in}), \qquad (12)$$

where

$$\mathrm{Re}\,(Y_{in}) = \frac{1}{1 + (2k-1)\cos^2\theta},$$

and

$$|E_1|^2 = \frac{I^2[1 + (2k-1)\cos^2\theta]^2}{Y_0^2\left\{[2 + (2k-1)\cos^2\theta]^2 + \frac{2}{k\tan^2\theta}[k - 1 - (2k-1)\cos^2\theta]^2\right\}},$$

so that

$$P_{in} = \frac{I^2[1 + (2k-1)\cos^2\theta]}{Y_0\left\{[2 + (2k-1)\cos^2\theta]^2 + \frac{2}{k\tan^2\theta}[k - 1 - (2k-1)\cos^2\theta]^2\right\}}. \qquad (13)$$

This power is maximum when $\theta = \pi/2$, which corresponds to the design center frequency of the ring and is equal to the maximum available power from the source, or

$$P_{in(\theta=\pi/2)} = \frac{I^2}{4Y_0}. \qquad (13a)$$

By normalizing (13) with respect to (13(a)), an expression is obtained showing the power loss when the frequency is other than at design center

and

$$p = \frac{P_{in}\left(\theta = \frac{\pi}{2}\right)}{P_{in}} = \frac{[2 + (2k-1)\cos^2\theta]^2 + \frac{2}{k\tan^2\theta}[k - 1 - (2k-1)\cos^2\theta]^2}{4[1 + (2k-1)\cos^2\theta]}. \qquad (14)$$

Equation (14) defines a response curve for the wideband hybrid ring, and in the subject application it is desirable that the bandwidth be maximum. Although an expression for bandwidth can be derived and differentiated with respect to k to find the optimum value of k, it is easier here to differentiate p with respect to k for any given angle of θ and set the differential equation equal to zero to obtain the optimum k. Thus

$$\frac{dp}{dk} = \frac{1}{4}\left\{-\frac{[(1 - \cos^2\theta) + 2k\cos^2\theta]\frac{2}{\tan^2\theta}}{k^2} + \left[1 + \frac{2}{k\tan^2\theta}\right]2\cos^2\theta\right\} = 0. \qquad (15)$$

Solving (15) for k,

$$k = 1. \qquad (16)$$

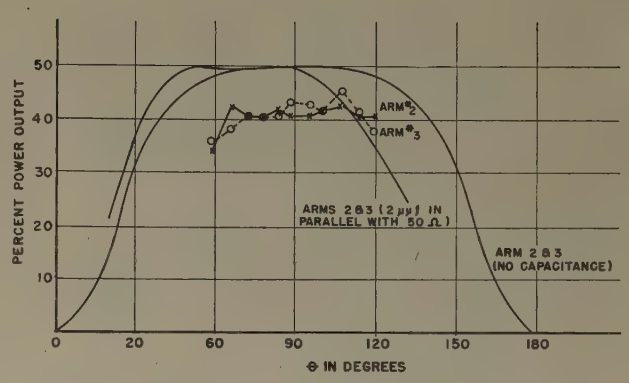

Fig. 4—Theoretical and experimental power outputs at terminals 2 and 3 versus frequency.

A plot of the reciprocal of p with $k = 1$ is shown in Fig. 4, and the half-power bandwidth is approximately 130 degrees. Assuming a band center frequency of 680 mc, this corresponds to a bandwidth of almost 1000 mc.

Since the variation of power output with frequency is due to mismatch at the input terminals, (14) can be used to determine the voltage standing-wave ratio, and the variation with frequency can be inferred from Fig. 4.

The voltage standing-wave ratio may be obtained from the expression

$$\rho = \frac{1 + \left|\frac{1 - y_{in}}{1 + y_{in}}\right|}{1 - \left|\frac{1 - y_{in}}{1 + y_{in}}\right|}. \qquad (17)$$

After substituting the value of $Y_{(k=1)}$ in the above equation, (17) becomes

$$\rho = \frac{1+\sqrt{\dfrac{\cos^6\theta+\cos^4\theta}{\cos^6\theta-3\cos^4\theta+4}}}{1-\sqrt{\dfrac{\cos^6\theta+\cos^4\theta}{\cos^6\theta-3\cos^4\theta+4}}}. \qquad (18)$$

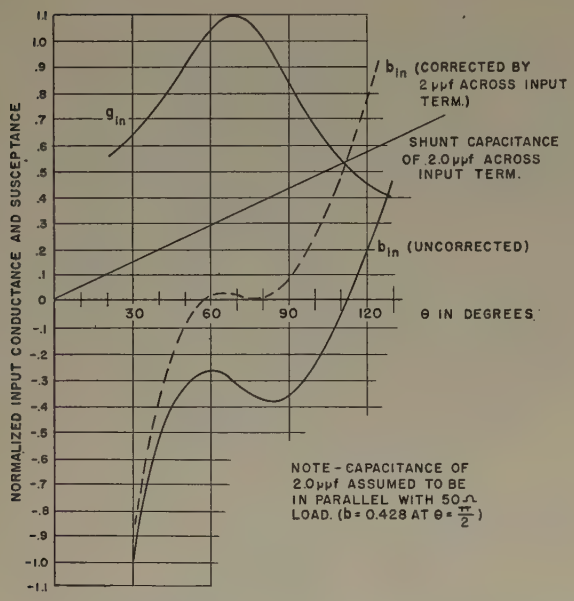

Fig. 5—Input admittance versus frequency of wide-band hybrid ring with capacitance at terminals 2 and 3.

While the preceding analysis was carried out for purely resistive terminations, parallel capacitance is invariably encountered in practice. To accommodate the parallel RC load at terminals 2 and 3, Y_{22} becomes

$$Y_{22} = \frac{Y_0}{k} + 2Y_1 + 2Y_{12} + Y,$$

where

$$Y = JB = J\omega C \quad \text{and} \quad \frac{B}{Y_0} = b.$$

When Y_{22} is substituted in (7), the normalized admittance for $k=1$ becomes

$$y_{in} = g_{in} + J\left[\frac{\sqrt{2}}{\tan\theta}(g_{in}-1) - g_{in}b\right], \qquad (19)$$

where

$$g_{in} = \frac{1}{\sin^2\theta\left[1+\left(\dfrac{\sqrt{2}}{\tan\theta}-b\right)\right]}. \qquad (20)$$

Normalized input conductance and susceptance for the special case where $b=0.428$ at $\theta=\pi/2$ has been plotted in Fig. 5. As might be expected, the capacitive loading reduces the line lengths necessary; the graph also shows that the input susceptance can be made small over a wide band if equal capacitors equivalent to $b=0.428$ at $\theta=\pi/2$ is placed across terminals 1 and 4.

The response of this capacity-loaded hybrid ring can then be evaluated from the normalized input admittance which becomes

$$y_{in} = g_{in} + J(g_{in}-1)\left(\frac{\sqrt{2}}{\tan\theta}-b\right), \qquad (21)$$

where g_{in} is defined by (20) and $b=0.428$ at $\theta=\pi/2$. The response curve as plotted in Fig. 4 is obtained from

$$\rho = \frac{(g_{in}+1)^2+(g_{in}-1)^2\left(\dfrac{\sqrt{2}}{\tan\theta}-b\right)}{4g_{in}}. \qquad (22)$$

Some Practical Considerations and Experimental Results

The hybrid ring shown in Fig. 1(b) was built by cutting four lengths of 75-ohm twin-lead transmission line a quarter wave length at the center frequency and connecting them to 50-ohm connectors as indicated in the diagram. Two such networks were assembled and one intended for balanced feed was mounted on an insulating material, in this case glass-bonded mica, and the other employing unbalanced feed was mounted on copper sheet. Photographs showing the size and configuration of two typical rings, together with a printed circuit version, are shown in (a) and (b) of Fig. 6.

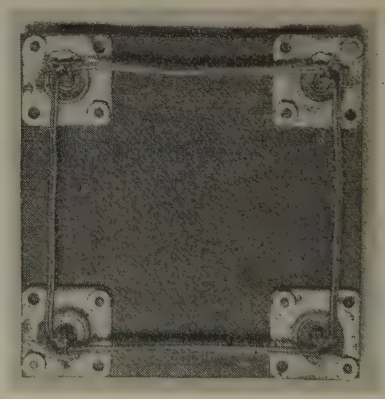

Fig. 6(a)—Wide-band hybrid ring with balanced feeds.

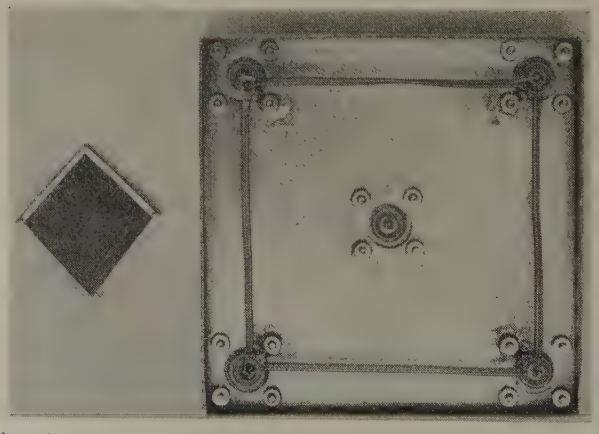

Fig. 6(b)—Printed circuit wide-band hybrid ring and twin-lead version using unbalanced feeds.

As inferred above, the π phase shift was approximated by a reversal of twin-lead connections at one termination. Although no absolute measurement was

made to determine the exact phase shift and its variation with frequency, these considerations can be evaluated from the measurements made on the experimental ring. The deviations are most readily apparent in the determination of insertion loss of the ring using balanced feed from terminals 1 to 4, or 4 to 1. The experimental curve, Fig. 7, shows a maximum loss of 33 db with the isolation being somewhat frequency dependent. Similar results were obtained with the ring employing unbalanced feed. A comparison of these results with those obtained using a $6\lambda/4$ hybrid ring[6] are shown on Fig. 7, and the broad-band property of this wide-band ring is apparent. With greater care in balancing the wide-band ring, rejections as high as 45 db may be obtained; however, the results above appear to represent the practical case.

The response of the ring as determined by (14) is very broad and considerations such as (6) shows that the power absorbed by the ring is divided equally between the two load conductances at terminals 2 and 3.

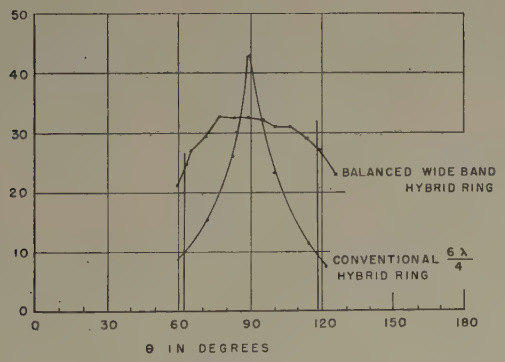

Fig. 7—Isolation from terminals 1 to 4 versus frequency for conventional and wide-band hybrid rings.

Measurements of the power at each of these terminals show the ring to be somewhat lossy, but that the wide-band feature is still maintained. These measurements are plotted on Fig. 4.

Applications

Power Splitting and Addition

One of the most obvious applications for the wide-band hybrid ring at uhf is that of splitting a single input into a multiple of outputs, as shown in Fig. 8. Thus a single antenna, or other power source, can feed a number of uhf receivers in production testing, receiver display rooms, and other multiple-receiver installations. In this application the isolation feature of the hybrid ring serves to isolate receivers by offering considerable attenuation to the oscillator radiation, with a well-designed hybrid ring giving a minimum of 26-db isolation over the band.

The inverse process of addition can also be accomplished through the use of a hybrid ring, so as to obtain the summation of outputs from a number of low-power generators. When maximum power output is desired, the two input voltages at terminals 2 and 3 in Fig. 1(b) should be of equal magnitude and should bear a phase relationship of 0 or 180°. If the voltages are in phase, the summation of powers appears at terminal 1 with zero power appearing at terminal 4. For a 180° phase relationship the power outputs are reversed.

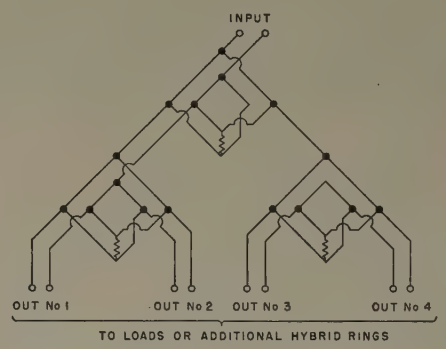

Fig. 8—Power splitting with hybrid rings.

Since the power output at terminals 1 or 4 can be made to vary from complete addition to one of complete cancellation as the phase is varied over 180°, a variable attenuator[7] can be built for the uhf television frequencies as illustrated in Fig. 9. An experimental unit built

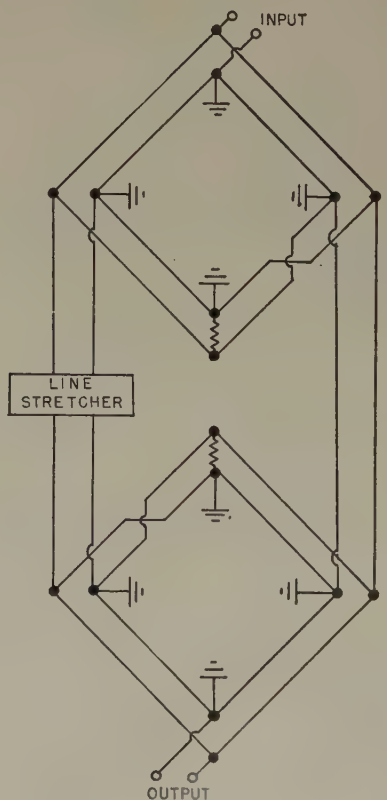

Fig. 9—UHF variable attenuator.

[6] W. H. Sayer, Jr., and J. M. De Bell, Jr., "Television antenna diplexers," *Electronics*, vol. 23, pp. 75–77; July, 1950.

[7] R. H. Dicke, "Waveguide Transmission System," U. S. Patent 2,593,120.

using 75-ohm twin lead in an unbalanced hybrid ring, for 50-ohm systems, produced an attenuation range of approximately 1 to 40 db.

Harmonic Generation

Although harmonic generation by use of nonlinear impedances such as crystals is widely known, the use of a hybrid ring for harmonic generation has certain advantages. In addition to the increase in power output through the use of a second crystal, the hybrid ring also eases the selectivity requirements for a filter circuit choosing the desired harmonic. If a push-pull signal is applied to terminals A–B in Fig. 10, a Fourier expansion of the voltages at terminals 2 and 3 shows, that for equivalent crystal characteristics, the two voltages will be identical except for difference in sign for the odd harmonics. Thus at terminal 1, where the two powers add, the odd harmonics will cancel, while at terminal 4 the even harmonics will disappear. In practical applications where crystals do not have completely identical characteristics, complete cancellation does not take place, but 20-db suppression was found reasonable. For a further improvement in suppression to 40 db it was found necessary to insert variable bias resistors in series with both crystals. The bias resistors are not only desirable in balancing the ring, but are also found useful to maximize the desired harmonic output.

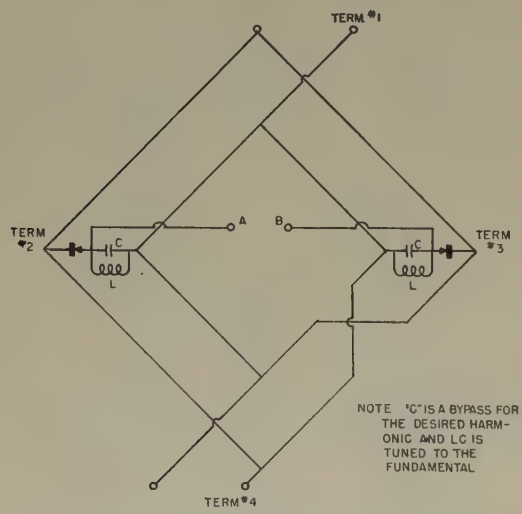

Fig. 10—Harmonic generator.

Mixer[8]

The hybrid ring is employed at microwave frequencies as a mixer not only because it affords a convenient method of injecting oscillator energy into the crystals with minimum oscillator energy at the antenna terminals but also because of the suppression of local oscillator noise. Although at ultra-high television frequencies local oscillator noise is not a problem, the oscillator injection features of the wide-band hybrid ring are useful. Other considerations that bear mentioning are the band-pass filter action shown in Fig. 4 and the suppression of IF beats arising from incoming signals separated by IF.

Recent development of low-cost vacuum tubes for amplifier and mixer use in the uhf band suggests the possibility of eventual displacement of crystal mixers from uhf tuners and converters. However, crystals are theoretically capable of extremely low noise figures; and while vacuum tubes for uhf receiver applications are subject to further development, the possible improvement in crystal design and manufacturing technique also cannot be discounted. At the present state of the art selected silicon crystals when used with 2.0-db noise figure, IF amplifiers can give noise-figure performance as low as 9.0 db.

Small-Signal Modulation

The inverse process to detection can be used to translate a low-frequency signal into one of higher frequency. If a low-frequency signal is applied in push-pull to the terminals A–B in Fig. 10 and a local oscillator is injected in terminals 1 or 4, the output at terminal 4 or 1 will consist of suppressed carrier and sidebands. This method provides a simple method of converting a vhf television signal to one at uhf with a minimum of equipment. The vhf signal can be taken directly off the air, amplified if necessary, and a standard signal generator can be used as a local oscillator. To preserve the order of sound and picture carrier the receiver should then be tuned to the upper sideband. For production testing a convenient arrangement is to supply a single modulated uhf signal to several hybrid rings with separate uhf oscillators. The desired sidebands can then be combined into a single line and fed to individual test positions by means of hybrid rings. An alternative arrangement for more intensive tests is to provide a vhf signal and variable oscillator at each test position so that the uhf receiving equipment can be checked over the entire band.

Large-Signal Modulation[9]

An experimental hybrid-ring modulator was arranged to determine the feasibility of deriving uhf local oscillator power by beating a vhf oscillator with one of higher frequency. Using conventional oscillator tubes, a 6J6 at 80 mc and 6AF4 at 620 mc, the output at 700 mc was sufficient to obtain approximately 3 ma of detected current in an unbalanced 1N72 mixer. Since this is more than enough power to drive two crystals, a possible uhf tuner design is suggested.

[8] W. V. Tyminski and A. E. Hylas, "UHF Hybrid Ring Mixers," presented at National I.R.E. Convention, Symposium on UHF Receivers, New York, N. Y.; March 5, 1952.

[9] W. R. Bennett, "A general review of linear varying parameters and non-linear circuit analysis," Proc. I.R.E., vol. 38, pp. 259–263; March, 1950.

A system of reception similar to that described by Scandurra[10] would use a decimal system with the "unit" switch actuating a low-frequency oscillator in 6-mc step, and the "tens" switch moving the higher frequency oscillator in 60-mc steps. The difficulty associated with this suggestion is the large number of frequencies generated in the mixing process. These consist of f_0, the high-frequency oscillator, nf_m, where n is any integer and f_m is the low-frequency oscillator, and $f_0 \pm nf_m$. The use of a hybrid-ring modulator serves to suppress the carrier and odd or even harmonics, depending upon the connection used, and in the uhf spectrum all responses will be at least 30 db down from the upper and lower sideband response, $f_0 \pm f_m$. A tuned circuit can then be used to choose the desired sideband and further suppress other spurious signals. Probably the most difficult spurious signal to suppress is one which falls directly into the band that is being received, but by proper choice of modulating frequencies this condition can be avoided.

The availability of a uhf local oscillator output controllable by a lower frequency oscillator also permits the use of automatic frequency control techniques to stabilize the uhf oscillator output.

[10] A. M. Scandurra, "An 82-Channel U.H.F.-V.H.F. Turret Tuner," presented at National I.R.E. Convention, Symposium on UHF Receivers, New York, N. Y.; March 5, 1952.

Comparison Bridge

The wide-band hybrid ring can also be considered as a bridge where for an input signal at terminal 1, the output at terminal 4 is an indication of the mismatch in the loads at terminals 2 and 3. Thus unknown susceptances can be compared to calibrated stubs. If a double-stub with variable spacing[11] is provided, a wide range of loads can be matched to the ring, further extending the usefulness of the wide-band hybrid ring as a measuring instrument.

Conclusions

In applications using hybrid rings, the wide-band ring removes the frequency limitations of the conventional $6\lambda/4$ ring, and thus extends the usefulness of this technique. Because of simplicity and small physical size, the wide-band hybrid ring is particularly useful in the uhf television spectrum.

[11] R. W. P. King, H. Mimno, and A. Wing, "Transmission Lines Antennas and Wave Guides," McGraw-Hill Book Co., Inc., New York, N. Y., pp. 48–50; 1945.

Ferrites at Microwaves*

N. G. SAKIOTIS†, ASSOCIATE, IRE, AND H. N. CHAIT†

Summary—**After a preliminary discussion of the propagation of waves in an unbounded ferromagnetic medium, and in waveguides containing ferrites, the results of an experimental study of the propagation characteristics of waveguides containing ferrites are presented for some samples of commercially available ferrites. Some of the applications of ferrites to microwave circuitry are briefly described.**

Introduction

RECENTLY there have appeared on the microwave scene new materials under the generic name of "ferrites." Consisting of metallic oxides having a spinel structure and a general chemical formula XFe_2O_4, where X represents a bivalent metal such as magnesium, nickel, or cobalt, the ferrites furnish an interesting microwave propagation medium. The high resistivity of the oxide components together with the ferromagnetic properties of the iron component classify the ferrites as ferromagnetic dielectrics. Because of their high magnetic susceptance at low frequencies, the ferrites furnish a microwave medium whose properties may be varied over quite a large range by magnetizing the ferrite with a controlled static magnetic field.

Among their other ferromagnetic properties, the ferrites exhibit a strong Faraday Effect. This phenomenon was first observed by Faraday in 1848 when he passed a plane polarized light beam through a thin sheet of magnetic material magnetized in the direction of propagation. The following results were observed and have recently been obtained in the microwave region.[1]

1. The plane of polarization is rotated in passing through the medium, the angle of rotation being proportional to the thickness of material traversed.

2. The direction of rotation of plane of polarization depends only on the direction of the applied static magnetic field. Relative to an observer looking along the direction of the magnetic field, the sense of rotation of a linearly polarized wave will be the same whether the wave is traveling toward or away from him.

3. The angle of rotation is a function of the strength of the magnetic field.

The Infinite Ferromagnetic Medium

The observed phenomena may be explained[2] by considering the linearly polarized wave to be made up of two

* Decimal classification: R282.3. Original manuscript received by the Institute, September 29, 1952.

† Antenna Research Branch, Radio Division I, Naval Research Laboratory, Washington 25, D. C.

[1] F. F. Roberts, "A note on the ferromagnetic Faraday effect at centimetre wavelengths," *Le Jour. De Phys. et le Radium*, vol. 12, pp. 305–307; March, 1952.

[2] The following is based on the explanation given by M. Abraham and R. Becker, "Theorie der Elektrizitat," Taubner, Leipzig, vol. II, p. 27; 1933.

circular components, one right-handed and the other left. Upon application of the magnetic field the material becomes anisotropic in such a way as to have different indices of refraction for right- and left-hand circular polarization. Thus, in passing through the material, a relative phase shift is introduced between the two circularly polarized components which then recombine to give a rotated linear polarization at the output. The above explanation may be expanded in mathematical terms as follows:

Let a linearly polarized plane wave propagate through a lossless, semi-infinite medium in the direction of the applied field intensity $\overline{H}$. If we erect rectangular axes x, y, and z with the z-axis parallel to $\overline{H}$, the E-vector of the plane wave will lie in the x-y plane. We will specify the magnitude of E to vary as $\cos(\omega t-\beta_0 z)$:

$$|\overline{E}| = E_0 \cos(\omega t - \beta_0 z),$$

or if $\bar{i}_x$ and $\bar{i}_y$ are unit vectors along the x and y axes,

$$\overline{E} = [E_{0x}\bar{i}_x + E_{0y}\bar{i}_y] \cos(\omega t - \beta_0 z)$$
$$\overline{E} = |\overline{E}| \cos\theta \bar{i}_x + |\overline{E}| \sin\theta \bar{i}_y$$
$$\overline{E} = \mathrm{Re}(|\overline{E}| e^{j\theta})\bar{i}_x + \mathrm{Im}(|\overline{E}| ej^{\theta})\bar{i}_y.$$

We see from the last equation that we can derive the x- and y-components of $\overline{E}$ from the real and imaginary parts of the scalar $|\overline{E}|e^{j\theta}=E_0e^{j\theta}\cos(\omega t-\beta_0 z)$. Thus, $e^{j\theta}$ in this system of notation indicates spatial orientation rather than a time phase as is more usual. In this notation, then, a right-hand circularly polarized wave would be represented by $Ee^{j\omega t}$, a left-hand by $Ee^{-j\omega t}$, where E may be complex.

In accordance with the description of the Faraday effect given above, we will let $\theta=az$, where θ is the angle rotation of the plane of polarization assuming the wave enters the medium aligned with the x-axis, at $z=0$. Then the expression for $|\overline{E}|e^{j\theta}$ is

$$E_0 e^{j\theta}\cos(\omega t-\beta_0 z) = \frac{E_0}{2} e^{jaz}\left[e^{j(\omega t-\beta_0 z)} + e^{-j(\omega t-\beta_0 z)}\right]$$
$$= \frac{E_0}{2}\left[e^{j[\omega t-(\beta_0-a)z]} + e^{-j[\omega t-(\beta_0+a)z]}\right].$$

Let $(\beta_0-a)=\beta_+$ and $(\beta_0+a)=\beta_-$. Then,

$$|\overline{E}| e^{j\theta} = \frac{E_0}{2} e^{j(\omega t-\beta_+ z)} + \frac{E_0}{2} e^{-j(\omega t-\beta_- z)}$$

and

$$\overline{E} = \bar{i}_x \frac{E_0}{2}\cos(\omega t-\beta_+ z) + \bar{i}_y \frac{E_0}{2}\sin(\omega t-\beta_+ z)$$
$$+ \bar{i}_x \frac{E_0}{2}\cos(\omega t-\beta_- z) - \bar{i}_y \frac{E_0}{2}\sin(\omega t-\beta_- z).$$

It can be seen by inspection of the above expression that the rotating plane wave is equivalent to two circularly polarized plane waves traveling along the z-axis, with different phase velocities. One is circularly polarized in the same sense as the angle of rotation of the linearly polarized wave and has a phase constant $\beta_+=\beta_0-a$, while the other is circularly polarized in the opposite sense having $\beta_-=\beta_0+a$.

The rate of rotation a, and also the angle of rotation θ, can then be expressed as

$$a = \frac{\beta_- - \beta_+}{2},$$

$$\theta = \frac{\beta_- - \beta_+}{2} z. \qquad (1)$$

It must be emphasized that the β_0 is the phase constant for a rotating linearly polarized wave in the medium and is not necessarily identical with the phase constant of an ordinary nonrotating, linearly polarized wave traveling through the medium. We may express β_0 in terms of β_+ and β_-,

$$\beta_0 = \frac{\beta_- + \beta_+}{2}.$$

Since θ is a function of the magnetic field, β_0, β_+, and β_- will then be functions of the magnetic field as well as of the material. These functions will have to be determined by an analysis of the interaction of the material and the applied fields.

The above model shows that in order that the Faraday effect take place the material must exhibit different phase velocities for the two senses of circularly polarized waves. Since the direction of rotation of the plane wave depends only on the direction of the applied static field, the phase velocity of each of the circularly polarized components will depend upon which sense of polarization the component has with respect to the applied field, not upon which sense it has with respect to the direction of propagation. Thus, in order to prevent confusion, we will have to abandon the usual nomenclature of right- and left-hand circular polarization since it depends on the direction of propagation. Instead, a wave circularly polarized in the sense that would advance a right-hand screw in the direction of the static field will by definition have a positive sense of polarization and will be characterized by a phase velocity β_+ irrespective of whether it propagates in a direction parallel or antiparallel to the static field. The opposite sense will be the negative sense with phase velocity β_-. Therefore a given circular polarization will change sense if the direction of the applied field is reversed with respect to the direction of propagation.

Polder[3] has shown that a ferromagnetic medium which is homogeneously magnetized to saturation is characterized by a tensor permeability. That is, RF magnetic field intensity $\bar{h}$ and flux density $\bar{b}$ are related by

$$\bar{b} = [T]\bar{h},$$

where $[T]$ is a tensor of the form

[3] D. Polder, "On the theory of ferromagnetic resonance," *Phil. Mag.*, vol. 40, pp. 99–115; January, 1949.

$$[T] = \begin{bmatrix} \mu & -j\alpha & 0 \\ j\alpha & \mu & 0 \\ 0 & 0 & \mu_0 \end{bmatrix},$$

where the tensor components, μ and α, are functions of the static field strength, flux density, and magnetization as well as the frequency of the microwave field.

Uniform plane-wave solutions of Maxwell's equations have been obtained[3,4] for such a saturated ferromagnetic medium magnetized in an arbitrary direction with respect to the direction of propagation. In general, two solutions are obtained, representing two elliptically polarized waves propagating in the same direction but with different velocities. In the case of the medium magnetized parallel to the direction of propagation, the two solutions represent contrarotating circularly polarized waves with phase velocities

$$\beta_- = \omega\sqrt{\epsilon(\mu + \alpha)}, \quad \beta_+ = \omega\sqrt{\epsilon(\mu - \alpha)}.$$

In the case of the medium magnetized perpendicularly to the direction of propagation, the two solutions represent orthogonal linearly polarized waves. One wave has its E-vector polarized parallel to the direction of magnetization and travels with the phase velocity

$$\beta_\parallel = \omega\sqrt{\epsilon\left(\frac{\mu^2 - \alpha^2}{\mu}\right)},$$

while the other is polarized perpendicularly to the magnetization and travels with the phase velocity

$$\beta_\perp = \omega\sqrt{\epsilon\mu_0},$$

which is clearly not a function of the magnetization of the medium.

Ferrites in Waveguide

While the above discussion was based upon an infinite medium, the results have been found to be useful guides in qualitatively understanding the results obtained in the case of a circular waveguide with a small rod of ferrite placed on the axis of the waveguide. On the other hand, the infinite medium propagation constants have not been useful in understanding the data obtained in the case of a waveguide of rectangular cross section containing ferrite material.

The μ-tensor given above seems to be an inherent property of magnetized media and is therefore applicable to all analyses of ferrite propagation phenomena irrespective of the geometry of the medium. The phase velocity and the configuration of the fields, however, depend on the geometry involved. Thus, in order to analyze the propagation of energy through waveguides containing ferrite media, solutions must be found to Maxwell's equations with the ordinary scalar permeability replaced by the tensor permeability and subject to the waveguide boundary conditions.

[4] M. Born, "Optik," Springer, Berlin, pp. 363–365; 1933.

Formal solutions have been obtained by Kales[5] and by Suhl and Walker[6] for the modes in a completely filled circular waveguide magnetized in the axial direction. The rectangular waveguide case is also under investigation and some of the modes that may exist in the filled rectangular waveguide magnetized in the transverse plane have been obtained by Van Trier.[7] These theoretical investigations indicate that the modes which exist in a magnetized medium are quite different from the usual TE or TM waveguide modes. However, before the formal solutions can be used to obtain mode configurations and phase velocities, numerical solutions are necessary which require the knowledge of the μ-tensor components as functions of the applied field. This requires μ and α to be obtained experimentally for values of applied field at least below saturation. We are not at present aware of a satisfactory experimental method of measuring μ and α.

We have been engaged in an experimental study of the propagation characteristics of both circular and rectangular waveguide containing pieces of standard commercial ferrites at 9,375 mc. Let us consider first the case of the circular waveguide. It can be seen from (1) that the angle of rotation of the plane of polarization may be obtained from measurements of the phase velocity of the circularly polarized components. The transmission loss, reflections and changes in ellipticity of a linearly polarized wave may also be deduced from measurements made upon circularly polarized waves. Because of the more fundamental nature of the information obtained by studying the propagation of circular polarization, most of the measurements are being made with circularly polarized waves using the apparatus shown in Fig. 1(a). A right-hand circularly

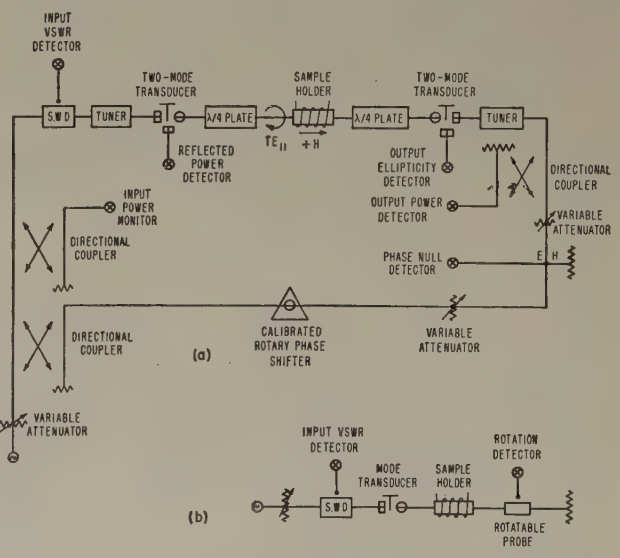

Fig. 1—Schematic diagram of the measuring apparatus.

[5] M. L. Kales, "Modes in Waveguides Containing Ferrites," NRL Report #4027, August 8, 1952.

[6] H. Suhl and L. R. Walker, "Faraday rotation of guided waves," *Phys. Rev.*, vol. 86, no. 1, pp. 122–123; April 1, 1952. (Letters to the Editor.)

[7] Van Trier, "Anomalous wave types in waveguides containing ferromagnetics," *Phys. Rev.*, vol. 87, no. 1, pp. 227–228; July 1, 1952. (Abstract of talk given at meeting of A.P.S. in Washington, D. C.)

polarized TE_{11} mode is incident upon a ferrite cylinder mounted coaxially in a length of 0.9375 inch diameter waveguide by means of a polyfoam spacer. The ferrite is magnetized in the axial direction by a solenoid wound around the waveguide. When the applied field is in the direction of propagation, the incident wave is by definition polarized in the positive sense. Upon reversal of the applied field, the incident field must be regarded as polarized in the negative sense.

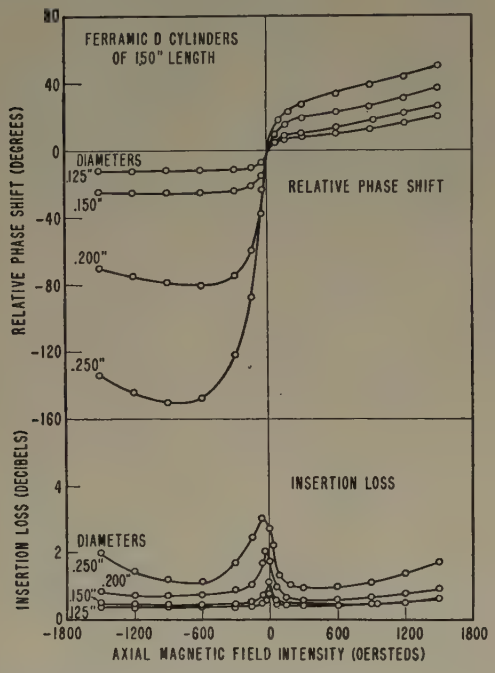

Fig. 2—Relative phase shift and insertion loss versus applied axial magnetic field intensity with the diameter of the sample as a parameter in the case of circularly polarized wave propagation.

As can be seen from the schematic, all reflections as well as changes in ellipticity are measured. The power absorbed by the ferrite can then be calculated from the measured insertion loss, the difference in readings of the input monitor, and the output power detector. It has been found, however, that for most samples the power absorbed is at least 90 per cent of the insertion loss.

The change in the phase constant $(\beta_{\pm}-\beta^0)$ due to the application of the magnetizing field was measured by observing the amount of phase shift that had to be introduced in the reference line to maintain a minimum reading at the phase null indicator. The phase shift was introduced by means of a calibrated rotary phase shifter capable of producing any change of phase within an accuracy of at least ± 2 degrees. In terms of ϕ, the difference in settings of the phase shifter for the magnetized and unmagnetized states, $\beta_{\pm}$, is given by

$$\beta_{\pm} l = \beta^0 l - \phi_{\pm},$$

where l is the length of the sample and the subscripts $+$, $-$ refer, as before, to the phase velocities for the positive and negative senses while the superscript, 0, refers to the phase velocity in the unmagnetized medium. The angle of rotation for a plane polarized wave can then be calculated from

$$\theta = \frac{\phi_+ - \phi_-}{2} l.$$

The angle of rotation was measured directly in the apparatus shown schematically in Fig. 1(b) to an accuracy of at least ± 2 degrees and found to be in agreement with calculated values within experimental errors.

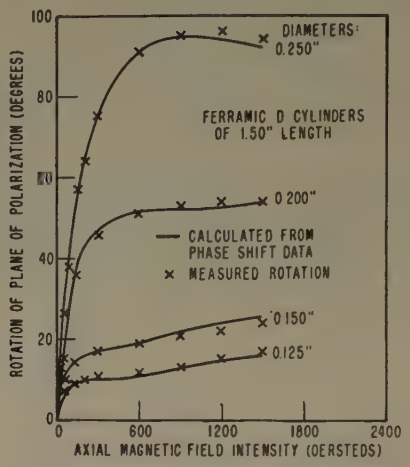

Fig. 3—Calculated and measured angle of rotation of the plane of polarization versus applied axial magnetic field intensity.

The curves of ϕ and insertion loss versus external applied field H are shown in Fig. 2 for samples of Ferramic D of the same length but different diameters. The angle of rotation calculated from these curves as well as the measured rotation is shown in Fig. 3. The effect of changing only the length of the sample can be seen in Fig. 4. The corresponding curves of angle of

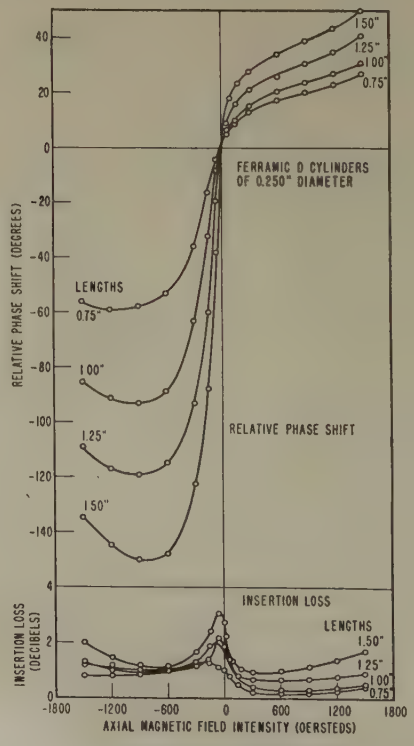

Fig. 4—Relative phase shift and insertion loss versus applied axial magnetic field intensity with the length of the sample as a parameter in the case of circularly polarized wave propagation.

rotation are presented in Fig. 5. The general shape of the curves is seen to be the same as the physical dimensions are changed, only the magnitude apparently being affected.

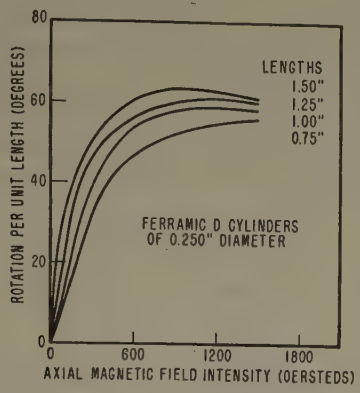

Fig. 5—Calculated angle of rotation of the plane of polarization versus applied axial magnetic field intensity.

The horizontal shift of the peaks of the phase and insertion loss curves as the length or diameter is changed may be a result of the change of the demagnetization factor as the dimensions are changed, resulting in different internal fields for the same applied field, as well as end effects producing lumped phase shifts at the ends of the cylinder. These factors may also explain why the rotation per unit length curves do not coalesce into a single curve as would be expected from (1).

The origin of the peak which is present in the insertion-loss curves is not yet fully understood. There are some indications that it may be a shape resonance since as one goes to much larger diameters in some ferrites more peaks appear. We have found, however, that if in addition to the axial field a magnetic field is applied transverse to the axis of the waveguide a substantial reduction can be made in the magnitude of the peak in many cases. This is shown in Fig. 6, where the parameter is the value of the transverse field, the dimensions of the sample being held constant.

Because of the limitations of space, only the curves for Ferramic D are shown. These were chosen since this particular ferrite exhibits the lowest absorption loss of the materials we have tested. The rest of the samples,

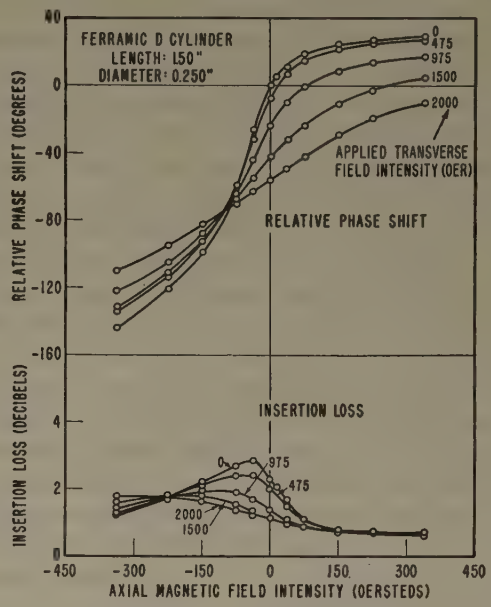

Fig. 6—Relative phase shift and insertion loss versus applied axial magnetic field intensity with the applied transverse magnetic field intensity as a parameter in the case of circularly polarized wave propagation.

with the exception of three, exhibit phase and insertion loss curves having the same general shape as those shown for Ferramic *D*, the difference between curves for individual materials of the same size being one of magnitude rather than of shape. A résumé of the values of the ϕ and insertion loss curves at the more interesting points is given in Table I for 0.250-inch×1.50-inch cylinders of the materials tested. The three exceptions are Ferramic B, Ferramic H, and Ferroxcube 4B. These three materials give ϕ and insertion loss curves which seem to have the same general trend, but differ markedly in

TABLE I

Ferrite	Peak of ϕ_-	Magnitude of loss peak	Loss at $H=0$	ϕ_+ at $H=1000$ *oe*	Loss at $H=+1000$ *oe*	Loss at $H=-1000$ *oe*
Ferramic[8] A	−145°	3.4 db	2.6 db	43°	0.8 db	1.2 db
Ferramic A-34	−188°	2.1 db	0.6 db	95°	0.3 db	1.5 db
Ferramic C	−244°	11.5 db	6.0 db	35°	0.9 db	5.4 db
Ferramic D{D[1]	−150°	3.0 db	2.7 db	41°	1.2 db	1.2 db
Ferramic D{D[2]	−350°	4.4 db	3.2 db	35°	1.0 db	3.2 db
Ferramic E	−540°	12.5 db	3.0 db	35°	1.1 db	8.6 db
Ferramic G	−650°	26.0 db	5.5 db	30°	1.0 db	6.0 db
Ferramic H_1	−238°	26.0 db	3.5 db	98°	0.25 db	18.0 db
Ferramic I	−490°	20.0 db	5.5 db	123°	0.8 db	19.4 db
Ferramic J	−305°	11.5 db	6.0 db	40°	1.0 db	6.5 db
Ferroxcube[9] 4D	−312°	15.0 db	6.2 db	38°	1.2 db	9.7 db
Ferroxcube 4E	−170°	2.8 db	1.7 db	42°	0.5 db	0.8 db
Crolite[10]	−570°	21.0 db	5.5 db	35°	1.0 db	6.5 db

[8] General Ceramics and Steatite Corp., Keasbey, N. J.
[9] Ferroxcube Corporation of America, New York, N. Y.
[10] Henry L. Crowley and Co., West Orange, N. J.

form from the other materials. An unusual feature of these materials is that over the range of values measured ϕ_+ is less than ϕ_-; hence, negative rotation is obtained.

The data presented is intended to give a qualitative rather than a quantitative picture of what may be expected. In view of the nonuniformity of commercial ferrite materials with respect to their microwave properties, exactly reproducible results cannot in general be expected for materials having the same commercial designation. Thus, for example, we have been able to separate our Ferramic D samples into two groups from their phase- and insertion-loss characteristics which we designate as D^1 and D^2. The differences in the characteristics between these two forms of Ferramic D can be seen from Table I. The data presented applies to Ferramic D^1.

In the rectangular waveguide case, experiments have been conducted with various physical dimensions and relative orientations of the waveguide and the ferrite. It is interesting to note that the transmission loss depends not only on the intrinsic properties of the ferrite material but also on the particular physical configuration used. For example, it has been found that when a small rectangular piece of ferrite is inserted in the center of a standard X-band waveguide the loss is much higher than if the same piece of ferrite were placed adjacent to the narrow wall of the waveguide.

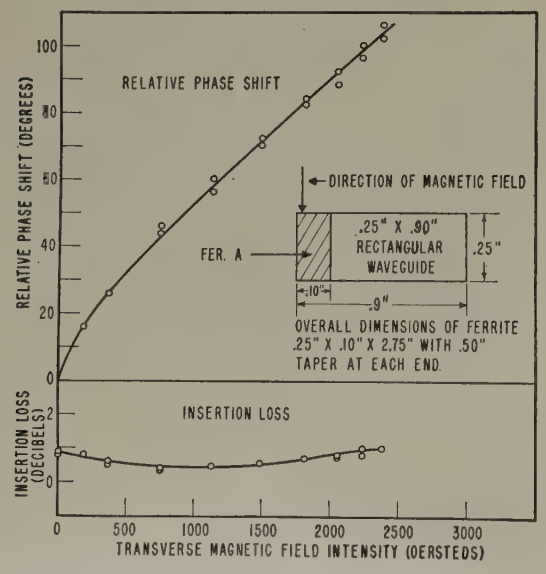

Fig. 7—Relative phase shift and insertion loss versus applied transverse magnetic field intensity for rectangular waveguide case.

On the other hand, the range of phase shift is not appreciably changed. A possible explanation is that the reduction in the loss is due to a reduction in the dielectric loss which results from placing the ferrite in a part of the waveguide where the electric field is small. Figs. 7 and 8 show the phase shift and loss as a function of transverse field obtained from two different physical arrangements.

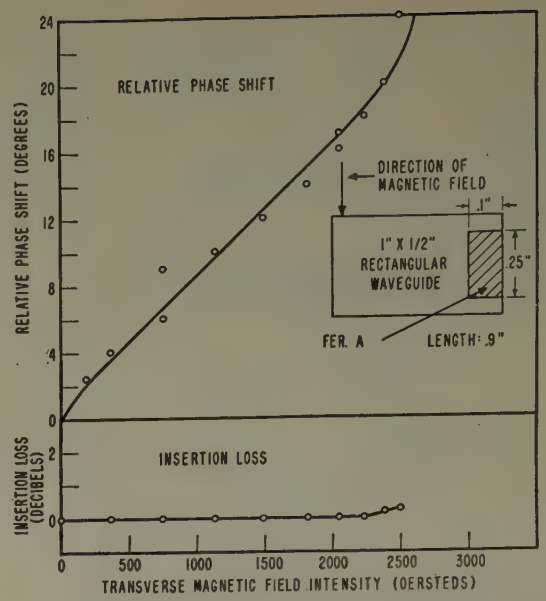

Fig. 8—Relative phase shift and insertion loss versus applied transverse magnetic field intensity for rectangular waveguide case.

Applications

Since it is possible, by means of ferrite devices, to vary electrically the phase or polarization of microwave fields, the ferrites should have many applications in microwave systems. Before such applications may be realized, however, the absorption losses of the ferrite materials must be minimized and further study must be made of their power-handling capabilities and the dependence upon frequency and temperature of their propagation characteristics. In view of the fact that commercially available ferrites were developed as relatively-low frequency transformer cores, it is not to be expected that they are optimum at microwave frequencies. Thus, it is quite possible that new ferrite materials can be developed with loss so low that they will be practical for many applications.

A direct application of the Faraday Rotation in ferrites has been made by Luhrs in his microwave switch.[11] Essentially, the Luhrs' switch consists of a section of dielectric-filled circular waveguide in which a piece of ferrite rod is axially located. A coil is wound on the circular waveguide to provide an axial magnetic field. The input to the ferrite section is a rectangular waveguide and the output another length of rectangular waveguide which is rotated 90° about its axis with respect to the input waveguide. Thus with the ferrite unmagnetized, there is about 50-db isolation between the crossed waveguides. When the proper current is supplied to the coil, the ferrite rotates the plane of polarization 90° and the input and output guides are coupled. The transmission loss in the "on" state is about 0.25 db. If a square waveguide having two outputs is used at the output, one could electrically switch between the two output channels. A number of two-channel switches,

[11] C. H. Luhrs and Co., Hackensack, N. J.

if cascaded, could form an organ-pipe scanner[12] with no moving parts. A rod of ferrite magnetized to produce 45° of rotation and located on the axis of a circular waveguide terminated at each end by a two-mode transducer produces a very interesting device called a "circulator," the properties of which are described by Hogan.[13] In the same paper, Hogan describes a one-way π phase shifter utilizing a 90° rotator. This device produces a phase shift of π for linearly polarized waves traveling in one direction. If the direction of propagation is reversed, no phase shift is introduced.

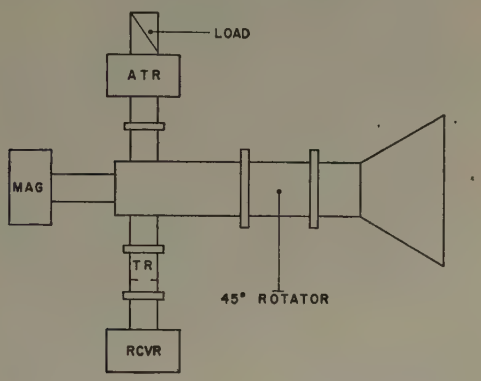

Fig. 9—Diagram of ferrite isolating device.

Another important possible application is the isolation of the generator from the load. If successful, it may make possible many antenna designs, particularly for scanning antennas, which in the past have had to be rejected because of the variable impedance presented to the generator. Fig. 9 shows a typical possible arrangement. When the magnetron fires, both the *TR* and *ATR* are closed. The output of the magnetron is rotated 45° in passing through the 45° rotator, and then proceeds to the antenna. If any power is reflected by the antenna, it comes back down the line, passes through the rotator, and is rotated another 45° in the same direction, making a total of 90°. The reflected wave therefore cannot enter the input and must proceed up one of the two side arms. Since the *TR* and *ATR* are still closed, the reflected wave proceeds to the upper arm and is absorbed in the load. By the time the target reflection reaches the antenna, both the *TR* and *ATR* are open and thus the target energy proceeds to the receiver instead of the load.

The electrical variation of phase made possible by the ferrites makes these materials especially useful in the design of scanning antennas, since one can scan a radar beam by controlling the phase distribution over the radiating aperture. We are at present developing an array whose beam can be electrically scanned. The array consists of shunt slots cut along the edge of a rectangular waveguide. Pieces of ferrite are located between the slots and energized by small electromagnets in such a way as to progressively change the phase at each slot, thus causing the radiated beam to scan.

A phase shifter utilizing the variation in phase velocity of circular polarization will be nonreciprocal since a wave traveling in one direction will suffer a phase shift which differs from that of the wave traveling in the reverse direction. However, such a device can be made reciprocal by the addition of a 45° ferrite rotator at each end.[14]

We have described only a few of the many possible applications of ferrites in present-day microwave systems. The field is relatively new and there is much more to be learned about ferrites at microwave frequencies.

Acknowledgments

The authors wish to thank Dr. M. L. Kales of the Naval Research Laboratory for his many helpful comments and suggestions and the many persons who ably assisted in taking the experimental data.

[12] K. S. Kelleher and H. H. Hibbs, "Organ pipe radar scanner," *Electronics*, vol. 25, pp. 126–127; May, 1952.
[13] C. L. Hogan, "The ferromagnetic Faraday effect at microwave frequencies and its applications—the microwave gyrator," *Bell Sys. Tech. Jour.*, vol. 31, pp. 22–26; January, 1952.
[14] N. G. Sakiotis, A. J. Simmons, and H. N. Chait, "Microwave-antenna ferrite applications," *Electronics*, vol. 25, pp. 156–166; June, 1952.

Characteristics of the Magnetic Attenuator at UHF*

FRANK REGGIA† AND ROBERT W. BEATTY†, MEMBER, IRE

Summary—**Certain ferromagnetic materials such as ferrites have considerable loss at frequencies in excess of 30 mc. This loss can be controlled by producing a magnetic field in the material by external means, such as an electromagnet. This principle is used in the small electrically controlled variable attenuator for coaxial lines which is described. The performance of the attenuator at ultra-high frequencies is given for a specific attenuator using a number of suitable materials. The design and applications of the attenuator are also discussed.**

* Decimal classification: R396.9. Original manuscript received by the Institute, October 10, 1952.
† National Bureau of Standards, U. S. Dept. of Commerce, Washington 25, D. C.

Introduction

CERTAIN FERROMAGNETIC MATERIALS such as ferrites,[1,2] which have relatively high permeability and low loss at radio frequencies below approximately 30 mc, become quite lossy at higher frequencies. Investigation has shown that the losses at

[1] C. L. Snyder, E. Albers-Schoenberg, and H. A. Goldsmith, "Magnetic ferrites," *Elec. Manu.*, vol. 44, no. 6, pp. 86–91; December, 1949.
[2] M. J. O. Strutt, "Ferromagnetic materials and ferrites," *Wireless Eng.*, vol. 27, no. 327, pp. 277–284; December, 1950.

higher frequencies are not caused mainly by hysteresis and eddy currents, but are associated with changes in the internal magnetic structure of the material such as domain wall relaxation and rotation of domains.[3,4,5] The losses have been shown to be a function of the magnetic field within the material, and certain resonance effects have been observed in the microwave region. The field is usually produced by an electromagnet which permits electrical control of the loss in the material.

This phenomenon is the basis for several devices which make use of the dissipative properties of ferromagnetic materials at high frequencies. An electrically controlled *X*-band waveguide attenuator was made by Miller,[6] using a mixture of polystyrene and iron powder. The properties of this attenuator were in many ways inferior to other types of waveguide attenuators. An electrically controlled coaxial attenuator has been developed by Reggia,[7] using ferrite materials to obtain excellent loss characteristics over a broad frequency range. An *X*-band waveguide microwave switch made by Luhrs[8] uses a ferrite material to obtain rotation of polarization in the guide. The amount of rotation is controlled by an electromagnet. A somewhat similar device has been developed by Hogan[9] using a ferrite to produce Faraday rotation of polarization in a waveguide. The circuit element is called a "gyrator" and has many uses in addition to its application as an attenuator.

The electrically controlled coaxial variable attenuator developed by Reggia fills the need for a continuously variable coaxial attenuator having a low minimum loss of the order of a few decibels. The performance of this attenuator has been investigated at ultra-high frequencies for a number of commercially available ferromagnetic materials. The purpose of this paper is to describe the attenuator, present the performance data, and discuss the design and applications of the device.

Description of the Attenuator

As shown in Fig. 1, the magnetic attenuator consists of two principal parts: a short section of coaxial transmission line containing a suitable dissipative material filling the space between the inner and outer conductors, and an electromagnet which produces a magnetic field in the dissipative material.

The coaxial-line section and the dissipative material are shown in the photograph of Fig. 2. The respective

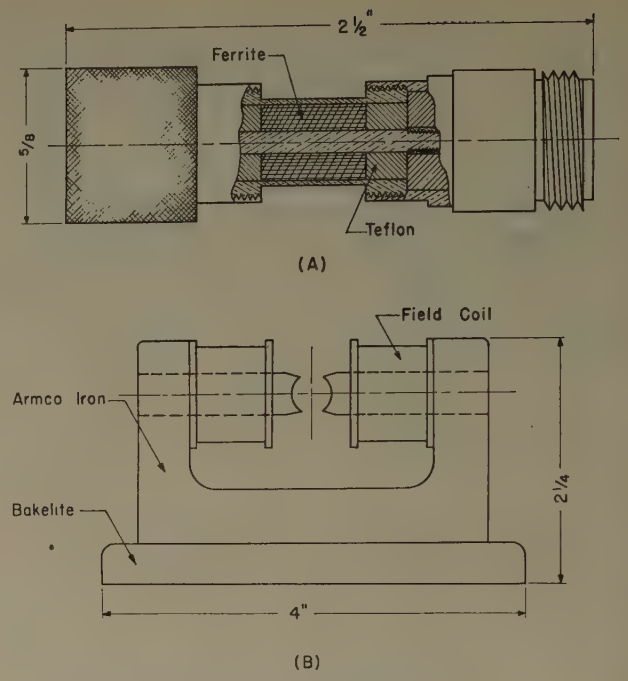

Fig. 1—Essential parts of the magnetic attenuator: (A) a short section of transmission line containing a dissipative material, (B) the electromagnet used to produce a magnetic field in the material.

diameters of the inner and outer conductors at the center of the line section are 0.100 inch and 0.355 inch. The dimensions of the line are varied at the ends to permit use of 50-ohm Type N connectors. The wall thickness of the outer conductor at the center of the

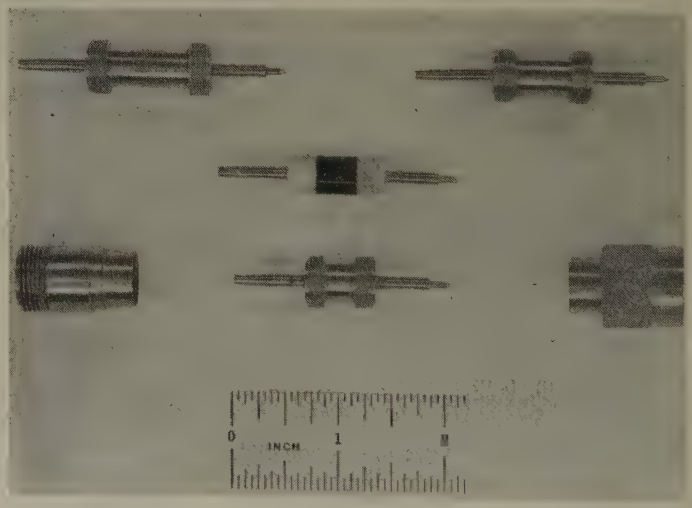

Fig. 2—Short section of transmission line showing the end connectors, the ferrite material, and three sizes of material housings for holding inserts of different lengths.

line section is 0.010 inch and conforms to the standard dimensions for Type N connectors at the ends. The connectors are designed to unscrew from the line section, permitting quick removal of the dissipative material insert.

The insert of dissipative material is a cylindrical slug having a length of one-half inch, with an axial hole to accommodate the center conductor. The dissipative ma-

[3] J. B. Birks, "The properties of ferromagnetic compounds at centimeter wavelengths," *Proc. Phys. Soc.* (London B), vol. 63, pp. 65–74; February, 1950.
[4] D. Polder, "Ferrite materials," *Proc. I.E.E.* (London), vol. 97, pt. II, pp. 246–256; April, 1950.
[5] G. T. Rado, R. W. Wright, and W. H. Emerson, "Ferromagnetism at very high frequencies. III. Two mechanisms of dispersion in a ferrite," *Phys. Rev.*, vol. 80, no. 2, pp. 273–280; October, 1950.
[6] T. Miller, "Magnetically controlled wave-guide attenuators," *Jour. Appl. Phys.*, vol. 20, pp. 878–882; September, 1949.
[7] "NBS magnetic attenuator," *Nat. Bur. Standards Tech. News Bull.*, vol. 35, pp. 109–111; August, 1951.
[8] H. W. Herman, "Performance Tests on the C. H. Luhrs Microwave Switch," Naval Research Laboratory Report 3883, 10 pages; December, 1951.
[9] C. L. Hogan, "The microwave gyrator," *Bell Sys. Tech. Jour.*, vol. 31, pp. 1–10; January, 1952.

terial appears black in the photograph and fits between two teflon insulators. It is possible to obtain ferrite inserts of the required size (to fit snugly between the inner and outer conductors) directly from the manufacturers, thus avoiding the difficulties of machining[10] the hard and brittle ferrite materials.

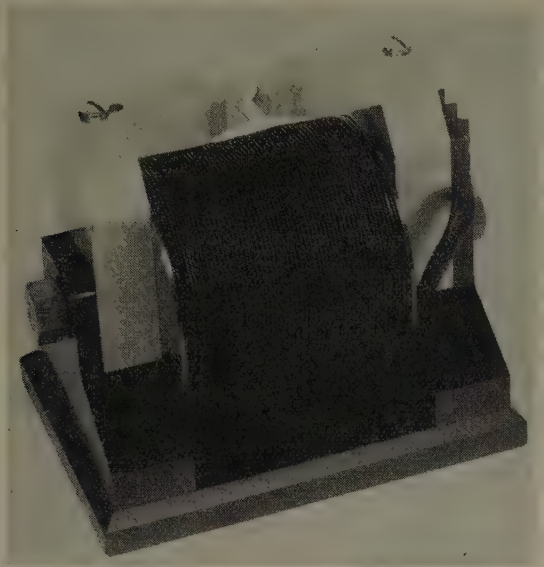

Fig. 3—Large electromagnet capable of carrying several amperes of current.

The electromagnet may be of any convenient design. A large electromagnet capable of carrying several amperes of current is shown in Fig. 3 and a smaller electromagnet (using field coils taken from relays) is shown in Fig. 4. Both electromagnets have adjustable pole pieces

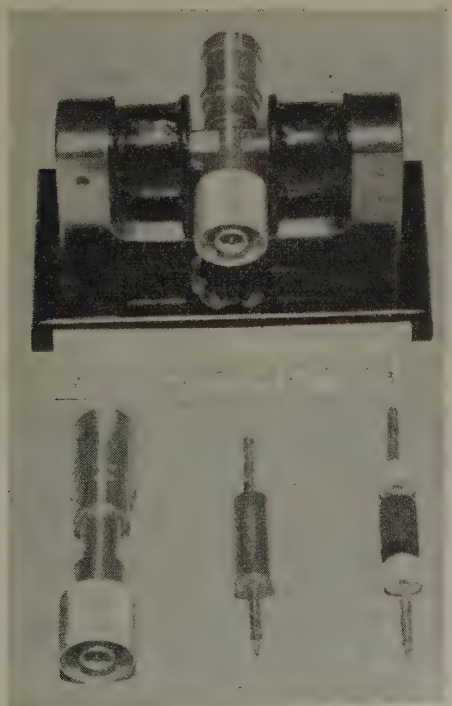

Fig. 4—Assembled magnetic attenuator using the small electromagnet and internal parts of the attenuator.

[10] A. A. Feldmann, "The Machining of Powdered Iron Materials and Ferromagnetic Ferrites," NBS Report No. 1530, 7 pages.

to facilitate installation and removal of the coaxial-line section. The pole pieces and yoke of both magnets were made of pure iron. The assembled attenuator consisting of the line section fitting snugly between the curved pole pieces of the electromagnet is shown in Fig. 4.

Experimental Data

Two properties of the magnetic attenuator were investigated, the attenuation and input impedance. The attenuation is defined to be the insertion loss which occurs when the attenuator is placed in a matched, 50-ohm coaxial transmission-line system having Type N connectors. The arrangement for the measurement of attenuation by direct substitution is shown in the block diagram of Fig. 5. The input impedance was measured with the attenuator terminated in a matched 50-ohm load.

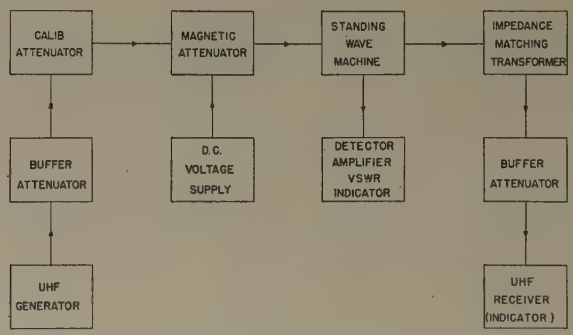

Fig. 5—Block diagram of the circuit used for attenuation measurements.

The above properties were investigated to determine their dependence on the following factors:

1. Type of ferromagnetic material.
2. Frequency of operation of the transmission-line system.
3. Strength of the magnetic field.
4. Orientation of the magnetic field.

Additional experiments were made to determine the effect of the dimensions of the insert, power level, temperature, and hysteresis, but complete data could not be obtained because of limited time and manpower.

The attenuation in decibels versus the electromagnet current in amperes is shown in Fig. 6 for an attenuator operating at ultra-high frequencies using various dissipative materials. The length of the dissipative material is one-half inch and the diameter is three-eighths of an inch in each case. The electromagnet of Fig. 3 was used to produce the magnetic field. The field strength is roughly proportional to the electromagnet current below the saturation point in the iron pole pieces and yoke. It is difficult to estimate the magnetic field strength in the material because of the nonuniform magnetic circuit, but measurements in the air gap of the electromagnet with the attenuator removed yield field strengths up to 4000 gauss with 4 amperes of current. The actual field strength in the material is higher than this, depending upon its permeability.

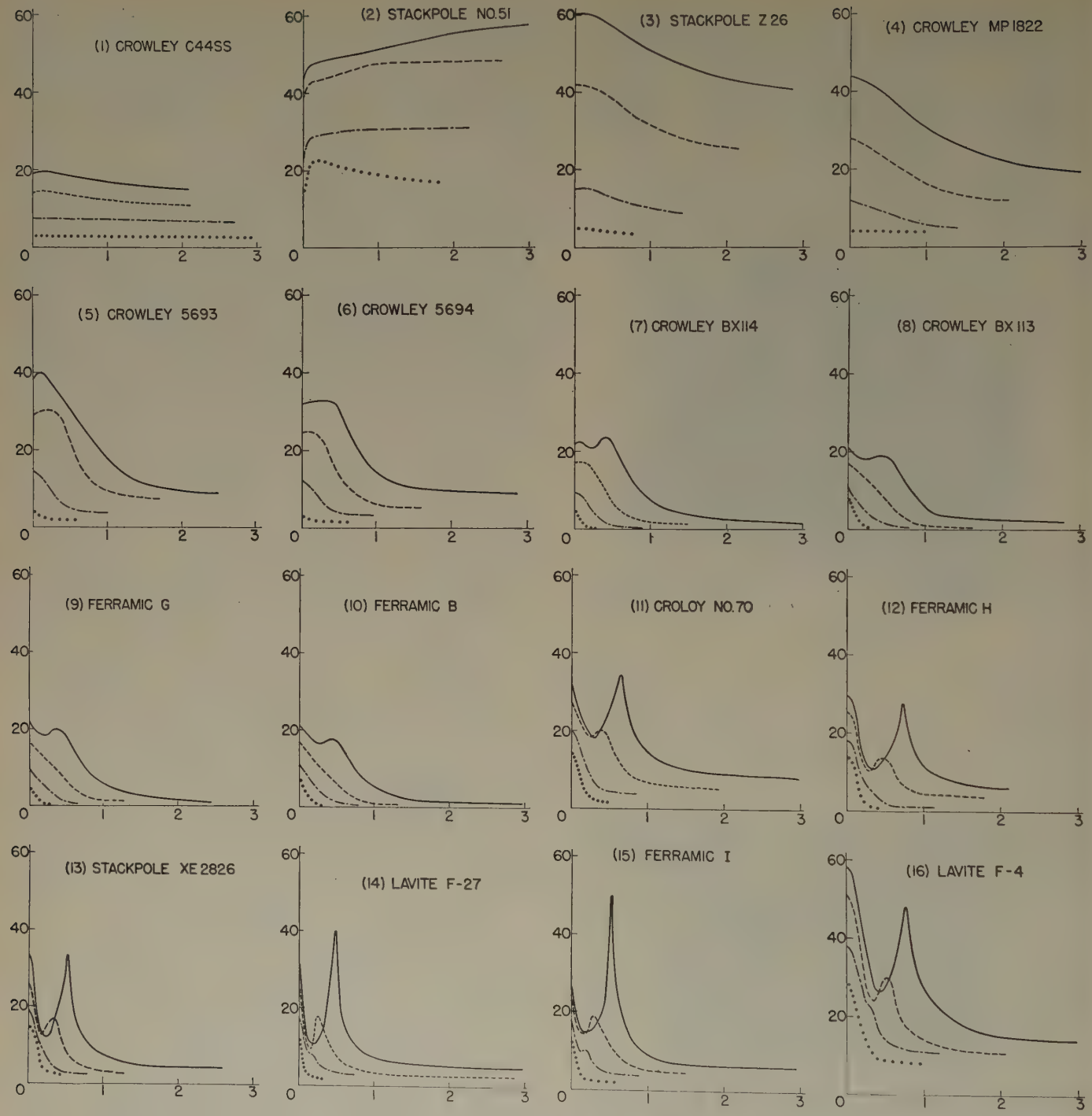

Fig. 6—Attenuation in decibels versus electromagnet current in amperes is shown for the magnetic attenuator using various dissipative materials. The name of the material is shown on each family of curves. In each case, the solid curve represents a frequency of operation of 3000 mc and the other curves correspond in descending order to frequencies of 2000, 1000, and 300 mc.

Inspection of the graphs reveals many interesting things. Some materials such as Crowley C44SS (Fig. 6-1) are not at all suitable for use with magnetic attenuators at ultra-high frequencies because the attenuation does not change appreciably with magnetic field strength. In most cases, the attenuation ultimately decreases as the magnetic field strength is increased, but in the attenuator using Stackpole No. 51 (Fig. 6-2) the reverse is true.

Attenuators using polyiron such as Crowley MP1822 (Fig. 6-4) have a decreasing attenuation characteristic at frequencies of 1000 mc and above. At lower frequencies, both the total attenuation and the change in attenuation are very small.

The materials are arranged in order to show the gradual increase in the ferromagnetic resonance[11] effect. A slight dip is noted at 3000 mc in the Crowley BX114 characteristic (Fig. 6-7) and the dip has widened out to give a pronounced absorption peak at 0.65 ampere in

[11] K. J. Standley, "Ferromagnetic resonance phenomena at microwave frequencies," *Sci. Prog.*, vol. 38, no. 150, pp. 231–245; April, 1950.

the 3000-mc curve of Croloy No. 70 (Fig. 6-11). Perhaps the sharpest observed peak occurs in the 3000-mc curve for Ferramic I (Fig. 6-15). The materials which exhibit ferromagnetic resonance in or near the uhf band yield the greatest attenuation sensitivity to changes in the magnetic field and are best suited for use in control circuits and modulators. The minimum attenuation that can be reached is of interest in switching applications, and it is seen that a material such as Ferramic B (Fig. 6-10) is superior to many others in this respect.

Additional data on ferromagnetic resonance is shown in Fig. 7 for Croloy No. 20 material. The resonance is observed to occur at higher magnetic field strengths as the frequency is increased. The highest observed resonance peak occurs at a frequency of approximately 3200 mc.

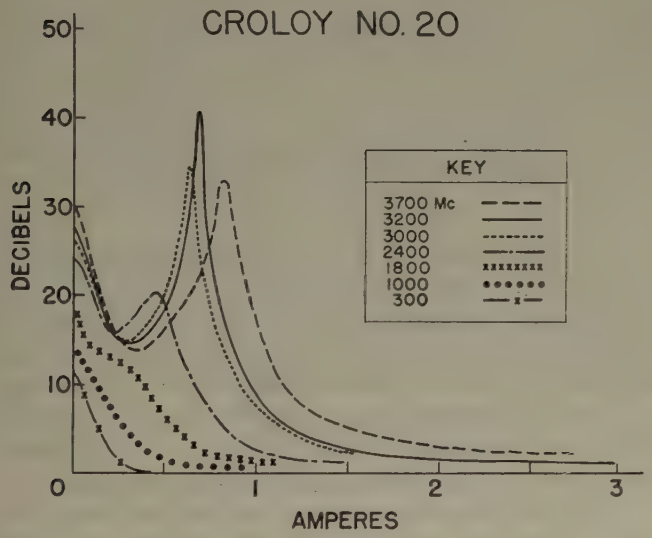

Fig. 7—Attenuation versus electromagnet current (showing ferromagnetic resonance) for a magnetic attenuator using Croloy No. 20 as the dissipative material.

Using the small electromagnet shown in Fig. 4, good control of the attenuation can be obtained with small currents when certain dissipative materials are used in the attenuator. Fig. 8 shows a variation of 11 db at 325 mc, with a total current change of 10 m amps when using a Ferramic H ferrite. The corresponding curve shown in Fig. 6–12 indicates that similar control can be obtained using this material over the entire uhf band. Other suitable materials include Lavite F-27 and Stackpole XE2826.

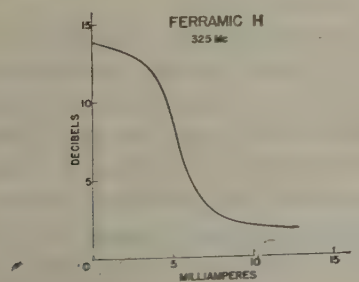

Fig. 8—Control of attenuation using small electromagnet.

In some cases, rotation of the coaxial-line section containing the ferromagnetic material with respect to the electromagnet produces a change in attenuation. This effect is quite small or absent in most cases except at ferromagnetic resonance. This phenomenon is shown in Fig. 9 for a particular attenuator using Ferramic B. It is

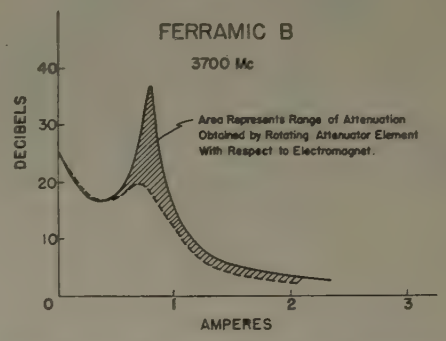

Fig. 9—Effect of rotating magnetic field of an attenuator operating near ferromagnetic resonance and using anisotropic dissipative material.

to be presumed that the particular sample of the material used is anisotropic.

The variation of input impedance at ultra-high frequencies with change of magnetic field strength is shown for attenuators using Croloy No. 20 in Fig. 10,

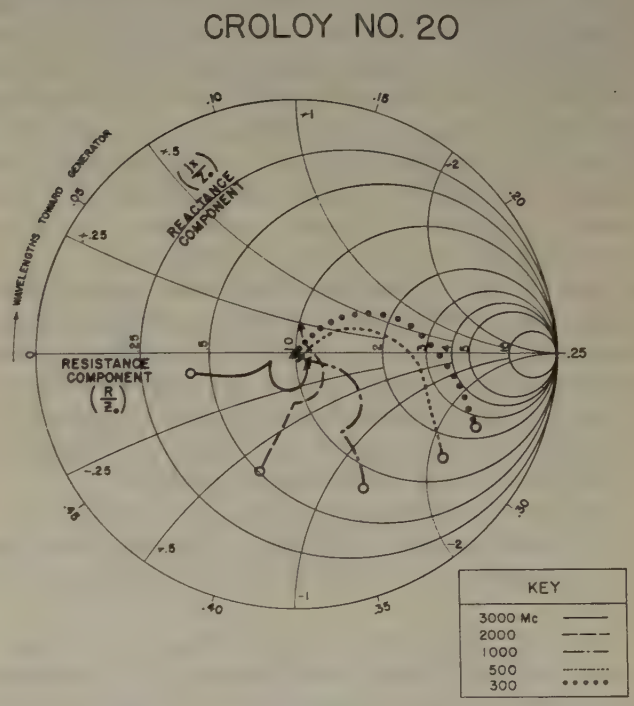

Fig. 10—Impedance characteristics at ultra-high frequencies of a magnetic attenuator using Croloy No. 20 material. The circles correspond to the normalized impedance with no magnetic field applied. As the field is increased, the impedance changes in the direction of the arrows.

Croloy No. 70 in Fig. 11, and Ferramic H in Fig. 12. The curves of normalized impedance are plotted with an arrow on circular transmission-line (Smith) charts to show the direction of increasing field strength. In each case, the beginning of the curve corresponds to zero electromagnet current.

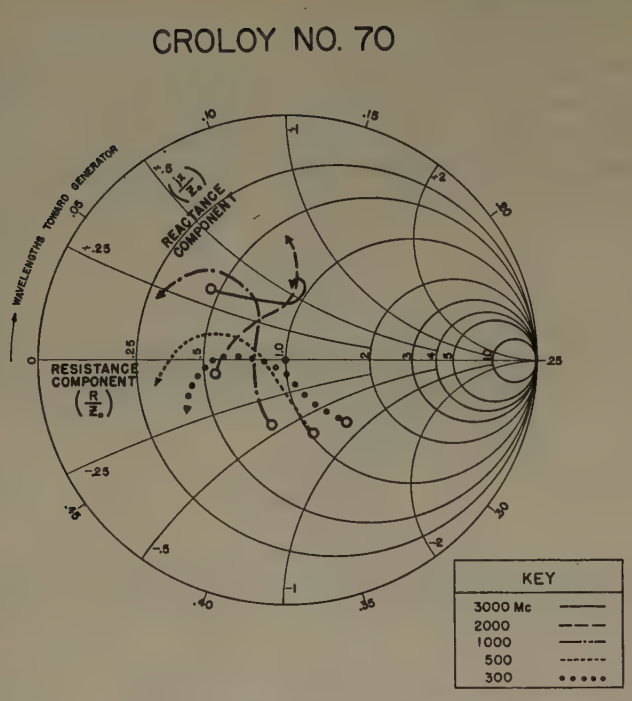

Fig. 11—Impedance characteristics at ultra-high frequencies of a magnetic attenuator using Croloy No. 70 material.

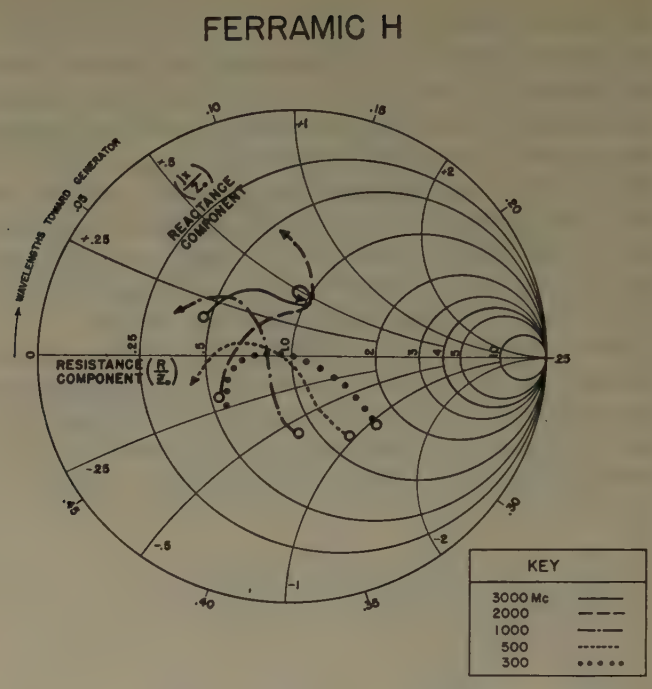

Fig. 12—Impedance characteristics at ultra-high frequencies of a magnetic attenuator using Ferramic H material.

It can be seen that the attenuator impedance curves are quite similar in shape at the lower frequencies, but assume individual characteristics at frequencies near ferromagnetic resonance. A good impedance match is obtained in a number of cases and the voltage standing-wave ratio (vswr) is at all points less than 4.0. It is apparent that attenuators can be designed for use as absorption modulators having good impedance characteristics. This can be readily seen from the three-dimensional figure shown in the photograph of Fig. 13. In this figure, the data in the impedance plane correspond to the 2000 and 3000 mc curves of Fig. 10 for an attenuator using Croloy No. 20. The attenuation corresponding to each impedance value is plotted vertically. It can be seen that large changes in attenuation can be obtained with small impedance changes if the attenuator is operated near ferromagnetic resonance.

The effect of dimensions, power level, temperature, and hysteresis on the attenuation characteristics are not shown graphically, but can be briefly summarized as follows:

The attenuation at zero electromagnet current generally increases linearly with the length of the insert. Some deviation from linearity may be experienced at higher electromagnet currents if the distribution of magnetic field in the material is changed due to the increased size of the poles of the electromagnet.

The diameter of the insert and the relative diameter of the inner and outer conductors have their principal effect on the input impedance. The size of the insert chosen for the uhf magnetic attenuator gives a fairly good impedance match and efficient control of attenuation with most materials used.

At power levels up to 10 watts, some heating was observed but no noticeable change[12] in the attenuation characteristic was observed. At 2000 mc and with no external magnetic field applied, an attenuator using a Ferramic H ferrite as the dissipative material was heated to a temperature above 105°C and no noticeable change in its attenuation characteristics was observed. One hour was required for a complete heating cycle.

There was practically no noticeable hysteresis effect when increasing or decreasing the external magnetic field. With any one attenuator, measured data could be repeated within the accuracy of the measurements.

Applications

Several applications of the magnetic attenuator are apparent and others may be found.

The magnetic attenuator fills the need for a continuously variable coaxial attenuator having a low minimum attenuation. Piston attenuators used for this purpose have a minimum attenuation of approximately 20 db. Coaxial variable attenuators using a resistive flap inserted through a slot in the coaxial line are nonlinear and have a relatively small attenuation and frequency range. There are few other types of coaxial variable attenuators available.

The magnetic attenuator may be used as an absorption modulator. With cw input to the attenuator, an ac modulating field is superimposed on the dc field, producing an amplitude modulated output. The modulating field may be produced by varying the electromagnet current about a chosen bias[13] value, or by using an addi-

[12] Changes in attenuation less than 0.2 db.

[13] If the attenuator is biased at the linear portion of its attenuation characteristic, undistorted modulation may be obtained.

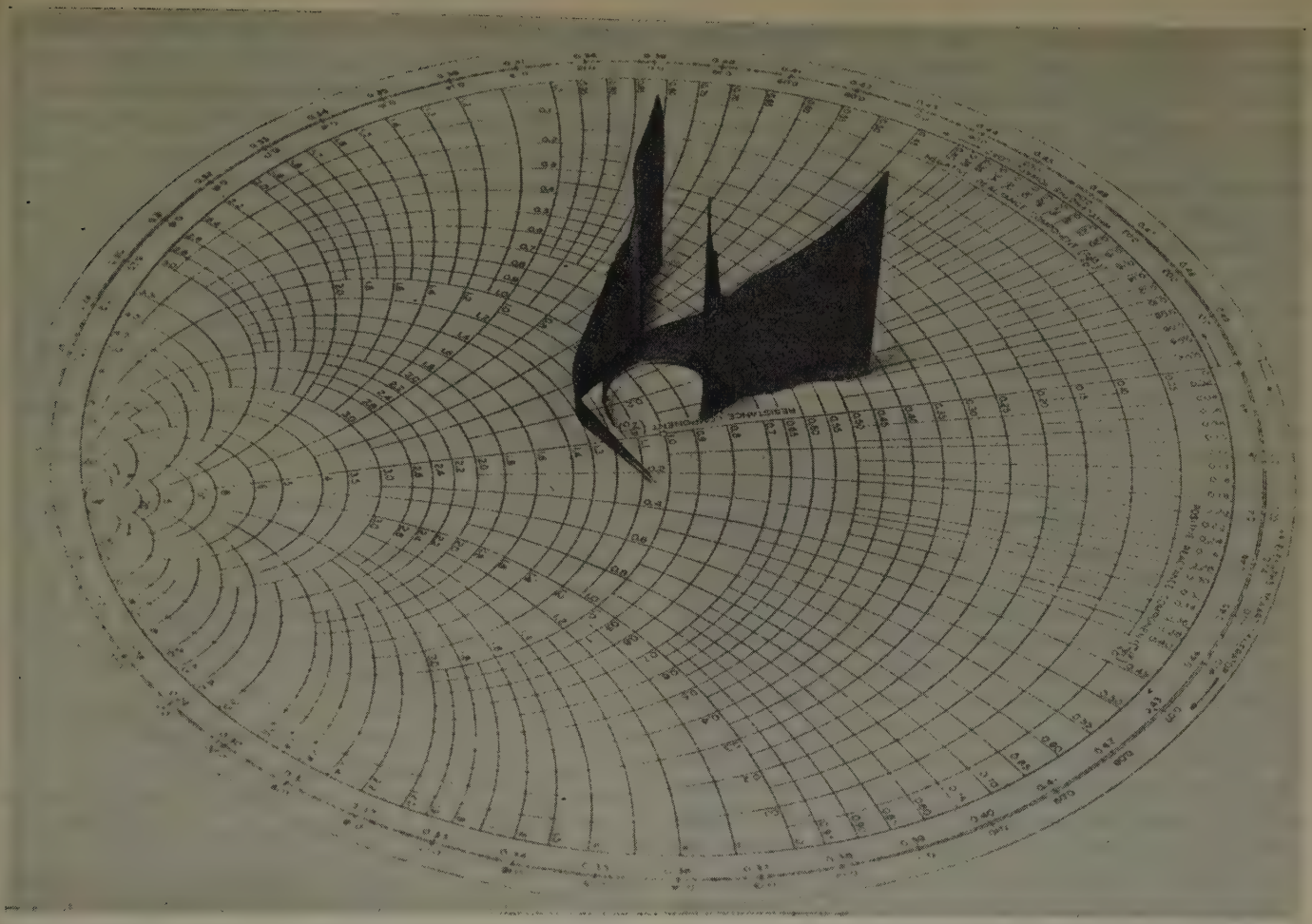

Fig. 13—Photograph of a three-dimensional plot of the attenuation and impedance changes obtained with a magnetic attenuator as the electromagnet current is increased from zero to 3 amperes. Two graphs are shown, one for an operating frequency of 3000 mc (on the right) and the other for a frequency of 2000 mc. Attenuation is plotted vertically, the two horizontal lines corresponding to 10 and 20 db. The normalized impedance is shown on the horizontal Smith chart. The dissipative material is Croloy No. 20.

tional modulating coil on the yoke of the electromagnet. This is often easier to accomplish than direct modulation of the oscillator which usually produces unwanted frequency modulation. The impedance characteristics can be improved by proper choice of the dc biasing field to reduce pulling of the oscillator due to changes of loading. Modulation frequencies from dc to 10,000 cycles have been used successfully with the attenuator assembly shown in Figs. 1 and 4.

If suitable dissipative materials are chosen, the magnetic attenuator can be used as a transmission switch, which alternately transmits or attenuates high-frequency energy as the electromagnet current is varied between two fixed values.

As shown in Fig. 14, the magnetic attenuator can be used as a control device in a degenerative feedback network to stabilize automatically the power output of a uhf generator. A small amount of RF power taken from the coaxial transmission line is detected, amplified, compared against a dc reference voltage, and used to control the output voltage of the dc power supply which supplies the electromagnet current that controls the RF power level through the attenuator.

The rotational effect shown in Fig. 9 can be used to provide additional control in connection with an angular rotation which may be of value in certain applications.

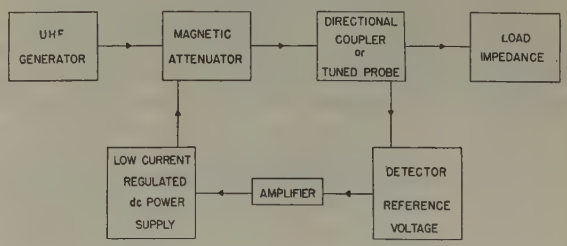

Fig. 14—Block diagram showing amplitude stabilization of the output of the uhf generator using a magnetic attenuator.

Design Considerations

The design of a magnetic attenuator depends upon its application requirements. A certain amount of trial and error may be necessary to find the best material for a given application. It is good practice to choose a standard size for the insert of dissipative material and make the line section in such a way (see Fig. 2) that it is easily disassembled to accommodate inserts of various materials.

Since the physical properties of the magnetic ferrites closely resemble those of ceramics, special machining techniques are required to shape the materials to the desired dimensions. Diamond-surfaced grinding wheels and drills are required throughout. In most cases, it is possible to have the ferrite molded in prescribed shapes by special arrangement with the manufacturer.

The outer conductor of the line constitutes a high reluctance gap in the magnetic circuit between the dissipative insert and the pole pieces of the electromagnet. It is advisable to reduce this reluctance by making the outer conductor very thin.

In applications involving modulation, the fields from eddy currents in the outer conductor may reduce the ac modulating field in the dissipative material. If high modulating frequencies are used, it may be necessary to axially laminate the electromagnet poles and a section of the outer conductor to reduce eddy currents.

Another method for high-frequency modulation is as follows: A second electromagnet is placed about the attenuator element perpendicular to the electromagnet previously described. This electromagnet differs from the first in that a ferrite material is used for the yoke and pole pieces. Holes are cut in the outer conductor of the attenuator so that the pole pieces can contact the dissipative material. Leakage of uhf energy may be prevented by extending the outer conductor back over the pole pieces a short distance, forming cylindrical waveguides which are below cutoff at ultra-high frequencies.

Field coils used with the electromagnet need not be specially wound in all cases, but can be chosen for their voltage or current ratings, shape, and size and can be readily obtained from commercially available ac or dc relays. For some applications, several windings can be used to accommodate both ac and dc control fields and can be operated in series or parallel.

Appendix

A partial list of commercially available dissipative materials suitable for use in the uhf magnetic attenuator is shown in Table I. The approximate attenuation at 1000 mc when no external magnetic field is applied is shown for each material, together with the manufacturers' name and address.

TABLE I

Dissipative material		Zero field attenuation (db/in) at 1000 mc	Manufacturer
Ferramic	B	22	General Ceramic and Steatite Corp., Keasbey, N. J.
	G	19	
	H	35	
Croloy	20	29	H. L. Crowley and Co., Inc., West Orange, N. J.
	70	40	
	BX113	22	
Lavite	F27	35	D. M. Steward Manufacturing Co., Chattanooga, Tenn.
	F15	34	
	F4	72	
XE2826		38	Stackpole Carbon Company, St. Marys, Pa.

A Microwave Magnetometer*

P. J. ALLEN†

Summary—**Faraday rotation in ferrites at microwave frequencies is applied experimentally to a new magnetometer technique expected to attain extreme sensitivity. The microwave output voltage is linearly related to the magnetic field. Sensitivity is a function of microwave carrier level, length and initial permeability of the ferrite rotator. Experimental response curves are given for two different rotator lengths. Magnetic increments of the order of one gamma have been detected. The prospect of attaining the extreme sensitivity inherent in the microwave magnetometer principle suggests the magnetic detection possibilities of a micro-magnetometer.**

Introduction

UNTIL RECENTLY the term Faraday effect has been associated principally with a magneto-optical rotation phenomenon observed when a polarized light beam is transmitted through a transparent material in the direction of an applied magnetic field. Materials generally considered are nonmagnetic substances such as liquids, glasses and the like in which optical rotation, expressed by Verdet's constant, is of the order of 1/1,000 of a degree or less per cm path per oersted of applied field. Because of the very small rotations obtainable in available materials, with reasonable fields, the Faraday effect at optical wavelengths has achieved slight practical significance. At microwave frequencies, however, the Faraday effect reasserts itself.

Hogan[1] has reported Faraday rotations of the order of 1/10 degree per cm per oersted applied field in various ferro-magnetic ferrites at a frequency of 9,000 mc, thus confirming the predictions of Polder[2] that at microwave frequencies ferromagnetic substances should show appreciable Faraday rotation. With such large rotations at microwave frequencies being a practical reality, and much larger rotations to be expected, the Faraday effect and related gyromagnetic phenomena take on new meaning. This is well illustrated by Hogan's application

* Decimal classification: R282.3. Original manuscript received by the Institute, October 2, 1952.

† Naval Research Laboratory, Washington 25, D. C.

[1] C. L. Hogan, "The microwave gyrator," *Bell Sys. Tech. Jour.*, vol. 31, pp. 1–31; January, 1952.

[2] D. Polder, "On the theory of magnetic resonances," *Phil. Mag.*, vol. 40, pp. 99–115; January, 1949.

of the phenomenon to the realization of a new circuit element, the microwave gyrator. Other applications of gyromagnetic phenomena in ferrites at microwave frequencies are reported by Sakiotis, Simmons, and Chait.[3] The present paper proposes application of microwave Faraday rotation to a new magnetometer technique expected to attain extreme sensitivity.

Magnetometer Principle

The microwave magnetometer is essentially a microwave counterpart of the familiar optical system used for measuring Faraday rotations with known applied magnetic fields. In the magnetometer application, however, the magnetic field is the unknown and is determined from the readily-measured Faraday rotation imparted to the polarized microwave field in passing through the Faraday plate or rotator. The principle is illustrated in Fig. 1. Radiation from a microwave carrier source, S, is incident on a polarizer which transmits only a plane-polarized wave as represented by the vector A. The wave travels through the "transparent" Faraday rotator and in the presence of a magnetic field component, H, parallel to the direction of propagation, experiences a rotation θ.[1] The electric field now is represented by the vector A' which can be resolved into the components B and C. Component B lies in the acceptance plane of the analyzer and is transmitted through to the detector, D. Component C, on the other hand, lies in a plane normal to the acceptance plane of the analyzer, is thus rejected, and the detector senses only the component $B = A' \sin \theta$. It is apparent that for small angles of rotation B and θ are linearly related.

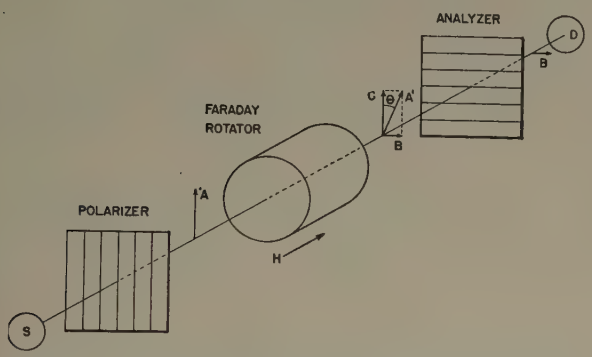

Fig. 1—Optical analogy of the microwave magnetometer.

Now a change in the applied field, H, produces a change in the rotation θ and a corresponding change in the amplitude of component B reaching the detector. If θ is proportional[4] to H, then for small angles component B is proportional to H, and the RF voltage reaching the detector is a direct indication of the applied field, H. On reversing the direction of H, vector B also is reversed, effecting a 180-degree relative phase change in the RF wave reaching the detector. It is obvious that by means of a suitable phase-sensing detector, the relative direction as well as the magnitude of the applied magnetic field, H, can be derived from B.

Microwave Aspects

In application of the principle at microwave frequencies, dominant-mode rectangular waveguides, aligned axially and with crossed electric planes, make effective polarizer and analyzer. The microwave Faraday rotator, which accomplishes direct intimate physical linkage between magnetic field and RF field, takes the form of a circular cylinder of ferrite material enclosed in a length of circular waveguide. This permits a closed microwave circuit with the waveguide polarizer and analyzer directly connected to the ends of the rotator waveguide.

One effective rotator design[5] consists of a pencil of ferrite imbedded in the center of a teflon-filled circular waveguide. This design provides good mechanical support for the ferrite rod, yet maintains reasonably good impedance match when in direct abutment with the rectangular waveguide. Variations of this design have been used in the magnetometer experiments.

In using a rectangular waveguide for the analyzer, component C (Fig. 1) will be totally reflected back through the Faraday rotator to the signal source unless absorbed by some means. If the transmission loss of the Faraday rotator is not small, the reflected wave reaching the generator may be sufficiently attenuated as to be of no consequence. On the other hand, if the Faraday plate is low-loss, an absorbing septum placed between Faraday rotator and analyzer and in the plane of vector C will dissipate this residual component while allowing the desired component, B, to enter the analyzer.

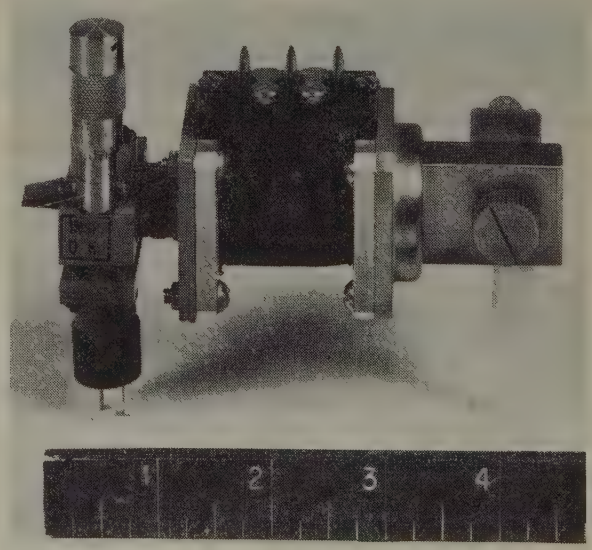

Fig. 2—Microwave elements of basic magnetometer.

The microwave carrier required in the magnetometer can be furnished by a klystron oscillator. The signal detector is some form of sensitive microwave receiver. Various possibilities suggest themselves.

The waveguide elements of a basic microwave magnetometer are shown in Fig. 2 and consist simply of a

[3] N. G. Sakiotis, A. J. Simmons, and H. N. Chait, "Microwave-antenna ferrite applications," *Electronics*, vol. 25, pp. 156; June, 1952.

[4] H. Suhl and L. R. Walker, "Faraday rotation of guided waves," *Phys. Rev.*, vol. 86, pp. 122–123; April 1, 1952.

[5] Due to C. H. Luhrs and Co., Hackensack, N. J.

klystron signal source, a Faraday rotator (with solenoid used for applying a magnetic bias or bucking field), and a crystal detector. A complete magnetometer requires only the addition of a klystron power supply and an indicating amplifier. Such a magnetometer is sufficiently sensitive to detect field changes of a small fraction of an oersted.

Regarding Sensitivity

If one assumes the magnetic induction, B_z, in the direction of propagation to be constant throughout the length of the ferrite rod, then for small rotations the angle through which the plane of polarization of the incident wave is rotated in passing through the Faraday plate can be expressed as

$$\theta = RlB_z.$$

Here, l is the length of the ferrite rotator and R is a factor (corresponding to Verdet's constant) expressing the rotation per unit length per unit induction in the particular microwave rotator being considered. If no loss occurs in the ferrite, then the RF output voltage reaching the detector is

$$E_0 = E_i \sin \theta,$$

where E_i and E_0 are magnitudes of input and output voltages, respectively, and correspond to vectors A and B of Fig. 1. Since we are dealing with small angles of rotation in the magnetometer application,

$$\sin \theta \simeq \theta, \quad \text{and} \quad E_0 = E_i\theta = E_iRlB_z.$$

Now,

$$B_z \cong \mu_a H_a,$$

where μ_a is the apparent permeability of the ferrite rod, and H_a is the longitudinal component of the applied magnetic field, thus $E_0 = E_iRl\mu_aH_a$.

If we define the sensitivity of the magnetometer as

$$\Delta E_0/\Delta H_a,$$

then

$$\Delta E_0/\Delta H_a \simeq E_iRl\mu_a,$$

where factors on the right-hand side of the expression are independent of H_a. It is seen that with R constant, the sensitivity of the magnetometer can be increased by increasing the RF input voltage, E_i, by increasing the length, l, of the ferrite rotator, and by increasing the apparent permeability, μ_a, of the rotator. However, because of demagnetizing effects[6,7] in the ferrite rod, μ_a itself is a function of the true permeability, μ_0, and of the length of the ferrite cylinder. Curves, found in footnote reference 6 show that in general, as the length-to-diameter ratio, l/d, of the magnetic rod is increased, a proportionate increase occurs in the apparent permeability, μ_a, until $\mu_a \simeq \frac{1}{2}\mu_0$. Beyond this the curves begin to flatten and μ_a approaches μ_0 asymptotically as l/d approaches infinity. Further, the larger μ_0, the larger the l/d ratio which may be used to advantage. Thus if $\mu_0 = 20$, an l/d ratio of 15 is a practical maximum; however, if $\mu_0 = 1{,}000$, an l/d ratio of 100 or more may be used to advantage. As a consequence, if one selects a material having a high "true" permeability, the apparent permeability, μ_a, increases as l/d, and with constant rod diameter, sensitivity of the microwave magnetometer increases approximately as the *square* of the length up to large ratios of l/d for the ferrite rod.

In expressing the sensitivity of the magnetometer the longitudinal component of induction, B_z, has been assumed uniform throughout the length of the Faraday rotator. This is not strictly true in the case being considered, as the induction in a rod[7] diminishes toward the ends. An accurate expression for sensitivity thus involves integration of the longitudinal component of induction over the length of the cylinder. Also, in the foregoing expressions for sensitivity the Faraday plate has been assumed lossless. For long rotators, however, the insertion loss may become significant, resulting in a reduction of sensitivity by the factor $e^{-\alpha l}$ where $-\alpha l$ is the absorption in nepers of the rotator. Thus for long rotators, the use of a low-loss material is important.

It appears that reducing the diameter of the ferrite rod also should increase sensitivity since this increases the rod induction. However, it is not known at what point one reaches diminishing returns since the dependence of the rotation constant, R, on rod diameter is not known.

For detecting small increments of magnetic field change in the presence of a relatively large residual field, a controllable fraction of the carrier generator power, properly phased, can be fed to the detector to essentially annul the residual RF signal to the order of the incremental variation to be detected. This technique permits the available sensitivity of the detecting receiver to be used to best advantage.

For still larger residual magnetic fields, an opposing magnetic bias can be applied to the rotator by means of a concentric solenoid.

If the Faraday rotator introduces negligible loss, the sensitivity can be doubled by extracting component B after component A' has been totally reflected back through the rotator, doubling the total angle of rotation, consequently doubling the amplitude of component B. However, if the rotator introduces appreciable loss, this approach can actually result in a decrease in sensitivity, depending on the one-way absorption loss of the rotator.

The answer to the question of what limits ultimate sensitivity remains moot. The limit of sensitivity in any practical case will be determined by the noise level of

[6] R. M. Bozorth and D. M. Chapin and "Demagnetizing factors of rods," *Jour. Appl. Phys.*, vol. 13, p. 322; May, 1942.

[7] H. van Suchtelen, "Ferroxcube aerial rods," *Elec. Appl. Bull.*, vol. 13, pp. 88–100; June, 1952.

the system. However, assuming a noise-free carrier source, any ultimate limitation appears to be whatever microwave noise is introduced to the system by the presence of the ferrite material in the waveguide.

Experimental Results

A nonreversible curve, typical of the response of the magnetometer of Fig. 2, is shown in Fig. 3. Relative RF voltage across a matched detector is plotted against the applied magnetic field, beginning with a completely demagnetized Faraday rotator. While the upper portion of the curve is not reversible due to hysteretic effects in the ferrite, the lower portion is reversible for applied fields up to several oersteds.

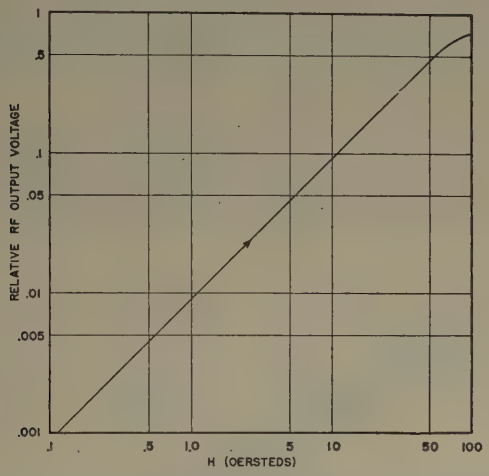

Fig. 3—Typical nonreversible response curve for basic microwave magnetometer of Fig. 2, operating at 9,300 mc.

Using the arrangement shown in Fig. 4, reversible experimental curves were obtained for two different lengths of ferrite sample in the Faraday rotator. The applied magnetic field, H, was controlled by varying the current in a long solenoid surrounding the rotator. The

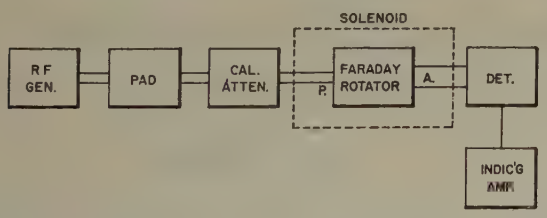

Fig. 4—Microwave test setup for measuring magnetic response of Faraday rotator.

intercept of each curve with the vertical axis of Fig. 5 indicates the minimum relative signal level at the detector which was obtained at zero applied magnetic field. The upper line shows the result of the first attempt to measure the properties of a rotator containing a Ferramic "D" rod $4\frac{7}{8}$ inches long. The curvature and relatively large output at zero magnetic field strength was found to be due to lack of perfect electrical symmetry

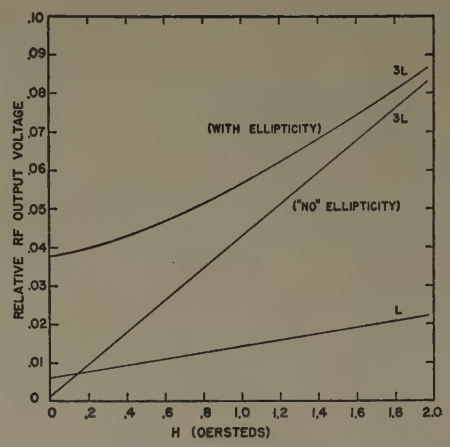

Fig. 5—Reversible response curves made at 9,300 mc for two Faraday rotators of different length, showing the effect of residual ellipticity in the rotator waveguide on the response of the longer rotator ($L=1\frac{5}{8}$ inches, $3L=4\frac{7}{8}$ inches).

in the circular waveguide rotator, resulting in slight ellipticity in the output. This was remedied by the use of special flanges as shown in Fig. 6, which allowed the circular waveguide to be rotated about its own axis, independent of the polarizer and analyzer waveguides.

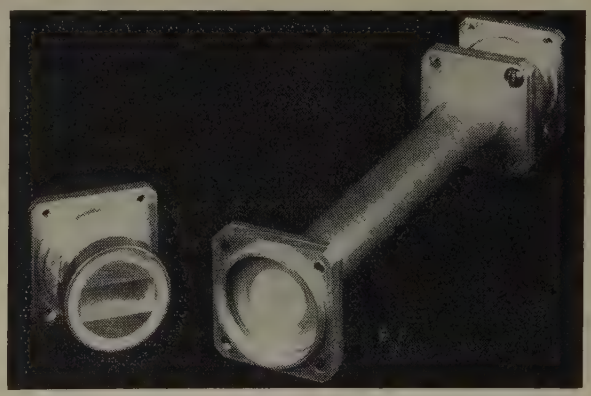

Fig. 6—Faraday rotator and special flanges which allow independent orientation of unit to reduce ellipticity in output.

Orienting the imperfect circular waveguide section in this manner established electrical symmetry about the polarization plane of the wave being propagated, thus preventing the production of a cross-polarized component in the output. On rotating the circular waveguide section independently, without applied magnetic field, the ellipticity ratio could be varied from about 30 db to something over 80 db. The consequence of "eliminating" the ellipticity is seen in a second curve of Fig. 5, applying to the same rotator, which shows that the minimum transmission has been considerably reduced, and the lower portion of the curve has become linear. The third curve is for a shorter Ferramic "D" rod, $1\frac{5}{8}$ inches long.

These curves indicate actual experimental sensitivities of the two different rotators if used as magnetometer elements, and include the effect of insertion loss of the individual rotators. The sensitivity (slope) data are

compiled in Table I along with data for two other similar length rotators using Ferramic "*A*" rods. The column of "corrected sensitivity" is the sensitivity obtained after correcting the experimental sensitivity for the transmission loss of the actual rotator, and represents the sensitivity one would obtain if the rotator were lossless. From the corrected sensitivity, the total rotation angle is found for an applied field of one oersted. With the longer Ferramic "*D*" rod, a rotation of nearly 16 degrees was obtained, or a rotation of about $1\frac{1}{4}$ degrees per cm per oersted. It is seen that although the absorption loss of the Ferramic "*D*" rotator is greater than for the corresponding "*A*" rotator, the actual sensitivity of the "*D*" rotator is the higher. Magnetic increments of the order of one gamma (10^{-5} gauss) have been detected with a relatively simple magnetometer in the laboratory.

While agreement between experimental and expected sensitivity as a function of rotator length thus far has been poor, experimental sensitivities have been consistently higher than those expected from the foregoing expressions. The principal source of error is believed to be in assuming both R and B_z to be constant throughout the length of the ferrite rod.

Conclusion

Numerous considerations regarding both theoretical and practical aspects of the microwave magnetometer remain to be investigated. Further development of ferrites for microwave applications should result in materials of lower loss at low inductions than those now in use, making feasible longer Faraday rotators. Such factors as mechanical and thermal stability, ratio of carrier power to receiver sensitivity, and maximum practical RF carrier level require further study. In fact, the practical limitation of sensitivity has yet to be determined.

Two similar rotator units in a microwave bridge circuit may offer certain advantages in practical magnetometer applications. Incorporation of the principle in a three-co-ordinate version is suggested as a means of indicating magnitude and direction of the total field vector with a fixed magnetometer unit.

The prospect of attaining the extreme sensitivity inherent in the microwave magnetometer principle suggests the magnetic detection possibilities of a *micromagnetometer*.

TABLE I

Experimental Data for Four Different Ferrite Faraday Rotators, Operating at 9,300 mc.

Ferrite Rod Data				Rotator transmission loss (db)	$e^{-\alpha l}$	Experimental sensitivity $(1/E_i) \cdot \Delta E_0/\Delta H_a$	Corrected sensitivity $[1/(E_i e^{-\alpha l})] \cdot \Delta E_0/\Delta H_a$	Rotation θ (degrees per oersted)
"Ferramic" ferrite type	Length, l, (inches)	Diam., d, (inches)	l/d Ratio					
D	$1\frac{5}{8}$	0.25	6.5	5.0	0.562	0.008	0.014	0.8
D	$4\frac{1}{8}$	0.25	19.5	16.5	0.147	0.040	0.272	15.8
A	$1\frac{5}{8}$	0.25	6.5	1.1	0.881	0.003	0.0034	0.195
A	$4\frac{1}{8}$	0.25	19.5	3.6	0.661	0.025	0.038	2.2

A UHF and Microwave Matching Termination*

ROBERT C. ELLENWOOD†, and WILLIAM E. RYAN‡, associate, ire

Summary—**Coaxial transmission line and waveguide terminations are described which employ a double-slug transformer and a lossy dielectric load to provide an impedance match. Electromagnetic waves reflected from the load are canceled out by adjusting the positions of the two dielectric transformer slugs relative to the load, by means of bakelite rods which extend axially through the end of the termination. The terminations can be matched over wide frequency ranges; they are simple in operation and construction, having no critical dimensions.**

* Decimal classification: R117.3×R310. Original manuscript received by the Institute, February 4, 1952; revised manuscript received September 11, 1952.

† Bureau of Ships, Navy Dept., Washington, D. C. Formerly with Central Radio Propagation Laboratory.

‡ Central Radio Propagation Laboratory, National Bureau of Standards, Washington, D. C.

I. Introduction

IN ULTRA-HIGH-FREQUENCY (uhf) and microwave measurements, transmission-line terminations are needed which can be adjusted to match the impedance of the line or to provide a given voltage-standing-wave ratio (vswr) in the line. These loads are useful, for example, in the evaluation of discontinuities in transmission-line components, such as connectors or slotted-line standing-wave machines. Other applications of these adjustable terminations are power and attenuation measurements and the calibration of probes under matched-load conditions.

This paper describes a simple termination composed of two low-loss dielectric slugs and one lossy dielectric,

which are moved back and forth in a waveguide or coaxial line by means of bakelite rods parallel to the axis of the guide.[1] The two low-loss dielectrics operate together as a double-slug transformer to cancel out the multiple reflections, and the lossy dielectric which is backed by a brass short absorbs the electromagnetic energy. The termination (used with a fixed probe) is adjusted for an impedance match by varying the distances between the three dielectrics with the rods which extend out the end of the guide. A match is indicated if no standing wave is observed as the three dielectrics are slid back and forth together with the spacing between them fixed.

The dimensions of the components of the termination are not critical and most of them were chosen arbitrarily. The major requirement is that both transformer slugs be a quarter wavelength long at some suitable frequency, as is explained later.

II. Coaxial Termination

This design was adopted especially for a 7/8-inch coaxial termination (Fig. 1) for use in the uhf range from 300 to 3,000 mc. The 7/8-inch coaxial model is

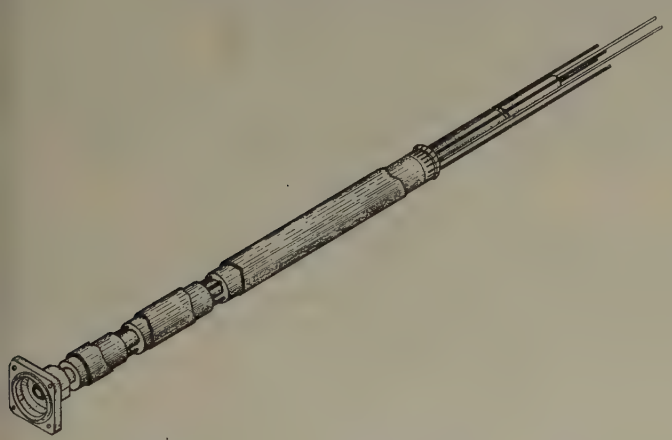

Fig. 1—Cutaway view of $\frac{7}{8}$-inch coaxial-line termination.

built of 4-foot conductors from ordinary machine brass stock, a type which has nominal tolerances of 0.003 to 0.005 inch. To ensure free movement of the dielectric cylinders, about 0.008-inch clearance was allowed between them and the conductors.

The brass short attached to the end of the lossy dielectric has bronze fingers with a spring fit in order to prevent leakage, help to center the inner conductor, and maintain a fairly constant short circuit as the slugs are slid back and forth in the line. Three pairs of long rods of 0.113-inch diameter extending through 0.125-inch holes in the short are used to position the three dielectric slugs as it was found that two rods were necessary for proper mechanical control of each slug. One pair of rods, made of brass, is screwed through the short into the lossy dielectric load in order to fasten them together, and is used to position not only the lossy dielectric load but also the complete termination after the transformer has been tuned. A brass slug beyond the end of the conductors (not shown in Fig. 1) with holes through which the rods may slide and screws to tighten on the rods, was used to fix the relative positions of the slugs once the transformer was tuned. The other two pairs of rods, which must be dielectric (bakelite was chosen for mechanical strength), extend through holes in the load and screw into their respective transformer slugs. The pair of rods attached to the slug furthest from the load passes also through 0.125-inch diameter holes in the other transformer slug.

Because of the presence of these bakelite drive rods and the loose fit of the slugs in the transmission line, accurate calculations of the electrical properties of the load are impractical. It is simpler and more accurate to determine the vswr or reflection coefficient of the termination by direct measurement. The general approximation for the attenuation of a lossy dielectric in a coaxial transmission line is[2]

$$\alpha = \frac{8.686\pi\sqrt{\epsilon}\,\tan\delta}{\lambda}\ \text{db per inch},$$

where λ is the wavelength in air in inches, ϵ the real part of the complex dielectric constant relative to air, and $\tan\delta$ the loss tangent, or ratio of the imaginary to the real component of the complex dielectric constant.

A plastic, Catalin (700 base), was chosen as the lossy dielectric because of its high loss-tangent and excellent machinability. Its loss tangent is 0.15 to 0.20 and its dielectric constant approximately 5. This results in an attenuation of about $\frac{1}{2}$ to 3 db per inch in the uhf range. After the measurement of the vswr of various lengths of Catalin loads, a 13-inch length was chosen as a suitable compromise for a load with a small reflection coefficient and a reasonably short length. VSWR of Catalin load is shown as a function of frequency in Fig. 2(a).

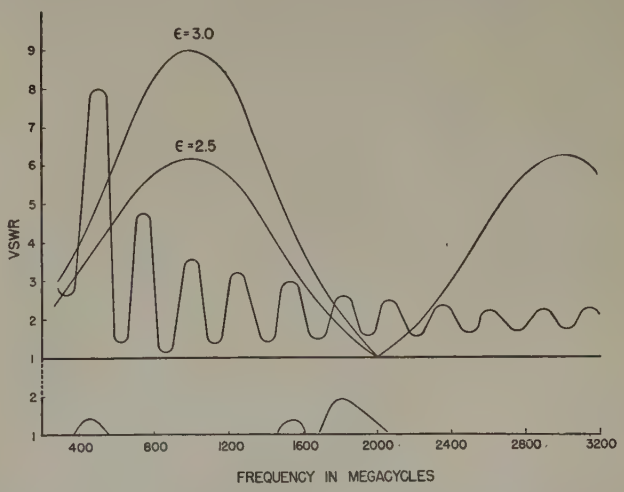

Fig. 2—(a) at the top. Measured vswr before matching of 13-inch length of Catalin in $\frac{7}{8}$-inch coaxial-line termination, together with curves showing theoretical matching capabilities of transformer slugs with dielectric constants of 2.5 and 3.0. (b) at the bottom. VSWR after matching using $\epsilon = 2.5$ transformer slugs.

[1] R. E. Grantham, in "A reflectionless waveguide termination," *Rev. Sci. Instr.*, vol. 22, pp. 828–834; November, 1951, describes another matching termination of somewhat different design.

[2] T. Moreno, "Microwave Transmission Design Data," McGraw-Hill Book Co., Inc., New York, N. Y. first ed., p. 65; 1948.

The vswr's can be matched to the transmission line by a double-slug transformer, a type which is effective over wide frequency ranges for fairly large vswr's. This transformer can match any impedance whose vswr does not exceed ϵ^2 for the dielectric of which the slugs are made. Though the transformer will match a vswr of this magnitude only at frequencies for which the slugs are an odd number of quarter-wavelengths long, it is sufficiently "broad-band" to match any vswr approaching this values at other frequencies according to the following equation,[3]

$$\text{vswr}_{\max} = 1 + \frac{b}{2} + \sqrt{b + \frac{b^2}{4}},$$

where

$$b = \left[1/2\left(\epsilon - \frac{1}{\epsilon}\right)(1 - \cos 2\beta_a l_a)\cos \beta_0 l_0 + \sqrt{\epsilon}\left(1 - \frac{1}{\epsilon}\right)\sin 2\beta_a l_a \sin \beta_0 l_0\right]^2,$$

and

$\beta_a l_a$ = electrical length of each slug,
$\beta_0 l_0$ = electrical distance between the slugs,
ϵ = dielectric constant of the slugs.

The curves marked $\epsilon = 2.5$ and $\epsilon = 3.0$ in Fig. 2(a) are plots of the above equation for slugs a quarter-wavelength long at 1,000 mc and indicate the maximum vswr's that can be matched at each frequency with slugs having these dielectric constants. It can be seen that, if the vswr's are not large, there is little increase in the matching band to be gained by using transformer slugs of large dielectric constant. Moreover, high dielectric-constant slugs were found to be more difficult to adjust for match than low dielectric-constant slugs, such as polystyrene, whose dielectric-constant is about 2.5. Transformer slugs of polystyrene are capable of matching the vswr of the Catalin termination over all but the lower end of the uhf range. The measured vswr of the 13-inch Catalin termination is also shown in Fig. 2(a).

The experimental performance of the adjustable coaxial termination is shown in Fig. 2(b). With the polystyrene slugs ($\epsilon = 2.5$) of Fig. 2(a) which were 1.87 inches long it was possible to obtain a match over more than 80 per cent of the uhf range. It is seen that the frequencies at which one could not obtain a match with this set of slugs (that is, where the vswr of the Catalin load exceeds the vswr matching capability of the transformer) are somewhat lower than the curves of Fig. 2(a) predict. This is probably caused by an effective increase in the dielectric constant of the transformer slugs due to the presence of the bakelite rods, so that the slugs were a quarter wavelength long at a frequency somewhat less than 1,000 mc.

[3] R. C. Ellenwood and E. C. Hurlburt, "The determination of impedance with a double-slug transformer," to be published in a forthcoming issue of the PROC. I.R.E.

With this coaxial termination it is possible to obtain a vswr measured with a differential vacuum-tube voltmeter less than 1.004 (reflection coefficient <0.002) without any difficulty. This small limitation in making a perfect match is apparently caused by a slight warping of the conductors so that, as the load moves along the line, the conductors go in and out of concentric positions, thus changing the characteristic impedance of the line.

At the lower frequencies the lossy termination results in larger vswr's. In order to match a vswr of the order of 6 to 10, it is necessary to use slugs of such material as bakelite or Dielectene, which have dielectric constants of 3 or more. The more critical adjustment of these high dielectric-constant slugs is partially compensated for by the fact that in this case they are being employed at the longer wavelengths. Of course, some decrease in the vswr at low frequencies can be obtained by the use of longer pieces of Catalin.

As the first set of polystyrene slugs could not match any appreciable vswr's near 2,000 mc, a second pair was made which was a quarter wavelength at 2,000 mc to cover that frequency range. Thus, with two or three pairs of transformer slugs the entire uhf band can be covered. With only one pair a match can be obtained over most of the range. In order that the sets may be easily changed, the slugs have threaded holes into which their respective drive rods may be screwed.

III. Waveguide Models

Though this termination was designed primarily for use with coaxial transmission lines, waveguide models were also built for the purpose of determining their performance at *X*-band (8,200–12,400 mc) and at *K*-band (18,000–26,500 mc).

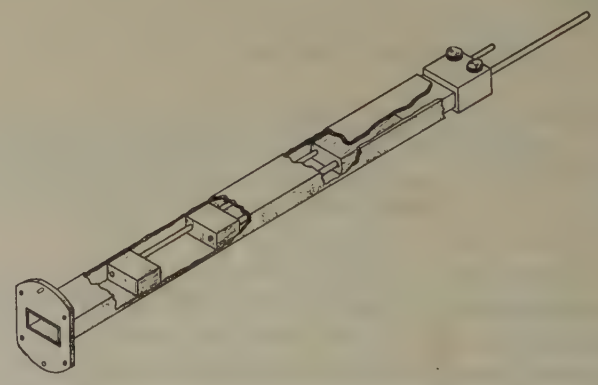

Fig. 3—Cutaway view of waveguide termination.

The waveguide model which is shown in Fig. 3 uses 2-inch lengths of Catalin for the lossy terminations in both the 0.900- by 0.400-inch *X*-band guide and the 0.420- by 0.170-inch *K*-band guide. These lengths are sufficiently lossy to reduce the vswr in the waveguide to a value less than three. At these frequencies this vswr is due mostly to the impedance mismatch at the air-Catalin interface. The Catalin in the waveguide is fastened to a 1.5-inch sliding brass block which serves

as a short circuit and as a centering device. The slugs and two 0.113-inch diameter drive rods in both waveguide models are made of polystyrene. In the X-band model the slugs are 0.675 inch long, three-quarters wavelength at 9,380 mc, and in the K-band model 0.475 inch long, five-quarters wavelength at 23,000 mc, in order to improve their rigidity and stability within the guide. The two thumb screws shown in Fig. 3 are tightened on the drive rods to anchor the slugs in position once they have been properly adjusted. In the waveguides a single drive rod was sufficient for mechanical control of each transformer slug. With each waveguide termination it was found that a match could be obtained to a vswr of 1.01 (reflection coefficient <0.005).

IV. Conclusion

This instrument is capable of covering wide frequency ranges. The coaxial termination will provide a match to a vswr of 1.004 with two pair of slugs over the entire uhf range. Similarly waveguide models will provide matches to 1.01 over their particular frequency ranges. Not only can these terminations provide a match, but they may also be adjusted to given values of vswr of the order of one to ten when for various reasons such a vswr is desired.

The outstanding features of this termination are its simplicity of construction and ease of tuning. There are no critical dimensions and the essential requirements are three dielectric slugs (one lossy) to fit loosely within a transmission line and the rods by which they may be moved. It takes but a short time to reduce the vswr to less than 1.01. The vswr could be reduced still further if closer tolerances and more refined components were used, such as a gearing arrangement to adjust the position of the slugs, with a sacrifice, of course, of some of the simplicity of construction.

A UHF Surface-Wave Transmission Line*

C. E. SHARP†, ASSOCIATE, IRE AND G. GOUBAU†, ASSOCIATE, IRE

***Summary*—A description is given of a surface-wave transmission-line unit developed to meet a requirement for an efficient, easy to install and maintain antenna feed line.**

Introduction

SINGLE-CONDUCTOR surface-wave transmission lines[1,2] are particularly advantageous as antenna feeds in the uhf range. In this frequency range the loss of flexible coaxial lines is usually too high, and rigid coaxial lines and waveguides are costly and difficult to install. Although there is a certain radiation loss inherently connected with the launching of surface waves, this loss is very small, if the launchers are properly designed. The efficiency of a surface transmission line is much greater than that of a coaxial line, assuming the diameter of the surface-wave conductor is comparable to that of the center conductor of the coaxial line. A surface-wave line is easily installed since it can be stretched directly between the antenna and the transmitter or receiver.

Since the field is on the outside of the conductor, the performance of a surface-wave transmission line is, to a certain extent, affected by weather conditions. It has been found that rain causes an appreciable increase of the transmission loss at the higher frequencies of the uhf band, if many drops form along the conductor. In the case of an antenna feed where the line is inclined from the ground, drops will not form and the effect of rain is negligible. Ice, if formed in thick layers, increases the transmission loss considerably, but the formation of ice can be prevented by heating the line electrically.

The surface-wave line assembly to be described was developed for operation in the frequency range from 1,700 to 2,400 mc. The electrical requirements were insertion loss for 150-foot line length, less than 3 db, and a standing-wave ratio not exceeding 1.5. Other requirements were ruggedness, simple installation and maintenance, and electric heating to prevent ice formation on the line.

Description

The conductor used for the surface-wave line is a number 10 (0.102-inch diameter) soft-drawn copper wire covered with an extruded layer of pigmented polyethylene of 0.014-inch thickness. The theoretical loss of this conductor, assuming a power factor of 5×10^{-4} for the dielectric, ranges from 0.7 db/100 feet at 1,700 mc to 0.95 db/100 feet at 2,400 mc. The phase velocity of the surface wave is about 1.2 per cent below the free-space velocity; the 90-per cent power radius of the field around the conductor at the center of the frequency range is about 4 inches.

Fig. 1 shows a cross-section view of a line termination or "launcher." The coaxial end section, I, together with the horn section, II, can be considered a tapered coaxial line in which the coaxial-wave mode is gradually converted into the surface-wave mode, or vice versa. The center conductor (1) is tapered down until it matches the diameter of the wire. The outer conductor (2) flares

* Decimal classification: R320.41×R117.1. Original manuscript received by the Institute, October 9, 1952.

† Signal Corps Engineering Laboratories, Fort Monmouth, N. J.

[1] G. Goubau, "Surface waves and their application to transmission line," *Jour. Appl. Phy.*, vol. 21, pp. 1119–1128; November, 1950.

[2] G. Goubau, "Single-conductor surface wave transmission lines," PROC. I.R.E., vol. 39, pp. 619–624; June, 1951.

out until it has little effect on the field as the surface wave is developed. The wire is connected to the center conductor by means of a specially designed wire fastener made of stainless steel. A cross-section drawing of this fastener is shown separately in Fig. 1. The connection is made in the following manner: The wire, after removing the insulation over a length of about 3 inches, is fed through the end (12) of this wire fastener at an angle of about 30 degrees to the axis of the fastener. Then the end of the wire is bent to form a hook and forced into the hole (13) and the slot (14). This method of fastening the wire has proven very satisfactory as it provides a smooth transition from the center conductor (1) to the wire. The holding strength of this connection is greater than the breaking strength of the wire. The collar (15) on the fastener compensates for the small electrical discontinuity at the junction (12) between wire and fastener.

The feed into section I is located at a quarter-wave distance from the shorted end. The coupling is made by a quarter-wave coaxial-line section, the inner conductor (3) of which is threaded into the center conductor (1); the outer conductor (4) is also the inner conductor of the coaxial feed section, III, shown separately in Fig. 1, which terminates in a standard LN-type connector (5). This coupling arrangement provides for uniform coupling over the frequency range and rejects low-frequency signals which may be received by the line acting as long wire antenna.

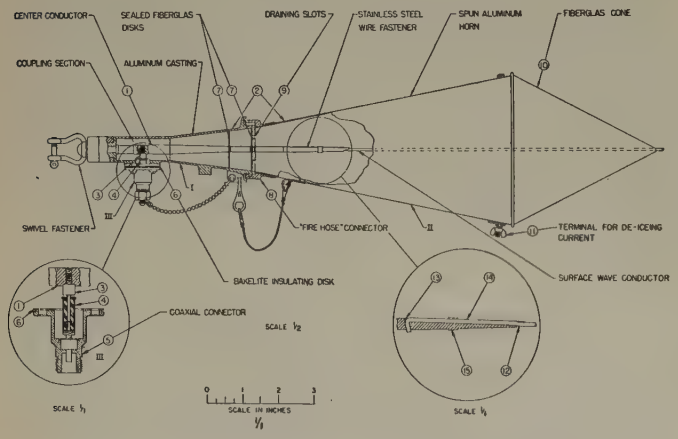

Fig. 1—Cross-section drawing of a launching unit.

The feed section, III, is insulated from section I by a bakelite disk (6). In this manner the current required for de-icing the line is entirely isolated from the equipment connected to the line assembly. Section I is sealed to prevent entry of water. The sealing is accomplished by two fiberglas disks (7) cemented in place. They are spaced about one quarter wavelength to compensate for reflection.

The horn section, II, is joined to the end section I by means of a "fire-hose" type connector (8). This connector has draining slots (9) on its circumference to avoid the collection of water in the horn. The opening of the horn is covered by a fiberglas cone (10) to prevent snow and insects from entering. The horn section contains a heating wire (not shown in the figure) for melting the snow which might collect on the outside of the fiberlas cone. One end of this heating wire is connected to the terminal (11), the other end to the metal horn.

Fig. 2—View showing one launching unit of the test-model line assembly.

The de-icing current enters at the terminal (11), passes through the heating wire, the metal horn, the outer and inner conductor of section I, the surface-wave line, and returns through the other line termination. Measurements in a cold chamber indicated that a heating power of 2 watts per foot of the line is more than adequate to prevent ice formation.

The line assembly is supported at both ends by swivel fasteners and kept under a constant tension of about 100 pounds by a spring assembly. Fig. 2 shows a launching unit of the installed line.

Performance Data

The insertion loss and the standing-wave ratio were measured for a line 130 feet in length. The results are shown in Fig. 3. Within the required operating range of 1,700 to 2,400 mc, the insertion loss measured between 2.1 and 2.4 db. The calculated loss, which takes into account the loss of the dielectric coated wire and the launching loss, is 0.5 db less than the measured value, but this discrepancy can be accounted for. It is known from measurement that the fiberglas cones contribute about 0.1 db each to the loss. There is also some additional loss in the launching units caused particularly by the two fiberglas disks and the wire fastener, which was not plated in the test model.

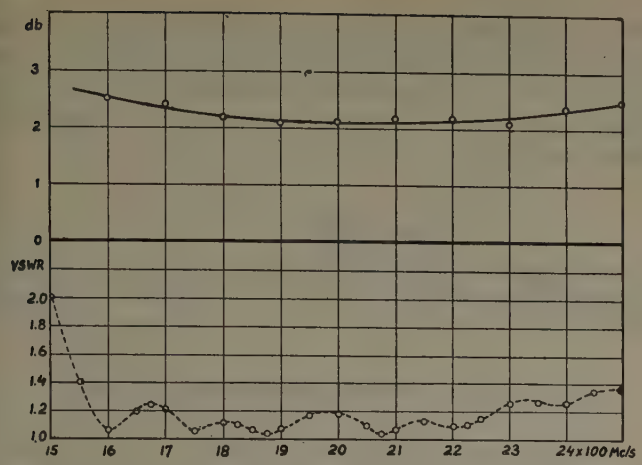

Fig. 3—Upper curve shows insertion loss of a 130-foot line assembly. Lower curve is a plot of voltage standing-wave ratio maxima.

The plot of the standing-wave ratio in Fig. 3 represents the maxima of this ratio with the line terminated in a 50-ohm load. Since some reflection occurs at the terminating launching unit, the standing-wave ratio has many maxima and minima within the frequency band. The standing-wave ratio is below 1.3 over the required band.

Acknowledgment

The authors wish to thank Messrs. John Hessel and Raymond Lacy for their foresight and encouragement. Credit is also due Mr. Wilhelm Schneider and the personnel of the Mechanical Engineering and Shop Sections of Coles Signal Laboratory for their valuable assistance on this development.

Gain of Electromagnetic Horns*

E. H. BRAUN†

***Summary*—Recent experimental evidence indicates that the measured gain of pyramidal electromagnetic horns may be considerably in error if the measurements are carried out at short distances, and the aperture to aperture separation between horns is used in the gain formula $G=(4\pi R/\lambda)\sqrt{P_R/P_T}$.**

Further experimental verification of this effect has been obtained and a theory developed which is in good quantitative agreement with present experimental data and demonstrates the physical reasons why the previous "far field" criterion of $2D^2/\lambda$ is invalid.

Curves are presented from which the error in gain measured at any distance may be obtained and applied as a correction.

Introduction

RECENT EXPERIMENTS[1] have indicated that considerable error may be incurred in measuring the gain of electromagnetic horns at short distances if the aperture to aperture distance between the horns is used in the gain formula

$$G=\frac{4\pi R}{\lambda}\sqrt{\frac{P_R}{P_T}}. \tag{1}$$

Previously, an aperture to aperture separation (R) of about $2D^2/\lambda$ (D = larger horn dimension) was considered adequate, but the above experiments indicate that an error of the order of 1 db may occur at this distance, and that the true Fraunhofer gain may not be realized even at distances several times $2D^2/\lambda$.

The present work provides a theoretical explanation of the failure of the $2D^2/\lambda$ criterion, together with further experimental data in good quantitative agreement with the theory. The theory replaces the $2D^2/\lambda$ criterion with a new criterion, and in addition makes it possible to calculate the error incurred when this criterion is not satisfied.

Theory

Two assumptions are implicit in the gain formula: (a) The power arriving at the receiving aperture varies as $1/R^2$; (b) the wave striking the receiving horn is sensibly plane, so that the effective cross section of the receiving horn is $(\lambda^2/4\pi)G_\infty$, where G_∞ is the true Fraunhofer gain.

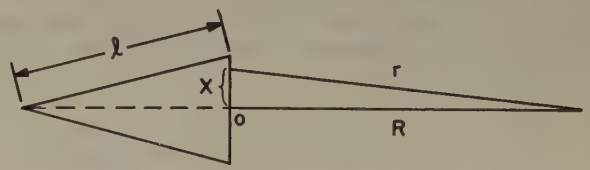

Fig. 1—Physical dimensions for computing the phase errors.

Actually, neither of these conditions is necessarily satisfied until the separation between the horn apertures is considerably greater than $2D^2/\lambda$. To show this qualitatively it should first be noted that the relative phases of contributions from different points in the aperture depend on the intrinsic phasing of the aperture and on the space phasing in exactly the same way; both are quadratic errors. Considering a sectoral horn for simplicity (Fig. 1), the intrinsic phase error can be shown[2] to be $-k(x^2/2l)$. The space phase error is $-k(r-R)=-k(\sqrt{R^2+x^2}-R)\cong-k(x^2/2R)$. The effect

* Decimal classification: R165×R265.2. Original manuscript received by the Institute September 29, 1952.

† Naval Research Laboratory, Washington, D. C.

[1] W. C. Jakes, Jr., "Gain of electromagnetic horns," PROC. I.R.E., vol. 39, pp. 160–162; February, 1951.

[2] S. A. Schelkunoff, "Electromagnetic Waves," D. Van Nostrand Book Co., New York, N. Y., p. 361, ff.; 1943.

of phase error on gain can now be discussed, keeping in mind that the phase error may be due either to intrinsic phasing or to space phasing.

Let us first make a qualitative comparison of the gains of transmitting apertures having maximum phase errors of 0, $\lambda/8$, and $\lambda/4$, respectively. In the case of zero phase error contributions from the various points of the aperture add in phase as shown in Fig. 2(a). In going from zero phase error to a phase error of $\lambda/8$ the vectors are all rotated through small angles less than 40 degrees. The resultant would not be expected to differ materially from the in-phase case (Fig. 2(b)).

Going from a phase error of $\lambda/8$ to an error of $\lambda/4$, each vector is again rotated through an angle of less than about 40 degrees, but in addition to this rotation, the upper vectors are all rotated by the lower ones. This means that many of the vectors are rotated through large angles, and the resultant for $\lambda/4$ may differ considerably from the resultant for $\lambda/8$ (Fig. 2(c)).

Hence in going from a zero phase error to a $\lambda/8$ phase error, the gain changes by a very small amount, whereas in going from $\lambda/8$ to $\lambda/4$ (again a change of $\lambda/8$) the gain changes by a considerable amount.

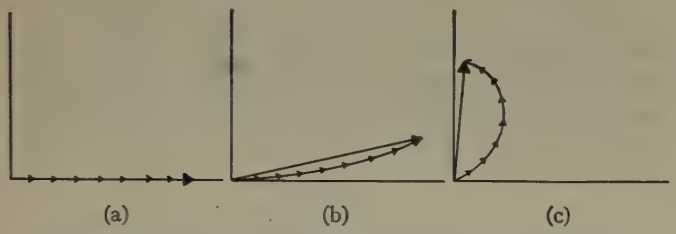

Fig. 2—Qualitative illustration of the effect of phase error on gain.

This may be seen more quantitatively from Schelkunoff's gain curves.[2] For a fixed aperture size "a," the phase error depends only on the slant height "l." For example, for $a/\lambda=6$, the slant height may be changed from $l=\infty$ (phase error $=0$) to $l=30\lambda$ (phase error $=0.15\lambda$), which represents a change in phase error of 0.15λ, with only about 2 per cent loss in gain, whereas in going from $l=30\lambda$ (phase error $=0.15\lambda$) to $l=15\lambda$ (phase error $=0.30\lambda$), also a change in phase error of 0.15λ, the gain decreases by about 12 per cent. Thus the larger the initial phase error, the more sensitive the gain becomes to further variations in phase error.

In the case of an electromagnetic horn, as one moves in from the Fraunhofer region to the Fresnel region, the space phasing effectively adds a quadratic phase error to the intrinsic quadratic error of the aperture, that is to say, it makes the wave front appear more curved. On the basis of the preceding argument, one would expect the measured gain to decrease, the decrease being a function of the intrinsic phasing, as well as the space phasing. Hence the point at which the true Fraunhofer gain is realized cannot be specified by a simple expression involving the aperture dimensions alone, e.g., $2D^2/\lambda$.

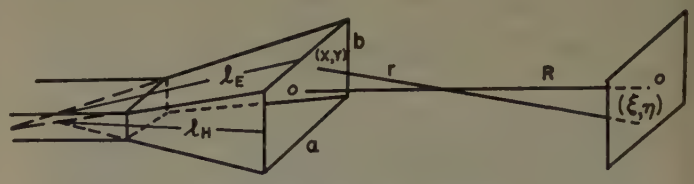

Fig. 3—Physical dimensions for calculating the gain.

To investigate the problem quantitatively, let us first calculate the amplitude of the field at any arbitrary point of the receiving aperture. The transmitting and receiving horn apertures are separated by a distance R, origins are chosen at the centers of the apertures, and points in the apertures are denoted by (x, y) and (ξ, η), respectively. The x and ξ axes are parallel to each other and to the E-vector, and the y and η axes are parallel to each other and to the H-vector. Pertinent dimensions are shown in Fig. 3.

Assuming the field at the aperture of the transmitting horn is the same as though the horn were continued,[2] the aperture distribution is given by

$$\mathcal{E}(x, y) = E_0 \cos\frac{\pi y}{a}\, e^{-jk(x^2/2l_E + y^2/2l_H)},$$

where l_E and l_H are the E and H plane slant heights, respectively.

From Fig. 3,

$$r = \sqrt{R^2 + (x-\xi)^2 + (y-\eta)^2} \cong R + \frac{(x-\xi)^2 + (y-\eta)^2}{2R}.$$

Hence, in the Fresnel approximation,

$$\mathcal{E}(\xi, \eta) = \frac{E_0}{\lambda R} e^{-jkR} \int\int \cos\frac{\pi y}{a}\, e^{-jk(x^2/2l_E + y^2/2l_H)} e^{-jk[(x-\xi)^2 + (y-\eta)^2]/2R} dx dy$$

Denoting $|\mathcal{E}(\xi, \eta)|$ by $E(\xi, \eta)$,

$$E(\xi, \eta) = \frac{E_0}{2\lambda R}\left| \int_{-a/2}^{+a/2} \left[e^{j(\pi y/a)} + e^{-j(\pi y/a)}\right] \cdot e^{-j(\pi/2)[(2/\lambda)(1/l_H + 1/R)y^2 - (4\eta/\lambda R)y]} dy \times \int_{-b/2}^{+b/2} e^{-j(\pi/2)[(2/\lambda)(1/l_E + 1/R)x^2 - (4\xi/\lambda R)x]} dx \right|$$

$$= \frac{E_0}{2\lambda R}\left| \int_{-a/2}^{+a/2} e^{-j(\pi/2)(Ay^2 - By)} dy + \int_{-a/2}^{+a/2} e^{-j(\pi/2)(Ay^2 - Cy)} dy \right|$$

$$\cdot \left| \int_{-b/2}^{+b/2} e^{-j(\pi/2)(Dx^2 - Fx)} dx \right|,$$

where

$$A = \frac{2}{\lambda}\left(\frac{1}{l_H} + \frac{1}{R}\right), \qquad B = 2\left(\frac{2\eta}{\lambda R} + \frac{1}{a}\right),$$

$$C = 2\left(\frac{2\eta}{\lambda R} - \frac{1}{a}\right), \qquad D = \frac{2}{\lambda}\left(\frac{1}{l_E} + \frac{1}{R}\right),$$

$$F = \frac{4\xi}{\lambda R}.$$

Completing the square in each exponent and factoring,

$$E(\xi, \eta) = \frac{E_0}{2\lambda R}\left| e^{j(\pi/2)(B^2/4A)} \int_{-a/2}^{+a/2} e^{-j(\pi/2)(\sqrt{A}\, y - B/2\sqrt{A})^2} dy \right.$$

$$\left. + e^{j(\pi/2)(C^2/4A)} \int_{-a/2}^{+a/2} e^{-j(\pi/2)(\sqrt{A}\, y - C/2\sqrt{A})^2} dy \right|$$

$$\times \left| e^{j(\pi/2)(F^2/4D)} \int_{-b/2}^{+b/2} e^{-j(\pi/2)(\sqrt{D}\, x - F/2\sqrt{D})^2} dx \right|.$$

Write

$$\frac{\pi}{2}(B^2/4A) = \epsilon + Q,$$

and

$$\frac{\pi}{2}(C^2/4A) = \epsilon - Q,$$

where

$$\epsilon = \frac{\pi\lambda}{4} \frac{Rl_H}{R + l_H}\left[\frac{4\eta^2}{\lambda^2 R^2} + \frac{1}{a^2}\right], \qquad Q = \frac{\pi\eta}{a} \frac{l_H}{R + l_H}.$$

Changing the variables, let

$$\alpha = \sqrt{A}\, y - B/2\sqrt{A}, \qquad dy = d\alpha/\sqrt{A}$$

$$\beta = \sqrt{D}\, y - C/2\sqrt{A}, \qquad dy = d\beta/\sqrt{A}$$

$$\psi = \sqrt{D}\, x - F/2\sqrt{D}, \qquad dx = d\psi/\sqrt{D}.$$

$$E(\xi, \eta) = \frac{E_0}{2\lambda R\sqrt{AD}}\left| \left[\int_{\psi_1}^{\psi_2} e^{-j(\pi/2)\psi^2} d\psi \right] \right.$$

$$\left. \cdot \left[e^{jQ} \int_{\alpha_1}^{\alpha_2} e^{-j(\pi/2)\alpha^2} d\alpha + e^{-jQ} \int_{\beta_1}^{\beta_2} e^{-j(\pi/2)\beta^2} d\beta \right] \right|, \qquad (2)$$

where

$$\alpha_1 = -\frac{1}{\sqrt{2}}\left[\frac{a}{\sqrt{\lambda}}\sqrt{\frac{R + l_H}{Rl_H}} + \left(\frac{\sqrt{\lambda}}{a} + \frac{2\eta}{R\sqrt{\lambda}}\right)\sqrt{\frac{Rl_H}{R + l_H}}\right]$$

$$\alpha_2 = +\frac{1}{\sqrt{2}}\left[\frac{a}{\sqrt{\lambda}}\sqrt{\frac{R + l_H}{Rl_H}} - \left(\frac{\sqrt{\lambda}}{a} + \frac{2\eta}{R\sqrt{\lambda}}\right)\sqrt{\frac{Rl_H}{R + l_H}}\right]$$

$$\beta_1 = -\frac{1}{\sqrt{2}}\left[\frac{a}{\sqrt{\lambda}}\sqrt{\frac{R + l_H}{Rl_H}} + \left(\frac{\sqrt{\lambda}}{a} - \frac{2\eta}{R\sqrt{\lambda}}\right)\sqrt{\frac{Rl_H}{R + l_H}}\right]$$

$$\beta_2 = +\frac{1}{\sqrt{2}}\left[\frac{a}{\sqrt{\lambda}}\sqrt{\frac{R + l_H}{Rl_H}} - \left(\frac{\sqrt{\lambda}}{a} - \frac{2\eta}{R\sqrt{\lambda}}\right)\sqrt{\frac{Rl_H}{R + l_H}}\right]$$

$$\psi_1 = -\frac{1}{\sqrt{2\lambda R}}\left[b\sqrt{\frac{R + l_E}{l_E}} + 2\xi\sqrt{\frac{l_E}{R + l_E}}\right]$$

$$\psi_2 = +\frac{1}{\sqrt{2\lambda R}}\left[b\sqrt{\frac{R + l_E}{l_E}} - 2\xi\sqrt{\frac{l_E}{R + l_E}}\right].$$

These can be converted to Fresnel integrals

$$\int_{x_1}^{x_2} e^{-j(\pi/2)x^2} dx = \int_0^{x_2} e^{-j(\pi/2)x^2} dx - \int_0^{x_1} e^{-j(\pi/2)x^2} dx$$

$$= [C(x_2) - C(x_1)] - j[S(x_2) - S(x_1)].$$

Equation (2) then reads

$$E(\xi, \eta) = \frac{E_0\sqrt{l_E l_H}}{4\sqrt{(R + l_E)(R + l_H)}}\, Y(\eta) X(\xi), \qquad (3a)$$

where

$$Y(\eta) = (\{\cos Q[C(\alpha_2) + C(\beta_2) - C(\alpha_1) - C(\beta_1)]$$

$$+ \sin Q[S(\alpha_2) + S(\beta_1) - S(\alpha_1) - S(\beta_2)]\}^2$$

$$+ \{\cos Q[S(\alpha_2) + S(\beta_2) - S(\alpha_1) - S(\beta_1)]$$

$$- \sin Q[C(\alpha_2) + C(\beta_1) - C(\alpha_1) - C(\beta_2)]\}^2)^{1/2}$$

$$X(\xi) = \{[C(\psi_2) - C(\psi_1)]^2 + [S(\psi_2) - S(\psi_1)]^2\}^{1/2}. \qquad (3b)$$

To determine the average power per unit solid angle radiated by the transmitting horn in the direction of the receiving horn, the Poynting vector must be integrated over the receiving aperture. The expression for $|E(\xi, \eta)|^2$ obtained from (3) is unfortunately too complicated to integrate directly, but calculation of the aperture field for a number of different horns shows that $Y(\eta)$ and $X(\xi)$ can be approximated by

$$Y(\eta) = Y\left(\frac{a}{2}\right) + \left[Y(0) - Y\left(\frac{a}{2}\right)\right] \cos^{1/2}\left(\frac{\pi\eta}{a}\right)$$

$$X(\xi) = X\left(\frac{b}{2}\right) + \left[X(0) - X\left(\frac{b}{2}\right)\right] \cos^{1/2}\left(\frac{\pi\xi}{b}\right),$$

where $Y(0)$ and $Y(a/2)$, and $X(0)$ and $X(b/2)$ are the values of $Y(\eta)$ and $X(\xi)$ at the center and edges of the aperture, respectively. The cosinusoidal term is quite small, so that deviations in this term from exact $\cos^{1/2} x$ behavior are unimportant. Alternatively, (2) can be expanded in a Taylor series in ξ and η, thus obtaining an expression which can be averaged. The author has done this, but the present expressions are more symmetric and the numerical difference between the two methods is small.

Using these expressions for $Y(\eta)$ and $X(\xi)$, the average value of E^2 over the receiving aperture is

$$\overline{E_{ap}^2} = \frac{E_0^2 l_E l_H}{(R + l_E)(R + l_H)}\, \theta^2 \omega^2,$$

where

$$\theta^2 = \frac{1}{4}\left\{Y^2\left(\frac{a}{2}\right) + 1.526\left[Y(0) - Y\left(\frac{a}{2}\right)\right]Y\left(\frac{a}{2}\right) + 0.636\left[Y(0) - Y\left(\frac{a}{2}\right)\right]^2\right\}$$

$$\omega^2 = \frac{1}{4}\left\{X^2\left(\frac{b}{2}\right) + 1.526\left[X(0) - X\left(\frac{b}{2}\right)\right]X\left(\frac{b}{2}\right) + 0.636\left[X(0) - X\left(\frac{b}{2}\right)\right]^2\right\}.$$

Taking the ratio of the receiving cross section to transmitting gain to be the same as that in the plane wave case, i.e., $A(R)/G(R) = \lambda^2/4\pi$, the power received is

$$P_R = \tfrac{1}{2}\sqrt{\epsilon/\mu}\,\overline{E_{ap}{}^2}\,(\lambda^2/4\pi)G(R).$$

Substituting this in the gain formula, (1), we have

$$G(R) = \frac{2\pi R^2\sqrt{\epsilon/\mu}\,\overline{E_{ap}{}^2}}{P_T} = \frac{2\pi R^2\sqrt{\epsilon/\mu}\,\overline{E_{ap}{}^2}}{(1/4)\sqrt{\epsilon/\mu}\,abE_0{}^2} = \frac{8\pi R^2\overline{E_{ap}{}^2}}{abE_0{}^2}. \tag{4}$$

The ratio of this gain measured at a distance R to the gain which would be measured at infinity is given from (3) and (4) by

$$\frac{G(R)}{G(\infty)} = \frac{8\pi R^2\overline{E_{ap}{}^2}/abE_0{}^2}{(8\pi l_H l_E/ab)[C^2(r) + S^2(r)]\{[C(u) - C(v)]^2 + [S(u) - S(v)]^2\}}$$

$$\frac{G(R)}{G(\infty)} = \frac{\theta^2}{(1 + l_H/R)\{[C(u) - C(v)]^2 + [S(u) - S(v)]^2\}} \cdot \frac{\omega^2}{(1 + l_E/R)[C^2(r) + S^2(r)]},$$

where

$$r = \frac{b}{\sqrt{2\lambda l_E}}, \qquad u = \frac{1}{\sqrt{2}}\left(\frac{\sqrt{\lambda l_H}}{a} + \frac{a}{\sqrt{\lambda l_H}}\right),$$

$$v = \frac{1}{\sqrt{2}}\left(\frac{\sqrt{\lambda l_H}}{a} - \frac{a}{\sqrt{\lambda l_H}}\right).$$

$G(R)/G(\infty)$ is thus a function of five independent variables, a, b, l_H, l_E, and R, and each of the two factors is a function of three independent variables, R being common to both. This makes it very difficult to express the results graphically, so that a separate calculation would have to be made for each set of horns to be tested. Since the calculation is tedious, it is fortunate that this expression can be re-written in terms of four new variables,

$$M = \frac{8\lambda R}{a^2}, \quad H = \frac{8\lambda l_H}{a^2}, \quad P = \frac{8\lambda R}{b^2}, \quad E = \frac{8\lambda l_E}{b^2}.$$

The first two depend on H plane dimensions only, and the second two on E plane dimensions only. M and P represent the reciprocals of the maximum phase errors across the aperture due to the space phasing, in the H and E planes, respectively. H and E represent the reciprocals of the maximum phase errors across the aperture due to intrinsic phasing, in the H and E planes, respectively.

In terms of these new variables, the final result becomes

$$\frac{G(R)}{G(\infty)} = \frac{\omega^2}{\left(1 + \frac{E}{P}\right)[C^2(r) + S^2(r)]} \cdot \frac{\theta^2}{\left(1 + \frac{H}{M}\right)\{[C(u) - C(v)]^2 + [S(u) - S(v)]^2\}},$$

where

$$r = 2/\sqrt{E}, \qquad u = \frac{\sqrt{H}}{4} + \frac{2}{\sqrt{H}}, \qquad v = \frac{\sqrt{H}}{4} - \frac{2}{\sqrt{H}}.$$

$$\theta^2 = \frac{1}{4}\left\{Y^2\left(\frac{a}{2}\right) + 1.526\left[Y(0) - Y\left(\frac{a}{2}\right)\right]Y\left(\frac{a}{2}\right) + 0.636\left[Y(0) - Y\left(\frac{a}{2}\right)\right]^2\right\}$$

$$\omega^2 = \frac{1}{4}\left\{X^2\left(\frac{b}{2}\right) + 1.526\left[X(0) - X\left(\frac{b}{2}\right)\right]X\left(\frac{b}{2}\right) + 0.636\left[X(0) - X\left(\frac{b}{2}\right)\right]^2\right\}$$

$$Y\left(\frac{a}{2}\right) = (\{\cos Q[C(h) + C(l) - C(g) - C(k)] + \sin Q[S(h) + S(k) - S(l) - S(g)]\}^2 + \{\cos Q[S(h) + S(l) - S(g) - S(k)] - \sin Q[C(h) + C(k) - C(l) - C(g)]\}^2)^{1/2}$$

$$Y(0) = \{[C(f) - C(e)]^2 + [S(f) - S(e)]^2\}^{1/2}$$

$$X\left(\frac{b}{2}\right) = \{[C(t) - C(p)]^2 + [S(t) - S(p)]^2\}^{1/2}$$

$$X(0) = [C^2(m) + S^2(m)]^{1/2}$$

$$h = +2\sqrt{\frac{H + M}{HM}} - \frac{1}{4}\sqrt{\frac{HM}{H + M}} - \frac{2}{M}\sqrt{\frac{HM}{H + M}},$$

$$l = +2\sqrt{\frac{H+M}{HM}} - \frac{1}{4}\sqrt{\frac{HM}{H+M}} + \frac{2}{M}\sqrt{\frac{HM}{H+M}},$$

$$g = -2\sqrt{\frac{H+M}{HM}} - \frac{1}{4}\sqrt{\frac{HM}{H+M}} - \frac{2}{M}\sqrt{\frac{HM}{H+M}},$$

$$k = -2\sqrt{\frac{H+M}{HM}} - \frac{1}{4}\sqrt{\frac{HM}{H+M}} + \frac{2}{M}\sqrt{\frac{HM}{H+M}},$$

$$f = +2\sqrt{\frac{H+M}{HM}} - \frac{1}{4}\sqrt{\frac{HM}{H+M}},$$

$$e = -2\sqrt{\frac{H+M}{HM}} - \frac{1}{4}\sqrt{\frac{HM}{H+M}},$$

$$p = -2\sqrt{\frac{E+P}{EP}} - 2\sqrt{\frac{E/P}{E+P}},$$

$$t = +2\sqrt{\frac{E+P}{EP}} - 2\sqrt{\frac{E/P}{E+P}},$$

$$m = +2\sqrt{\frac{E+P}{EP}},$$

$$Q = \frac{\pi}{2}\frac{H}{H+M},$$

$$M = \frac{8\lambda R}{a^2},\quad H = \frac{8\lambda l_H}{a^2},\quad P = \frac{8\lambda R}{b^2},\quad E = \frac{8\lambda l_E}{b^2}.$$

(If all dimensions are given in wavelengths, set $\lambda = 1$ wherever it appears.)

Since the expression for $G(R)/G(\infty)$ has the form of a product of two factors, one depending on M and H alone, and one depending on P and E alone, each factor can be plotted separately in db as a one parameter family of curves, and the total correction to the gain will then be given by the sum of the corrections read off the two graphs (Figs. 4 and 5).

Since essentially the same assumptions are made in calculating $G(R)$ and $G(\infty)$, it might reasonably be expected that the percentage error is nearly the same for each, and hence the percentage error in the ratio is quite small. That this is so has been verified experimentally in a number of cases.

Use of Curves

In measuring the gain of a particular set of horns, one first wants to know the minimum aperture separation between horns which will give the correct far-field gain figure. Calculating H (and E) from the horn dimensions selects the proper curves on the two graphs for the particular horn in question. To find the minimum aperture separation for which the true Fraunhofer gain will be measured, one simply follows each curve out to the zero correction line, and arrives at two values of R, one for each plane. The larger value is the minimum aperture separation required.

In many cases this distance will be found to be prohibitively large, either because adequate space is not

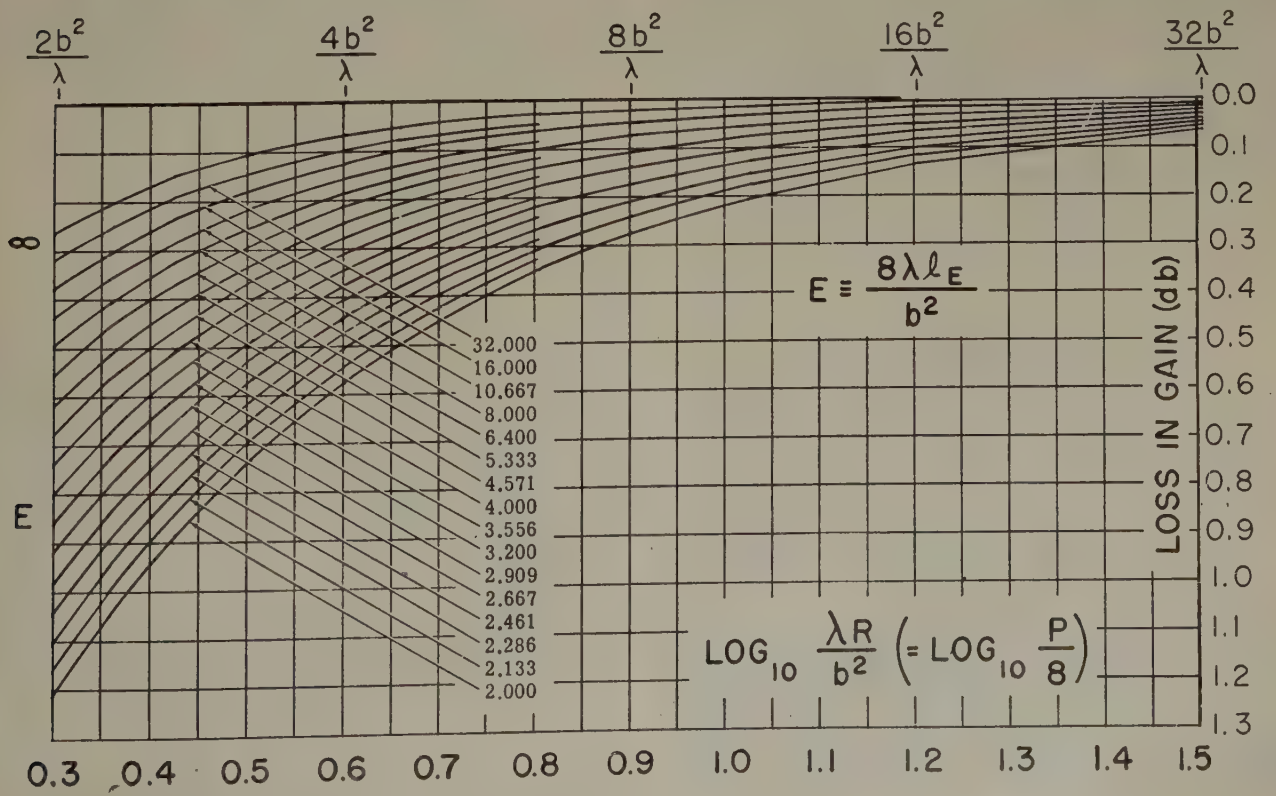

Fig. 4—*E*-plane correction curves.

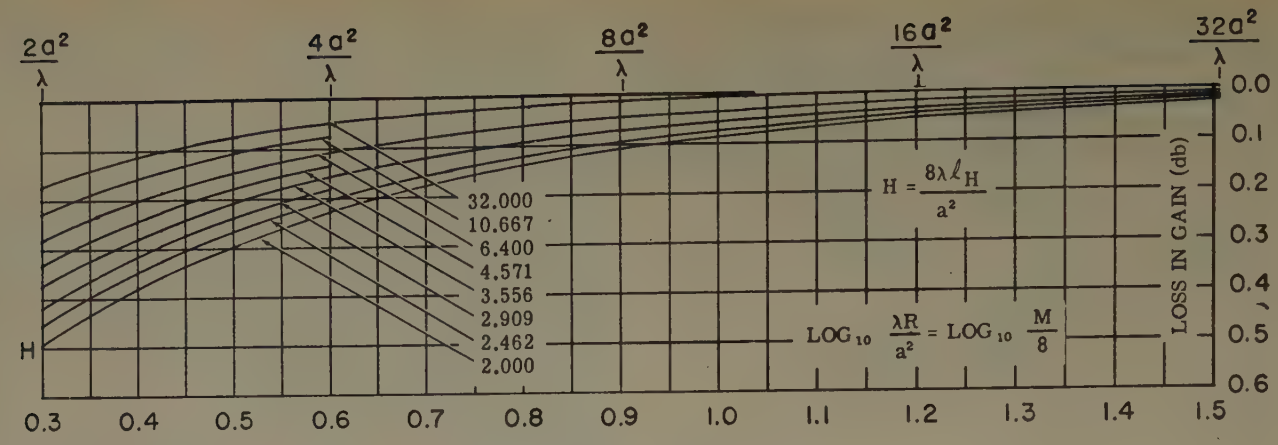

Fig. 5—*H*-plane correction curves.

available in which to perform the measurements, or because serious reflections are encountered when the distance to neighboring objects becomes comparable with the aperture to aperture separation. At some wavelengths, errors due to reflections may be appreciable even after considerable precautions have been taken to minimize them.

The alternative in this case is to make the measurements at shorter distances, and to then correct the measured values to obtain the true gain. This correction factor is obtained directly from the curves (by adding the corrections in db read off the two separate curves) for each distance at which measurements are carried out.

To afford the convenience and accuracy of linear interpolation, $\log M/8 = \log \lambda R/a^2$ and $\log P/8 = \log \lambda R/b^2$ are plotted on the H and E plane graphs, respectively, instead of M and P themselves.

For example, suppose one wishes to measure the gain of a horn having the following dimensions: $a = 4.69\lambda$, $b = 3.78\lambda$, $l_H = 6.52\lambda$, $l_E = 5.94\lambda$. A measurement is to be carried out at $R = 2a^2/\lambda$. What correction to the measured value is necessary to give the true gain?

Calculating E, H, $\log \lambda R/a^2$, and $\log \lambda R/b^2$, the following results are obtained.

$$E = \frac{8\lambda l_E}{b^2} = \frac{(8)(5.94)}{(3.78)^2} = 3.326,$$

$$H = \frac{8\lambda l_H}{a^2} = \frac{(8)(6.52)}{(4.69)^2} = 2.371,$$

$$\log \frac{\lambda R}{a^2} = \log 2 = 0.301,$$

$$\log \frac{\lambda R}{b^2} = \log \frac{2a^2}{b^2} = \log \frac{(2)(4.69)^2}{(3.78)^2} = 0.488.$$

Looking at the H-plane curves for $H = 2.371$ and $\log \lambda R/a^2 = 0.301$ shows a correction of 0.47 db. Looking at the E-plane curves for $E = 3.326$ and $\log \lambda R/b^2 = 0.488$ shows a correction of 0.49 db. Hence 0.96 db must be added to the "gain" measured at this distance to obtain the correct gain.

Experimental Results

Measurements have been carried out on a number of horns, and some of the results are given in Figs. 6 and 7. In each case the lower curve A is the uncorrected curve, and the upper curve B represents the average of the corrected points. The corrected points are also shown. The arrow is a "check point" obtained by comparing the horn with a small gain standard which was actually calibrated in the Fraunhofer region, or by actually measuring the gain of the horn in the Fraunhofer region when this was possible. All of the corrected points lie

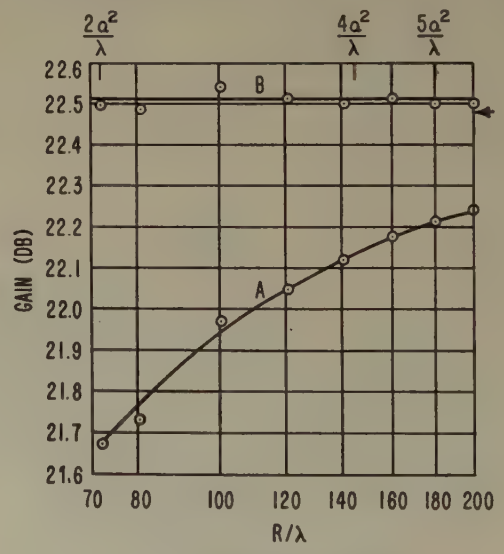

Fig. 6—Experimental results.

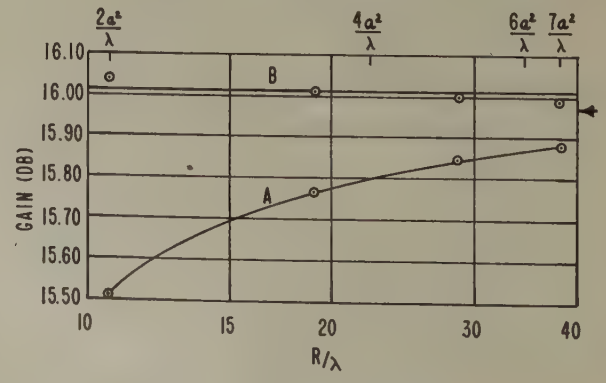

Fig. 7—Experimental results

within about 0.1 db of their average, and this average lies within about 0.1 db of the check point in every case. The horns tested represent phase errors ranging from about 1/16 to 1/2 wavelength. It can be seen that any attempt to use the uncorrected points to compute the gain will in general lead to large errors.

Considerable care was required in performing the experimental work, since the desired accuracy of measurement is very high. One of the principal difficulties was that encountered due to reflections from the walls of the room and from other objects. These were carefully minimized by the use of absorbing screens. Amplifiers and meters were calibrated, and each measurement was carried out at several different power levels. Bolometers were used as detectors. Whenever the ratio of P_R/P_T became too low (at large horn separations), P_T was measured by use of a calibrated directional coupler. It was felt that the calibration of the directional coupler would be less liable to change than that of a variable or fixed attenuator. It was found that the measurements could be repeated to better than ± 0.1 db on different days and using different pieces of equipment.

It has been suggested[1] that the correct gain figure may be obtained from the experimental data by measuring the distance "R" in the gain formula (1) between points located behind the apertures rather than between the apertures themselves. These points are located by the requirement that the received power fall off as $1/r^2$ when the separation "r" between the points, rather than between the apertures, is used.

However, if one attempts to locate these points experimentally one finds that the log P_R/P_T versus log r curve never becomes exactly a straight line with slope -2 for any location of the points, but that a set of curves is obtained, several of which approximate such a straight line over part of their length. Since one has no basis for choosing one curve above another, the location of these points, and hence the gain, remains indeterminate.

The author has also shown theoretically that such points are not fixed with respect to the horn apertures, but that their location is also a function of horn separation, and hence does not exist in the sense suggested above. This is the reason that experimental curves plotted with these points fixed are not straight lines.

The value of this method in determining the correct gain is therefore open to question.

Conclusions

Further experimental verification of the observed variation in measured gain with aperture separation for electromagnetic horns has been obtained. A theory has been developed which is in good quantitative agreement with the experimental data, and demonstrates the physical reasons why the previous "far field" criterion of $2D^2/\lambda$ is invalid. The $2D^2/\lambda$ criterion has been replaced by a generic set of curves from which the error in gain measured at any distance may be determined directly, and applied as a correction. The minimum aperture separation for which zero correction is required marks the beginning of the true Fraunhofer region.

Acknowledgment

The author would like to thank William T. Slayton of the Naval Research Laboratory for his assistance throughout the experimental part of this work, and C. H. Chrisman of the Operational Research Branch of the Naval Research Laboratory for arranging most of the numerical computation.

UHF Radio-Relay System Engineering*

J. J. EGLI†, ASSOCIATE, IRE

Summary—**UHF radio-relay transmission is affected by atmospheric conditions, obstructions, distance, antenna height, and path clearances. It is important that paths be engineered with adequate clearance. A nomograph is presented for rapid determination of the required clearance from path parameters and operating frequency.**

Various types of transmission paths with means of minimizing fading are discussed, and a method is derived for determining from the path profile the required spacing of receiving antennas for space diversity.

A single-hop system is evaluated in terms of equipment parameters and displayed on a level diagram. This is followed by a discussion of the system performance and reliability of a number of hops in tandem.

* Decimal classification: R480. Original manuscript received by the Institute, October 8, 1952.

† Signal Corps Engineering Laboratories, Fort Monmouth, N. J.

I. Introduction

UHF RADIO-RELAY SYSTEMS must be engineered to provide as high a degree of reliability as other communications systems. This reliability must be achieved at the expense of many relay stations in tandem. The frequencies used for these systems are so high that radio transmission in this spectrum behaves very much like light waves. The radio waves travel in approximately straight lines and can be reflected or refracted. Radio waves travelling along the ground are heavily attenuated. Waves travelling upward are not reflected by the ionosphere as in the case of lower frequencies; however, these waves may be reflected by discontinuities in the lower atmosphere due to unusual conditions of temperature and humidity,

or they may be reflected when striking the surface of a body of water or a good conducting earth. In addition to reflection, the waves are bent or refracted in the atmosphere due to gradual changes in pressure and humidity. Because of these factors, it is very important to locate radio-relay antennas where a good line-of-sight path is available. The amount of clearance required and techniques for overcoming various propagation difficulties are included in the paper.

A microwave radio-relay link, in order to operate satisfactorily, must have an over-all system gain which exceeds the system attenuations by an amount which accounts for the fading and results in the desired reliability. The level diagram[1] is used to display the equipment parameters and attenuations for a single-hop system. Nomograms and conversion charts are included which rapidly transform system characteristics into gains or losses in terms of decibels. Multiple-hop systems are evaluated and must take into account (a) the tandem reliability of fading, which is the combined reliability of each path taken separately, and (b) the degradation of the signal-to-noise ratio of the communication, unless this intelligence can be regenerated at the repeater points as in pulse-code modulation.

II. Wave-Propagation Phenomena

UHF radio relay is in a frequency range which eliminates attenuation considerations due to oxygen, rain, fog, snow, and clouds. The medium of transmission is the troposphere which is the layer of atmosphere directly adjacent to the earth's surface and extends upward approximately six miles.

Propagation of radio waves in the troposphere is materially influenced by the distributions of temperature, pressure, and water vapor. The variation of these quantities with height is expressed conveniently by the index of refraction which decreases linearly with height in a so-called standard atmosphere. The condition most nearly approximated in the temperate zone has been accepted as the standard atmosphere. Since the index of refraction normally decreases with height, the upper portions relative to the earth of a wave front moves with higher velocity than the lower portion, and the wave path may be represented by rays curved slightly downward toward the earth. As a result, the distance to the radio horizon is some 15 per cent greater than the geometrical line-of-sight distance from the transmitter to the horizon. This curvature of the rays by the atmosphere is called "refraction."

Over a line-of-sight path the radio waves arriving at the receiver are the vector sum of the radiations arriving by way of both the direct and reflected ray paths. The contribution from the reflected ray path depends primarily on the manner in which the earth or sea acts as a reflecting body. Over water and salt flats, for instance, the reflection is essentially 100 per cent. Over land areas with gentle rolling country having some vegetation, the reflection is only approximately 10 per cent complete. Since the angle of reflection to be taken into account in radio-relay siting is very small, consideration need not be given to polarization effects, that is, whether the antenna is horizontally or vertically polarized. For the same reason the phase lag of the reflected wave with respect to the incident wave at the point of reflection is for all practical purposes 180 degrees.

The mechanism by which radio waves curve around edges and penetrate into the shadow region behind an opaque obstacle is called "diffraction." This effect is of importance because it allows a limited extension of the line-of-sight path length.

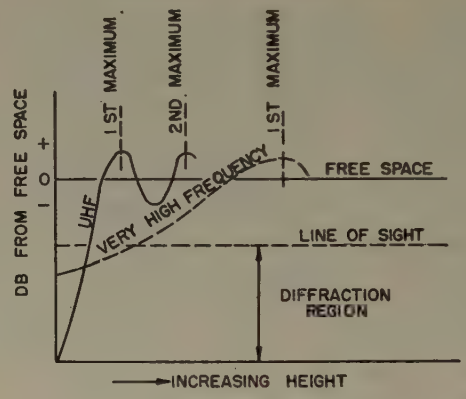

Fig. 1—Height-gain curves.

As the receiving antenna is elevated from ground level, the received signal strength due to diffraction rises rapidly until line-of-sight is reached. (See Fig. 1.) Above line-of-sight, the direct and reflected waves interfere and result in maxima and minima patterns called the "Fresnel pattern." The first maximum occurs when the difference in path length between the direct and reflected wave is one-half wave length, since the reflected signal undergoes a 180-degree phase reversal at the reflecting point. The succeeding maxima are odd multiples of half-wave lengths. The magnitude of the first maximum and minimum with relation to the free-space field is dependent on the magnitude of the reflection coefficient. The height required to obtain the first maximum clearance at uhf is much less than that required at "very high frequencies" since the wavelength at microwaves is measured in inches and at vhf in feet. It should be noted that in the diffraction region the signal strength for microwave frequencies falls more rapidly than for "very high frequencies."

III. Fading

The troposphere is continually undergoing changes in dielectric constant which affects the field strength of the received signal. The fading range ordinarily increases with increase in distance since the effects of atmospheric refraction are more pronounced at greater

[1] R. Guenther, "Radio relay design data 60 to 600 mc," Proc. I.R.E., vol. 39, p. 1027; September, 1951.

distances. Changes in atmospheric refraction appear to change the transmission path curvature. Drawn on 4/3 earth profile paper, the earth may appear to bulge in a more convex curve (equivalent earth radius factor K less than 4/3) or may appear to be less convex (K greater than 4/3). In most localities the earth's radius factor[2] is rarely less than 0.8 or greater than 3. As an example of the effect of change in earth curvature, Table I has been prepared to show required antenna heights for various values of K and distances to the horizon. The signals received on twin antennas separated vertically (space diversity) under these conditions are affected alike.

TABLE I

REQUIRED ANTENNA HEIGHT IN FEET

Earth radius factor K	Horizon distance		
	15 miles	30 miles	50 miles
0.8	180	800	2300
1	150	620	1800
4/3	120	480	1300
2	75	300	950
3	50	200	600

Another common cause of fading, called "multiple path transmission," is one in which two, three, or more signal components are found to arrive at the receiving station at various angles in the vertical plane. The extent of this type of fading is dependent on the relative amplitudes and delays of each of the components. This fading, which is a fine structure, can be thought of as being superimposed on the fading described above. The signals received on two antennas separated vertically under these conditions are affected differently.

TABLE II

MIDPATH CLEARANCE VARIATION IN FEET NORMALIZED ON $K=4/3$. $f=2000$ mc

K	Midpath clearance in feet		
	30 miles	60 miles	100 miles
0.8	20	−206	−852
1	50	−26	−352
4/3	80	114	148
2	125	294	498
3	150	394	848

In Table I, the columns marked 15, 30, and 50 miles correspond to path lengths of 30, 60, and 100 miles. The variation in height around the 4/3 earth radius can be thought of as the variation of the clearance of an engineered path. Table II shows the free-space height required at midpath for a K factor of 4/3 at an operating frequency of 2,000 mc and the variation of this clearance over the range of K values which can normally be expected. The minus sign in this table indicates the extent to which the signal is in the shadow region. It will be noted that the 30-mile path is clear over this entire range of K. A 60-mile path, on the other hand, may appear to be in the shadow region or may appear as a path which has excessive height. At 100 miles this variation is even more marked.

During the time when the field strength appears to be in the shadow region, diversity is not useful since the signal strength on both of the diversity antennas fade simultaneously.

These wide variations which occur on long path lengths are taken into account in radio-relay systems engineering by limiting the path lengths to approximately 30 miles. Longer path lengths, 40 to 50 miles, may be used in areas where the climate is dry and propagation fading is not influenced greatly by changes in humidity. Again path lengths longer than 30 miles may be engineered by increasing the fade margin (by use of larger antenna dishes and/or power amplifiers) or by accepting less system reliability.

Sites engineered to path lengths of 30 miles, and provided with free-space clearance in the uhf range, should for most operation result in a propagation reliability in which the depth of fades which can be expected a certain percentage of the time with its corresponding percentage of reliability is approximated in Table III. This reliability, while a good rule of thumb, is approximate for 3,000 to 4,000 mc. As the operating frequency is increased, a decrease in reliability can be expected, and likewise for lower operating frequencies the reliability will be increased.

TABLE III

Fade in db	Per cent of the time	Reliability
10	10	90
20	1	99
30	0.1	99.9
40	0.01	99.99

It is unusual for more than one path to experience the same depth of fade simultaneously. Therefore, the system reliability of a number of paths in tandem is the combined reliability of each path taken separately. This results in a system reliability which is less than that of the individual path.

The correlation between received field strengths and meteorology conditions is as yet in its infancy. The statistical information which relates depth of fading to percentages of the time takes into account the fact that at various times throughout the day, month, and year the atmospheric conditions may be such as to form low-level ducts, high-level ducts, substandard refraction, super refraction, temperature inversions, and other meteorological effects. In locations where one or more of these meteorological effects are pronounced, the depth of fade for a given percentage of the time may be greatly affected. Restricted path lengths may be necessary in such locations, but apparently conditions of this type are the exception rather than the rule.

[2] K. Bullington, "Radio propagation at frequencies above 30 megacycles," PROC. I.R.E., vol. 35, pp. 1122–1136; October, 1947.

IV. Siting

The free-space Fresnel clearance required for radio-relay engineering is the clearance which at any point in the path results in a direct and reflected path difference of $\frac{1}{6}$ wavelength. This can be expressed as an ellipse (Fig. 2) since the property of an ellipse is that $TP+RP=2a$, where $2a$ is a constant. If the axis of the ellipse is taken at T so that path distances to an obstruction can be measured from one end of the path, the equation for the ellipse is

$$\frac{(X-D/2)^2}{a^2}+\frac{y^2}{a^2-(D/2^2)}=1, \qquad (1)$$

where for free space $2a=D+\lambda/6$.

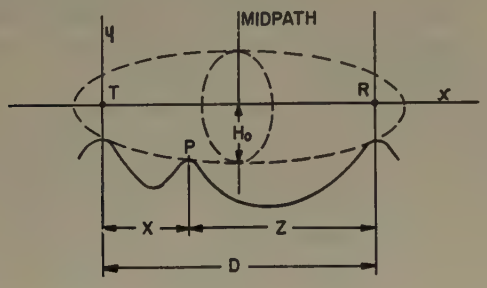

Fig. 2—Free-space clearance.

Substituting this in (1) and eliminating factors very much smaller than $(D/2)^2$,

$$\frac{(X-D/2)^2}{(D/2)^2}+\frac{y^2}{\frac{D\lambda}{12}}=1. \qquad (2)$$

The free-space clearance (H_0) required at midpath, when $X=D/2$, is

$$H_0=\sqrt{\frac{D\lambda}{12}}, \qquad (3)$$

all expressed in the same units. When H_0 is expressed in feet, D in miles, and λ as $1/f$ where f is in megacycles,

$$H_0=658\sqrt{D/f}. \qquad (4)$$

To determine the free-space clearance required at any high elevation H on a profile, (2) may be written as

$$\frac{(X-D/2)^2}{(D/2)^2}+\frac{H^2}{H_0^2}=1,$$

substituting the value of H_0 as given in (4) and solving for the required clearance

$$H=658\sqrt{D/f}\sqrt{1-\frac{(x-D/2)^2}{(D/2)^2}}. \qquad (5)$$

Reducing this expression by use of $D=X+Z$, $H=1316\sqrt{XZ/Df}$, where H is in feet; D, X, Z are in miles and f in megacycles. This expression is shown in the form of a nomograph (Fig. 3).

The selection of sites suitable for stations of a radio-relay system may be made from contour maps or stereoscopic photographs. Recently commercial and government agencies concerned with geological surveys have been experimenting with electronic airborne profile recorders which can produce an elevation profile record. The instrument is basically an altimeter which uses a radar beam projected downward from aircraft to measure the actual clearance between the aircraft and the ground.

It is well to choose several alternate locations for each site, if possible, so that after profiling, factors other than path clearance which then become important may be taken into consideration. The choice of the most suitable sites may well be influenced by: (a) accessibility to the site from an installation, operational, and maintenance standpoint; and (b) proximity to roads, which frequently means that primary power from commercial sources is readily available.

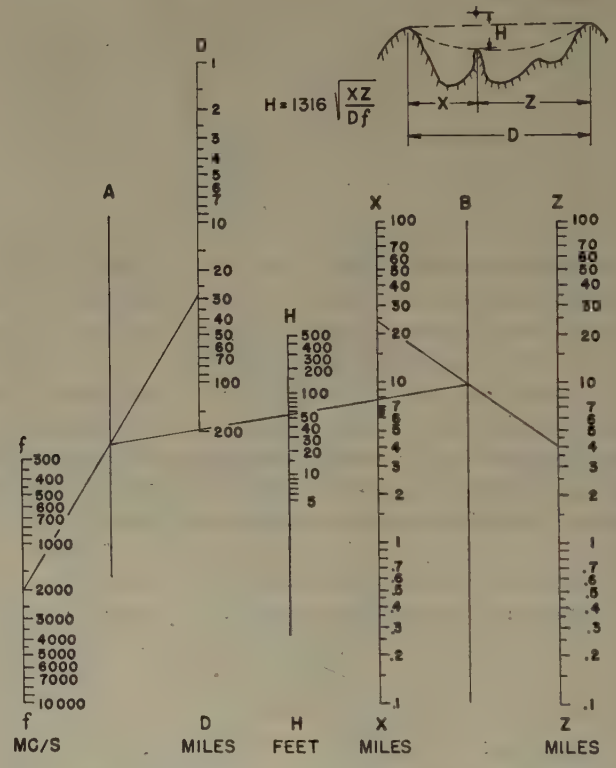

Fig. 3—Nomogram for determining free-space path clearance.

Contour maps generally lack information regarding trees, buildings, and other obstacles. Facilities such as power lines and smaller roads may not appear on the map. Also, the contour map may be in serious error. It is well, therefore, to make a preliminary survey of proposed paths, noting the above information on the contour maps. This survey can be made by air reconnaissance or vehicle.

Contours may be plotted on linear paper and corrected for 4/3 earth radius by means of the correction $X^2/2$, where X is the distance in miles from the reference point and the correction is in feet. A preferable method which requires no correction of the profile for

the curvature of the earth is to plot the points selected from the contour map directly on profile graph paper, (Fig. 4) which self corrects for 4/3 earth curvature.

Once the profile of the path is available, it must be studied to determine the following points:

1. Is the path including available tower heights clear of objects? If not, another path perhaps of shorter length must be plotted.

2. If the path is clear, by how many feet does the line drawn between the sites clear high contours? The determination of this clearance must include the height of trees and other objects. The clearance should also be maintained in all directions relative to the line drawn between the sites. The procedure in determining whether a path has the required clearance and what the required tower heights must be is as follows:

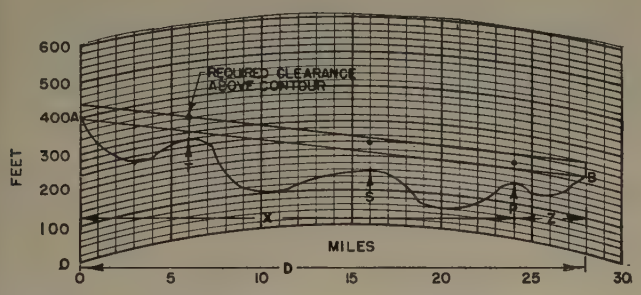

Fig. 4—Plotting profiles on profile paper (4/3 earth profile paper)

Assume equipment with a radio carrier frequency $f=2{,}000$ mc and a path as in Fig. 4, in which the path distance is $D=28$ miles between proposed sites. The high contour at point P is $X=24$ miles from A and is $Z=4$ miles from B. Referring to Fig. 3:

a. Set a straight edge across the f and D scales and draw a line from $f=2{,}000$ mc to $D=28$ miles.
b. Set a straight edge across the X and Z scales and draw a line from $X=24$ miles and $Z=4$ miles.
c. Set a straight edge across the A and B scales and draw a line from the points intersected on the A and B scales by the above two operations.
d. Read the H scale. This reading, which is the required clearance above point P, is $H=55$ feet.

This procedure is followed for other high contours, such as point S on Fig. 4. It will be noted that the line drawn between the f and D scales for a particular profile remains the same for all high contours under investigation. Point S is $X=16$ miles from A and is $Z=12$ miles from B and requires a clearance of 78.5 feet. Point T is $X=6$ miles from A and is $Z=22$ miles from B and requires a clearance of 65 feet. The required clearance above the high contours are on Fig. 4 by large dots.

3. Having determined the clearance above high contours, it remains only to determine the tower heights required at the sites.

a. In the event that a line drawn on the profile paper between the sites is below a required clearance point, as in Fig. 4, towers must be provided to clear this point. On Fig. 4 the required tower height is 40 feet. If the required tower height is excessive, new sites must be surveyed.
b. In the event that the line just passes above required clearance, then a tower height of, for example, 6 to 8 feet or one section of tower may be used at each site. If the site in the direction of transmission is not clear of trees, tower heights which extend above the tree tops must be used.
c. If the line between sites is well above required clearance, for example, two or more times the required midpath clearance, sites at tower elevations usually more desirable should be chosen.

4. The profiles of the proposed paths are now available and are ready for on-location checking. Aerial reconnaissance by helicopter, liaison plane, or vehicle along the propagation path should be made to determine the reliability of the information on the profile. During flight the propagation path should be viewed for obstructions such as trees, buildings, and other landmarks which were not shown on the profile. At the sites themselves it is well to observe whether the land is cleared and accessible by vehicle. In terrain where there is considerable visibility, visual exploration at one site may determine the line-of-sight properties to the other site. For nighttime observation of the line-of-sight properties of selected sites, search lights may be used. Portable towers[3] with path-attenuation measuring facilities are another method of checking path reliability before costly site commitments are made.

V. Transmission Paths

Irregular terrain, such as is encountered in rolling countryside, is generally suitable from a propagation standpoint. Smooth terrain, such as salt flats, should be avoided, if possible. If it becomes expedient to use such paths, however, a high-low type of siting (Fig. 5(a)) should be employed. This technique uses one site highly elevated so as to provide the required clearance and the other site located near ground level. Reflection point is essentially near the "low" site, so geometrically reduces variation between direct and reflected paths that would otherwise occur if reflection point were near midpath (Fig. 5(d)).

Overwater paths should be avoided, if possible. In the event that such a path must be used, the high-low technique may again be applicable. Furthermore, one site is highly elevated and the other site located a few feet above ground level so that the reflection point occurs over land. This is shown in Fig. 5(b). This type of siting should, in many locations, provide the reliable communications required. Where fading difficulties are still experienced, space diversity will be required. Where the overwater path is such that this technique cannot be applied, but the profile is such as to provide

[3] *Bell Lab. Rec.*, pp. 6; January, 1948.

screening, this technique should be used. This is shown in Fig. 5(c). The high contour which serves as the screen must have free-space clearance. Space diversity may still be required in the event of severe fading. Where the overwater paths are such that these techniques cannot be applied, diversity must be used.

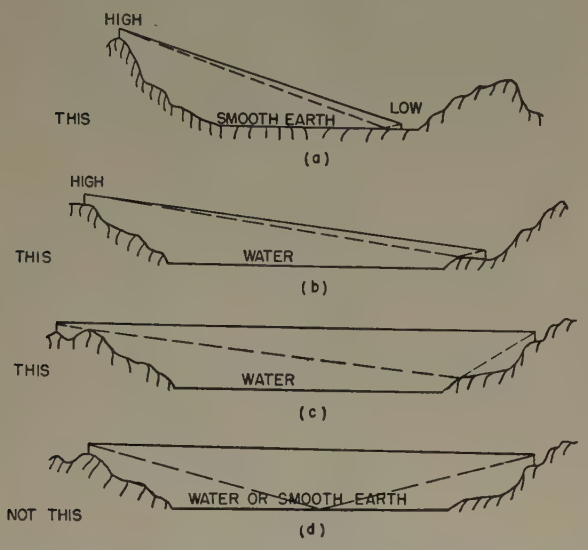

Fig. 5—Transmission paths. (a) High-low technique. (b) High-low technique. (c) Screening technique. (d) Undesirable path.

A highly elevated path, that is, one which has an Nth Fresnel clearance or excessive lobing, such as may be encountered in going from one mountain top to another, is generally to be avoided. Where the intervening terrain has a small coefficient of reflection, the signal strength will fluctuate between the maxima and minima of the reflection pattern and provide reliable transmission. If the coefficient of reflection approaches unity, such as overwater paths and salt flats, the maxima and minima of the pattern is widely separated in amplitude. Diversity is not a cure-all for such paths, but it does reduce the per cent of the time deep fades occur. The reason diversity may still result in deep fades is that the atmosphere is not homogeneous. The lobes are therefore caused to move in random fashion in front of the antenna. These lobes are relatively close together at higher elevations since the spacing between successive maxima decrease with increasing height. For example, at 2,000 mc with a path difference of 30 miles, the spacing between the first and second maxima is approximately 200 feet and the spacing between the 21st and 22nd maxima is approximately 45 feet if the transmitting antenna remains fixed and the receiving antenna is the variable. Excessive heights may also result in fading due to reflections caused by temperature inversions which are generally present at around 3,000 to 7,000 feet above the earth's surface. At lower heights with ranges of approximately 30 miles, the high inversion is usually outside the beam width of the antenna. One method of avoiding this type of path is to provide a repeater station near midpath. Another method is the high-low technique described above. Still another alternative is to select sites at lower elevations which may still result in path lengths of approximately 30 miles. In the event that these alternates are not possible, these highly elevated paths may require diversity antennas.

Selected sites which contain partially overland and overwater paths are satisfactory if the reflection point is on the land portion of the path. In the event that the reflection point is overwater, it is advisable to move one of the sites. This is generally accomplished by moving one site a relatively short distance.

VI. Diversity Spacing for Receiving Antennas

Referring to the height-gain curve Fig. 1, the first maximum occurs when the difference in path length between the direct and reflected waves is $\frac{1}{2}$ wavelength. The first minimum occurs when the difference in path length is one wavelength. The path difference in wavelengths between the direct and reflected waves for successive maximum and minimum fields is

$$1/2_{(\max)},\ 1_{(\min)},\ 3/2_{(\max)},\ 2_{(\min)},\ 3/2_{(\max)} \cdots \frac{n}{2},\ \frac{n+1}{2},$$

and for successive free-space field values

$$1/6_{(\max)},\ 4/6_{(\min)},\ 7/6_{(\max)},\ 10/6_{(\min)} \cdots \frac{3n-2}{6},\ \frac{3n+1}{6}.$$

The midpath clearance for the first free-space field (see (3)) is

$$H_0 = \sqrt{\frac{\lambda D}{12}},$$

for the n^{th} free-space field,

$$H_n = \sqrt{\frac{(3n-2)\lambda D}{12}} = H_0\sqrt{3n-2}, \qquad (6)$$

and for the $(n+1)$ free-space field,

$$H_{n+1} = \sqrt{\frac{(3n+1)\lambda D}{12}} = H_0\sqrt{3n+1}.$$

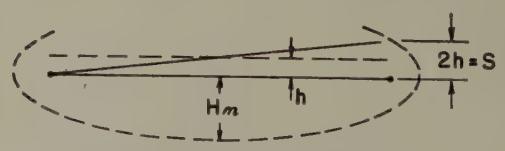

Fig. 6—Diversity spacing.

The clearance difference at midpath (h) of any two successive Fresnel free-space fields, n and $n+1$, is

$$h = H_{n+1} - H_n \quad \text{and} \quad h = H_0(\sqrt{3n+1} - \sqrt{3n-2}).$$

From simple geometry of Fig. 6 it can be seen that h must be doubled to obtain the diversity spacing S of the antennas or

$$S = 2h = 2H_0(\sqrt{3n+1} - \sqrt{3n-2}). \qquad (7)$$

The clearance height required at midpath H_n for any given height E along a path (see Fig. 9) is given by (5), with the proper transposition of symbols as

$$H_n = \frac{E}{\sqrt{\dfrac{1(X - D/2)^2}{(D/2)^2}}} = E/C.$$

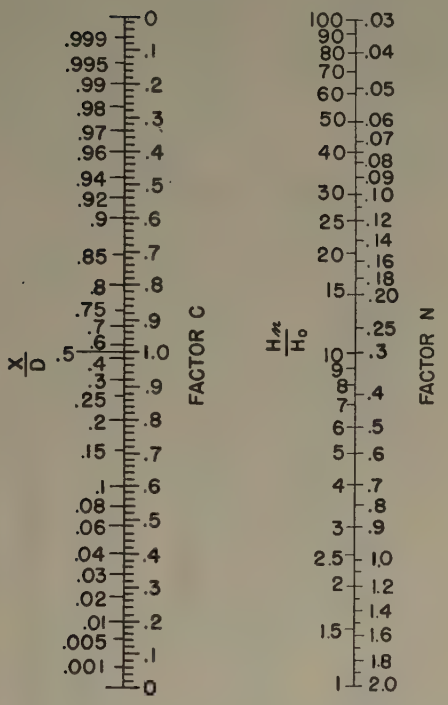

Fig. 7

Fig. 8

Fig. 7—Path-clearance determining factor.
Fig. 8—Diversity antenna spacing factor.

The radical reduces to

$$2\sqrt{\frac{X}{D}\left(1 - \frac{X}{D}\right)},$$

and values of C versus X/D are shown on the conversion scale (Fig. 7). It will be noted from (6) that the relation between the midpath height H_n, of any path is related to the first free-space clearance H_0 of a path of the same length by the expression

$$\frac{H_n}{H_0} = \sqrt{3n-2}, \text{ which can be solved for } n.$$

This value of n can then be substituted in (7) to determine the value of antenna diversity spacing S.

This procedure can be simplified for field use by the conversion scale (Fig. 8) of

$$\frac{H_n}{H_0} = \sqrt{3n-2}$$

versus

$$N = 2(\sqrt{3n+1} - \sqrt{3n-2}).$$

The vertical distance between receiving antennas is therefore determined as follows:

All high points of a profile should be investigated to determine which one results in the smallest required midpath height. This high contour is therefore the path-clearance determining point. Referring to Fig. 9, the line AB which connects the two sites is essentially the direct path between the transmitting antenna and the lower diversity receiving antenna. The height $E = 1{,}040$ feet is the extent to which the direct path AB clears the high contour T. The required midpath clearance H_n is this clearance divided by the path-clearance determining factor C, which may be obtained from Fig. 7. The point T is $X = 17$ miles; therefore, $X/D = 11/28 = 0.392$, which from Fig. 7 corresponds to a C factor equal to 0.97. The midpath clearance H_n is therefore $E/C = 1{,}040/0.97 = 1{,}072$ feet. A similar calculation for the high contour S will result in a midpath clearance which is larger than the one for T. Therefore, the point T is the path-clearance determining point.

For convenience, the frequency and path length are assumed as being the same as in the example given under siting. Find the clearance H_0, at midpath from Fig. 3, using $X = 14$, $Z = 14$, $D = 28$, and $f = 2{,}000$. H_0 will be found to be 79 feet. Then $H_n/H_0 = 1{,}072/79 = 13.6$. Referring to Fig. 8, this corresponds to a diversity antenna spacing factor $N = 0.21$. The required vertical spacing between antennas is $N \times H_0 = 0.21 \times 79 = 17$ feet.

Where the spacing is larger than a reasonable tower height required by transmission without diversity, the second antenna should be located close to the base of the tower provided clearance above nearby trees and other obstructions is obtained.

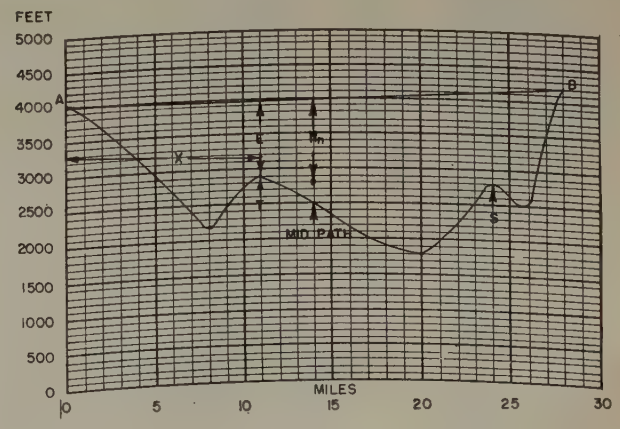

Fig. 9—Large clearance path (4/3 earth profile paper).

VII. System Evaluation

The elements which contribute to the over-all system gain of a radio-relay link are the transmitter power, transmitting antenna gain, the receiving antenna gain, and the wide-band gain. Elements that contribute to the over-all system attenuation are antenna line loss,

and free-space path attenuation for the given distance between stations and the frequency used. The system evaluation extends from the audio or broad-band terminals of the modulator in the transmitter to the audio or broad-band terminals of the demodulator in the receiver.

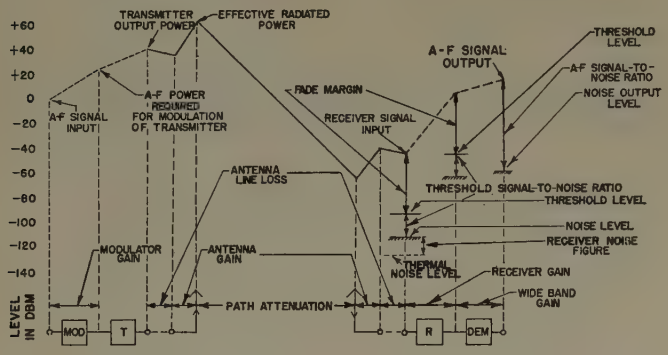

Fig. 10—One-hop system—level diagram.

The various factors for system evaluation may be displayed on a level diagram as in Fig. 10. The level diagram shows a one-hop system from the transmitter audio-frequency signal level input to the audio-frequency signal level output of the receiver. The level

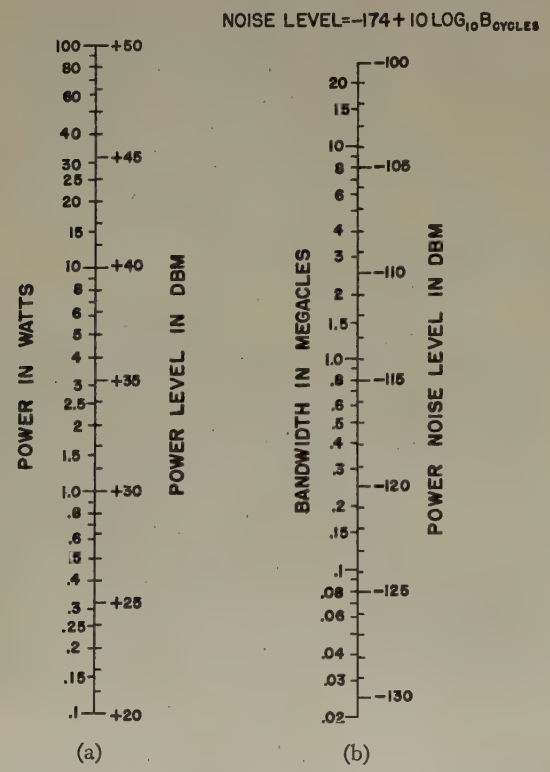

Fig. 11—(a) Conversion of power to dbm. (b) Conversion of bandwidth to thermal noise level.

diagram for all practical purposes starts with the transmitter output power if it is assumed that the transmitter modulation does not introduce noise.

1. The transmitter output ordinarily given in watts is converted to decibels above 1 mw (dbm) by means of the conversion scale of Fig. 11(a).

2. The loss in the antenna transmission line expressed in decibels (db) will depend upon the type and length of line used and, on the level diagram, causes the level of power transmitted to go down.

3. In a microwave radio-relay link the energy radiated from a transmitting antenna is wasted unless it is directed toward the receiving antenna. To obtain this directivity a paraboloidal reflector or dish is ordinarily used to focus the radio waves. The gain of a paraboloidal reflector referred to a dipole antenna expressed in decibels (db) may be determined from Fig. 12. The antenna gain raises the level on the diagram to a point known as the "effective radiated power."

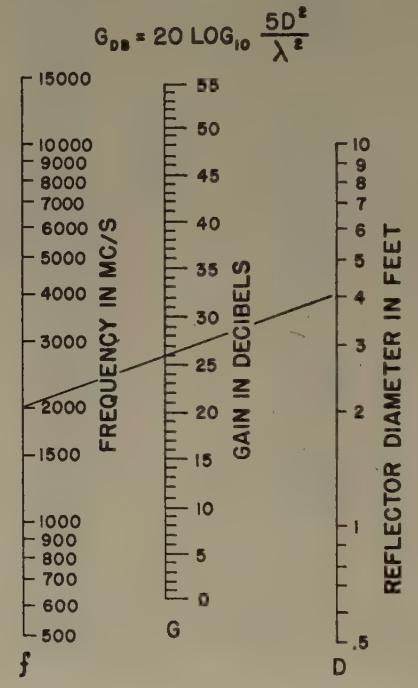

Fig. 12—Parabolic antenna gain referred to a dipole.

4. The path attenuation is the free-space attenuation (Fig. 13) because the path has been engineered to provide this clearance.

5. As in 3 above, the receiver antenna gain raises the level on the diagram by an amount equal to the gain in decibels of the antenna over a dipole.

6. The transmission-line loss between antenna and receiver lowers the level of the diagram by an amount equal to the line loss. The resulting level is the receiver signal input.

To determine the fade margin available for operation, the receiver signal input must be compared with the noise which is present at the receiver input.

(1) External noise is extremely low in the microwave region and the noise level of the receiver may thus be determined from the thermal noise generated in the antenna plus the fluctuation noise produced by the receiver. The thermal noise generated in the antenna is dependent on the bandwidth of the receiver. The noise level in dbm for a given receiver bandwidth may be obtained from the conversion chart of Fig. 11(b). The level

is shown on the diagram by a dashed line below the receiver signal input level.

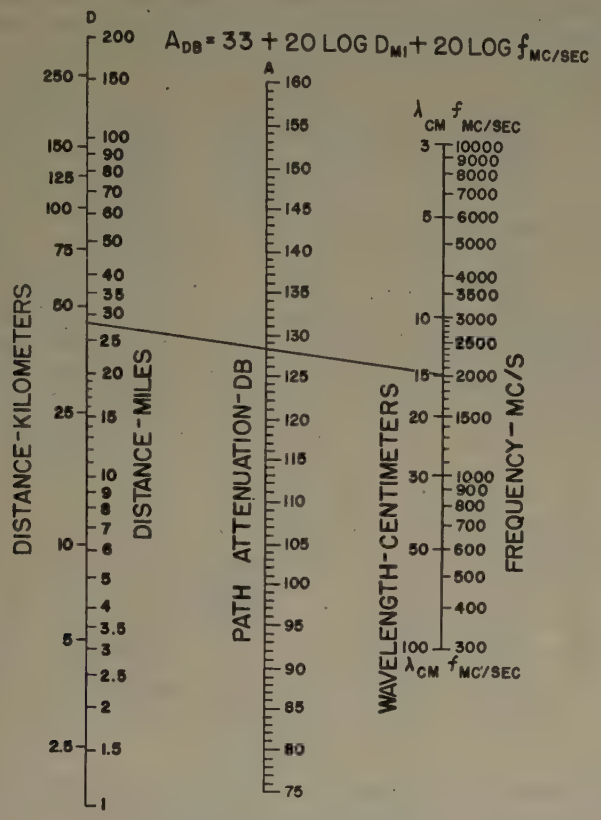

Fig. 13—Path attenuation between dipole antennas for free-space propagation.

(2) The fluctuation noise produced by a receiver is usually given in terms of noise figure. The noise figure indicates the amount of deterioration of signal-to-noise ratio which occurs while signal and noise pass through the equipment. This noise figure expressed in decibels is added to the thermal noise level and the resulting level is the receiver noise level.

(3) The difference between the receiver signal input level and receiver noise level is the signal-to-noise ratio at the input to the receiver. Since the gain in the linear portion of the IF of the receiver holds for the signal as well as the noise, the levels of both rise as shown in the level diagram. This rise will depend upon the gain of the equipment only and does not affect the system evaluation with respect to the signal-to-noise ratio. Thus the signal-to-noise ratio at the input to the receiver is the same as the signal-to-noise at the input to the demodulator.

(4) In conventional amplitude-modulation (AM) systems with 100-per cent modulation, the signal-to-noise ratio at the input to the demodulator will also be the signal-to-noise ratio in the audio output of the receiver. If wide-band modulation is applied, such as frequency modulation, pulse modulation, and so forth, the AF signal-to-noise ratio will be improved in comparison to the IF signal-to-noise ratio. The amount of improvement is called "wide-band gain," which is realized only if the signal remains at a level above the noise level by an amount depending on the type of modulation. This level is called the "threshold" level of the receiver, and for FM is about 10 to 13 db above the noise level. (See level diagram, Fig. 10.) If the signal fades below the threshold level, the transmission fails completely. Thus the wide-band signal-to-noise ratio at the audio-frequency output is greater than the signal-to-noise ratio at the receiver input when above threshold. The exception to this is in conventional AM systems in which the modulation is less than 100 per cent and the wide-band gain is negative (loss).

For convenience a step-by-step process in accordance with the flow of the level diagram from transmitter to receiver, as in the preceding paragraphs, is shown in Table IV. The equipment data is assumed for purposes of illustration.

It will be noted from Table IV that with a fade margin of 32 db the reliability will be in excess of 99.9 per cent. It must be remembered however that during a 30-db fade the AF wide-band signal-to-noise ratio will be reduced from 65 to 35 db. A fade greater than 32 db will result in a breakdown of the system.

TABLE IV

Signal Level	Assumed Data	Level or S/N Ratio
Transmitter power. Converting 10 watts by use of Fig. 11(a)	10 watts	+40 dbm (trans. output power)
Transmitter antenna line loss	3 db	+37 dbm
Transmitter antenna gain at 2000 mc, 4 ft dia dish from Fig. 12	26 db	+63 dbm (effective radiated power)
Path attenuation for $D=28$ miles and $f=2000$ mc/s from Fig. 13	128 db	−65 dbm
Receiving antenna gain (same as trans ant gain)	26 db	−39 dbm
Receiving antenna line loss	3 db	−42 dbm (receiver signal input)
Assume a nominal gain for IF of	42 db	0 dbm
Assume a nominal gain for AF of	10 db	+10 dbm
RECEIVER NOISE LEVEL		
Thermal noise for a bandwidth of 10 mc from Fig. 11(a)	10 mc	−104 dbm
Noise figure	17 db	−87 dbm (receiver noise level)
RF AND IF SIGNAL TO NOISE RATIO		
Receiver signal input level (−42 dbm) minus receive noise level (−87 dbm)		45 db S/N
AF SIGNAL-TO-NOISE RATIO WHEN ABOVE THRESHOLD		
RF signal to noise ratio (45 db) plus wide-band gain	20 db	65 db S/N
FADE MARGIN		
Receiver signal input level (−42 dbm) minus threshold level	−74 dbm	32 db (margin)
THRESHOLD SIGNAL-TO-NOISE RATIO		
RF signal-to-noise ratio (45 db) minus fade margin (32 db)		13 db S/N
AF SIGNAL-TO-NOISE RATIO BREAKPOINT		
AF signal-to-noise ratio above threshold (65 db) minus fade margin (32 db)		33 db S/N

VIII. Multiple-Hop System Evaluation

The discussion above is limited to single-hop systems. In evaluating a multiple-hop system additional factors must be taken into consideration. The audio noise level

of a multiple-hop system is higher than for a single-hop system; therefore, the AF system signal-to-noise ratio will be smaller. Also, in a multiple-hop system the reliability from a propagation viewpoint is reduced.

Consider a multiple-hop system in which, for convenience, the path distance for each hop is approximately 30 miles and the paths are provided with free-space clearance. Assume first, that no propagation fading is taking place. The single-hop RF and AF signal-to-noise can then be calculated as in preceding paragraphs.

1. The RF and audio signal level, receiver noise level, and threshold level will remain the same at each repeater receiver and at the terminal receiver.

2. The audio noise level will rise in each successive receiver, starting at the receiver nearest the terminal transmitter, and will be a maximum level at the terminal receiver. The amount of increase in noise level is dependent on the number of jumps. The conversion scale (Fig. 14(a)) shows the increase in audio noise level for a system of a given number of hops.

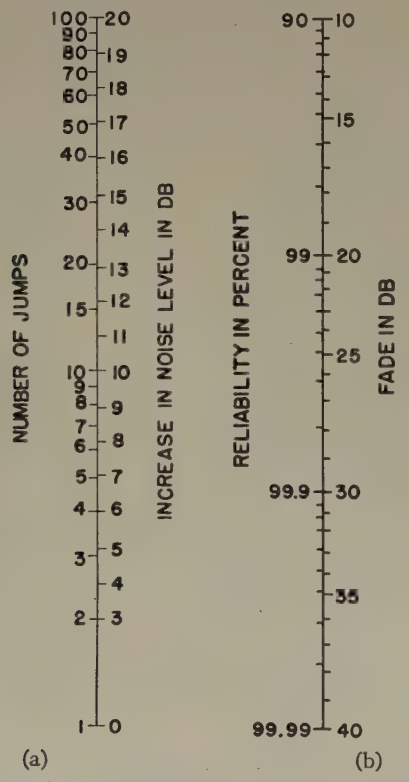

Fig. 14—(a) Noise-level increase for multiple hops. (b) Fading reliability.

In the preceding illustrative example the audio signal-to-noise ratio is 65 db S/N. If a multiple-hop system of 8 jumps, for example, is assumed, then from Fig. 14(a) a rise in noise level of 9 db will result in an AF signal-to-noise ratio of 56 db. It will be noted that the RF and IF signal-to-noise ratio remains the same for each jump. The fade margin in each hop, therefore, remains the same, that is, 32 db. The AF signal-to-noise break point for the 8-hop system is the AF signal-to noise ratio of 56 db minus the fade margin of 32 db. The AF break point is therefore 24 db S/N.

The other factor which must be taken into account in system evaluation is the system reliability from a wave-propagation standpoint. The multiple-hop reliability

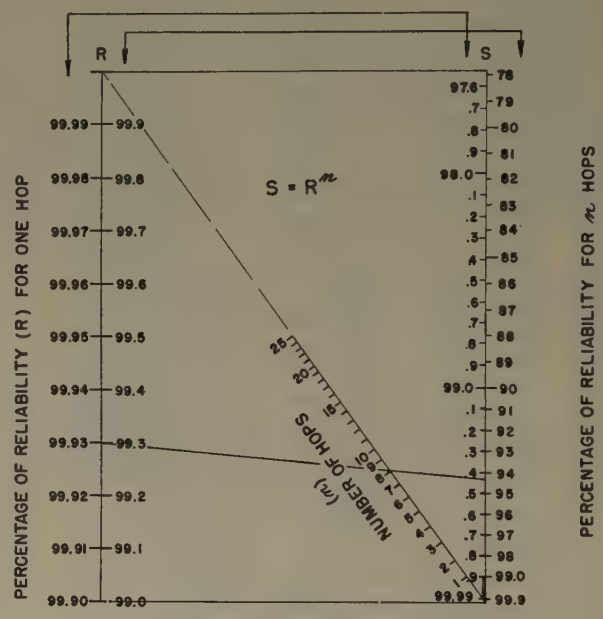

Fig. 15—System reliability.

compared to single-hop reliability is lower and the system reliability of a number of paths in tandem is the combined reliability of each path taken separately. The nomograph of Fig. 15 shows how the system reliability due to propagation is affected by multiple-hop radio relay. This chart assumes all paths approximately 30 miles long and provided with free-space clearance. Thus, continuing the illustrative example, a fade of 32 db occurs approximately 0.1 per cent of the time, or from Fig. 14(b), a path with a fade margin of 32 db has a reliability of 99.93 per cent. For an 8-jump system using the nomograph of Fig. 15, draw a line between $R=99.93$ and $n=8$. Read the value where the line crosses the S scale or $S=99.4$. This is the system reliability due to propagation. Another way of evaluating the system is to state the system reliability for a given number of jumps, and then determine the single-hop fade and reliability required. Thus if an 8-hop system with a reliability of 99.4 per cent is desired, draw a line between the n and S scales at $n=8$ hops and $S=99.4$ per cent. Read the percentage of reliability for one hop, 99.93 per cent on the R scale.

Acknowledgment

The author wishes to express his appreciation to R. E. Lacy, under whose guidance this paper was written, for the many valuable suggestions received. This work was carried out at the Signal Corps Engineering Laboratories, Fort Monmouth, New Jersey, in order to provide the military with a technical bulletin for field use. The high-low technique of siting is directly due to informal talks with personnel of Bell Telephone Laboratories.

An FM Microwave Radio Relay*

R. E. LACY†, SENIOR MEMBER, IRE, AND C. E. SHARP†, ASSOCIATE MEMBER, IRE

Summary—**The design features of an experimental 8,000–8,500-mc radio relay are reviewed. The technical innovations mentioned are the result of research and engineering accomplished for the design of a military radio-relay system.**

A duplexing antenna system comprised of a waveguide hybrid tee, a waveguide mast structure, an off-center fed parabolic reflector antenna assembly, and a waveguide cavity preselector for the receiver is described.

A mechanically and electronically tuned cw communications magnetron, which provides a carrier power in excess of 50 watts, is included and is capable of being frequency modulated. A unique frequency stabilization circuit maintains the carrier center frequency, improves the linearity of the modulation, and reduces the carrier-noise frequency variations.

Introduction

IN THE DESIGN of microwave radio-relay equipment for transportable military radio communication systems, there are many factors that must be considered. Compromises are usually necessary in the interest of obtaining the utmost simplicity in design and maximum performance with a minimum of weight and complexity. Some of the novel features and components devised in an attempt to attain these desired characteristics in one type of radio-relay equipment design, with a brief description of their functioning, are presented. A stable but tunable FM equipment was desired to transmit and receive a 20-kc intelligence band via any pair of approximately fifty radio-frequency channels in the super high-frequency range.

The antenna and feed systems are described initially, followed by a résumé of the modulation and frequency-control means, along with an indication of the results of tunable FM magnetron research.

Antenna Duplexing

Duplexing an antenna system to accomplish both the transmitting and receiving functions provides a method of reducing equipment weight and installation time by one-half, since only one antenna per relay terminal would be necessary. This was accomplished by application of a balanced waveguide hybrid junction,[1] generally known as the "Magic T." The "Magic T" is most simply described as a symmetrical combination of a waveguide E-plane T and an H-plane T, having a shunt and a series arm, a balance arm, and an output arm, and it may be considered as analogous to the familiar hybrid coil of telephone practice.

Fig. 1 illustrates the arrangement of the antenna duplexing T. As shown, the shunt and series arms of the hybrid are connected to the transmitter and the receiver, respectively. One end of the balance arm of the T is terminated by a matched load, capable of dissipating at least one-half the transmitter power output; the other end of the balance arm is connected to the waveguide sections assembled within a forty-eight foot sectional tubular mast, which is terminated at the top by the radiating assembly.

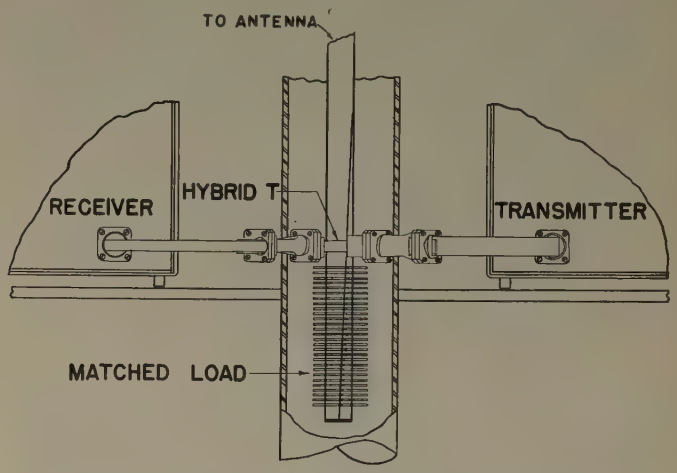

Fig. 1—Arrangement of the antenna duplexing T shown connected to the RF assemblies.

The RF energy from the transmitter is divided equally between the matched load and the antenna, with the result that approximately one-half of the available power from the magnetron is dissipated while the other half is delivered to the antenna. The received energy at the antenna passes down the waveguide mast to the hybrid T where it is divided equally between the series and shunt arms, with one-half the available received energy being lost in the transmitter magnetron. A well-balanced waveguide hybrid T will provide about 30 db of isolation between the transmitter and receiver.

Tunable Preselector

The isolation provided by the hybrid was not sufficient between the receiver input and the transmitter output to permit the channel spacing required within the frequency band; therefore, a preselector was included in the receiver to reduce the possibility of interference to the desired signal due to spurious responses which might otherwise be generated within the receiver. The preselector, as constructed, is a very compact, band-pass two-cavity waveguide filter. This filter is continuously tunable over the frequency band by a single control knob, enabling selection of the desired signal and effectively rejecting the local transmitter frequency which may be only 50 mc removed.

* Decimal classification: R480×R561. Original manuscript received by the Institute, September 15, 1952. Presented, IRE National Convention, New York, N. Y., March 6, 1952.

† Signal Corps Engineering Laboratories, Fort Monmouth, N. J.

[1] L. D. Smullin and C. G. Montgomery, "Microwave Duplexers," Radiation Laboratory Series 14, McGraw-Hill Book Co., Inc., New York, N. Y., pp. 350–372; 1948.

Radiating Assembly

The radiating assembly atop the waveguide mast, consists of a section of a paraboloidal reflector, illuminated by a horn feed. Fig. 2 illustrates the manner in

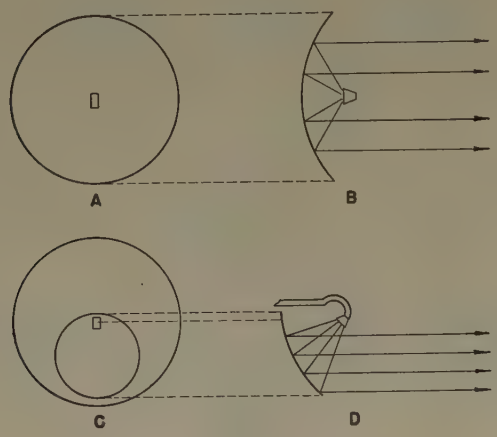

Fig. 2—Derivation of the antenna section.

which this section is derived. A and B of this sketch show two views of the conventional paraboloidal reflector. C shows the portion of the reflector which is cut out for use in this type of antenna. In D it may be seen from the ray diagram that, although the horn is placed at approximately the original focal point, it is now directed at a point near the center of the new reflector section. This type of antenna design represents an improvement over the conventional type since it greatly reduces the screening effect of a horn assembly placed in the center of the field of radiation. Gain of the antenna is thereby increased as there is a reduction of the side lobes. Also the standing-wave ratio in the waveguide is improved, as less energy is reflected back into the horn.

Fig. 3 is a view of the antenna assembly mounted directly on the hybrid T, without the mast sections inserted. As was illustrated by the ray diagram in Fig. 2(d), the reflector is in its normal position for a horizontal beam. The gain of the antenna is 34 db above that of a dipole; the half-power beam-width is 4 degrees in both the E and H planes.

RF Power and FM Magnetron

To determine the amount of radio-frequency power required from the transmitter, the usual considerations and calculations of the principal transmission factors, comprising the "power-balance" equation for one radio-relay link over a 50-mile path, show that the minimum required transmitter power output is in the order of 30 watts.

A cw oscillator capable of being both frequency modulated and continuously tunable over the 8,000- to 8,500-mc band, and having this power-output requirement, was not available at the initiation of the equipment development. However, based principally on a design by Raytheon Manufacturing Company of an FM magnetron for the 4,000-mc frequency range, new models were developed for 8,000 mc capable of being mechanically tuned and electronically frequency modulated and stabilized. These magnetrons operate at an anode voltage around 1,500 volts and have a power output of about 50 watts, with anode efficiencies of approximately 40 per cent. Frequency modulation of this magnetron oscillator is made possible by the introduction of an additional heater and cathode known as a "halo" because of its shape. The space charge, and consequently the resonant frequency of the magnetron cavities, can be varied by changing the voltage on the "halo" cathode, permitting frequency modulation of the magnetron up to 20 kc with modulator power of less than 1 watt. Mechanical tuning is accomplished by means of a diaphragm-tuned external cavity closely coupled to one of the magnetron cavities.

Fig. 3—Antenna assembly shown mounted directly on the hybrid T and RF equipment support.

Frequency Stabilization

Since the inherent frequency stability of a magnetron oscillator is inadequate for a communication system, many methods were tried in order to achieve the required stability via a system which was tunable yet relatively simple in operation. Finally, a unique method of frequency control or stabilization[2] meeting these requirements was developed.

[2] George G. Bruck, "Stabilizing frequency of reflex oscillators," *Electronics*, pp. 170–176; February, 1948.

This stabilization method as developed is all electronic and has less critical circuit-components than the previously devised methods. This frequency stabilizer, based on a duplex heterodyne principle, incorporates as the frequency reference, a high Q tunable cavity resonator of high thermal stability. This frequency reference cavity is in a servocontrol circuit, which in event of magnetron oscillator frequency drift applies a frequency correcting voltage to the electronic tuning element of the magnetron.

Operation of Frequency-Control Circuit

The operation of this frequency-control circuit may best be explained by reference to Fig. 4.

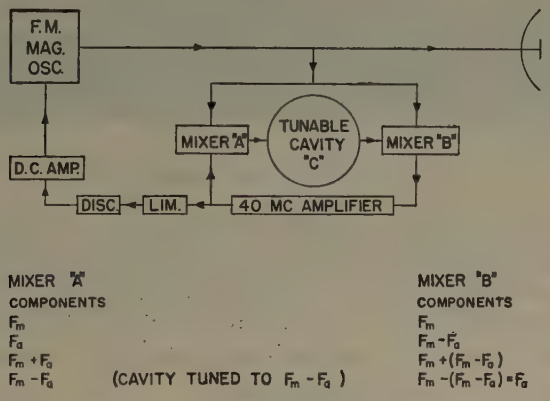

Fig. 4—Block diagram of the frequency stabilization circuit. Arrows indicate direction of the principal frequency components.

A small amount of the RF power output from the FM magnetron (a few milliwatts) is coupled to the crystal mixers designated "A" and "B." With the frequency control cavity "C" resonated, for example, 40 mc lower than the magnetron frequency, the 40-mc amplifier oscillates due to an external feedback path provided through mixer "A," cavity "C," and mixer "B."

Oscillation occurs in the following manner: At mixer "A," the magnetron output frequency (F_m) is mixed with the 40-mc amplifier output frequency (F_a) and the difference frequency ($F_m - F_a$) is transmitted through the control cavity "C" to mixer "B." This difference frequency from the cavity mixes again with the magnetron output frequency, and the resultant difference frequency (F_a), the original 40 mc, becomes the amplifier input. The positive feedback loop thus formed will cause oscillation at 40 mc, as long as the net phase shift around the loop is zero. If, however, the magnetron frequency should start to drift, for any reason, the cavity will no longer be excited at its resonant frequency and there will be a phase shift. The frequency of oscillation of the amplifier loop will then change to the frequency at which the net loop phase-shift is again zero. Since this frequency will not be 40-mc there will be a dc output from the 40-mc discriminator. This dc, after amplification by the dc amplifier, will change the voltage on the magnetron electronic tuning element in the proper polarity to shift the magnetron frequency back toward the point from which it drifted. As the magnetron is shifted back toward its original frequency, the magnitude of the correcting voltage will be decreased, until a condition of equilibrium is reached.

Fig. 5 shows a practical arrangement of the reference cavity and crystal mixers assembled on the waveguide. The crystal mixers "A" and "B" mounted on opposite sides of the waveguide are coupled to the guide through small holes. The open top ends of the mixers are covered by the bottom of the cylindrical resonant cavity. The bottom of this cavity is solid except for one small round glass-covered hole or iris centered over each low-Q mixer cavity. These holes provide the input and output path through the cavity.

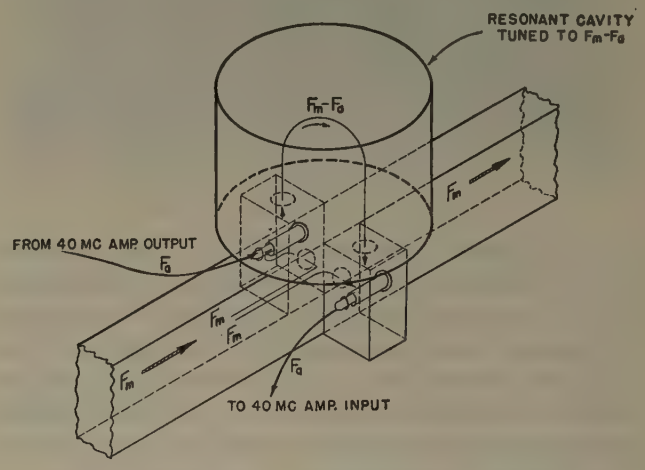

Fig. 5—Arrangement of the tunable frequency reference cavity and crystal mixers.

Performance of Frequency Stabilizer

The frequency stabilization circuit performs two other important functions besides stabilizing the frequency of the magnetron anywhere within its tuning range. It also reduces the effects of modulation distortion arising from any nonlinearity of the halo-cathode frequency-voltage characteristic. Furthermore, it reduces the internally generated magnetron noise-frequency variations, correspondingly improving the carrier-to-noise ratio by virtue of the large amount of inverse feedback introduced.

The transmitter carrier-to-noise improvement ratio due to the effectiveness of the frequency stabilizer was observed by open circuiting the inverse feedback loop and then measuring the increased carrier noise level at the receiver. By closing the loop and again measuring this noise level, the improvement ratio was obtained. The amount of improvement observed, in general, varied from about 40 db with a newly installed magnetron down to about 20 db for a magnetron with several hundred hours of service.

RF Equipment Assemblies

Figs. 6 and 7 show the engineering models of the transmitter and receiver radio-frequency assemblies. The compact construction and comparative simplicity for a microwave equipment of both units is apparent.

The transmitter assembly (Fig. 6) contains the FM magnetron, frequency reference cavity, and stabilizing circuits. Adjustment to a desired frequency channel is simply accomplished by first setting the precalibrated dial on the reference cavity, then, with the aid of the panel meters in the stabilizing circuit, by precisely adjusting the magnetron mechanical tuning to correspond. The receiver assembly (Fig. 7) includes a balanced mixer, intermediate amplifier and audio circuits, reflex klystron oscillator, and associated frequency reference cavity and stabilization circuit. Tuning of the receiver is similar to that of the transmitter, except that, in addition, the precalibrated preselector dial is also set to the desired frequency channel.

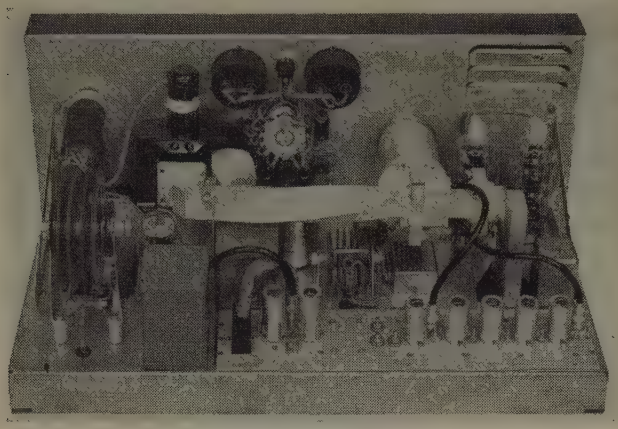

Fig. 6—Transmitter RF assembly.

Fig. 7—Receiver RF assembly.

Results and Conclusions

The results of operational tests conducted with the equipment have shown the antenna system to be efficient and satisfactory, especially in regard to its ease of installation and operation which is especially important for transportable military equipment.

The fact that 50 watts of power at 8,000 mc is readily obtainable from a tube with an anode efficiency of 40 per cent shows attractive possibilities for tunable FM magnetrons for SHF microwave communications equipments.

The operational tests have also demonstrated that by utilizing a selected magnetron and by careful transmitter adjustments over-all one-jump system signal-to-noise ratios as high as 50 db could be realized. However, noise reduction, comparatively short life, and linearity of modulation still remain as important problems to be solved before FM magnetrons are entirely satisfactory for communications equipment.

Acknowledgment

Acknowledgment is made to the engineering personnel of the Belmont Radio Corporation and the Raytheon Manufacturing Company, particularly to Mr. R. M. Sprague and Mr. P. Pontecorvo of the Microwave Equipment Department, for the detailed development of the engineering models of the above equipment under Army Signal Corps contract.

A Microwave Correlator*

R. M. PAGE†, fellow, ire, A. BRODZINSKY†, and R. R. ZIRM†, associate, ire

Summary—**A method is presented for the measurement of auto- or cross-correlation functions of wide-band uhf signals. A novel method of frequency translation is used to obtain a transformation of the spectrum into a more convenient form for computation. This method involves the generation of a line spectrum of local oscillator frequencies throughout the bandwidth of the signal, and subsequent summing of the frequency differences into a narrower band of video signals containing all the correlative characteristics of the original signal. A theoretical analysis of the operation is presented along with experimental results obtained with this correlator on a 200-mc bandwidth noise signal centered at 1.1 kmc.**

IN THE ANALYSIS of experimental data it has become popular in recent years to supplement the classical techniques of Fourier analysis by counterpart techniques in the time domain, derived from the concepts of statistical mechanics, and dealing with the statistical properties of the data. In this realm of ideas the autocorrelation function of a sample of data is the counterpart of the power spectrum in Fourier analysis. A number of devices for computing the correlation functions of arbitrary data have been developed.[1,2,3] In general these devices are adequate to fulfill their intended purposes, where frequency and bandwidth requirements are not severe. It is sometimes desirable, however, to measure these functions at microwave frequencies and at video or greater than video bandwidths.

* Decimal classification: 621.375.2. Original manuscript received by the Institute, October 8, 1952.

† Naval Research Laboratory, Washington 25, D. C.

[1] H. E. Singleton, "A digital electronic correlator," Proc. I.R.E., vol. 38, pp. 1422–1428; December, 1950.

[2] A. E. Hastings, and J. E. Meade, "A device for computing correlation functions," *Rev. Sci. Instr.*, vol. 23; July, 1952.

[3] A. H. Schooley, "A Simple Instrument for Evaluating Correlation Functions," Natl. Elec. Conference, Cleveland, Ohio; September 10, 1952.

In such regions existing techniques offer somewhat less than desired performance.

The essential functions performed by a correlator are delay, multiplication, and integration. These functions must be performed in the order stated. The delay component must be linear and must operate at data frequency, i.e., bandwidth must equal or exceed the data signal bandwidth, and its frequency of operation must include the spectrum of the data signal, or one to which the data signal may be shifted by heterodyne methods. For sufficiently great bandwidths a suitable length of radio-frequency cable or waveguide makes a satisfactory delay device. The integrator is a relatively low bandwidth device and presents no problem of great difficulty. The more difficult problem of immediate interest is the multiplier.

It is doubtless possible to design a multiplier that will operate satisfactorily at ultra-high frequencies with very great bandwidth. In some cases, however, it may be simpler to first transform the data signal to a narrower bandwidth, and then perform the multiplication process in the more convenient narrow bandwidth form. This may be accomplished without loss of information, providing that phase significance is preserved in the bandwidth transformation. A process that meets this condition will now be described.

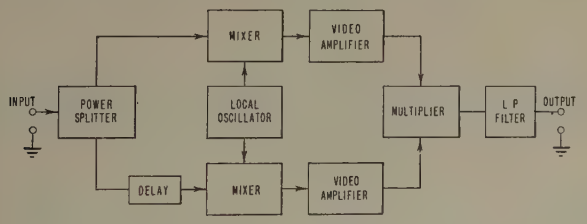

Fig. 1—Basic correlator block diagram.

A signal of a given bandwidth in one part of the radio-frequency spectrum may be transformed to a similar signal of the same bandwidth in another part of the spectrum by heterodyning with a reference oscillator and filtering to retain one sideband of the heterodyned signal. This is the well-known principle of the familiar superheterodyne receiver. In the process, phase significance is preserved in the signal. Two signals occupying the same frequency band may be similarly translated to a different frequency band by separately heterodyning the two signals with a common reference oscillator. Frequency and phase relationships between the two signals will not be disturbed in the process. Specifically, the cross-correlation function of the two signals measured at output will be identical with that measured at input, providing the delay necessary to correlation measurement is made on input signal, before heterodyning. This is true even when the frequency of the heterodyning oscillator lies within the same frequency band that is occupied by the signals. By placing the heterodyning oscillator at the center frequency of the signal, the output bandwidth is reduced to one half the original signal bandwidth, with one limit at zero frequency. Such a system is shown in block diagram form in Fig. 1.

Bandwidth may be further reduced before multiplication by using a second heterodyne oscillator whose frequency is one third the bandwidth of the original signal, or two thirds the cutoff frequency of the low-pass filter appropriate to the output of the first heterodyne. The output of this second heterodyne will contain all the phase and frequency information of the original signals necessary to the correlation process in one sixth the bandwidth of the original signal, and may be followed by a low-pass filter with cutoff frequency at one half the heterodyne oscillator frequency. The process may be repeated as many times as desired before multiplication. Each added heterodyne will further reduce the bandwidth by a factor of three.

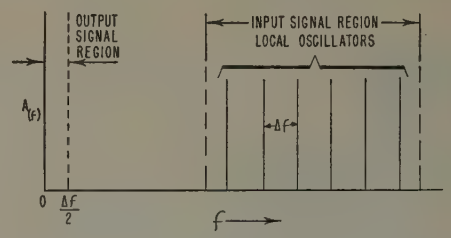

Fig. 2—Mixer input and output spectra.

A somewhat similar result may be obtained in a single step of bandwidth transformation if the original signal is heterodyned with a reference signal composed not of one frequency but of a series of frequencies uniformly spaced and distributed throughout the spectrum of the signal. The heterodyne process is then followed by a low-pass filter with cutoff frequency equal to half the frequency separation of the heterodyne frequencies. Fig. 1 also illustrates this method when the local oscillator frequency is multivalued as necessary to the process. The local oscillator spectrum is shown in its relation to the input and output signal spectra in Fig. 2.

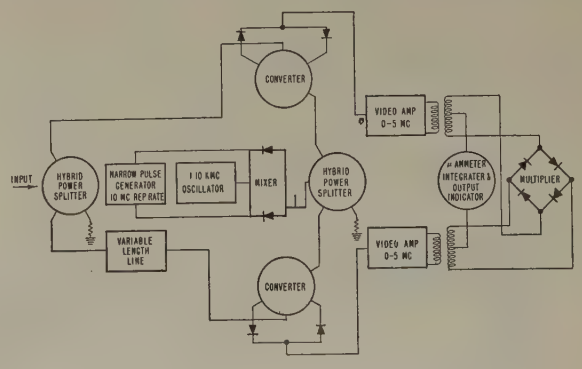

Fig. 3—UHF correlator functional diagram.

There is no theoretical limit to the local oscillator frequency spacing, and therefore no limit thus imposed on the degree of bandwidth narrowing possible. The limit on bandwidth reduction is determined by the bandwidth requirement in the output, which is set by the time allocated to a reading.

A more detailed functional diagram of an experimental uhf correlator is shown in Fig. 3. The signal of

interest occupies the 200-mc band from 1 to 1.2 kmc. Hybrid rings are found to give adequate channel separation over this band. A combination of fixed and variable length transmission lines is used to obtain delay times extending from 0 to 50 mμ sec. The line spectrum local signal is generated with 10-mc frequency spacing by operating a narrow pulse generator at a 10-mc rate[4] and mixing this in a balanced converter with a 1.1-kmc single-frequency signal. By operating the balanced converter slightly off balance, the carrier component at 1.1 kmc is made equal to the amplitude of the sideband components. This local oscillator signal is then fed through a hybrid-ring power splitter to each of two balanced crystal mixers.

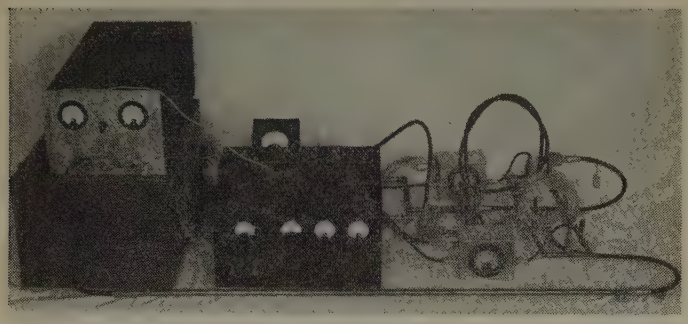

Fig. 4—Experimental 1.1-kmc 20-per cent bandwidth correlator.

The output of each mixer is amplified and filtered by a 5-mc bandwidth video amplifier. The balanced outputs of the two video amplifiers feed the product detector which, in turn, multiplies the two channel signals together. A galvanometer at the output provides adequate integration of the product signal and, at the same time, an output indication. A photograph of the correlator is shown in Fig. 4.

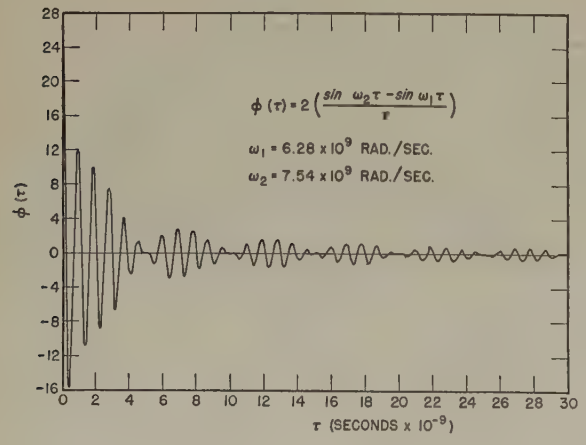

Fig. 5—Calculated autocorrelation function.

The calculated autocorrelation curve of a perfectly square band of noise 200 mc wide and centered at 1.1 kmc is shown in Fig. 5. The autocorrelation curve of an approximately square band of noise approximately 200 mc wide and centered at 1.1 kmc is shown in Fig. 6, as measured with the microwave correlator. Considering that the experimental signal spectrum was neither ideally flat nor ideally band-limited, the agreement is sufficiently good to illustrate the validity of the method.

A Microwave Correlator

Mathematical Appendix[5]

Given a function of time whose power spectrum is distributed over a finite bandwidth, it is desired to show that the autocorrelation function may be correctly determined when the delay operation is followed with a heterodyne operation in which both delayed and undelayed ensembles are identically reduced in both frequency and bandwidth before multiplication. Let the given function have a power spectrum $p(\omega)$ whose value is unity between the bandwidth limits ω_1 and ω_2, and zero outside these limits. The autocorrelation function $\phi(\tau)$ is the Fourier cosine transform of the power spectrum; so

$$\Phi(\tau) = 2\int_0^{+\infty} p(\omega) \cos \omega\tau d\omega.$$

Under the stated conditions, this integrates directly to

$$\Phi(\tau) = 2(\sin \omega_2\tau - \sin \omega_1\tau)/\tau.$$

This equation represents a sine wave of angular frequency $(\omega_1+\omega_2)/2$, with the modulation envelope of the form

$$\frac{\sin \frac{1}{2}(\omega_2 - \omega_1)\tau}{\frac{1}{2}(\omega_2 - \omega_1)\tau},$$

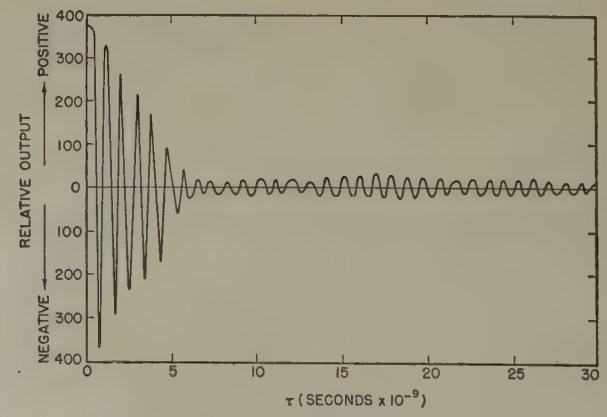

Fig. 6—Measured autocorrelation function.

[4] M. G. Morgan, "A modulator producing pulses of 10^{-7} sec duration," Proc. I.R.E., vol. 38; May, 1950.

[5] "Threshold Signals," Rad. Lab. Series No. 24, McGraw-Hill Book Co., Inc., New York, N. Y.; 1950.

which is the well-known autocorrelation function of ideally band-limited white noise.

As shown by Rice,[6] ideally band-limited white noise may be represented as a function of time by the relation

$$V(t) = \sum_{n=N_1}^{N_2} C_n \cos (n\Delta\omega t + \phi_n)$$

in the limit as $n\to\infty$ and $\Delta\omega\to 0$; C_n and ϕ_n are amplitude and phase variables, either or both of which may vary randomly with time, and $\Delta\omega$ is an arbitrary frequency increment, so that

$$\omega_1 = N_1\Delta\omega, \qquad \omega_2 = N_2\Delta\omega.$$

The mean-square signal power in each incremental frequency component $\Delta\omega$ is then

$$\overline{[V(t)]^2}_{n\Delta\omega} = \tfrac{1}{2}C_n^2\Delta\omega \to p(\omega)d\omega.$$

The signal represented by $V(t)$ is now to be mixed with a heterodyning signal whose spectrum consists of a series of k discrete frequencies of equal amplitude V_0, equally spaced throughout the spectrum of $V(t)$, which is $\omega_2-\omega_1=\beta$. The angular frequency of the p^{th} heterodyning signal is given by

$$\omega_p = \omega_1 + \frac{\beta}{k}(p - 1/2).$$

The total heterodyning signal is therefore given as

$$V_H = V_0\sum_{p=1}^{k} \cos \omega_p t.$$

The following operations are now to be performed:

1. $V(t)$ is to be heterodyned with V_H under the condition $V_0 \gg C_n$ so that products of the components of $V(t)$ alone will be negligible relative to products of the components of $V(t)$ and V_H.
2. DC terms in the output are to be eliminated by ac coupling.
3. All output frequencies greater than $\beta/2k$ are to be eliminated by filtering.

By these processes the only terms that remain are product terms between each component of $V(t)$ and the nearest single component of V_H. These may be written directly as

$$V_1 = 2V_0\sum_{p=1}^{k}\left[(\cos \omega_p t)\sum_{n=N_1+(p-1)\beta/k}^{N_1+p\beta/k} C_n \cos (n\Delta\omega t - \phi_n)\right],$$

whence

$$V_1 = V_0\sum_{p=1}^{k}\sum_{n=N_1+(p-1)\beta/k}^{N_1+8p\beta/k} C_n \cos (n\Delta\omega t - \omega_p t + \phi_n)$$

since the frequencies corresponding to $n\Delta\omega+\omega_p$ are rejected by the low-pass filter.

In order to determine the autocorrelation function of $V(t)$, the original $V(t)$ must be delayed by the delay parameter τ and then multiplied by its corresponding undelayed value. If the delayed value is represented by $V(t)$, then the undelayed value will be represented by $V(t+\tau)$, and may be written

$$V(t+\tau) = \sum_{n=N_1}^{N_2} C_n \cos [n\Delta\omega(t+\tau) + \phi_n].$$

If identical operations are performed on $V(t+\tau)$ as were performed on $V(t)$, one may by analogy write directly

$$V_2 = V_0\sum_{r=1}^{k}\sum_{m=N_1+(r-1/k)\beta}^{N_1+(r/k)\beta} C_m \cos [m\Delta\omega(t+\tau) - \omega_r t + \phi_m].$$

The next operation is to multiply V_1 by V_2 and filter out all ac terms, retaining only dc terms, to obtain the autocorrelation function. If samples are of sufficient length to be considered stationary, the product V_1V_2 may be averaged over the random variables C_n, C_m, ϕ_n, ϕ_m instead of integrated in time, to obtain the same result. Thus

$$\Phi(\tau) = \overline{V_1V_2}^{n,m}.$$

However, when $n\neq m$, the functions V_1 and V_2 are statistically independent and their average product is zero. Also, when $n=m$, $p=r$ by definition. Thus,

$$\Phi(\tau) = V_0^2\sum_{p=1}^{k}\sum_{n=N_1+(p-1)\beta/k}^{N_1+(p/k)\beta} \overline{\tfrac{1}{2}C_n^2}\left[\overline{\cos (n\Delta\omega\tau)} + \overline{\cos (2n\Delta\omega t + n\Delta\omega\tau - 2_p\omega t + 2\phi_n)}\right].$$

Since the average of a sinusoid over all phases is zero, the term containing ϕ_n drops out. Then since

$$\sum_{p=1}^{k}\sum_{n=N_1+(p-1)\beta/k}^{N_1+(p/k)\beta} = \sum_{n=N_1}^{N_2},$$

there remains

$$\Phi(\tau) = V_0^2\sum_{n=N_1}^{N_2} \overline{\tfrac{1}{2}C_n^2}\cos (n\Delta\omega\tau).$$

This summation may be converted to an integral by passing to the limit as $n\to\infty$ and $\Delta\omega\to 0$, with the relation $\omega=n\Delta\omega$ and with the substitution $\overline{\tfrac{1}{2}c_n^2}=p(\omega)d\omega$; the function then becomes

$$\Phi(\tau) = V_0^2\int_{\omega_1}^{\omega_2} p(\omega)\cos \omega\tau d\omega.$$

As before, this integrates directly to

$$\Phi(\tau) = V_0^2(\sin \omega_2\tau - \sin \omega_1\tau)/\tau.$$

Since the function may be normalized to any amplitude, the desired proof is demonstrated.

[6] S. O. Rice, "Mathematical analysis of random noise," *Bell Sys. Tech. Jour.*, vol. 23, p. 282; 1944; vol. 25, p. 46; 1945.

Radio Transmission Beyond the Horizon in the 40- to 4,000-MC Band*

KENNETH BULLINGTON†, ASSOCIATE, IRE

Summary—**Reliable signals have been received at distances of several hundred miles at frequencies of 500 and 3,700 mc. The median signal levels are 50 to 90 db below the free-space field, but are hundreds of db (in one case 700 db) stronger than the value predicted by the classical theory based on a smooth spherical earth with a standard atmosphere. Antenna gains and beam widths are maintained to a first approximation and no long delayed echoes have been found. The experimental results are compared with other available data, and it appears that roughly the same median signal levels are obtained for frequencies from 40 to 3,700 mc.**

Introduction

IT IS WELL KNOWN that radio frequencies below about 30 mc are useful for transmission over hundreds and thousands of miles because these signals are returned to the earth by the ionosphere. Frequencies higher than about 40 to 50 mc are ordinarily not returned by the ionosphere, and as a first approximation, these waves are frequently assumed to be limited to almost line-of-sight paths.

Although this first approximation is based on common experience with visible light, it is a rather crude one. It has long been recognized that some energy is bent around the curvature of the earth by both refraction and diffraction, but the magnitude of the received signals has generally been assumed to be too weak and too variable to be useful very far beyond the horizon.

During 1950 and 1951 the Bell Telephone Laboratories conducted a series of experiments at about 500 and 3,700 mc which show that reliable signals can be obtained at distances up to 200 or 300 miles. The signals vary from instant to instant, but the rate of fading is within the compensating capabilities of modern equipment design. The median signal levels are 50 to 90 db below the free-space field, but are hundreds of decibels in excess of the computed value based on the classical theory of smooth spherical earth with a standard atmosphere. The median values are reasonably steady from day to day and no long delayed echoes such as those that distort long-distance ionospheric transmission have been found.

3,700-MC Test

The 3,700-mc test used an experimental transmitter at Whippany, N. J. which generates 1.5-μsec pulses with a peak power of about 300 kw. This energy was fed through 250 feet of waveguide to a 10-foot paraboloid antenna mounted on top of a 150-foot tower. The receiving antenna was a 57-inch "dish" mounted on top of the truck that carried the receiving and recording apparatus. The measurements consisted of recording the received signal for several days to a week at each of several locations from 22 to 285 miles northeast of the transmitter. These sites were on high ground relative to the local terrain, but were all beyond the optical line-of-sight. The most distant site was at Mt. Washington, N. H., where the optical line-of-sight from the transmitter was nearly 8 miles above the receiving antenna, in spite of the material elevation. The principal transmission paths are shown by the long dash lines on the map in Fig. 1.

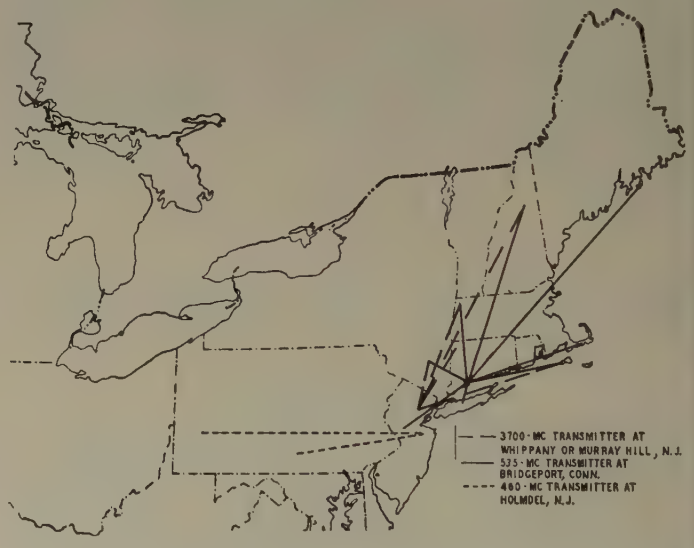

Fig. 1—Paths used in radio tests beyond the horizon.

The median signals obtained at the various locations are shown by the crosses on Fig. 2 in terms of the decibels below the intensity that would have been expected in free space with the same power and antenna gains. At Mt. Washington, for example, the median received signal was about 82 db below free space during the tests in May, 1950 and about 75 db below free space on a return trip the following August. On the basis of the smooth spherical earth theory, the expected signal would have been more than 700 db below free space. Attempts were made in both May and August to pick up a signal near Bar Harbor, Me., a distance of 400 miles, but the sensitivity of the receiver was only about 90 db below free space at this distance and no recognizable signals were found.

The signal fluctuations as seen on an oscilloscope indicated a fading rate of several cycles per second, and on one or two occasions a substantial change was noted between two successive frames of motion pictures

* Decimal classification: R355.914.31. Original manuscript received by the Institute, March 17, 1952; revised manuscript received August 11, 1952. Presented at the IRE National Convention, March, 1952.

† Bell Telephone Laboratories, Inc., 463 West St., New York, N. Y.

taken at a speed of 64 frames per second. The signal as recorded on an Esterline Angus Recorder did not vary more than ±2 db from minute to minute, but the actual fluctuations were smoothed by means of a 2-second time constant associated with the recording apparatus.

In addition to the rapid fading, a slow variation in the average signal occurred over a period of hours and from day to day. These changes rarely exceeded ±15 db, and no drop-outs occurred during any of the tests. At locations far beyond the line-of-sight, there was no obvious correlation of the fading with the time of day or with weather conditions. On shorter paths, however, where the receiver was only moderately below the line-of-sight, an increase of signal level of 20 to 30 db was noted at night and during the passage of cold fronts.

The received pulse was not appreciably widened, and, with one exception, no separate delayed echoes were found. This result indicates that the delays were ordinarily not more than 0.1 or 0.2 μsec, which in turn indicates that bandwidths of several megacycles may be possible. The one exception occurred at Gay Head on Martha's Vineyard, Mass. during very unusual weather conditions. A small hurricane was off the Atlantic coast and ionospheric and magnetic disturbances were observed in Washington, D. C. During a period of about 8 hours the signal level was 35 to 40 db stronger than normal, and it was found that signals were received over an azimuthal angle of about 30° instead of the usual 5°. As the antenna steered counterclockwise in azimuth starting with a northerly point where no signals were received, a pulse appeared which grew in amplitude. As this pulse approached full amplitude, a second pulse appeared approximately 1.5 μsec after the first. As the antenna continued to scan counterclockwise, the second pulse grew to full amplitude and the area between the two began to fill in. This condition represented the "on bearing" pointing toward the transmitter. Further counterclockwise scanning caused the first pulse to diminish in strength and disappear. Then finally the delayed pulse decreased in strength and disappeared. The picture described was not constant with time, and when the antenna was left fixed, the display would change markedly in a few minutes. This phenomenon was followed by a period during which the signal was 10 to 15 db below normal for a period of several hours. All transitions were gradual and the signal finally returned to what was considered its normal value.

Except for the above instance, the antenna beam widths were not widened more than 2 or 3 degrees in either azimuth or elevation. These values are only approximate since antenna patterns are particularly difficult to measure with rapidly varying signals. As a further check on some of the recent theories, measurements were made on the antenna gain that is obtained at locations far beyond the horizon. An open-ended waveguide was substituted for the 57-inch receiving antenna and the received signal decreased by 26±1 db, as would be expected in free space. The substitution of a 19-db horn or an open-ended waveguide for the 39-db transmitting antenna decreased the received signal beyond the horizon by approximately the same amount observed on a line-of-sight control path.

Tests were made on top of Mt. Greylock, Mass. (145 miles) and at three sites located about 800, 1,200, and 1,500 feet below the summit in the direction of Pittsfield. The differences in median signal varied from 2 to 8 db in an irregular manner with changes in elevation, and it was not clear whether these differences were the result of the change in effective antenna height or normal variations during the time required to change locations.

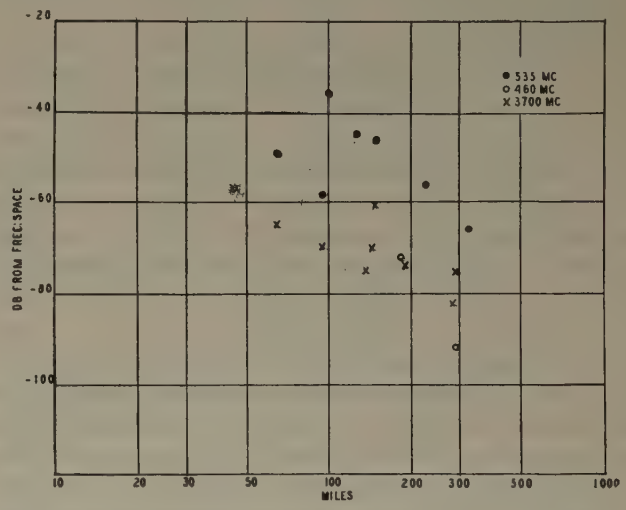

Fig. 2—Median signal levels measured at 460, 535, and 3,700 mc.

The polarization of the received signal was checked at the 100-mile point by substituting a 19-db horn for the receiving antenna and then rotating the horn. The transmitted signal was vertically polarized, and as the horn was rotated, the signal decreased, as expected, until it was lost in the noise.

Although the received pulses were not widened appreciably, the shape varied rapidly, and at times the pulse seemed to break into two or more separate pulses of much shorter duration. However, the frequency of the transmitter changed more than a megacycle during the time of each pulse, and it is believed that the unwanted frequency modulation coupled with multipath transmission is the principal reason for the distortion of the received pulses.

535 MC Test

A second series of tests made use of the 534.75-mc sound channel of an experimental television transmitter operated by National Broadcasting Company at Bridgeport, Conn. These measurements lasted for several hours to several days on each of the transmission paths shown by the solid lines on Fig. 1. The receiving antenna was a corner reflector with a gain of about 10 db above a half-wave dipole and was mounted on top of a truck.

The median signal obtained for various distances from Bridgeport are shown by the solid dots on Fig. 2.

The longest path was about 325 miles to a point near Bar Harbor, Me., and was half over land and half over water. The 225-mile path was entirely over land to Mt. Washington, N. H., and the 125-mile path was almost entirely over sea water to Gay Head on Martha's Vineyard.

The average rate of fading around the median value was about 1 cycle every 5- to 10-seconds with a maximum rate of about 10 cps. By automatically sampling the field intensity every second, it was established that the received signal during a 5- to 10-minute interval follows the Rayleigh distribution. For periods of time measured in terms of hours or days, the received signal measured in decibels follows the normal, or Gaussian probability law.

The quality of the received sound appeared to be limited only by noise, which indicated that no troublesome echoes were present. In addition, no significant changes in the effective antenna gain and beam width were found. These results are not as conclusive as the 3,700-mc test in which pulse transmission provided greater accuracy in measuring delays and narrow beam antennas provided sharper angular discrimination.

460 MC Test

As a result of the tests in New England on 535 and 3,700 mc, a 1-kw transmitter operating at 459.05 mc was set up at Holmdel, N. J. The transmitting antenna gain was about 20 db above a half-wave dipole. The receiving antenna had a gain of about 15 db above a half-wave dipole and was mounted on top of a truck. Two principal receiving sites were selected along the New York-Chicago microwave relay route, one near Chambersburg, Pa. (183 miles) and the other in Pittsburgh. These paths are shown by the short dashed lines on Fig. 1. Approximately two weeks of data were obtained near Chambersburg and several days records were taken at Pittsburgh. The median values are shown by the circles on Fig. 2. The 20- to 30-db difference between these data and the 535-mc data for the same distance may be due in part to the different type of terrain, and in part to seasonal effects. The New England tests were conducted in the summer of 1950 while the Pennsylvania tests were made in early spring of 1951. Several attempts were made to pick up the signal at distances of 400 miles and beyond, but no recognizable signal was found.

A series of tests on antenna beam widths and gain were conducted on the 183-mile path to the site near Chambersburg. These tests indicated that the signals were coming from the horizon along the great circle route and that the antenna beam widths were not widened by more than 1 or 2 degrees in either azimuth or elevation. The substitution at either terminal of half-wave dipoles for the gain antennas resulted in a loss of signal equal to the difference in free-space antenna gain.

Frequency-modulated speech transmission over the 183-mile path showed high quality during periods of relatively strong signal and marginal intelligibility during periods of relatively low signal. The loss in intelligibility seemed to result entirely from low signal level, and no evidence of delay distortion was found.

The receiving antenna was located on a mountain with a sharp drop of about 1,500 feet in the direction of the transmitter. A later test at the base of the mountain, where the effective antenna height was only 50 to 100 feet above the immediate foreground, indicated less than 6-db decrease in median signal level.

Summary of Previously Available Data

The principal data that have been published previously on transmission beyond the horizon are summarized in Fig. 3. The crosses show 3,300-mc data over

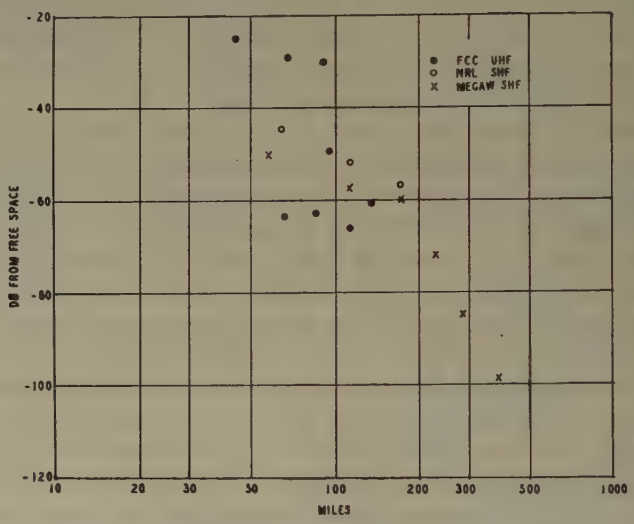

Fig. 3—Median signal levels at uhf and shf (from previously published material.

sea water as reported by Megaw.[1] The circles also show 3,300-mc data over sea water as given by Katzin, Bauchman, and Binnian of the Naval Research Laboratory.[2] The dots represent median values over land in the 400- to 550-mc range which have been obtained from several sources and summarized by the Federal Communications Commission.[3]

The data shown in Figs. 2 and 3 for the 300- to 4,000-mc band are combined in Fig. 4 in which the crosses and dots represent frequency ranges rather than the source of the data. Considering the differences in frequency, terrain, antenna heights, and duration

[1] E. C. S. Megaw, "Scattering of electromagnetic waves by atmospheric turbulence," *Nature*, vol. 166, p. 1100; December, 1950.

[2] M. Katzin, R. W. Bauchman, and W. Binnian, "3- and 9-Centimeter propagation in low ocean ducts," Proc. I.R.E., vol. 35, pp. 891–905; September, 1947.

[3] H. Fine and F. V. Higgins, "Long Distance Tropospheric Propagation in the Ultra High Frequency Band 288–700," Federal Communications Commission T.R.R. Report No. 2.4.10; October 13, 1950.

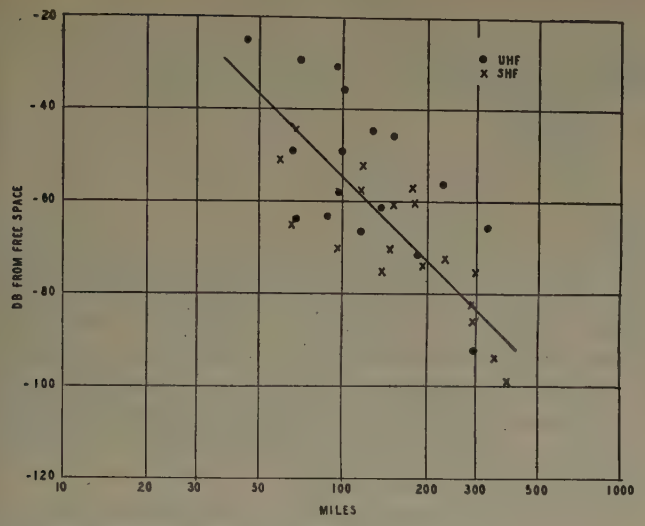

Fig. 4—Median signal levels in 300- to 4,000-mc band.

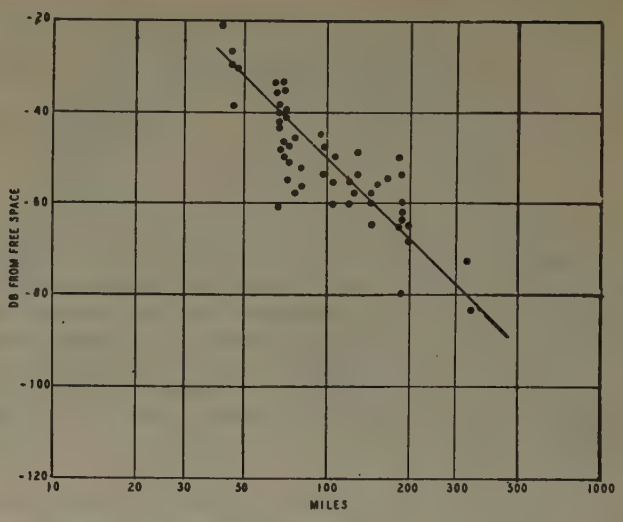

Fig. 5—Median signal levels in 40- to 300-mc band.

of tests, the spread in experimental results is not as large as might have been expected. The data in each frequency range are within about ± 15 db and are approximately equally distributed about an empirical line which indicates a median signal of 55 db below free space at 100 miles and 85 db below free space at 300 miles.

Similar long, distance propagation at frequencies below about 300 mc have been known for several years. Most of the data are in the 40- to 50-mc range, and on many paths experimental data are available for six months to a year or more. The median signal levels shown on Fig. 5 have been obtained from the summaries published by the FCC.[4,5] In most cases, the transmitting antenna height was several hundred feet above the immediate foreground, while the receiving antenna height was only 30 to 50 feet above the ground. The effect of antenna height is most pronounced at and within the optical horizon and becomes less important as the distance beyond the horizon increases.

A comparison of Figs. 4 and 5 shows that the short-term median signal levels in the 300- to 4,000-mc range decrease with distance in approximately the same manner as the long term data in the 40- to 300-mc range.

Conclusions

The most significant conclusion to be obtained from the available data is that the received power at points far beyond the horizon is relatively independent of frequency, antenna height, and weather effects. These parameters have an important effect at or near the horizon, but their importance decreases gradually with increasing distance. The decrease in signal level in going from within the horizon to slightly beyond is greater at shf than at vhf, but once this loss is accepted, the signal decreases much more slowly with increasing distance than the exponential decrease predicted by the classical smooth-earth theory.

The median signal levels far beyond the horizon seem to decrease approximately 18 db for doubling the distance in addition to the 6-db extra free-space loss. The median values are relatively independent of diurnal effects and day-to-day variations, which means that the over-all reliability is much greater than would be expected from the duct theory.

The experimental result that the free-space antenna gains and beam widths are realized beyond the horizon is inconsistent with the initial predictions of the scattering theory. It seems difficult to modify the parameters in the scattering theory to account for both this result and the relatively high observed signal levels.

Although the signal levels are much higher than was commonly expected, high transmitter power and large antennas are needed to obtain reliable voice channels over distances of 200 miles or more. The high-gain antennas needed at both transmitter and receiver indicate that the most likely application of long-path transmission will be for point-to-point service over difficult terrain.

Acknowledgment

The measurement and interpretation of the experimental data described above have involved many individuals, and the author wishes to acknowledge particularly the valuable help and co-operation given by Messrs. R. P. Booth, G. H. Baker, R. C. Shaw, W. Strack, and W. R. Young.

[4] E. W. Allen, W. C. Boese, and H. Fine, "Summary of Tropospheric Propagation Measurements and the Development of Empirical VHF Propagation Curves (Revised)," Federal Communication Commission T.I.D. Report No. 2.4.6; May 26, 1949.

[5] G. V. Waldo, "Summary of Recent VHF Tropospheric Propagation Measurements over Southern and Mid-Western Paths," Federal Communications Commission T.R.R. Report No. 2.4.8; October 16, 1950.

Prediction of the Nocturnal Duct and Its Effect on UHF*

L. J. ANDERSON† AND E. E. GOSSARD†

Summary—**A method is described for predicting diurnal variation in uhf field strengths, which is based on the micrometeorology governing the nighttime refractive-index profiles. Using surface meteorological data from past years, predictions are made of the probability distribution of the diurnal field variations to be expected on 100 and 1,000 mc over CRPL links in Colorado. The predictions are compared with field-strength observations taken in 1952, and the agreement is encouraging.**

NONOPTICAL PROPAGATION of uhf radio energy over land is generally characterized by a diurnal change in received signal strength. Although this effect is superimposed upon other trends, it is often the dominant feature of signal distributions, particularly in regions of low humidity.

The purpose of this paper is to describe a convenient method of predicting, from surface meteorological data, nocturnal duct formation and associated effects upon uhf propagation. The method has been used to predict propagation conditions on 100 and 1,000 mc in eastern Colorado, and these predictions have been compared with observations.

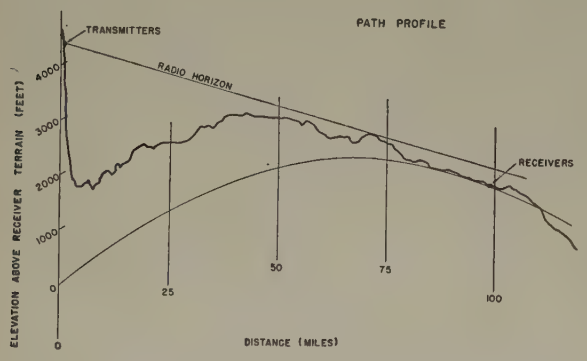

Fig. 1—Path profile for CRPL Cheyenne Mountain links.

The link is operated by the Central Radio Propagation Laboratory, Boulder, Colo., to whom we are indebted for the data on observed fields as well as the path profile (Fig. 1). Observations to date have been made for February through July of 1952. The transmitter is located on Cheyenne Mountain, some 4,400 feet above the general terrain at the receiver. The heights of the receiver antennas are 43 feet for 1,000 mc and 18 feet for 100 mc. Path distance is 98 miles. It may be seen from Fig. 1 that the path is somewhat beyond the optical region under standard propagation conditions.

Predictions of the monthly distributions of the diurnal range in signal were made on a statistical basis from three and a half years of surface meteorological data taken at Dodge City, Kan. No attempt has been made to predict signal behavior on a day-to-day basis from current data, since the complex time and space variation of refractive index profiles make it difficult to predict representative detailed meteorological conditions. However, on a statistical basis, the results show good agreement with observation.

The meteorological processes underlying diurnal propagation effects are nocturnal radiation and heat conduction, since the nighttime temperature profile is a result of the interaction of these processes. Associated refractive-index profiles are such that a radio duct begins forming about sunset. It develops rapidly in the early evening hours, more slowly in early morning, and dissipates rapidly after sunrise. The trend is occasionally modified when condensation takes place early in the evening.

It is shown later in this paper that nocturnal modification may be considered to be largely confined to a layer between the surface and a height $\delta(t)$, which can be computed from surface meteorological observations. The extreme stability often present in nocturnal inversions makes it necessary to use a modification of the usual boundary-layer approach in making such computations.

In the region between δ and the usual height at which surface meteorological data are taken, the profile of refractive index, modified to 4/3 earth, is virtually logarithmic and may be described in terms of δ and the diurnal variation of refractive index at the surface. Thus, the profile may be expressed in terms of the parameter:

$$\gamma = \frac{B_\delta - B_s}{\log \frac{\delta}{s}},$$

where s is the height of the instrument shelter in which the surface meteorological data are taken, and B is refractive index modified to 4/3 earth.

Propagation Prediction

We may now consider the effect of the nocturnal duct upon the diurnal variation in field strength observed for certain links on the Cheyenne Mountain Path. We assume that the B profile is vertical ($\gamma = 0$) near sunset, and that the surface duct development proceeds from then through the night until early morning. At that time, the duct, as described by the parameter γ, is fully developed and remains so until sunrise, when it rapidly deteriorates and the B profile again becomes essentially

* Decimal classification: R113.616. Original manuscript received by the Institute, October 1, 1952.

† United States Navy Electronics Laboratory, San Diego, Calif.

vertical until the following sunset. The diurnal signal variation is thus the difference caused by γ changing from 0 to its maximum value on any given night.

It has been adequately established that, within a given duct, beyond the optical horizon, the signal decreases more or less exponentially with distance; hence, the field expressed in db decreases linearly at a rate less than the standard diffracted field. The problem is to establish this attenuation rate as a function of γ over the observed range. Analysis of data taken on a 100-mile path at 100 mc in Texas shows that for a given distance the attenuation is a linear function of γ.

The remaining problem is to determine the slope of the line—the diurnal signal change (Δ db) versus γ—for the particular link under consideration. When Δ db is determined at one γ value, the prediction of diurnal field-strength variations is complete.

Examination of the path profile (Fig. 1) shows that a direct ray from transmitter to horizon enters the region of appreciable diurnal effect (approximately 300 feet above the surface), about 50 miles from the transmitter. If one can assume negligible diurnal variation over this first portion of the path, then the diurnal variation at the horizon ridge should be very similar to that observed on Arizona desert paths[1] (transmitter, 200 feet; receiver, 0–200 feet; distance, 26 miles). Similarly, the path from ridge to receiver is well approximated by the same link. Thus, the diurnal variation at the receiver should be the sum of, (1) variations observed in Arizona with a 200-foot transmitter and a low receiver plus (2) similar variations with a low transmitter and with the receiver height corresponding to that used in Colorado. For $\gamma = 5$, these variations are 7 db for 100 mc and 20 db for 1,000 mc.

It would be academically more satisfying if one could derive these figures on a theoretical basis, but to date no theoretical treatment of the duct has been found to agree satisfactorily with observations over the wide range of meteorological conditions considered. Therefore, we are forced to make use of the empirical approach in these predictions. In this instance, data were available which enabled close simulation of the path under consideration. Since such data exist for a wide variety of paths, this approach can be applied in many cases.

Verification

There are various ways of defining diurnal signal change. For example, it may be considered as the difference between signals at two specific times, such as afternoon and early morning; or it may be considered as the variation between late afternoon and the maximum occurring any time during the night. The latter concept is perhaps more useful for our analysis, since several factors may cause the highest signal to occur at a time other than the early morning hours. Such factors include:

1. The occurrence of a change in air mass.
2. A significant increase in average wind speed some time during the night.
3. The occurrence of precipitation during the night.
4. The temperature falling to the dew point thus preventing a further increase in B_s during the night.

The observational data obtained over the Cheyenne Mountain links were analyzed in terms of the maximum signal occurring during the night, and the corresponding theoretical prediction therefore has been based on the same concept. Since our purpose was to examine the diurnal signal change, those cases in which a significant air-mass change occurred simultaneously with the diurnal signal change were neglected when analyzing the meteorological observations. However, the curves of observed signal include all times, regardless of whether steady-state meteorological conditions were realized.

For the forecast, hourly surface observational weather data for three and a half years of the period from 1948 to 1951, taken at Dodge City, Kan., were analyzed in terms of the diurnal change in refractive index at instrument-shelter height, and of the mean-wind velocity from sunset to the time at which the maximum refractive index occurred. The frequency distribution of the parameter γ was computed for each month and the diurnal range in db obtained as indicated previously.

The predictions, plotted on probability paper, are compared with observation in Figs. 2, 3, 4, and 5. Of the six months of observational data available (February to July, 1952), the months of February and June, in which the greatest number of hours of data were obtained, were selected to show the seasonal trends. The dashed portion of the observed curves indicates the minimum existing variation, since in this portion the nighttime signal often went off scale. However, the median-diurnal change for each month should usually be unaffected by the "off-scale" periods, and Fig. 6 indicates the predicted seasonal change in the median-diurnal variation as compared with the observed.

In view of the fact that the predictions are based on an average year, and that the extent to which the year 1952 departs from the average would cause departure of observation from prediction, it is felt that the agreement shown is very encouraging. Analysis of Dodge City data for June, of 1949, 1950, and 1951, shows that the departure of observation from prediction in 1952 is within the normal year-to-year variation to be expected.

Meteorology

In order to derive expressions for refractive-index profiles when the atmosphere is quite stable, we use the work of Deacon,[2] based on detailed wind and temperature observations taken at Porton, England.

[1] J. P. Day and L. G. Trolese, "Propagation of short radio waves over desert terrain," Proc. I.R.E., vol. 38, p. 165; February, 1950

[2] E. L. Deacon, "Vertical diffusion in the lowest layers of the atmosphere," *Quart. Jour. R. Met. Soc.*, vol. 75, no. 323, pp. 89–103; 1949.

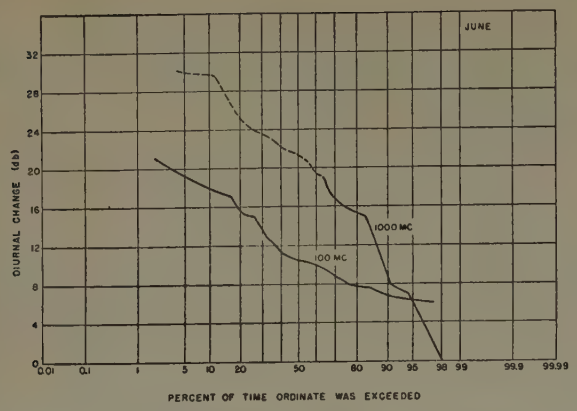

Fig. 2—Frequency distribution of observed diurnal change in June.

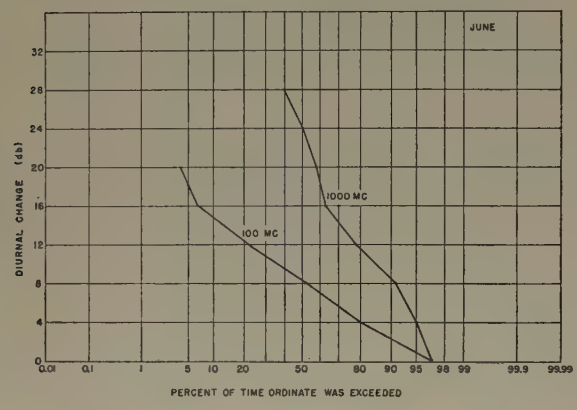

Fig. 3—Predicted frequency distribution of diurnal change in June.

Deacon concludes from these data that the eddy diffusivity is given by:

$$K = k_0 U_* z_0^{1-\beta} z^{\beta}, \qquad (1)$$

where U_*, the friction velocity, is given by

$$U_* = \frac{k_0(1-\beta)}{\left(\frac{z}{z_0}\right)^{1-\beta} - 1} U_z, \qquad (2)$$

where

k_0 is 0.40 (Von Karman's constant),
z_0 is a surface roughness parameter, which may be obtained from wind-profile measurements, or from tables such as that given by Deacon,[3]
z is height,
U_z is wind speed at height z and,
β is a profile index, assumed to be a function of atmospheric stability (as defined by Richardson's Number).

Taking the conventional expression for heat flux, we may write

$$F = \rho c_p K \frac{\partial \theta}{\partial z} = \rho c_p k_0 U_* z_0^{1-\beta} z^{\beta} \frac{\partial \theta}{\partial z}, \qquad (3)$$

where

ρ is density of air,
c_p is specific heat of air at constant pressure, and
θ is potential temperature.

[3] E. L. Deacon, "Vertical profiles of mean wind velocity in the surface layers," *Gt. Brit. Porton*, Technical Paper, no. 39; 1948.

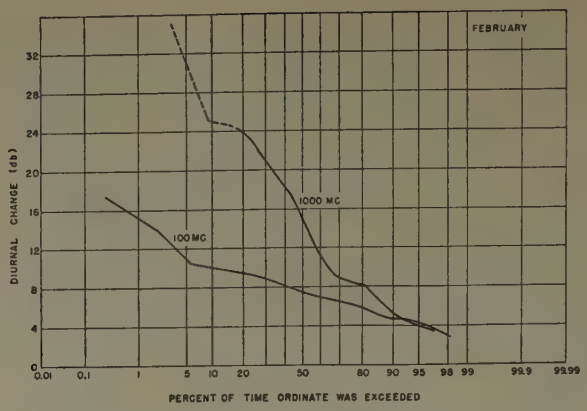

Fig. 4—Frequency distribution of observed diurnal change in February.

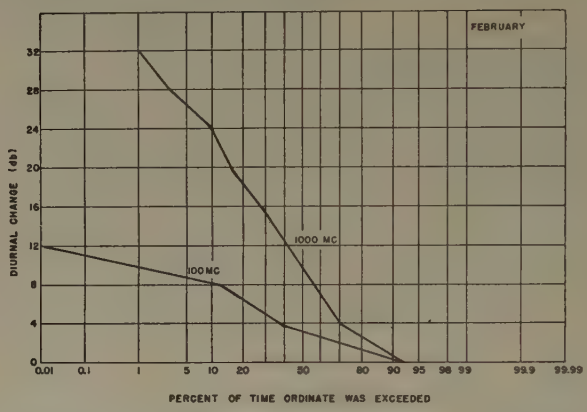

Fig. 5—Predicted frequency distribution of diurnal change in February.

Now, if we make the approximation that flux is independent of height over the height range in which we are interested, and integrate (3) between limits of z_0 and δ, we obtain:

$$F_{z_0} = \frac{\rho c_p k_0 U_* (\theta_\delta - \theta_0)}{\left(\frac{\delta}{z_0}\right)^{1-\beta} - 1}. \qquad (4)$$

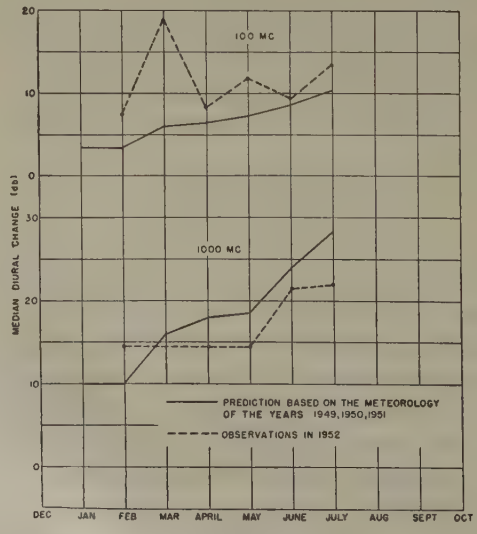

Fig. 6—Observed versus predicted median-diurnal change (January to July).

This defines a height $\delta(t)$ which may be considered an effective depth of modification of the lower atmosphere under nocturnal radiation conditions. Furthermore, if we assume like Frost[4] that flux at the surface is constant through the night, and note that ρc_p is essentially constant through our height range, we have

$$F_{z_0} t = \rho c_p \int_{z_0}^{\delta(t)} (\theta_\delta - \theta_z) dz. \tag{5}$$

Taking the height distribution of temperature to follow the Deacon distribution, we have

$$\frac{\theta_0 - \theta_z}{\theta_0 - \theta_\delta} = \frac{\left(\frac{z}{z_0}\right)^{1-\beta} - 1}{\left(\frac{\delta}{z_0}\right)^{1-\beta} - 1}.$$

Substituting, and integrating (5), we have an expression from which the flux may be eliminated by using (4). If we then note that in general

$$1 - \beta\left(\frac{\delta}{z_0}\right)^{2-\beta} \gg (2-\beta)\left(\frac{\delta}{z_0}\right)^{1-\beta} - 1,$$

we arrive finally at the expression for δ

$$\frac{\delta}{z_0} = \left(k_0(2-\beta)\frac{U_* t}{z_0}\right)^{1/(2-\beta)}. \tag{6}$$

Thus, knowing wind at some anemometer height (and therefore knowing U_*) and having z_0 (computed from wind profiles or obtained from tables), we need only choose a time t and determine β in order to solve for δ.

The above technique is somewhat parallel to the Karman-Polyhausen method for dealing with boundary-layer problems in aerodynamics, and the corresponding approximations are of about the same order. The height δ is, of course, a fictitious height, and the discontinuity in the height derivative of temperature at this point is in reality smoothed. From a mathematical standpoint, it is a very convenient concept, and the functional dependence of the temperature profile on wind speed and time is quite reliable.

In the Deacon relationship, β is assumed to be a function only of stability as defined by the Richardson's Number

$$J = \frac{g}{\theta} \frac{\frac{d\theta}{dz}}{\left(\frac{du}{dz}\right)^2}$$

at a given height.

Deacon[3] further points out that if the ratio of the wind velocities at two fixed heights is uniquely related to Richardson's Number, then it must also be uniquely related to $\theta_2 - \theta_1/(U_2)^2$, where the subscripts 2 and 1 indicate heights. Thus, if this latter parameter can be related to β, we can obtain β from simple surface observations. Such a relationship was obtained empirically by Deacon[3] for his particular instrument heights and surface roughness. His curve may also be translated to other conditions of roughness and instrument heights. It is to be noted that at great stabilities (low winds and large positive temperature gradients) β appears to approach a constant value of about 0.75. At high winds and small temperature differences, β approaches 1.00, which means the profile is logarithmic. The fact that conditions are very stable in nocturnal inversions makes the Deacon modification of the conventional logarithmic profile quite important when computing δ. It is also true, however, that even for the case of a quite stable lapse rate (say $\beta = 0.75$), the profile above a few feet from the surface would appear essentially logarithmic within the accuracy of most observations. Therefore let us, for simplicity, take the distribution of potential temperature and potential vapor pressure to be approximately logarithmic from instrument shelter height s (about 5 feet), up to the height δ. Now, it can be shown that the distribution of refractive index (expressed in terms of B)[5] closely approximates the same functional height variation as that of potential temperature and potential vapor pressure. We then finally have

$$B - B_s = \frac{B_\delta - B_s}{\log \frac{\delta}{s}} \log \frac{z}{s}. \tag{7}$$

But the value of B_δ is assumed to be nearly constant throughout the night and equal to the late afternoon value of B_s. Late in the afternoon B is virtually constant with height, and since for a given set of conditions δ is only a function of wind and β at any particular time, in (7), we have expressed the distribution of refractive index aloft in terms of surface measurements.

If we define the profile constant on the right-hand side of (7) as γ, we have

$$\gamma = \frac{B_\delta - B_s}{\log \frac{\delta}{s}},$$

which is the critical meteorological parameter used in the propagation predictions earlier in this paper. It is a parameter which may be conveniently determined from standard data taken by all Weather Bureau stations.

[4] R. Frost, "Calculation of night minimum temperatures," *Gt. Brit. Met. Off. Professional Notes*, no. 95, pp. 1–6; 1948.

[5] $B = \frac{77.6}{T}\left(P + \frac{4{,}800e}{T}\right) + 0.012z.$

where: T is temperature (°A),
e is vapor pressure (mb),
p is pressure (mb).

Field Strength of KC2XAK, 534.75 MC Recorded at Riverhead, N. Y.*

G. S. WICKIZER†, SENIOR MEMBER, I.R.E.

Summary—**Field strength was recorded for 22 months over a nonoptical path, at a distance of 33 miles. Over-all variation was approximately 12 db in winter and 33 db in summer, with relatively small variation in the median level. On this transmission path, fading 10 db or more below the median occurred during the summer months and was about evenly divided between daylight and darkness for the normal hours of operation.**

THE EXPANSION of television broadcasting into the uhf spectrum has brought new problems of many kinds to the design engineer. In addition to changes in equipment techniques, there remains the question of propagation and field-strength behavior at the higher frequencies. With the object of extending the scope of available data on this subject, the RCA Laboratories Division has recorded the field strength of an experimental uhf television transmitter in Bridgeport, Connecticut for a period of nearly two years.

The audio channel, being frequency modulated, maintained a constant power output with varying modulation, and was thus better adapted to field-strength recording than the video channel. The audio transmitter of KC2XAK operated on a frequency of 534.75 mc, with effective radiated power of 6,800 watts, horizontally polarized.

The transmission path, from southern Connecticut, across Long Island Sound to eastern Long Island, is shown on the map of Fig. 1. The profile of Fig. 2 reveals a more complex situation than the map indicates since the optical portion of the path was over water while the path beyond the optical horizon was over land.

Fig. 1—Map showing transmission path.

The receiving site was located on level ground at the southern edge of the village of Riverhead, with the area in front of the antenna clear of trees, wires, or other objects for a distance of about 300 feet. Beyond this distance, the transmission path traversed a small residential area with trees estimated to be 25 to 40 feet in height. The remainder of the distance over land passed through another small residential section and about five miles of farm land, with open fields and wooded areas.

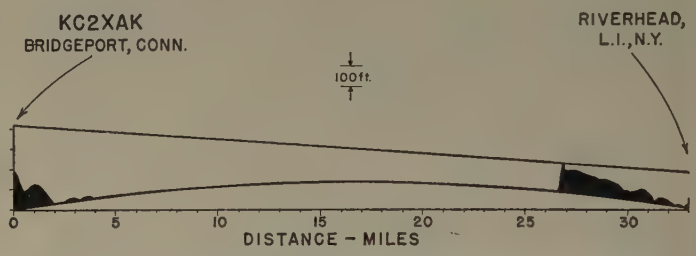

Fig. 2—Profile from KC2XAK, Bridgeport, Conn. to Riverhead, N. Y. 4/3 earth's radius.

The receiving antenna was a parabolic dish 76 inches in diameter, mounted with its center 30 feet above ground. The gain of the antenna, as calculated from its directive pattern, was 17.5 db over a half-wave dipole. The antenna was connected to the receiving equipment by 33 feet of RG-14/U coaxial cable, having an estimated attenuation of 2 db. The net gain of the antenna and transmission line was thus 15.5 db relative to a half-wave dipole.

The receiver was a superheterodyne employing double conversion, and equipped with automatic frequency and gain controls. A record of receiver output was obtained from a Bristol moving-pen recorder connected in the receiver diode-load circuit. Analysis of the field-strength record was simplified by the use of a totalizer unit[1] which operated from the amplified agc voltage in the receiver. The totalizer contained twelve adjustable levels which were set at intervals of 4 db from 25.5 to 69.5 db above 1 μv/m.

The normal operating schedule of the transmitter was approximately 9 a.m. to 11 p.m., Tuesday through Saturday. This permitted the receiver calibration to be checked before each day's operation, with the exception of Saturday. The totalizer readings and the deflection of the recorder at the various totalizer levels were recorded manually as a part of the calibration procedure. This permitted the daily totalizer figures to be corrected for

* Decimal classification: R271.3. Original manuscript received by the Institute, October 9, 1952.

† RCA Laboratories Division, Radio Reception Laboratory, Riverhead, L. I., N. Y.

[1] R. W. George, "Signal strength analyzer," *Electronics*, vol. 24, pp. 75–77; January, 1951.

each day's operation to agree with the true signal performance as interpreted from the recorder chart. In this way, each day's results were corrected as a unit and the monthly results were a summation of these units.

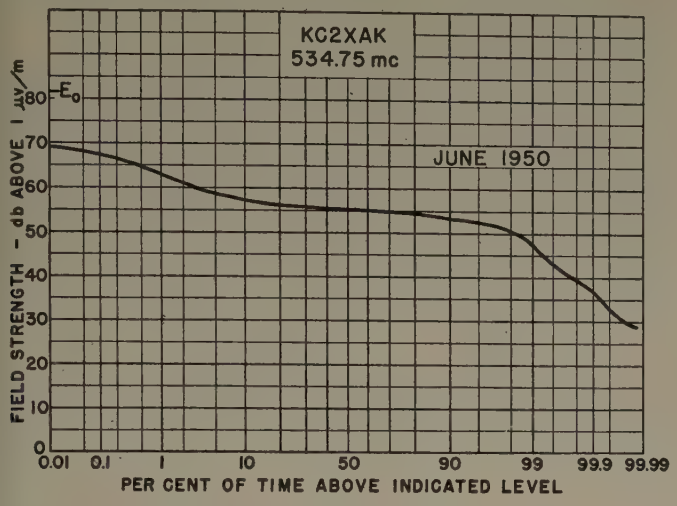

Fig. 3—Typical field-strength distribution for summer months.

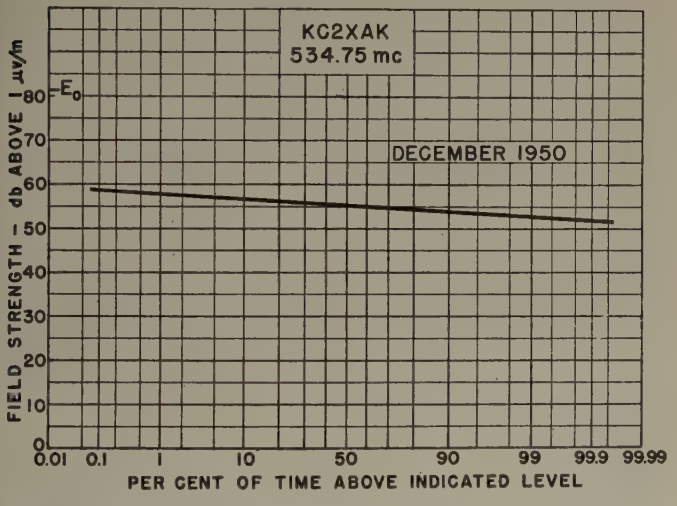

Fig. 4—Typical field-strength distribution for winter months.

Typical examples of the monthly field-strength performance curves are found in Figs. 3 and 4. Relatively little variation occurred during the winter months, while the performance in summer was characterized by occasional deep fading, with slower and somewhat smaller excursions to higher values. The seasonal nature of field-strength variation on this path becomes more apparent when the monthly curves are combined in summary form, as in Fig. 5. Although the maximum and minimum levels exhibit relatively large variations, the median value shows an over-all variation of only 2.3 db. Dotted portions of the curves indicate extrapolated points on the monthly time analyses.

Field strength at the obstruction shown in the profile of Fig. 2 was calculated to be 1.5 db above the free-space value (E_0). This figure was confirmed by measurements made in the same general area. However, calculation of the field strength at the receiving site, based on simple diffraction theory, was found to be 9 to 16 db above the measured median value. This discrepancy is not surprising, as previous measurements[2] have indicated appreciable attenuation at these frequencies when passing through wooded areas. As indicated in Fig. 5, the median field strength at the receiving site was 25 to 26 db below E_0.

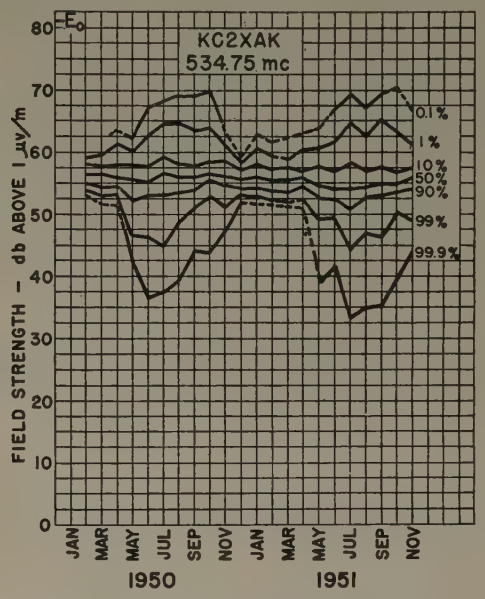

Fig. 5—Summary, field-strength analysis for entire recording period.

The refraction effects which are troublesome from a service viewpoint are deep fades, which occurred on this path during the summer months. These fades were usually of short duration, but might be as much as 20 or 30 db below the median value. In general, the deeper the fade, the shorter its duration, suggesting the combination of two paths of equal amplitude and opposite phase. This condition is possible when strong refraction exists above the elevation of the normal direct-ray path.

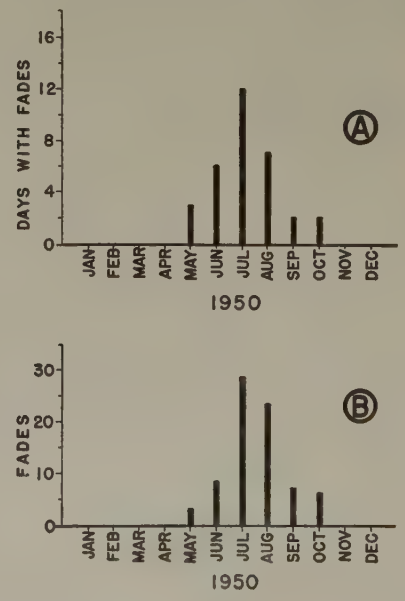

Fig. 6—Summary of fading 10 db or more below median field strength. (A) Number of days with fading. (B) Number of individual fades.

[2] B. Trevor, "Ultra-high-frequency propagation through woods and underbrush," *RCA Rev.*, vol. V, pp. 97–100; July, 1940.

Since the normal field intensity was roughly 25 db below E_0, the interfering ray would only have to attain this strength to cause cancellation when the phase difference was 180 degrees. Maximum fields were about 14 db above the median, which indicates that at times the energy refracted around the obstruction was the dominant factor in determining field strength at the receiver.

The distribution of fades, which dropped 10 or more db below the median, have been plotted for 1950 in Fig. 6. As would be expected from Fig. 5, the severe fading was restricted to the summer months, especially July and August, in 1950.

Further analysis of the fading data indicated that slightly more fades took place in the daylight hours than at night. A large proportion of the daylight fading may be attributed to refraction on the over-water portion of the transmission path. This large body of water served both as a source of water-vapor and as a stabilizing influence on the lower layers of the atmosphere during the daylight hours.

The particular transmission path over which KC2XAK was recorded is not sufficiently representative of general conditions to permit drawing any broad conclusions. It can be stated however that field-strength variation was much less in the winter, and that attenuation beyond the optical horizon may depend considerably on local conditions such as terrain, vegetation, or other obstacles.

Toward a Theory of Reflection by a Rough Surface*

W. S. AMENT†

Summary—**A rough, perfectly reflecting surface is first specified by the statistics of noise theory. If illuminated by a plane electromagnetic wave, such a surface would reflect statistically predictable fields. An attempt is made to formulate the problem of predicting the fields in terms of the statistics of the surface. The result is a series of integral expressions in which averages of the currents induced in the surface appear as unknown functions. Owing to mathematical complexities, these expressions are not solved for the average currents; however, a qualitative discussion is given of a known formula for the specular reflection coefficient of a gently rolling surface.**

Introduction

IN TRYING to predict theoretically the effect of oceanic swell and chop on the propagation of microwaves, we are interested primarily in average effects, such as the average power scattered per unit area of sea surface, or the average specular reflection coefficient. This paper will be concerned with a possible method of mathematically combining the statistics of a model sea-surface with Maxwell's equations so that, in principle, such averages can be deduced.

As the paper deals with methods rather than predictions, it is best to start with a descriptive outline of the problem and the physics behind the attempted mathematical formulation. We consider a surface obtained when an infinite, horizontal, perfectly conducting plane is randomly corrugated. The "randomness" is specified statistically, so that many somewhat similar specific surfaces have to be considered in taking an "average." When a plane wave (with electric vector parallel to the corrugations) is incident from above on one such surface, currents are induced in the surface. These currents radiate fields and the total field (incident plane wave plus fields reradiated by all currents) must vanish on the surface. For a single surface, this fact can be formulated mathematically as an integral equation, which can be solved in principle for the induced currents. For the statistically specified surface, we have to consider many somewhat similar specific integral equations. Thus we should first solve a large number of integral equations for the currents, and then somehow average the fields scattered by these currents over all possible surfaces. Instead, we consider all of the integral equations at once, and try to take the average before solving any one of them. This leads to a set of integral relations in which *averages* of the induced currents are the unknown functions, and in which appears the statistical description of the randomly corrugated horizontal surface.

Since these integral relations are complicated, we reduce the complication by restricting the generality of the unknown average currents. In the final formulation the average current is considered to be basically a function only of altitude above the horizontal mean-plane. With this approximation, all portions of the surface at a single altitude are considered to have the same induced current density, regardless of whether or not a portion is shadowed by another, higher, part of the surface. Even with this approximation, the resulting integrals still are not readily evaluated. However, by using a heuristically justifiable approximate current density of this restricted type, we deduce a reasonable expression for the average specular reflection coefficient of the rough surface, and are able to discuss qualitatively the validity of the expression.

Mathematical Formulation

We first prescribe a perfectly conducting, continuous surface $(x, h(x))$ in some statistical way, so that the general behavior of the surface height h is about the same at all points of the x axis. For this purpose we consider $h(x)$ to depend on x in the same way that a filtered

* Decimal classification: R113.307. Original manuscript received by the Institute, October 17, 1952.
† Naval Research Laboratory, Washington 25, D. C.

noise voltage depends on time. For the statistical properties of the surface, we then can use results from noise theory.[1] In particular, we require a first probability density $W(h)$, a conditional probability $P(h; h', \Delta)$, and a second probability density

$$W(h, h', \Delta) = W(h')P(h; h', \Delta). \tag{1}$$

$W(h)$ may be defined with reference to Fig. 1:

$$W(h)dh = \lim_{N\to\infty} \sum_{i=-N}^{N} \Delta x_i \div (x_N - x_{-N}).$$

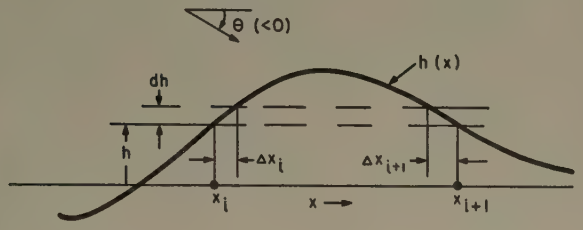

Fig. 1

If $F(h)$ is an arbitrary function of h, integrable over the range $-\infty < h < \infty$, then

$$\lim_{T\to\infty} \frac{1}{2T} \int_{-T}^{T} F[h(x)]dx = \int_{-\infty}^{\infty} F(h)W(h)dh.$$

The noise-theoretic formula for $W(h)$ is

$$W(h) = (2\pi\bar{h}^2)^{-1/2} e^{-h^2/(2\bar{h}^2)}, \tag{2}$$

where $\bar{h}^2$ is the mean-square value of h, the mean value of h being taken as zero. $P(h; h', \Delta)dh$ may be described as the probability that $h(x)$ lies between h and $h+dh$ when $h(x+\Delta) = h'$:

$$P(h; h', \Delta) = (2\pi\bar{h}^2)^{-1/2}[1 - \rho^2(\Delta)]^{-1/2} \cdot \exp\left\{-[h - h'\rho(\Delta)]^2/[2\bar{h}^2\{1 - \rho^2(\Delta)\}]\right\}, \tag{3}$$

where the autocorrelation function $\rho(\Delta)$ can be calculated through

$$\bar{h}^2\rho(\Delta) = \lim_{T\to\infty} \frac{1}{2T} \int_{-T}^{T} h(x)h(x+\Delta)dx = \int_{-\infty}^{\infty}\int_{-\infty}^{\infty} hh'W(h, h', \Delta)dhdh'. \tag{4}$$

Through $\rho(\Delta)$ and $\bar{h}^2$ the statistical behavior of the surface is completely specified.

Now let us assume a plane wave incident on this surface from above (from $y \gg (\bar{h}^2)^{1/2} > 0$), the electric vector of this wave being parallel to the z-axis of the rectangular co-ordinate system. Then there are currents induced in the surface, and these currents reradiate fields in such a way that the total field (incident field plus fields reradiated from all parts of the surface) vanishes on the perfectly conducting surface. We also know that the total field vanishes *below* the surface. Let us express these statements mathematically for a particular $h(x)$, and then try to introduce the statistics of the surface. First we may assume that the incident wave is expressed by

$$\psi_0 = \exp(ikx\cos\theta - iky\sin|\theta|) \tag{5}$$

and satisfies the wave equation

$$\psi_{0xx} + \psi_{0yy} + k^2\psi_0 = 0.$$

(The time-factor $\exp(-i\omega t)$ is suppressed.) The field radiated from a unit current at $(x', y') = p'$ to a point $p = (x, y)$ is

$$\frac{i}{4} H_0^{(1)}[k\{(x - x')^2 + (y - y')^2\}^{1/2}] = G(x, y; x', y') = G(x', y'; x, y).$$

Now let the current in the surface per unit length along the x axis be given by $j(x)\exp(ikx\cos\theta)$. Then we must have for all x,

$$\psi_0[x, h(x)] + \int_{-\infty}^{\infty} j(x')e^{ikx'\cos\theta}G[x', h(x'); x, h(x)]dx' = 0, \tag{6}$$

and

$$\psi_0(x, y) + \int_{-\infty}^{\infty} j(x')e^{ikx'\cos\theta}G[x', h(x'); x, y]dx' = \begin{cases} \psi_{\text{total}}, & y > h(x) \\ 0, & y < h(x). \end{cases} \tag{7}$$

The integral (6) in principle completely determines $j(x)$, and (7) (in the case $y < h(x)$) must follow from (6) as a mathematical identity, or else $j(x)$ would in general have to satisfy two contradictory requirements.

As $h(x)$ is known only statistically, we are driven to the use of average values of the currents $j(x)$ rather than exact values. For instance, with the aid of Fig. 1, we can define an average current $J(h)$ as

$$J(h) = \lim_{N\to\infty, dh\to 0} \sum_{i=-N}^{N} \Delta x_i j(x_i) \div \sum_{i=-N}^{N} \Delta x_i. \tag{8}$$

Thus if $F(h)$ is the previous integrable function,

$$\lim_{T\to\infty} \frac{1}{2T} \int_{-T}^{T} F(h(x))j(x)dx = \int_{-\infty}^{\infty} W(h)J(h)F(h)dh.$$

Similarly, one can loosely define a more complicated $J(h; h', \Delta)$ as the average value of $j(x)$ when $h(x) = h$ *and* when $h(x+\Delta) = h'$. (For further generality and complication, one could define a probability density for $j(x)$: $W(j, h)dj$ is the probability that $j(x)$ lies between j and $j+dj$ when $h(x) = h$, and so forth.) For consistency we must have, for all Δ,

$$J(h) = \int_{-\infty}^{\infty} J(h; h', \Delta)P(h'; h, -\Delta)dh'. \tag{9}$$

To introduce statistics into (6), we first rewrite it by using (5) and factoring out $\exp(ikx\cos\theta)$:

[1] Lawson and Uhlenbeck, "Threshold Signals," Radiation Laboratory Series, M.I.T., Cambridge, Mass., vol. 24, chap. 3; 1950.

$e^{-ikh(x)\sin|\theta|}$

$$+\int_{-\infty}^{\infty} j(x+\Delta)e^{ik\Delta\cos\theta}G[\Delta, h(x); 0, h(x+\Delta)]d\Delta = 0.$$

Now this must hold whenever $h(x) = h$, i.e., at each point x_i of Fig. 1. Thus

$$0 = (2N+1)e^{-ikh\sin|\theta|} + \int_{-\infty}^{\infty} e^{ik\Delta\cos\theta}d\Delta \cdot$$

$$\cdot \sum_{i=-N}^{N} j(x_i+\Delta)G[\Delta, h; 0, h(x_i+\Delta)].$$

Dividing by $(2N+1)$ and letting $N\to\infty$, we get

$$0 = e^{-ikh\sin|\theta|} + \int_{-\infty}^{\infty} d\Delta \int_{-\infty}^{\infty} dh' e^{ik\Delta\cos\theta} \cdot$$

$$\cdot P(h'; h, -\Delta)J(h'; h, -\Delta)G[\Delta, h; 0, h']. \quad (10)$$

This relation does not suffice to determine $J(h; h,'x)$, a function of three independent variables. Thus additional relations in $J(h; h', x)$ are required, and are found from (7).

But before expressing (7) statistically, we should first list some properties of the average scattered field. In the first place, it is rather obvious that the average reradiated *field* above the surface is of the form $R\exp(ikx\cos\theta + iky\sin|\theta|)$, and below the surface, of the form $T\exp(ikx\cos\theta - iky\sin|\theta|)$, where $T=-1$ to satisfy (7). For we may first consider that portion of the field reradiated by currents lying between the horizontal dotted lines of Fig. 1. We can calculate this field at some point (x, y) far above the surface by Fresnel zone methods, and by further increasing y, we can make the Nth Fresnel zone arbitrarily long, so long, in fact, that the effective current-density in the zone approaches $J(h)W(h)dh$ arbitrarily closely. The result of the Fresnel zone calculation is then

$$\frac{i}{2k\sin|\theta|} W(h)dhJ(h)e^{-ikh\sin|\theta|}e^{ik(x\cos\theta+y\sin|\theta|)}.$$

Adding the fields from all similar horizontal strips, we get

$$R = \frac{i}{2k\sin|\theta|}\int_{-\infty}^{\infty} J(h)W(h)dh\, e^{-ikh\sin|\theta|}. \quad (11)$$

Similarly, for large negative y we get

$$T = \frac{i}{2k\sin|\theta|}\int_{-\infty}^{\infty} J(h)W(h)dh = -1. \quad (12)$$

The latter equation obviously does not contain sufficient additional information to determine either $J(h)$ or, when combined with (9) and (10), to determine the more general $J(h; h', x)$.

For further information we use the fact that, below the surface, no power flows in *any* direction. To calculate the power flux per unit angle, traveling in a direction ϕ, per unit length of surface, we first write, in terms of $j(x)$, the flux P scattered from a length $2T$ of surface.

$$Pd\phi = d\phi C\int_{-T}^{T} j(x)e^{ikx\cos\theta}e^{-ikh(x)\sin\phi}e^{-ikx\cos\phi}dx$$

$$\cdot\int_{-T}^{T} j^*(x')e^{-ikx'\cos\theta}e^{ikh(x')\sin\phi}e^{ikx'\cos\phi}dx'.$$

Here C is a proportionality constant, j^* represents the complex conjugate of j, the asymptotic expansion of G has been used, and k is considered real. Now we divide both sides by $2T$ and let $T\to\infty$, thus obtaining average power flux at angle ϕ per unit angle per unit length equals

$$C\int_{-\infty}^{\infty}\int_{-\infty}^{\infty}\int_{-\infty}^{\infty} J(h; h', \Delta)J^*(h'; h, -\Delta)W(h, h', \Delta)dhdh'd\Delta$$

$$\cdot e^{ik\Delta(\cos\phi-\cos\theta)}e^{ik(h'-h)\sin\phi}. \quad (13)$$

This is an approximation, not an equality, as the average of a product is not necessarily equal to the product of the averages of the factors. The reason we are forced to this approximation is that we wish further specification of $J(h; h', x)$ and do not wish to consider more complicated averages involving $j(x)$. When $0<\phi<-|\theta|$ and when $-|\theta|<\phi<-\pi$, (13) must vanish, or, on the average, energy is transmitted through the continuous, perfectly conducting surface. This is the further restriction on $J(h; h', x)$. (The case $\phi=\theta$ has already been considered in (12).)

In the opinion of the writer, the system of integral expressions (9), (10), (12), and (13) (equated to zero for negative $\phi\neq\theta$) can be solved for $J(h; h', x)$ uniquely, in principle. The aim so far has been to show the possibility of mathematically formulating the problem of finding a statistical description of the fields reflected by a statistically described surface (i.e., of statistically determining the currents induced in the surface). The resulting mathematical problem seems formidable, and we now resort to formidable approximations to reach a solution in a particular case. We replace $J(h; h', x)$ by $J(h)$ and write down the resulting equations in order of decreasing exactitude.

$$\frac{i}{2k\sin|\theta|}\int_{-\infty}^{\infty} J(h)W(h)dh = -1. \quad (14)$$

(Equation (12) was exact.)

$$0 = e^{-ikh\sin|\theta|} + \int_{-\infty}^{\infty}\int_{-\infty}^{\infty} d\Delta dh' P(h'; h, -\Delta)\cdot$$

$$\cdot J(h')G[\Delta, h; 0, h']. \quad (15)$$

(Equation (10) was exact.)

$$P(\phi) = C\int_{-\infty}^{\infty}\int_{-\infty}^{\infty}\int_{-\infty}^{\infty} dhdh'd\Delta J(h)J^*(h')W(h, h', \Delta)\cdot$$

$$\cdot e^{ik\Delta(\cos\phi-\cos\theta)}e^{ik(h'-h)\sin\phi}$$

$$= \begin{cases} \psi_{\text{total}} & 0 < \phi < \pi \\ 0, & -\pi < \phi < 0; \phi \neq \theta. \end{cases} \quad (16)$$

(Equation (13) was approximate.)

In the integrals of (15) and (16), it is effectively assumed that the current density in a surface element at height h is always $J(h)$, regardless of whether the element is illuminated or shadowed by other portions of the surface. Thus we have made a major physical concession in order to simplify the mathematical expressions. In this regard, it is again the opinion of the writer that (14) and (16) can be solved for $J(h)$. But now (15) is an integral equation completely specifying $J(h)$; the consistency of these equations is still an open question.

To dodge this question, we use a slight modification of Schwinger's variational principle.[2] Let us multiply both terms of (15) by $J(h)W(h)$ and integrate with respect to h over $(-\infty, \infty)$. Thus, from (1) and (11) we have

$$-i2k\sin|\theta|\,R + \int_{-\infty}^{\infty}\int_{-\infty}^{\infty} dhdh'J(h)J(h')\cdot \cdot \int_{-\infty}^{\infty} W(h, h', \Delta)G[\Delta, h; 0, h']d\Delta = 0, \quad (17)$$

or

$$R\int_{-\infty}^{\infty}\int_{-\infty}^{\infty} dhdh'J(h)J(h')\cdot \cdot \int_{-\infty}^{\infty} W(h, h', \Delta)G[\Delta, h; 0, h']d\Delta\cdot = \frac{-i}{2k\sin|\theta|}\left\{\int_{-\infty}^{\infty} J(h)W(h)e^{-ikh\sin|\theta|}dh\right\}^2. \quad (18)$$

The last equation may seem a trivial consequence of (17) and (11), but it provides an excellent formula for calculating an approximate R from an approximate J. Furthermore, since J appears quadratically on both sides, we get the same R from, for example, $7J$ as from J. This means that (14) can be satisfied automatically merely by multiplying, by a suitable constant, whatever J is used to calculate R. Finally, (16) may not be satisfied for negative ϕ, but can perhaps be used as a criterion of accuracy.

We now try to apply some of the foregoing mathematical apparatus to a surface for which $h(x)$ varies so slowly with x that, in the neighborhood of each x, the surface is approximately a plane parallel to the x axis. Then to a first approximation, the induced current $j(x)$ is $J_0\exp(-ikh(x)\sin|\theta|) = J_1[h(x)]$, where J_0 is the current that would have been induced in the perfectly reflecting x-axis, for which the reflection coefficient is -1. Thus from (11) and (2),

$$\frac{R_1}{-1} = \frac{\int_{-\infty}^{\infty} e^{-i2kh\sin|\theta|}W(h)dh}{\int_{-\infty}^{\infty} W(h)dh},$$

or

$$R_1 = -\exp\left[-2k^2\bar{h}^2\sin^2\theta\right]. \quad (19)$$

(This result was derived by Pekeris and, independently, by MacFarlane during World War II.) Now J_1 satisfies (14) since J_0 satisfied the corresponding equation for the plane surface. If J_1 is substituted into (16), the integrand is an even function of ϕ times the phase-factor $\exp[ik(h'-h)(\sin\phi + \sin|\theta|)]$; here the phase changes more rapidly with $(h'-h)$ when, for example, $\phi=A>0$ than when $\phi=-A$. Through this fact, it is apparent that $P(A)<P(-A)$. This means that, by using J_1, one predicts that more power flows *through* the surface at nonspecular angles than the surface reflects at nonspecular angles. Thus we have used (16) qualitatively to show that J_1 is a poor approximation to $j(x)$.

Although $\rho(x)$ does not appear in (19), there are still things to be said in favor of this formula. We know that, regardless of the form of $\rho(x)$, the surface becomes perfectly reflecting both at extreme grazing incidence ($\theta\cong 0$) and when the mean-square surface height, measured in wave-lengths, becomes small compared with unity ($k^2\bar{h}^2 \ll 1$). R_1 satisfies both requirements.

To use (16) quantitatively, we need a specific expression for $\rho(x)$. Here the most convenient forms seem to be $\rho(x)=e^{-ax^2}$, appropriate to white noise filtered by a conventional narrow-band filter, or $\rho(x)=e^{-b|x|}$, which is more appropriate to the velocity of a particle in Brownian motion.[3] The writer is unable to perform the Δ-integration of (16), using either of these forms. In trying to get an improved estimate of R by substituting J_1 into (18), one finds similar difficulties with the integral on the left.

Now we discuss the validity of the R_1 of (19) as an approximation to the specular reflection coefficient of the rough surface. The same expression is obtained if the incident plane wave is considered as a bundle of rays, if all such rays bounce off the surface in the specular direction, and if all reflected rays are added in the phase appropriate to the heights above the x-axis of their points of reflection. This ray-picture applies when the surface height varies extremely slowly, i.e., when $\rho(x)\cong 1$ for very large x. As the integrals (16) and (18) have eluded approximate evaluation, there is presently no specification of "extremely slowly" or "very large."

[2] N. Marcuvitz, "Waveguide Handbook," Radiation Laboratory Series, M.I.T., Cambridge, Mass., vol. 10, p. 143, 1951.

[3] S. Chandrasekhar, "Stochastic problems in physics and astronomy," *Rev. Mod. Phys.*, vol. 15, no. 1, pp. 1–89; January, 1943.

Concluding Remarks

We have approached the two-dimensional problem of finding the specular reflection coefficient R of a perfectly conducting surface which is specified statistically through a mean-square height $\bar{h}^2$ and an autocorrelation function $\rho(x)$. Through a series of approximations, we have obtained an expression of R through the variational formula (18). This formula will be useful for calculating R from approximate average current densities J when methods of evaluating the integral on the left are found. In the absence of such methods, we are unable to estimate the error made in using the approximation (19) for R, in which $\rho(x)$ does not appear at all.

Transmission Loss in Radio Propagation*

KENNETH A. NORTON†, FELLOW, IRE

Summary—**The utility of the concept of transmission loss in radio-propagation analysis is explored. The transmission loss of a radio system is defined to be the ratio of the power radiated from the transmitting antenna to the resulting signal power available from a loss-free receiving antenna. After discussing some methods of measuring transmission loss, its calculation for representative systems is discussed. It is shown that a measure of transmission loss often adopted, namely the attenuation relative to the free-space value, sometimes leads to errors and confusion in the presentation of the results of measurements and in applications to radio systems; the use of the over-all transmission loss of a system avoids these pitfalls.**

A discussion is given of the expected variation with time (fading) of the transmission loss expected for radio systems involving ionospheric or tropospheric propagation. This discussion involves the theory of the Rayleigh distribution and its limitations in such applications.

A definition is then derived for the effective noise figure of a radio system which includes the external noise picked up on the receiving antenna. This definition is used to explain the method of determining the maximum range of a radio system.

Finally a discussion is given of the maximum range of a radio system as limited by interference from other radio signals plus noise rather than from noise alone.

1. Introduction

THE PURPOSE of this paper is to point out the advantages of the use of the concept of transmission loss in studies of radio wave propagation and in the application of the results of these studies to the engineering of successful radio communication, navigation, and control systems.

It is convenient to define the "transmission loss" in a radio system involving propagation between antennas to be the ratio of the power radiated from the transmitting antenna divided by the resulting signal power available from an equivalent loss-free receiving antenna.

$$\text{Transmission loss} \equiv \frac{\text{power radiated from the transmitting antenna}}{\text{resulting signal power available from the loss-free receiving antenna}} \equiv (p_r/p_a). \quad (1)$$

We see that the transmission loss of a system is a dimensionless number greater than unity and that it will often be convenient to express this in decibels, i.e., ten times the logarithm to the base 10 of the ratio given by (1). The transmission loss, L,[1] expressed in decibels, is thus always positive:

$$L = 10 \log_{10} p_r - 10 \log_{10} p_a \equiv P_r - P_a. \quad (1(a))$$

This particular choice of definition excludes from "transmission loss" the transmitting- and receiving-antenna circuit losses[2] and any loss which occurs in any transmission lines which may be used between the transmitter and the transmitting antenna or between the receiving antenna and the receiver. This exclusion appreciably increases the difficulty in measuring the transmission loss, particularly at the lower frequencies, but has the advantage that it results in a measure of loss which is attributable solely to the transmission medium including the effective gains of the transmitting and receiving antennas. We will see in what follows that the greatest advantage in the use of this concept of transmission loss arises simply from the fact that it does lump together the gains and losses arising from these three components of the system: the transmitting antenna, the transmission medium, and the receiving antenna. Much complication and confusion in measuring and expressing the results of radio-propagation studies often arises from an attempt to separate the effects of these three system components. It will be shown that this separation is often practically impossible although, whenever feasible, it does have considerable advantage over the above lumped concept of transmission loss.

Although apparently dependent upon the transmitter power, the "transmission loss" is actually independent of the power used since this transmitter power is contained as a factor in the received power. (See Section 3.)

Before discussing some of the advantages of this concept of transmission loss in more detail, it will be ad-

* Decimal classification: R112×R247. Original manuscript received by the Institute, November 11, 1952.

† National Bureau of Standards, Boulder, Col.

[1] Throughout this paper capital letters will be used to denote the ratios, expressed in decibels, of the corresponding quantities designated with lower-case type.

[2] Antenna circuit loss includes the ground losses arising from the induction field of the antenna, but excludes those due to the radiation field.

vantageous to describe the methods of measuring it and of calculating its expected value in various representative systems.

2. Measurement of Transmission Loss

One of the principal advantages of the use of transmission loss as a measure of the characteristics of a radio system is the comparative ease and precision with which it may be measured. Thus, it is only necessary to measure separately the numerator and denominator of (1) and then determine their ratio.

The power radiated from the transmitting antenna is simply equal to

$$p_r = i^2 r_a, \tag{2}$$

where p_r is expressed in watts, i in amperes, and r_a in ohms; i is the transmitting antenna current and r_a its radiation resistance, both determined at the same point, ordinarily at the input terminals. When (2) is used for determining p_r, it will be necessary to calculate, rather than measure, the value of r_a unless the antenna circuit losses may be considered to be negligibly small. In some cases it will be more convenient to measure the power input, p_i, by replacing the transmitting antenna with a calorimeter (water-cooled dummy load) of the same impedance as that of the input terminals of the transmitting antenna and then measuring the radio frequency power absorbed by the calorimeter; the radiated power, p_r, is then determined by subtracting the thermal power lost in the antenna circuit from p_i. In practice it may be more convenient to place the calorimeter near the transmitter and separately measure or calculate the power lost in the transmission line. Summarizing the above, if we let P_t denote the actual transmitter power expressed in decibels above one watt and measured at the input terminals of the transmitting antenna transmission line, and if we let L_t, expressed in decibels, denote the transmitting-antenna circuit losses together with the transmitting-antenna transmission-line losses, then

$$P_r = P_t - L_t. \tag{3}$$

The signal power available from an equivalent loss-free receiving antenna will usually be measured differently in those cases (usually at frequencies above, for example, 2 mc) where the antenna is not grounded and the antenna circuit losses are negligibly small, and in those cases (usually vertical polarization at frequencies below 2 mc) where the antenna is grounded and thus subject to appreciable circuit loss.

The high-frequency case is simplest; the signal power available from the receiving antenna is usually measured by (1) tuning out the receiving-antenna reactance, (2) matching the receiving-antenna radiation resistance to the signal-generator output resistance, and (3) using a radio-frequency voltmeter to compare the signal voltage from the receiving antenna with that from the signal generator. When these two voltages are made equal, the signal power available from the receiving antenna is given by

$$p_a = \frac{v_0^2}{4r_g} \tag{4}$$

(applicable when antenna circuit losses are negligible), where p_a is expressed in watts, v_0 in volts, and r_g in ohms; r_g is the resistance of the signal generator output, and v_0 is its open-circuit voltage.[3] Equation (4) is strictly applicable, of course, only when the receiving-antenna circuit losses are negligible; but this is a valid assumption for a wide range of applications. These circuit losses include, of course, those associated with the transformer used to match the receiving-antenna radiation resistance to that of the signal generator.

At the lower frequencies, particularly when grounded receiving antennas are used, the signal power available from a loss-free antenna will usually be considerably greater than that available at the input to the receiver, and various methods are available for making the measurements in this case. A good discussion of this problem is contained in a recent report prepared by Crichlow.[4] At these lower frequencies it has been common practice to express the results of measurements of the signal power available from an equivalent loss-free receiving antenna in terms of microvolts per meter. The intimate relation between these two essentially equivalent quantities is discussed in Section 3, and advantages of the available received-signal-power concept explained.

The radio-frequency voltmeter used in comparing the received and the signal-generator voltages is ordinarily simply a receiver with its output circuits so arranged that it is possible to compare input signals with levels varying throughout the range expected with the system under test. When the received signal power is varying in intensity (fading), it is often convenient to record the receiver output, and thus the transmission loss, on a meter which may be calibrated directly, by means of the signal generator, in terms of the signal power available from the receiving antenna. In fact, since the transmitter power is usually constant, the calibration may often be conveniently expressed simply in terms of transmission loss. It should be noted that it is not necessary to match the receiver to the antenna. In fact, if the receiver has a good noise figure, and adequate gain, it will usually be desirable at frequencies greater than 100 mc to over-couple the receiver to the antenna since this will improve its ability to measure weak signals.[4,5]

At frequencies below about 100 mc, atmospheric and cosmic noise will be mixed with the signal of the transmission system for which the loss is being measured,

[3] Some signal generators read directly in open-circuit voltage, while the scale on others gives the value of $v_0/2$.

[4] W. Q. Crichlow, "The Effects of Antenna Circuit Loss, Receiver Noise and External Noise on Radio Reception in the Frequency Band from 50 to 5000 Kilocycles," National Bureau of Standards, Central Radio Propagation Laboratory Report 4-4; May 3, 1948.

[5] H. T. Friis, "Noise figures of radio receivers," Proc. I.R.E., vol 32, pp. 419–422; July, 1944.

and this noise power must be subtracted from the recorded signal-plus-external noise-power output from the receiving antenna. This external noise power may be measured with the transmitter off the air. This correction will, of course, only be of consequence when the received signal power is of the same order of magnitude, or less than, the received external noise power. An alternate procedure for eliminating the effects of this external noise is to introduce the calibrating signal from the signal generator in parallel with the receiving antenna and with the transmitter off the air. With this method of measurement the signal generator is left in the circuit and simply turned off when the transmitter is turned on for a transmission-loss measurement. Under these circumstances (4) directly represents the proper calibration for the signal power alone which is available from the receiving antenna rather than the signal-plus-external noise power. The signal-plus-external noise power available to the comparison voltmeter will be 3 db less with this latter method of calibrating; but this loss in resolving power of the receiver will often be unimportant since the external rather than the receiver noise will be the limiting factor under many circumstances for which this method of calibration would be indicated. This loss in resolving power may be avoided by a variation of this method in which the signal generator is loosely coupled across the antenna for a calibration in the presence of the noise with the transmitter off the air; the absolute values from the loosely coupled signal generator are then established by a calibration in which the antenna is replaced by the signal generator. The above methods of measurement are valid only under the assumption that the external noise power during the time the transmitter is off the air is the same as it is during the time of reception of the desired signal. In those cases for which it is inconvenient to turn the transmitter off for an external noise measurement, it may be practicable to tune the receiver to an adjacent signal-free channel for a measurement of the external noise level.

Examples of the application of the transmission-loss concept to analyses of experimental data are given by Chambers, Herbstreit, and Norton[6] and by Norton.[7]

3. Expected Transmission Loss for Representative Systems

An idealized, perfectly conducting, isotropic transmitting antenna in free space produces a field intensity of $p_r/4\pi d^2$ watts per square meter at a distance d, expressed in meters. The absorbing area of a perfectly conducting, isotropic receiving antenna in free space is equal to $\lambda^2/4\pi$ square meters, where λ is the free-space wavelength expressed in meters or $\lambda = 299.79/f_{mc}$, with f_{mc} equal to the radio frequency expressed in mc per second. The signal power available from such a receiving antenna is thus $p_r\lambda^2/(4\pi d)^2$ and the transmission loss for this basic system is

$$\left.\begin{array}{l}\text{transmission loss for perfectly conducting, isotropic transmitting and receiving antennas separated a distance, } d, \text{ in free space}\end{array}\right\} = (4\pi d/\lambda)^2. \quad (5(a))$$

The above equation is applicable at distances $d \gg \lambda$.[8]

If we let L_b denote the transmission loss of this basic system, we may write

$$L_b = 20 \log_{10} d + 20 \log_{10} f_{mc} - 27.552, \quad (5(b))$$

or

$$L_b = 20 \log_{10} D + 20 \log_{10} f_{mc} + 36.581, \quad (5(c))$$

where D is the distance expressed in miles.

For a system in which the transmitting and receiving antenna effective gains are G_t and G_r db relative to a perfectly conducting isotropic antenna and for which the propagation path attenuation is A db relative to the free-space value, the expected system transmission loss will be

$$L = L_b - G_t - G_r + A. \quad (6)$$

It is of interest to see how the above simple concept of transmission loss is related to the more complex procedures sometimes adopted in radio-propagation studies. Usually, a determination is first made of the "effective radiated power" of the transmitter; expressed in db above one watt this is simply equal to $(P_r + G_t) \equiv (P_t - L_t + G_t)$. Similarly, at the receiver a measurement is usually made of w, the field intensity in watts per square meter, i.e., the square of the field strength in volts per meter divided by the impedance, z, of free space; expressed in db above one watt per square meter, this is simply equal to

$$W \equiv P_a + 10 \log_{10} (4\pi/\lambda^2) - G_r. \quad (7)$$

The attenuation factor, A, for the propagation path under consideration relative to free-space transmission may now be determined by subtracting the field intensity, W,[9] and the free-space attenuation loss $10 \log_{10} (4\pi d^2)$ from the "effective radiated power,"

$$\begin{aligned} A &= P_r + G_t - W - 10 \log_{10} (4\pi d^2), \quad (8(a)) \\ &= P_r + G_t - P_a + G_r - 10 \log_{10} (4\pi/\lambda^2) \end{aligned}$$

[6] G. R. Chambers, J. W. Herbstreit, and K. A. Norton, "Preliminary Report on Propagation Measurements from 92-1046 Mc at Cheyenne Mountain, Colorado," National Bureau of Standards Report No. 1826; July 23, 1952.

[7] K. A. Norton, "Transmission Loss of Space Waves, Propagated Over Irregular Terrain," Trans. IRE Professional Group on Antennas and Propagation, No. PGAP-3, August, 1952; Also published as National Bureau of Standards report No. 1737; June 16, 1952.

[8] At very short distances ($d \ll \lambda$), the induction field exceeds the radiation field, for which (5(a)) is computed, by the factor $(\lambda/2\pi d)^2$, and thus in this region the transmission loss should be equal to $4(2\pi d/\lambda)^4$. Note, however, that this implies a negative transmission loss, i.e., a gain, at distances $d/\lambda < 2\pi\sqrt{2}$, and we conclude that our formula will be inapplicable at such short distances, presumably because of interaction between the transmitting and receiving antennas.

[9] If we let E denote the field strength expressed in db above 1 μv per meter, then $W = E - 120 - 10 \log_{10} z = E - 145.760$; thus we see the intimate relation between the field intensity in watts per square meter and the field strength in microvolts per meter.

$$- 10 \log_{10} (4\pi d^2), \quad (8(b))$$

$$= L + G_t + G_r - L_b. \quad (8(c))$$

Upon comparison, we see that (6) and (8(c)) are identical.

Thus, in those cases where it is feasible to determine the effective values of the transmitting- and receiving-antenna gains,[10] G_t and G_r, (8) may be used for the determination of A, the path attenuation relative to free space. However, it becomes impossible to separate the transmitting- and receiving-antenna gains from the transmission loss under some operating conditions, such as when the transmission takes place by scattering in the troposphere or when multipath signals are present in the case of ionospheric propagation. Under these circumstances it will be shown below that the only values which can be measured are the values of P_r and P_a; thus neither L_b nor A can be determined separately, and we must be satisfied simply with a value for the effective transmission loss, L.

A good discussion of the impropriety of expressing the results of the received scattered signal power in terms of field intensities and effective radiated powers has been given by Schott.[11]

Consider as an example the signal power available from the receiving antenna for a transmission system involving different transmission paths through the ionosphere. Let d_j denote the distance and a_j the voltage-attenuation factor corresponding to the jth ionospheric path, and let g_{tj} and g_{rj} denote the power gains of the transmitting and receiving antennas for this path. The effects of ground reflection at each terminal are most conveniently included in g_{tj} and g_{rj}. Assuming a variable relative phase relation for the signals received on the various paths, the average signal power available from the receiving antenna in this case will be equal to

$$\bar{p}_a = p_r \lambda^2 \sum_{j=1}^{m} a_j^2 g_{tj} g_{rj} / (4\pi d_j)^2. \quad (9)$$

The above is simply a generalization of the antilogarithmic form of (6), and is obtained by adding the signal powers available from the m separate paths. The average transmission loss for this case is thus equal to

$$L_a = - 10 \log_{10} \left[\lambda^2 \sum_{j=1}^{m} a_j^2 g_{tj} g_{rj} / (4\pi d_j)^2 \right]. \quad (10)$$

It is important to notice that the distance as well as the transmitting- and receiving-antenna gains are inextricably combined under the summation sign, and it is thus impossible to separate out either an inverse distance factor or the values of the "effective radiated power" and of the received field intensity. Under some circumstances it may, of course, be possible to resolve the separate modes of propagation by means of pulses and, in this case, the free space and path attenuations may, in principle, be determined separately for each mode. Usually, however, this cannot be done very satisfactorily with pulses, and it is, of course, impossible with continuous wave transmissions. Consequently, comparison between theory and observation may be made in this continuous wave case only between the calculated and measured values of the instantaneous and of the average transmission losses.

As another example, consider the formula for the average transmission loss for propagation via scattering in a turbulent atmosphere.

$$L_a = - 10 \log_{10} \left[\lambda^2 \int \frac{g_t g_r \sigma}{(4\pi r_0)^2 r^2} dv \right], \quad (11)$$

where the integration is to be taken over the volume of that part of the turbulent atmosphere which is both illuminated by the transmitting antenna and is within line of sight of the receiving antenna; r_0 and r are the distances of the volume element dv from the transmitting and receiving antennas, respectively, and σ represents the scattered power per unit solid angle, per unit incident power density, and per unit element of volume. A discussion of the derivation of (11) has been given by Booker and Gordon;[12] an amplification and clarification of this derivation have been given by Staras.[13] The application of this theory to the explanation of tropospheric fields at large distances is developed in a paper by Herbstreit, Norton, Rice, and Schafer.[14] Here again it will be observed that the antenna gains and the distance are inextricably combined under the integral sign. Thus, only the over-all instantaneous or average transmission losses can be measured and compared with the results to be expected from theory.

4. Expected Variations of Transmission Loss with Time

The instantaneous signal power available on long circuits involving transmission through the ionosphere or troposphere will vary with time (i.e., fade) due, in part, to phase interference between the components arriving along the various transmission paths. Over short periods of time, during which transmission conditions may be regarded as constant, the instantaneous power of a radio signal may, in some cases, be regarded as distributed in

[10] These antenna gains are the free-space, plane wave front, values. They may be calculated values or may be measured by determining the transmission loss at short distances where A may be calculated, or by comparing the transmission loss over an appropriately chosen path with that from a standard antenna such as a half-wave dipole.

[11] F. W. Schott, "On the response of a directive antenna to incoherent radiation," Proc. I.R.E., vol. 39, pp. 677–680; June, 1951.

[12] H. G. Booker and W. E. Gordon, "A theory of radio scattering in the troposphere," Proc. I.R.E., vol. 38, pp. 401–412; April, 1950.

[13] H. Staras, "Scattering of Electromagnetic Energy in a Randomly Inhomogeneous Atmosphere," National Bureau of Standards Report No. 1662; May 12, 1952; *Jour. App. Phy.*, vol. 23, pp. 1152–1156; October, 1952.

[14] J. W. Herbstreit, K. A. Norton, P. L. Rice, and G. E. Schafer, "Radio wave scattering in tropospheric propagation," submitted for later possible publication in Proc. I.R.E..

a Rayleigh distribution,[15] to a good approximation. This gives

$$Q(p_a > y) = 100 \exp(-y/\bar{p}_a), \qquad (12)$$

where p_a is the instantaneous power, $\bar{p}_a$ is the average power, and Q is the percentage of time that the instantaneous power exceeds some given value y.

The above short-time distribution is applicable only in those cases for which the signal power available from no one of the transmission paths is comparable to, or large in comparison to, the sum of the powers from the other components. In particular, then, it will not be applicable in that range of distances where one of the received-signal components consists of a comparatively strong ground wave. Appropriate distribution curves for this latter case are given in a recent paper by the author and applied to the case of tropospheric propagation.[16] Such modified distribution curves have also been used by Vandivere[17] for an explanation of the variations in the transmission loss of a combined ground wave and ionospheric wave and by Norton[18] in the case of the ground-reflected wave in air-to-air propagation over rough terrain; in this latter case the large component was identified with a wave specularly reflected from the ground, and it was found that this component increased with respect to the remaining scattered components as the transmission path approached grazing incidence.

It should be noted that the above probability distributions are to be expected only over those short periods of time for which the average power, $\bar{p}_a$, is constant and the fading is thus due only to phase interference. It has been found experimentally that $\bar{p}_a$ usually varies relatively slowly and, as a consequence, it is customary in the analysis of either ionospheric or tropospheric field intensities to determine the hourly median values of p_a which we may designate by p_h.

In those cases for which the Rayleigh distribution is applicable to the instantaneous distribution within the hour, i.e., for which the average received power is relatively constant during the hour and for which there is no single strong component, we may determine the relation between p_h and $\bar{p}_a$ by setting $Q=50$ and $y=p_h$ in (12) and solving for the ratio $(p_h/\bar{p}_a)$. Thus we find for this case that $p_h=(\log_e 2)\bar{p}_a=0.69315\ \bar{p}_a$, that is, the average power in a Rayleigh distributed received field will be 1.5915 db greater than the median power or, alternatively, that the average transmission loss will be 1.5915 db less than the median transmission loss.

It has been determined experimentally that the hourly median ionospheric or tropospheric fields, p_h, for a given time of day and a given season of the year are log-normally distributed.[19,20] For example, if we study the distribution of the 30 daily values of p_h determined for 8 to 9 p.m. in June, it is found that these values will appear to be samples from a log-normal population of such values. It follows directly from this that the median transmission loss, L_h, expressed in db, is normally distributed for such samples; thus a complete description of the expected distribution of the hourly median (or average) transmission loss for a specified time of day and season of the year can be given in terms of the two parameters, the median (of the hourly medians from day to day) and the standard deviation (of these hourly medians), both expressed in db.

5. Applications of the Transmission-Loss Concept to the Solution of Systems Problems

One of the principal applications of transmission-loss data or theory is for the determination of the maximum effective range of a radio system. This maximum range is determined when the desired signal becomes so weak that it becomes obscured by the presence of noise or of other types of interference.

Consider first the effect of noise. This is most readily developed by means of a generalization[21] of Friis'[5] definition of the noise figure of a radio receiver. Consider the network of Fig. 1. It will be convenient to compare the desired signal power with the noise power in network (a), i.e., in the loss-free receiving antenna. We write p_n

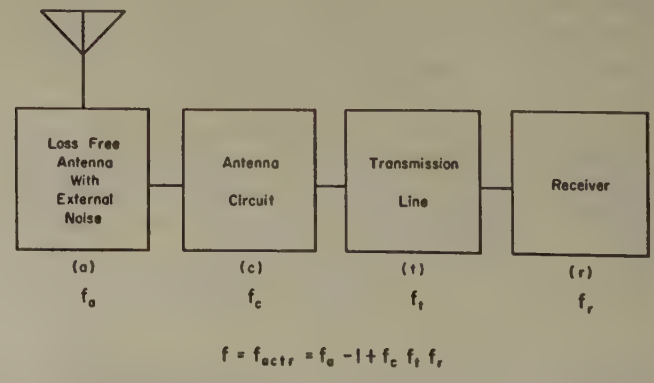

Fig. 1—Network for definition of f, the effective receiver noise figure.

[15] Lord Rayleigh, "On the resultant of a large number of vibrations of the same pitch and of arbitrary phase," *Phil. Mag.*, vol. 10, pp. 73–78; August, 1880; and vol. 27, pp. 460–469; June, 1889. See also, "Theory of Sound," 2nd ed., paragraph 42a; 1894; *Scientific Papers*, "On the problem of random vibrations and of random flights in 1, 2 or 3 dimensions," vol. 1, p. 491. Lord Rayleigh, *Phil. Mag.*, vol. 37, pp. 321–347; April, 1919.

[16] K. A. Norton, "Propagation in the FM Broadcast Band," "Advances in Electronics," Academic Press, Inc., New York, N. Y., vol. I, pp. 406–408; 1948.

[17] E. F. Vandivere, "Some Notes on Probability Functions and Distributions," Appendix to the report of Federal Communications Commission Committee III in preparation for the Clear Channel Hearing, Docket 6741.

[18] K. A. Norton, "Propagation Over Rough Terrain," Report of Symposium on Tropospheric Wave Propagation, U. S. Navy Electronics Laboratory, San Diego, Cal., pp. 101–105; July 1949.

[19] N. Smith and M. B. Harrington, "The Variability of Sky-Wave Field Intensities at Medium and High-Frequencies," National Bureau of Standards Report CRPL-1-6; April 15, 1948.

[20] Report of the Ad Hoc Committee for the Evaluation of the Radio Propagation Factors Concerning the Television and Frequency-Modulation Broadcasting Services in the Frequency Range Between 50 and 250 Mc, Federal Communications Commission Mimeo Nos. 36728; May 26, 1949; 36830; May 31, 1949; and 54382; July 7, 1950.

[21] K. A. Norton and A. C. Omberg, "The maximum range of a radar set," Proc. I.R.E., vol. 35, pp. 4–24; January, 1947.

for the average external noise power[22] in such an antenna and set

$$p_n \equiv f_a ktb \text{ (watts)}, \tag{13}$$

where k is Boltzmann's constant and is equal to 1.38×10^{-23}, t is the absolute temperature in degrees K, and b is the effective bandwidth in cycles per second as defined by Friis.[5] Thus (13) effectively defines the noise figure, f_a, of network (a). Network (c) has a noise figure, f_c, where f_c is a number greater than 1 which is simply the loss factor of the antenna circuit. Similarly, the transmission-line loss is equivalent to a noise figure, f_t, which is also a number greater than 1. Finally, we may denote the noise figure of the receiver itself by f_r. Using Friis' method for combining the noise figures of several networks in tandem, we obtain for the effective noise figure at the input to the loss-less receiving antenna,

$$f \equiv f_{actr} = f_a - 1 + f_c f_t f_r. \tag{14}$$

Finally, if we write r for the minimum signal-to-noise power ratio which will provide a satisfactory reception, then the minimum signal power available at the terminals of the receiving antenna which will provide satisfactory reception may be expressed,

$$p_m = rfktb \text{ watts}. \tag{15}$$

Expressed in db, (15) becomes

$$P_m = R + F + B - 204, \tag{16}$$

where $R\equiv10\log_{10} r$, $F=10\log_{10} f$, $B=10\log_{10} b$, and t is taken as 288.48° K (60° F).[23]

The transmitter power, P_t, required for satisfactory reception with a given transmission loss, L, may now be expressed;

$$P_t = L + L_t + P_m = L + L_t + R + F + B - 204. \tag{17}$$

For the basic free-space system we may substitute L_b, as given by (5c), for L, and we obtain

$$P_t = 20\log_{10} D + 20\log_{10} f_{mc} + L_t + R + F + B - 167.419. \tag{18}$$

The above equation demonstrates several basic characteristics of the power required for communication between isotropic antennas in free space, i.e., its dependence on distance, radio frequency, effective noise figure, and effective receiver bandwidth. Equation (18) may easily be generalized, in those cases for which this is appropriate, to actual antennas and a propagation path with attenuation, A, relative to the free-space value, by subtracting G_t and G_r and adding A (see (6)).

For a proper evaluation of F_r it is necessary to know the value of f_a; this has been given by Crichlow[4] (in his notation $f_a=\overline{EN}$) for atmospheric noise as a function of radio frequency in the range 50 to 5,000 kc and for several geographical locations and seasons of the year. Using the results in a recent paper by Cottony and Johler,[24] values of f_a may also readily be determined for cosmic noise from their values of equivalent black-body temperatures of the cosmic noise; thus our f_a is simply their measured value of t divided by 288.48. It should be noted that f_a will usually be somewhat dependent upon the receiving antenna directivity, the published values of f_a quoted above corresponding to a vertical electric antenna for atmospheric noise, and a horizontal electric dipole for cosmic noise. It is interesting to note that f_a does not depend upon the receiving antenna gain in the case where the noise may be assumed to reach the antenna uniformly from all directions.

Consider next the problem of the limitation of service range due to interference from other radio signals. Let p_u be the available signal power from the loss-less receiving antenna arising from a transmission system other than the desired system. If we write r_u for the minimum signal-to-interference power ratio at the terminals of the loss-less receiving antenna which will provide satisfactory reception, then $p_a=r_u p_u$ at the maximum range of the system. It follows from this that the following relation must hold at the maximum range of the system:

$$L_d = L_u - R_u + P_{rd} - P_{ru}. \tag{19}$$

In the above $R_u\equiv\log_{10} r_u$ and the subscripts d and u refer to the desired and undesired systems, respectively. The above equation defines a service area within which satisfactory reception of the desired system may be expected provided noise is not a limiting factor, that is, provided $p_a\gg p_m$ throughout this service area. It is important to notice, provided $p_a\gg p_m$, that the interference-limited service area is independent of the absolute power used by either system, being dependent only on the ratio of the powers radiated from the transmitting antennas of the desired and undesired systems.

When m undesired signals of comparable magnitude are present and noise is also present in objectionable degree, an approximate determination of the minimum signal power, p_m', which will provide satisfactory reception may be determined from

$$p_m' = rfktb + \sum_{u=1}^{m} r_u p_u, \tag{20}$$

where r, and the several values of r_u, are to be measured

[22] At frequencies less than about 20 mc, this external noise will arise either from man-made sources or, more probably, from thunderstorms; in the range from 20- to 200-mc cosmic and solar sources, rather than thunderstorms, constitute the principal source of noise picked up by the antenna. At still higher frequencies the effects of external noise are usually negligible, the noise picked up by the antenna being a measure of the temperature of the atmosphere and the ground in the vicinity of the antenna.

[23] Friis suggested $t=290$, for which $kt=4\times10^{-21}$ watts per cycle bandwidth, whereas we have chosen $t=288.48°$ so that $-10\log_{10} kt=204$ db relative to 1 watt per cycle bandwidth.

[24] H. V. Cottony and J. R. Johler, "Cosmic radio noise intensities in the VHF band," Proc. I.R.E., vol. 40, pp. 1053–1060; September, 1952. Also published in somewhat greater detail as National Bureau of Standards Report No. 1098, August 3, 1951; For the present application, see Figs. 4, 6, 7, and 8 in the IRE paper or Figs. 7, 8, 9, 11, and 13 in the NBS report.

with these individual sources of interference present alone.[25] It should be noted that r and r_u have been so defined that they are independent of the transmission loss and depend only on the method of modulation and the characteristics of the receiving system, e.g., its selectivity and noise or interference suppression characteristics. Using this definition of p_m', we may write

$$P_{td} = L_d + L_{td} + P_m', \tag{21}$$

where $P_m' = 10 \log_{10} p_m'$ and the subscript d refers to the desired system.

For most radio systems it is satisfactory to determine an approximate effective service area as the region within which none of the sources of interference cause unsatisfactory reception when acting alone; such an approximate effective service area may be determined by separately solving (17) and then (19) for each undesired system. However, in the case of some systems involving a large number of interfering sources, this approximation may not be very satisfactory. An example illustrating the method of solution by means of the more complex (21) was developed in vol. II of the FCC Ad Hoc Committee[20] and a digest of this method was presented in a paper by Norton, Staras, and Blum.[26]

Discussions of some of the factors entering into the determination of values of R and of R_u appropriate for various types of radio systems are presented in the documents of the VIth Plenary Assembly of the CCIR.[27]

[25] Since interference of different types may affect the observer in different ways, (20) represents merely a convenient formal method of adding these effects. An example of a joint interference not even approximately represented by (20) would be two tone-modulated interfering transmissions, with the same carrier frequency, for which neither tone by itself appears in the pass band of the receiver but for which the beat note between the tones is very objectionable. It should be noted, however, that this is a very special case and that (20) will, for the more usual case of random types of interference, usually give results within, say, 1 db of the correct answer. In fact, in the limiting case where the several interfering sources are completely random in character and thus representable by white noise, (20) becomes exact.

Acknowledgments

The author wishes to acknowledge the assistance in the formulation of this paper of his colleagues, William Q. Crichlow and Ross Bateman. The methods of presentation of several aspects were developed in discussions with them.

[26] K. A. Norton, H. Staras, and M. Blum, "A Statistical Approach to the Problem of Multiple Radio Interference to FM and Television Service," Trans. IRE Professional Group on Antennas and Propagation, PGAP-1, pp. 43–49; February, 1952.

[27] Documents of the VIth Plenary Assembly of the International Radio Consultative Committee, Vol. I, Geneva, 1951, International Telecommunication Union, Geneva, Switzerland.

Calibrating Ammeters above 100 MC*

H. R. MEAHL†, SENIOR MEMBER, IRE AND C. C. ALLEN†, ASSOCIATE, IRE

Summary—**A survey is made of the progress to date in measuring current above 100 mc. The types of vacuum thermocouples available for ultra-high frequency current measurement are discussed and the several methods of calibration are reviewed. A calorimeter method and a thermistor bridge method are presented. The advantages and limitations of the calibrating methods are brought out. The electrodynamic method is particularly suited to large currents, the calorimeter method to medium currents, and the thermistor bridge method to small currents. The importance of obtaining agreement between methods that do not depend on the same principles is emphasized.**

I. Introduction

THE ACCURATE MEASUREMENT of current at frequencies above 100 mc per second is made difficult by the fact that an appreciable discontinuity is generally introduced into an uhf circuit by an instrument that would have a negligible effect on that circuit when operated at lower frequencies. In addition, the instrument itself may behave as a complex network because of increased inductive and decreased capacitive reactances in the instrument. The first difficulty must be overcome by careful attention to the placement and manner of connection of the instrument in the circuit. The second difficulty requires that the instrument be accurately calibrated to determine its usable frequency range.

This paper is concerned with methods of calibration for both large and small currents. It is possible to use large current instruments, which have been properly calibrated, directly in the power circuits of commercial equipment. The calibration for small currents has greater application in the use of measuring instruments, such as field-strength meters which are often calibrated by means of a known current. The commercial expansion in the region from 100 to 1,000 mc has increased the need for uhf measuring instruments and calibration equipment.

The principles of the oscillating ring electrodynamic ammeter are reviewed, and techniques for its use are described. Other calibrating methods which have been used in the past are appraised, and precautions concerning their use are given. A calorimeter method and a thermistor bridge method, which were developed for the calibration of low-current vacuum thermocouples, are presented.

II. A Primary Standard

A. Oscillating Ring Electrodynamic Ammeter

The form of electrodynamic ammeter in which the short-circuited ring is allowed to oscillate freely

* Decimal classification: R242. Original manuscript received by the Institute, October 1, 1952.

† General Engineering Laboratory, General Electric Co., Schenectady, N. Y.

(Fig. 1) is an absolute standard of current at high frequencies: its characteristics are calculable from measurements of length, mass, and time.[1,2,3] The period of mechanical oscillation of the short-circuited ring is a function of the strength of the electromagnetic field in which it is immersed and hence of the current associated with that field. The correction resulting from skin effect in the ring decreases as the frequency increases because skin effect is an asymptotic function. The correction for the suspension becomes negligible at high currents because the torque increases with current. It is therefore

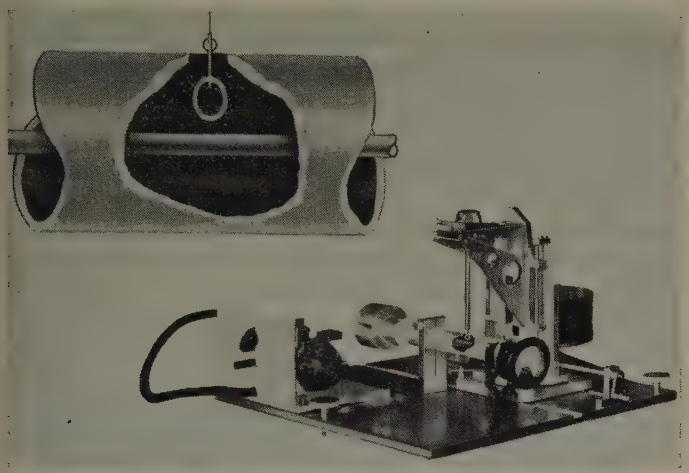

Fig. 1—Electrodynamic ammeter with thermocouple ammeter mounted for calibration.

best at high current and high frequency, the area in which it previously has been so difficult to work. The lower current limit depends upon the fineness of the ring suspension and upon the effects of air currents on the oscillation of the ring. In practice, this has been found to be approximately 1 ampere with a ring in air and 1/10 ampere with the ring in a vacuum. The lower frequency limit depends upon the reactance-to-resistance ratio of the ring. The practical limit is approximately 1 mc per second. The upper frequency limit has not been determined closely. Tests at the General Electric Company on a scaled-up model actually operated at approximately 300 mc indicated that satisfactory operation at 3,000 mc is probable. Gundlack,[4] at a later date, reported work at 2,100 mc. Nor has the upper current limit been determined. It appears to be limited only by the ability of a source to maintain the current at a fixed value long enough that a satisfactory observation of the period of mechanical oscillation may be made. The oscillating-ring type electrodynamic ammeter is not likely to be used much except in the laboratory for calibrating other types of ammeters which are direct reading. However, it should be noted that an engineer who knows the principles upon which this ammeter operates could make a more accurate measurement of 200 amperes at 200 mc with a loop of antenna wire, a silk thread, and a stop watch than could an engineer, without such knowledge, with commercially available current measuring equipment.

The oscillating ring electrodynamic ammeter is especially well adapted to calibrating ammeters at frequencies greater than 100 mc per second, First, because it can always be adjusted to cause negligible reaction on the current being measured and second, because it causes negligible diversion of current around the ammeter being calibrated. The first results from the fact that the ring oscillates about a position of minimum coupling and that it is easy to make accurate determinations of the mechanical period of oscillation of the ring using low amplitudes, 3 degrees or less. The second is the result of the small size of the ring. Calibrations accurate within 1 per cent have been obtained for currents from 3 to 10 amperes over the frequency range 1 to 350 mc.

B. Techniques

One ammeter calibrating circuit which has been used over the frequency range of 1 to 350 mc is shown in Fig. 1. It may be seen from Fig. 1 that the ammeter being calibrated is located at the end of a short section of coaxial transmission line and that provision has been made for moving the oscillating ring along the line. This was done in order that it might be used at frequencies for which the coaxial line is an appreciable part of a wavelength and hence has a standing wave on it. One technique is to calculate the expected current distribution on the line knowing the impedance of the ammeter used as a termination, then to measure the current at from three to five positions along the line and compare the two current distribution curves. Good agreement between calculated and measured values allows a correction for position on the line to be applied. This technique was not needed at frequencies less than 300 mc because the current 3.0 cm from the end of the line was the same as that 1.5 cm from the end, and therefore the same as that in the terminating ammeter. Another technique which could be used is that of making the coaxial line at least one-half wave length long and then locating the oscillating ring one-half length from the terminating ammeter. A correction can be made for line loss when necessary.

In the electrodynamic ammeter of Fig. 1 the period of mechanical oscillation of the ring was determined by means of a light beam which was reflected from a mirror attached to the ring and operated one pen of a chronograph electronically. A standard second and also 60 cycles per second from a quartz-crystal-controlled frequency standard were used to operate the other pen of the two-pen chronograph. This resulted in measurements of the period of mechanical oscillation accurate within one part in five thousand.

A two-plate variable capacitor was built into the input end of the coaxial line and was used to resonate the

[1] H. M. Turner and P. C. Michel, "An electrodynamic ammeter," Proc. I.R.E., vol. 25, p. 1367; 1937.
[2] H. R. Meahl, "A bearing type high frequency electrodynamic ammeter," Proc. I.R.E., vol. 26, pp. 734–744; June, 1938.
[3] M. Solow, "Theoretical study of an electrodynamic ammeter for very high frequencies," CRPL Preprint 50-15, U. S. Dept. of Commerce, National Bureau of Standards; January 12, 1950.
[4] F. W. Gundlack, "Electrodynamic ammeter," *Hochfreq. und Elecktroak.*, vol. 55, p. 169; 1940.

line with the ammeter attached in order that relatively low-power oscillators (20 watts) could be used to obtain currents as high as 8 amperes. Usually, satisfactory operation could be obtained by inductively coupling the oscillator coil directly to the coaxial line through the slot shown in Fig. 1, but at some frequencies an additional series resonant coupling link was used which had a loop at each end and a variable capacitor in series with one lead at the center. This gave greater purity of waveform in the coaxial line and hence in the ammeter being calibrated.

In this electrodynamic ammeter the ring was mounted on a fine fused quartz filament which was protected by means of a glass tube fastened to the movable carriage at the top so as to move with it. Further protection from air currents was obtained by covering the slot in the coaxial line with cylindrical segments of plastic.

The fine quartz filament was made by melting a rod of fused quartz in a flame, then suddenly pulling the two ends of the rod apart and putting the molten part in a jet of air simultaneously. The resulting cloud of filaments was caught on a piece of black velvet cloth hung up in line with the blast. The final grading of the filaments was done by suspending a ring on each in turn and measuring the natural period of mechanical oscillation. The one with the longest period of natural oscillation is, of course, the finest. One having a period of 29 seconds was obtained after trying five others. The use of adjustable strong oblique lighting was needed to make it visible against black velvet. Great care was required in handling since it would float away on a slight draft of air. The ends were fastened by means of small drops of glyptal cement.

The ring was adjusted to a known position with respect to the center conductor of the coaxial line by means of a fine adjusting screw on the movable carriage. The technique used was to lower the ring until it just touched the center conductor, then to raise it a specified number of turns of the screw. The point of touching was observable by eye and by touch when no ammeter was at the end of the line, and it was found that it could be set precisely by touch. Use of a dial gage following vertical motion of the head showed that reset of the ring to a chosen height within one ten-thousandth of an inch was feasible with care. The position of the center conductor with respect to the outer conductor was maintained by means of triangular spacers made of plastic. Most of the dielectric was removed by drilling holes so as to cause a minimum disturbance in the electric field and yet give firm mechanical support. Teflon is the best material available for such purposes. The spacers were arranged with a point down so that the ring could be moved past them without interference.

The oscillating ring electrodynamic ammeter may be used as an absolute standard of current in any circuit for which it is possible to calculate the coupling between the ring and the rest of the circuit. It may also be used as a transfer standard if desired by calibrating at a low frequency by means of a thermocouple or other type ammeter whose low-frequency characteristics are known. Then it may be used at high frequencies by using a calculated correction for the effect of increasing the frequency.

III. Other Standards

A. Hot-Wire Air Thermometer

The hot-wire air thermometer has been called a standard of current at frequencies greater than 100 mc.[5] It is a transfer standard and may be used as long as the assumption that currents having equal heating power are equal, independent of frequency, is true. It is obvious that if the frequency is increased far enough a standing wave will exist on the high-frequency half of the hot-wire air thermometer and a measurable part of the high-frequency power will be radiated, which causes the equality to be lost. In one form of this device, two hot-wires are used, one in the radio-frequency circuit and the other in a direct-current circuit. The relation of the heating effects is indicated by a colored drop in a horizontal capillary connecting the two columns of air heated by the two hot-wires so that equality may be determined easily.

In spite of the difficulties caused by thermal inertia and the continuous comparison technique, this is still one of the best means for calibrating ammeters in the range of 10 to 500 ma at frequencies greater than 100 mc because of the simplicity of the heating wire and its consequent small disturbance of the high-frequency circuit.

B. Photoammeter

Another form of hot-wire ammeter which has been widely used is the photoammeter.[6] A photocell and galvanometer are used to indicate the high-frequency current in an incandescent wire. In practice, this also is a transfer standard being calibrated with direct current and used on high frequencies, assuming that equal light output results from equal currents independent of frequency. The errors encountered at the higher frequencies because of standing waves on the heater are generally appreciable here since the heater is usually of finely coiled tungsten wire. Precision is obtainable by means of the photoammeter because the galvanometer current is approximately the sixth power of the radio-frequency current, and the close agreement which has been obtained between photoammeters and conventional thermocouple ammeters has led some to claim high accuracy for it.[7] It should be noted that the photoammeter and the thermocouple ammeter operate on the same basic principle, and are therefore subject to the same errors. This has resulted in good agreement between them over a wide frequency range because the

[5] A. Shiebe, "Jahrbuch der Drahtlosen Telegraphie und Telephonie," *Hochfreq. und Electroak.*, vol. 25, p. 12; 1925.
[6] H. Schwarz, *op. cit.*, vol. 39, p. 160; 1932.
[7] J. H. Miller, "Thermocouple ammeters for ultra-high frequencies," Proc. I.R.E., vol. 24, p. 1567; December, 1936.

errors were so nearly alike. The photoammeter uses more power from the circuit than the other hot-wire types because it takes more power to make a wire emit light. It seems likely that future use of this device will be limited to precise indication of constancy of high-frequency currents in the range of 0.1 to 1 ampere, i.e., an application in which its precision is used and its lack of accuracy is not detrimental. Errors as large as 60 per cent have been found at 5 amperes and 200 mc.

IV. Calorimeter and Thermistor Bridge Methods

Calorimeter and thermistor bridge methods of calibrating vacuum thermocouples have been developed at Worcester Polytechnic Institute[8] and an extensive measurements study is now in progress. Both of these methods were developed for use with coaxial transmission line equipment to calibrate vacuum thermocouples over the 100- to 1000-mc region.

In certain applications, it is desirable to use a vacuum thermocouple connected to a separate millivoltmeter rather than a self-contained thermocouple ammeter. In such cases, the errors in current measurement at ultra-

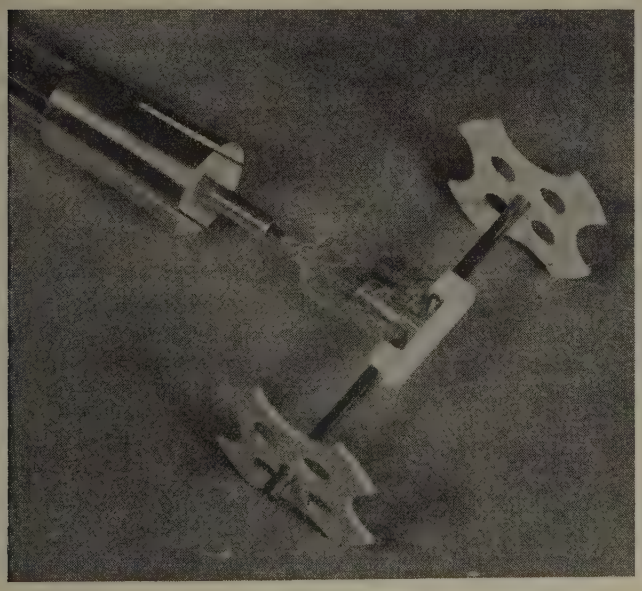

Fig. 2—Vacuum thermocouple mounted for calibration.

high frequencies are caused primarily by the inductance, capacitance, and skin effect of the vacuum-thermocouple heater circuit provided that adequate precautions are taken to isolate the thermal junction leads from the heater circuit.

The American-made vacuum thermocouple best suited for measurements at these frequencies is constructed with the thermal junction leads brought out at the opposite end of the glass envelope from the heater leads as shown in Fig. 2. The planes of the heater circuit and the thermal junction are at right angles to further minimize coupling. The heater and the thermal junction are thermally connected but electrically insulated by a small ceramic bead. In a typical vacuum thermocouple of this construction the lumped values of heater circuit inductance and capacitance are approximately 0.024 μh and 0.39 $\mu\mu$f. If the parallel combination of these values is taken as an approximation to the actual distributed constants of the heater circuit, the heater circuit would be parallel resonant at 1,650 megacycles per second. At 1000 mc, the actual heater current would be 62 per cent higher than that supplied to the leads, while at 100 mc, the heater current would be 0.4 per cent too great.

The error caused by the heater circuit inductance and capacitance can be greatly reduced by the use of a vacuum thermocouple having a straight-through type of heater circuit as shown in Fig. 3. Vacuum thermo-

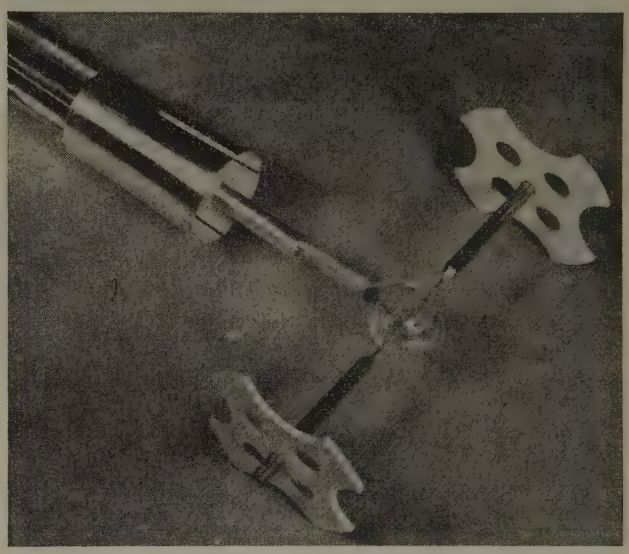

Fig. 3—Vacuum thermocouple with straight heater mounted for calibration.

couples having this collinear type of heater and lead construction are now available from a manufacturer in England. The electrically insulated thermal junction in a plane perpendicular to the heater is also featured. These vacuum thermocouples have been used in the measurements at Worcester Polytechnic Institute.

A. Calorimeter Method

The calorimeter constructed at Worcester Polytechnic Institute is shown in Fig. 4. This consists of a small cylinder of Teflon in which a special resistor is concentrically located. The principles of this calorimeter method are illustrated in Fig. 5. A current, I, passed through the resistor, R, will generate heat at the rate of I^2R. When the temperature of the cylinder has been increased sufficiently to make the rate of heat flow away from the cylinder by way of the resistor leads and the surrounding air equal to I^2R, an equilibrium condition of temperature and heat flow will be reached. The major heat-flow terms are proportional to the temperature rise; hence, the temperature rise is essentially propor-

[8] C. C. Allen, "A Coaxial Calibration Standard for Ultra-High-Frequency Current," Master of Science Thesis, Worcester Polytechnic Institute, Worcester, Mass.; June, 1950.

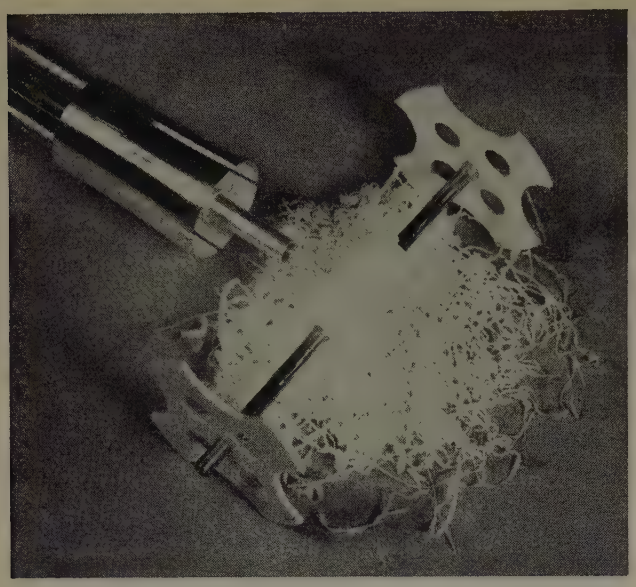

Fig. 4—Calorimeter interior with Teflon heat insulation.

tional to the current squared. The temperature rise is indicated by measuring the voltage difference between a thermal junction imbedded in the cylinder and a second junction kept at normal temperature. Because of its low value, this voltage should be measured with a potentiometer.

The best resistor for use in the calorimeter is made by metalizing the surface of a glass or ceramic rod. Such a resistor, when properly designed and aged, has essentially the same resistance to both ultra-high-frequency and direct current. The diameter of the resistor is made the same as the center conductor of the coaxial line with which the calorimeter is used, and the end connections are made as smooth as possible. The distributed inductance and capacitance of the line is thereby not altered at the calorimeter. The resistor is short and has a resistance which is small compared with the characteristic impedance of the line. The net effect, therefore, is the insertion of a small resistance in the line. This sets up a small standing wave for which a correction can easily be made.

After equilibrium has been obtained with uhf current, direct current is then passed through the calorimeter and adjusted to give the same equilibrium temperature-rise indication. The calibration is then made directly in terms of the accurately measured direct current. If a resistor having unequal uhf and dc resistances is used in the calorimeter, the ratio of uhf current to direct current for equal equilibrium temperature-rise indications is obtained from the square root of the dc to uhf resistance ratio.

The calorimeter method as originally developed calls for insertion of the calorimeter in series with the center conductor of a coaxial line terminated in its characteristic impedance. The thermal junction leads are brought out through the hollow center conductor of a one quarter wavelength-long isolation stub with suitable bypass condensers.

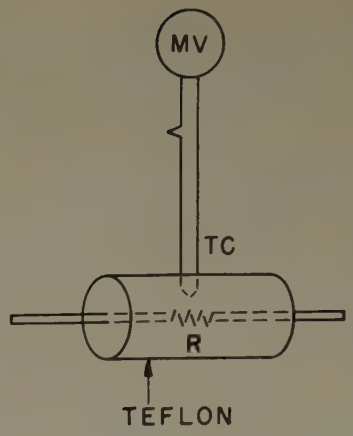

Fig. 5—Principle of calorimeter method. Same indication: $I_{uhf}^2R_{uhf}=I_{dc}^2R_{dc}$.

The present calorimeter employs a 30-ohm resistor and is used with a coaxial line having a characteristic impedance of 149 ohms. This design is suitable for currents from about 50 to 200 ma when used as discussed above. Another arrangement suitable for measuring currents from about 20 to 100 ma is described in the following.

The alternate arrangement for employing the calorimeter method consists of using the calorimeter as the termination for the coaxial line together with matching stubs to terminate the line in its characteristic impedance, Z_0. Under these conditions, since Z_0 is essentially a pure resistance at ultra-high frequencies, the uhf power supplied to the calorimeter by a given line current, I_{uhf}, is $I_{uhf}^2Z_0$, neglecting any loss in the matching stubs. This is then equated to the measured dc power required to give the same equilibrium temperature-rise indication. Since Z_0 can be accurately determined from the dimensions of the line, the value of uhf line current, I_{uhf}, is readily obtained.

B. Thermistor Bridge Method

The thermistor bridge method is similar in application to the alternate calorimeter method just described. Since a thermistor is a semiconductor having a negative tem-

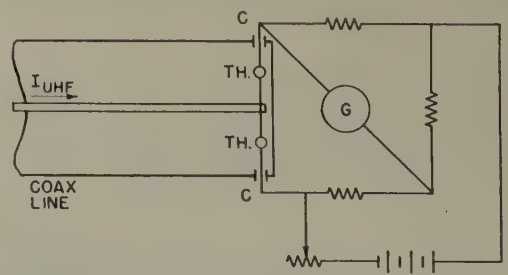

Fig. 6—Principle of thermistor bridge method. For balance: $I_{uhf}^2Z_0=\Delta P_{dc}$ in TH.

perature coefficient of resistance, a balanced direct-current bridge having two thermistors in series in one arm will be unbalanced by the change in resistance if the power supplied to the thermistors is changed. By mounting the thermistors as a capacitively coupled termination for a coaxial line as shown in Fig. 6, they

will be in parallel for the uhf current; hence, the uhf-voltage drop will balance out in the bridge arm. The only effect of applying uhf current will then be to heat up the thermistors and decrease their resistance.

If the thermistors are made to properly terminate the coaxial line in its essentially resistive characteristic impedance, Z_0, by suitable stub matching with some direct current supplied from the bridge, uhf power absorbed by the thermistors will be $I_{uhf}^2 Z_0$ where I_{uhf} is the uhf line current. If the dc bridge is balanced under this condition and the uhf power is then shut off, the increase in dc power that must be supplied to the thermistor arm to rebalance the bridge for direct current can be measured and equated to $I_{uhf}^2 Z_0$. Since Z_0 can be accurately determined from the line dimensions, the value of I_{uhf} is readily obtained.

The thermistor bridge method is suitable for measuring small currents from about 5 to 15 ma when used with a coaxial line having a characteristic impedance of 149 ohms. The use of wire barretters would permit somewhat greater currents to be measured.

C. Techniques

The calorimeter and thermistor bridge methods of measuring uhf current were developed primarily for the calibration of vacuum thermocouples, and are intended for use with coaxial transmission-line equipment designed for that purpose. If the calibration is to be practical, it must not be limited to the particular coaxial line and connections used for the calibration, but must be readily adaptable to all types of circuit connections. This requires that the vacuum-thermocouple heater circuit act essentially as a series impedance inserted in the center conductor of the line, the ends of the center conductor should add negligible shunt capacity across the heater circuit, and the heater circuit should add negligible shunt admittance across the line. If these conditions are fulfilled and the effective series impedance of the vacuum-thermocouple heater circuit is determined at the time it is calibrated, the calibration may then be converted for any circuit connections, provided that the shunt capacity which the connections place across the heater circuit can be determined or estimated.

A small center conductor which minimizes the shunt capacity across the heater circuit is also desired so that the calorimeter resistor can be made to have the same diameter as the center conductor and be of reasonable size. This is important if the resistor is to act essentially as a pure resistance inserted in the line. The outer conductor should have a large inner diameter to permit mounting the vacuum thermocouples within the line and to minimize the increment of shunt admittance across the line due to vacuum-thermocouple heater eccentricity. A large outer conductor also makes the increment of shunt admittance of the calorimeter have negligible effect.

The equipment which has been constructed at Worcester Polytechnic Institute for use with these methods employs a 1.500-inch inner diameter outer conductor having a 0.200-inch wall and a 0.1250-inch diameter center conductor. These values give a characteristic impedance, Z_0, of 148.9 ohms. The only disadvantage of this high characteristic impedance is the greater input power required to supply a given value of current.

The over-all assembly for calibrating vacuum thermocouples is shown in Figs. 7 and 8, and consists of a suitable source of uhf power with an appropriate input

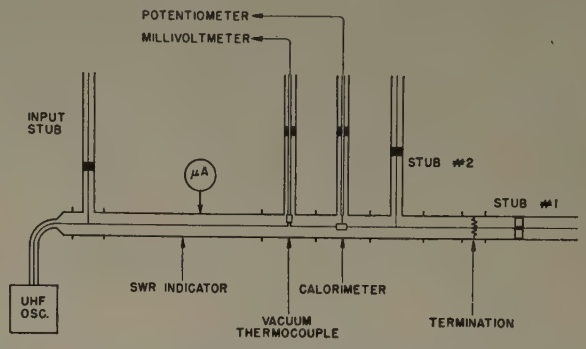

Fig. 7—Diagram of vacuum-thermocouple calibrating equipment.

matching system and dc blocking capacitors, a 12-foot slotted section for measuring voltage standing-wave ratios, a section for mounting the vacuum thermocouples, a calorimeter section, and a termination assembly with matching stubs that will terminate the line in its characteristic impedance with either a resistance or a thermistor termination. By proper design of the resistance termination the matching stubs are kept less than one quarter wavelength long, which is important when working down to 100 mc per second. The dc blocking is provided to permit direct current to be supplied rapidly to the vacuum thermocouple and the calorimeter without removing those sections. The vacuum thermocouple and calorimeter sections are provided with isolation stubs having center conductors of tubing through which the thermal junction leads can be brought out and by-passed. Matching stub 1 in the

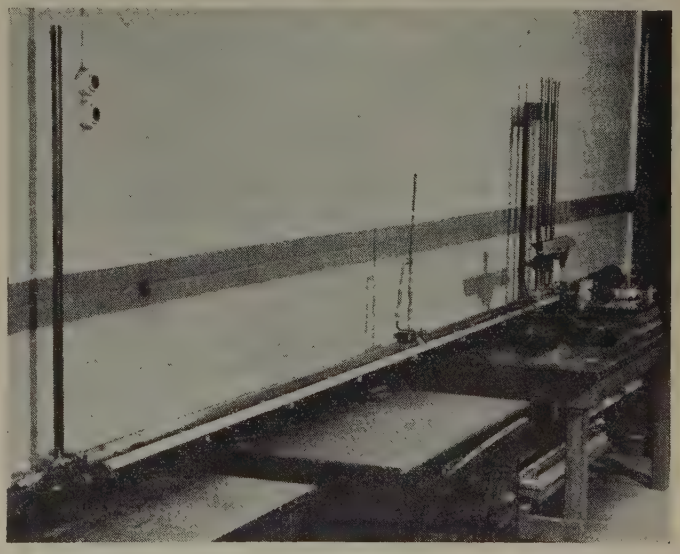

Fig. 8—Vacuum-thermocouple calibrating equipment.

termination assembly is made collinear with the line to provide complete shielding.

When calibrating by the calorimeter method, the termination assembly using the resistance termination is first connected to the slotted section and adjusted for unity voltage standing-wave ratio, vswr. The calorimeter section is then inserted and its vswr is measured with the isolation stub adjusted to give the minimum vswr. A study of the conditions involved shows that the calorimeter is at a voltage maximum when its vswr is a minimum; hence, the measured vswr of the calorimeter is used to apply a correction to the current, I_c, at the calorimeter to obtain the actual current, I_{th}, at the vacuum thermocouple location. The correction equation is

$$I_{th} = I_c\left(\cos\frac{2\pi x}{\lambda} + j\text{vswr}_{cal}\sin\frac{2\pi x}{\lambda}\right),$$

where x is the distance between the vacuum thermocouple and the calorimeter and λ is the wavelength. The magnitude of the parenthetic multiplier term is about 1.007 at 100 mc and 1.200 at 750 mc for the equipment described. After the calorimeter vswr has been measured, the vacuum-thermocouple section is inserted between the calorimeter and the slotted section. The vacuum-thermocouple isolation stub is adjusted for minimum vswr. When the calorimeter has reached equilibrium, the calorimeter output voltage is read with a potentiometer and the vacuum-thermocouple output voltage is read on a millivoltmeter.

The uhf current is then shut off and batteries are connected to the dc input jack with a means of controlling the current and with an accurate meter to measure it. The current is adjusted to give the same equilibrium calorimeter output voltage as was obtained with the uhf current and the dc input is read. This value of direct current is converted to the equivalent uhf current by multiplying it by the square root of the ratio of dc to uhf calorimeter resistance if the resistances are not the same. The calorimeter vswr correction is then applied to the equivalent uhf current to obtain the actual uhf current that was supplied to the vacuum-thermocouple heater circuit. Several values of actual uhf current at a particular frequency may be plotted versus the corresponding millivoltmeter readings to obtain a direct uhf calibration.

After the calibration has been completed, the calorimeter section is removed and the uhf current is reapplied. The effective series impedance of the vacuum-thermocouple heater circuit is then determined by measuring the vswr and noting the position of the voltage minimum.

The alternate method of using the calorimeter may be employed to calibrate vacuum thermocouples having smaller current ratings. For this method, the calorimeter is used as the termination and the matching stubs are adjusted for unity vswr on the slotted line before inserting the vacuum-thermocouple section. A dc blocking capacitor must be used to connect the calorimeter to matching stub 1 which has a tubing center conductor through which the dc lead from the calorimeter may be brought out. The output voltage of the vacuum thermocouple is read on a millivoltmeter and the calorimeter output voltage is measured with a potentiometer with uhf current applied. The uhf current is then shut off and direct current applied to the calorimeter and adjusted to obtain the same calorimeter output voltage as with uhf current. The dc power thus supplied to the calorimeter is determined and equated to $I_{uhf}^2Z_0$, from which the uhf current, I_{uhf}, that was supplied to the vacuum thermocouple is determined. A direct calibration for a particular ultra-high frequency is obtained by plotting several values of uhf current against the corresponding millivoltmeter readings. The vacuum-thermocouple vswr and voltage minimum position for determining the heater circuit series impedance can be obtained at the same time as the uhf current readings.

To calibrate vacuum thermocouples by the thermistor bridge method, the resistance termination in the termination assembly is replaced by the thermistor mount. The termination assembly is connected to the slotted section and the thermistors are connected to a suitable dc bridge. With reduced direct-current input to the thermistors from the bridge, the matching stubs are adjusted to obtain unity vswr on the line. This adjustment is not simple since the resistance of the thermistors changes as the stub adjustments change the amount of uhf current supplied to the thermistors. The adjustment is further complicated by the requirement that the bridge be balanced for direct current with the uhf current supplied and unity vswr on the line. This adjustment is best made by setting a reasonable coupling for uhf current into the line and then balancing the bridge for each adjustment of the stubs until unity vswr is obtained. If the desired condition is outside the range of dc input adjustment, the coupling of uhf current into the line should be reset and the process repeated.

Once the termination assembly has been adjusted to give unity vswr with the bridge balanced, the vacuum-thermocouple section is inserted in the line. This will change the uhf current which reaches the termination assembly, and thus cause the bridge to be unbalanced and the line to be improperly terminated. To restore the desired condition, the bridge adjustments should be left unchanged, but the coupling of uhf current into the line should be adjusted until the bridge is returned to a balanced condition. The uhf current supplied to the termination system from the vacuum-thermocouple location will then be the same as when the adjustment for unity vswr was made. The uhf power supplied to the termination system is $I_{uhf}^2Z_0$ since with unity vswr the line is terminated in its essentially resistive characteristic impedance, Z_0. This power is all absorbed by the thermistors if the stubs are lossless. A correction can be applied for stub loss when necessary. The vacuum-thermocouple output voltage is read on a millivoltmeter, and the uhf current source is then shut off.

The increase in dc power that must be supplied to the thermistor arm of the bridge to rebalance it can be measured on the rebalancing type of bridge, or is determined by the amount of bridge unbalance on the calibrated type of bridge. In either case, this dc power is equal to the uhf power that was previously supplied to the thermistors. The uhf current with correction for stub loss is then given by

$$I_{\text{uhf}} = \sqrt{\frac{P_{\text{dc}} + \text{stub loss}}{Z_0}}.$$

As with the previous methods, a direct calibration for a particular ultra-high frequency is obtained by plotting several values of uhf current against the corresponding millivoltmeter readings.

The measurement of the vswr and voltage minimum position for determining the heater circuit series impedance can be made right after the millivoltmeter reading for uhf current is taken. The line is properly terminated at that time; hence, the standing wave is due only to the heater circuit impedance.

The lower power rating of thermistors, or other forms of barretters, places a limitation on the value of current for which this method may be used. Since the uhf power is a rather large increment of the total thermistor power, it is best to use a rebalancing type of bridge.

An alternate method of presenting the results of the calibration is in terms of a correction to dc calibration rather than as stated uhf calibration. For this, the value of direct current necessary to obtain the same vacuum-thermocouple output voltage (millivoltmeter reading) as was obtained using uhf current is measured. The difference between the direct current and the uhf current is the amount by which the dc calibration is too high at the particular ultra-high frequency. This error may be expressed as a percentage of the direct current and will apply at other current levels of the same frequency since the heater circuit is essentially linear. With a negative sign, this error becomes a percentage correction to be applied to the dc calibration. When the error has been determined for several frequencies, a curve of correction versus frequency may be plotted for the particular vacuum thermocouple.

The coaxial calibrating equipment which has been constructed for use with the calorimeter and thermistor bridge methods lends itself well to the air milliammeter method which has been used by Gainsborough[9] with other equipment. It is expected that an air milliammeter unit will be built at Worcester Polytechnic Institute to serve as a check on the calorimeter and thermistor bridge methods. The air milliammeter has the advantage that no leads must be brought out from it as is required with the calorimeter. The resistors will be of the metalized glass-rod type having the same diameter as the coaxial-line center conductor used in the calorimeter.

[9] G. L. Gainsborough, "Experiments with thermocouple milliammeters at very high radio frequencies," *Jour. IEE* (London), vol. 91, pt. 3, p. 156; September, 1944.

V. General Precautions

An examination of the equivalent circuit together with the knowledge that a thermocouple ammeter gives a reading proportional to the total heating effect of a current should cause one to be critical of the purity of waveform of the energy used in making a calibration and to take steps to insure the total harmonic content being low enough not to affect the accuracy of the calibration. The waveform may be improved by judicious use of link-coupled resonant circuits and Faraday screens between the energy source and calibrating circuit.

An essential for any calibrating work is stability of amplitude so that there is no doubt that the standard and the ammeter being calibrated are indicating the same current. Since resonance effects are always present in practical circuits at frequencies greater than 100 mc, good frequency stability in the energy source is one essential to good amplitude stability in the calibrating circuit. Other contributors to such stability are an electronically regulated power supply for the RF source, proper shielding and freedom from interfering sources of RF energy (high-power broadcasting stations, radar transmitters, electronic heaters, arc welders, and the like can cause great difficulties, particularly when the effects are intermittent and the cause unsuspected), sturdy construction of the whole equipment, freedom from mechanical vibration and shock, protection from rapid changes in temperature, and protection from drafts.

Another difficulty likely to be encountered in calibrating ammeters at frequencies greater than 100 mc is that caused by lack of appreciation for the difference between accuracy and precision. An ammeter may have excellent precision and yet be quite inaccurate, but it cannot be accurate without having precision equal to or better than the order specified in naming its accuracy. This is because precision is self-consistency, ability to give the same indication within close limits each time it is subjected to the same current, and accuracy connotes comparison with an absolute standard.

VI. Conclusions

It has been found that the basic orderliness of the universe is present in high-frequency circuits; i.e., the same current occurs each time the same circuit is subjected to the same set of conditions.

It is imperative that at least two instruments depending upon different principles agree to establish a value of current. It is desirable that this agreement be obtained over a wide frequency range to eliminate agreement resulting from compensating errors.

Acknowledgments

The authors wish to express their appreciation to Dr. E. D. Cook, of the General Engineering Laboratory, General Electric Company, and to Professors T. H. Morgan and H. H. Newell, of the Worcester Polytechnic Institute, for their interest and encouragement in the work on which this paper is based.

Correspondence

Electronic Sleep-Teaching* (4475)

Sleep-teaching may be defined as the art of producing knowledge in a brain by repeated stimuli without any conscious mental effort on the part of the student patient. This art, bordering on the fields of extrasensory perception, hetero-suggestion, and hypnotism, including the state of semi-wakefulness, is beginning to gain commercial applications. It is becoming apparent that the associated techniques provide a tool in the psychotherapy field, perhaps a tool for unlearning of habits, ignoring the patient's feeling in the matter. Twenty years ago, phonograph records for sleep-teaching and "suggestive attitude" listening were sold in the market; today the activities are concentrated more usefully on the teaching of languages.

In the language field, the pioneer work of Max Sherover, President of the Linguaphone Institute, is well-known through magazine articles and otherwise. His Linguaphone technique, with the Dormiphone apparatus, represents a milestone in the history of sleep-teaching, and his early research brought medical experts into the field and established a basis of sound scientific approach.

The present scientific study of sleep in the neurophysiological field has revealed characteristics such as the significance of various sleep levels and sleep-level transfers. Via encephalographic and other investigations, this study has shed light on the question of retention percentage of repeated stimuli (in the form of signals reaching the cerebral cortex via a sensory receptor, such as the ear).

In 1947, while experimenting with brain waves, the author discovered that many hours of sleep-teaching, using a patient in "steady" sleep, sometimes gave less encouraging results than just a few minutes of sleep-teaching when the patient transferred between different sleep levels. The equipment used was very crude (see Fig. 1), and the conclusion drawn should not be given

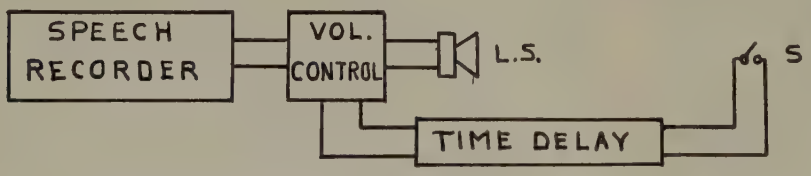

Fig. 1

too much significance. The equipment consisted of a wire recorder with the text to be learned, a loudspeaker, and a time-delayed on-off switch, in which open contacts corresponded to maximum loudness. The patient's hand, operating the switch S, opened up when the condition of sleep was entered into, causing a gradual increase in loudspeaker output. Sufficiently awake to become "disturbed" by the loudspeaker, the patient closed his hand, thus reducing the sound intensity by closing the contact S, and again fell asleep.

A partly developed, improved apparatus is shown in Fig. 2. It makes use of the brain potentials derived from the frontal and occipital areas of the scalp, overlying one hemisphere. While the effect of sleep-level transfers on these cortical potentials is rather complex, a certain simplicity is achieved if either the frequency changes of one particular output in the frequency domain is selected, or if the amplitude changes of the entire frequency spectrum is selected. For these two alternatives, a switch S with two positions, a and b, has been arranged, following the electrode leads amplifier. Switch position a connects to a frequency discriminator and rectifier, together providing an FM detector, so that a deviation in frequency yields an output voltage of certain polarity. Switch position b connects to a rectifier, followed by an integrator, so that the output voltage level becomes a direct function of the integrated brain potentials. Thus, in either switch position, the deepening of sleep, or transfer into a different level of sleep, can be made to vary a direct voltage, utilized as bias voltage on a relay tube, turning on more or less loudspeaker output of recorded text to be learned.

With such equipment as described above, medical research begins. Much investigation is needed for proper recording of the retention percentage of repeated stimuli under various conditions. Still more investigation is needed to find out the beneficial effect, if any, of simultaneously applied drugs. It is seen from Fig. 2 that a feedback loop exists via the sensory receiver, the nervous system, and the cortical activities. The sign of the feedback should be negative so that if the patient tends to change from one sleep level to another in the direction toward wakefulness the loudspeaker output is reduced, the compensation action maintaining an equilibrium. This also means that the system will make up for some of its own weaknesses; therefore, if a tube in either amplifier should go bad, the loss in gain will limit itself in an effort to compensate. Again, the complexity of the cortical activities implies

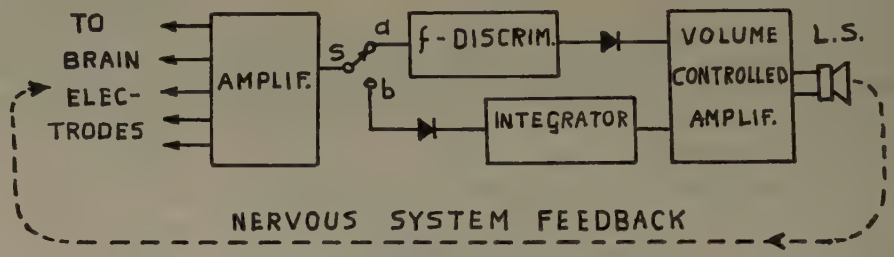

Fig. 2

variational conditions, which symbolically may be expressed as a βA of the nervous system, vulnerable to sudden 180-degree phase shifts. Positive feedback would not only enhance the poor qualities of the system but might also most abruptly wake up the patient, and if repeated, lead to complications of a psychiatric nature. In view of these difficulties, one should not hook up the circuit indicated in Fig. 2 and expect immediate gratifying results, maintaining, by chance, the patient in a desired condition of high receptivity and retention percentage to such stimuli as a voice reading off the multiplication table or a sequence of mathematical formulas.

The above has been written merely to call attention to the fact that sleep-teaching results in a definite and measurable gain in learning, and that electronic sleep-teaching control is possible, and perhaps even promising; however, a considerable amount of work has to be done before it becomes practical.

HARRY STOCKMAN
Stockman Electronics Research Company
543 Lexington Street
Waltham 54, Massachusetts

* Received by the Institute, October 6, 1951.

Engineering Unity* (4476)

Those who have been working for some years in one or more of the attempts to find a basis for unity in the engineering profession will read Dean Evans' letter[1] with a great deal of sympathy and understanding.

The difficulties inherent in obtaining the opinions of the members have caused the publicly proposed plans to be small in number. This is particularly true of the work of the Exploratory Group and its Planning Committee. All now must be aware, however, that in proposing the adoption of Plan A as a first step, most of the members of the Exploratory Group were seeking to find a way to provide a better forum for discussion of future modifications and of final plans.

* Received by the Institute, July 30, 1952.
[1] See Correspondence section, PROC. I.R.E., December 1952.

Correspondence

Very few believe that Plan A is a permanent answer.

It would be most unfortunate at this time to take a *binding* vote of the members which would determine whether Plan A is or is not to be adopted. Let us rather look on Plan A as merely a move to improve the facilities of EJC for the study of the question and to enable it to lay before the engineers of the country the various suggestions and to obtain from them proposals for plans better and more detailed than any that have yet been prepared.

Dean Evans refers to Plan E of the Florida Section of the ASCE. This plan in a great many respects is similar to Plan C of the Exploratory Group. It has, however, certain characteristics which may not be favored by the membership of organizations such as the IRE. Among these are:

(a) limitation to founders soceties which, in turn, would become only technical divisions of the Unity Organization;
(b) apparent lack of provision in the organization for societies such as the IRE;
(c) provision that all officers (national, state or local) as well as officers of the technical divisions should be registered engineers. The idea that only registered engineers represent the profession is not pleasing to those of us who have come into engineering through the sciences. Only a small proportion of the IRE membership is composed of registered engineers.

Plan E, therefore, in so far as it differs from Plan C, would seem to make it unavailable to organizations such as IRE.

It is most helpful to have Dean Evans' letter and also to have his proposals in reference to the Florida Plan. Members may be of assistance by sending their ideas to the Editor or to the Secretary of the Institute.

B. E. Shackelford
IRE Member on the Exploratory Group
Radio Corporation of America
RCA Building
30 Rockefeller Plaza
New York 20, N. Y.

Tests Concerning the Inverse Current in Selenium-Iron Rectifiers* (4477)

About 14 years ago I made a number of tests on selenium-iron rectifiers. In view of the present-day interest in the subject, I report a summary of this work. The tests were made with a magnetic oscillograph, the results being recorded on photographic film.

The inverse current which flows in a selenium-iron rectifier is a function of the past history of the device. If such a rectifier has been idle for a long period of time (months), the application of a dc inverse voltage will cause a dc inverse current to flow which begins at a comparatively large value and gradually decreases to a steady state. This process usually takes several hours.

A peculiar phenomenon is noted, however, if the circuit is interrupted for a few milliseconds. Upon reclosure, the inverse current shows a transient pulse lasting a few microseconds. This pulse is of greater magnitude than the current flowing at the original circuit closure. After the transient pulse, the inverse current falls to a very low value and then gradually *builds up* to the steady-state value. This build-up also involves several hours. The inverse current behavior is about the same if the circuit is interrupted for several hours, rather than for several milliseconds.

Douglas E. Mode
Electrical Engineering Dept.
Lehigh University
Bethlehem, Pa.

* Received by the Institute, June 30, 1952; revised manuscript received July 11, 1952.

Auroral Effects on Television* (4478)

In the Ithaca fringe area an odd interference in television reception has been noticed and has been correlated with the aurora borealis. The effect seems to be similar to the auroral propagation discovered in this frequency range by the radio amateurs,[1] and it is also similar to the radar echoes from the aurora which have been reported.[2,3]

This television interference appears intermittently on the screen as horizontal, indistinct, black bands not only over the synchronized picture but also on channels which have no stations normally received in this area. The width of these bands is approximately equal to their spacing, and the number observed depends on the channel to which the set is tuned (see Fig. 1–3). On the lowest frequency channel No. 2 (54–60 mc) only two or three bands appear and, on successively higher channels, correspondingly more bands come in, up through channel No. 6 (82–88 mc). As yet, we have not observed this phenomenon on the high frequency channels No. 7–13 (174–216 mc).

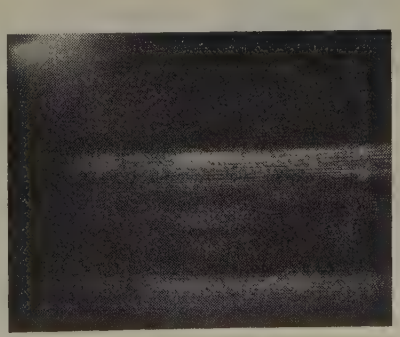

Fig. 1—Channel 2. No station. July 3, 1951. Ithaca, New York.

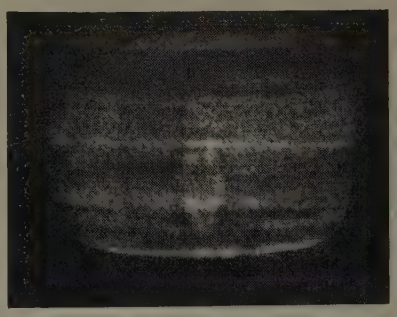

Fig. 2—Channel 4. Station WBEN-TV. July 3, 1951. Ithaca, New York.

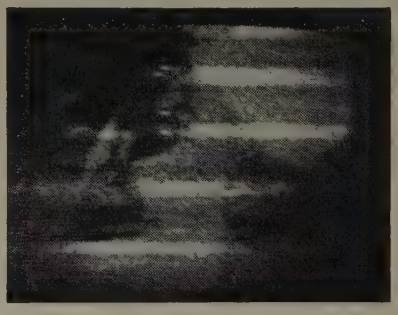

Fig. 3—Channel 6. Station WHAM-TV. July 3, 1951. Ithaca, New York.

This disturbance was first noticed in March, 1951 by Prof. W. C. Ballard of the Electrical Engineering School, Cornell University, and it was suggested by him that the aurora might be the cause. Since then there have been several correlations of this effect with the observation of visible auroras.

Even further evidence was gained by discovering the directional characteristic of this interference. The two strongest, low channel stations received here are located north of Ithaca; WSYR-TV, channel 5 in Syracuse, is 50 miles NNE, and WHAM-TV, channel 6 in Rochester, is 80 miles NW. The black bands come in very strong from the north at disturbed times, but when the antenna is rotated to the south side of the peak signal by an equal angle, the black bands are completely absent (reception is normal).

Thus, we are led to believe that there is some type of radio scattering from the ionized portions of the aurora structure which makes possible such unusual propagation. More widespread data on these phenomena would be interesting.

Roger E. Thayer
School of Electrical Engineering
Cornell University
Ithaca, New York

* Received by the Institute, August 3, 1951.

[1] R. K. Moore, "A VHF propagation phenomenon associated with aurora," *Jour. Geophys. Res.*, vol. 56, p. 47; March, 1951.
[2] A. Aspinall and G. S. Hawkins, "Radio echo reflections from the Aurora borealis," *Jour. Brit. Astron. Assoc.*, vol. 60, p. 130; April, 1950.
[3] P. A. Forsyth, W. Petrie, F. Vawter, and B. W. Currie, "Radio reflections from Auroras," *Nature* (London), vol. 165, p. 561; April, 1950.

Contributors to Proceedings of the I.R.E.

Charles C. Allen (S'47–A'51) was born in New York City on March 1, 1921. He received the B.S. degree in electrical engineering "with high distinction" from Worcester Polytechnic Institute in 1949, and his M.S. degree in electrical engineering in 1950, during which time he held a Gerard Swope Fellowship for his research on uhf current measurement.

C. C. Allen

In 1950 Mr. Allen joined the General Electric Company as a development engineer in the electronic systems and measurements division of the General Engineering Laboratory, where he is presently engaged in development of microwave components and antennas.

Mr. Allen is a member of Tau Beta Pi, and an associate member of Sigma Xi and the A.I.E.E.

❖

P. J. Allen was born in Whitinsville, Mass., on December 30, 1919. After two years of sub-professional employment with General Radio Company, he entered Pennsylvania State College, and in 1944, received the B.S. degree in physics.

P. J. Allen

Since 1944, Mr. Allen has been associated with Radio Division III at the Naval Research Laboratory, Washington, D. C., where he has been engaged in developing microwave components and antenna feeds, and in the development of automatic tracking radar systems.

Since 1951 Mr. Allen has been Section Head of the New Techniques Section of Radar I Branch.

❖

William Sterling Ament was born in Pomona, Calif. on September 13, 1918. He was graduated with honors in physics from Pomona College in 1939, where he was graduate assistant in physics until 1940.

W. S. Ament

After two years as graduate student in mathematics at Brown University, Mr. Ament was employed by the Naval Research Laboratory in 1942. His work there has been in the field of radio wave propagation and radar. He serves on two radio subpanels of the Research and Development Board, and is a member of RESA.

❖

L. J. Anderson was born in Salt Lake City, Utah, in 1917. He graduated from the University of California at Los Angeles in 1939 and received the M.A. degree in 1942. He then joined the U. S. Navy Electronics Laboratory in San Diego, where he has been since.

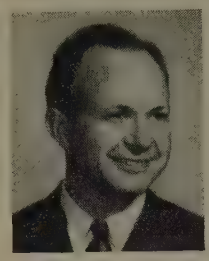

L. J. Anderson

While at N.E.L., his main fields of interest have been in tropospheric propagation and in the meteorological effects upon vhf and higher frequencies. Mr. Anderson has also been engaged in the development of special instrumentation for measuring meteorological parameters affecting electromagnetic propagation.

Mr. Anderson is at present head of the radio-meteorology section whose function is the prediction of propagation conditions from meteorological information.

❖

William J. Armstrong was born January 18, 1918, near Dubuque, Ia. He received his B.A. degree in 1947, majoring in chemistry and mathematics.

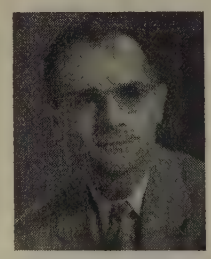

W. J. Armstrong

He worked as a research assistant at Collins Radio Company in 1946 and 1947. In 1947 and 1948 Mr. Armstrong was a graduate assistant at the University of Iowa. He was in U.S.A.A.F. communications from 1941 to 1945.

Mr. Armstrong rejoined Collins Radio as a development engineer in 1947 to work on a cyclotron project. He has since joined the resnatron development division and been instrumental in developing 200 mc, 400 mc, 600 mc, and 1,200 mc resnatrons.

❖

R. W. Beatty (S'43–A'45–M'50) was born in York, Pa. on May 31, 1917. He received the B.S. degree in electrical engineering in 1939 from the George Washington University and the S.M. degree in electrical communication from the Massachusetts Institute of Technology in 1943. From 1940 until 1942 he was associated with the Naval Research Laboratory and served as an officer in the U. S. Naval Reserve from 1943 until 1946.

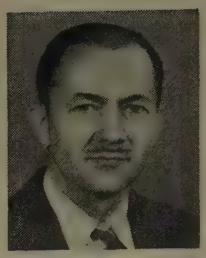

R. W. Beatty

Mr. Beatty has had several years' experience in the field of consulting radio engineering. At the present time he is in charge of the uhf group of the Microwave Standards Section at the National Bureau of Standards in Washington, D. C.

❖

Wilfred P. Bennett (S'43–A'46–M'51) was born in Milford, Mich., on October 9, 1922. He received the B.S. degree in electrical engineering from Michigan State College in 1944.

W. P. Bennett

Upon graduation, Mr. Bennett was engaged by the Radio Corporation of America at Lancaster, Penn. where he is at present in the power tube engineering group working on the design and development of tubes for uhf television and pulse applications.

Mr. Bennett is a member of Tau Beta Pi.

❖

Edward H. Braun was born in New York, N. Y., on March 27, 1925. He majored in physics at Columbia University, receiving his bachelor's degree in 1948 and master's degree in 1950. Previous to this he served in the U. S. Army for two and a half years.

E. H. Braun

Mr. Braun is currently engaged in research and development work on microwave antennas and related components as a member of the Antenna Research Branch at the Naval Research Laboratory in Washington.

❖

Albert Brodzinsky was born in Buffalo, N. Y. on July 7, 1920. He received the B.E.E. degree from Cornell University in 1942 and the M.S. degree from the University of Maryland in 1951.

A. Brodzinsky

After working briefly for the Buffalo Niagara Electric Corporation, Mr. Brodzinsky joined the Naval Research Laboratory staff in 1942 working on pulse circuitry and electronic navigation systems.

Contributors to Proceedings of the I.R.E.

Except for a brief period of active duty in the U. S. Naval Reserve, he has worked at N.R.L. on air navigation systems and is, at present, head of the Avigation Branch.

❖

Kenneth Bullington (A'45) was born in Guthrie, Okla., on January 11, 1913. He received the B.S. degree in electrical engineering in 1936 from the University of New Mexico, and the M.S. degree in 1937 from the Masachusetts Institute of Technology. Since his graduation he has been a member of the technical staff of the Bell Telephone Laboratories, where he is engaged in wire and radio transmission problems.

K. Bullington

❖

Herman N. Chait was born in Boston, Mass., on February 15, 1924. He attended Northeastern University, and transferred to Tufts College, obtaining a B.S. degree in electrical engineering in 1945. He has since done graduate work at the University of Maryland.

H. N. Chait

After three years service as an Electronics Technician in in the U. S. Navy, Mr. Chait joined the Naval Research Laboratory, doing research and development work in the microwave region. He has done research on the design of signal generators and test equipment. At present he is a member of the Antenna Research Branch at NRL doing research on antennas and microwave applications of ferrites.

❖

H. W. A. Chalberg (J'36–S'40–A'43–M'51–SM'51) was born in Evanston, Ill., on September 30, 1916. He received the B.S.E.E. degree in 1941 from Purdue University.

H. W. A. Chalberg

Except for one year Mr. Chalberg has been with the General Electric Company since 1941. He is a graduate of the Creative Engineering Program and from 1945 to 1947 was assigned to the mechanical design engineering group of the industrial control division, Electronics Section. In 1948 he transferred to the Electromedical Section of the General Electric X-Ray Corp. In 1950 he became section leader of the advanced circuit laboratory of the Receiving Tube Division in Owensboro, Ky. At present he is located in Chicago as commercial engineer for the Electronics Department.

Mr. Chalberg is an associate, member of Sigma Xi and the A.I.E.E. He is past chairman of the Evansville-Owensboro section of the I.R.E.

❖

Marvin Chodorow (A'43–SM'47) was born on July 16, 1913, in Buffalo, N. Y. He received the B.A. degree in physics from the University of Buffalo in 1934, and the Ph.D. degree from the Massachusetts Institute of Technology in 1939.

M. Chodorow

During 1940 he was a research associate at Pennsylvania State College. Dr. Chodorow was an instructor of physics at the College of the City of New York from 1941 to 1943, when he became associated with the Sperry Gyroscope Company as a senior project engineer. He remained at Sperry until 1947, when he joined the physics department of Stanford University, where he is now associate professor.

Dr. Chodorow is a member of the American Physical Society, and of Sigma Xi.

❖

Charles E. Dean (A'29–M'36–SM'43) was born in South Carolina in 1898. He attended Harvard, obtaining the A.B. degree in 1921. Following graduation he joined the engineering department of the Western Electric Company (which later became the Bell Telephone Laboratories). During this time he received the M.A. degree in physics at Columbia. In 1927 he received a doctorate in physics at Johns Hopkins, and joined the American Telephone and Telegraph Company.

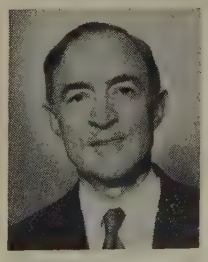

Charles E. Dean

Dr. Dean became a member of the Hazeltine Corporation staff in 1929 and has remained with this group. Here he has engaged in legal engineering work, editorial activity, and the direction of a staff of instruction-book writers At present he is assembling material for a book on color television.

John J. Egli (A'47) was born on October 22, 1911, in Teaneck, N. J. He received the B.S. degree in electrical engineering from Cooper Union in 1933, the E.E. degree from New York University in 1940, and graduate credit from Rutgers University in 1948. From 1929 to 1936, Mr. Egli was in the engineering department of the Mackay Radio and Telegraph Company, concerned with radio-telegraph equipment design and installation. From 1936 to 1941, with the Commercial Products Department of the Bell Telephone Laboratories, he participated in the design of radio-broadcast equipment, magnetic tape recorders, and voder equipment.

J. J. Egli

Since 1941, Mr. Egli has been associated with the Signal Corps Engineering Laboratories as chief of the design and construction section, of the Communication Engineering Branch; chief of the radio-relay and microwave section, of the Radio Communication Branch; and at present is a consultant on matters pertaining to wave propagation and radio-systems engineering.

Mr. Egli is a member of the Panel on Antennas and Propagation of the Research and Development Board, International Radio Consultative Committee, and of Eta Kappa Nu.

❖

For a photograph and biography of Robert C. Ellenwood, see page 1729 of the December, 1952 issue of the Proceedings of the I.R.E.

❖

Sin-pih Fan was born in Changsha, Hunan, China, on October 10, 1921. He graduated from the Yuyeng High School, Changsha, Hunan, in 1939. In 1944 he received the B.S. degree in electrical engineering from the National Central University, Chunking, China.

Sin-pih Fan

From 1944 to 1947 Dr. Fan was a teaching assistant in the aforementioned university. He then entered Stanford University, where he received the M.S. degree in 1949 and the Ph.D. degree in 1951, both in electrical engineering. During 1949 through 1951 he was a graduate research assistant in the Microwave Laboratory, Stanford University.

In 1952, Dr. Fan joined the tube laboratory of the research division of Burroughs Adding Machine Co., Philadelphia, where he

Contributors to Proceedings of the I.R.E.

is doing research on special tubes used in electronic computers.

Dr. Fan is a member of Sigma Xi.

❖

Max Garbuny was born on November 22, 1912 in Koenigsberg, Germany. He studied physics at the Technische Hochschule, Berlin, graduating with the Dipl. Ing. 1936 and the Dr. Ing. in 1938. His thesis work concerned the application of spectroscopy to atomic and nuclear physics problems.

M. Garbuny

Dr. Garbuny was associated with the Allen-Bradley Company, Milwaukee, Wisconsin, from 1939 to 1943 doing research and development work on arc discharges and timing devices. He then joined the physics department of Princeton University, teaching until 1944.

Since 1944 Dr. Garbuny has been with the Westinghouse Electric Corporation, connected at first with development work on ignitrons and engaged, after 1946, as a senior physicist at the Westinghouse Research Laboratories. He worked for several years on particle accelerators instrumental to nuclear-physics problems. Later his responsibilities concerned the theory and practice of resnatrons and general consulting in the field of microwave tubes. He is at present manager of the optical physics section at the Laboratories.

❖

For a photograph and biography of L. J. Giacoletto, see page 1607 of the November 1952 issue of the Proceedings of the I.R.E.

❖

E. E. Gossard was born in Eureka, Calif., on January 8, 1923. He received the A.B. degree in meteorology in 1948 and the M.S. degree in physical oceanography in 1951, both from the University of California at Los Angeles.

E. E. Gossard

In 1948 Mr. Gossard joined the U. S. Navy Electronics Laboratory as a meteorologist, and has since been engaged in research in the meteorology and micrometeorology of the troposphere and its effect on microwave propagation for the purpose of achieving more accurate operational predictions of radio and radar performance.

For a photograph and biography of Georg Goubau see page 871 of the July, 1952 issue of the Proceedings of the I.R.E.

❖

Alwin Hahnel was born in Karlsruhe, Germany, on September 9, 1912. He received his Dipl. Ing. degree in 1941 and the Dr. Ing. degree in 1942, both from the Karlsruhe Technical University. From 1943 to 1945 he was employed in research. He established the Radio Research Station Salzburg, Austria, and was in charge of it.

Alwin Hahnel

From 1945 to 1947 Dr. Hahnel was technical and personnel director of the decimeter communication network of the American and British occupation zones of Germany and simultaneously director of the Decimeter Laboratories of Mannheim, Germany. Since 1948, Dr. Hahnel has been a consultant at the Signal Corps Engineering Laboratories in Fort Monmouth, N. J.

❖

Clifford E. Horton (A'45–M'47) was born in Worcester, Mass., October 19, 1922. He received the B.S. degree in electrical engineering from Purdue University in 1943.

C. E. Horton

From 1943 to 1946 Mr. Horton was employed by the RCA Victor Division of RCA in the power tube development section, Lancaster, Pa.

Mr. Horton joined the General Electric Company in 1946, and was assigned circuit development work in the General Engineering Laboratory. From 1946 to 1949 he took General Electric's Advanced Course, transferring in 1947 from the Laboratory to rotating engineering assignments, which are a part of the Advanced Engineering Program. In 1949 Mr. Horton became a member of the advanced development section in General Electric's receiving-tube engineering organization at Owensboro, Ky.

Hsiung Hsu (S'46–A'51) was born in Nantung, Kiangsu, China, on January 24, 1920. He received his B.S. degree in electrical engineering from the National WuHan University, China, in 1941. From 1941 to 1945, he was employed as an engineer with the International Broadcasting Station (XGOY) in Chungking, China. He came to this country in 1945 and attended the Moore School of Electrical Engineering, University of Pennsylvania. His graduate studies were continued at Harvard University where he obtained a M.S. degree in communication engineering in 1946 and a Ph.D. degree in engineering sciences and applied physics in 1950. While at Harvard, he received a Gordon McKay scholarship and a Teaching Fellowship.

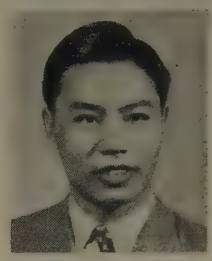

H. Hsu

During the summer of 1949, Dr. Hsu was employed by the RCA Laboratories Division of the Radio Corporation of America in Princeton, N. J. After graduation he worked in the Cyclotron Laboratory at Harvard University. Since 1950 he has been with the advanced development section of the General Electric Company in Owensboro, Ky. His work has been concerned primarily with the development of uhf receiving tubes.

Dr. Hsu is a member of Sigma Xi and the American Institute of Physics.

❖

Albert E. Hylas was born in New York, N. Y., on February 1, 1920. After graduating from the R.C.A. Institutes in 1939, he was employed at the R.C.A. Frequency Bureau. During World War II he served as Captain in charge of group radar in the Air Force Antisubmarine Command and Heavy Bomber Command. In 1947 he obtained the S.B. degree in electrical engineering from the Massachusetts Institute of Technology.

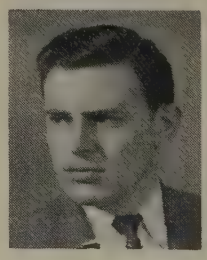

A. E. Hylas

Mr. Hylas then joined the Federal Telephone and Telegraph Laboratories in Nutley, N. J. where he engaged in studies of deposited carbon resistors and antenna systems. In 1948 he joined the research division of the Allen B. Du Mont Laboratories, where he has been engaged in studies of delay lines, transients in television transmitters, uhf and vhf television receivers and uhf tuners and converters.

Contributors to Proceedings of the I.R.E.

Robert L. Jepsen was born on June 16, 1920 in Valley, Wash. He received his B.S. degree in electrical engineering at Washington State College in 1944 and his Ph.D. degree in physics at Columbia University in 1951.

R. L. JEPSEN

He was employed by the Radio Corporation of America between 1944 and 1946 in the special development division (magnetrons). Between 1946 and 1951 he was a research associate at the Columbia Radiation Laboratory. Dr. Jepsen has published several papers on magnetron cathodes and other aspects of electron tube improvement, and holds patents in this field. He joined Varian Associates as a research engineer in 1951 and is at present director of research there.

Dr. Jepsen is a member of Tau Beta Pi, Sigma Xi and the A.P.S.

❖

Harwick Johnson (SM'45) received his B.S. degree in electrical engineering from the Michigan College of Mining and Technology in 1934 and the M.S. and Ph.D. degrees from the University of Wisconsin in 1940 and 1944, respectively.

H. JOHNSON

From 1939 to 1942 he was a research fellow and teaching assistant in the Department of Electrical Engineering at the University of Wisconsin. Since 1942 he has been associated with the RCA Laboratories Division at Princeton, N. J.

Dr. Johnson is a member of Tau Beta Pi, Gamma Alpha, and Sigma Xi.

❖

Henry F. Kazanowski (S'46–A'48–M'51) was born in Terryville, Conn., on May 11, 1923. From 1943 through 1946 he served with the U. S. Army Signal Corps in the European Theater, where he worked on the installation and operation of telephone carrier repeater equipment. He received the B.S. degree in electrical engineering in 1948 from Northeastern University.

H. F. KAZANOWSKI

Following graduation, Mr. Kazanowski was employed by the RCA Victor Division and entered their specialized training program. In 1949 he was assigned to the power tube group at Lancaster, Penn. where he worked on the design and development of tubes for uhf television.

Mr. Kazanowski has been an active amateur radio operator since 1939, having held the call letters W1NCV, W2YMX and, currently, W3PSK.

❖

L. L. Koros (A'43–SM'46) was born on July 4, 1903 in Hungary. He graduated in 1925 from the Royal Joseph Engineering University of Budapest. He then joined a European subsidiary of the International Telephone and Telegraph Company of New York.

L. L. KOROS

In order to exploit his patents in the electronic voltage control field, the Stabilovolt Companies of Holland and Germany were founded and in 1932 he became the managing director. After the outbreak of World War II Mr. Koros went to Argentina and worked for the Fabrica Argentina de Transmisores Guntsche, in Buenos Aires.

In 1943 he joined RCA Victor Argentina, S.A. and became chief design engineer of the engineering products department, in charge of engineering and manufacturing. Since 1948 he has been working in the RCA Victor Division, Camden, N. J. on advanced development projects.

❖

Raymond E. Lacy (SM'46) was born on March 17, 1916 at Camden, N. J. He obtained the B.S. and M.S. degrees, both in electrical engineering, from Drexel Institute of Technology in 1938 and New York University in 1940, respectively. From 1940 to 1948 he took additional technical graduate studies at the Polytechnic Institute of Brooklyn and from 1950–1951, personnel administration and management courses in the Graduate Division of Public Service, N.Y.U.

R. E. LACY

During 1933–1938 Mr. Lacy worked in various design engineering jobs with the Potomac Electric Power Co., Washington, D. C., and with Philco Corporation and Chubbuck and Patrick, consulting engineers, Philadelphia, Pa. He was a member of the electrical engineering faculty of N.Y.U. from 1938 to 1940, when he joined the Signal Corps Laboratories at Fort Monmouth, N. J. as a radio engineer. He has been associated directly in research and development for all types of radio communication systems. At present he is chief of communication research.

Mr. Lacy is a member of Tau Beta Pi and Eta Kappa Nu.

❖

Richard J. Lindeman (A'52) was born in Grand Rapids, Mich., on December 14, 1924. He attended Grand Rapids Junior College in 1942, and then spent the following three years in the U. S. Navy. At the end of World War II Mr. Lindeman entered the University of Michigan, where he received the B.S. degree in electrical engineering in 1949.

R. J. LINDEMAN

Since graduation, Mr. Lindeman has been employed as a member of the Engineering Development and Licensee Group of Hazeltine Corporation. His work has been concerned with the design and development of uhf television tuners and converters and with the design modification of vhf television tuners.

Mr. Lindeman is a member of both the Tau Beta Pi and Eta Kappa Nu societies.

❖

R. L. McCreary (SM'50) was born in Morning Sun, Ohio, on December 23, 1916. He received the B.S. degree from Miami University of Ohio in 1938 and the Ph.D. in physics from the University Rochester in 1942.

R. L. MCCREARY

Dr. McCreary then joined the Radiation Laboratory at Massachusetts Institute of Technology and worked on experimental radar systems with the overseas field service group. In 1945 he joined the physics department of National Research Corporation and worked on vacuum research. In 1946 Dr. McCreary became research associate in the physics department at the University of Rochester, where he assisted in development of the 130-inch synchrocyclotron. In 1949 he joined the research division of Collins Radio Company and is now head of Research and Engineering Dept. I.

Dr. McCreary is a fellow of the American Physical Society and a member of Sigma Xi.

Contributors to Proceedings of the I.R.E.

Sterling G. McNees (M'47) was born in Harrisburg, Pa., November 14, 1921. He received his B.S. degree in physics from Allegheny College in 1943.

S. G. McNees

From 1943 to 1945 Mr. McNees was employed as a special research associate at the Radio Research Laboratory at Harvard University, except for several periods with the American-British Laboratory in Great Malvern, England. From 1945 to 1946 he was employed at the Woods Hole Oceanographic Institute at Woods Hole, Mass.

Since 1946 Mr. McNees has been with Collins Radio Company of Cedar Rapids, Ia., as a project engineer, mostly concentrating on development of the resnatron.

❖

H. R. Meahl (A'28–M'45–SM'46) was born on March 16, 1905 in Jamesport, Mo. He graduated from the State College of Washington in 1927 with the B.S. degree in electrical engineering. There he was elected to Tau Beta Pi and Phi Kappa Phi.

H. R. Meahl

In 1927 Mr. Meahl joined the General Electric Company, where he was concerned first with 100-kw vacuum tubes. Before attaining his present position of section engineer in the Electronic Systems and Measurements Division in the General Engineering Laboratory he was a development engineer in radio transmitter work.

For the last sixteen years Mr. Meahl has been associated with the development of standards of frequency, current, voltage, resistance, inductance, and capacitance. He is presently interested in an electronic moisture monitor for the paper industry, an application of high-frequency measuring techniques to industry.

Mr. Meahl is a member of A.I.E.E. In 1948 he received the Coffin Award for his outstanding work in developing precision wavemeter equipment of an accuracy and usefulness never before obtained.

❖

Theodore Moreno (S'41–A'44) was born in Palo Alto, Calif. on September 2, 1920. He received his A.B. degree in electrical engineering with great distinction from Stanford University in 1941 and his M.A. there in the same field in 1942. In 1949 he received the Sc.D. degree in electrical engineering from the Massachusetts Institute of Technology. From 1942 to 1946 he was employed as a project engineer on research and development of microwave components and measuring equipment at Sperry Gyroscope Company. From 1946 to 1949 he was a research associate at M.I.T., and from 1949 to 1951 he was a research physicist in the guided missiles division of Hughes Aircraft Company. He joined Varian Associates in 1951 and is presently manager of the department for design and development of electron tubes.

T. Moreno

Dr. Moreno is the author of "Microwave Transmission Design Data" and of numerous papers on technical journals and handbooks, and holds several patents in the field of microwaves. He is a member of Phi Beta Kappa, Tau Beta Pi and Sigma Xi.

❖

Clayton E. Murdock (A'51) was born in Westminster, Calif., in 1908. He graduated from San Diego State College in 1932 with the A.B. degree. He received the General Secondary Teaching Credential at the University of California in 1934.

C. E. Murdock

From 1933 through 1941 Mr. Murdock was an instructor in the Oakland, Calif., public schools. Since 1941 he has been with Eitel-McCullough, Inc., working on the research and development of radar and high-powered vacuum tubes.

❖

For a photograph and biography of K. A. Norton see page 491 of the April, 1952 issue of the Proceedings of the I.R.E.

❖

I. D. Olin (S'49–A'50) was born on June 24, 1928, in Brooklyn, N. Y. He received the B.S. degree in electrical engineering in 1949 from the Newark College of Engineering, and the M.S. degree in 1951 from Rutgers University.

While working for the M.S. degree, Mr. Olin was a research assistant for two years in the electrical engineering department at Rutgers University.

I. D. Olin

Since 1951 Mr. Olin has been employed by the Naval Research Laboratory in Washington, D. C. where he is presently engaged in radar research with Radio Division III.

❖

R. M. Page (SM'45–F'47) was born in St. Paul, Minn. on June 2, 1903. He received the B.S. degree in physics from Hamline University, St. Paul, Minn. in 1927; the M.S. degree in physics from George Washington University, Washington, D. C. in 1932, and the Hon. D.Sc. degree from Hamline University in 1943.

R. M. Page

From 1927 to the present Dr. Page has been at the Naval Research Laboratory, where his work has been precision instrumentation in the field of electronics. In 1934 he completed the first pulse radar in the world for detection of aircraft, for which he has received the U. S. Navy Distinguished Civilian Service Award, the Presidential Certificate of Merit, and an IRE Fellowship. He is now Superintendent of Radio Division III and Associate Director of Research for Electronics at the Naval Research Laboratory.

❖

Donald H. Preist (M'44) was born in Tunbridge Wells, England, on January 18, 1916. He received the B.Sc. degree from King's College, London University, in 1936, and subsequently entered the British Government Service as a member of the first radar team in England under Sir Robert Watson-Watt. Until 1946 he was associated with various aspects of radar development; in particular, early experiments on detection of ships, and development of high-power ground radar transmitters and the MKV IF and beacon system. From 1943 to 1945 he was with the combined research group at the Naval Research Laboratory in Washington, D. C.

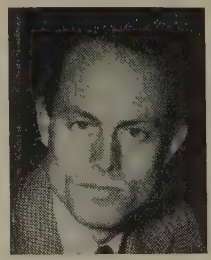

D. H. Preist

Contributors to Proceedings of the I.R.E.

During 1946 he served in the British Ministry of Supply, London, on the application of radio and radar to civil aviation, and represented the ministry at PICAO international conferences as a scientific advisor.

Mr. Preist served as a flight lieutenant in the Royal Air Force in connection with the establishment of radar in France, and later with Combined Operations Headquarters.

In 1946, Mr. Preist joined the research laboratory staff of Eitel-McCullough, Inc., San Bruno, Calif., where he is engaged as projected engineer on problems of high-power vacuum tube and circuit development.

Mr. Preist is an associate member of the Institution of Electrical Engineers, London.

❖

Frank Reggia was born in Northumberland, Pa. on October 30, 1921. He attended George Washington University, and is a graduate of Radio Materiél School at the Naval Research Laboratory in Washington, D. C. While a member of the Armed Forces, he served as an electronic specialist in both the United States and in the Pacific Theatre. Following separation in 1945, he joined the staff of the Microwave Standards Section of the National Bureau of Standards, where he has since been engaged in research and development in a uhf standards program

FRANK REGGIA

❖

William E. Ryan (S'43–A'45) was born in Springfield, Mass., on February 6, 1920. He received a B.S. degree in electrical engineering and mathematics from the University of Michigan in 1943. Since 1946 he has been attending evening classes in the physics department of George Washington University Graduate School.

WILLIAM E. RYAN

From 1943 to 1944 he was employed by the Naval Research Laboratory as a radio engineer assisting in tests of anti-aircraft gun directors. Since 1944 Mr. Ryan has been employed by the National Bureau of Standards in Washington, D. C., assisting in the development of field intensity standards. At present he is associated with the Ultra-High Frequency Standards Group of the Microwave Standards Section.

Mr. Ryan is a member of Eta Kappa Nu and Sigma Pi Sigma.

Nicholas G. Sakiotis (S'48–A'50) was born in Lakeland, Fla., on March 5, 1928. He received the B.E.E. degree at the College of the City of New York in 1950.

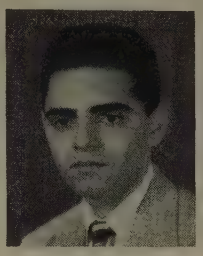

N. G. SAKIOTIS

After working with the Glenn L. Martin Company and the Marine Radar Design Branch of the Bureau of Ships, Mr. Sakiotis joined the Antenna Research Branch of the Naval Research Laboratory in 1951. While with the Laboratory, he has investigated figure-of-revolution scanners and is at present engaged in a study of the microwave properties of the ferrite materials.

❖

Chester E. Sharp (A'51) was born on June 2, 1906 at Long Branch, N. J. In 1940 he joined the Field Radio Section of the Signal Corps Laboratories, where he was concerned with the design of the first portable frequency-modulated military field radio equipment. In 1942 Mr. Sharp was assigned to investigation work on microwave receiver designs and components. As project engineer with the Radio Relay and Microwave Section on microwave transceiver designs in 1944, he developed the first man pack radio-relay equipment. His present assignment is with the Radio Communication Research Section, Coles Signal Laboratory, Fort Monmouth, N. J.

C. E. SHARP

❖

Walter V. Tyminski was born on July 19, 1924 in Cliffside, N. J. He received the B.S. degree in electrical engineering from Newark College of Engineering in 1948, and the M.S. degree in engineering sciences and applied physics from Harvard University in 1949.

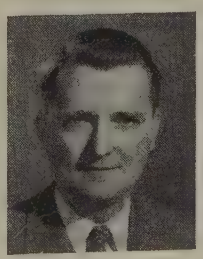

W. V. TYMINSKI

Upon graduation he joined the Spencer Kennedy Laboratories of Cambridge, Mass., where he was engaged in the development of distributed amplifiers. During 1950, Mr. Tyminski was associated with Industrial Television, Inc. of Clifton, N. J., and in 1951 joined the research division of the Allen B. Du Mont Laboratories, Inc., Passaic, N. J. At Du Mont he has been engaged in studies of agc systems, vhf and uhf television receivers and uhf tuners and converters.

Mr. Tyminski is a member of Tau Beta Pi.

❖

For a photograph and biography of G. S. WICKIZER, see page 1731 of the December, 1952 issue of the PROCEEDINGS OF THE I.R.E.

❖

John J. Woerner was born in Oakland, Calif., on September 26, 1914. He attended the University of California at Berkeley from 1933 to 1936, majoring in mechanical engineering.

J. J. WOERNER

Mr. Woerner joined the engineering staff of Eitel-McCullough, Inc., in 1940, working mainly on vacuum tubes and vacuum-tube test equipment design, including work on a number of high-power hard-tube modulators. Since 1950 he has been project engineer in charge of the development of high power uhf klystrons.

Mr. Woerner is a registered professional engineer in the State of California and a licensed radio amateur.

❖

Rudolph R. Zirm (A'51) was born in Jersey City, N. J. on August 3, 1923. He received the B.S. degree in electrical engineering from the Newark College of Engineering in 1944. Since then he has been associated with the U. S. Naval Research Laboratory as an electronic scientist, and is at present head of the Command Guidance Section of the Avigation Branch of Radio Division III. He has been engaged principally in experimental research on electronic guidance systems, data transmission, and applications of communication theory.

R. R. ZIRM

Mr. Zirm is an associate member of the A.I.E.E., and a registered professional engineer in the District of Columbia.

Institute News and Radio Notes

Calendar of COMING EVENTS

IRE-AIEE Meeting on High-Frequency Measurements, Washington, D. C., January 14–16

IAS-IRE-RTCA-ION Symposium on Electronics in Aviation, New York, N. Y., January 26–30

IRE-AIEE Western Computer Conference, Hotel Statler, Los Angeles, Calif., February 4–6

IRE Southwestern Conference and Electronics Show, Plaza Hotel, San Antonio, Tex., February 5–7

IEE Symposium on Insulating Materials, London, Eng., March 16–18

1953 IRE National Convention, Waldorf-Astoria Hotel and Grand Central Palace, New York, N. Y., March 23–26

IRE New England Radio Engineering Meeting, Storrs, Conn., April 11

9th Joint Conference of RTMA of United States and Canada, Ambassador Hotel, Los Angeles, Calif., April 16–17

IRE Seventh Annual Spring Technical Conference, Cincinnati, Ohio, April 18

SMPTE Convention, Statler Hotel, Los Angeles, Calif., April 26–30

NARTB Convention, Biltmore Hotel, Los Angeles, Calif., April 28–May 1

1953 IRE National Conference on Airborne Electronics, Dayton, Ohio, May 11–14

1953 Electronics Parts Show, Conrad Hilton Hotel, Chicago, Ill., May 18–21

1953 IRE-RTMA Radio Fall Meeting, Toronto, Ont., October 26–28

IRE Founders Award Established

The Institute's Board of Directors recently established an IRE Founders Award to be given on special occasions in recognition of an outstanding leader in the radio industry. The award commemorates the three radio pioneers who founded the Institute of Radio Engineers forty years ago—Alfred N. Goldsmith, Editor of the Institute and consulting engineer; John V. L. Hogan, president of Hogan Laboratories, New York, N. Y.; and Robert H. Marriott, deceased.

Brigadier General David Sarnoff, Chairman of the Board of the Radio Corporation of America, is the first recipient of the new award which will be presented at the IRE Annual Banquet, Hotel Waldorf Astoria, New York, N. Y., March 25, during the IRE National Convention. General Sarnoff is to be given the award "for outstanding contributions to the radio engineering profession through wise and courageous leadership in the planning and administration of technical developments which have greatly increased the impact of electronics on the public welfare."

IRE Officers for 1953 Announced

At its meeting on November 6, 1952, the Board of Directors announced the results of the elections for officers and directors of the Institute as follows:

President, 1953: James W. McRae, Bell Telephone Laboratories, Inc., New York, N. Y.

Vice President, 1953: S. R. Kantebet, Government of India Overseas Communications Service, Bombay, India.

Directors-Elected-at-Large, 1953–1955: Stuart L. Bailey, Jansky and Bailey, Washington, D. C.; B. E. Shackelford, License Department, RCA International Division, New York, N. Y.

Regional Directors, 1953–1954: Region 2, John R. Ragazzini, Columbia University, New York, N. Y.; Region 4, Conan A. Priest, General Electric Company, Syracuse, N. Y.; Region 6, Archie W. Straiton, University of Texas, Austin, Tex.; Region 8, John T. Henderson, National Research Council, Ottawa, Ont., Canada.

Technical Committee Notes

The **Standards** Committee convened on October 9. M. W. Baldwin took the chair in the absence of A. G. Jensen. A. F. Pomeroy, representing A. G. Clavier, Chairman of the Symbols Committee commented on the distribution of the ASA Y32/2 Standard on Graphical Symbols. Mr. Baldwin then asked the Committee to consider a proposed list of personnel which was to be published with the Receiver Standard (52 IRE 17. S1). The Commiteee then gave consideration to the Modulation Definitions. Reviewing completed, these definitions will be collated with the first half of the Modulation Definitions which were approved in September. After L. G. Cumming presented the Color Television Terms (52 IRE 22. PS1), he then summarized the background work done by the Television Subcommittee in its preparation of the 43 definitions. It was decided that no action should be taken during this meeting, and Chairman Baldwin was asked to revise the introduction for presentation at the next Committee meeting, which met on November 13, under the Chairmanship of A. G. Jensen. During this meeting, the Committee devoted most of the discussion to two tentative standards; the Proposed Standards on Television: Definitions of Color Terms (52 IRE 22. PS1), and the Standards on Sound Recording and Reproducing: Methods of Measurement of Noise in Sound Recording and Reproducing Systems (51 IRE 19. PS1). The Committee adopted both documents, to be presented to the Executive Committee at an early date. A motion was passed for the Standards Committee to adopt for the IRE the proposed ASA Y32/2 Standard on Graphical Symbols, with the proviso that the Symbols Committee prepare a suitable preface to the effect that the standard represents the joint effort of several organizations to whom due credit is to be given. The Standards Committee is to be acquainted also with any editorial changes made on the draft.

On November 7, the **Electron Devices** Committee met, under the Chairmanship of G. D. O'Neill. The Annual Review material on klystrons, traveling-wave tubes, and magnetrons was submitted by G. A. Espersen, and copies were distributed for possible additions to the bibliographies. T. J. Henry reported that he was in the final stages of assembling and adding to the material already collected on receiving tubes, by E. M. Boone and R. W. Slinkman, for the Subcommittee on SSHVT. W. H. Hall is co-ordinating the material on semiconductor devices. It was moved that the Klystron, Magnetron, and Traveling-Wave Tube Definitions, which were appended to the July 11, 1952 minutes, be approved except for the two Klystron Definitions, Electronic Efficiency and Circuit Efficiency which are to be rewritten. No specific action was taken on the Storage Tube Definitions, Appendix B, minutes of the September 12 meeting, in the absence of Subcommittee Chairman R. B. Janes. A report on the deliberations of the October 17 meeting of the Ad Hoc Committee on Reorganization was submitted by L. S. Nergaard in the absence of M. E. Hines. An extensive and detailed estimate had been made of the kind and amount of work facing the Electron Devices Committee in preparing revised standards in all categories, for a hypothetical deadline in 1958.

The **Information Theory and Modulation Systems** Committee met on September 15, under the Chairmanship of W. G. Tuller. Considerable discussion was held on the information theory terms, message, information, and information content.

On October 31, the **Navigation Aids** Committee met under the Chairmanship of P. C. Sandretto. Winslow Palmer presented comments on the terms "A and R Scope," and discussion ensued on the use of "scope" versus "display." A motion was passed that all definitions referring to various types of scopes should be changed to ready various types of displays. The Committee then completed the first half of the list of terms submitted by Harry Davis.

The **Receivers** Committee convened at Syracuse, N. Y., on October 22, under the Chairmanship of Jack Avins. Chairman Avins announced the resignation of the following Committee members: S. C. Spielman, C. R. Miner, and W. F. Sands. Members who have joined the Committee since its

(*Continued on following page*)

500 Attend September Cedar Rapids Technical Conference on Communications

A. A. Collins delivers the keynote and welcoming address.

The banquet session during the Conference.

L. V. Berkner (center) is greeted by A. W. Graf. At left is Jim Hollis, Chairman of Section.

(Technical Committee Notes cont'd)

last meeting are: L. E. Closson (Philco), D. E. Harnett (GE), and I. J. Melman (CBS). The scope of the Committee was reviewed. Due to the absence of K. W. Jarvis, no report was available on the activities of Subcommittee 17.3 (Single Sideband Receivers). R. F. Shea, Chairman of Subcommittee 17.4 on Spurious Radiation, reported that the Supplement to 51 IRE 17. S1 had been passed by the Standards Committee. Additional work remains on the standardization of uhf radiation measurements specification of standard antenna for range between 88–174 mc and 216–470 mc. Progress in standardization of test methods for sweep radiation was to be reported following the subcommittee meeting held in October. Chairman Avins commented on the excellent work done by the Spurious Radiation Subcommittee, since its formation, and its great value to the industry. The Annual Review report was discussed by L. M. Harris, and several items for inclusion were suggested which will be circulated among Committee members for their comments. The Chairman reported that the Definitions on Receivers were in galley form and would be published in the December, 1952 issue of the Proceedings. Subcommittee 17.6, therefore, is deactivated with a vote of thanks to its personnel. R. DeCola's group (IEC Task Group), reviewing the proposed International Electrotechnical Commission Standards for Testing AM Receivers, has completed its work, a report having been submitted August, 1952. As a byproduct of this group's work, data are now available on the differences between the IEC and IRE standards, which should be useful in future revisions of the IRE standard. W. O. Swinyard has accepted the chairmanship of the Subcommittee on the Revisions of Methods of Testing (Monochrome) TV Receivers, due to the past resignation of W. F. Sands. In connection with the manuscript on Methods of Testing AFC (local oscillator frequency stabilization) prepared by F. B. Uphoff, it was decided to defer action on this until a standard broader in scope might be prepared. This action is desirable, in view of the present status of the committee scope and the wide use of AFC in other than home entertainment receivers.

FCC Asks JTAC to Study Radiation Interference

The Joint Technical Advisory Committee was requested by the FCC in a letter dated December 3, 1952 from Chairman P. A. Walker to supplement its volume, "Radio Spectrum Conservation," with a study of the problems relating to spurious radiations from transmitters, receiver emissions, and noncommunication services. The FCC suggested that the study be considered in the following topics:

(a) The limits that should be established for radiations, which are incidental to the operation of equipment and which do not fall within allocated frequency bands, to assure safe and reasonable protection from interference to radio broadcasting, communication, and navigation services.

(b) Review the technical problem of reducing spurious radiation from various devices to determine the feasibility of the suppression measures necessary to accomplish the radiation limitations determined under Item 1.

(c) Review the problem of instrumentation necessary to effectuate a national program of the control of spurious radiation. The study should consider the practical problems of quality control measurements for the factory and simple tests that may be applied in the field to completed installations.

(d) Study the procedures and organizations activity in this field to determine whether additional effort is required to coordinate interference reduction efforts.

(e) Determine any needed action to co-ordinate the external performance of receivers with the engineering of service and station allocations.

As a result of meetings held on December 9 and December 18, Chairman Ralph Bown informed the FCC that the JTAC would accept the task.

Southwestern Conference Promises Huge Success

Over 1,200 IRE members, friends, and associates are expected for the Southwestern IRE Conference and Electronics Show February 5–6, 1953, at the Plaza Hotel, San Antonio, Tex.

The 3 days of double technical sessions will cover a wide variety of subjects including reports on new fields such as space travel and guided missiles. The Electronics Show will fill 46 exhibit booths and a seven-room "audio center." Over 95 per cent of the available space has been sold for exhibits and demonstrations of the latest equipment in the industry.

Highlighting the speakers will be a keynote address by A. T. Waterman, director of the National Science Foundation, and IRE President J. W. McRae, is scheduled tentatively to address a technical session or banquet meeting.

Among the social events will be the annual banquet, an informal party, and tours. Arrangements are being made for a ladies' program which will include special visits to many of the historical landmarks and points of interest in and near San Antonio.

For further information concerning the conference write to: A. W. Straiton, Electrical Engineering Department, University of Texas, San Antonio, Tex.

Notice!

PGQC-1 TRANSACTIONS

A limited supply of the Transactions of the Professional Group on Quality Control, containing papers of the Radio Fall Meeting in Toronto, Ont., October, 1951, and the Quality Control papers presented at the 1952 IRE National Convention, are still available.

Copies may be obtained for $1.20 for members of the Group, $1.80 for IRE members, and $3.60 for nonmembers by writing to: The Institute of Radio Engineers, 1 East 79 Street, New York 21, N. Y.

The Second Annual Professional Group Broadcast Symposium

G. Edward Hamilton

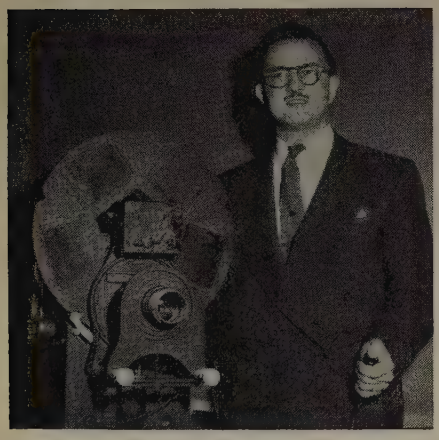

Alfred Jenkins

C. Robert Paulson

An enthusiastic audience, of several hundred, representing broadcasters and members of industry from all parts of the country, convened during the Second Annual Broadcast Symposium of the IRE Professional Group on Broadcast Transmission Systems, at Franklin Hall on October 27, and heard a striking report on broadcasting.

The meeting was highlighted by a series of operational exhibits which supplemented many of the papers. On view, and in some instances in operation, were complete rear-screen projection equipment, special-effect devices, tape recorders, a uhf klystron, audio switching units, high-power uhf tubes, flying-spot scanner mechanisms, and the 35 foot Telemobile which was used by NBC during the recent political conventions in Chicago. Surveyed at the sessions, held during the morning, afternoon, and evening, were special effects and their relation to camera design and pickup, the characteristics and applications of film scanners, audio techniques, ultra-high tubes and station facilities, and special-event practices.

A series of papers was offered on camera special-effect systems: Alfred Jenkins, Trans-Lux Corp., covered rear-screen projection; C. Robert Paulson, Audio-Video Products, discussed TV broadcasting production techniques; and G. Edward Hamilton, ABC, analyzed gray-scale considerations of a TV system. These talks were followed by four discussions on flying-spot scanners: Jesse Haines, Allen B. DuMont Labs, presented a paper on flying-spot scanner optics; R. E. Graham, Bell Labs., probed flying-spot scanner design; and J. W. Wentworth, RCA, discussed flying-spot scanner gamma-correction circuits. Through the courtesy of BBC, London, Arthur S. R. Toby, of the New York office, presented a recorded talk by R. H. Hammans on flying-spot telecine equipment and its use at BBC.

In a session on the ultrahighs, F. J. Bias, G.E., covered a high-power uhf broadcasting system, and Robert Manfredi, also of G.E., reviewed the subject of power tubes for uhf TV service. John S. McCullough, Eitel-McCullough, Inc., presented a paper on the operational characteristics of the klystron amplifier.

(*Continued on page 171*)

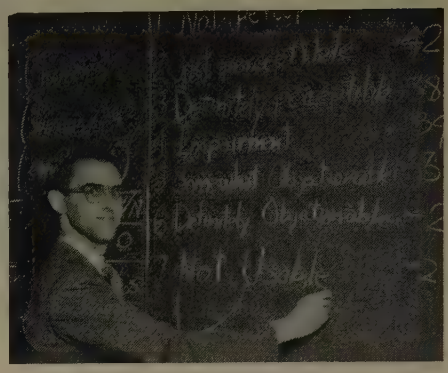

J. W. Wentworth

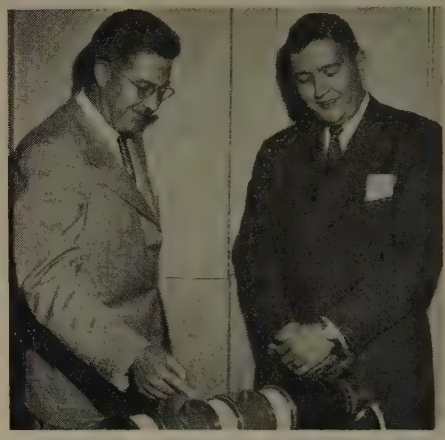

(l.) Jack McCullough, (r.) J. S. McCullough

(l.) R. E. Manfredi and (r.) F. J. Bias

Giant "Telemobile" on view during symposium

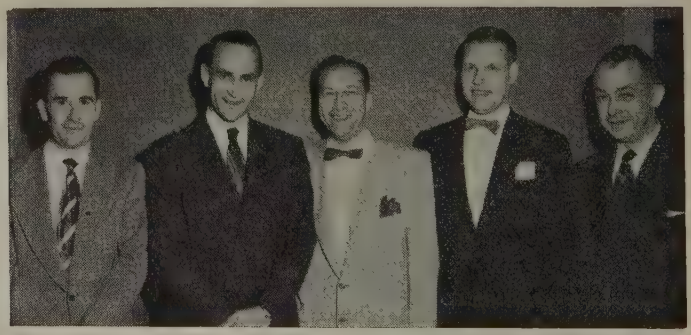

(l. to r.) William Trevarthen, Orville Sather, Lewis Winner, Rodney Chipp and F. A. Wankel

Professional Group News

Computers Proceedings Available

The "Review of Electronic Digital Computers," proceedings of the joint AIEE-IRE Computer Conference, held in Philadelphia, December, 1951, is still available in bound-volume form for $3.50.

Orders may be placed by writing to: The Institute of Radio Engineers, 1 East 79 Street, New York 21, N. Y.

Antennas and Propagation

A meeting of the Chicago Chapter of the Professional Group on Antennas and Propagation was held recently at the Western Society of Engineers Building, Chicago, Ill. J. S. Brown presided.

During the meeting, Edward Dyke, Motorola Inc., presented a paper on "Antenna Design for Microwave Relays," in which he discussed various phases in the design of antennas for microwave relays, including choice of frequency, type of antenna, type of feed, and so forth.

A set of slides illustrated such phases as a series of calculations of antenna performance with respect to impedance and bandwidth, and showed typical installations.

Audio

A petition for the formation of an Albuquerque Audio Group Chapter has been approved by the Executive Committee. D. V. Couden, Sandia Corporation, is organizer of the Chapter.

Circuit Theory

The Los Angeles Group Chapter on Circuit Theory held their November meeting at the Institute for Numerical Analysis, UCLA. Louis Weinberg, Hughes Aircraft Co., Chairman of the Group, spoke on, "Network Synthesis—What It Means."

Communications

A symposium on Military Communications was sponsored by Professional Group on Communications, recently, at Coles Signal Laboratory, Fort Monmouth, N. J.

The latest developments in Signal Corps, Air Force, and Navy communications were discussed, as well as varied contributions of electronic manufacturers to the military.

Speakers and their subjects were: John Hessell, Coles Signal Laboratory, who spoke on tactical military radio communications systems; W. C. Lent, Andrews Air Force Base, who spoke on global communications systems planning; J. A. Krcek, Navy Bureau Ships, who spoke on aspects of naval communications systems; and J. E. Smith, Raytheon Manufacturers Co., who discussed the manufacturer's contributions to military communications.

Electron Devices

R. W. Slinkman, Sylvania Electric Products Inc., is Chairman of the newly organized Group Chapter on Electron Devices in Emporium, Pa.

Engineering Management

The Professional Group on Engineering Management has announced the official approval of a chapter in Washington, D. C.

Professional Group Chapters

Forty-one chapters of the IRE Professional Groups now are operating officially, 14 in the West, 18 in the mid West, and 9 in the East. Petitions are being circulated for an additional 6 to be established.

Microwave Theory and Techniques

A Symposium on Microwave Circuits, sponsored by the Professional Group on Microwave Theory and Techniques, was held November 7, Western Union Auditorium, New York, N. Y. Representatives from many parts of the country were among the more than 200 members and guests.

Ben Warriner, Chairman of the Group, opened the meeting with a brief discussion on the Group's current state and its future plans. It was pointed out that new members are needed for the Executive Committee and can be nominated by petition from Group members who are in good standing.

The technical sessions were led by A. G. Clavier and G. C. Southworth, who were the chairmen of the morning and afternoon sessions. Outstanding papers were presented in the fields of microstrip, transmission lines, multimode waveguides, ferrites, and microwave components. Some of the papers presented may be published in a forthcoming Transactions of the Professional Group on Microwave Theory and Techniques.

Officers for the symposium included R. E. Henning, Chairman of the Publicity Committee; A. L. Witten, Chairman of the Arrangements Committee; and A. C. Beck, Chairman of the Papers Committee.

(*Professional Broadcast Symposium, cont'd*)

A comprehensive review of the audio installation at the ABC center in New York City was offered by A. C. Angus, G.E., and E. P. Vincent and John Bourcier, ABC, with Vincent presenting the paper.

The inside story of radio-TV special-event coverage at the Chicago political conventions was told by representatives of the networks. Orville Sather, CBS, discussed the TV industry pool; Rodney Chipp, DuMont TV Network, analyzed the pool master control setup; F. A. Wankel, NBC, reviewed network coverage, and William Trevarthen, ABC, discussed AM facilities, and the human side of special-event coverage.

George Lewis of WCAU, Clifford C. Harris of WIP and Louis E. Littlejohn of WFIL, moderated the three sessions. Scott Holt of Allen B. DuMont, Clure Owen of ABC, and Lewis Winner, Chairman of the group, arranged the program. Chairman Winner also served as session commentator.

Preprints of most of the papers were available at the meeting. All of the papers will be included in a special Transaction issue for mailing to paid group members who were unable to attend. Those who have not paid their assessment can obtain copies of the Transactions upon payment of the $2.00 assessment fee.

TRANSACTIONS OF IRE PROFESSIONAL GROUPS

The following issues of Transactions have recently been published by IRE Professional Groups and additional copies are available from the institute of Radio Engineers, Inc., 1 East 79 Street, New York 21, N. Y., at the prices listed below.

Sponsoring Group	Publication	Group Members	IRE Members	Non-members*
Airborne Electronics	PGAE-5; "A Dynamic Aircraft Simulator for Study of Human Response Characteristics" (8 pages)	$0.30	$0.45	$0.90
	PGAE-6; "Ground-to-Air Co-channel Interference at 2,900 MC" (29 pages)	0.30	0.45	0.90
Antennas and Propagation	PGAP-4; IRE Western Convention, August, 1952 (136 pages)	2.20	3.30	6.60
Audio	PGA-10; November-December Issue (28 pages)	0.70	1.05	2.10
Circuit Theory	PGCT-1; IRE Western Convention, August, 1952 (100 pages)	1.60	2.40	4.80
Electron Devices	PGED-1; Papers from IRE Conference on Electron Tube Research and IRE-AIEE Conference on Semiconductor Research, June, 1952 (32 pages)	0.80	1.20	2.40

* Public libraries and colleges can purchase copies at IRE Member rates.

1953 IRE National Convention News

MORE THAN 30,000 radio engineers and scientists from all parts of the world will convene on March 23 through 26, at the Waldorf-Astoria Hotel and Grand Central Palace in New York City for the most important technical event of the year—the 1953 IRE National Convention. Plans for the convention, now nearing completion, indicate that the convention theme, "Radio-Electronics, A Preview of Progress," will be faithfully carried out by an outstanding program of technical papers and exhibits, affording members the unique opportunity to "preview" the major developments in all branches of the radio engineering field.

❖

Annual Meeting

Of particular interest to members will be the innovations which are planned for the Annual Meeting of the Institute on the first day, March 23. This opening meeting of the Convention, to be held at 10:30 A.M. in the Grand Ballroom of the Waldorf-Astoria, will feature William R. Hewlett, Vice President of Hewlett Packard Co., as principal speaker, and will include reports of IRE officers on the status and operations of the Institute. Among the added features of the meeting will be the presentation of the gavel of office to IRE President J. W. McRae by his predecessor, D. B. Sinclair, and the awarding of special pins to nine Charter Members of the IRE, commemorating the three founders of the Institute, Alfred N. Goldsmith, John V. L. Hogan, and Robert H. Marriott. Messrs. Goldsmith and Hogan, and the family of R. H. Marriott will be present during the ceremonies.

❖

Technical Program

Under the chairmanship of Lloyd DeVore, the Technical Program Committee in co-operation with IRE Professional Groups, is planning a papers program of particular interest and significance this year, consisting of some 43 sessions and about 220 papers. Particularly noteworthy is the role that the Professional Groups are playing in organizing the program. At last count, nine Professional Groups are planning eleven special symposia on subjects of particular and timely interest in their respective fields. In addition, all Groups are assisting the Technical Program Committee in scheduling regular technical sessions comprising voluntarily contributed papers in their special fields.

Technical Sessions will be held in the Grand Ballroom, the Jade Room, and Astor Gallery on the third floor of the Waldorf-Astoria Hotel; in the Gold and Blue Halls on the third floor of the Grand Central Palace, a convenient two blocks from the Hotel; and in the Moderne Room of the Belmont Plaza.

❖

Exhibits

The Grand Central Palace will be the scene of what has become the most comprehensive technical display of radio-electronic apparatus and their applications in the world. Exhibits Manager William C. Copp reports that this year's Radio Engineering Show will be larger than ever with about 400 exhibitors completely filling four floors of the Grand Central Palace. The exhibits will run the entire gauntlet of products from subminiature circuits to complete communications systems, affording engineers an unparalleled opportunity for visual examination of the latest products in every field and consultation with the manufacturers' representatives.

For the convenience of those interested in specialized fields, many of the exhibits located on the third and fourth floors of the Palace will be grouped according to such subjects as audio, nuclear, components, instruments, mobile equipment, military radio, airborne equipment, and computers. Several theaters will be provided for the demonstration of audio and television equipment. As noted above, both lecture halls will be located on the third floor this year.

❖

Social Events

A "get-together" Cocktail Party will be held on the first evening of the convention, March 23, in the Waldorf Astoria's Grand Ballroom. In these spacious surroundings, members and guests will have an excellent opportunity to renew old acquaintances and make new ones.

The Annual IRE Banquet will be held in the Grand Ballroom of the Waldorf on Wednesday evening, March 25, at which time the Institute awards for 1953 will be presented by President McRae. The major address will be delivered by General David Sarnoff, the first recipient of the IRE Founders Award. His speech promises to be of great interest, not only to professional engineers, but to the entire electronics industry.

❖

Women's Activities

Mrs. Raymond F. Guy, Chairman of the Women's Activities Committee, reports that an attractive program has been arranged for the wives of members and guests. Activities will include fashion shows, tours of points of interest, luncheons, and matinee performances of leading Broadway shows.

❖

Further Details

As convention plans progress they will be reported in these pages in subsequent issues, and the Convention (March) issue of the PROCEEDINGS will contain a complete program of events, together with 100-word abstracts of all papers to be delivered at the convention.

IRE/AIEE Meeting on High-Frequency Measurements

HOTEL STATLER, WASHINGTON, D. C., JANUARY 14–16, 1953

Wednesday, 9:30 A.M., January 14

Registration

Wednesday, 1:30 P.M., January 14

MEASUREMENT OF FREQUENCY, WAVELENGTH AND TIME

Chairman, Harold Lyons, National Bureau of Standards

"Welcome and Introductory Remarks," A. V. Astin, National Bureau of Standards

"Precision Measurements of the Velocity of Electromagnetic Waves and the Refractive Indices of Gases at Microwave Frequencies," L. Essen, National Physical Laboratory

"Precision Microwave Measurement of Propagation Velocity of Electromagnetic Waves," W. W. Hansen,* W. J. Barclay,† K. Bol,‡ Stanford University

"The Measurement of Resonant Cavity Characteristics," G. L. Hall and B. Parzen, Federal Telecommunications Laboratories, Inc.

"Current Microwave Frequency Calibration Procedures at the National Bureau of Standards," A. E. Wilson, National Bureau of Standards

"New Techniques with Frequency and Time Counters," A. S. Bagley, Hewlett-Packard Co.

"Performance and Reliability Considerations of Underground Quartz-Crystal Resonators," T. A. Pendleton, National Bureau of Standards

* Deceased 1948, † now at Oregon State College, ‡ now at Sperry Gyroscope Company.

(*Continued on following page*)

(*High-Frequency Measurements Meeting cont'd*)

"Electronic Chronograph," W. E. Leavitt, Naval Research Laboratory

Thursday, 9:30 A.M., January 15

MEASUREMENT OF POWER AND ATTENUATION

Chairman, E. W. Houghton, Bell Telephone Laboratories, Inc.

"Measurement of High Power Breakdown in Transmission Line Components," M. S. Tanenbaum, Sperry Gyroscope Co.

"Water Calorimeters in Pressurized Rectangular Wave Guides," H. H. Grimm, General Electric Co.

"40–4,000 Microwatt Power Meter," R. W. Lange, Bell Telephone Laboratories, Inc.

"A Microwave Double Detection Measuring System with a Single Oscillator," D. H. Ring, Bell Telephone Laboratories, Inc.

"A Rectangular-Waveguide Below-Cutoff Attenuator as a Standard of Microwave Attenuation," R. W. Hedberg, National Bureau of Standards

"A Broad-Band Precision Waveguide Attenuator," B. P. Hand, Hewlett-Packard Co.

Thursday, 12:15 P.M., January 15

Luncheon, Hotel Statler

Chairman, E. P. Felch, Chairman, Joint AIEE-IRE Committee on High Frequency Measurements

Thursday, 2:00 P.M., January 15

Inspection Trips, Chartered Buses Leave from Hotel Statler

Thursday, 8:15 P.M., January 15

Demonstration Lectures, Interior Department Auditorium, Annual Joint Meeting of the Washington Sections of AIEE and IRE.

Chairman, F. Hamburger, Jr., Chairman AIEE Group, Joint AIEE-IRE Committee on High Frequency Measurements

"Microwave Propagation on Dielectric Rods and in Ferromagnetic Media," A. G. Fox, Bell Telephone Laboratories, Inc.

"A New Transistor for High Frequency Use," R. L. Wallace, Jr., Bell Telephone Laboratories, Inc.

Friday, 9:30 A.M., January 16

MEASUREMENT OF TRANSMISSION AND RECEPTION

Chairman, J. W. Kearney, Airborne Instruments Laboratory

"Frequency Considerations in the Transcontinental Radio Relay System," H. E. Curtis and J. B. Maggio, Bell Telephone Laboratories, Inc.

"A Waveguide Cavity for an Externally Tuned Reflex Oscillator at 9 KMC," N. A. Spencer and David Dettinger, Wheeler Laboratories

"Recent Developments on a New Type of Wide Range Electronically Tunable Oscillator," S. F. Kaisel, Electronics Research Laboratory, Stanford University

"Millimeter Waves from Harmonic Generator," W. Johnson, Radiation Laboratory, The Johns Hopkins University

"A Microwave Correlator," R. M. Page, A. Brodzynsky, Naval Research Laboratory

"A Note on the Stability of Microwave Noise Generators," W. W. Mumford, Bell Telephone Laboratories, Inc.

"Signal Generator Terminations for Receiver Measurements," Emerick Toth and L. S. Bearce, Naval Research Laboratory

Friday, 2:00 P.M., January 16

MEASUREMENT OF IMPEDANCE

Chairman, F. J. Gaffney, Polytechnic Research and Development Co.

"Swept Wide-Range SWR Indicators for 100 through 1,350 Megacycles," W. P. Peyser, Airborne Instruments Laboratory

"Balance Measurements on Balun Transformers," O. M. Woodward, Jr., RCA Laboratories Division

"Measurement of Crystal Mixer Dynamic IF Admittance," W. T. Doolittle, Jr. and A. Ackerman, Sperry Gyroscope Co.

"Design, Performance, and Application of a New Hybrid Junction," M. D. Adcock, Hughes Aircraft Co.

"The Design and Construction of a Relatively Inexpensive Long Slotted Line," C. F. Miller, The Johns Hopkins University

"Accurate Comparison of High SWR-Application to the Attenuation Constant of a Waveguide," Georges Deschamps, Federal Telecommunication Laboratories, Inc.

"Precision Measurements of Dielectric Constants and Attenuation Constants at Microwave Frequencies," H. M. Altschuler and A. A. Oliner, Microwave Research Institute

IRE People

John Ruze (S'39–A'40–M'46), has been appointed director of research of the Gabriel Company Laboratories.

JOHN RUZE

Dr. Ruze was born in New York, N. Y. in 1916, and received the B.S. degree in electrical engineering from the College of the City of New York in 1938. He received the M.S. degree from Columbia University and the D.Sc. degree from the Massachusetts Institute of Technology.

During World War II, Dr. Ruze became associated with the Signal Corps Engineering Laboratories, and from 1942–1946, he headed the antenna design section at the Evans Laboratory. In 1946, he joined the Air Force Cambridge Electronic Research Laboratory, where he served as assistant chief of the antenna laboratory until 1948. He later worked at the radar laboratory of that organization.

Dr. Ruze is a member of the American Physical Society, Epsilon Chi, Tau Beta Pi, and Eta Kappa Nu.

Robert E. Samuelson (SM'45) has been appointed chief engineer of the Motorola, Inc. research laboratories, Phoenix, Ariz. He has been head of the communications research section for the company.

R. E. SAMUELSON

A native of Minnesota, Mr. Samuelson received the B.S. degree from the University of Minnesota in 1933. From 1934–1938 he was a radio engineer for the Collins Radio Company in Cedar Rapids, Iowa, where he worked on the design and development of portable and aircraft radio equipment. He then joined the Hallicrafter Company in Chicago, Ill., in charge of all transmitters and audio amplifiers and later became the chief engineer.

After serving as president of the Voice and Vision Company in Chicago, Mr. Samuelson joined Motorola, Inc., in 1950.

Mr. Samuelson has been active on panel 14 of RTPB and several committees of RMA. He is a member of the Radio Engineers Club of Chicago.

Edwin J. Rudisuhle (A'50) has been appointed to the sales engineering department of Lenkurt Electric Company, San Carlos, Calif. Previously Mr. Rudisuhle was chief of the ninth region Civil Aeronautics Administration.

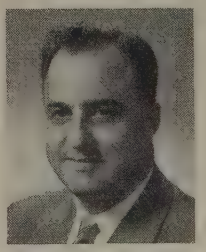

E. J. RUDISUHLE

Mr. Rudisuhle was born in Minnesota, and received the B.E.E. degree from the University of Minnesota in 1940. From 1941–1943, he was a radio engineer for the Federal Communications Commission working with high-frequency direction finding and monitoring. During World War II, he served with the communications operation division of the United States Coast Guard, traveling widely in his work with direction finding installations.

After the war, Mr. Rudisuhle joined the Civil Aeronautics Administration to handle engineering problems for the foreign section and later directed the engineering of air navigation and communications facilities in the Pacific Area.

IRE People

J. H. Dellinger (F'23) has been elected president of honor of the International Scientific Radio Union. He is a past chairman of the United States National Committee and retiring vice president of URSI.

J. H. DELLINGER

Dr. Dellinger was born on July 3, 1886, in Cleveland, Ohio, where he attended Western Reserve University. He received the B.A. degree in 1908 from George Washington University, and the Ph.D. degree from Princeton University in 1913. In 1932, he was awarded the D.Sc. degree from George Washington University.

During 1907–1948, Dr. Dellinger held successive posts at the National Bureau of Standards of physicist, chief of the radio section, and chief of the Central Radio Propagation Laboratory. During 1928–1929, he was chief engineer of the Federal Radio Commission and from 1922–1948, served as a representative of the United States Department of Commerce on the Interdepartment Radio Advisory Committee. He has been associated with numerous international radio conferences and commissions throughout his career.

Dr. Dellinger was IRE President in 1925, and an IRE Director from 1924–1927. He received the IRE Medal of Honor in 1936, and was Chairman of the Washington Section during 1932–1933. He also has been active on various committees of the Institute and has acted as its Representative at meetings of the American Documentation Institute and American Standards Committee.

❖

W. C. Fisher (A'42–M'45–SM'49) has become a member of the sales engineering service section of the Lenkurt Electric Company, San Carlos, Calif. Previous to joining Lenkurt, Mr. Fisher was vice president of Norwesto Communications Ltd., Kenora, Ont.

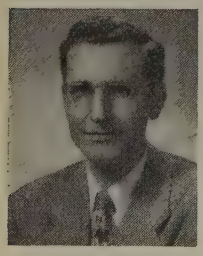

W. C. FISHER

Mr. Fisher, a native of Canada, received the B.S. and M.S. degrees in 1935 and 1938, from the University of Saskatchewan, and did post-graduate work at Purdue University.

During 1938–1939, Mr. Fisher was a mechanical radio inspector for Rogers-Majestic Ltd., in Toronto, and a sound engineer for Dominion Sound Equipments Ltd., in Montreal. From 1939–1940, he was an engineer in the receiver development laboratories for RCA Victor Ltd., Montreal. He served as a Wing Commander in the signals branch of the Royal Canadian Air Force from 1940–1945, and returned to RCA Victor as a senior engineer of the engineering products department until 1946. Mr. Fisher was also a sales engineer for this company in Winnipeg.

Mr. Fisher has been Chairman of the Winnipeg IRE Subsection, and is a member of the Association of Professional Engineers of the Province of Manitoba and a member of the Engineering Institute of Canada.

❖

Charles B. Aiken (A'25–M'35–SM'43), vice president and director of research of Electro-Mechanical Research, Inc., Ridgefield Conn., died this past year, it was learned recently by the Institute.

Dr. Aiken was a native of Lousiana where he received the B.S. degree from Tulane University in 1923. He received the M.S. degree in 1924, the M.A. degree in 1925, and the Ph.D. degree in 1933, from Harvard University.

Dr. Aiken's professional positions included his work as a research engineer at Mason, Slichter, and Hay, a technical staff member of Bell Telephone Laboratories, Inc., a lecturer in electrical engineering at Columbia University, associate professor at Purdue University, and consulting engineer of McCutchen and Aiken.

Dr. Aiken was a member of the American Institute of Electrical Engineers.

Robert M. Page (SM'45–F'47), superintendent of Radio III Division and consultant in electronics to the director of research at the Naval Research Laboratory, has been honored by Hamline University, St. Paul, Minn., in a dedication of their new laboratory. The Robert M. Page Laboratory of Electronics was dedicated "in tribute to the profound role (he has) played in the development of radar."

R. M. PAGE

A native of St. Paul, Dr. Page received his B.S. degree from Hamline University in 1927, and the M.A. degree from George Washington University in 1932. He received the doctorate from Hamline in 1943.

Dr. Page has served with the Naval Research Laboratory since 1927 in various positions and recently returned from a three-month survey of electronics developments in Germany for the State Department. He is the holder of several awards including the United States Navy Civilian Service Award, The Certificate of Award from the Office of Scientific Research and Development, and the President of the United States Certificate of Merit. Dr. Page has contributed numerous technical articles to scientific publications and has been issued approximately 20 patents. He has been a member of the IRE Board of Editors since 1946.

❖

M. Glenn Jarrett (A'38–VA'39–SM'49), transmission engineer of the Bell Telephone Company, Pittsburgh, Pa., died recently at the age of 47.

Mr. Jarrett, a native of Pennsylvania, received the B.S. degree in electrical engineering from the University of Pennsylvania in 1927. From that time, he worked with Bell Telephone in their transmission department. During World War II he was a member of the Bell Telephone laboratories, assigned to the staff of the school for training military personnel on fire-control radar equipment. In 1946, he was made responsible for engineering of radiotelephone systems to meet current transmission objectives.

Mr. Jarrett was Secretary-Treasurer of the IRE Pittsburgh Section, 1940–1942; Vice Chairman, 1948–1949; Chairman, 1949–1950.

Axel G. Jensen (A'23–M'26–F'42), director of television research of the Bell Telephone Laboratories, has been presented the 1952 David Sarnoff Gold Medal Award by the Society of Motion Picture and Television Engineers. The medal is given in recognition of recent technical contributions to the art of television.

A. G. JENSEN

Mr. Jensen also has been awarded a certificate of service by the American Standards Association in recognition of his work in the development of American Standards. Mr. Jensen is a member of the ASA Standards Council representing the IRE, and is especially active on ASA Committees on Radio (C-16), and on Definitions of Electrical Terms (C42).

Earlier this year Mr. Jensen was presented the G. A. Hageman Gold Medal Award by the Royal Technical College in Copenhagen, Denmark, where he received the E. E. degree in 1920, and was an instructor before coming to the United States. He has been a member of the Bell Telephone staff since 1922, when he finished post-graduate work at Columbia University as a fellow of the American Scandinavian Foundation. In 1926 Mr. Jensen went to London to initiate short-wave radio reception from the United States and returned in 1930 to work on the development of the coaxial system. He has been engaged in television research for Bell Telephone since 1938.

Mr. Jensen has been active on numerous IRE committees and has been an IRE Representative for various technical organizations and committees.

Books

Pulse Techniques by Sidney Moskowitz and Joseph Racker (4479)

Published (1951) by Prentice-Hall, Inc., 70 Fifth Ave., New York 11, N. Y. 259 pages+6-page index +35-page appendix+viii pages. 202 figures. 6×8¼. $6.65.

Sidney Moskowitz is on the staff of the Federal Telecommunications Laboratories, Inc., Nutley, N. J. Joseph Racker is microwave link consultant of the Joseph Racker Co., New York, N. Y.

Quoting from the book, "The primary objective of this text is to enable individuals with electrical engineering background to analyze and design circuits for transmission and utilization of pulses."

The book is divided into nine chapters and a mathematical appendix as follows: (1) Characteristics of Pulses; (2) Transient Response of Linear Networks; (3) Design of Pulse Networks; (4) Linear Pulse Amplifiers; (5) Pulse-Shaping and Clamp Circuits; (6) Pulse Generation; (7) Pulse Measurements and Instruments; (8) Pulse Communication Systems; (9) Aerial Navigation Aids; Appendices, Review of Complex-Variable Theory, Pulse Response of Cascaded Wave Filters, and Pulse Response of Transmission Lines.

The authors assume that the reader has had previous exposure to complex-variable theory. In Chapter 2, we are given a clear exposition of Fourier and Laplace transform theory with illustrative examples. However, numerous misprints and the use of undefined nonstandard symbols may tend to make the book confusing for the student. The authors seem to have purposely excluded the variable of integration under an integral sign. For example, in the mathematical appendix, page 263 contains two misprints, an undefined integral, the use of both j and i for $\sqrt{-1}$, and two undefined symbols whose meaning was very puzzling to the reviewer.

A few other inclusions may have been desirable in the material. For instance, no mention is made of RF pulses, and the important problem of providing selectivity for such signals is omitted. The treatment of delay lines in chapter 3 does not include the modern development of delay lines.

The best part of the book is chapter 5 on pulse shaping and clamp circuits in which the authors get together with the subject and pulses are treated as waveforms. However, even here, coincidence detectors are overlooked and "pulse-moding" (arranging pulses in a predetermined pattern for multiplexing) is dismissed after a short description of its use to provide synchronization in ppm.

The reader who may wish to supplement the book's information with further investigation is referred to the Radiation Laboratory Series, Volume 19, on "Waveforms."

CHARLES J. HIRSCH
Hazeltine Corporation
Little Neck, N. Y.

Most Often Needed 1952 Radio Diagrams and Servicing Information Compiled by M. N. Beitman(4480)

Published (1952) by Supreme Publications, 3727 West 13 St., Chicago 23, Ill. 168 pages including index, models, and diagrams. 10¾×8¼. $2.50.

This book contains a collection of manufacturers circuit diagrams and service notes for "1952" radio receivers. It is the twelfth volume of a series that starts with receivers of the year "1926." Also included is servicing information on the automatic record changers connected with some of these receivers. The book does not present information on every receiver manufactured, but as the title implies, it presents representative designs. In this respect it is successful in covering nearly all variations of AM and FM receiver designs for "1952."

Most of the schematic diagrams and service notes presented are reproductions of the manufacturers service notes, which has led to some minor inconsistencies and omissions. For example, fairly complete alignment instructions are given for some models while no information other than the schematic diagram is given for others. However, this may be an omission of the manufacturer's rather than the compiler's.

The volume, intended primarily for servicemen, seems quite adequate for the one experienced in this field. It also might provide a handy reference for the engineer interested in keeping abreast of design trends in the broadcast receiver field.

With practically no exceptions the circuit diagrams are clearly reproduced and component values are read easily. The index is clear and concise and, in general, the book is a worthwhile contribution in its field.

DAVID SILLMAN
Hazeltine Corporation
Little Neck, N. Y.

Radio Antenna Engineering by Edmund A. Laport (4481)

Published (1952) by McGraw-Hill Book Company Inc., 330 West 42 St., New York 18, N. Y. 526 pages +11-page index+27-page appendix+xii pages. 496 figures. 6×9. $9.00.

Edmund A. Laport is chief engineer of RCA International Division, New York, N. Y.

This new 563-page book presents the electrical and mechanical design aspects of radio antennas for communication and broadcast frequencies below about 30 mc. Because of its comprehensive coverage of the subject this book should be of great value to the engineer starting a career in this field. It should provide also much useful reference material for the practicing engineer in the field of radio antenna design.

In general, the book discusses the propagation characteristics, circuitry, and mechanical configurations of antennas constructed of wires, masts, and towers for all of the important antenna types in the so-called low-, medium-, and high-frequency bands. Much of the "hard-to-find" information which the engineer normally gathers only through long experience in the antenna field is presented in lucid fashion.

The first chapter discusses low-frequency antenna types such as the multiple-tuned antenna, the wave or beverage antenna, the adcock antenna used for low-frequency four-course radio ranges, and various flat-top designs. This is followed by a chapter discussing medium-frequency broadcast tower radiators and directional broadcast tower arrays with their associated feeder systems. Sample computations included are very helpful. Photographs illustrate structural details of broadcast antennas.

Following, is a chapter which occupies approximately one-third of the book, and is devoted to the high-frequency antenna types. It delves into the propagation characteristics of high-frequency electromagnetic waves and describes the many ramifications of high-frequency directional antenna arrays. Foster's stereographic projection method of analyzing the more complicated antenna radiation patterns, such as those of rhombic antennas, is included.

A chapter on transmission lines and another on impedance matching are presented; both subjects being closely associated with antenna design and both treated, for engineering purposes, largely from the time saving graphical view-point. A final chapter deals with the logarithmic-potential theory, a highly practical tool for the antenna engineer.

The book, carefully written and orderly arranged, includes bibliographies at the end of each chapter as well as a general bibliography at the end of the book, enabling the reader to pursue in greater detail any particular phase of the subject on which he may require further information.

PHILLIP H. SMITH
Bell Telephone Labs., Inc.
Whippany, N. J.

Measurements at Centimeter Wavelength by Donald D. King (4482)

Published (1952) by D. Van Nostrand Company, Inc., 250 Fourth Ave., New York 3, N. Y. 309 pages +8-page index+7-page glossary+vii pages. 220 figures plus tables. 6×9. $5.50.

Donald D. King is the assistant director, Radiation Laboratory, The John Hopkins University, Baltimore, Md.

The author presents a systematic exposition of wave phenomena as related to centimeter measurements in the wavelength range of three meters to ten millimeters. The manner of writing is aimed toward presenting "practical formulas and facts" based upon impedance, standing-wave ratio, and reflection coefficient concepts. Most of the topics are well referenced.

Following an introduction which briefly evaluates the effects of increasing frequency on lumped and distributed constant circuits, the author qualifies the use of impedance, power, and frequency as fundamental measurable quantities. In proceeding chapters, the subject matters discussed include transmission line equations and various alternate forms, surface-wave transmission, instruments for measuring power and frequency, characteristics of several classes of generators, methods for measuring impedance, vswr, attenuation with requirements on range and accuracy, and measurements relating to antenna field patterns. Full use is made of transmission line charts, summary tables, and block diagrams. An attempt is also made to describe the structural design of line components and required performance. The tangent method for determining the circuit parameters of four-terminal networks is introduced.

The text is valuable as a handbook of methods with brief regard of techniques. Although the topics are not sufficiently treated to stimulate the experimenter, the book with its broad coverage should be of great interest to experienced microwave engineers.

ANTHONY B. GIORDANO
Polytechnic Institute of Brooklyn
Brooklyn, N. Y.

Sections*

Chairman		Secretary
I. L. Knopp 628 Ecton Rd. Akron, Ohio	AKRON (4)	Buford Smith, Jr. 1831 Ohio Ave. Cuyahoga Falls, Ohio
W. L. Fattig Box 788 Emory Univ., Ga.	ATLANTA (6)	H. W. Ragsdale 654 Cooledge Ave., N.E. Atlanta, Ga.
C. E. McClellan 1306 Tarrant Rd. Glen Burnie, Md.	BALTIMORE (3)	C. D. Pierson, Jr. 1574 Waverly Rd. Baltimore, Md.
L. W. McDaniel 3385 Timberwood Lane Beaumont, Tex.	BEAUMONT-PORT ARTHUR (6)	C. B. Trevey 2555 Pierce St. Beaumont, Tex.
J. H. Merchant 2 Cedar St. Binghamton, N. Y.	BINGHAMTON (4)	R. F. New 654 Chenango St. Binghamton, N. Y.
F. D. Lewis 275 Massachusetts Ave. Cambridge, Mass.	BOSTON (1)	A. J. Pote Cyclotron Laboratory Cambridge, Mass.
I. C. Grant San Martin 379 Buenos Aires, Arg.	BUENOS AIRES	C. A. Cambre Olazabal 5255 Buenos Aires, Arg.
R. T. Bozak 90 Montrose Ave. Buffalo, N. Y.	BUFFALO-NIAGARA (4)	R. R. Thalner 254 Rano St. Buffalo, N. Y.
J. L. Hollis 2900 "E" Ave., N.E. Cedar Rapids, Iowa	CEDAR RAPIDS (5)	J. W. Smith 1136 27, N.E. Cedar Rapids, Iowa
A. R. Beach Loueridge Circle E. Eau Gallie, Fla.	CENTRAL FLORIDA (6)	Hans Scharla-Nielsen Radiation Inc. P. O. Drawer Q Melbourne, Fla.
R. M. Krueger 5143 N. Neenah Ave. Chicago, Ill.	CHICAGO (5)	J. J. Gershon 2533 N. Ashland Ave. Chicago, Ill.
J. P. Quitter 509 Missouri Ave. Cincinnati, Ohio	CINCINNATI (5)	D. W. Martin Box 319-A, RR 1 Newtown, Ohio
J. L. Hunter 3901 E. Antisdale Rd. S. Euclid, Ohio	CLEVELAND (4)	H. R. Mull R.F.D. 3, Elyria, Ohio
J. H. Jaeger 361 Oakland Park Ave. Columbus, Ohio	COLUMBUS (4)	R. W. Masters 1633 Essex Rd. Columbus, Ohio
John Merrill 16 Granada Terr. New London, Conn.	CONNECTICUT VALLEY (1)	H. E. Rohloff The So. New Eng. Tel. Co. New Haven, Conn.
R. A. Arnett 4073 Rochelle Dr. Dallas, Tex.	DALLAS-FORT WORTH (6)	J. A. Green 6815 Oriole Dr. Dallas, Tex.
J. L. Dennis 3005 Shroyer Rd. Dayton, Ohio	DAYTON (5)	A. B. Henderson 801 Hathaway Rd. Dayton, Ohio
W. R. Bliss 1426 Market St. Denver, Colo.	DENVER (5)	R. E. Swanson 1777 Kipling St. Denver, Colo.
W. L. Cassell Iowa State College Ames, Iowa	DES MOINES-AMES (5)	R. E. Price 1107 Lyon St. Des Moines, Iowa
P. L. Gundy 55 W. Canfield Ave. Detroit, Mich.	DETROIT (4)	E. J. Love 9264 Boleyn Detroit, Mich.
D. E. Reynolds 4116 Memphis St. El Paso, Tex.	EL PASO (7)	J. E. Hoefling Box 72 Fort Bliss, Tex.
L. R. Maguire 4 E. 6 St. Emporium, Pa.	EMPORIUM (4)	J. B. Grund Sylvania Elec. Prods. Emporium, Pa.
H. L. Thorson General Electric Co. Owensboro, Ky.	EVANSVILLE-OWENSBORO (5)	A. P. Haase 2230 St. James Ct. Owensboro, Ky.
R. B. Jones 4322 Arlington Ave. Fort Wayne, Ind.	FORT WAYNE (5)	J. J. Iffland 1008 Madison St. Fort Wayne, Ind.
Arthur Ainlay RR 6, Mt. Hamilton Hamilton, Ont., Canada	HAMILTON (8)	John Lucyk 77 Park Row S. Hamilton, Ont.
F. L. Mason Elec. Office Naval Shipyard Pearl Harbor, Oahu, T.H.	TERRITORY OF HAWAII (7)	J. W. Anderson 4035 Black Pt. Rd. Honolulu, T. H.
H. T. Wheeler 802 N. Avenue "A" Bellaire, Tex.	HOUSTON (6)	J. K. Hallenburg 1359 DuBarry Lane Houston, Tex.
F. D. Meadows 5915 N. Oxford Indianapolis, Ind.	INDIANAPOLIS (5)	J. T. Watson 2146 Admiral Dr. Indianapolis, Ind.
D. L. Ewing 108-A Byrnes China Lake, Calif.	INYOKERN (7)	F. S. Howell 313-B Tyler St. China Lake, Calif.
D. G. Wilson Univ. of Kansas Lawrence, Kan.	KANSAS CITY (5)	Mrs. G. L. Curtis Radio Industries, Inc. Kansas City, Kan.
G. H. Scott American Radio & TV Inc. N. Little Rock, Ark.	LITTLE ROCK (5)	V. L. Dillaplain 203 S. Pine St. Little Rock, Ark.
R. B. Lumsden 332 Hale St. London, Ont., Canada	LONDON, ONTARIO (8)	J. D. B. Moore 27 McClary Ave. London, Ont., Canada
W. G. Hodson 10806 Smallwood Ave. Downey, Calif.	LOS ANGELES (7)	B. S. Angwin 238 N. Frederic St. Burbank, Calif.
M. C. Probst Rt. 7, Box 415 Louisville, Ky.	LOUISVILLE (5)	G. W. Yunk 2236 Kaelin Ave. Louisville, Ky.
H. W. Mehrling 365 La Villa Dr. Miami Springs, Fla.	MIAMI (6)	M. C. Scott, Jr. Station WIOD Miami, Fla.
D. E. Mereen 3260 N. 88 St. Milwaukee, Wis.	MILWAUKEE (5)	H. J. Zwarra 722 N. Broadway Milwaukee, Wis.
N. R. Olding Canadian Broad. Corp. Montreal, P.Q., Canada	MONTREAL, QUEBEC (8)	R. W. Cooke 17 De Castelneau St. Montreal, P. Q., Canada
C. W. Carnahan 3169-41 Pl., Sandia Base Albuquerque, N. M.	NEW MEXICO (7)	L. E. French 107 S. Washington Albuquerque, N. M.
H. T. Budenbom 82 Wellington Ave. W. Short Hills, N. J.	NEW YORK (2)	A. B. Giordano 85-99 Livingston St. Brooklyn, N. Y.
V. S. Carson N. C. State College Raleigh, N. C.	NORTH CAROLINA-VIRGINIA (3)	J. G. Gardiner 3502 Kirby Dr. Greensboro, N. C.
C. E. Harp 524 E. Macy St. Norman, Okla.	OKLAHOMA CITY (6)	E. G. Crippen 3829 N.W. 23 St. Oklahoma City, Okla.
C. W. Rook Univ. of Nebraska Lincoln, Neb.	OMAHA-LINCOLN (5)	V. H. Wight 1411 Nemaha St. Lincoln, Neb.
E. L. R. Webb 31 Dunvegan Rd. Ottawa, Ont., Canada	OTTAWA, ONTARIO (8)	D. V. Carroll Box 527 Ottawa, Ont., Canada
C. M. Sinnett 103 Virginia Ave. Westmont, N. J.	PHILADELPHIA (3)	S. C. Spielman Walton Rd. Huntingdon Valley, Pa.
R. E. Samuelson 1401 E. San Juan Ave. Phoenix, Ariz.	PHOENIX (7)	Z. F. McFaul 4242 N. 2nd Dr. Phoenix, Ariz.
J. G. O'Shea 104 N. Fremont St. Pittsburgh, Pa.	PITTSBURGH (4)	J. H. Greenwood 166 N. Sprague Ave. Pittsburgh, Pa.
E. D. Scott 4424 S.W. Twombly Ave. Portland, Ore.	PORTLAND (7)	J. M. Roberts 5927 S.E. 23 Ave. Portland, Ore.
W. H. Bliss Princeton Univ. Princeton, N. J.	PRINCETON (3)	Jerome Kurshan RCA Laboratories Princeton, N. J.
Garrard Mountjoy 100 Carlson Rd. Rochester, N. Y.	ROCHESTER (4)	R. N. Ferry 196 Lafayette Pkwy. Rochester, N. Y.
W. F. Koch 1340-33 St. Sacramento, Calif.	SACRAMENTO (7)	H. C. Slater 1945 Bidwell Way Sacramento, Calif.
H. J. Hicks 62 Whitehall Ct. Brentwood, Mo.	ST. LOUIS (5)	R. W. Benson 818 S. Kingshighway St. Louis, Mo.

* Numerals in parentheses following Section designate Region number

Sections

	Chairman	Secretary
Salt Lake City (7)	Stanley Benson Box 1707 Salt Lake City, Utah	M. E. Van Valkenburg Univ. of Utah Salt Lake City, Utah
San Antonio (6)	A. H. LaGrone Box F, Univ. Station Austin, Tex.	Paul Tarrodaychik 215 Christine Dr. San Antonio, Tex.
San Diego (7)	C. R. Moe 4669 E. Talmadge Dr. San Diego, Calif.	R. A. Kirkman 6306 Celia Dr. San Diego, Calif.
San Francisco (7)	W. E. Noller 1229 Josephine St. Berkeley, Calif.	O. J. M. Smith Univ. of Calif. Berkeley, Calif.
Schenectady (2)	E. S. Sampson 1243 Chrisler Ave. Schenectady, N. Y.	D. E. Norgaard 1908 Townsend Rd. Schenectady, N. Y.
Seattle (7)	J. E. Hogg 4107 Sunnyside Ave. Seattle, Wash.	H. M. Swarm Univ. of Washington Seattle, Wash.
Syracuse (4)	Samuel Seely Syracuse University Syracuse, N. Y.	W. H. Hall Gen. Elec. Co. Syracuse, N. Y.
Toledo (4)	W. M. Stringfellow 136 Huron St. Toledo, Ohio	G. H. Eash 845 W. Woodruff Ave. Toledo, Ohio
Toronto, Ontario (8)	G. E. McCurdy 74 York St. Toronto, Ont., Canada	Clive Eastwood 658 Pharmacy Ave. Dawes Rd. P.O. Toronto, Ont., Canada
Tulsa (6)	C. E. Buffum Box 591 Tulsa, Okla.	W. J. Weldon 2530 E. 25 St. Tulsa, Okla.
Twin Cities (5)	O. A. Schott 4224 Elmer Ave. Minneapolis, Minn.	F. S. Hird 224 S. 5th St. Minneapolis, Minn.
Vancouver (8)	A. H. Gregory 150 Robson St. Vancouver, B. C. Canada	Miles Green 2226 W. 10th Ave. Vancouver, B. C. Canada
Washington (3)	M. W. Swanson 1420 Mt. Vernon Memorial H'way Alexandria, Va.	T. B. Jacocks 777 14 St., N.W. Washington, D. C.
Williamsport (4)	J. H. Canning 1701 Chestnut St. Williamsport, Pa.	R. C. Lepley R.D. 2 Williamsport, Pa.

Subsections

	Chairman	Secretary
Amarillo-Lubbock (6) (Dallas-Ft. Worth Subsection)	R. F. Lee 2704-31 St. Lubbock, Tex.	C. M. McKinney Texas Tech. College Lubbock, Tex.
Centre County (4) (Emporium Subsection)	Carl Volz 160 W. Hamilton Ave. State College, Pa.	R. L. Riddle Penn. State College State College, Pa.
Charleston (6) (Atlanta Subsection)	F. G. McCoy Rt. 4, Box 452-J Charleston, S. C.	C. B. Lax Sergeant Jasper Apts. Charleston, S. C.
Huntsville (6) (Atlanta Subsection)	S. L. Johnston 207 Edgewood Dr. Huntsville, Ala.	R. C. Haraway 603 College Hill Apts. Huntsville, Ala.
Lancaster (3) (Philadelphia Subsection)	L. B. Headrick RCA Victor Div. Lancaster, Pa.	C. G. Landis Safe Harbor, Box 6 Conestoga, Pa.
Long Island (2) (New York Subsection)	C. J. Hirsch Hazeltine Elec. Corp. Little Neck, L. I., N. Y.	B. F. Tyson 49-16 Douglaston Pkwy. Douglaston, N. Y.
Mid-Hudson (2) (New York Subsection)	R. T. Blakely Merry Hill Titusville Rd. Poughkeepsie, N. Y.	
Monmouth (2) (New York Subsection)	S. D. Robertson Box 107 Red Bank, N. J.	G. F. Senn 81 Garden Rd. Little Silver, N. J.
Northern N. J. (2) (New York Subsection)	A. G. Richardson 180 Vreeland Ave. Boonton, N. J.	P. S. Christaldi Box 111 Clifton, N. J.
Palo Alto (7) (San Francisco Subsection)	O. G. Villard, Jr. 2050 Dartmouth St. Palo Alto, Calif.	J. V. Granger 772 Paul Ave. Palo Alto, Calif.
Rome (4) (Syracuse) Subsection)	A. A. Kunze Lee Center New York, N. Y.	J. M. Thompson Box 1245 Haselton Br. P.O. Rome, N. Y.
South Bend (5) (Chicago Subsection)	George Weiler 1429 E. Monroe South Bend, Ind.	A. R. O'Neil WSBT-WSBT-TV South Bend, Ind.
Wichita (Kansas City Subsection)	H. G. Swift Rte. 2 Derby, Kan.	P. A. Bunyar 1328 N. Lorraine Wichita, Kan.
Winnipeg (8) (Toronto Subsection)	R. F. Tinkler 166 Portage Ave., E. Winnipeg, Canada	H. R. Gissing 65 Rorie St. Winnipeg, Canada

Professional Groups

	Chairman
Airborne Electronics	George Rappaport Wright Field, Dayton, Ohio
Antennas and Propagation	A. H. Waynick Pennsylvania State College State College, Pa.
Audio	J. J. Baruch Massachusetts Institute o fTechnology Cambridge, Mass.
Broadcast and Television Receivers	D. D. Israel 111 8 Ave. New York, N. Y.
Broadcast Transmission Systems	Lewis Winner 52 Vanderbilt Ave. New York, N. Y.
Circuit Theory	R. L. Dietzold 34 W. 11 St. New York, N. Y.
Communications Systems	G. T. Royden 67 Broad St. New York, N. Y.
Electron Devices	George D. O'Neill Sylvania Electric Products, Inc. Bayside, L. I., N. Y.
Electronic Computers	M. M. Astrahan I.B.M. Plant. no. 2 Poughkeepsie, N. Y.
Engineering Management	Ralph I. Cole Griffiss A.F.B., Rome, N. Y.

	Chairman
Industrial Electronics	Eugene Mittlemann 549 W. Washington Blvd., Chicago, Ill.
Information Theory	Nathan Marchand Sylvania Electric Products Inc. Bayside, L. I., N. Y.
Instrumentation	I. G. Easton General Radio Co. Cambridge, Mass.
Medical Electronics	L. H. Montgomery, Jr. Vanderbilt University Nashville, Tenn.
Microwave Theory and Techniques	Ben Warriner Gen. Elec. Co., Advanced Electronics Center, Cornell Univ., Ithaca, N. Y.
Nuclear Science	L. R. Hafstad Atomic Energy Comm. Rm. 132, 1901 Constitution Ave. Washington, D. C.
Quality Control	Leon Bass General Elec. Co. Schenectady, N. Y.
Radio Telemetry and Remote Control	M. V. Kiebert, Jr. Bendix Aviation Corp. Teterboro, N. J.
Vehicular Communications	F. T. Budelman Budelman Radio Corp. Stamford, Conn.

Abstracts and References

Compiled by the Radio Research Organization of the Department of Scientific and Industrial Research, London, England, and Published by Arrangement with that Department and the *Wireless Engineer*, London, England

NOTE: The Institute of Radio Engineers does not have available copies of the publications mentioned in these pages, nor does it have reprints of the articles abstracted. Correspondence regarding these articles and requests for their procurement should be addressed to the individual publications, not to the I.R.E.

The number in heavy type at the upper left of each Abstract is its Universal Decimal Classification number and is not to be confused with the Decimal Classification used by the United States National Bureau of Standards. The number in heavy type at the top right is the serial number of the Abstract. DC numbers marked with a dagger (†) must be regarded as provisional.

The Annual Index to these Abstracts and References, covering those published in the PROC. I.R.E. from February, 1951, through January, 1952, may be obtained for 2s.8d. postage included from the *Wireless Engineer*, Dorset House, Stamford St., London S.E., England. This index includes a list of the journals abstracted together with the addresses of their publishers.

ACOUSTICS AND AUDIO FREQUENCIES

016:534 3298

References to Contemporary Papers on Acoustics—R. T. Beyer. (*Jour. Acous. Soc. Amer.*, vol. 24, pp. 421–426; July, 1952.) Continuation of 2675 of November.

534.2 3299

Sound Scattering by Thin Elastic Shells—M. C. Junger. (*Jour. Acous. Soc. Amer.*, vol. 24, pp. 366–373; July, 1952.) Theory previously developed by Faran (2611 of 1951) for scattering by solid cylinders and spheres is extended to take account of the modification of the scattering pattern due to the forced vibrations excited in the elastic shell by the incident wave. The influence of the ambient medium is discussed.

534.231:621.3.018.78† 3300

Two Applications of the Concept of Spatial Distortion—J. Bernhart. (*Onde élect.*, vol. 32, pp. 334–343; July, 1952.) Spatial distortion is regarded as including all defects of reproduction which detract from the directional effect, whether they originate in the pickup of a sound or in its transmission or reproduction. Two cases are considered: (*a*) the distortion introduced at the origin of a transmission chain by classical methods of sound pickup, stereophonic reproduction being treated as a particular case, (*b*) the spatial distortion in the reproduction of sound. A detailed study is presented of the Elipson "radiation transformer"; its use for directing the maximum amount of sound energy toward an audience is explained. See also 2108 of September (Forestier).

534.232+621.395.612.4 3301

The Radiation Impedance of Ribbon-Type Sound Radiators, and the Vibro-motive Force on Them—T. Nimura and K. Shibayama. (*Sci. Rep. Res. Inst. Tohoku Univ. Ser. B*, vol. 3, pp. 77–85; September, 1951.) Mathieu functions are used to derive formulas for the acoustic radiation from a ribbon with a baffle of finite width, and for the acoustic scattering by a rigid ribbon. The analysis is applicable to ribbon microphones.

534.232 3302

Calculation of the Directivity Index for Various Types of Radiators—H. Stenzel. (*Jour. Acous. Soc. Amer.*, vol. 24, pp. 417–418; July, 1952.) Discussion on 3289 of 1948 (Molloy).

534.232 3303

Observations on Edge-Tones—M. Mokhtar and H. Youssef. (*Acustica*, vol. 2, no. 3, pp. 135–139; 1952.) The mechanism of edge-tone production is studied from the following aspects, (*a*) distribution of wind velocity between slit and edge, (*b*) paths of the vortices, (*c*) velocity/frequency relation. Particular attention is paid to the frequency-jump stage.

534.232:537.228.1 3304

On the Characteristics of Miscellaneous Piezoelectric Vibrators in Stiffness Control—S. Honda. (*Sci. Rep. Res. Inst. Tohoku Univ., Ser. B*, vol. 3, pp. 95–114; March, 1952.) Investigation of the characteristics of electromechanical transducers of the longitudinal- and shear-vibration types and of twin-plate flexure and torsion types. Formulas for the electrical and mechanical constants of the different types are tabulated.

534.232:[537.228.2+538.652 3305

On the Effective Attenuation of Some Electroacoustic Transducers at their Conjugate Electrical Matching—Y. Kikuchi and H. Shimizu. (*Sci. Rep. Res. Inst. Tohoku Univ., Ser B*, vol. 3, pp. 13–18; September, 1951.)

534.232:538.652 3306

On the Effective Attenuation of Ring-Type Magnetostriction Transducers—Y. Kikuchi and H. Shimizu. (*Sci. Rep. Res. Inst. Tohoku Univ., Ser. B*, vol. 3, pp. 1–5; September, 1951.)

534.24 3307

The Reflection of a Transient [sound] Pulse by a Parabolic Cylinder and a Paraboloid of Revolution—W. Chester. (*Quart. Jour. Mech. Appl. Math.*, vol. 5, pp. 196–205; June, 1952.) An adaptation of Lamb's analysis for the case of an incident harmonic wave train is used to derive the corresponding transient solutions.

534.321.9 3308

Linear Magnetostrictive Ultrasonic-Wave Generation using Crossed Magnetic Fields—H. H. Rust and E. Bailitis. (*Acustica*, vol. 2, pp. 132–135; 1952. In German.) With linear magnetostrictive generators the actual maximum elongation is given by the difference of the elongations in the remanence and the saturation states. If the vibrating body, a cube of ferromagnetic material, is enclosed in two pairs of coils at right angles to each other, one of each pair providing a permanent magnetic field, the other carrying alternating current, an alternation of maximum elongation and contraction will take place in the direction of the wave vector. At these maxima the Weiss vectors will be normal to each other, and remanence will temporarily vanish. The expected increase in elongation with the above arrangement is $\sim 45.10^{-6}$ for Ni, and it should thus be possible to use less costly materials, e.g., Fe-Ni alloy with 4 per cent Ni content, as magnetostrictive elements.

534.321.9 3309

Considerations and Suggestions on the Concentration of Ultrasonic Energy—A. Barone. (*Ricerca sci.*, vol. 22, pp. 679–684; April, 1952.) Reflection types of concentrator, two of which are described, are preferable to acoustic lenses. One equipment uses a parabolic reflector to obtain a converging beam; the other makes use of reflections at the surfaces of two conical holes bored in the ends of a metal cylinder arranged in front of the ultrasonic generator. By suitable design of cone lengths and angles, and the internal diameter where the holes meet, the energy can be concentrated, within certain limits, over a prescribed area.

534.321.9:534.22:[546.264+547.313.2 3310

Propagation of Ultrasonic Waves in Vapours near the Critical Point—H. D. Parbrook and E. G. Richardson. (*Proc. Phys. Soc.* (London), vol. 65, pp. 437–444; June 1, 1952.) An experimental study of the velocity and absorption of ultrasonic waves at frequencies of 0.5, 1 and 2 mc in CO_2 and C_2H_4 at pressures up to 100 atm, using a variable-path acoustic interferometer.

534.414 3311

Multiple Helmholtz Resonators—C. S. McGinnis and V. F. Albert. (*Jour. Acous. Soc. Amer.*, vol. 24, pp. 374–379; July, 1952.) The equations of motion for the fluid in any resonator network are obtained by application of Lagrange's method. The number of resonances found is equal to the number of distinct cavities. Calculated values of resonance frequency agree with values found experimentally. The work is relevant to investigations of the mechanism of voice production.

534.612.4 3312

A Simplified Technique for the Pressure Calibration of Condenser Microphones by the Reciprocity Method—A. K. Nielsen. (*Acustica*, vol. 2, pp. 112–118; 1952.) Calibration technique is much simplified if the transfer impedance is determined, the open-circuit voltage

of the receiver microphone and the current through the source microphone being measured directly. A suitable method and precautions necessary are explained. Discussion shows that the noise level of the cathode-follower preamplifier used can be reduced to a tolerable value of suitable circuit design.

534.613:534.321.9 3313
Absolute Method of Measurement of Acoustic Power in an Ultrasonic Beam in a Liquid, based on the Radiation Pressure exerted on a Liquid/Gas Interface—C. Florisson. (*Compt. Rend. Acad. Sci.* (Paris), vol. 235, pp. 27–28; July 7, 1952.)

534.78:519.271 3314
An Experimental Study of Speech-Wave Probability Distributions—W. B. Davenport, Jr. (*Jour. Acous. Soc. Amer.*, vol. 24, pp. 390–399; July, 1952.)

534.833.4-13/-14 3315
General Theory of the Absorption of Sound in Gases and Liquids taking Account of Transport Phenomena—J. Meixner. (*Acustica*, vol. 2, pp. 101–109; 1952. In German.)

534.84 3316
Recent Progress in Architectural Acoustics—A. C. Raes. (*Onde élect.*, vol. 32, pp. 321–330; July, 1952.) Review of methods of determining the acoustic properties of rooms or halls, and of test methods for sound-absorbent materials.

534.84:621.396.619.13 3317
Frequency Modulation in Architectural Acoustics—J. Pujolle and R. Lamoral. (*Onde élect.*, vol. 32, pp. 331–333; July, 1952.) An investigation of the optimum values of frequency and frequency swing of a warble-tone generator for room-acoustics measurements.

534.84:621.396.712.3 3318
New Studios of Radiodiffusion Française—J. Pujolle. (*Ann. Télécommun.*, vol. 7, pp. 305–309; July/August, 1952.) Description of studios at Nancy, Lille and Nice, and at the Center Bourdan, Paris, with particular reference to the acoustic treatment of walls, ceilings, etc.

534.843 3319
The Acoustic Significance of the Amplitude and Phase of Harmonics Present in a Source of Sound in a Room—J. G. Robbins. (*Jour. Acous. Soc. Amer.*, vol. 24, pp. 380–383; July, 1952.) Report of a study of the acoustic properties of a rectangular room, using both subjective listener-response tests and objective measurements of the modulation of the sound-decay curve. The sound source covered the fundamental frequency range 50–3000 cps, the amplitude and phase of the first four harmonics being adjustable. A large majority of listeners cannot distinguish between two steady-state sounds differing only in the relative phase of a harmonic.

534:844.1/.2 3320
The Reverberation Times of Ten British Concert Halls—P. H. Parkin, W. E. Scholes, and A. G. Derbyshire. (*Acustica*, vol. 2, pp. 97–100; 1952.) Measurements at frequencies of 125, 500, 2000 and 4000 cps are tabulated and are discussed with reference to the opinions of 42 professional musicians regarding the acoustic quality of the halls. In general, the reverberation times of the "good" halls lie on or near the Knudsen optimum line.

534.844.2 3321
Reverberation Times in Baroque Churches—W. Lottermoser. (*Acustica*, vol. 2, no. 3, pp. 109–111; 1952. In German.) Measurements for five churches in Upper Swabia and one in Alsace are reported. The many bays in the side-walls and the stucco ornamentation combine to "mix" the sound waves thoroughly, so that good intelligibility of speech and music results. A significant feature is the maximum reverberation time occurring between 500 and 1000 cps.

534.861:534.322.1 3322
Quadratic and Cubic Distortion in the Transmission of Music—G. Haar. (*Frequenz*, vol. 6, pp. 199–206; July, 1952.) Report of tests to find how much distortion can be introduced in a transmission system before listeners notice a deterioration of musical quality. Results are shown graphically. Cubic distortion has a greater effect than quadratic distortion.

534.861:534.843.2 3323
The Effect of the Direct and the Reflected Sound on the Sound Pattern—J. Grunert. (*Tech. Hausmitt. NordwDtsch. Rdfunks*, vol. 4, pp. 138–141; July/August, 1952.) Discussion of the characteristics of the sound picked up by a single microphone in a studio, as affected by reflection from the interior, and of problems of balance when two microphones are used, as in the case of a soloist and orchestra.

534.861:621.396.8 3324
Use of Electronic Sound Sources of Broadcasting—W. Meyer-Eppler. (*Tech. Hausmitt. NordwDtsch. Rdfunks*, vol. 4, pp. 130–135; July/August, 1952.) Discussion of the technical possibilities of sound film, electronic organs, and similar devices.

534.861:782/785 3325
The Musical Work of Art in Electrical Transmission—H. Husmann. (*Tech. Hausmitt. NordwDtsch. Rdfunks*, vol. 4, pp. 135–137; July/August, 1952.) General discussion of technical and physiological problems connected with the faithful transmission of music.

621.395.623.7 3326
Studies on Cone-Type Loudspeakers: Part 1—On the Extensional Vibration of a Conical Shell—T. Nimura and K. Shibayama. (*Sci. Rep. Res. Inst. Tohoku Univ., Ser. B*, vol. 3, pp. 56–75; September, 1951.) Theoretical and experimental investigations are reported.

621.395.623.73 3327
Studies on Cone-Type Loudspeakers: Part 2—On the Inextensional Vibration of a Conical Shell—T. Nimura and K. Shibayama. (*Sci. Rep. Res. Inst. Tohoku Univ., Ser. B*, vol. 3, pp. 189–198; March, 1952.) Resonance modes of vibration of conical diaphragms in which bending is chiefly involved are analyzed. Theoretical and experimental results are in good agreement with those of Bordoni (1976 of 1947) and McLachlan. Part No. 1: 3326 above.

621.395.623.73 3328
Studies on Cone-Type Loudspeakers: Part 3—The Upper Frequency Limit of Cone-Type Loudspeakers—T. Nimura and E. Matsui. (*Sci. Rep. Res. Inst. Tohoku Univ., Ser. B*, vol. 3, pp. 199–213; March, 1952.) Discussion of effects depending on cone edge conditions and derivation of a formula for the upper limiting frequency. Part 2: 3327 above.

621.395.623.74:537.58 3329
The Ionophone—S. Klein. (*Onde élect.*, vol. 32, pp. 314–320; July, 1952.) An account of the principles of operation of the ionophone, its construction and associated receiver circuits, with results of performance tests as a microphone and as an ultrasonic transmitter See also 896, 897 and 898 (Bonhomme) of May.

621.395.625 3330
Comparison of Sound-Recording Methods—H. Schiesser. (*Elektrotech. Z.*, vol. 73, pp. 366–371; June 1, 1952.) Review of the development and application of photoelectric, mechanical and magnetic recording techniques. Features of modern equipment are noted.

621.395.625.2 3331
Disk Recording and Reproduction—P. Gilotaux. (*Onde élect.*, vol. 32, pp. 289–294; July, 1952.) Further discussion of modern techniques. See also 2970 of 1950.

621.395.625.3 3332
Progress and Trends in High-Fidelity Magnetic Recording—F. Gallet. (*Onde élect.*, vol. 32, pp. 295–301; July, 1952.) Discussion of harmonic distortion, background noise, tape characteristics, etc., with a view to the choice of optimum recorder adjustments.

621.395.625.3:539.23:538.221 3333
Experiments on the Anisotropy of the Magnetization of Magnetic-Recorder Tapes J. Greiner. (*NachrTech.*, vol. 2, pp.197–201; July, 1952.) Investigation of the influence of particle material, shape and arrangement on the properties of magnetic tapes. A considerable increase in remanence was obtained by applying, prior to drying, a dc field of 500 oersted to a tape coated with a mixture of ferromagnetic particles and insulating material.

621.395.625.3:539.23:538.221 3334
Crystalline Structure and Electroacoustic Properties of Magnetic Tapes—A. Lovichi and J. P. Deriaud. (*Onde élect.*, vol. 32, pp. 275–288; July, 1952.) A comparison is made between the properties of high-speed and low-speed tapes. The differences are attributed to differences of crystalline structure of the iron oxides used for the tape coatings. From relations established for the magnetic properties of these oxides predictions of the electroacoustic characteristics of the two types of tape can be made.

621.395.92(083.74) 3335
The Problem of the Standardization of Hearing Aids and Their Test Methods—P. Chavasse and R. Lehmann. (*Onde élect.*, vol. 32, pp. 302–313; July, 1952.) A review of the special problems of bone-conduction and air-conduction types of hearing aid, and of standard equipment and test methods adopted in various countries, together with a proposed scheme of standard methods for testing complete hearing-aid apparatus of the air-conduction type. 34 references. See also *Acustica*, vol. 2, pp. 119–131; 1952.

ANTENNAS AND TRANSMISSION LINES

621.3.018.78†:621.315.212 3336
Distortion of a Signal Transmitted by a Perfectly Uniform Coaxial Line—R. Cazenave. (*Câbles & Trans.* (Paris), vol. 6, p. 264; July, 1952.) Corrections to paper abstracted in 1194 of June.

621.315.212.2:621.315.687.1 3337
Reflectionless Joints for Coaxial Pairs—R. J. Turner. (*P.O. Elec. Eng. Jour.*, vol. 45, pp. 72–76; July, 1952.) Design theory is given for joints producing no reflection of signals transmitted along a cable, with practical details for a 0.375-inch coaxial-pair cable with polythene-disk spacers.

621.392.09 3338
Surface-Wave Transmission Lines—A. C. Grace and J. A. Lane. (*Wireless Eng.*, vol. 29, pp. 230–231; September, 1952.) An account is given of experiments at frequencies of 3.3 and 9.4 kmc, using single-conductor lines of 18 swg copper wire bare, tinned or enamelled, with launching and receiving horns of small flare angle. Oscillator output power and received power were measured by a bolometer bridge method. The results are in good agreement with values calculated from Goubau's theory (812 and 2636 of 1951). The effect of bending the line was investigated.

621.392.09 3339
Propagation of Electromagnetic Waves along a Conducting Wire with Thin Dielectric

Covering—A. Fromageot and B. Louis. (*Bull. Soc. franç. Élect.*, vol. 2, pp. 349–353; June, 1952.) Discussion of paper abstracted in 317 of March.

621.392.09:621.396.611.31 3340

Interaction between Surface-Wave Transmission Lines—A. A. Meyerhoff. (PROC. I.R.E., vol. 40, pp. 1061–1065; September, 1952.) Interaction may occur between two surface-wave transmission lines or between one line and a near-by conductor. Analysis is presented for the case of two parallel lossless lines whose separation is large compared with the diameters. Interaction is found to be a maximum when the two lines are identical, the complete power transfer from one line to the other is possible under suitable conditions. Numerical examples are discussed.

621.392.21 3341

An Approach to the Standard Equations for a Uniform Transmission Line—H. R. Harbottle. (*P.O. Elec. Eng. Jour.*, vol. 45, pp. 30–34 and 80–82; April and July, 1952.) The standard equations for a uniform line are derived without the use of the differential calculus. The propagation of voltage and current through a chain of similar symmetrical resistance sections is first considered. The results obtained are applied to the general case of propagation through a chain of impedance sections simulating a uniform transmission line.

621.392.26 3342

Waveguide Systems with Negative Phase Velocities—L. B. Mullett and B. G. Loach. (*Nature*, (London), vol. 169, p. 1011; June 14, 1952.) A fundamental wave with genuinely negative phase velocity is possible in the case of the helix and folded-strip transmission line. A diagram shows how the propagation constant of a rectangular waveguide loaded on one broad face with a reactive sheet changes with the loading reactance; to obtain a slow wave with negative phase velocity the reactive sheet must be capacitive. The abnormal behavior below cut-off for the H_{01} mode is confirmed in two experimental arrangements.

621.392.26 3343

Theory of Waveguide-Fed Slots Radiating into Parallel-Plate Regions—H. Gruenberg. (*Jour. Appl. Phys.*, vol. 23, pp. 733–737; July, 1952.) A formula is derived for the conductance of a longitudinal slot in a rectangular waveguide when the slot is radiating into a space bounded by parallel plates. The influence of plate spacing and slot position is discussed. Theoretical and experimental results are in good agreement.

621.392.26 3344

The Principle of Limiting Absorption in a Waveguide—A. G. Svenshnikov. (*Compt. Rend. Acad. Sci.* (URSS), vol. 80, pp. 345–347; September 21, 1951. In Russian.)

621.392.26 3345

Notes on Methods of Transmitting the Circular Electric Wave around Bends—S. E. Miller. (PROC. I.R.E., vol. 40, pp. 1104–1113; September, 1952.) Theory and results concerning the propagation of TE_{01} waves in round guides, published by various authors, are reviewed and three alternative solutions of the problem of transmitting these waves round bends in the guide are discussed in detail.

621.392.26 3346

Study of Obstacles in Rectangular Waveguides and of Waveguide Filters—J. Dockès. (*Câbles & Trans.* (Paris), vol. 6, pp. 221–242; July, 1952.) A method is described for determining the susceptance of a waveguide diaphragm from measurements of the reflection or the transmission coefficient, and a theoretical and experimental study is presented of resonant cavities enclosed between diaphragms in rectangular waveguides. Band-pass filters constituted by a series of such resonant cavities coupled by $\lambda g/4$ (or $3\lambda g/4$) lines are discussed and design formulas derived. Application is made to the design of (*a*) a 3-cavity filter with a pass band of 52 mc centered on 3.92 kmc, (*b*) a 5-cavity filter with a similar pass band centered on 3.69 kmc.

621.392.26 3347

Completeness Relations for Loss-Free Microwave Junctions—T. Teichmann. (*Jour. Appl. Phys.*, vol. 23, pp. 701–710; July, 1952.) Using a method which is the electromagnetic analogue of the scattering-matrix formalism in the theory of nuclear reactions, two "sum rules" are derived for the frequency-independent coefficients occurring in the admittance matrix relating the currents and voltages in a loss-free microwave junction. The results are used to estimate the effect on the admittance matrix of the higher modes, both of the guides, and of the junction proper.

621.392.26 3348

A Compact Broad-Band Microwave Quarter-Wave Plate—A. J. Simmons. (PROC. I.R.E., vol. 40, pp. 1089–1090; September, 1952.) Theory is presented for a device using three capactivie pins in a round waveguide to obtain a 90° phase difference between two orthogonal TE_{11} waves. With an experimental X-band unit only 1 inch long, a voltage ellipticity ratio <1.1 and a voltage swr<1.2 is maintained over a 12 per cent frequency band.

621.392.5 3349

Cable Operating Parameters in the Transmission of Energy in the Decimeter and Metre Wavebands—H. Ebert. (*Fernmeldetech. Z.*, vol. 5, pp. 239–240; May, 1952. Quadripole theory is applied to determine the equivalent circuit of a lossy transmission line, attenuation and phase coefficients being accounted for by separate networks in a symmetrical arrangement. The dependence of the transfer ratio on the line attenuation coefficient and the terminal mismatch is hence derived.

621.396.67:621.392.076.12 3350

Increase of Aerial Bandwidth by means of Compensation Circuits—R. Goublin. (*Rev. tech. Comp. franç. Thompson-Houston*, no. 17, pp. 61–73; July, 1952.) The problem of bandwidth increase reverts to that of finding a quadripole which, when terminated on the antenna, has an impedance lying within a certain circle in the complex plane. A detailed discussion is given of various methods of compensation by circuits or transmission-line sections. Methods of calculation for certain types of auto-compensated antenna such as folded dipoles, are outlined.

621.396.677 3351

An Improved Theory of the Receiving Antenna—R. King. (PROC. I.R.E., vol. 40, pp. 1113–1120; September, 1952.) "The theory of the center-loaded receiving antenna is improved by introducing the expansion parameter of King and Middleton, and generalized to take account of a load consisting of a two-wire line with finite spacing. First-order formulas for the distribution of current are obtained, together with approximate second-order formulas for the complex effective length of the antenna. Theoretical results are compared with experiment."

621.396.677 3352

A Design Method for a Directive Antenna Consisting of Two Elements, Projector and Reflector—R. Sato and K. Nagai. (*Sci. Rep. Res. Inst. Tohoku Univ., Ser. B*, vol. 3, pp. 125–133; March, 1952.) Methods used in the measurement of antenna input impedance, power gain and directional characteristic are described. The data thus determined have been applied to the construction of a chart from which design details can be derived for antennas with specified characteristics.

621.396.677 3353

A Directive Aerial with Increased Line-Wavelength—U. Finkbein. (*Frequenz*, vol. 6, pp. 206–213; July, 1952.) Discussion of a system of two conductors in line, fed at the inner ends and with capacitors inserted at regular intervals which are small compared with the wavelength used. The line wavelength is in this case greater than the free-space wavelength. The radiation diagram for such an antenna is determined, and also the radiation resistance and power gain.

621.396.677 3354

Wide-Band Aerial for U.S.W. Beam Links—H. Körner and W. Stöhr. (*Frequenz*, vol. 6, pp. 154–162; May/June, 1952. Corrections, *ibid.*, vol. 6, p. 215; July, 1952.) A detailed account of the development of directive antennas for a radio link, of length 213 km, between Berlin and the Harz mountains, about 90 km of the path being beyond the limit of vision. Two methods of measuring the input impedance of dipoles are described and the results obtained on different types of dipole assembly are compared with theoretical results. The antenna arrays finally adopted consist of groups of four or six units, each unit including four stacked whole-wavelength dipoles fed in phase, with reflectors. Satisfactory operation has been maintained with these antennas over a period of $1\frac{1}{2}$ years, even under conditions of severe icing.

621.396.677 3355

Experimental Results for a Lattice Lens for Centimetre Waves—J. Moussiegt. (*Compt. Rend. Acad. Sci.* (Paris), vol. 234, pp. 2263–2265; June 4, 1952.) Report of preliminary tests of a rough model of a lattice lens (3004 of December), made up of 312 resonant elements cut from 0.05-mm Al foil and of length 16 mm and breadth 4 mm, arranged in three parallel planes 16 mm apart, at their intersections with four paraboloids, the largest nodal circle having a diameter of 37.5 cm. Power is reduced by a half at 3.5° on either side of the axis, and the gain relative to that of an isotropic source is 42.

621.396.677:538.566:513.433 3356

Laws of Propagation of Electromagnetic Waves in a Conical Horn—H. Buchholz. (*Arch. Elektrotech.*, vol. 40, pp. 346–362; 1952.) Analysis of the propagation of any partial wave of the infinite system of TM and TE waves. The phase velocity, complex energy flow, and the em energy stored in a thin conical capsule within the horn, are calculated. Calculation of the group velocity by the usual formula, assuming an exponential law of propagation, gives satisfactory results for large values of rk, where r is the distance from the apex of the cone and k the wave-equation constant. For medium and small values of rk, however, the usual formula fails completely and even gives negative group velocities. A formula is derived which can be used throughout the range $0<rk<\infty$. For large values of rk it agrees, to a first approximation, with the usual formula. The attenuation is also calculated and the dependence of the amplitude on the value of rk determined.

621.396.677.3 3357

Sharpness of Aerial Beam Cut-Off—L. G. Chambers. (*Wireless Eng.*, vol. 29, p. 142; May, 1952.) A note suggesting that the angle required for the field distribution at infinity to fall from 1/2 of its value to 1/10 of its peak value, i.e., for the gain to fall from 1/2 to 1/100 of its peak value, a drop of nearly 17 db, affords a practical basis for specifying the sharpness of cut-off.

621.392.26 3358

Waveguide Handbook. [Book Review]—N. Marcuvitz (Ed.). Publishers: McGraw-Hill, London, Eng., 1951, 428 pp., 64s. (*Nature* (London), vol. 169, p. 1071; June 28,

1952.) No. 10 of the M.I.T. Radiation Laboratory Series. "... it may certainly be recommended as a standard text of reference."

CIRCUITS AND CIRCUIT ELEMENTS

621.3.012.3 3359

The Resolution of Complex Quantities—N. H. Crowhurst. (*Electronic Eng.*, vol. 24, pp. 426–428; September, 1952.) A chart using logarithmic scales is presented for facilitating calculations involving complex quantities; its use is illustrated by examples.

621.3.015.3:517.942.82 3360

Treatment of Transient Phenomena by means of the Laplace Transformation—U. Kirschner. (*Funk u. Ton*, vol. 6, pp. 369–373; July, 1952.) A simple explanation of the essential steps in applying the Laplace transform to the determination of the transient response of a system.

621.3.015.7:621.392.5 3361

A Transmission-Line Pulse Inverter—R. W. Rochelle. (*Rev. Sci. Instr.*, vol. 23, pp. 298–300; June, 1952.) Description and theory of a device for reversing the polarity of pulses with rise times of the order of 10^{-9} seconds. It consists of two coaxial cables joined so that the inner conductor of one is connected to the outer conductor of the other and vice versa, the junction being shielded. Normalized design graphs aid in the calculation of inverter characteristics.

621.314.3† 3362

Magnetic Amplifiers—W. Schilling. (*Arch. tech. Messen*, no. 197, pp. 139–142; June, 1952.) Review of the properties of basic types in reference to their use for control purposes in industry.

621.314.634:621.314.222 3363

The Characteristics of the New Siemens Flat Se Rectifier, and the Internal Resistance of the Associated Transformer—R. Kühn. (*Funk u. Ton*, vol. 6, pp. 337–350; July, 1952.) Description of the construction of Type-SSF rectifiers, with a table of dimensions and ratings, derivation of approximate formulas and curves for the internal resistance of transformers using standard M-type or E-I-type stampings, and examples of their application in the design of half-wave and full-wave rectifiers.

621.316.86 3364

Nonlinear Resistors with Sintered-Semiconductor Base—N'Guyen Thien-Chi and J. Suchet. (*Ann. Radioélect.*, vol. 7, pp. 106–114; April, 1952.) Complementary to paper abstracted in 1219 of June. Two recently developed types of thermistor are described Type RD (1-W rating) and Type RH (15- or 25-W rating). Their dc and ac characteristics are discussed and their applications are illustrated.

621.318.4:621.318.3 3365

Rapid Coil Calculations for Magnetic Devices—A. E. Maine. (*Jour. Brit. IRE*, vol. 12, pp. 403–410; July, 1952.) The equations and charts presented are primarily for designing coils associated with solenoid-operated devices, but are not restricted in their scope.

621.392.4/.5 3366

Realization of Positive Reactance Functions for Practical Use—P. Behrend and K. Scheuermann. (*Frequenz*, vol. 6, pp. 190–199; July, 1952.) The realization of positive reactance functions has applications in all section of quadripole theory. The general problem is here treated by a symbolism which a practical engineer can use without elaborate mathematics. The rational positive function corresponding to the impedance of a 2-pole network is first obtained and the result is extended to the case of a quadripole. Essential matrix and function theory is given. A scheme for realizing reactance functions in the form of 2-pole and 4-pole networks is explained and illustrated by practical examples, including the realization of (*a*) a positive matrix as the resistance matrix of a quadripole, (*b*) a quadripole equivalent to a 10.5-km length of wideband cable.

621.392.4.014.8.015.4 3367

Electrical Resonance—W. Alexander. (*Electrician*, vol. 148, pp. 1857–1861; June 6, 1952.) General discussion of resonance conditions in series and parallel RLC circuits, with correction of some common mis-statements and loose or ambiguous definitions. Relevant formulas are collected in two tables.

621.392.5 3368

Synthesis of Shunt-Resistance Networks with Given Resonance and Antiresonance Frequencies by the Partial-Network Method—T. O'Callaghan. (*Frequenz*, vol. 6, pp. 185–190; July, 1952.) The use of the method is explained for extension of a given network to one with new resonance and antiresonance frequencies, and for the synthesis of a network from elements with assigned resonance and antiresonance frequencies. See also 66 of February.

621.392.5 3369

The Transfer Function of General Two-Terminal-Pair RC Networks—A. Fialkow and I. Gerst. (*Quart. Appl. Math.*, vol. 10, pp. 113–127; July, 1952.) The present study is completely general in relation to the types of network treated, in contrast to an earlier paper (350 of March) which deals with particular types. The investigation establishes the properties characteristic of the transfer functions of this class of network, and indicates how to synthesize the network being given a transfer function having these properties. The adaptation of the analysis of RL and LC networks is indicated.

621.392.5 3370

Network Analysis by Least-Power Theorems—F. L. Ryder. (*Jour. Frank. Inst.*, vol. 254, pp. 47–60; July, 1952.) Theorems relating to electrical power, analogous to the theorem of least work applicable to mechanical deformation, are applied to the solution of the general linear network (*a*) without use of Kirchhoff's second law in the mesh-analysis case, (*b*) without use of Kirchhoff's first law in the nodal-analysis case. The theorems are put into a form suitable for practical network analysis and are extended to ac networks including transformers and complex impedances.

621.392.5 3371

Approximations in Network Design—W. Saraga. (*Wireless Eng.*, vol. 29, pp. 280–281; October, 1952.) The relation between the Taylor and Tchebycheff approximations is demonstrated. See 2461 of October (Linvill).

621.392.5 3372

Positive Feedback Operator Networks—A. W. Keen. (*Jour. Brit. IRE*, vol. 12, pp. 395, 402; July, 1952.) A feedback system using a passive bilateral shaping network in the forward path and a unidirectional unit-gain transformer in the return path can be made to perform a prescribed mathematical operation on an input quantity. This generalized network is basic to certain hitherto uncorrelated circuits, including Beale and Stansfield's integrator /differentiator (British Patent No. 453887), Schmitt and Tolles' feedback differentiator (2174 of 1942) and Newsam's "bootstrap" integrator (British Patent No. 493843). Instability is prevented by including local negative feedback in the main return path. The system is compared with a more conventional arrangement using negative feedback.

621.392.5 3373

"Non-canonical" Symmetrical Lattice Networks—R. Leroy. (*Câbles & Trans.* (Paris), vol. 6, pp. 193–210; July, 1952.) In "canonical" lattice networks the opposite impedances are equal for both pairs of branches, while in "non-canonical" units the impedances of only one pair are the same. The solution of the general equation for such networks is considered particularly for networks comprising reactive elements, which enable the number of elements required for a filter to be reduced. The design is discussed of filters (*a*) passing neither zero nor infinite frequency, (*b*) passing either zero or infinite frequency and rejecting the other, (*c*) passing both zero and infinite frequency. Filters with a single pass-band, comprising reactances (*a*) with zeros both at the origin and at infinity, (*b*) with zeros at the origin and poles at infinity, are also dealt with and the necessary design formulas derived.

621.392.5:512.94 3374

Quaternion Calculus and Chain Arrangements of Quadripoles—J. A. Ville. (*Câbles & Trans.* (Paris), vol. 6, pp. 211–220; July, 1952.) The elements of quaternion calculus are explained. A quadripole can be represented by a matrix, and its image-impedance attenuation by the logarithm of a matrix. A method is described for deriving the image parameters of a chain of quadripoles by a particular form of addition of the image parameters of the constituent units.

621.392.5:621.396.645 3375

Networks with Maximally Flat Delay—W. E. Thomson. (*Wireless Eng.*, vol. 29, pp. 256–263; October, 1952.) Discussion of the application of these networks (310 of 1950) to the design of low-pass and band-pass multistage wide-band amplifiers and pulse-shaping networks. The treatment is more general and complete than that of Laplume (951 of May) which deals with 2-, 3-, and 4-stage amplifiers. The impulse response can be made more and more symmetrical and free from overshoot by increasing the order of n of the system, the Gaussian curve being approached as n tends to infinity. Numerical examples are worked out.

621.392.52 3376

On the Redundant Information Supplied in Practical Applications by the Time and Frequency Phase Responses of a System—M. Levy. (*Jour. Appl. Phys.*, vol. 23, pp. 801–802; July, 1952.) In determining the transient response of a system from its frequency phase characteristics, or vice versa, curves are obtained which include redundant information whose elimination simplifies the problem. Three main cases are discussed in relation to low-pass systems. See also *Proc. NEC* (Chicago), vol. 7, p. 73, 1951 (abstract only), and 2750 of November.

621.392.52 3377

Formulation of the Characteristic Functions and Calculation of the Attenuation of Symmetrical and Antimetrical Filters—K. H. Haase. (*Frequenz*, vol. 6, pp. 168–176, 182; May/June, 1952.) The term "characteristic function" is applied to the quotient of two polynomials determining the transmission properties of a quadripole. The different forms of these functions are tabulated for low-pass, high-pass, band-pass and band-stop filters of both the symmetrical and the antimetrical type, the latter being such as are changed into the dual form on exchange of input and output [see 959 of 1940 (Piloty)]. The normalized characteristic functions are applied to determine the over-all attenuation, for which approximate tolerances for the transmission and blocking regions can be derived. Numerical calculations for a practical band-pass filter illustrate the theory.

621.396.611.21.029.3 3378

Quartz Vibrators for Audio Frequencies—J. E. Thwaites. (*Proc. IEE* (London), part IV, vol. 99, pp. 83–91; April, 1952.) Full paper. See 2472 of October.

621.396.611.3 3379
Theory of Pull-In Effect—H. Fack. (*Frequenz*, vol. 6, pp. 141–145; May/June, 1952.) An approximate solution is obtained of the system of nonlinear differential equations for the oscillations in an oscillatory circuit subjected to an applied alternating voltage of frequency different from the natural circuit frequency, a simplified type of characteristic being assumed.

621.396.611.3:621.392.26 3380
Multi-element Directional Couplers—S. E. Miller and W. W. Mumford. (PROC. I.R.E., vol. 40, pp. 1071–1078; September, 1952.) Theory is presented that facilitates the treatment of directional couplers using any number of coupling elements from two up to infinity. The backward wave in a directional coupler is related to the shape of the function describing the coupling between transmission lines by the Fourier transform. This facilitates the design of directional couplers with arbitrary directivities over any prescribed frequency band. Directional couplers with tight coupling are analyzed in simple terms; any desired loss ratio, including complete power transfer between lines, can be achieved. The theory is verified by experiments on waveguide models at frequencies of 4, 24 and 48 kmc.

621.396.615 3381
RC Tuned Oscillators—H. Stibbé and P. Kundu. (*Jour. Brit. IRE*, vol. 12, pp. 392–393; July, 1952.) Discussion on 2955 of 1951, with analysis of the oscillator shown in Fig. 5(*a*).

621.396.615 3382
Cascade LCR Phase-Shift Oscillators—F. Butler. (*Wireless Eng.*, vol. 29, pp. 264–268; October, 1952.) By including inductance in the feedback network the energy dissipation can be reduced in comparison with that for a RC network producing the same phase shift, thus facilitating the sustaining of oscillations. Several one-tube and transistor oscillator circuits are described, intended primarily for operation at audio and low radio frequencies; some of them incorporate quartz crystals for frequency control. A simplified theory of operation is presented.

621.396.615.17:537.533.9:530.12 3383
Possibility of Frequency Multiplication and Wave Application by Means of Some Relativistic Effects—K. Landecker. (*Phys. Rev.*, vol. 86, pp. 852–855; June 15, 1952.) Discussion of the possibility of converting the frequency of an em wave to a higher frequency by reflection from an electron cloud moving with relativistic velocity. Such a cloud can be realized by compressing all or part of the beam of an electron accelerator into one or more groups. A gain of wave energy should result from such reflection. It is estimated that a 1-mm wave, with a power of at least 1 mw, can be generated by reflecting a 3-cm wave from the beam of a small betatron. Equipment to test this is being designed.

621.396.615.18 3384
A New Frequency Divider—J. A. Fitzgerald. (*Electronic Eng.*, vol. 24, pp. 413–415; September, 1952.) The divider described is a development of the balanced-modulator type. A single tube is used, having in its anode circuit the tuned primary of a transformer whose secondary is connected back to the modulator bridge. Satisfactory operation is obtained with division ratios from 2:1 to 5:1. By modifying the circuit slightly, fractional ratios are also obtainable.

621.396.645 3385
The Effective Bandwidth of Video Amplifiers—F. J. Tischer. (PROC. I.R.E., vol. 40, p. 1060; September, 1952.) See 3050 of December.

621.396.645 3386
Amplifier Frequency Response—A. E. Ferguson and D. A. Bell. (*Wireless Eng.*, vol. 29, pp. 281–282; October, 1952.) Comment on 2482 of October and author's reply.

621.396.645 3387
Amplifiers and Superlatives—D. T. N. Williamson and P. J. Walker. (*Wireless World*, vol. 58, pp. 357–361; September, 1952.) Requirements of a good amplifier [2715 of 1947 (Williamson)] are first listed. Amplifier efficiency and trouble-free production are important factors in design. The operation and the merits of different output circuits are discussed. A triode-connected tetrode and a distributed-load tetrode give about the same quality, the efficiencies being 27 per cent and 36 per cent respectively. Similar quality can be obtained with a conventional tetrode circuit if appropriate feedback is applied, preferably by way of multiple loops in order to avoid instability.

621.396.645:621.314.7 3388
Transistor Power Amplifier—R. F. Shea. (*Electronics*, vol. 25, pp. 106–108; September, 1952.) Discussion of the best methods of obtaining maximum power gain and efficiency from junction-type transistors when used in class-A and class-B af amplifiers, with illustrations of practical circuits for gramophone and speech amplifiers and for intercommunication systems.

621.396.645:621.314.7:621.396.822 3389
Noise Figures of Transistor Circuits—Y. Watanabe. (*Sci. Rep. Res. Inst. Tohoku Univ., Ser. B*, vol. 3, pp. 151–187; March, 1952.) An alternative definition of noise figure is proposed, based on the relation between source power and output power on load. Comparison is made between the values of noise figure thus defined and the values in terms of available power for some simple amplifier circuits, cascade types of network, and for a circuit including a tube amplifier. Reasons are given for preferring the author's alternative definition, and on this basis noise figures are determined for transistor amplifiers with either base, emitter or collector electrode grounded, and the variation of noise figure with load resistance is considered.

621.396.645:621.396.619 3390
On the Theory of Doherty's Power-Amplifier Circuit—A. Simon. (*Fernmeldetech. Z.*, vol. 5, pp. 201–210; May, 1952.) The operation of the circuit is analyzed. Expressions for voltage, efficiency etc. of the individual amplifier chains and their typical values for an 80 kw power stage are listed. The latter are based on the characteristics of a Siemens Type-RS566 tube which does not operate with grid secondary emission. Two methods of reducing distortion are discussed: (*a*) insertion of a correction circuit in the input, (*b*) using a grounded-grid circuit for the main amplifier.

621.396.645.029.42 3391
Low-Pass RC Amplifier for Very Low Frequencies—G. Hoffmann. (*Frequenz*, vol. 6, pp. 162–165; May/June, 1952.) Description, with full circuit details, of an ac amplifier with a fixed lower frequency limit of about 0.3 cps and upper limit adjustable stepwise to 1, 2, 4, 8, 16 or 32 cps. The amplifier is particularly suitable as a balance indicator in bridge measurements at frequencies down to 1 cps.

621.396.645.36 3392
The Differential Amplifier with a Useful Modification—B. F. Davies. (*Electronic Eng.*, vol. 24, pp. 404–407; September, 1952.) An analysis is given of the manner in which an amplifier comprising a cathode-coupled pair of triodes discriminates between push-pull and push-push signals. By suitably adjusting the input to one of the pair, via a potentiometer, the discrimination is made infinitely great without an inconveniently high value of hv being required.

621.396.645.371:621.396.61:621.396.712 3393
C.F.T.H. Applications of Negative Feedback—Warnier. (See 3590.)

621.396.662 3394
Saturable Reactors as R.F. Tuning Elements—E. Newhall, P. Gomard and A. Ainlay. (*Electronics*, vol. 25, pp. 112–115; September, 1952.) New ferrite materials are used in saturable reactors for remote tuning of rf circuits, the inductance of the coils wound on the ferrite cores being varied by changing the dc producing the magnetizing field.

GENERAL PHYSICS

06.055.5(45):53:538.56.029.6 3395
Centre for the Study of the Physics of Microwaves [Florence, Italy]—N. Carrara. (*Ricerca sci.*, vol. 22, pp. 643–647; April, 1952.) Director's report for the year 1951.

535.22 3396
A Check Determination of the Velocity of Light—E. Bergstrand. (*Ark. Fys.*, vol. 3, pp. 479–490; July 3, 1952. In English.) Further measurements, using improved equipment, termed a "geodimeter," were made to check the determination previously reported (324 of 1951). The final value deduced is $c=299793 \pm 0.2$ km.

535.43 3397
Scattering of Plane Waves by Soft Obstacles: Part 3—Scattering by Obstacles with Spherical and Circular Cylindrical Symmetry—E. W. Montroll and J. M. Greenberg. (*Phys. Rev.*, vol. 86, pp. 889–898; June 15, 1952.) A new variational method is devised for obtaining the "best" parameters for trial wave functions of a given type for insertion in the integral equation for the scattering by soft obstacles. The differential and total scattering cross sections for scattering by Gaussian, exponential, and screened Coulomb potentials are obtained in simple closed forms. Part 1: 2139 of 1951 (Hart and Montroll). Part 2: 2317 of 1951 (Hart).

537.226:546.391.85 3398
On the Theory of the Dielectric, Piezoelectric, and Elastic Properties of $NH_4H_2PO_4$—T. Nagamiya. (*Progr. theor. Phys., Osaka*, vol. 7, pp. 275–284; March, 1952.)

537.226.2/.3:[546.212+547.261+547.262 3399
Dielectric Dispersion in Pure Polar Liquids at Very High Radio Frequencies: Part 1—Measurements on Water, Methyl and Ethyl Alcohols—J. A. Lane and J. A. Saxton. (*Proc. Roy. Soc. A*, vol. 213, pp. 400–408; July 8, 1952.) Measurements were made at wavelengths of 6.2 mm, 1.24 cm and 3.21 cm by a waveguide technique similar to that of Collie et al. (2508 of 1948). The temperature range covered was from $-10°$ to $+50°$C and results were obtained for water in the supercooled state. Values of the absorption coefficient and refractive index for the three liquids are tabulated. The electrical characteristics of water vary in a continuous manner down to at least $-8°$C. The results for the alcohols indicate that both, like water, have relatively high atomic polarizations. Part 2: 3400 below.

537.226.2/.3:[546.212+547.261+547.262 3400
Dielectric Dispersion in Pure Polar Liquids at Very High Radio Frequencies: Part 2—Relation of Experimental Results to Theory—J. A. Saxton. (*Proc. Roy. Soc. A*, vol. 213, pp. 473–492; July 22, 1952.) Analysis of the results given in part 1 (3399 above) indicates that a single relaxation time as a function of temperature is sufficient to account for the observed dielectric properties of water, at any rate for wavelengths greater than a few millimetres. The results for methyl and ethyl alcohols for wavelengths near to 1 cm, which apparently indicate a distribution of relaxation times, can be explained in terms of resonance absorption, with postulated bands centered at

wavelengths of 2.5 mm and 5 mm in methyl and ethyl alcohol respectively. Further measurements at wavelengths between 1 mm and 1 cm are required. The close relation between dipole rotation and viscous flow in the three liquids is discussed.

537.311.33 3401

The Influence of Surface [energy] Levels on the Chemical Potential and Work Function of a Semiconductor—G. E. Pikus. (*Zh. eksp. teor. Fiz.*, vol. 21, pp. 1227–1238; November, 1951.) A discussion based on the assumption of a surface zone in which the number of levels is equal to the number of surface cells of the crystal.

537.311.33 3402

On the Diffusion Theory of Rectification—P. T. Landsberg. (*Proc. Roy. Soc. A*, vol. 213, pp. 226–237; June 24, 1952.) The Einstein relation $eD=\mu kT$ between the mobility μ and diffusion coefficient D has not so far been established theoretically or experimentally for rectifiers. Analysis of experimental results for a copper-oxide rectifier in terms of a Schottky barrier on the basis of the diffusion equation in which μ and D are retained, suggests that the values of μ and D differ for forward and reverse characteristics. The diffusion equation is developed from the formal theory of conduction using Fermi-Dirac statistics; the μ and D of this equation are to be regarded as average values throughout the barrier, as both depend on the concentration distribution of conduction electrons in the barrier.

537.523.4 3403

Mechanism of Positive Spark Discharges with Long Gaps in Air at Atmospheric Pressure—H. Norinder and O. Salka. (*Ark. Fys.*, vol. 3, pp. 347–386; July 3, 1952. In English.) Report of experiments made to determine to what extent the streamer theory is applicable in the case of long gaps. A sphere-to-plane or point-to-plane arrangement was used, with the point or sphere always at the positive potential; gap lengths ranged from 5 to 155 cm. 41 references.

537.523.4:546.17-1 3404

Electrical Breakdown of Gases: Part 2—Spark Mechanism in Nitrogen—J. Dutton, S. C. Haydon and F. L. Jones. (*Proc. Roy. Soc. A*, vol. 213, pp. 203–214; June 24, 1952.) The growth of the pre-breakdown ionization currents in uniform fields in nitrogen was measured for various field strengths, pressures, gap widths and sparking potentials. The sparking distances and potentials measured were found to be exactly in accordance with those predicted by the Townsend equation. There were strong indications that the secondary ionization is a cathode process. Possible effects of space charge are considered. Part 1: 3405 below.

537.523.4:546.217 3405

Electrical Breakdown of Gases: Part 1—Spark Mechanism in Air—F. L. Jones and A. B. Parker. (*Proc. Roy. Soc. A*, vol. 213, pp. 185–202; June 24, 1952.) Experimental investigations show that the pre-breakdown growth of small ionization currents in air in uniform electric fields can, for certain conditions, be represented by the well-known Townsend relation. This indicates the existence of a secondary mechanism throughout the complete breakdown process. Measurement of the primary and secondary ionization coefficients gave agreement between the calculated and observed sparking potentials.

537.533 3406

The Dispersion of Electron Beams in Gases—P. F. Little and A. von Engel. (*Proc. Phys. Soc.* (London), vol. 65, pp. 459–460; June 1, 1952.) Discussion of the mechanism of dispersion based on the discovery that an electron beam accelerated at 3–10 kv in nitrogen remains well concentrated at pressures of about 1 mm Hg. The ultimate cause of beam concentration is the presence of positive ions in and around the beam.

537.533:519.21 3407

Probabilities relating to a Continuous Electron Beam—P. Mourmant. (*Radio franç.*, no. 6, pp. 19–24; June, 1952.) In the case of currents involving the movement of a very large number of electrons, simple statistical methods of treatment result in theories of practical value for engineers. For feeble currents, however, where the number of electrons concerned may be relatively small, statistical methods are not satisfactory and discussion of certain probabilities concerning individual electrons appears preferable. The probable number of electrons passing across a certain section of an electron beam in a given time interval, and the probable time interval between the passage of consecutive electrons, are discussed, with numerical examples. Application of certain probability invariants in the case of modulated or unmodulated beams is also considered.

537.533.7:537.226 3408

Free Paths of Electrons in Crystals, Electroluminescence Effects and Phenomena of Dielectric Breakdown—D. Curie. (*Jour. Phys. Radium*, vol. 13, pp. 317–325; June, 1952.)

537.533.8 3409

A Note on Wooldridge's Theory of Secondary Emission—E. M. Baroody. (*Phys. Rev.*, vol. 86, pp. 915–916; June 15, 1952.) Re-examination of Wooldridge's theory shows that the broad maximum which he obtained in the curve of secondary-emission coefficient against primary energy is a result of inconsistency in approximations, rather than an essential result of his theory. See also 107 and 110 of February, and 108 and 109 of February (Brophy).

537.562 3410

Wave Theory of Plasmas—D. Gabor. (*Proc. Roy. Soc. A*, vol. 213, pp. 73–86; June 5, 1952.) A critical review is given of various theories. The spectral law of energy distribution in plasma waves is discussed and a thermodynamical upper limit is shown to exist for the energy. The momentum and energy interchange of electrons with plasma waves is very weak, and quite insufficient to explain the existence of the Maxwellian energy distributions in low-pressure arcs observed by Langmuir, for which a fresh interpretation is required.

537.562:538.566 3411

High-Frequency Oscillations in an Electron Plasma—A. I. Akhiezer and Ya. B. Faynberg. (*Zh. eksp. teor. Fiz.*, vol. 21, pp. 1262–1269; November, 1951.) If a beam of charged particles enters an electron plasma, the fluctuations of density and velocity in the beam are propagated in the form of waves with increasing amplitude.

537.562:538.566 3412

On Magneto-hydrodynamic Waves in Gases—V. L. Ginzburg. (*Zh. eksp. teor. Fiz.*, vol. 21, pp. 788–794; July, 1951.) Formulas are derived which for high frequencies are transformed into corresponding expressions determining the propagation of radio waves in the ionosphere, taking account of the effect of the magnetic field. At low frequency, below the gyromagnetic frequency for ions, the results obtained coincide with those derived from the hydrodynamic approximation. See also 2152 of 1951 (Åström).

538.114 3413

Molecular-Field Treatment of Ferromagnetism and Antiferromagnetism—J. S. Smart. (*Phys. Rev.*, vol. 86, pp. 968–974; June 15, 1952.) A modified Weiss treatment of magnetism in crystals in which both first and second nearest-neighbor interactions, with all four combinations of signs, are considered.

538.221 3414

Antiferromagnetic Arrangements in Ferrites—Y. Yafet and C. Kittel. (*Phys. Rev.*, vol. 87, pp. 290–294; July 15, 1952.) Néel's molecular-field treatment is extended to take into account the exchange interactions within the two magnetic sublattices.

538.3 3415

A Method for determining the Electromagnetic Field inside a Closed Spherical Envelope with Nonuniform Permittivity—R. G. Mirimanov. (*Compt. Rend. Acad. Sci.* (U.R.S.S.), vol. 80, pp. 361–364; September 21, 1951. In Russian.) An equation (10) is derived establishing the relation between the total fields on both sides of the envelope. The total field in this case is made up of the field due to the external sources, which induce corresponding currents in the envelope, and the field excited by these currents in space. Methods are indicated for determining the secondary field, and a linear differential equation (22) is derived from which the required solution can be found.

538.3 3416

Matrix and Tensor Form of the Fundamental Relations of Magneto-ionic Theory—H. Arzeliès. (*Compt. Rend. Acad. Sci.* (Paris), vol. 234, pp. 2430–2432; June 16, 1952.) Matrix relations are developed from Maxwell's equations which give all the characteristics of waves, including phase velocity and polarization. Formulas such as the Appleton-Hartree formula are included as particular cases. The system can be put into tensor form.

538.521 3417

The Dromgoole Effect—R. H. Frazier. (*Wireless Eng.*, vol. 29, p. 253; September, 1952.) Comment on 2491 of September, indicating the relation between the Dromgoole effect and the well known Wiedemann effect.

538.56:535.42 3418

Diffraction by a Semi-infinite Metallic Sheet—T. B. A. Senior. (*Proc. Roy. Soc. A*, vol. 213, pp. 436–458; July 22, 1952.) "In spite of the considerable attention which has been focused on diffraction by perfectly conducting structures, little success has so far been achieved when finite conductivity is introduced. It is now shown that with the assumption of suitable boundary conditions, the problem of diffraction at a metal sheet is capable of exact solution. Corresponding to each of two fundamental polarizations, a pair of Wiener-Hopf integral equations is derived from which to determine the electric and 'magnetic' currents present in the sheet. One of these equations is subjected to a rigorous solution, and from it the solutions of the other three are deduced by symmetry considerations. Use of the generalized method of steepest descent then serves to determine the diffracted fields. The case of a circularly polarized incident wave is also briefly discussed and a comparison presented between the theoretical and experimental forms of the scattered field; good agreement is obtained."

538.56:621.3.011.21:523.14 3419

The Characteristic Impedance of Vacuum, an Important Universal Constant—E. Hallén. (*Bull. Soc. franç. Élect.*, vol. 2, pp. 377–380; June, 1952.) Discussion of basic formulas of electromagnetic theory. See also 1397 of 1950 (Tanasescu: Brylinski) and back references.

538.566.2 3420

The Concept of Group Velocity—P. Poincelot. (*Compt. Rend. Acad. Sci.* (Paris), vol. 234, pp. 2426–2427; June 16, 1952.) Discussion for the case of propagation from one medium to another with different refractive index, justifying the methods applied to the study of the ionosphere. See also 2179 of September.

GEOPHYSICAL AND EXTRA-TERRESTRIAL PHENOMENA

523.72+523.85]:621.396.822.029.6 3421

Cosmic Radio-Noise Intensities in the V.H.F. Band—H. V. Cottony and J. R. Johler. (Proc. I.R.E., vol. 40, pp. 1053–1060; September, 1952.) Results of continuous observations made at the National Bureau of Standards during 1948 and 1949 on frequencies in the range 25–110 mc are reported. A regular daily variation in noise was found to correspond with the movement of the principal sources of cosmic rf noise across the receiving antenna system. The results are presented in terms of the observed daily maxima and minima. Periods of abnormally high noise levels, generally associated with periods of unusual solar activity, were also recorded.

523.752:523.746.5 3422

Prominence Activity and the Sunspot Cycle—R. Ananthakrishnan. (*Nature* (London), vol. 170, pp. 156–158; July 26, 1952.) Analysis of solar-prominence records at Kodaikanal from 1905 to 1950 shows a marked correlation with the sunspot cycle. The region of most intense prominence activity on the sun is at about latitude 50°–55° in both hemispheres some three or four years before sunspot maximum.

523.854:621.396.822.029.62 3423

Measurements of the Radiation from the Milky Way on 255 Mc/s—I. Atanasijević. (*Compt. Rend. Acad. Sci.* (Paris), vol. 235, pp. 130–132; July 16, 1952.) Preliminary report of results obtained with the 7.5-m paraboloid of the Institut d'Astrophysique, Paris, with a diagram showing the 255-mc radio-isophotes for the region of the Milky Way investigated.

537.311+537.226.2]:546.331.31-145.1 3424

Electrical Properties of Sea Water—J. A. Saxton and J. A. Lane. (*Wireless Eng.*, vol. 29, pp. 269–275; October, 1952.) The results of recent measurements of the dielectric properties of aqueous NaCl solutions at frequencies between 9.4 and 48 kmc are applied to the calculation of the electrical properties of sea water. The static dielectric constant has values of about 75 and 69 respectively at 0° and 20°C, the corresponding values for pure water being 88 and 80. The reflection coefficient of sea water is given as a function of the angle of incidence at frequencies between 30 mc and 30 kmc, and it is shown how the dipolar and ionic conductivities govern the attenuation of pure, fresh and sea water at radio frequencies.

550.386:523.78 3425

Micro-magnetic Variations during the Solar Eclipse of February 25, 1952—N. F. Astbury. (*Nature* (London), vol. 170, pp. 68–69; July 12, 1952.) A preliminary account of observed variations of the horizontal component of the geomagnetic field at Khartoum. A region of minimum disturbance occurred about 10 minutes after totality; recovery to the pre-eclipse level was prolonged for 4–5 hours after the last contact. It is suggested that the magnetic variations are largely due to plasma oscillations in the lower levels of the ionosphere.

551.510.535 3426

Nocturnal Disturbances of Ionization in the Lower Ionosphere—E. A. Lauter and K. Sprenger. (*Z. Met.*, vol. 6, pp. 161–173; June, 1952.) The observations made on 245-kc sky waves, reported previously [1377 of 1951 (Lauter)], are analyzed statistically and the types of disturbance are classified. Though there is generally close correlation with geomagnetic activity, some of the phenomena observed cannot be explained by accepted corpuscular-radiation theories. Observations on long waves should yield useful information not only about the mechanism of disturbances in the lower ionosphere, but also about the wind systems in the upper atmosphere.

551.510.535:621.396.11.029.53 3427

Weak Echoes from the Ionosphere with Radio Waves of Frequency 1.42 Mc/s—S. Gnanalingam and K. Weekes. (*Nature* (London) vol. 170, pp. 113–114; July 19, 1952.) Note of results obtained by a sensitive FM method suitable for detecting echoes at times of high absorption. In January and February, reflections were obtained from heights between 75 and 80 km. The effective reflection coefficient was found to be $<3\times10^{-4}$. On days when the absorption was less, discrete reflection heights were noted near 90, 96 and 112 km. From mid-March the reflection height was consistently in the range 102–105 km.

551.54:550.386 3428

Atmospheric Pressure and Geomagnetic Disturbance—R. P. W. Lewis and D. H. McIntosh. (*Nature* (London) vol. 169, pp. 1059–1060; June 21, 1952.) Discussion of possible relations between geomagnetic disturbances and atmospheric pressure variations in the light of results for selected days in years of low sunspot number between 1900 and 1945.

551.594.6:551.515.3 3429

Identification of Tornadoes by Observation of Atmospherics Waveform—H. L. Jones and P. N. Hess. (Proc. I.R.E. vol. 40, pp. 1049–1052; September, 1952.)

LOCATION AND AIDS TO NAVIGATION

621.396.9 3430

Narrow-Band Link relays Radar Data—J. L. McLucas. (*Electronics*, vol. 25, pp. 142–146; September, 1952.) Description, with detailed circuit diagrams, of equipment for scanning the ppi display on a radar cr tube at a slow rate, thus integrating the display data and enabling a video signal, of bandwidth 2.3 kc, to be derived for transmission over telephone lines or a radio link to any desired point, where an adapter unit generates the signals necessary to operate a display which is a reasonably good reproduction of the original.

621.396.9 3431

A Survey of Requirements for Port Radar—L. S. Le Page. (*Jour. Inst. Nav.*, vol. 5, pp. 285–295; July, 1952.) General discussion of the advantages and limitations of a port radar system, based on the results of an official investigation. The trial equipment set up at Sunderland (1388 of 1951) and now permanently installed is described. Details are given of the operating procedure. Other existing and projected shore installations in various parts of the world are listed, with descriptive notes.

621.396.9 3432

Operational Requirements for the Harbour Radar Installation at Ijmuiden—E. Goldbohm. (*Tijdschr. ned. Radiogenoot.*, vol. 17, pp. 156–167; July, 1952. Discussion, p. 167.) The special problems introduced by local weather and tidal conditions are indicated. Design features discussed include choice of wavelength (3.26 cm) and resolving power (17 m radial, 0.7° half beam-width), screen excitation, ranges (10 km maximum), scale of display and accuracy. Details are given of the parabolic-cylinder antenna with offset horn feed; rotation rate is 20 r.p.m. Communication is effected by FM radiotelephone operating in the 160-mc band.

621.396.9:621.317.75 3433

The Indicator of the Harbour Radar Installation at Ijmuiden—J. A. Grosjean. (*Tijdschr. ned. Radiogenoot.*, vol. 17, pp. 182–190; July, 1952. Discussion p. 190.) The indicator comprises two similar independent units each equipped with a 16″ metal-cone cr tube for panoramic display. A direct indication of bearing and distance of object is provided. The sweep is performed by a rotating-coil mechanism driven from the antenna by a servo link. Permanent magnets of ferroxdure are used to offset the display to give bearing and distance from the harbor mouth rather than from the transmitter. See also 3432 above.

621.396.9:621.396.61/.62 3434

The Transmitter and Receiver of the Harbour Radar Installation at Ijmuiden—J. Verstraten. (*Tijdschr. ned. Radiogenoot.*, vol. 17, pp. 168–180; July, 1952. Discussion, p. 181.) A magnetron transmitter with a peak power of 7 kw is used in conjunction with a heterodyne receiver including Si detector and klystron oscillator with afc. The IF is 30 mc and the pulse repetition frequency 3 kc. Circuit design details for attaining the required resolution, range and accuracy of location are discussed. Some notes on the mechanical construction are included. See also 3432 above.

621.396.9:621.396.8 3435

Fluctuations of Ground Clutter Return in Airborne Radar Equipment—T. S. George. (*Proc. IEE* (London), part IV, vol. 99, pp. 92–99; April, 1952.) Full paper. See 2514 of October.

621.396.932/.933 3436

Decca Navigator—(*Wireless World*, vol. 58, p. 338; September, 1952.) A map shows the locations of European Decca stations, including those of the South-West British chain opened on 29th July 1952, with its central station near Plymouth.

621.396.932/.933].1+621.396.97 3437

Common-Wave Broadcasting and Hyperbolic Navigation: Part 2—M. Pohontsch. (*Telefunken Ztg*, vol. 25, pp. 93–97; June, 1952.) Discussion of the accuracy of hyperbolic navigation systems and of the possibility of using the transmissions of the German Decca stations as frequency standards for common-wave transmitters in the medium-wave range and even for the control of usw transmitters. 37 references. Part 1: 2515 of October.

MATERIALS AND SUBSIDIARY TECHNIQUES

535.37 3438

Induced Conductivity and Light Emission in Different Luminescent Type Powders—H. Kallmann and B. Kramer. (*Phys. Rev.*, vol. 87, pp. 91–107; July 1, 1952.) Experimental and theoretical investigation of various (Zn:Cd)S phosphors.

535.37 3439

Electroluminescence of Single Crystals of ZnS:Cu—W. W. Piper and F. E. Williams. (*Phys. Rev.*, vol. 87, pp. 151–152; July 1, 1952.) Application of direct or alternating voltage causes luminescence. Observations are explained on the basis of semiconductor theory.

535.371:546.472.21 3440

A Study of the Electron Traps in Zinc Sulfide Phosphor—A. W. Smith and J. Turkevich. (*Phys. Rev.*, vol. 87, pp. 306–308; July 15, 1952.)

535.376 3441

Recent Research on Radio-luminescence—G. F. J. Garlick. (*Brit. Jour. Appl. Phys.*, vol. 3, pp. 169–172; June, 1952.) Investigations of the excitation of single crystals by single particles, using sensitive photomultipliers, indicate much simpler relations between luminescence intensity and particle energy than those previously found for phosphors of complex structure. In many inorganic crystals the luminescence is proportional to the energy absorbed; deviations from proportionality provide indications of the nature of the processes involved. Further theoretical research is needed on the nature of the nonradiative processes which consume at least 80 per cent of the energy absorbed by ordinary phosphor screens.

535.376:[546.41.786-31+546.47−31 3442

The Decay of Calcium-Tungstate and Zinc-Oxide Phosphors after Electron-Beam Ex-

citation—H. Gobrecht, D. Hahn and H. Dammann. (*Z. Phys.*, vol. 332, pp. 239–247; June 23, 1952.) Oscillograms of the decay characteristics are examined. That of $CaWO_4$ is exponential, of ZnO hyperbolic. Luminescence is assumed to be a monomolecular process in $CaWO_4$, and to be due to a recombination mechanism in ZnO.

537.224 3443
Investigation of the Thermal Conductivity of Electrets—J. van Calker and R. Arnold. (*Z. Phys.*, vol. 132, pp. 318–329; June 23, 1952).

537.226 3444
Thermodynamic Theory of the Ferroelectric Properties of Crystals of the Barium Titanate Type—M. Ya. Shirobokov and L. P. Kholodenko. (*Zh. eksp. teor. Fiz.*, vol. 21, pp. 1239–1249; November, 1951.)

537.226 3445
The Ferroelectric Properties of Crystals of the $BaTiO_3$ Type near the Curie Point in the Presence of Elastic Stresses—L. P. Kholodenko and M. Ya. Shirobokov. (*Zh. eksp. teor. Fiz.*, vol. 21, pp. 1250–1261; November, 1951.)

537.228.2:538.652 3446
On the Theory of Electrostriction Vibration—Substitution of Magnetostriction Theory—Y. Kikuchi. (*Sci. Rep. Res. Inst. Tokohu Univ., Ser. B*, vol. 3, no. 1, pp. 7–12; 1951.)

537.311.3 3447
The Electrical Resistance of Binary Metallic Mixtures—R. Landauer. (*Jour. Appl. Phys.*, vol. 23, pp. 779–784; July, 1952.) A theory is developed which assumes a random mixture of the two components, conduction proceeding as if each crystal is surrounded by a homogeneous medium whose properties are those of the mixture. The variation of resistivity with composition as computed from the theory is compared with curves obtained experimentally; agreement is satisfactory for one group of mixtures, but totally unsatisfactory for another group.

537.311.33:537.565 3448
Effects of Dislocations on Mobilities in Semiconductors—D. L. Dexter and F. Seitz. (*Phys. Rev.*, vol. 86, pp. 964–965; June 15, 1952.) The scattering of electrons or holes in semiconductors by the dilatation of the lattice around rigid randomly arranged edge-type dislocations is treated by the method of the deformation potential. The contribution of this scattering to the electrical resistance is determined from the Boltzmann transport equation.

537.311.33:537.58 3449
Thermal Ionization of Trapped Electrons—R. Kubo. (*Phys. Rev.*, vol. 86, pp. 929–937; June 15, 1952.) The rate of thermal ionization of electrons trapped on impurity atoms is treated on a quantum mechanical basis. Approximate formulas based on an Einstein model are derived for the total ionization rate. Reasons are given for expecting much greater rates than those given by Goodman, Lawson and Schiff (2453 of 1947).

537.311.33:546.24-1 3450
Semiconducting Properties of Tellurium—P. Aigrain, C. Dugas, J. Legrand des Cloiseaux and B. Jancovici. (*Compt. Rend. Acad. Sci.* (Paris), vol. 235, pp. 145–146; July 16, 1952.) Measurements of the conductivity and Hall effect of single crystals, of dimensions several millimeters, were made at different temperatures between that of liquid N and 50°C. The results show that Te is a *p*-type semiconductor with intrinsic activation energy of 0.34 ev and impurity activation energy of about 0.039 ev. At room temperature the mobility of electrons was found to be 910 cm per v/cm, and that of holes 570 cm per v/cm.

537.311.33:546.28-1 3451
Study of the Conductivity of Silicon—M. Perrot and J. Tortosa. (*Compt. Rend. Acad. Sci.* (Paris), vol. 235, pp. 143–145; July 16, 1952.) Films of Si were deposited by evaporation on to glass between two Ag electrodes 100–300 μ apart. For thicknesses 300 mμ the resistance was nearly constant for applied voltages up to 1.5 kv/cm, but the thinnest films showed considerable departures from Ohm's law, the resistance of 70-mμ and 160-mμ films being 15 times greater at 1.5 kv/cm than at zero voltage.

537.311.33:546.289 3452
The ABC's of Germanium—J. P. Jordan. (*Elec. Eng.* (N.Y.), vol. 71, pp. 619–625; July, 1952.) Discussion of mechanisms governing the properties and applications of Ge crystals.

537.311.33/:546.289:537.568 3453
Electron-Hole Recombination in Germanium—R. N. Hall. (*Phys. Rev.*, vol. 87, p. 287; July 15, 1952.) Measurements show that the rate of recombination varies linearly with carrier concentration over a wide range of concentration and of temperature. This can be explained on the assumption that recombination takes place largely through the agency of recombination centers distributed throughout the Ge. The Fermi level of these centers is estimated as about 0.22 ev above the valence band or below the conduction band.

537.311.33:546.772.21 3454
Semiconductor Properties of Molybdenite—F. Regnault, P. Aigrain, C. Dugas and B. Jancovici. (*Compt. Rend. Acad. Sci.* (Paris), vol. 235, pp. 31–32; July 7, 1952.) Measurements of conductivity and Hall effect were made at temperatures between that of liquid H and 300°C. The curve showing the logarithm of the number of free carriers plotted against the reciprocal of absolute temperature is not a straight line in all cases, indicating the presence of both types of impurity.

538.221 3455
New Magnetic Material—(*Elec. Rev.* (London) vol. 150, p. 1246; June 6, 1952.) A few details are given of a new Ni-Fe alloy, developed by Standard Telephones, to be known as "Permalloy F." It has a very nearly rectangular hysteresis loop, low coercive force, and is very suitable as a core material for all types of saturable reactor. A flux density of nearly 14,000 gauss can be obtained with magnetizing fields <0.1 oersted. A list of proposed core sizes is given.

538.221 3456
The Magnetic Structure of Alnico 5—E. A. Nesbitt and R. D. Heidenreich. (*Elec. Eng.* (N.Y.), vol. 71, pp. 530–534; June, 1952.) Revised text of A.I.E.E. Winter General Meeting paper, January 1952. Detailed discussion of (*a*) the mechanism which enables the alloy to respond to heat treatment in a magnetic field, (*b*) the mechanism resulting in the high coercive force of 600 oersted. See also 2530 and 2531 of October.

538.221 3457
Rare-Earth Ferrites with Two Curie Points—H. Forestier and G. Guiot-Guillain. (*Compt. Rend Acad. Sci.* (Paris), vol. 235, pp. 48–50; July 7, 1952.) Continuation of work noted previously (2532 of 1950).

538.221:534.232:538.652 3458
Magnetostrictive Vibration of Prolate Spheroids. Ni-Fe and Ni-Cu Alloys—J. S. Kouvelites and L. W. McKeehan. (*Phys. Rev.*, vol. 86, pp. 898–904; June 15, 1952.) A study of various magnetic properties of Ni-Fe and Ni-Cu alloys determined from longitudinal magnetostrictive vibrations of spheroidal samples. See also 1929 of August (Beck et al.).

538.221:537.226.2/.3 3459
Dielectric Investigations on Ferrites—G. Möltgen. (*Z. angew. Phys.*, vol. 4, pp. 216–224; June, 1952.) Measurements of dielectric constant s_r and dielectric loss between 50 cps and 20 mc indicate an inhomogeneous structure. Extremely high values of s_r at low frequencies are attributed to very thin air layers between the ferrite crystals. At frequencies of a few kc s_r falls to a constant value of about 10; this is maintained up to 4 kmc.

538.221:621.318.2 3460
A New Permanent-Magnet Material of Nonstrategic Material—F. G. Brockman. (*Elec. Eng.* (N.Y.), vol. 71, pp. 644–647; July, 1952.) An account of the properties of the Philips material ferroxdure. See also 2824 of November (Went et al.).

538.221:621.318.2 3461
Determination of the Characteristics of Permanent-Magnet Materials—E. Meyer. (*Arch. Elektrotech.*, vol. 40, pp. 363–366; 1952.) A graphical method is described for determining the maximum induction that can be obtained in the air-gap of a magnet made from specified material.

538.221:621.318.2 3462
A Graphical Method for Determining the Optimum Working Point of Permanent-Magnet Systems—W. Breitling. (*Arch. Elektrotech.*, vol. 40, pp. 366–369; 1952.)

538.221:669.14.018.582-15 3463
The Influence of Heat Treatment on Magnetic Viscosity in Permanent-Magnet Alloys—R. Street, J. C. Woolley and P. B. Smith. (*Proc. Phys. Soc.* (London), vol. 65, pp. 461–462; June 1, 1952.)

538.221:669.15.782 3464
Low Remanence and the Temperature Variation of Permeability of Silicon-Iron Alloys—E. W. Lee. (*Proc. Phys. Soc.* (London), vol. 65, pp. 455–456; June 1, 1952.)

538.221.029.5/.6 3465
The Magnetic Spectra of the NiZn Ferrites at Radio Frequencies—L. A. Fomenko. (*Zh. eksp. teor. Fiz.*, vol. 21, pp. 1201–1208; November, 1951.) The influence of frequency on the elastic and viscous permeabilities of ferrites is considered. The Ni-Zn ferrites have a continuous magnetic spectrum with sharply defined dispersion bands of elastic permeabilty and absorption bands of viscous permeability at frequencies from 0.75 to 360 mc.

546.23.161:621.317.335.3 3466
The Dielectric Constant and Loss of Amorphous Selenium at a Wavelength of 3 cm—H. A. Gebbie and D. G. Kiely. (*Proc. Phys. Soc.* (London), vol. 65, p. 553; July 1, 1952.) Results of waveguide measurements are in good agreement with values previously found for infrared wavelengths.

546.26-1:537.582 3467
The Thermionic Constants of Metals and Semi-conductors: Part 1—Graphite—S. C. Jain and K. S. Krishnan. (*Proc. Roy. Soc.* A, vol. 213, pp. 143–157; June 24, 1952.) Experimental determination of the saturation vapor pressure of the electron gas from graphite as a function of temperature T by an effusion method, yielding a value for the work function of 4.62 ev and for the effusion constant of 60 $A/cm^2/T^2$.

546.47-31 3468
The Photoconductivity of Zinc Oxide—H. Weiss. (*Z. Phys.* vol. 132, pp. 335–353; June 23, 1952.) An investigation of the photoconductivity of evaporated ZnO films as a function of temperature and of the wavelength of the incident light. The quantum efficiency is determnied from the initial rise of current. Normal relations connecting dark and light current and rate of current change hold at temperatures down to 87°K.

546.47-31:[537.533.9+535.215.2 3469
The Energy Conversion in Light or Electron Irradiation of Thin Zinc-Oxide Films—G.

Heiland. (*Z. Phys.*, vol. 132, pp. 367–383; June 23, 1952.) A simple model is proposed which affords a theoretical explanation of the effects previously described (3470 below).

546.47-31:537.533.9 3470
Conductivity Variations of Thin Zinc-Oxide Films due to Electron Irradiation—G. Heiland. (*Z. Phys.*, vol. 132, pp. 354–366; June 23, 1952.) Irradiation by electrons of energy 1–6 kev produced a reversible increase of the conductivity; a quantitative estimation of the energy conversion was made from the initial increase of current.

621.3.042.143 3471
Tape-Wound Magnetic Cores—A. L. Morris. (*Electronic Eng.*, vol. 24, pp. 416–417; September, 1952.) The advantages of tape-wound cores for use in transformers and magnetic amplifiers are indicated, and various constructions are discussed. Flux distribution can be made satisfactorily uniform by means of series, parallel or tertiary compensating windings.

621.314.63 3472
Further Results in the General Theory of Barrier-Layer Rectifiers—P. T. Landsberg. (*Proc. Phys. Soc.* (London), vol. 65, pp. 397–409; June 1, 1952.) Formulas are derived for the temperature variation of the zero-voltage resistance of a rectifier with an arbitrary distribution of impurity centers. These formulas are applied to interpret experimental results and to determine the dependence on temperature of (*a*) the effective mass of current carriers in Ge rectifiers and (*b*) the mobility of current carriers in Se rectifiers. Thermal instability and current creep are discussed.

621.314.632:549.328.1 3473
Rectification Phenomena exhibited by Natural and Sulphurized Galena—A. L. Reimann and J. V. Sullivan. (*Proc. Phys. Soc.* (London), vol. 65, pp. 480–487; July 1, 1952.) According to the sulphurization treatment given, either the rectification properties of specimens of *n*-type galena were improved, or the polarity was changed to *p*-type. The results of tests with dc and at 3 kmc were discussed in the light of present-day theory.

621.314.634+621.383.42]:546.49-13 3474
The Influence of Mercury Vapour on Selenium Rectifiers and Selenium Photoelements—P. Selényi. (*Proc. Phys. Soc.* (London), vol. 65, p. 552; July 1, 1952.) If Se rectifiers are exposed to Hg vapor, they lose their high resistance in the blocking direction and become useless. A similar destructive effect has been observed with Se photocells. The effect, which is due to the formation of mercuric selenide, an excess semiconductor of high conductivity, is discussed with reference to Schottky's barrier-layer theory.

621.315.61:537.311.1 3475
Electronic Conduction in Crystalline Insulating Materials—W. Franz. (*Z. Phys.*, vol. 132, pp. 285–311; June 23, 1952.) Systematic development of a theory of conduction and breakdown.

621.315.612.6:666.1 3476
Dielectric Losses in Glass—J. M. Stevels. (*Philips tech. Rev.*, vol. 13, pp. 360–370; June, 1952.) Losses at different temperatures due to (*a*) conduction, (*b*) after effect and (*c*) resonance are discussed. The influence of chemical composition and structure is investigated, with special attention to the borate glasses. Methods of reducing the losses in certain frequency ranges are described.

621.315.612.6:677.021/.024 3477
Fibreglass in Electrical Insulation—A. R. Henning. (*Distrib. Elec.*, vol. 25, pp. 154–158; July, 1952.) An account of modern methods of producing, spinning and weaving glass fibres, and of the application of glass-fibre yarn, braid, cloth, etc., for cable insulation and other purposes.

621.315.616.9:621.396.822 3478
Random Noise in Dielectrics—H. Bauss and R. F. Boyer. (*Jour. Appl. Phys.*, vol. 23, pp. 802–803; July, 1952.) The fluctuating currents previously observed [2550 of 1950 (Boyer)], on applying direct voltage across thin films of certain polymers, tend to disappear on cooling the sample below the second-order transition temperature. This is interpreted as supporting the theory that the fluctuations are due to the diffusion of ions.

621.318.1 3479
Magnetodynamics of Cores and Sheaths with Air-gaps—P. M. Prache. (*Câbles & Trans.* (Paris), vol. 6, pp. 265–277; July, 1952.) Continuation of a previous paper (2246 of September). A physical explanation is given of the action of air-gaps in increasing the frequency at which skin effects begin to cause a decrease of coil inductance and *Q* factor. Formulas and charts are given which enable quantitative estimation of the improvement due to the use of air-gaps; experiments confirm their validity.

621.318.2 3480
Permanent Magnets for Spectrographs and Nuclear Physical Research—D. Hadfield and D. L. Mawson. (*Brit. Jour. Appl. Phys.*, vol. 3, pp. 199–202; June, 1952.) Descriptions are given of recently designed permanent-magnet systems for producing constant strong fields in large air gaps; modern anisotropic alloys are used. Where small variations can be tolerated, auxiliary electromagnets are used to facilitate adjustment of field strength; alternatively control may be effected by artificial aging.

621.396.611.21 3481
High-Frequency Crystal Units for Primary Frequency Standards—A. W. Warner. (PROC. I.R.E., vol. 40, pp. 1030–1033; September, 1952.) Description of the characteristics of and production methods for a new type of crystal unit suitable for mass-production techniques. An AT cut is used and one face of the crystal has a spherical contour whose radius is chosen to give minimum series-resonance resistance. Both faces are polished, with gold-film electrodes of limited area. Overtone operation is used, final frequency adjustment to within 1 cps per megacycle/second being effected by control of the final stage of the gold-film deposition. Such crystals operate in the range 3–20 mc, have very high *Q* values and very low temperature coefficients, and are highly stable under conditions of vibration or shock.

MATHEMATICS

517.942.93 3482
Separability Conditions for the Laplace and Helmholtz Equations—P. Moon and D. E. Spencer. (*Jour. Frank. Inst.*, vol. 253, pp. 585–600; June, 1952.) The necessary and sufficient conditions are deduced for separation of the variables in the Helmholtz and Laplace equations. The wave equation and the damped-wave equation can be reduced to the Helmholtz equation by separation of the time term, and Poisson's equation can be reduced to the Laplace equation by change of variable. Results are tabulated for Euclidean *n*-space and for Euclidean 3-space.

681.142 3483
Modern Computing Machines—G. T. Hunter. (*Jour. Frank. Inst.*, vol. 253, pp. 567–583; June, 1952.) A review of some American digital computers, with particular reference to the I.B.M.-Harvard calculators and their operation. Practical applications are mentioned.

681.142:512.37 3484
A New Construction Principle for Electrical Machines for Determination of the Roots of Algebraic Equations—D. Mitrovic. (*Compt. Rend. Acad. Sci.* (Paris), vol. 234, pp. 2519–2521; June 23, 1952.) Voltages defined by certain relations among the coefficients of the equation are applied in the various branches of a ladder type of network comprising a set of simultaneously variable impedances μ in series and a set of equal fixed-value impedances λ in parallel. By adjusting to obtain zero current in the first mesh of the network, the roots of the equation can be directly determined from the ratio μ/λ.

MEASUREMENTS AND TEST GEAR

531.76:621.318.572 3485
A Dekatron Timer—J. McAuslan and K. J. Brimley. (*Electronic Eng.*, vol. 24, pp. 408–409; September, 1952.) A circuit including a 1-kc crystal-controlled oscillator is used to measure detonator delay times from 25 ms to 12 seconds. The counting is done by four Type-GC10/B dekatrons which display the result in decimal form.

621.3.018.41(083.74):621.396.611.21 3486
High-Frequency Crystal Units for Primary Frequency Standards—Warner. (See 3481.)

621.316.726.078.3:538.569.4.029.64 3487
The Application of Molecular Resonance to Microwave Frequency Stabilization—H. R. L. Lamont and E. M. Hickin. (*Brit. Jour. Appl. Phys.*, vol. 3, pp. 182–188; June, 1952.) A description is given of apparatus for stabilizing an oscillator at wavelengths near 1.25 cm; the method is based on that of Hershberger and Norton (2953 of 1948 and 2140 of 1950), making use of the absorption lines of ammonia. Factors affecting performance are discussed. An N.P.L. test gave a measured stability figure of ± 6 parts in 10^7; it should be possible to improve on this by using a larger waveguide and a lower temperature, and especially by finding substances with sharper absorption lines.

621.317.015.33 3488
Parameters and Operation Constants of Surge Waves with Different Time Characteristics—R. Höfer. (*Elecktrotech. Z. Ed. A.*, vol. 73, pp. 461–462; July 11, 1952.) The different forms of surge waves are discussed and the theoretical relations between their parameters are explained, numerical results being tabulated and shown graphically.

621.317.32.029.64:621.396.611.4:537.52 3489
Methods of Measuring the Properties of Ionized Cases at High Frequencies: Part 2—Measurement of Electric Field—D. J. Rose and S. C. Brown. (*Jour. Appl. Phys.*, vol. 23, pp. 719–722; July, 1952.) Three cavity-resonator methods are described, the field being determined in terms of the power incident on the cavity and the standing-wave pattern on the input line. Two of the methods are applicable to high-*Q* cavities, with simple and complex field configurations respectively, while the third is applicable to low-*Q* cavities. Part 1: 3496.

621.317.329:621.392.26 3490
The Electric Polarizability of Apertures of Arbitrary Shape—S. B. Cohn. (PROC. I.R.E., vol. 40, pp. 1069–1071; September, 1952.) Report of further electrolyte-tank measurements. See also 725 of April.

621.317.335.3 3491
The Effect of Reactance in a $\lambda/4$ Lecher System on Measurements of Dielectric Constant—I. V. Zhilenkov and A. N. Efremov. (*Zh. eksp. teor. Fiz.*, vol. 21, pp. 839–844; July, 1951.) Results are given of an experimental investigation of the effects of the inductance of the capacitor leads, the shunting action of the coupling loop, bending of the leads, etc., on measurements of capacitance and dielectric constant. The advantages of direct immersion of the open end of the system in the dielectric and of the use of a three-plate capacitor are indicated.

621.317.335.3+621.317.374]:621.392.2 3492
The Tuned Coaxial $\lambda/2$ Lecher Line as

Measurement Line for Determination of Loss Angle and Dielectric Constant at Decimetre and Centimetre Wavelengths—E. Löb. (*Arch. elekt. Übertragung*, vol. 6, pp. 288–298; July, 1952.) A method is described for determining dielectric properties from the resonance curve of a coaxial $\lambda/2$ line provided with short-circuiting disks. The loss angle is found in the usual way from the width of the resonance curve at half the maximum height, and the dielectric constant by comparison of the resonance frequencies for the air-filled and the dielectric-filled resonator. The losses occurring in the resonator itself are calculated for different ratios of the diameters of the inner and outer conductors, minimum losses occurring for a ratio of 3.6. Numerical results are given for the losses in a brass resonator of optimum dimensions, for wavelengths of 40 cm and 55 cm.

621.317.335.3.029.64:546.217 3493
An Airborne Microwave Refractometer—C. M. Crain and A. P. Deam. (*Rev. Sci. Instr.*, vol. 23, pp. 149–151; April, 1952.) An account of the adaptation of the equipment previously described [2565 of 1950 (Crain)] to measurements in aircraft. Results are to be published later.

621.317.335.3.029.64:551.578.4 3494
The Dielectric Properties of Ice and Snow at 3.2 Centimeters—W. A. Cumming. (*Jour. Appl. Phys.*, vol. 23, pp. 768–773; July, 1952.) Report of an investigation to establish the relation between the reflection coefficients of snow-covered surfaces and the dielectric properties of ice and snow. Permittivity and loss-tangent measurements were made using waveguide techniques; values of reflection coefficient calculated from these measurements are compared with values found from measurements of the radiation pattern of a slotted-waveguide antenna mounted at a variable height above a snow-covered surface.

621.317.336:621.315.212 3495
Reflections in a Coaxial Cable due to Impedance Irregularities—G. Fuchs. (*Proc. IEE* (London), part IV, vol. 99, pp. 121–136; April, 1952.) Full paper. See 2554 of October.

621.317.337.029.64:621.396.611.4:537.52 3496
Methods of Measuring the Properties of Ionized Gases at High Frequencies: Part 1—Measurement of Q—S. C. Brown and D. J. Rose. (*Jour. Appl. Phys.*, vol. 23, pp. 711–718; July, 1952.) Measurements of the field associated with a gas discharge at microwave frequency commonly involve prior determination of the power absorbed in a resonant cavity. Methods are described for determining the impedance, Q and resonance wavelength of such cavity systems from measurements of the voltage distribution on the line terminated by the cavity; the series losses in the coupling between cavity and transmission line are taken into account.

621.317.35:621.396.61 3497
A Method to Estimate Attenuation of Spurious Emission of Very-High-Frequency Transmitter—H. Uchida. *Sci. Rep. Res. Inst. Tohoku Univ., Ser. B.*, vol. 3, pp. 87–94; September, 1951.)

621.317.35:621.396.615.17 3498
Synthetic Waveforms speed Wave Analysis—A. A. Mahren. (*Electronics*, vol. 25, pp. 132–135; September, 1952.) Description, with circuit details, of a generator for producing particular waveforms by addition of harmonics to a fundamental whose frequency can be varied from 25 cps to 3 kc. Both the amplitudes and phases of the individual harmonics up to the fifth are variable over very wide ranges. Typical synthetic waveforms are reproduced.

621.317.443 3499
Some Developments and Simplifications in Permeameters—A. M. Armour, A. J. King and J. W. Walley. (*Proc. IEE* (London), part IV, vol. 99, pp. 74–82; April, 1952.) Problems of strains in specimens and nonuniformity of field are solved for a precision-type instrument. One of the simplified instruments described uses a rotatable permanent magnet to vary the magnetization of the specimen. The associated magnetometer, covering a range 1–3000 oersted, has a low-permeability moving magnet of silmanal, 3 mm² in volume.

621.317.723 3500
The Vibrating-Condenser-Type Electrometer—S. Hamada, E. Takagi and A. Sato. (*Sci. Rep. Res. Inst. Tohoku Univ., Ser. B*, vol. 3, pp. 233–249; March, 1952.) Description of the instrument used in the Research Institute of Tohoku University. Minimum difference of potential measurable is about 0.1 mv.

621.317.725 3501
A Differential Voltmeter using a Temperature-Limited Diode—V. H. Attree. (*Jour. Sci. Instr.*, vol. 29, pp. 226–229; July, 1952.) A type-29C1 diode forms one arm of a resistance bridge. A center-zero instrument in the anode circuit gives an accurate indication of the supply voltage. A typical instrument has a range 215–245 v and consumes 10 w.

621.317.725 3502
Mean-Square Vacuum-Tube Voltmeter—L. A. Rosenthal and G. M. Badoyannis. (*Electronics*, vol. 25, pp. 128–131; September, 1952.) Description, with full circuit details, of an instrument which uses a nonlinear thyrite element in a rectifier bridge circuit for squaring the input signal. A suitable resistive shunt across the thyrite element results in a square-law characteristic accurate to within ± 2.5 per cent for a current range of 50:1. The upper frequency limit of the meter is 500 kc. A thermostat may be used to reduce the temperature error of the thyrite element.

621.317.725 3503
Valve Voltmeter TVL25—A. V. J. Martin. (*Télévision*, no. 25, pp. 161–168; July/August, 1952.) Constructional details of an inexpensive linear-scale instrument with a range 3 v−1 kv. Probe fittings extend the range to 30 kv and adapt the instrument for measurement of alternating voltages with an upper frequency limit of 250 mc.

621.317.733 3504
The Elimination of Errors due to Stray Capacitances in certain Schering-Bridge Measurements—H. C. Hall. (*Jour. Sci. Instr.*, vol. 29, pp. 224–225; July, 1952.) The simple circuit is modified to include three variable capacitors and a switch connecting the junction of the resistive arms either to earth E or to the high-voltage terminal A. The value of stray capacitance included in the equation for balance with the switch at E is unaltered when measurement is made with the switch at A. A Wagner earth is not required.

621.317.733:621.311.6 3505
Precision Voltage Source—V. H. Attree. (*Wireless Eng.*, vol. 29, pp. 226–230; September, 1952.) A tungsten-lamp nonlinear bridge, run from a mains transformer, provides an ac source for the rapid and accurate checking of amplifier gain. The bridge is switched to dc for calibrating.

621.317.733.011.22 3506
A Note on the Sensitivity of Electrical Bridge Networks—M. Romanowski and A. F. Dunn. (*Canad. Jour. Phys.*, vol. 30, pp. 342–347; July, 1952.) An analytical solution is presented of the problem of determining accurately the value of a resistance when the bridge used for its measurement is very nearly but not quite balanced. Application is made to the use of the Kelvin double bridge for the comparison of precision standard resistors.

621.317.733.011.5 3507
A High-Voltage Schering Bridge for Dielectrics Research—B. Salvage and T. R. Foord. (*Distrib. Elec.*, vol. 25, pp. 160–162; July, 1952.) Description of a doubly screened bridge with automatic compensation of stray capacitance by use of a cathode-follower circuit to maintain the inner screen at the potential of one of the detector terminals, thus avoiding the need for balance by successive approximations, as with the Wagner circuit. An amplifier and moving-coil rectifier instrument are used as detector. A new hv standard capacitor for the bridge, with units of 200, 350 and 700 pf, is described.

621.317.733.029.62 3508
A Bridged-T Impedance Bridge for the V.H.F. Waveband—R. F. Proctor. (*Proc. IEE* (London), part IV, vol. 99, pp. 47–50; April, 1952.) Full paper. See 2557 of October.

621.317.755.029.51/.62 3509
High-Frequency Curve Tracer for 100 kc/s–230 Mc/s—A. Klemt. (*Funk u. Ton*, vol. 6, pp. 357–362; July, 1952.) Description of signal generator and cro equipment for display of the response curves of amplifiers, oscillatory circuits, filters, etc. Ranges of 100 kc–110 mc and 170–230 mc, with frequency marker pips derived from a quartz-crystal oscillator, are provided. A frequency wobble of 0–20 mc can be applied.

621.317.77 3510
A Simple Variable-Frequency Phase-Measuring Device—J. C. West and J. Potts. (*Electronic Eng.*, vol. 24, pp. 402–403; September, 1952.) The phase shift produced by the network under test is compared oscillographically with that produced by a calibrated 4-tube phase-shifting network with a frequency-independent response over the range 100 cps–25 kc. The error in the phase-angle measurement is $<\frac{3}{4}°$.

621.317.794 3511
Accuracy of Bolometric Power Measurements—H. J. Carlin and M. Sucher. (Proc. I.R.E., vol. 40, pp. 1042–1048; September, 1952.) When a bolometer is calibrated at LF, errors of measurements at RF are minimized by using a convectively cooled wire with a large length/diameter ratio. Analysis shows that the error for a Wollaston wire in air is less than that for a corresponding wire mounted in vacuo, and that the advantage of the air-mounted wire increases as the wire length becomes an appreciable fraction of the wavelength. Wollaston-wire bolometers, if properly designed and mounted, can be used to measure cw power over a range of wavelengths down to millimetre waves with an accuracy approaching that of LF measurements.

621.396.615.029.426/.51 3512
A Note on "A Precision Decade Oscillator"—J. A. B. Davidson. (Proc. I.R.E., vol. 40, pp. 1124–1125; September, 1952.) Comment on 2237 of 1951 (Edwards), pointing out that Muirhead & Co. have been producing precision decade oscillators since 1940 with a frequency accuracy within 0.1–0.2 per cent over the range 1 cps–100 kc, four decade dials giving 1-cps steps up to 10 kc and 10-cps steps up to 100 kc. Special features of these oscillators are mentioned. Other types with ranges of 100 cps–40 kc and 0.1 cps–20 kc respectively are also noted.

OTHER APPLICATIONS OF RADIO AND ELECTRONICS

534.321.9:620.179.16 3513
Thickness Gauge—(*Overseas Eng.*, vol. 25, p. 440; July, 1952.) Oscillations from a variable-frequency ultrasonic generator are transmitted into the plate or other structure whose thickness is to be measured, a film of oil or grease being used to give good coupling. When the wave reflected from the back face is in phase with the transmitted wave, a maximum signal is picked up by a probe. The thickness is at

once obtained as the quotient of the speed of sound in the material by twice the fundamental frequency, which is read directly. Accuracy is within about 1 per cent. The complete equipment weighs only 23 lb.

534.321.9:620.179.16:625.8 3514
An Apparatus for Determining the Velocity of an Ultrasonic Pulse in Engineering Materials—E. N. Gatfield. (*Electronic Eng.*, vol. 24, pp. 390–395; September, 1952.) A detailed description of equipment for investigating road materials, particularly concrete. The time of propagation between quartz transducers separated by the thickness of the material is measured and indicated on a cro. The frequency used is 200 kc and the pulse repetition rate 50 per second.

535.336.2.071:621.316.728 3515
Power Supply for a Thermionic Ion Source—C. Reuterswärd. (*Jour. Sci. Instr.*, vol. 29, pp. 184–185; June, 1952.) Stabilized power is supplied to emissive filaments investigated in mass spectroscopy by means of regulated oscillation generators; the laboratory unit described delivers 15 w.

537.228.1:531.768.087 3516
The Reciprocity Calibration of Piezoelectric Accelerometers—M. Harrison, A. O. Sykes and P. G. Marcotte. (*Jour. Acous. Soc. Amer.*, vol. 24, pp. 384–389; July, 1952.) Theoretical and experimental evaluation of an absolute technique for the frequency range 100 cps–10 kc.

621.384.6:621.319.3.027.89 3517
Tested Construction of Electrostatic Generator for Nuclear Research, giving Very High Voltage and using a Dust Stream—M. Morand, A. Raskin and L. Winand. (*Compt. Rend. Acad. Sci.* (Paris), vol. 234, pp. 2450–2452; June 16, 1952.) Discussion of problems in the development of a generator giving a current of the order of 1 ma at over 1 mv. Very finely powdered glass is used for the dust stream. A generator of this type has been in regular use for over five years without giving trouble. For the first description and theory of such generators see 3451 of 1937 (Pauthenier and Moreau-Hanot), 3725 and 4117 of 1939 (Pauthenier).

621.384.622.2 3518
Axial Motion of an Electron in a Constant-Wave-Velocity Section of a Linear Accelerator—D. Caplan and E. Akeley. (*Jour. Appl. Phys.*, vol. 23, pp. 774–778; July, 1952.)

621.385.833 3519
The Derivation of Paraxial Constants of Electron Lenses from an Integral Equation—H. Bremmer. (*Appl. Sci. Res.*, vol. B2, no. 6, pp. 416–428; 1952.)

621.385.833 3520
The Current in the Electron Immersion Objective—L. Jacob. (*Proc. Phys. Soc.* (London), vol. 65, pp. 421–425; June 1, 1952.) Analysis showing that the emission current under conditions of constant cut-off voltage is uniquely defined by the cross-over potential.

621.385.833 3521
The Reliability of Internal Standards for Calibrating Electron Microscopes—J. H. L. Watson and W. L. Grube. (*Jour. Appl. Phys.*, vol. 23, pp. 793–798; July, 1952.)

621.385.833 3522
Specimen Charging in the Electron Microscope and some Observations on the Size of Polystyrene Latex Particles—S. G. Ellis. (*Jour. Appl. Phys.*, vol. 23, pp. 728–732; July, 1952.)

621.385.833 3523
A Method for the Electron and Optical Microscopic Examination of Identical Areas—E. D. Hyam and J. Nutting. (*Brit. Jour. Appl. Phys.*, vol. 3, pp. 173–176; June, 1952.)

621.387.4.087.6 3524
A Printing Recorder for use in Conjunction with Scaling Units—A. R. Lang. (*Jour. Sci. Instr.*, vol. 29, pp. 176–178; June, 1952.) Description of a machine designed for use with an automatic X-ray counter spectrometer. The counts, together with an angle given in degrees and minutes, are recorded on a paper roll 6 inches wide.

621.387.42 3525
The Parallel-Plate Counter as a Self-Quenching Particle-Counting Apparatus—E. Bagge and J. Christiansen. (*Naturwiss.* vol. 39, p. 298; July, 1952.)

621.387.462:549.211 3526
Electrical Counting Properties of Diamonds—F. C. Champion. (*Proc. Phys. Soc.* (London), vol. 65, pp. 465–472; July 1, 1952.) About 25 out of 200 gem-quality diamonds responded to both α- and β-particles. Pulse heights given by 5-mev α-particles were only about three times those for 1-mev β-particles. Results are discussed.

621.387.462:549.211 3527
Electrical Counting Response of Two Large Diamonds under Beta-Irradiation—K. Stratton and F. C. Champion. (*Proc. Phys. Soc.* (London), vol. 65, pp. 473–480; July 1, 1952.) Report and discussion of tests on removal of space charge, variation of counting rate with time, variation of pulse height with applied field, and comparison with a Geiger counter.

621.387.464 3528
Characteristics of Scintillation Counters—G. F. J. Garlick and G. T. Wright. (*Proc. Phys. Soc.* (London), vol. 65, pp. 415–421; June 1, 1952.) Experimental study to determine the factors responsible for the pulse-amplitude distribution in α-particle counters.

771.36.537.228.4.531.557 3529
Electro-optical Shutters for Ballistic Photography—B. J. Ley and P. Greenstein. (*Electronics*, vol. 25, pp. 123–125; September, 1952.) Equipment for operating Kerr-type shutters gives either a single 1-μs pulse or ten identical pulses spaced 25, 50 or 100 μs apart, with amplitudes up to 50 kv.

PROPAGATION OF WAVES

621.396.11 3530
Sweep-Frequency Oblique-Incidence Ionosphere Measurements over a 1150-km Path—P. G. Sulzer and E. E. Ferguson. (Proc. I.R.E., vol. 40, p. 1124; September, 1952.) Preliminary account of results obtained in simultaneous transmission and reception experiments at both Sterling, Virginia, and St. Louis, Missouri, as well as in vertical-incidence virtual-height/frequency recordings at the midpoint of the path. Values of muf determined from the oblique-incidence records are in good agreement with those calculated from midpoint data by the transmission-curve method [3042 of 1939 (Smith)].

621.396.11 3531
On the Propagation of Electric Waves behind a Mountain—Y. Nomura. (*Sci. Rep. Res. Inst. Tohoku Univ., Ser. B*, vol. 3, pp. 115–124; March, 1952.) Formulas for the field strength are derived on the assumption that the mountain can be regarded as a vertical screen (*a*) with upper edge horizontal and inclined at 90° or any other angle to the vertical plane through transmitter and receiver, (*b*) with upper edge not horizontal.

621.396.11+535.222]:535.417 3532
Determination of the Velocity of Short Electromagnetic Waves by Interferometry—K. D. Froome. (*Proc. Roy. Soc. A*, vol. 213, pp. 123–141; June 5, 1952.) A full account of the equipment used and the method of measurement, an outline of which has previously been given (2313 of May).

621.396.11.029.51 3533
The Ionospheric Propagation of Radio Waves with Frequencies near 100 kc/s over Short Distances—K. Weekes and R. D. Stuart. (*Proc. IEE* (London), part IV, vol. 99, pp. 29–37; April, 1952.) Full paper. See 2577 of October.

621.396.11.029.51 3534
The Ionospheric Propagation of Radio Waves with Frequencies near 100 kc/s over Distances up to 1000 km—K. Weekes and R. D. Stuart. (*Proc. IEE* (London), part IV, vol. 99, pp. 38–46; April, 1952.) Full paper. See 2578 of October.

621.396.11.029.55 3535
Investigations of High-Frequency Echoes: Part 3—H. A. Hess. (Proc. I.R.E., vol. 40, pp. 1065–1068; September, 1952.) See 3139 of 1950. Part 2: 3523 of 1949.

621.396.81 3536
Ionospheric-Propagation Predictions for Any Two Points on the Earth's Surface by the "Spanish Method"—R. Gea Sacasa. (*Rev. Telecommunicación*, Madrid, vol. 8, pp. 11–26; June, 1952.) Graphs are given for the month of June and N-S direction of propagation showing the optimum working frequency for any latitude at any time of day for four distances, viz., 400, 1000, 1300 and 2000 km. From these the optimum working frequencies for the E-W direction of propagation and/or for distances >2000 km can be simply determined. Similar curves can be constructed for other months.

621.396.812.029.62 3537
Cross Polarization of Scattered Radio Waves—A. H. LaGrone. (Proc. I.R.E., vol. 40, pp. 1120–1123; September, 1952.) Extension of analysis previously given (1412 of June) to include study of the polarization of the scattered waves. Formulas are derived for the response of dipole antennas oriented horizontally, vertically, or axially relative to a linearly polarized source. Numerical calculations for selected values of the scattering parameters are compared with measurements on 102.9-mc signals, initially horizontally polarized, arriving over a 147-mile path.

621.396.812.5 3538
Analysis of Observed Variations of Absorption of Electromagnetic Waves in the Ionosphere. G. Lange-Hesse. (*Naturwiss.*, vol. 39, pp. 297–298; July, 1952.) Published absorption figures have been analyzed by Bartels' method (883 of 1951). In equatorial latitudes (Singapore) monthly mean values of absorption correlate closely with the relative sunspot number. For temperate latitudes (Slough) such correlation exists only for the summer months. Prediction of monthly mean absorption is possible in principle. The mean variation during the sun's 27-day cycle is far greater than that of the monthly means from month to month. Frequent marked increases of absorption of 2 to 20 hours duration occurring in polar latitudes show correlation with geomagnetic disturbances and are limited to the auroral zone.

RECEPTION

621.396.62+621.397.62]:061.4 3539
19th National Radio Exhibition [London, 1952]: State of Development in Television and Sound Receivers—(*Wireless Eng.*, vol. 29, pp. 275–279; October, 1952.)

621.396.621.54 3540
Approximate Formulae for Alignment of Superheterodyne Receivers—H. W. Paehr. (*Frequenz*, vol. 6, pp. 133–138; May/June, 1952.) Formulas are derived for three-point alignment of circuits with ganged capacitors of the same plate area; their use is illustrated by a worked-out example.

621.396.813:621.396.97 3541
Quality of Broadcasting Transmissions—H. Kösters. (*Tech. Hausmitt. NordwDtsch. Rdfunks*, vol. 4, pp. 127–130; July/August, 1952.) General discussion of problems asso-

ciated with faithful transmission and reproduction, in particular of original sound patterns such as are provided by orchestral music.

621.396.822 3542
On the Evaluation of Noise Samples—A. J. F. Siegert. (*Jour. Appl. Phys.*, vol. 23, pp. 737–742; July, 1952.) Criteria are developed for use in deciding whether a given noise sample can reasonably be assumed to have come from a Gaussian noise with predetermined parameters.

STATIONS AND COMMUNICATION SYSTEMS

621.39.001.11 3543
Channel Capacity and Transmission Time—K. Küpfmüller. (*Arch. elekt. Übertragung*, vol. 6, pp. 265–268; July, 1952.) The capacity of a transmission channel depends in general on the channel transmission time. Only in the case of transmission times greater than a certain value can the limiting value of channel capacity given by Shannon's formula be approximately reached. This minimum transmission time is about equal to twenty times the reciprocal of the bandwidth. A formula is derived for the channel capacity corresponding to a given finite transmission time.

621.39.001.11 3544
Information Theory—"Cathode Ray." (*Wireless World*, vol. 58, pp. 365–370; September, 1952.) An outline of the subject in simple terms, indicating its significance and application.

621.39.001.11:621.39.7.5 3545
Quantized Signals in Communications Technique—F. Schröter. (*Bull. schweis. elektrotech. Ver.*, vol. 43, pp. 497–508; June 14, 1952. In German.) Practical means for using the equivalence of bandwidth and the logarithm of the signal/noise ratio in the Hartley-Shannon theory are discussed, and the principles of quantization for the reduction of bandwidth are illustrated. A "double-amplitude" system giving a further reduction of bandwidth is proposed. This is a form of binary coding of the quantized signal so that the final pulse amplitude represents $kx+y$, where k is a constant defined by the number of quantum stages, and x, y are the partial amplitudes of the quantized signal. Examples of quantization processes discussed include the coding of text and of color television. See also *Telefunken Ztg*, vol. 25, pp. 115–127; June, 1952.)

621.394.14 3546
A Method for the Construction of Minimum-Redundancy Codes—D. A. Huffman. (Proc. I.R.E., vol. 40, pp. 1098–1101; September, 1952.)

621.394.14:621.392.5 3547
Coding with Linear Systems—J. P. Costas. (Proc. I.R.E., vol. 40, pp. 1101–1103; September, 1952.)

621.394.441:621.396.619.13 3548
Two New Voice-Frequency Telegraphy Systems—H. Gardère. (*Câbles & Trans.* (Paris), vol. 6, pp. 243–264; July, 1952.) A system using phm has been described previously (1100 of May). A similar account is here given of a FM system. A subsequent paper will give results of a comparison of the two systems.

621.395.44:622 3549
"Montavox," Equipment for High-Frequency Telephony in Mining—H. Ukrow. (*Telefunken Ztg*, vol. 25, pp. 98–104; June, 1952.) Description of a transmitter-receiver housed, together with its efficient Ag-Zn alkaline accumulator, in a cylindrical watertight container which can be carried in one hand. Communication is effected by coupling with a flexible loop to any continuous metal system such as compressed-air pipes, tramway lines or lighting cables. Operating frequency is about 200 kc, power 0.1–0.2 w. The locally generated oscillation of the 5-tube heterodyne receiver serves, after frequency transformation, to control the power stage of the transmitter. A signal lamp, whose switch is operated by a magnetic device in the receiver, indicates when the carrier of the "called" station is being received. Ranges up to 1000 m are practicable.

621.396:061.3 3550
The Extraordinary Administrative Radio Conference, Geneva, 1951—C. F. B. (*P.O. Elec. Eng. Jour.*, vol. 45, pp. 85–86; July, 1952.) A brief outline of the main provisions of the agreement reached at the conference, 15th August—3rd December 1951. See also 2599 of October (Pressler).

621.396.4:621.396.619.13 3551
Theoretical Performance of Simple Multichannel Systems using Frequency Modulation—E. G. Hamer. (*Jour. Brit. IRE*, vol. 12, pp. 411–415; July, 1952.) Frequency-sharing and time-sharing systems using small numbers of channels are considered, formulas commonly used for systems with large numbers of channels being adapted. The same basic assumptions are made regarding signal bandwidth and noise as those made by Feldman and Bennett (454 of 1950). Advantages obtainable with the frequency-sharing system due to nonsimultaneous loading, and with the time-sharing system by use of companding, are discussed and illustrated by practical examples.

621.396.41 3552
Fundamental Aspects of Linear Multiplexing—L. A. Zadeh and K. S. Miller. (Proc. I.R.E., vol. 40, pp. 1091–1097; September, 1952.) In a linear multiplex system the channel separation is achieved by the use of linear time-variant or time-invariant filters. The sets of signals associated with the different channels are linear and disjoint, and the signals belonging to such sets can be transmitted simultaneously and separated at the receiving end by means of linear, generally time-variant, filters. Frequency-band compression cannot be effected with linear systems. Analysis of the filtering process is based on resolution of signals into a set of complex exponential component signals. Methods of synthesis of linear multiplex systems are indicated for types other than those using frequency or time division. See also 3028 of December (Zadeh).

621.396.5:621.396.932 3553
Portable Radiotelephony Equipment for Communication between Ship and Port—W. A. Krause. (*Frequenz*, vol. 6, pp. 146–149; May/June, 1952.) Port facilities such as those for Liverpool, where a single radar station suffices, are quite unsuitable for the long approach up the Elbe to Hamburg, where there are five radar stations with overlapping ranges and a similarly distributed set of hf telephony stations. Illustrations are given of portable send-receive equipment as used at Liverpool and Sunderland, and of several German types, one of which weighs only 3.1 kg. All operate in the range 156–174 mc.

621.396.619.13:517.564.3 3554
Spectrum of a Frequency-Modulated Wave—W. C. Vaughan. (*Wireless Eng.*, vol. 29, p. 254; September, 1952.) Corrections to paper noted in 2892 of November.

621.396.619.16:621.396.4 3555
Nonsynchronous Time Division with Holding and with Random Sampling—J. R. Pierce and A. L. Hopper. (Proc. I.R.E., vol. 40, pp. 1079–1088; September, 1952.) A detailed description of the system, of which a shorter account has been given by Hopper (3231 of December).

621.396.619.16:621.396.41:621.396.822.1 3556
Crosstalk in Time-Division-Multiplex Communication Systems using Pulse-Position and Pulse-Length Modulation—J. E. Flood. (*Proc. IEE* (London), Part IV, vol. 99, pp. 64–73; April, 1952.) Full paper. See 2606 of October.

621.396.712:623.98 3557
Project "Vagabond"—J. W. Seymour. (*Electronics*, vol. 25, pp. 120–122; September, 1952.) Description of some of the equipment installed in the U. S. Coast Guard cutter *Courier* for relaying Voice-of-America programs. One 150-kw transmitter operates anywhere in the range 540–1600 kc and there are also two 35-kw sw transmitters.

621.396.932/.933].1+621.396.97 3558
Common-Wave Broadcasting and Hyperbolic Navigation: Part 2—Pohontsch. (See 3437.)

621.396.97:621.396.8 3559
Quality in Broadcasting, and Compressor-Expandor Systems—A. Warnier. (*Onde élect.*, vol. 32, pp. 261–274; July, 1952.) A survey of the performance achieved in broadcasting as regards musical quality indicates that in the reception, e.g., of orchestral music, the results obtained are definitely inferior, even with a high-fidelity receiver, to those obtained from modern gramophones. Improvement is practicable by the use of compressor-expander systems, the characteristics of which are discussed. Equipment is described which has given results comparable with studio quality.

621.396.97.029.62+621.397.61.029.62]:061.3 3560
The European Broadcasting Conference [C.E.R.], Stockholm, 1952—W. Stepp. (*Tech. Hausmitt. NordwDtsch. Rdfunks*, vol. 4, pp. 144–145; July/August, 1952.) An outline of the proceedings, with analysis of the standards adopted for usw broadcasting and television. For a fuller account, in Danish, see *Teleteknik, Copenhagen*, vol. 3, pp. 149–155; August, 1952.

SUBSIDIARY APPARATUS

621-52:621.316.728 3561
A Device for the Automatic Control of Electrical Power up to 2 kW—W. T. Bane and J. S. Appleby. (*Jour. Sci. Instr.*, vol. 29, pp. 174–176; June, 1952.) Description of a closed-loop control system in which a voltage proportional to the consumed power is continuously compared with a voltage representing the desired power consumption. Control to within $\pm\frac{1}{4}$ per cent has been achieved.

621.311.62 3562
Variable-H.T. Power Pack—A. H. B. Walker. (*Wireless World*, vol. 58, pp. 374–376; September, 1952.) Details are given of an easily constructed unit providing continuously variable output up to about 400 v. The rectifier circuit comprises two triodes with a center-tap cathode-follower connection. The control voltage applied to the grids is derived from one half of the center-tapped mains-transformer secondary via a miniature metal rectifier.

621.311.62:621.316.722.1 3563
New Constant-Voltage Source of High Control Accuracy—E. Helmes. (*Elektrotech. Z., Ed. A*, vol. 73, p. 458; July 11, 1952.) Description of equipment for supplying heater currents at voltages from 2.5 to 6 v, constant to within ± 0.1 per cent. Variation of output voltage produces a deflection in a mirror galvanometer controlling the illumination of a photocell, which, in turn, governs a tube anode current feeding the primary of the output transformer.

621.313.323.029.3 3564
The Theory of the Operation of a Phonic Motor—D. E. Caro. (*Proc. IEE* (London), part IV, vol. 99, pp. 51–63; April, 1952.) "A mathematical analysis of the operation of a phonic motor is presented. Expressions are developed for the motor currents and voltages, power output, efficiency, etc. Both polarized and unpolarized motors are treated, and operation from high- and low-impedance sources is considered. A method for obtaining the motor constants experimentally is given and the predicted power output is compared with experimental results. Power ripple and motor

hunting are both analyzed. The possibility of multi-phase motors is discussed and some applications of phonic motors are described."

621.314.63 3565
Special Rectifier Circuits—D. B. Corbyn. (*Electronic Eng.*, vol. 24, pp. 418–419; September, 1952.) Some new hv circuits with improved regulation are described, and "center-tapped" circuits are discussed briefly.

621.314.63 3566
The High-Frequency Properties of the Boundary-Layer Rectifier—W. Schottky. (*Z. Phys.*, vol. 132, pp. 261–284; June 23, 1952.) In dry rectifiers with specific impurity-center semiconductivity, delay in achieving an equilibrium condition can only affect the impedance characteristic if the impurity centers remain largely undissociated. This is the condition for a reserve boundary layer to be formed. The total boundary layer capacitance for small ac loads decreases with increasing frequency to a value many times smaller and finally corresponding to the thickness of the reserve layer. The "kinetic" frequency ω_{kin} characterizing the transition from conductive to capacitive action is given by the product of the recombination coefficient α and the electron density. Since the dielectric relaxation frequency ω_{rel} can be represented as the product of the electron density and a constant factor dependent on mobility μ and permittivity ϵ, the ratio $\omega_{kin}:\omega_{rel}$ is determined completely in terms of α, μ and ϵ, and is apparently in every case $\ll 1$. The capacitive shunt appearing across the reserve layer as frequency increases, is due to lack of the necessary rapid transfer of charge by the impurity centers. Values of α of about 5×10^{-10} cm^3 sec^{-1} obtained from impedance measurements on Cu_2O rectifiers support the theory. This is extended by considering a two-stage recombination process. The effect of reaction inertia on the rectification process is discussed. The effective increase of boundary-layer thickness at high frequencies can greatly improve the performance of a rectifier with a poor static characteristic.

621.314.63:546.824-3 3567
Titanium-Dioxide Rectifiers—(*Electronics*, vol. 25, pp. 164, 166; September, 1952.) Short note on rectifiers, developed at the National Bureau of Standards, consisting of a layer of semiconducting TiO_2 on a sheet of Ti, with a counter electrode of some other conducting material such as Ag. The most satisfactory oxide films are formed by heating Ti plates in steam at 600°C for about three hours. The counter electrodes are then applied by electroplating. The easy-flow direction is opposite to that for Cu_2O rectifiers. The TiO_2 rectifiers withstand reverse voltages of about 20 v per plate.

621.314.634.015.5 3568
Breakdown in Selenium Rectifiers—R. Cooper. (*Proc. Phys. Soc.* (London), vol. 65, pp. 409–414; June 1, 1952.) Experiments show that breakdown may occur at higher reverse voltages as the ambient temperature is raised, and as the thermal-dissipation constant is lowered. At voltages near to and beyond the knee of the current voltage characteristic the temperature coefficient of the rectifier is negative, i.e., rise in temperature causes the leakage current to decrease. Results do not support the thermal-instability theory of breakdown.

621.314.653:621.311.62:621.396.712 3569
Use of Thyratron Rectifiers in Broadcasting Transmitters—C. Wait. (*Rev. tech. Comp. franç. Thomson-Houston*, no. 17, pp. 33–40; July, 1952.) The characteristics and mode of operation of thyratron rectifiers are described, with illustrations of the waveforms of the cathode and anode voltages for various 3-phase arrangements. An outline scheme is shown for a complete rectifier unit for the medium and high voltages required for a broadcasting transmitter.

621.316.722:621.396.645.029.3 3570
Supply Problems at Low Frequency—L. Chrétien. (*TSF et TV*, vol. 28, pp. 223–227; July/August, 1952.) Discussion of methods of stabilizing the anode voltage of an af amplifier, with details of a practical circuit.

621.355.5 3571
Reversible Cell with Electrolyte a Thin Crystal Layer deposited by Evaporation—A. Sator. (*Compt. Rend. Acad. Sci.* (Paris), vol. 234, pp. 2283–2285; June 4, 1952.) Layers of Ag, $PbCl_2$ and Ag are deposited successively on a glass support. Repeated charging (at 0.5 μA) and discharging results in the reversible cell $+Ag/AgCl/PbCl_2/Pb/Ag$ with a terminal voltage of 0.44 v, which only drops to 0.41 v after 90 minutes discharge at about 1 μA.

TELEVISION AND PHOTOTELEGRAPHY

621.397.24/.26 3572
Paris-London Television—T. H. Bridgewater. (*Electronic Eng.*, vol. 24, pp. 410–412; September, 1952.) Discussion of problems encountered by the B.B.C. in connection with the cross-channel relay of July 1952. See also 2902 of November.

621.397.3 3573
Build-Up Curve and Bandwidth Utilization in Television—E. Schwartz. (*Frequenz*, vol. 6, pp. 138–141; May/June, 1952.) The relations between the steepness of the build-up curve, overshoot, Kell factor [3942 of 1940 (Kell et al.) and 2639 of 1950], and width of scanning aperture are discussed. Curves given show that the build-up curve is steepest for unity Kell factor, and that overshoot is greatest for a factor of 0.5 and practically vanishes for a factor of 2.0. Optimum bandwidth represents a compromise between the effects of the various factors involved. The method described by Goldmark and Hollywood (828 of April) for increasing the steepness of the build-up curve by a factor of 2 is noted.

621.397.5:621.39.001.11 3574
Quantized Signals in Communications Technique—Schröter. (See 3545.)

621.397.5(485) 3575
Television in Sweden—F. Bernard. (*Télévis. franç.*, nos. 84/85, p. 36; July/August, 1952.) Note of transmission equipment operating experimentally in Stockholm. A public service is to start in 1953.

621.397.61 3576
C.S.F. Television Transmitters—J. Polonsky, L. Amster and G. Melchior. (*Ann. Radioélect.*, vol. 7, pp. 151–165; April, 1952.) The units described are designed for service in France or abroad. Their frequency ranges are 41–85 mc and 174–216 mc. Powers of 5 and 20 kw are obtained by adding extra units to the 3-bay 500-w transmitter. The hf amplifier chain and synchronization system are described. The antenna coupling circuits include a band-suppression filter, a dummy antenna in the form of a lossy coaxial line, and diplexing equipment for feeding both vision and sound signals to one antenna. The functions of a maintenance bay are illustrated by diagrams of the signal-generator output waveforms suitable for checking and monitoring the transmitter performance.

621.396.62+621.397.62]:061.4 3577
19th National Radio Exhibition [London, 1952]: State of Development in Television and Sound Receivers—(*Wireless Eng.*, vol. 29, pp. 275–279; October, 1952.)

621.397.62:535.514 3578
Surfaces with Multiple Planes of Polarization Application to Television—P. Toulon. (*Compt. Rend. Acad. Sci.* (Paris), vol. 234, pp. 2591–2592; June 30, 1952.) A study has been made of synthetically produced rectangular plates of optically polarizing material in which the plane of polarization varies as a periodic function of distance parallel to one edge of the plate. The distance between successive lines corresponding to the same plane of polarization is a characteristic parameter, termed the pitch. Various optical effects can be obtained by combinations of such plates. They have been applied successfully in the manufacture of variable-color screens for color television reception.

621.397.62:621.396.677.1 3579
The Detection of Television Receivers—W. J. Bray. (*P.O. Elec. Eng. Jour.*, vol. 45, part 2, pp. 49–51; July, 1952.) Description of equipment fitted in a van and suitable for detecting and locating television receivers that are being operated. Three horizontal loop antennas mounted on the roof of the van pick up energy radiated from the line-scanning coils of a receiver, and switching arrangements for intercomparison of the signal strengths from the three loops enable the receiver to be located, the discrimination being sufficient to distinguish between receivers in adjacent houses on the same side of a road.

621.397.621.2 3580
Line-Scan Circuit with Economy Transformer—R. Andrieu. (*Telefunken Ztg.*, vol. 25, pp. 107–114; June, 1952.) Simplifying assumptions enable the relations between the most important parameters of this circuit to be determined and design data to be derived.

621.397.621.2 3581
Low-Power Deflection for Wide-Angle C.R. Tubes—C. V. Bocciarelli. (*Electronics*, vol. 25, pp. 109–111; September, 1952.) The use of a narrow-neck tube with a specially shaped deflection yoke enables tubes to be produced with deflection angles up to 90° and with a considerable increase of the ratio of face diameter to tube length.

621.397.645.37 3582
New Amplifier Techniques—V. J. Cooper. (*Jour. Brit. IRE*, vol. 12, pp. 371–391; July, 1952.) Three types of television amplifier are discussed, viz., the cathode repeater (2168 of 1950), the shunt-regulated amplifier (2562 of 1951) and the feedback amplifier with desired frequency response characteristics (642 of April). Practical circuits and experimental results are given in each case.

621.397.8 3583
Various Factors affecting the Quality of Television Pictures—R. Monnot. (*Radio franç.*, no. 6, pp. 1–15; June, 1952.) Discussion of factors affecting picture detail, contrast, distortion, stability, etc., including scanning methods, number of lines, camera optics, transmission bandwidth, transient response of video amplifier, cr tube deflection system, projection methods, ambient light, and the characteristics of the different elements of the television chain. The interconnection between technical and economic aspects of television is indicated.

621.397.812 3584
The Effect of Atmospheric Variations on Picture Quality—P. Lemeunier. (*Télévis. franç.*, nos. 84/85, p. 31; July/August, 1952.) A diagram based on 3 years' observations correlates in general terms the quality of television reception with local weather conditions.

621.397.828 3585
Noise Limiters for Television Sound—R. T. Lovelock. (*Wireless World*, vol. 58, pp. 339–342; September, 1952.) In the series peak limiter for suppression of pulsed RF interference, shunt capacitance must be low to obtain good frequency discrimination. For the shunt limiter, a very low forward impedance is essential. A combination of these circuits is described which uses Ge diodes Type GEX34 and GEX03 in the series and shunt circuits respectively; the harmonic distortion introduced is negligible.

TRANSMISSION

621.396.61:621.317.35 3586
A Method to Estimate Attenuation of Spurious Emission of Very-High Frequency Transmitter—H. Uchida. (*Sci. Rep. Res. Inst. Tohoku Univ., Ser. B*, vol. 3, pp. 87–94; September, 1951.)

621.396.61:621.396.712 3587
The Latest C.F.T.H. Developments in Broadcasting Transmitters—M. Guérineau. (*Rev. tech. Comp. franç., Thomson-Houston*, no. 17, pp. 9–26; July, 1952.) Illustrated descriptions, with diagrams showing circuit arrangements, of 100/150-kw and 5/10-kw medium-wave transmitters and a 50-kw sw transmitter.

621.396.61.029.53 3588
A New 150-kW Medium-Wave Broadcasting Transmitter—H. Campet and S. Odartchenko. (*Ann. Radioélect.*, vol. 7, pp. 139–150; April, 1952.) The first transmitter of a new type constructed by the Société Française Radioélectrique was put into service in Luxembourg in 1951. The circuit and lay-out of equipment are shown. Features described include the over-all-feedback system, high-power triodes with ac filament heating for the modulation amplifier, and Hg-vapor rectifiers which are liquid-cathode tetrodes. Performance figures are given.

621.396.619.23 3589
Bases of Application and Calculation of Frequency-Modulation Pulse Trains—D. Bünemann and H. Pethke. (*Fernmeldetech. Z.*, vol. 5, pp. 226–231; May, 1952.) The principles and operation of the serrasoid modulator [342 of 1949 (Day)], and of a pulse-counting discriminator system being developed for FM monitoring are described. A formula is derived for direct calculation of the lf and hf spectra of a series of FM pulses. See also 3267 of December (Gundlach).

621.396.645.371:621.396.61:621.396.712 3590
C.F.T.H. Applications in Negative Feedback—A. Warnier. (*Rev. tech. Comp. franç., Thomson-Houston*, no. 17, pp. 53–60; July, 1952.) Brief discussion of the use of negative feedback for reducing distortion and background noise, and description of a two-path negative-feedback system which has been applied in broadcasting transmitters with excellent results.

TUBES AND THERMIONICS

537.525.92 3591
Some Considerations on the Space-Charge Equation—M. Matsudaira, M. Wada and T. Koda. (*Sci. Rep. Res. Inst. Tohoku Univ., Ser. B*, vol. 3, pp. 215–231; March, 1952.) The limit of application of the three-halves power law is considered and a solution of the space-charge equation is obtained which expresses the characteristics of a tube with an oxide cathode and close electrode spacing.

621.314.632:621.396.822 3592
The Theory of Noise in the Crystal Rectifier—Y. Watanabe and N. Honda. (*Sci. Rep. Res. Inst. Tohoku Univ., Ser. B*, vol. 3, pp. 39–46; September, 1951.) The noise-producing effect of impurities in Si and Ge rectifiers is considered. Fluctuations in the concentration of surface-state electrons affect the height of the potential barrier and produce noise. Calculations based on Richardson's diffusion model (1391 of 1950) give results in good agreement with those obtained experimentally by Miller (2567 of 1947). See also 870 of April.

621.383.2:621.396.822 3593
Measurement of Fluctuations in a Photomultiplier—F. Lenouvel. (*Compt. Rend. Acad. Sci.* (Paris), vol. 234, pp. 2594–2596; June 30, 1952.) The output current of a 19-stage multiplier is measured directly by means of a galvanometer. An optical system comprising lamp, galvanometer mirror and photocell detector in conjunction with appropriately masked lenses is used to record either the mean value of the multiplier output current or the mean square of the fluctuations. Results are tabulated together with values calculated from theory.

621.383.27 3594
Photoelectric Characteristic in the Ultraviolet down to 1500 Å of an Electron Multiplier using a Copper/Beryllium Alloy—V. Schwetzoff, S. Robin and B. Vodar. (*Jour. Phys. Radium*, vol. 13, pp. 369–370; June, 1952.) Measurements on a 12-stage multiplier sealed into a pyrex tube with a quartz window are reported. The photoelectric threshold is at about 4 ev (3000 Å), and the photoelectric efficiency is 6 to 8 times less than that of Ag-O-Cs electrodes over the range 1608–2000 Å. The advantage of this alloy is its stability on exposure to the atmosphere.

621.383.4:546.817.221 3595
Impedance Measurements on PbS Photoconductive Cells—E. S. Rittner and F. Grace. (*Phys. Rev.*, vol. 86, pp. 955–958; June 15, 1952.) Analysis of existing and new impedance measurements indicates that the observed decrease in parallel resistance with frequency is attributable to a known effect of distributed capacitance.

621.383.4:546.817.221 3596
Industrial Applications of Semiconductors: Part 4—Lead Sulphide Photocells—C. J. Milner and B. N. Watts. (*Research* (London), vol. 5, pp. 267–273; June, 1952.) Discussion of the mechanism of photoconductivity, the production and properties of PbS photocells, and their various applications.

621.385.029.6:621.396.822 3597
Calculation of the Noise Figure of the Travelling-Wave Valve: Part 2—W. Kleen. (*Arch. elekt. Übertragung*, vol. 6, pp. 299–303; July, 1952.) Methods of investigation similar to those described in part 1 (3276 of December) are applied to tubes in which the electron beam is subjected to potential jumps at points between field-free sections. With suitable choice of the lengths of these sections, an improvement of the noise figure can be obtained compared with that for the beam system considered in part 1. The effect of various parameters on the noise figure of the traveling-wave tube with helical delay line and different beam-generator systems is discussed.

621.385.029.64:168.2 3598
A Symbolism for Microwave-Valve Classification—G. M. Clarke. (*Proc. IEE* (London), part IV, vol. 99, pp. 24–28; April, 1952.) Full paper. See 2658 of October.

621.385.032.216 3599
Characteristic Shifts in Oxide-Cathode Tubes—W. P. Bartley and J. E. White. (*Elec. Eng.* (N. Y.), vol. 71, p. 496; June, 1952.) Summary of A.I.E.E. Winter General Meeting paper, January 1952. Investigations have shown that an oxide-cathode tube operating in the space-charge-limited condition may have its transconductance changed with time as a result of change of one or more of the following factors: interface impedance, contact pd, coating resistance, and peak emission. In the Type-6SN7GT tubes studied, the only significant effects over a considerable period were resistive and contact-pd shifts, the most important component of resistance, in active base-metal cathodes, being the interface compound between the oxide coating and the base metal. Such interface resistances did not develop in passive-cathode tubes in 3000 hours under normal operating conditions, but the resistance of the coating itself changed enough to affect the transconductance.

621.385.032.216 3600
Thermionic Emitters under Pulsed Operation—R. Loosjes, H. J. Vink and C. G. J. Jansen. (*Philips Tech. Rev.*, vol. 13, pp. 337–345; June, 1952.) See 2380 of September (Loosjes and Jansen) and back references.

621.385.032.216.2:539.16 3601
The Use of Radioactive Isotopes in a Study of Evaporation from Thermionic Cathodes—W. F. Leverton and W. G. Shepherd. (*Jour. Appl. Phys.*, vol. 23, pp. 787–793; July, 1952.) Radioactive Ba_{140}, Sr_{89} and Ca_{45} were incorporated in the coatings of mixed-carbonate cathodes on Ni bases. The cathodes were mounted in diodes having a removable electrode between cathode and anode to permit separate measurement of material evaporated during processing and during operation. The rates of transfer found for all three elements can be expressed as a function of absolute temperature by a single formula with appropriate constants. The effect on the rate of transfer of bombarding the anode by electrons was investigated.

621.385.15 3602
Research on Electron Multiplication and its Applications: Part 2—D. Charles. (*Ann. Radioélect.*, vol. 7, pp. 115–138; April, 1952.) The construction of a simple form of cylindrical-diode multiplier and techniques for forming secondary-emission layers of Cs, K and Ba are described. Emission characteristics of different layers at various voltages and frequencies are shown graphically. Theory developed is supported by experimental results. Part 1: 2368 of September.

621.385.15 3603
Secondary-Emission Valves—M. Hirashima. (*Wireless Eng.*, vol. 29, pp. 246–252; September, 1952.) The response of tubes using MgO-coated secondary emitters is investigated. Potentials of 10–100 v are built up on the surface of these emitters; as a result, single pulses or pulses at low repetition rate are distorted much more than pulses at a high repetition rate. The general trend of the waveform distortion is illustrated graphically by means of semiquantitative analysis of the experimental data obtained by Kawamura (*Proc. Phys. math. Soc. Japan*, vol. 24, p. 211; 1942.)

621.385.2:546.289:538.63 3604
Germanium Phenomenon—A. B. Kaufman. (*Radio & Telev. News, Radio-Electronic Eng. Section*, vol. 48, pp. 10, 29; July, 1952.) Experiments indicate that the forward resistance of a Ge diode increases appreciably when the diode is subjected to a strong magnetic field; an increase of about 0.5 per cent was noted for a field strength of 2800 gauss. Si diodes did not show this effect.

621.385.2.011.21 3605
The Admittance of a Diode with a Retarding Field—J. J. Freeman. (*Jour. Appl. Phys.*, vol. 23, pp. 743–745; July, 1952.) The contribution of space charge to the diode admittance is found by evaluating the current induced in an external circuit. The susceptance is capacitive at low frequencies and inductive at high frequencies. The expression for the conductance is the same as that derived by Begovich (2959 of 1949).

621.385.2/.3:621.396.615.141.2 3606
Magnetron Effect in High-Power Valves—A. M. Hardie. (*Wireless Eng.*, vol. 29, pp. 232–245; September, 1952.) The resultant magnetic field in the neighborhood of a squirrel-cage filament structure is calculated and the results are used to investigate theoretically the magnetron effect in tubes with this type of filament. The theoretical treatment is restricted to the condition when anode and grid are strapped, since the problem becomes intractable for the case of a triode with anode and grid at different potentials. Experiments on two diode-connected tubes gave results supporting the approximate theory. A tube with normal triode connections was also investigated

experimentally, using a pulse method; a qualitative explanation is given of the observed results.

621.385.3 3607

The Amplification Factor of a Triode: Part 2—A Cylindrical Triode having a Cage Grid with Arbitrary Electrode Dimensions—M. Wada. (*Sci. Rep. Res. Inst. Tohoku Univ., Ser. B*, vol. 3, pp. 19–38; September, 1951.) The analysis developed in part 1 (552 of March) for uhf planar triodes is extended to cover cylindrical arrangements of the type described by Rose et al. (501 of 1950). Results are compared with formulas derived by other workers.

621.385.3:621.318.572 3608

The Initial Conduction Interval in High Speed Thyratrons—J. B. Woodford, Jr. and E. M. Williams. (*Jour. Appl. Phys.*, vol. 23, pp. 722–724; July, 1952.)

621.385.3.012 3609

Calculations of Families of Characteristics for a Planar Triode with Negatively Biased Control Grid of Parallel Round Wires of Finite Thickness and Spacing—W. Dahlke. (*Telefunken Ztg*, vol. 25, pp. 83–92; June, 1952.) The known distribution function for the cathode-current density of a planar triode is applied to the evaluation of various tube parameters as dependent on operating voltages and physical dimensions. Results are shown graphically.

621.385.3.026.445 3610

A Coaxial Power Triode for 50-kw output up to 110 Mc/s—R. H. Rhéaume. (PROC. I.R.E., vol. 40, pp. 1033–1037; September, 1952.) Description of the construction and special features of the Type-ML5681 tube, which has a thoriated cathode, a reentrant anode with integral water-cooling jacket, and coaxial ring-seal terminals. The bandwidth is suitable for television broadcasting.

621.385.4 3611

Study on the Characteristics of a Beam Power Output Tube: Part 1—The Volt/Ampere Characteristics—M. Wada. (*Sci. Rep. Res. Inst. Tohoku Univ., Ser. B*, vol. 3, pp. 135–150; March, 1952.) Analysis for the case of plane parallel electrodes. The formulas derived give results in good agreement with measurements on Type-807 tubes.

621.385.4 3612

Effect of Electron Transit-Time on the Efficiency of Transmitting Tetrodes—H. Rothe and E. Gundert. (*Telefunken Ztg*, vol. 25, pp. 75–82; June, 1952.) The hf output of both triodes and tetrodes decreases with increasing frequency. This decrease is partly due to the finite transit time of the electrons between cathode and control grid, and between control grid and anode in triodes or between screen grid and anode in tetrodes. A quantitative analysis of transit-time effects in the space adjacent to the anode is presented and their contribution to power decrease is discussed. Under different operating conditions the calculated efficiency of tetrodes decreases almost linearly to about zero for a screen-grid/anode transit-time angle of 360°, but in practice the zero value is reached for much smaller angles, about 52° for Type-RS682 tubes and about 60° for Type-4X150A tubes. Effects of large and of small signal amplitudes on the efficiency are discussed.

621.385.832 3613

Ion Burn in Cathode-Ray Tubes: Metallized Screens and Ion Traps—R. Roulaud. (*Rev. gén. Élect.*, vol. 61, pp. 263–270; June, 1952.) The causes of ion burn are discussed and various methods adopted for eliminating this troublesome effect are described.

621.385.832:621.318.572 3614

A Decade Counter Valve for High Counting Rates—J. L. H. Jonker, A. J. W. M. van Overbeek and P. H. de Beurs. (*Philips Res. Rep.*, vol. 7, pp. 81–111; April, 1952.) A tube is described of the type having a ribbon beam deflected in one dimension to pass through a slotted screen over a target, ten discrete fixed positions of the beam being provided by means of feedback from the target to the deflection electrode. In each fixed position a part of the beam impinges on a fluorescent region of the wall, giving a visible numerical indication of its position. The beam is moved on by application of pulses to the deflection electrode. A detailed analysis is made of the flyback process. Time intervals <0.2 μs can be resolved by use of appropriate tubes in circuit with the counter tube.

621.396.615.14 3615

Properties of Lines with Periodic Structure—P. Guénard, O. Doehler and R. Warnecke. (*Compt. Rend. Acad. Sci.* (Paris), vol. 235, pp. 32–34; July 7, 1952.) The frequency dependence of the wave-transmission properties is studied. The expression for the field is written in a form corresponding to the superposition of progressive waves whose phase velocities form a series; these waves are designated as forward or backward according as the phase velocity has or has not the same sense as the energy velocity. For investigating the interaction between the wave field and an electron beam, it is convenient to consider the variation of the "retardation factor" (ratio of free-space velocity to phase velocity along line) with wavelength; this function is plotted and discussed in relation to the dispersion of the forward and backward waves.

621.396.615.14 3616

New U.H.F. Oscillator Valves with Wide Electronic Tuning Band—P. Guénard, O. Doehler, B. Epsztein and R. Warnecke. (*Compt. Acad. Sci.* (Paris), vol. 235, pp. 236–238; July 21, 1952.) An account of the basic principles of tubes depending on the interaction between an electron beam and a transmission line consisting of elements with periodic spatial distribution (3615 above). When the beam velocity is equal to the phase velocity of a forward wave along the line, additive effects are obtained in the direction of the beam and the arrangement can be used as an amplifier. When, however, the beam velocity is equal to the phase velocity of a backward wave, the additive effect is obtained in the backward direction and the amplitude of the field transported by the line increases towards the origin of the beam, so that oscillations can be produced, the frequency being dependent on the velocity of the beam and the dispersion curve of the line.

621.396.615.14 3617

Reflex Resnatron shows Promise for U.H.F. TV—G. E. Sheppard, M. Garbuny and J. R. Hansen. (*Electronics*, vol. 25, pp. 116–119; September, 1952.) In the reflex resnatron the negative repeller electrode reflects the electron beam back through the output cavity to the accelerator electrode. Wide-band modulation is effected with low power by varying the repeller voltage. Some details are given of the construction of an experimental tube capable of an output of 2.5 kw at 560 mc, with a bandwidth of 8 mc, power gain of ~5, and over-all efficiency of 38 per cent, the repeller voltage being 6.5 kv negative with respect to the accelerator voltage of 8 kv.

621.396.615.14 3618

Some Limitations on the Maximum Frequency of Coherent Oscillations—R. S. Elliott. (*Jour. Appl. Phys.*, vol. 23, pp. 812–818; August, 1952.) Electron-beam oscillator tubes are classified in two groups depending on whether or not they use resonant energy extractors; for those which do it is proved that a natural upper frequency limit exists. The limit is determined chiefly by the ac beam current density and the noise level in the resonant structure. For practical values of these parameters the limit is below the frequency of light.

621.396.615.141.2 3619

Study of the Magnetron in the Cut-Off Condition: Part 1—P. Fechner. (*Ann. Radioélect.*, vol. 7, pp. 83–105; April, 1952.) Various theories of space charge are discussed. The static distribution of the charge density is then calculated. In the case of electrons emitted with velocities obeying a statistical law, the electron density has a maximum value at a certain distance from the cathode, this distance depending on the anode voltage. The space charge takes the form of an extremely thin ring of very high density rotating round the cathode and including almost all the electrons circulating in the interelectrode space. An electron in the ring is in stable equilibrium and can oscillate with large amplitude if a resonance condition is established. Conditions of resonance in a multi-cavity magnetron are to be considered in part 2. See also 2678, 2680 and 2946 of 1950.

621.396.615.141.2 3620

The Magnetron in the Static Cut-Off State Experimental Study—J. L. Delcroix. (*Compt. Rend. Acad. Sci.* (Paris), vol. 234, pp. 2347–2349; June 9, 1952.) Investigations were carried out on carefully constructed magnetrons for which the ratio of anode to cathode diameter ranged from 1.25 to 7.5. Langmuir's law and the law governing the cut-off voltage (V_∞) were verified for each tube. Magnetic fields (H) of 50–150 gauss and anode voltages (v) of 50–500 v were used. A residual current was observed in the cut-off region; it is probably due to spontaneous space-charge oscillations and is of an order of magnitude 1000 times smaller than the thermionic currents which produce the space charge. It affords a means for studying the steady state and exhibits discontinuities for certain values of the applied voltage, the positions of the discontinuities only depending on the parameter m ($=V/V_\infty$) when H is varied. The residual current intensity depends on both H and m and increases with H when m is constant. The discontinuities fall into two classes, one class corresponding to transitions with small hysteresis of the order of 1–5 v, the other to transitions exhibiting very much greater hysteresis effects. Three distinct states have been distinguished these being the Brillouin state and the first two "bidromic" states. See also 3185 of 1951.

621.396.615.141.2 3621

Inverted Magnetron—J. F. Hull. (PROC. I.R.E., vol. 40, pp. 1038–1041; September, 1952.) Description of the construction and performance of a new type of magnetron in which the positions of the cathode and the segmented anode are the reverse of those in a normal magnetron. Tests on experimental tubes show that over-all efficiencies of 25–55 per cent can be achieved. Since a relatively low anode voltage and high anode current are required, it may be possible to operate such tubes from a gas-filled modulator tube without a pulse transformer.

MISCELLANEOUS

001.891/.892:621.39 3622

Army Communications—(*Wireless World*, vol. 58, pp. 353–354; September, 1952.) General account of the work of the Signals Research and Development Establishment at Highcliffe, near Christchurch.

621.38:061.4 3623

Electronic Instruments and Equipment. Exhibition in Manchester—C. A. Taylor. (*Nature* (London), vol. 170, pp. 407–408; September 6, 1952.) Short descriptions of some of the exhibits at the seventh annual exhibition of the North-Western Branch of the Institution of Electronics, July 1952.